# CHARACTERISATION OF MATERIAL PROPERTIES AND BEHAVIOUR OF COLD BITUMINOUS MIXTURES FOR ROAD PAVEMENTS

Lucas-Jan Ebels M.Sc. (Eng)

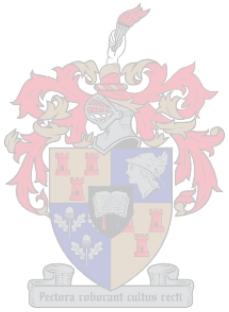


Dissertation presented for the degree of Doctor of Philosophy (Engineering) at Stellenbosch University, South Africa

Professor K. J. Jenkins Ph.D.
Promotor

March 2008

# DECLARATION

I, the undersigned, hereby declare that the work contained in this thesis is my own original work and that I have not previously in its entirety or in part, submitted it at any university for a degree.

Signature: ……

L. J. Ebels

Date: ……

*For Venesië, Tarren-Lee and Laycken*

# SUMMARY

The cold bituminous mixtures, which are the subject of this study, are obtained by mixing mineral aggregate with either bitumen emulsion or foamed bitumen at ambient temperatures. These techniques are frequently used in Cold In-Place Recycling whereby typically the top 150 – 250 mm of the existing pavement is reworked, as a rehabilitation measure when structural maintenance is required. To differentiate from the cold mixes for surfacing layers the term Bitumen Stabilised Materials (BSM's) is adopted here.

The increased use of BSM's, shortcomings in the existing design guidelines and manuals and ongoing developments in the concepts and understanding of these materials require further research into the fundamental properties and behaviour of BSM's. Achieving a better understanding of the fundamental performance properties of BSM's is the main objective of this study, with a view to using the extended knowledge for improvements to current mix design and structural design practices.

The state-of-the-art of bitumen emulsion and foamed bitumen techniques is reviewed in a literature study. Current best practices in the design of BSM's and pavements incorporating such materials is also included in this literature study. Shortcomings and areas for further improvement of the design practice have been identified. With new environmental legislation that recently came into effect in South Africa, the importance of BSM technology as an environmentally-friendlier and more sustainable construction technique is set to increase in the coming years.

A laboratory testing programme was set-up to study the properties and behaviour of BSM's and to establish links with the compositional factors, *i.e.* the type of binder used, the percentage of Reclaimed Asphalt Pavement (RAP) in the mix and the addition of a small dosage of cement as active filler. The mineral aggregates used were sourced in the USA and consisted of crushed limestone rock and RAP millings. These were blended in two different proportions of crushed rock : RAP, *i.e.* 3:1 (with 3.6 % residual binder) and 1:3 (with 2.4 % residual binder). Tri-axial testing (150 mm diamter) was carried out to determine shear parameters, resilient modulus and permanent deformation behaviour, while four-point beam testing was carried out to determine strain-at-break, flexural stiffness and fatigue behaviour.

It was found that the process of bitumen stabilisation improves the shear strength of the material, particularly in case 1 % of cement is added as active filler. This increase in shear strength is entirely the result of increased cohesion. There is a good correlation between the shear strength and the resilient modulus of BSM's. The resilient modulus of BSM is stress-dependent and the $Mr$-$\theta$ model is adequate to model the resilient modulus of the blends with a low percentage of RAP. For the blends with a higher percentage of RAP this model cannot be applied and the resilient modulus reduces in stiffness at higher deviator stress ratios.

A considerable part of the efforts of this study were dedicated to characterise and model the permanent deformation behaviour. The General Permanent Deformation

Law as originally developed by Francken applies also to BSM's. An improved non-linear method to converge at a solution for the model parameters that describe the tertiary flow part of this deformation law was developed as part of this study. Parameters that can be derived from the first stage of the permanent deformation test, *i.e.* initial strain and initial strain rate as defined in this study, were found that correlate well with the model parameters that describe the first linear part of the deformation law. Critical deviator stress ratios for the several mixes tested were determined. When BSM's are subjected to loading below these ratios, tertiary flow is unlikely to occur.

A high variability was generally found in the four-point beam test results, especially for the strain-at-break. Specimen preparation protocols and the quality of the beam specimens are of utmost importance when performing four-point beam tests on BSM's. This limits the practical applications of the strain-at-break test. Trends observed in the strain-at-break were also inconsistent and sometimes not in line with the other type of tests.

BSM's exhibit a visco-elastic behaviour, which was determined by flexural stiffness testing, however, to a lesser extent than HMA. Phase angles and Black Diagrams were developed for the BSM's tested, which also made it possible to determine the parameters of the Burgers Model, which is a mechanical model describing visco-elastic behaviour. Fatigue relationships were also developed for the BSM's tested. The fatigue performance of these mixes is lower than for selected HMA mixes. The foamed BSM generally showed better fatigue life than emulsion BSM, however, the lower initial stiffness of the foamed BSM's may contribute to a perceived longer fatigue life. For the mixes tested, the flexural stiffness of foamed BSM's is generally also lower than that of emulsion BSM's

It is recommended that the mix design of BSM's be split into two phases. During the first phase the usually large number of variables could be reduced to a selected few by means of UCS and ITS indicator testing. Subsequently, more fundamental parameters should be determined during the second phase, such as shear strength and resilient modulus, as well as permanent deformation behaviour. The fact that commercial laboratories in South Africa do not have tri-axial testing facilities is currently a practical limiting factor. Initiatives currently underway to develop "simple" shear tests are welcomed in this regard. It is proposed that classification of BSM is based on shear strength.

There are indications that shear failure in BSM is more critical than failure as a result of fatigue. The effect of curing resulting in an increase in BSM stiffness in the period after construction, *i.e.* typically 6 to 18 months, is currently ignored in structural design models. The rapid stiffness reduction of BSM's during the first period after construction in the current structural design models and also found during Accelerated Pavement Testing is not being observed in Long-Term Pavement Performance (LTPP). On the contrary, an increase in stiffness is observed in LTPP. This would indicate that stiffness reduction as a result of fatigue does not occur or is overshadowed by the effect of curing and that fatigue as a failure mechanism of BSM's is currently over-emphasized.

# OPSOMMING

Die onderwerp van hierdie studie is bitumen gestabiliseerde materiale (BSM) vir padbou doeleindes. Dit is mengsels wat bestaan uit minerale aggregaat wat by omliggende temperature gemeng word met bitumenemulsie of skuimbitumen. Hierdie tegniek word dikwels toegepas indien strukturele instandhouding vereis word waartydens die bestaande kroonlae (wat gewoonlik die boonste 150 – 250 mm van bestaande plaveisels verteenwoordig) hersirkuleer word. Om verwarring te voorkom met koue asfalt mengels vir oppervlak slytlae word die term bitumengestabiliseerde materiale (BSM) gebruik in hierdie proefskrif.

Die toename in die gebruik van BSM, tekortkominge in bestaande riglyne en handleidings asook nuwe insigte in die konsepte en begrip van hierdie materiale veroorsaak dat meer navorsing oor die fundamentele eienskappe en gedrag benodig word. Die hoofdoelstelling van hierdie studie is om ‘n better begrip te verkry van die fundamentele werksverrigtingseienskappe van BSM. Daar word beoog dat die verdieping in kennis gebruik kan word om verbeterings aan te bring aan die huidglike riglyne en handleidings vir mengselontwerp van BSM en die gepaardgaande strukturele ontwerp van plaveisels wat hierdie tipe materiale insluit.

Die huidige stand van die vakkennis op dié gebied word dmv ‘n literatuurstudie weergegee, asook die gebruikspraktyke vir die ontwerp van BSM en plaveisels met hierdie materiale. Tekortkominge en moontlike verbeteringe op hierdie gebied word ook geidentifiseer. Nuwe wetgewing met betrekking tot die omgewing is onlangs ingestel in Suid-Afrika. Hierdie wetgewing vereis meer omgewingsvriendelike en volhoubare konstruksietegnieke, wat toenemende gebruik van BSM alleen maar sal bevorder in die toekoms.

‘n Laboratoriumtoetsprogram is opgestel om die eienskappe en gedrag van BSM te bestudeer en om verbande te bepaal met samestellende faktore soos die tipe bindmiddel, die persentasie herwinde asfaltplaveisel (HA) in die mengels en die aanwending van klein hoeveelhede sement as aktiewe vulstof. Die minerale aggregaat wat gebruik is om die mengsel te maak is afkomstig van die VSA en bestaan uit gebreekte kalksteen en HA. Hierdie twee bestanddele is in twee verskillende verhoudings gemeng, *i.e.* 3:1 (met 3.6 % bindmiddelnhoud) en 1:3 (met 2.4 % bindminddelinhoud). Drie-assige skuiftoetse (150 mm deursnit) is uitgevoer om die skuifsterkte parameters, die veerkragmodulus en die blywende vervormingsgedrag te bepaal. Vierpuntbuigtoetse is uitgevoer om die breukrek, buigsterkte en vermoeiingslewe te bepaal.

Daar is bevind dat bitumenstabilisasie die skuifsterkte van granulêre materiale verbeter, spesifiek wanneer 1 % sement as aktiewe vulstof bygevoeg word. Hierdie verbetering in skuifsterkte kan geheel en al toegeskryf word aan die verhoging van die kohesie van die materiaal. Daar is ‘n goeie korrelasie gevind tussen die skuifsterkte en die veerkragmodulus van BSM.

Die veerkragmodulus is spanningsafhanklik en die *Mr-θ* model kan toegepas word om dit te modelleer. Dit geld egter net vir mengsels met ‘n lae persentatie HA. Vir mengsels met ‘n hoë persentasie HA kan hierdie model nie toegepas word nie en die veerkragmodulus verminder indien die uitwykspanning toeneem.

In hierdie studie is aansienlike aandag gegee aan die karakterisering en modellering van die blywende vervormingsgedrag van BSM. Die algemene wet vir blywende vervorming wat oorspronklik deur Francken ontwikkel is vir asfalt kan ook toegepas word op BSM’e. ‘n Verbeterde nie-lineêre metode om ’n oplossing daar te stel vir die modelparameters van die tersiêrevloei komponent van dié vervormingswet is ontwikkel tydens hierdie studie. Daar is ook bevind dat paramters wat afgelei kan word aan die hand van die eerste fase van die blywende vervormingstoets goed korreleer met die modelparameters van die vervormingswet wat die eerste reglynige deel beskryf. Kritiese uitwykspanningsverhoudings is ook vasgestel vir die verskeie mengsels wat getoets is. Dit is onwaarkynlik dat tersiêre vloei sal plaasvind in hierdie mengsels indien die aangewende belasting laer is as hierdie kritiese verhoudings.

‘n Groter mate van variasie is oor die algemeen gevind in die resultate van die vierpuntbuigtoetsresultate en in besonder vir die breukrektoetse. Die vervaardigingmetodiek van toetsmonsters asook die uiteindelike kwaliteit van dié toestsmonsters is van uiterste belang wanneer vierpuntbuigtoetse gedoen word. Dit sal in die praktyk die toepassing van die breukrektoets beperk. ‘n Bykomende faktor is dat die tendense in die breukrekresultate party keer teenstrydig is en nie ooreenstem met die ander toetse nie.

Die BSM vertoon ‘n visko-elastiese gedrag, wat bepaal is met behulp van die buigsterktetoetse, maar in ‘n mindere mate as die gedrag van asfalt. Fasehoeke is ook uitgewerk en Black-diagramme is saamgestel vir die verskeie BSM mengels. Dit maak dit moontlik om die parameters van die Burgersmodel te bepaal. Dié model is ‘n meganistiese model wat die visko-elastiese gedrag beskryf. Vermoeiingslyne is ook ontwikkel vir die BSM wat getoets is. Die vermoeiingswerksverrigting van hierdie mengsels is egter minder as in vergelyking met sekere asfaltmengsels. Die skuimbitumenmengsels toon oor die algemeen beter vermoeiingswerksverrigting as die bitumenemulsiemengsels. Die laer aanvangstyfheid van die skuimbitumenmengsels kan gedeeltelik bydra to hierdie waargenome beter vermoeiingslewe.

Daar word aanbeveel om die mengselontwerp van BSM te verdeel in twee fases. Tydens die eerste fase kan die aantal aanvanklike veranderlikes, wat gewoonlik groot is, herlei word tot enkele primêre veranderlikes deur gebruik te maak van eenassige druksterkte (EDS) en indirekte treksterkte (ITS) aanduidingstoetse. Tydens die tweede fase kan meer fundamentele eienskappe soos skuifsterkte en veerkragmodulus, asook die blywende vervormingsgedrag bepaal word. Die feit dat geen van die kommersiële laboratoriums in Suid-Afrika oor drie-assige skuiftoetsapparatuur beskik nie is tans ‘n beperkende faktor. Inisiatiewe wat tans aan die gang is om ‘n eenvoudige skuifsterktetoetsapparaat te ontwikkel word

ondersteun. Daar word aanbeveel dat die klassifisering van BSM gebaseer word op skuifsterkte.

Dit wil voorkom asof die skuifvloei van BSM meer krities is as die swigting as gevolg van vermoeiing. Die invloed van nabehandeling wat gepaard gaan met ‘n styfheidstoename van BSM’e tydens die eerste periode na konstruksie, dws tipies 6 tot 18 maande, word tans geignoreer in strukturele ontwerpmetodes. Die vinnige afname van die styfheid van BSM wat hierdie metodes wel voorspel vir die eerste periode na konstruksie en wat ook gevind is met versnelde plaveiseltoetse word nie gevind in opnames van langtermyn plaveiselwerksverrigting nie. In teendeel, ‘n toename in styfheid is wel gevind tydens hierdie opnames. Daar is moontlike aanduidings dat styfheidsafname as gevolg van vermoeïng nie voorkom nie of dat dit uitgekanseleer word deur die invloed van nabehandeling. Dit sal beteken dat daar tans in die ontwerpmetodes te veel klem geplaas word op vermoeïng as swigtingsmeganisme.

# ACKNOWLEDGEMENTS

I would like to express my sincere gratitude and appreciation to the following persons, without whom I would not have been able to successfully complete this study:

- My loving wife Venesië and daughters Tarren-Lee and Laycken, for inspiration, care and patience
- Jan and Maria Ebels, father and mother, for my upbringing, education and for forming me into the person I am
- Professor Kim Jenkins, promoter, for support, guidance, supervision, inspiration and for facilitating my studies at Stellenbosch University
- Professor Hugo, for support, kindness, the opportunities to interact with peers and for being an exemplary Engineer
- Annemieke Ebels, my only sister, this work is also for you
- Dirk and Sarah Williams, farther- and mother-in-law, for selfless support, generosity and for taking me in as a family member
- The Institute for Transport Technology and employees for financial and logistical support
- The Department of Civil Engineering, Professor Bester and staff, for the opportunity to study at Stellenbosch University
- A large part of the research used for this study formed part of a project for SemMaterials L.P. (USA). Their support and permission to publish the results is gratefully acknowledged
- Messrs. UWP Consulting, Zulch Lotter, Craig Northwood, Mike White and Adrian Skea for financial support and continued interest throughout my studies
- The Association of Asphalt Paving Technologist (USA) and their sponsors for the award of a scholarship in 2006
- Professors Molenaar and van de Ven, for guidance, advice and for educating me since 1995 in the field of pavement engineering and beyond
- Lee-Ann Mullins and Twagira Elias Mathaniya, MSc students, who undertook the largest part of the four-point beam testing as part of their thesis work
- Quintin Viljoen, BSc student, for assisting me with the monotonic tri-axial testing
- University and ITT secretaries Delysia Baard, Ansoné Jordaan, Janine Myburgh and Alett Slabbert

- Fellow students at the University, Riaan Burger, Thomas Glatz and Eben de Vos
- Sophia Arnolds, Ruth Sedeman, Kenny and Jenny Martin, Beryl Samuels and Rodney Davidse
- The workshop personnel, Oom Dries Rossouw, Louis Fredericks and Dion Viljoen
- The laboratory assistants Colin Isaacs and Gaven Williams
- All family, colleagues and friends that showed an interest in my studies

# TABLE OF CONTENTS

# LIST OF TABLES

# LIST OF FIGURES

# LIST OF ABBREVIATIONS AND SYMBOLS

## Abbreviations

| | |
|---|---|
| AASHO | American Association of Highway Officials, now AASHTO |
| AASHTO | American Association of Highway and Transportation Officials |
| APT | Accelerated Pavement Testing |
| ASTM | American Society for Testing and Materials |
| BFA | Beam Fatigue Apparatus |
| BSM | Bitumen Stabilised Materials |
| CBR | Californian Bearing Ratio |
| CCW | Counter-clockwise |
| CDAS | Control and Data Acquisition System |
| CIPR | Cold In-Place Recycling |
| CSIR | Council for Scientific and Industrial Research; based in Pretoria, South Africa |
| CW | Clockwise |
| EIA | Environmental Impact Assessment |
| EMC | Equilibrium Moisture Content; level at which the moisture content of granular material pavement layers stabilises |
| $ER_m$ | Expansion Ratio; foamed bitumen property |
| ETB | Emulsion (bitumen) Treated Base |
| EVT | Equiviscous Temperature; parameter used in the production of bitumen emulsion |
| FBTM | Foamed Bitumen Treated Material |
| FDR | Full-Depth Recycling; synonym for CIPR |
| FI | Foam Index; foamed bitumen property |
| GEMS | Granular Emulsion (bitumen) Mixes |
| HMA | Hot-Mix Asphalt |
| HSE | Health, Safety and Environment |
| HVS | Heavy Vehicle Simulator |
| ITS | Indirect Tensile Strength |
| LTPP | Long-Term Pavement Performance |
| LVDT | Linear Variable Differential Transformer |
| MEET | Minimum Emulsion Exit Temperature; parameter used in the production of bitumen emulsion |
| MPRD Act | Mineral and Petroleum Resources Development Act |
| MTS | Mechanical Testing and Simulation (MTS Systems®) |
| NEM Act | National Environmental Management Act |
| RAP | Reclaimed Asphalt Pavement |
| S.R. | Stress Ratio |
| SABITA | South African Bitumen Association |

| | |
|---|---|
| SABS | South African Bureau of Standards, now SANS, South African National Standards |
| SAMDM | South African Mechanistic (pavement) Design Method |
| SHRP | Strategic Highway Research Programme |
| S-N curve | Wöhler curve for fatigue characterisation |
| SU | Stellenbosch University |
| TG2 | Technical Guideline No. 2, published by the Asphalt Academy (2002) |
| TMH | Technical Methods for Highways |
| UCS | Unconfined Compressive Strength |
| UTM | Universal Testing Machine (UTM®) |

## Symbols

| | |
|---|---|
| $C$ | Cohesion |
| $E^*$ | Complex Modulus |
| $E_0$, $E_1$, $\lambda_0$, $\lambda_1$ | Burgers Model Parameters |
| $E_{sec}$ | Secant modulus |
| $E_{tan}$ | Tangent modulus |
| $M_r$ | Resilient modulus |
| $N_f$ | Number of load repetitions to failure |
| $S_{ini}$ | Initial stiffness (used for four-point beam testing) |
| $\delta$ | Phase angle (between applied strain and responsive stress) |
| $\varepsilon_b$ | Strain-at-break |
| $\varepsilon_f$ | Strain-at-failure |
| $\varepsilon_p$ | Permanent strain |
| $\theta$ | Bulk Stress = $\sigma_1 + \sigma_2 + \sigma_3$ |
| $\sigma$ | Normal stress |
| $\sigma_1$, $\sigma_2$, $\sigma_3$ | Major, intermediate and minor principal stress |
| $\sigma_d$ | Deviator stress = $\sigma_1 - \sigma_3$ |
| $\tau$ | Shear stress |
| $\tau_{½}$ | Half-life time; foamed bitumen property |
| $\varphi$ | Angle of internal friction |

# 1 INTRODUCTION

## 1.1 Cold bituminous mixtures

Bituminous mixtures for road pavements consist mainly of mineral aggregate and bitumen. The mineral aggregate can be divided into three fractions according to particle size, *i.e.* stone, sand and dust. Bitumen is a product that is obtained by refining crude oil and the standard product is called penetration grade bitumen. It is sometimes also referred to as asphalt-cement. The bitumen forms a mastic with the finest particles of the mineral aggregate, which glues the larger particles of the mineral aggregate together. The proportion of bitumen in bituminous mixtures varies depending on the type of mixture and application, but roughly ranges from 1% (added in the form of bitumen emulsion as compaction aid) up to 10% (guss-asphalt) by mass.

Penetration grade bitumen at ambient temperature has a high viscosity. In order to facilitate mixing with the mineral aggregate, the viscosity of the bitumen needs to be reduced. The following processes may be used to achieve this:

- Raising the temperature;
- Emulsifying;
- Foaming; and
- Adding selected petroleum solvents (cutting back).

In the first process, the temperature of the bitumen needs to be raised to approximately 155 – 175 ºC to reduce the viscosity sufficiently to facilitate proper mixing with the mineral aggregate. At the same time, the mineral aggregate itself needs to be heated to the same temperature to prevent an immediate reduction in the viscosity of the bitumen on first contact with the mineral aggregate, especially with the larger particles. The bituminous mixture obtained by this mixing process is called hot-mix asphalt, asphalt-concrete or in short, asphalt. Hot-mix asphalt mixtures need to be placed and compacted at sufficiently high temperatures, normally in excess of 110 ºC, before the viscosity of the bitumen, and thus of the mix, increases again as a result of lowering temperatures. At in-service temperatures the viscosity of the bitumen is high enough to provide sufficient stiffness to the asphalt mix.

The three other processes listed above differ from hot-mix asphalt in that the mineral aggregate does not need to be heated and can be mixed with the bitumen at ambient temperatures (depending on the type of cut-back bitumen it may sometimes be necessary to warm the aggregate). The technology is therefore referred to as cold-mix technology and the end-product is known as cold-mix asphalt or cold-mixes. These mixes can be placed and compacted at ambient temperatures.

There are certain other technologies, *inter alia* partially heating the mineral aggregate (half-warm mixes) or using certain additives to reduce the viscosity at

mixing temperature (Fisher-Tropsch waxes), but these fall outside the scope of this study.

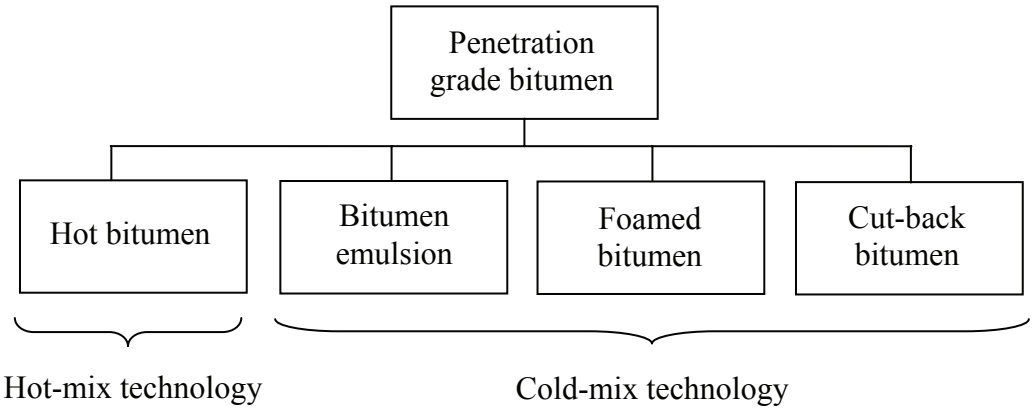


Figure 1: Mixing technologies for penetration grade bitumen

Emulsifying bitumen is generally done using a colloid mill. The bitumen temperature is raised sufficiently high, 140 – 180 ºC after which the bitumen is mixed with an aqueous solution and forced through a small gap in the colloid mill. In this process the bitumen is sheared into small droplets, approximately 5 – 10 micron in diameter, which are suspended in the continuous water phase. The bitumen is the discontinuous phase in the emulsion. The surfactants in the aqueous solution keep the droplets in suspension and give the emulsion its stability. Bitumen emulsions can be anionic or cationic, which refers to the particle charge of the bitumen droplets in the emulsion and depends on the type of emulsifier (surfactant) used. The residual bitumen content in emulsions is generally between 60 % and 65 %.

Bitumen emulsion can be mixed with the mineral aggregate at ambient temperatures. The mineral aggregate may be moist and there is no need to heat the aggregate. Once mixed with the aggregate, the emulsion starts to "break" and the emulsion water to evaporate. Breaking of the emulsion, also referred to as setting, is the process in which the state of the bitumen changes from being dispersed in the water phase to forming an adhesive layer on the surface of the aggregate. The rate of breaking depends on the type of emulsion, which can be from rapid-set, *e.g.* for spray applications to slow-set, *e.g.* for pre-mix applications.

Foaming of bitumen is the process in which cold water (foamant water) is injected into hot bitumen (approximately 150 – 170 ºC). The transition of the foamant water from a liquid to a gaseous form on contact with the hot bitumen results in expansion of the bitumen into foamed bitumen. This state of expansion is only temporary as the water vapour escapes from the foamed bitumen causing it to collapse. The expansion ratio and the half-life time characterise respectively the maximum expansion and the rate of collapse of foamed bitumen. During the short period of time during which the foamed bitumen is in an expanded state, its viscosity is sufficiently low for the bitumen to be mixed with the mineral aggregate. This mixing can be done at ambient temperatures and, as for bitumen emulsion mixes, the aggregate may be moist.

The process of adding selected petroleum solvents, such as kerosine or paraffin, is also referred to as "cutting-back" the bitumen. Cut-back bitumen contain solvents with a low boiling point that will evaporate from the mix with time. The evaporation of the solvent increases the viscosity of the bitumen and thus the stiffness of the cold-mix asphalt. During placing and compaction the solvent should not have evaporated yet and because the evaporation process takes time, the increase in mix stiffness is only slow after compaction and opening to traffic. Cut-back asphalt mixes are nowadays mainly used for patching application in small quantities. There are certain disadvantages in terms of health, safety and environment (HSE) associated with the use of cut-back asphalt. Cut-back asphalts fall outside the scope of this study.

## 1.2 Cold in-place recycling

The cold bituminous mixtures obtained by adopting the techniques described above as emulsifying and foaming of the bitumen are the focal point of this study. These mixes are often used in in-situ recycling of distressed pavements. This in-situ recycling process uses cold-mix technology and is therefore referred to as cold in-place recycling (CIPR). CIPR is a pavement rehabilitation measure that typically consists of the following operations, often all carried out in one-pass of a recycling machine:

- milling the existing pavement layers to depths of up to 300 mm;
- treatment with bitumen emulsion or foamed bitumen, often in combination with addition of a small percentage of active filler;
- adding compaction water; and
- replacing the mix.

In a CIPR process as described above the surfacing layer (reclaimed asphalt pavement, RAP) as well as part or whole of the granular or stabilised base layer are recycled. This is in contrast to certain recycling processes whereby only a part of the asphalt surfacing is milled up, treated and replaced. To distinguish these two processes, the process of milling through the surfacing layer(s) and including the base layer in the recycling operation is therefore referred in some countries referred to as full-depth recycling (FDR), particularly the United States. The principle of CIPR is shown in Figure 2.

The main focus of many road authorities around the world is to maintain their road network at high standards or even to upgrade it, rather than extending the network. The fact that the road network in South Africa consists mainly of high quality granular pavement layers with thin bituminous surfacing layers, combined with the fact that large parts of the network are in a state of distress, provides an ideal background for the use of CIPR in pavement rehabilitation and upgrading. The popularity of CIPR can be seen from the increase in the number of recycling machines in Southern Africa. The graph in Figure 3 shows a steady increase in total number of recycling machines during the 1990's and a sharper increase after the turn of the century.

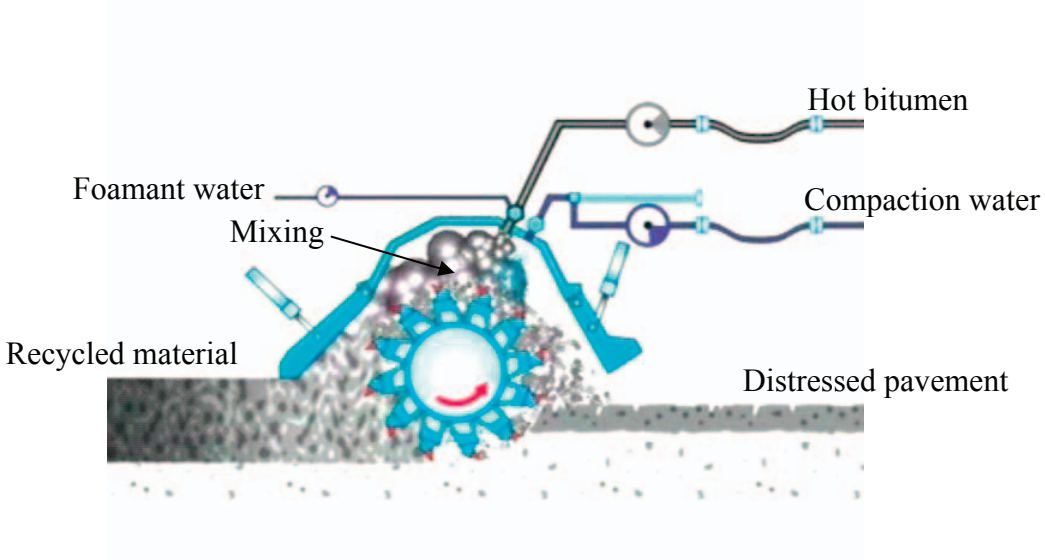


Figure 2: Schematic process of CIPR with foamed bitumen (Ebels *et al.*, 2005)

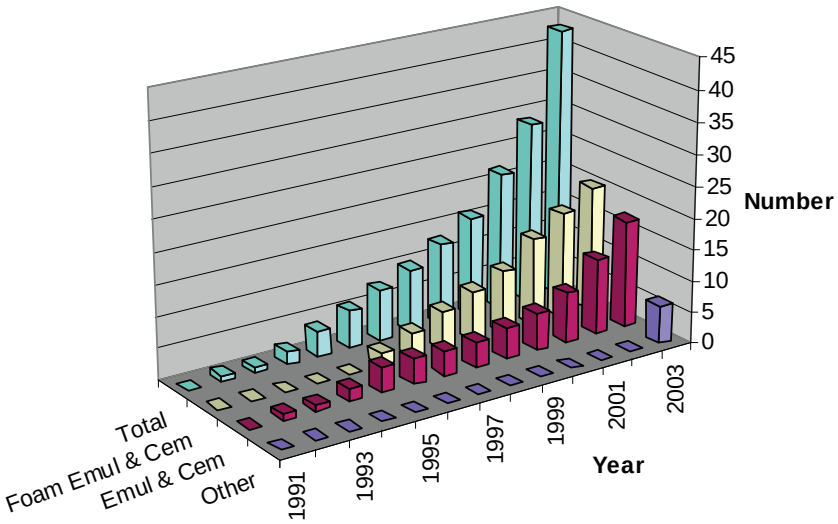


Figure 3: Number of recycling machines in Southern Africa (Ebels *et al.*, 2005)

The residual binder contents added to the mineral aggregate in the process of CIPR are generally low (< 4 %) in comparison to hot-mix asphalt. The recycled product is also not used as final surfacing layer but rather as base (or sometimes as subbase) layer. The end-product is therefore not a hot-mix asphalt equivalent, but a granular material of which the properties and performance have been improved by adding bitumen using cold-mix technology. The term Bitumen Stabilised Material (BSM) is adopted in this study to refer to these materials. BSM's typically fulfil a role in the pavement that is between the application range of hot-mix asphalt and unbound granular materials. The term BSM has also been adopted to prevent confusion with cold-mixes that are produced to act as hot-mix asphalt equivalents.

## 1.3 BSM design guidelines

The first experiments with BSM's in Southern Africa took place during the 1960's using cationic bitumen emulsions. The first guideline on the use of bitumen emulsions in construction and maintenance of roads was published in 1972. This manual however, dealt with general aspects of the use of bitumen emulsion and provided little guidance in terms of mix design of BSM's and structural design of pavements incorporating such materials.

It was not until 1993 that the Granular Emulsion Mixes (GEMS) Manual (SABITA, 1993) was published, which introduced laboratory test procedures, mix design procedures, evaluation criteria and structural design guidelines for granular bitumen emulsion mixes. Certain shortcomings that were identified in the GEMS Manual were updated in the Emulsion Treated Base (ETB) Manual, which was published six years later (SABITA, 1999). This manual provides extended guidelines on structural design, mix design, constructability and economic aspects. The mix design and structural design in the ETB manual are based on two material classes, *i.e.* E1 and E2. The mix design tests that govern this classification are the Californian Bearing Ratio (CBR) and Unconfined Compressive Strength (UCS) tests. The ETB Manual is to date the most recent guideline document published in South Africa that deals with the design and use of bitumen emulsion stabilised materials.

Because of the limited usage of foamed bitumen prior to the 1990's, no South African guidelines for the use of foamed bitumen were developed earlier on. Designers in Southern Africa mainly 'borrowed' from the available guidelines for bitumen emulsions, international foamed bitumen guidelines, as well as hot-mix asphalt mix design philosophy when designing for foamed bitumen treated materials. With the increased usage of foamed bitumen treatment by practitioners during the 1990's, the fundamental understanding of these materials required for mix design and structural design lagged behind.

The need for mix and structural design guidelines for foamed bitumen treated materials was partially addressed by research into foamed bitumen mix design aspects by Jenkins (2000). Subsequently an interim guideline (TG2) for foamed bitumen treatment was published (Asphalt Academy, 2002) based on this research and limited accelerated pavement testing (APT) testing with the Heavy Vehicle Simulator (HVS) on pavement structures with a foamed bitumen treated base layer. Extensive laboratory testing, including Indirect Tensile Strength (ITS), UCS, four-point beam testing and tri-axial testing, was also used to shape the TG2 Guideline, but only the ITS and UCS tests were selected for mix design. This was primarily on the basis of the capacity of the commercial laboratories to only carry out relatively unsophisticated tests. The guideline was launched as an interim guideline with the intention to update the manual once further research results became available.

Although at time of publication of the TG2 Guideline it was already evident that "true" shear properties would provide more reliable evaluation criteria compared to UCS and ITS testing, it was at the time decided that the industry was not ready for tri-axial testing as part of mix design procedures (Ebels and Jenkins, 2007). The use

of UCS and ITS tests for mix design purposes has certain limitations and the same applies to the CBR and UCS testing adopted in the ETB Manual. These shortcomings are discussed in this study.

Both the ETB Manual and the TG2 Guideline adopt a design philosophy for the structural design of pavements incorporating bitumen emulsion and foamed bitumen stabilised materials respectively that is based on the structural design of cement stabilised materials as developed in South Africa. This philosophy consists of a two-phased approach. Effective fatigue is considered to be the dominant behavioural mechanisms in the first phase, while in the second phase the material is considered to behave equivalent to granular material, although with a higher stiffness modulus, with shear failure as the critical mechanism.

In the structural design models for cemented materials a significant reduction in the stiffness of the cemented material takes place during the first phase. A similar reduction was found for BSM's during APT using the HVS. Fatigue with associated stiffness reduction thus plays an important factor in the structural design of BSM in the ETB Manual and the TG2 Guideline.

There is currently debate amongst researchers if the assumed rapid stiffness reduction of BSM's during the first phase for structural design is correct. Long-term Pavement Performance (LTPP) observations indicate that during the early life the stiffness of BSM's in the pavement increases (due to curing) rather than decreases. This being the case, there may currently be and over-emphasis on fatigue as a failure mechanism of BSM's.

To date the design and use of bitumen emulsion and foamed bitumen treated materials have been approached separately from each other and different documents exist for each type of BSM. Although different stabilisation techniques, the mix design criteria and structural design approach for each of them are to a large extent similar. Conceptual revisions to the latest guidelines for either of the two techniques would apply to the other as well. This begged the question whether there should not be a unified BSM design guideline. There are currently research initiatives underway to develop such a unified BSM design guideline (Jenkins *et al.*, 2006). The work discussed in this study also feeds into this unified BSM guideline.

## 1.4 Research objectives and limitations

The increased use of Bitumen Stabilised Materials (BSM's), shortcoming in the existing design guidelines and manuals and ongoing developments in the concepts and understanding of BSM requires further research into the fundamental properties and the behaviour of these materials. Increased knowledge would enable more informed decisions being made in the road-building industry, be it by the road authority, consulting engineer or contractor. This would lead to better performing pavements, more cost-effective solutions, more environmental-friendly construction techniques, improved sustainability and ultimately a better service to the civil society.

The main objective of this dissertation is therefore to research the fundamental material properties and behaviour of BSM's in order to extend the existing knowledge of these materials with a view to using the increased understanding for improvements to mix design and structural design of pavements incorporating these materials.

This objective is divided into the following sub-objectives:

1. To review the state-of-the-art of bitumen emulsion and foamed bitumen technology, critically analyse current BSM mix design and structural design guidelines and to evaluate material models that can be used to estimate material properties and behaviour.

2. To establish the following material properties of BSM's:
   - shear properties (cohesion and angle of internal friction);
   - stiffness (resilient modulus under axial loading and master curves of bending stiffness);
   - strain-at-break (in bending mode).

3. To establish the following laboratory behaviour of BSM's:
   - permanent deformation as a result of accumulation of plastic axial strain under repeated loading;
   - bending fatigue as a result of repeated loading.

4. To establish relationships between the properties and behaviour mentioned in Sub-objectives 2 and 3 above of BSM's and the following variable parameters:
   - The percentage of RAP in the mix (25 % vs. 75 %);
   - The percentage of active filler (0 % or 1 %) in the mixes with 25 % RAP;
   - The type of binder, *i.e.* two bitumen emulsions and one foamed bitumen.

5. To select appropriate existing material models to describe the observed material properties and laboratory behaviour, to determine the model parameters and to compare these model parameters with those of other materials.

6. To demonstrate and discuss how the results of Sub-objectives 4 and 5 above can be used to link laboratory test results to the performance of BSM's and to improve current design methods.

The BSM mixes investigated are limited to mixes that are typically obtained by CIPR and the mix variables were chosen within the requirements set by sponsors of the work. These variables are however realistic for South African applications. The BSM mixes tested in this study are generally used for base course construction and should not be regarded to replace hot-mix asphalt products, although improved understanding and use of BSM's may impact on the demands for such products.

The experimental testing is limited to tri-axial testing and four-point beam testing. Other tests such as unconfined compressive strength testing, indirect tensile testing

and other shear tests did not form part of this study. The experimental matrix is limited to nine mixes, allowing for the variables as described in Sub-objective 4 above to be investigated. Other parameters such as *inter alia* grading, density, curing and binder content that may have a significant influence on the performance and behaviour of BSM's are not varied in this study. Also, the compatibility of aggregate and bitumen emulsion has not been investigated here.

The modelling of the material behaviour in this study is limited to using existing material and behavioural models. The experimental investigations are limited to laboratory testing and no field testing or field performance monitoring was carried out during this study.

## 1.5 Reading guide

In Chapter 2 a comprehensive background is provided of bitumen emulsion and foamed bitumen. This background includes historic developments, technology and manufacture and aspects that are of particular importance to each of these technologies. A sound understanding of the technologies is considered of importance when dealing with BSM's. The use of BSM in Southern Africa is also discussed in this Chapter and an overview of guideline documents dealing with these materials is provided. Consideration is given to mix design and structural design of pavements incorporating BSM's and certain shortcomings have been identified. The Chapter closes with a brief discussion of some of the advantages of CIPR.

The literature study continuous in Chapter 3, but this Chapter focuses more on stress and shear stress and the material properties that can be derived from the engineering stress-strain diagram. The Chapter provides a literature overview of the available models to describe material properties and behaviour. These models form the basis for the interpretation and evaluation of the test results in the later chapters.

The materials and mixes tested in this study are in detail described in Chapter 4. This Chapter also includes the experimental matrix. The laboratory testing in this study focuses on tri-axial testing and four-point beam testing. The test protocols followed and the test conditions are described in this Chapter. The materials testing results are presented in the following Chapter 5. The information provided in Chapter 5 is presented in the form of tables of graphs, without any discussion or interpretation of the results. This follows in the subsequent Chapter 6.

The materials testing results are discussed test by test in Chapter 6 and where applicable the models discussed in Chapter 3 are used to evaluate the material properties and behaviour. The influence of the experimental variables, *i.e.* the percentage of RAP in the mix, the percentage of active filler in the mix and the type of binder, is discussed for each material property and type of behaviour tested.

Chapter 7 provides limited examples of how the test results obtained in this study can be used for pavement modelling and design. Limitations of the analysis methods

used are discussed and demonstrated. Within these limitations, however, useful information can be extracted and guidance to the practitioner be given.

In Chapter 8 a synthesis of the study results is provided. The importance of the parameters that were not varied in this study are discussed, *e.g.* compaction, grading, curing and moisture content. The performance of the different mixes and the influence of the experimental variables are compared over the full range of laboratory tests carried out. This performance is compared with other materials, such as hot-mix asphalt and granular materials, as well as similar materials from other research. Critical elements of the laboratory testing and the pavement design are brought together in this Chapter.

In the last Chapter the conclusion and recommendations that follow out of this study are presented. These conclusions and recommendations are broad and aimed at providing an overview of the overall performance of BSM's and with a view that the results of this study may contribute towards improving current design practice.

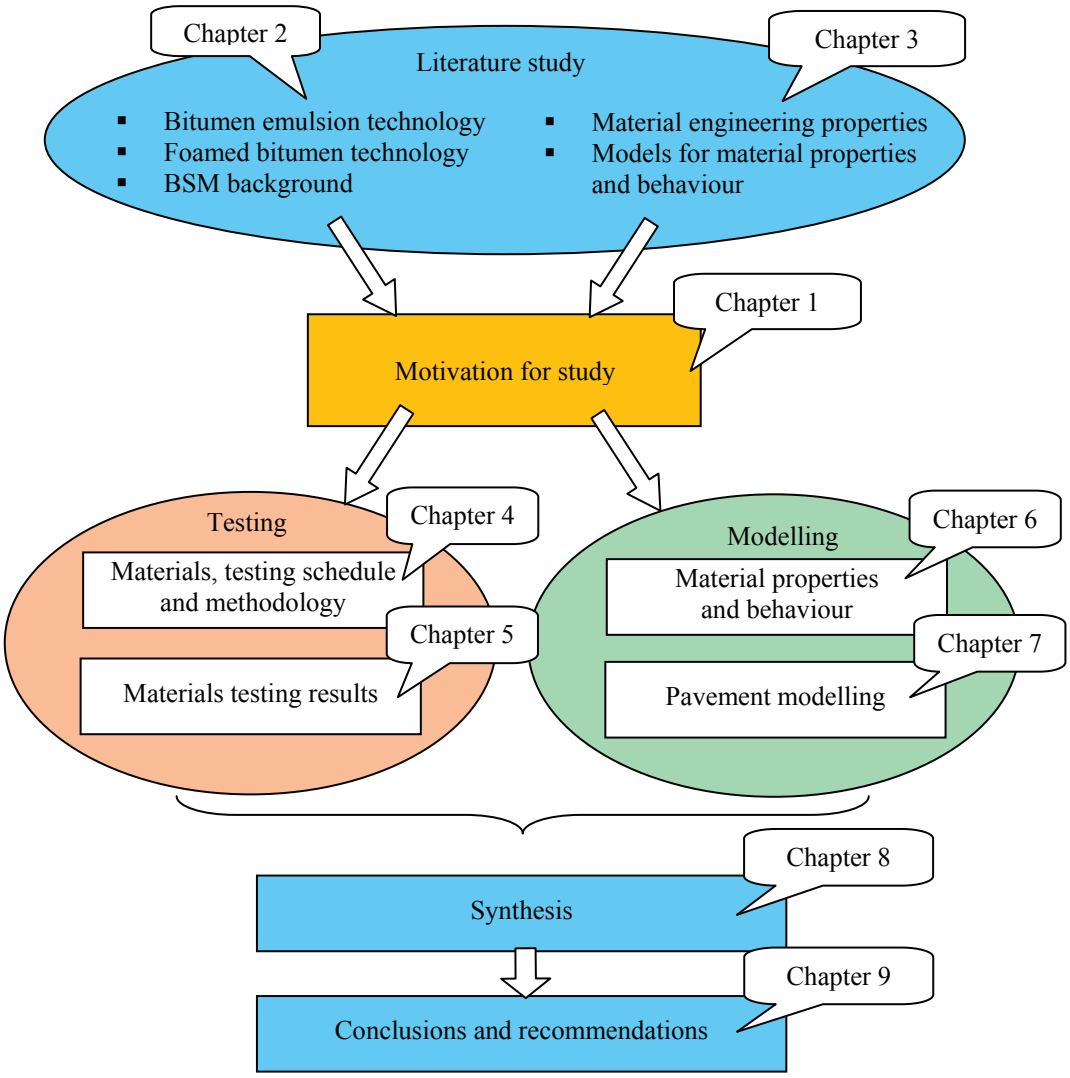


Figure 4 : Reading guide – structure of dissertation

## References

Asphalt Academy, *The design and use of foamed bitumen treated materials*. Interim Technical Guideline No. 2, Pretoria, South Africa, 2002

Ebels, L. J. and Jenkins, K. J., *Mix design of bitumen stabilised materials : Best practice and considerations for classification*, Proceedings of the 9th Conference on Asphalt Pavements for Southern Africa, Gaborone, Botswana, 2007

Ebels, L. J., Jenkins, K. J. and Collings, D., *Cold mix (bitumen stabilisation) technology in Southern Africa into the 21st Century*, International Symposium on Pavement Recycling, São Paulo, Brazil, 2005

Jenkins, K. J., Ebels, L. J. and Mathaniya E. T., *Updating Bituminous Stabilised Materials Guidelines: Mix Design Inception Study***.** Sabita and Gauteng Department of Transport, Roads and Public Works. Pretoria, South Africa, 2006

SABITA. *Manual 14: GEMS – The design and use of granular emulsion mixes*. Roggebaai, South Africa, 1993.

SABITA. *Manual 21: ETB – The design and use of emulsion-treated bases*. Roggebaai, South Africa, 1999

# 2 BACKGROUND TO COLD BITUMINOUS MIXTURES

## 2.1 Introduction

In pavement engineering two distinct categories are traditionally used to categorise pavements, *i.e.*:

- flexible pavements; and
- rigid pavements.

This categorisation is generally being used in the developed first world countries. In second and third world countries however, large parts of the road networks consist of unsurfaced roads. Because unsurfaced roads are constructed using different materials in the top layers compared to flexible pavements and are designed according to a different philosophy, unsurfaced roads are added here as a third category in the general discussion of the pavements. The material usage per pavement category in the different layers of the pavement structure is summarised in Figure 5.

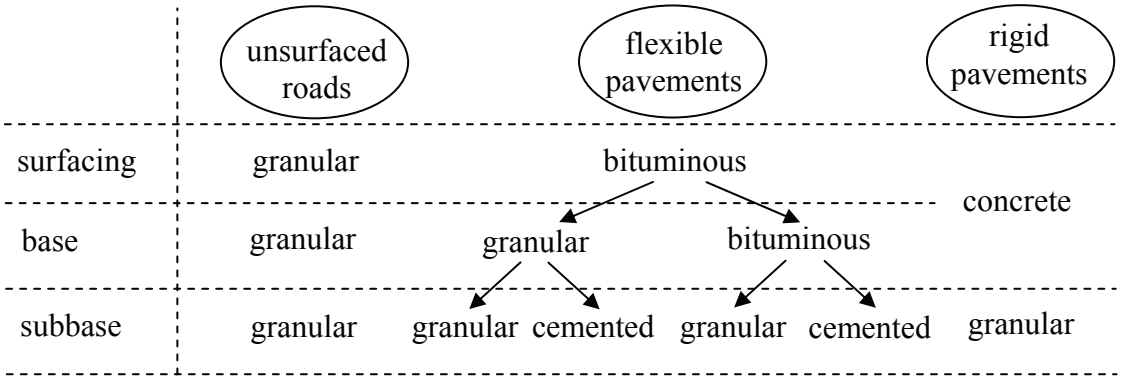


Figure 5: Pavement categories and material usage

Unsurfaced roads typically consist of only granular materials over the full depth of the pavement structure. There is scope for the use of CIPR in upgrading unsurfaced roads to surfaced standards. The material usage for concrete pavements is also relatively straight forward, *i.e.* concrete on a granular substructure. The design of rigid pavements is vastly different to that of flexible pavements. Neither unsurfaced roads, nor rigid pavements are discussed further in this study.

The largest variety in material usage can be found in flexible pavements. Flexible pavements are characterised by a bituminous surfacing or top layers. A distinction can be made between:

- thick (or full-depth) asphalt pavements; and
- thin asphalt pavements.

With thick asphalt pavements the base layer(s) also consist of bituminous material. Thick asphalt pavements are common in Europe, North America and other well developed countries, but are less common in countries like South Africa. Thin asphalt pavements generally consist of only a bituminous surfacing (typically < 50 mm) with a granular base layer. Bituminous surfacings such as chipseals and other microsurfacings also fall into this category. Thin asphalt pavements are widely used in South Africa, but also in many other developing countries.

In South Africa thin asphalt pavements are often constructed in combination with high quality crushed stone base layers and stiff cemented (stabilised) subbase layers. Pavement structures with such cemented subbase layers are sometimes also referred to as inverted pavement structures, because the granular base is supported by a stiffer cemented subbase. Granular materials show stress dependent behaviour and the stiff support of the subbase enables stiffer behaviour of the granular base than what would be the case with the same base layer on a less stiff granular subbase.

Thin asphalt pavements have in the past also been used in combination with very stiff cemented base layers. However, these highly cemented base layers exhibit shrinkage cracking similar to unreinforced concrete pavements. These shrinkage cracks quickly reflect through the thin bituminous surfacing and result in ingress of moisture and subsequent pumping. Thin asphalt pavements with highly cemented bases are no longer being constructed in South Africa nowadays and are therefore not discussed further here.

Bitumen Stabilised Materials (BSM's), being the subject of this study, are almost without exception used in flexible pavements. BSM's can be utilised both in base and subbase layers. The two main components of BSM's are granular and bituminous materials. The latter is either bitumen emulsion or foamed bitumen.

A background to these components of BSM's is given in the first section of this Chapter. Considerable attention has been given to the background of bitumen emulsion, as it was found that this information is not easily accessible and readily available in the public domain.

The use of BSM's in Southern Africa is discussed in the subsequent section of this Chapter. They are commonly applied in cold in-place recycling (CIPR). Existing guideline documents are discussed and consideration is given to mix design testing and BSM design philosophy. Certain shortcomings in the existing design methods have been identified. This Chapter ends with a discussion of the advantages of CIPR.

## 2.2 The material components of cold bituminous mixtures

### *2.2.1 Granular materials*

Granular material makes up the largest part (both in mass and volume) of a cold mix. Crushed stone, natural gravel, reclaimed asphalt pavement (RAP) and natural sand are amongst the granular materials used to produce BSM's. When cold in-place recycling (CIPR) is applied, there is limited choice in selection of aggregates and one has to work with the materials present in the existing pavement.

In answering the question whether the RAP in BSM acts as "black rock" or whether blending and rejuvenation of the aged old binder and fresh new binder takes place, it is important to consider the temperature at which mixing takes place as well as the condition of the old binder. In the case of hot-mix recycling the aged and fresh bitumen becomes a one-phase system. A so-called log-pen rule has been developed in the Netherlands to determine the penetration of the blended bitumen of a mix containing RAP. In a cold mixing process as used for BSM's no blending of the aged and fresh bitumen takes place and the resultant is a two-phase system (Voskuilen *et al.*, 2004). In the latter case, the RAP aggregate in a BSM should be regarded as "black rock". This concept has however not been investigated further in this study as it was not a study objective.

The binder content in mixes with a high percentage of RAP may be reduced to achieve similar mix properties because of the following:

- No binder absorption will take place in case of the RAP particles, because these are already coated with a bitumen film;
- Cohesion will be improved due to the higher affinity of the fresh bitumen with the RAP particles compared to virgin aggregates;
- Durability and moisture susceptibility is improved by the old binder on the RAP particles.

Typical percentages of RAP in the recycled mix in South Africa are in the order of 25% or less. This would approximately be obtained when recycling the top 200 mm of a pavement with a 40 mm asphalt wearing course.

The following properties of the parent material are among those that are of importance for the BSM properties:

- Geological origin;
- Soil classification;
- Grading after recycling.

An introduction to rock and soil, rock-forming minerals and the classification used for rock and soil is provided in Appendix A. This Appendix contains essential background information for the pavement materials engineer, because the geological source of the rock and the mineralogy influences the performance of BSM's and in particular the performance of bitumen emulsion mixes.

Most rock-forming minerals are silicates ($SiO_2$) and carbonates ($CO_2$ or $CO_3$). Rocks with high silicate content are acidic (low pH), while rocks with high carbonate content are alkaline (high pH). Cationic bitumen emulsions, which are acidic, generally react with all rock types, while anionic bitumen emulsions, which are alkali, have a greater affinity for alkaline rocks. Known incompatibility issues of anionic bitumen emulsions are with acidic rocks such as quartzite, granite, sandstone, rhyolite, syenite, felsite and sometimes tillite.

The grading of the aggregate is also an important factor in the performance of BSM's. The TG2 Interim Guideline for Foamed Bitumen Treated Materials (Asphalt Academy, 2002) provides guidelines for the grading of the granular material being stabilised with foamed bitumen. Aggregate gradings that approach the maximum density curve (Nijboer curve with n = 0.45) perform the best. The percentage passing the 0.075 mm sieve is of importance. A considerable percentage of filler (5 – 15% passing 0.075 mm) is required for optimal foamed bitumen mixes. Bitumen emulsion mixes generally perform better with a lower percentage of filler. Bitumen emulsion mixes are also less sensitive to gaps in the grading.

### *2.2.2 Bitumen emulsions*

2.2.2.1 Historic developments in bitumen emulsion

The first bitumen emulsions were produced and used in Europe at the beginning of the 20th century. During 1902 Ernest Guglielminetti, a Swiss physical doctor, established the French Anti-Dust Association for the purpose reducing dust generation by traffic on roads along the Mediterranean shoreline of Monaco. The association promoted the coating of road surfaces with hydrocarbons. The hydrocarbons were emulsified using ammonium based soap. In 1905 the first dedicated bitumen emulsion plant was commissioned in Lutterbach, Germany, by a chemist named Emile Feigel.

In 1908 the first International Road Congress was organised in Paris, which was attended by 1,600 delegates from 33 countries. About 20% of the papers were related to issues around reducing or preventing dust generation (Mom, 2004). Following this congress the Permanent International Association of Road Congresses (PIARC) was founded a year later.

During the 1920's Hugh Mackay, an English chemist, developed bitumen emulsions further and filed a patent on anionic bitumen emulsion in 1922. The trade mark was "Cold Spray" which was a few years later changed into "Cold Asphalt". This was later abbreviated into "COLAS" (Le Corroler, 2005). The use of bitumen emulsion for road works increased rapidly and within four years five countries had manufacturing plants; viz England, Germany, Denmark, Australia and India. The combined annual production of these five countries was estimated at 150,000 tons in 1926.

In South Africa, the company COLAS established the first bitumen emulsion manufacturing plant in 1928 in Bellville (Louw *et al.*, 2004).

The first anionic bitumen emulsions up to approximately 1950 were available in two types, i.e. Type A and Type B. These were a spray type and pre-mix type respectively that were specified in the British Standards. The emulsions were produced using fatty acids such as tall oils. These long chain fatty acids were neutralised using sodium hydroxide and imparted a negative loading on the bitumen droplets. The Type A and Type B emulsions were chemically not very stable. In combination with "hard water", cement or granular material with a high fines content the emulsion broke quickly.

During the late 1950's, a third type of anionic bitumen emulsion was developed. This was stable-mix type emulsion and was produced using Vinsol® resin, neutralised with alkali. The alkaline soaps derived from this complex resin derived from pinewood, are not destroyed by the action of aggressive mineral filler such as cement and the fines associated with crushed aggregate and natural gravel materials. Although some chemical reaction and precipitation occurs between the alkaline resin soaps and the cement, some residual functional groups in the resin are not affected by the presence of the cement, causing stabilisation of the emulsion in the presence of the aggressive compounds. Steric repulsion between the complex, branched alkaline resin molecules could also be responsible for this stable behaviour in the presence of aggressive fillers. Emulsions prepared with the alkaline resin soaps are thus very stable and breaking only takes place by evaporation or absorption of the emulsion water (Louw, pers. com., 2007).

With the stable-mix type emulsion it was now possible to use bitumen emulsions to make slurries (slurry seals, rut filling and micro-surfacings) and for stabilisation. The first slurry machine was brought into South Africa in 1962. During the early 1960's the first bitumen emulsion stabilised sand bases were constructed in South Africa

Another important milestone in the evolution of bitumen emulsions was the development of cationic emulsions, initiated by ESSO in 1951 (Le Corroler, 2005). The cationic emulsifiers are based on long chain amines. The amines are neutralised using acids such as hydrychloric, sulphuric and sometimes phosphoric acids. The bitumen droplets are positively charged when cationic emulsifiers are used. The cationic emulsions are also available in three types, i.e. spray, pre-mix and stable-mix type.

Cationic emulsions were first used in South Africa around 1965 (Louw, 2006). The first standard specification for cationic emulsion was SABS 548 dating from 1972. Globally, cationic emulsions quickly took over from anionic emulsions. Only ten years after the first cationic emulsions were manufactured, 50% of all bitumen emulsions produced was cationic. In 1972 more than 90% of all emulsion manufactured were cationic.

The split between cationic and anionic emulsions in South Africa differs considerably from that of the rest of the world. This is because there is a steady growth in the use of hot-applied (modified) binders for chip seals, at the expense of cationic spray grade emulsions, which were traditionally used for this purpose. The

popularity of the Cape Seals, texture slurries and emulsion treated base stabilisation has contributed to the increased use of anionic stable grade emulsions. The hot, dry climate in South Africa is conducive to the use of anionic emulsions for this purpose (Louw, pers. com. 2007). In addition, emulsifiers used for the production of anionic emulsions are cheaper compared to cationic emulsifiers.

2.2.2.2 Bitumen emulsion technology

Emulsions are dispersions of one immiscible fluid in another fluid. Any two immiscible fluids can be used to produce an emulsion. In the case of a bitumen emulsion the two fluids are bitumen and water. One can distinguish between three main types of emulsions (see Figure 6):

- Oil-in-water (O/W);
- Water-in-oil (W/O), also called inverted emulsion; and
- Multiple emulsions (W/O/W).

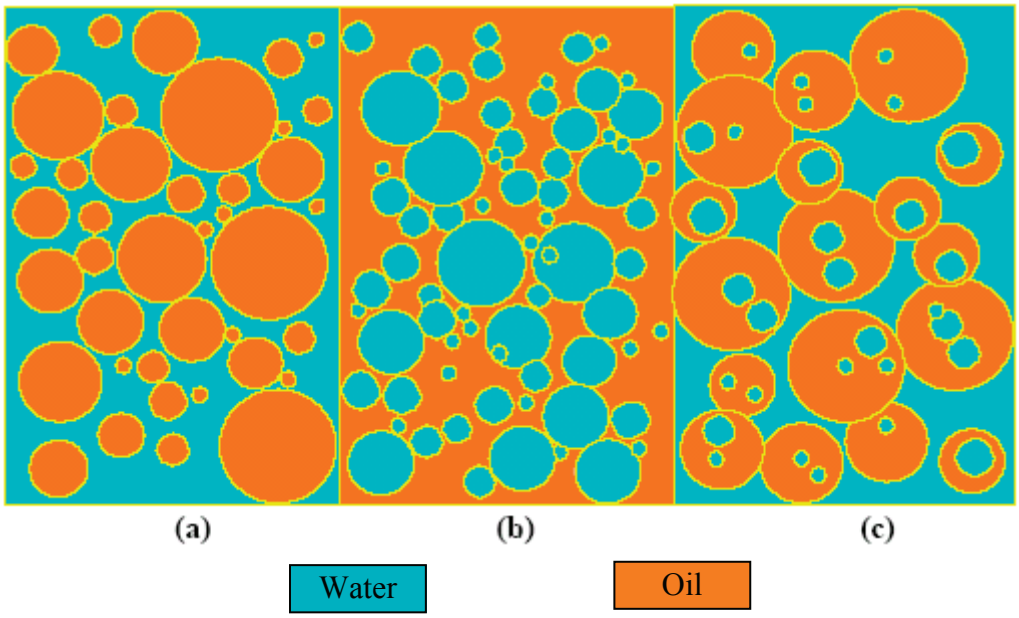


Figure 6: Types of emulsions: *(a)* O/W emulsion, *(b)* W/O emulsion, and *(c)* multiple W/O/W emulsion (James, 2006)

The oily fluid in emulsions is bitumen. In case of the O/W type emulsion, the bitumen droplets make up the dispersed phase in a continuous water phase. Multiple emulsions are like oil-in-water emulsions, except that the dispersed phase is not a homogeneous fluid, but a heterogeneous fluid, *i.e.* the dispersed fluid phase contains another phase. The phase contained in the dispersed phase is not necessarily the same as the continuous phase (water). This is illustrated by emulsion (c) in Figure 6. Multiple emulsions will be encountered in the cosmetic industry and are not used in road building applications.

Normally the bitumen content for O/W bitumen emulsions ranges from 30% (diluted emulsion) to approximately 75%. The upper limit of the bitumen content in an O/W emulsion depends on the distribution of the bitumen droplets sizes. When the

bitumen droplets are uniform in size, the maximum bitumen content of the emulsion is lower than when the droplets size distribution is more continuously. In the latter case the smaller droplets fit in between the larger droplets. The higher the bitumen content in the bitumen emulsion, the higher the viscosity of the emulsion.

The size of the bitumen droplets typically range from 1 micron to 20 micron in diameter. Emulsions with particle sizes in this range are referred to as macro-emulsions (James, 2006). Macro-emulsions are thermodynamically unstable and phase separation will eventually take place. As opposed to macro-emulsions, micro-emulsions are single phase-like solutions and thermodynamically stable. Micro-emulsions have droplets less than 0.1 micron in diameters in size (Akzo Nobel, 2001). Micro-emulsions require a specific emulsifier formulation and packing. Due to the exponential increased surface area as a result of smaller droplet sizes, much more emulsifier is required in micro-emulsion than in macro-emulsions. Bitumen emulsions are typically macro-emulsions. A particle (droplet) size distribution of a typical bitumen emulsion is shown in Figure 7. A microscopic image of the bitumen emulsion is shown in Figure 8.

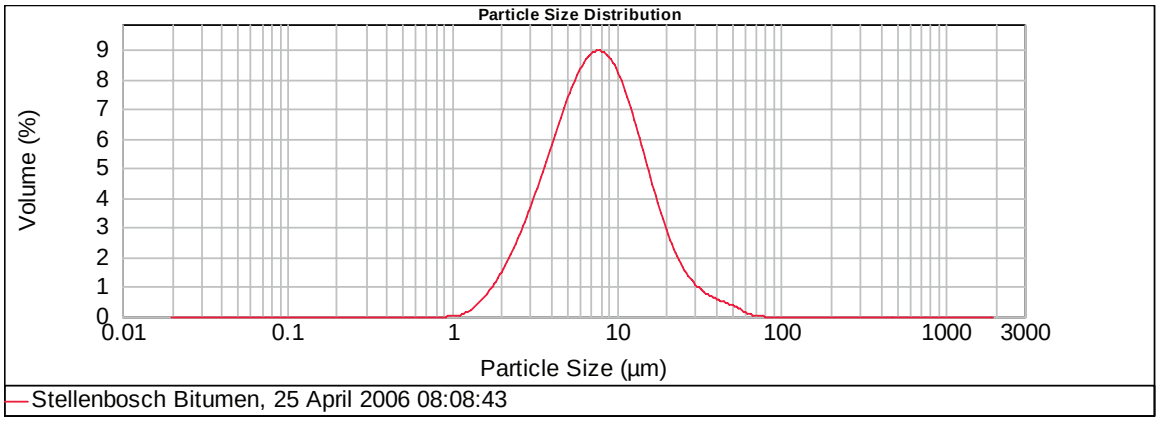


Figure 7: Typical particle (droplet) size distribution of an O/W bitumen emulsion (65% bitumen content)

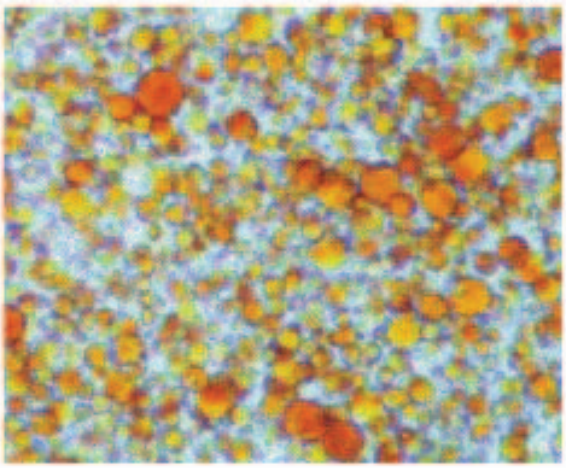

Figure 8: Microscopic image a of a bitumen emulsion (James, 2006)

The bitumen droplets in the emulsion are either positively (cationic) or negatively (anionic) charged. This electrostatic charge is caused by the emulsifier that is active on the surface of the bitumen droplet. The emulsifier is therefore a surface active agent, also called surfactant (Akzo Nobel, 2005). Due to the electrostatic charge on bitumen droplets, polar repulsion forces prevent the droplets to closely approach and adhere to each other (James, 2006).

When reaching the upper limit of the bitumen content, there is not enough space to accommodate more droplets without any external force. When there is enough energy available to overcome the electrostatic repulsion forces between the bitumen droplets, these droplets will start to flocculate. During flocculation the bitumen droplets adhere to one another. Water becomes trapped between the bitumen droplets during this process. Flocculation generally occurs if the bitumen content ranges from 70% to 80% (ScanRoad, 1983). Flocculation can be reversed by agitation, dilution or addition of more emulsifier. When the flocculated droplets of bitumen merge to form bigger droplets, it is called coalescence. Coalescence is non-reversible (James, 2006).

Factors that force bitumen droplets together and that will accelerate flocculation and coalescence are (James, 2006):

- Settlement under gravity;
- Evaporation of water;
- Shearing of the bitumen emulsion;
- Freezing of the bitumen emulsion.

During the process of flocculation and coalescence, as the water gets trapped between the flocculating droplets, the type of bitumen emulsion changes from oil-in-water (O/W) to water-in-oil (W/O). The water content of water-in-oil (W/O) emulsions is generally less than 20%. The different stage of full dispersion, flocculation and coalescence is illustrated in Figure 9.

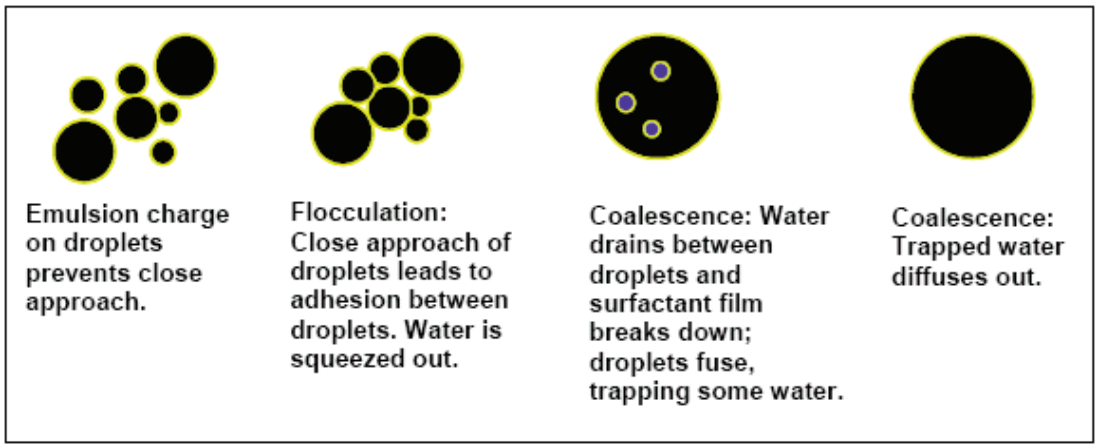


Figure 9: Different stages of the state of bitumen emulsion (James, 2006)

The interfacial area between the bitumen and the water is highly dependent on the droplet size of the dispersed bitumen. In one litre of a normal bitumen emulsion the total surface area of the bitumen may be as much as 5000 $m^2$ (ScanRoad, 1983).

Creation of this large interfacial area requires energy. Surfactants or emulsifiers reduce the interfacial surface tension and hence the energy required to produce and maintain the interfacial area.

Emulsifiers have a hydrophobic (water-fearing) part and a hydrophilic (water-loving) part. The hydrophobic part is also called the lipophilic (oil-loving) part. This part is the "tail" of the emulsifier, which is non-polar. The tail consists of a hydrocarbon chain of about 12 to 18 carbon atoms (James, 2006). ScanRoad (1983) reports hydrocarbon chains consisting of 8 to 22 carbon atoms. The hydrocarbon chain terminates with either a cationic or anionic group. This polar group is the functional head group of the emulsifier. The emulsifier orientates itself at the bitumen-water interface such that the hydrophobic and lipophilic tail is firmly adsorbed to the bitumen and the head group in the water phase (ScanRoad, 1983; Akzo Nobel, 2001). An example of an emulsifier molecule is shown in Figure 10. The orientation of the emulsifier on the bitumen-water interface is shown in Figure 11.

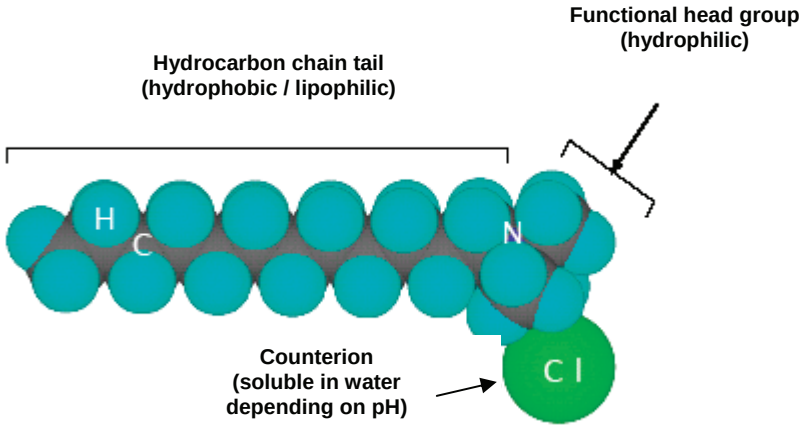


Figure 10: Cationic emulsifier (James, 2006)

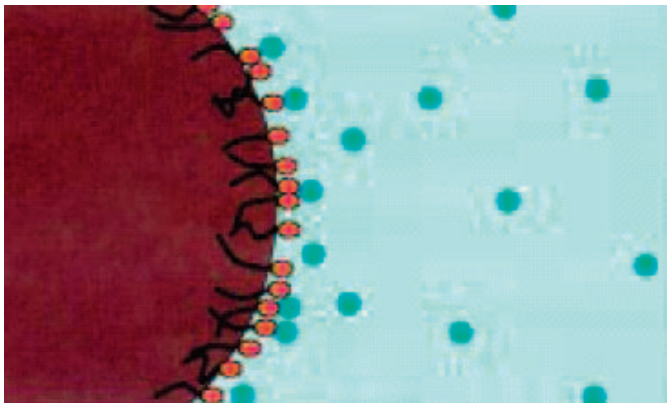

Figure 11: Orientation of emulsifier on the bitumen-water interface (Akzo Nobel, 2000)

The length of the emulsifier molecule is an order 1000 smaller than the diameter of a bitumen droplet in the emulsion (Akzo Nobel, 2000). Most emulsifiers are neutral and insoluble in water and need to be activated. Cationic emulsifiers are neutralised

with an acid, such as hydrochloric acid (HCl), phosphoric acid ($H_3PO_4$) or sulphuric acid ($H_2SO_4$). Hydrochloric acid is most commonly used to neutralise cationic emulsifiers. Anionic emulsifiers are neutralised with sodium hydroxide (NaOH), ammonium hydroxide ($NH_4OH$) or potassium (kalium) hydroxide (KOH). Sodium hydroxide is most commonly used in the production of anionic emulsions.

In chemical formulas of the emulsifier molecule the hydrocarbon chain is denoted by "R". Often amines or a distilled form of wood resin (Vinsol® Resin) is used in the production of cationic emulsifiers. The chemical process of neutralisation of a cationic emulsifier with hydrochloric acid is as follows:

$$\underset{\text{amine}}{R-NH_2} + \underset{\text{hydrochloric acid}}{HCl} \rightarrow \underset{\text{cationic soap}}{R-NH_3^+} + \underset{\text{counterion}}{Cl^-}$$

*$R - NH_3^+$ is the surfactant with a cationic functional group*

Fatty acid, tall oil and resins are used in the production of anionic emulsifiers. The neutralisation of an anionic emulsifier with sodium hydroxide is as follows:

$$\underset{\text{fatty acid}}{R-COOH} + \underset{\text{sodium hydroxide}}{NaOH} \rightarrow \underset{\text{anionic soap}}{R-COO^-} + \underset{\text{counterion}}{Na^+} + \underset{\text{water}}{H_2O}$$

*$R - COO^-$ is the surfactant with an anionic functional group*

The emulsifier is added to the water and neutralised before it is brought into contact with the bitumen. The quantity of emulsifier depends on the stability required (rapid setting, medium setting and slow setting). Slow setting emulsions require more emulsifier than the less stable rapid setting emulsions. Emulsion are categorised according to reactivity as shown in Table 1. Typical emulsifiers and levels are given in Table 2.

Table 1: Emulsion types

| Head group charge | Grade<br>ASTM D977, anionic<br>ASTM D2397, cationic | Type<br>SABS 309, anionic<br>SANS 548, cationic | Denotation |
|---|---|---|---|
| Anionic | Rapid setting | Spray | RS |
| | Medium setting | Pre-mix | MS |
| | Quick setting | | QS |
| | Slow setting | Stable-mix | SS |
| Cationic | Rapid setting | Spray | CRS |
| | Medium setting | Pre-mix | CMS |
| | Quick setting | | CQS |
| | Slow setting | Stable-mix | CSS |

Not all emulsifier is active in the interfacial area between the water and the bitumen. The emulsifier that is not adsorbed on the bitumen surface is called “free emulsifier”. This free emulsifier is dissolved in the water phase and more mobile than the bitumen droplets. The quantity of free emulsifier is dependent on the quantity of emulsifier initially added. Rapid setting emulsions (spray type) have the lowest emulsifier contents and hence have little free emulsifier. Slow setting (stable-mix type) emulsions have the highest quantity of emulsifier and hence also more free emulsifier.

Table 2: Typical emulsifiers and levels (Akzo Nobel, 2000)

| Emulsion type | Emulsifier type | Emulsifier level [%] | Soap solution pH |
|---|---|---|---|
| Cationic rapid-setting | Tallow diamine | 0.15 – 0.25 | 2 – 4 |
| Cationic medium-setting | Tallow diamine | 0.3 – 0.6 | 1.5 – 4 |
| Cationic slow-setting | Quarternary amine | 0.8 – 2.0 | 2 – 5 |
| Anionic rapid-setting | Tall acid | 0.2 – 0.4 | 10.5 – 12 |
| Anionic medium-setting | Tall acid | 0.4 – 0.8 | 10.5 – 12 |
| Anionic slow-setting | Non-ionic + lignosulphonate | 1.2 – 2.5 | 7.5 – 12 |

2.2.2.3 The manufacturing of bitumen emulsion

In order to produce an O/W bitumen emulsion, energy is required. This energy is both mechanical and physicochemical of nature. The mechanical energy is used to shear the asphalt into fine particles. The physicochemical energy reduces the interfacial tension between the bitumen and the water and adds stability to the emulsion (Baumgardner, 2006). The mechanical energy is provided by a mixer or mill and the physicochemical energy by the surfactants. Various types of mixers can be used to disperse the bitumen, however, a colloid type mill is most commonly used. A schematic diagram of a colloid mill is shown in Figure 12.

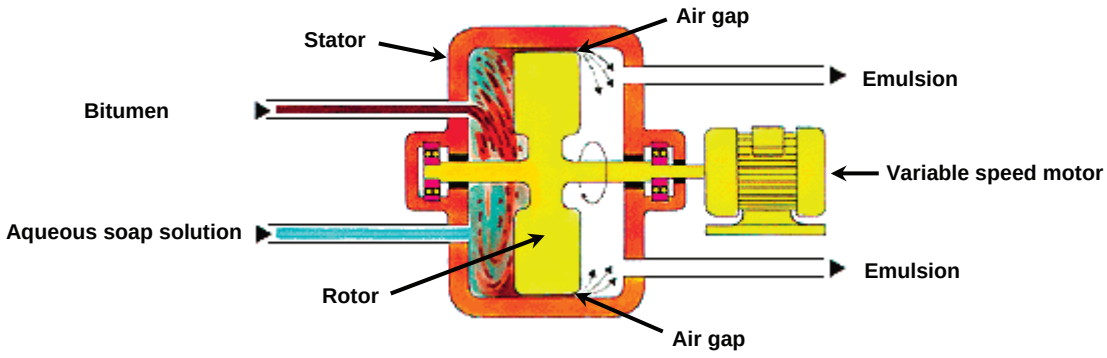


Figure 12: Colloid mill for the production of bitumen emulsion (after Louw, 2004)

The colloid mill consists of a static housing (stator) and a rotor. The rotor is driven by the rotor shaft, which is connected to an electrical motor. The rotor speed can be

varied. There is a small air gap (either fixed or variable) between the stator and the rotor. This gap is generally in the order of 0.5mm. There are two feeder lines into the colloid mill; one for the bitumen and one for the aqueous soap solution containing the surfactants. The bitumen and the aqueous soap solution are mixed when it enters the mill and is forced (by pumps not shown in Figure 12) through the air gap. The fluids forced through the air gap are subjected to high shear and hydraulic forces. These forces are dependent on the speed of the rotor and the size of the air gap. Through the gap the bitumen is sheared and dispersed into the water in fine droplets. The surfactants (or emulsifiers) firstly reduce the interfacial tension, which reduces the energy required to disperse the bitumen and secondly ensure that the emulsion has stability when it leaves the mill. The air gap spacing influences the emulsion fineness. The bitumen droplets size and the distribution thereof are highly dependent on the rotor speed (Baumgardner, 2006)

The colloid mill is the central spill in a bitumen emulsion manufacturing plant. Two types of bitumen emulsion plants can be distinguished:

- Batch emulsion plant; and
- In-line emulsion plant.

In the batch plant process the water phase (soap solution) preparation and the emulsion production are two separate processes. Batch tanks are required to hold the soap solution before it is added to the bitumen feed just before it enters the colloid mill. In the in-line process the water phase preparation is done continuously as part of the emulsion production process. It requires more sophisticated automated process controls. A flow diagram of an in-line bitumen emulsion plant is shown in Figure 13.

In order to be able to disperse the bitumen into the water phase, its viscosity needs to be relatively low. Baumgardner (2006) reports an optimum viscosity of 200 centipoises. The temperature at which this viscosity is obtained is called the equiviscous temperature (EVT). The EVT of bitumen, depending on the bitumen grade, generally ranges from 140ºC for softer bitumen and 180ºC for the harder bitumen.

The aqueous soap solution is prepared by dosing the correct quantities of emulsifier and activator into the water. Sometimes another chemical such as a stabiliser is also added. These stabilisers can be added to control the viscosity of the emulsion or improve the storage stability of the emulsion. The addition of the emulsifier and activator needs to be very precise as small changes in the dosage of especially the emulsifier have a great effect on the reactivity and stability of the emulsion. A static mixer and a dwell tank provide the necessary mixing and reaction time. The pH of the water phase is carefully monitored and adjusted to the correct level before the soap solution is added to the bitumen feed just before the colloid mill.

The temperature of the bitumen emulsion as it leaves the colloid mill needs to be carefully monitored. The emulsion exit temperature is an important manufacturing parameter. The emulsion stability during manufacturing, cooling and storage is improved if the emulsion exit temperature is maintained at or above a certain

Minimum Emulsion Exit Temperature (MEET). The MEET is considered to be equivalent to the temperature at which the viscosity of the bitumen is approximately 20,000 centipoises (Baumgardner, 2006).

The minimum soap solution temperature can be calculated and is a function of:

- the EVT;
- the MEET;
- the mix proportions of the bitumen and water phase;
- the colloid mill;

Proper activation of the emulsifying agents may put further requirements on the minimum soap solution temperature. If the emulsion exit temperature exceeds 100ºC, boiling of the emulsion may occur at atmospheric pressure because the emulsion temperature exceeds the boiling point of water. In such cases, the production of the emulsion and storage needs to be pressurised until such time that the temperature has fallen below the boiling point of water (Baumgardner, 2006). This would typically apply to the production of some modified bitumen emulsions (*e.g.* SBS modified bitumen emulsion).

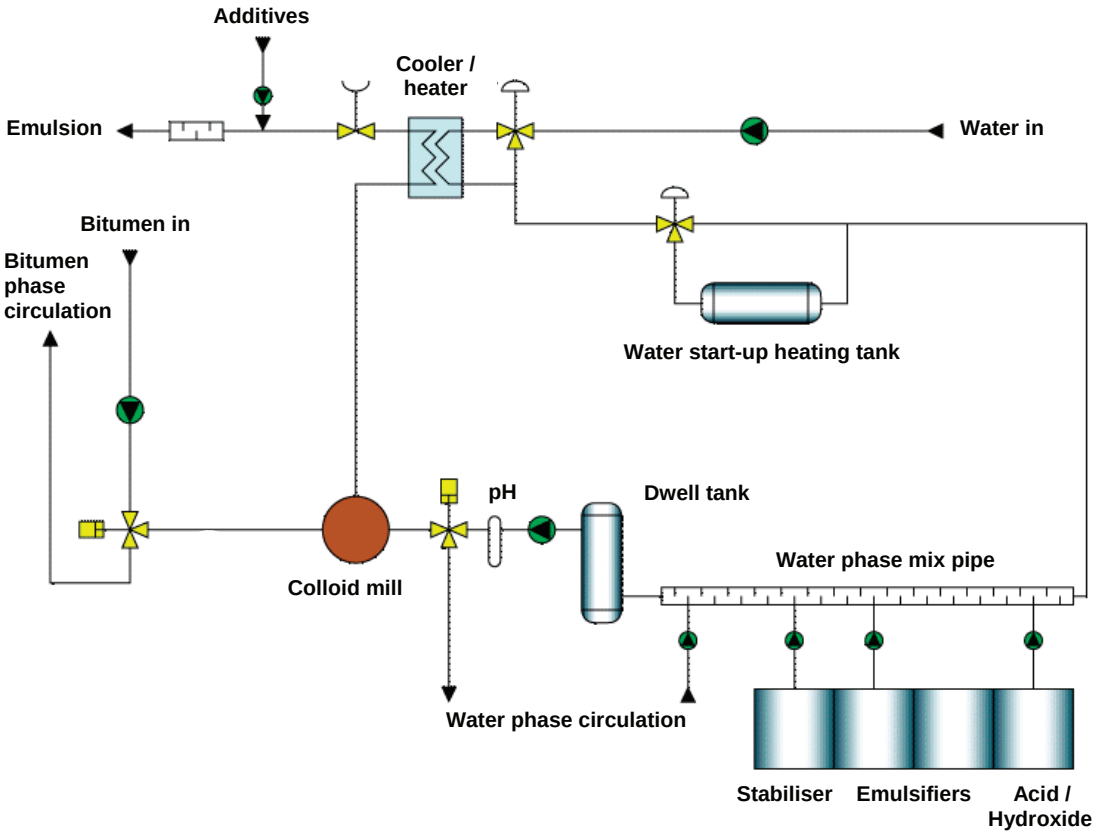


Figure 13: Flow diagram of an in-line bitumen emulsion plant (after Akzo Nobel, 2006)

2.2.2.4 The breaking of bitumen emulsion

The emulsifier contributes to the stability of the bitumen emulsion during manufacturing, storage and transportation. In case of stable-mix type emulsions used for the production of pre-mix asphalt or cold mix stabilisation, the emulsifier also provides stability during the mixing process of the emulsion with the mineral aggregate.

The terminology around the concept of stability is somewhat confusing, as it is sometimes used with a mechanical instead of a physicochemical meaning. The mechanical stability has to do with sedimentation. Sedimentation is concentration of the bitumen droplets in the bottom part of a bitumen emulsion during storage. The process of sedimentation is illustrated by Figure 14. Sedimentation is caused by gravity forces and the slight difference in specific gravity of bitumen and water. Sometimes bitumen emulsions with the ability to withstand sedimentation are referred to as stable emulsions (Lesueur and Potti, 2004).

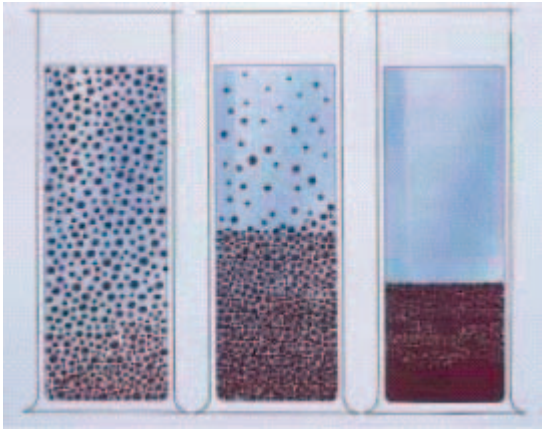

Figure 14: Different stages of sedimentation of a bitumen emulsion (VBW Asfalt, 2003)

Stability, however, more often refers to the physicochemical resistance to breaking. Although sedimentation can be one of the factors that start the process of flocculation and coalescence (which is illustrated in Figure 9) that form part of the breaking process, the electrostatic repulsion forces between the bitumen droplets determine to a great extent the stability of a bitumen emulsion and the breaking behaviour.

After manufacturing, storage, transportation and mixing, the emulsifier has fulfilled its role of keeping the bitumen droplets in dispersion. At this stage it is required that adhesion of the bitumen to the mineral aggregate surface develops. This change in state of the bitumen, from being dispersed in the emulsion to forming an adhesive layer on the surface of the mineral aggregate is called breaking of the bitumen emulsion. It is sometimes also referred to as setting of the bitumen emulsion.

The rate at which the emulsion should break depends on the type of application. For chip seal applications a fast breaking rate is required. For plant mixes with a low surface area (coarse or open-graded mixes) a more moderate breaking rate is required. For dense graded mixes, in-place mixes (recycling or stabilisation) and

slurries a slow breaking rate is required. The different types and classification of bitumen emulsion were summarised in Table 1. Typical applications of emulsions with different breaking rates are summarised in Table 3.

Table 3: Typical applications for emulsions with different breaking rates (After James, 2006)

| Application | Breaking or setting rate | | |
|---|---|---|---|
| | Rapid | Medium | Slow |
| Plant Mixes | | | |
| Open-graded | | ✓ | |
| Dense-graded | | | ✓ |
| RAP-mixes | | ✓ | ✓ |
| Stockpile mix | | ✓ | |
| Pre-coated chips | | ✓ | ✓ |
| Mix paving | | | |
| Open-graded | | ✓ | |
| Slurry seal | | | ✓ |
| Slurry for Cape Seal | | | ✓ |
| Microsurfacing | | | ✓ |
| In-place mixes | | | |
| RAP-mixes | | ✓ | ✓ |
| Dense-graded | | | ✓ |
| In situ recycling (full depth) | | | ✓ |
| Stabilisation | | | ✓ |
| Spray applications | | | |
| Chipseal | ✓ | | |
| Fog seal | ✓ | ✓ | |
| Tack coat | | ✓ | ✓ |
| Prime coat | | | ✓ |
| Dust palliative | | | ✓ |
| Penetration macadam | ✓ | | |

Breaking of an emulsion takes place when the repulsive forces between the bitumen droplets are either:

- overcome;
- reduced; or
- removed.

Overcoming the repulsive forces has been discussed in Section 2.2.2.2 and occurs when the localised bitumen content of the bitumen emulsion is high. This can also be the result of evaporation of water out of the mix. The repulsive forces between the bitumen droplets are reduced when the electrostatic charge of these droplets reduces. This can be brought about by a reduction in the quantity of emulsifier molecules around the bitumen droplets or by a neutralisation of the charge of the functional head group of the emulsifier.

A reduction in the quantity of emulsifier molecules around the bitumen droplets can be the result of migration of the emulsifier from the bitumen droplet to the aggregate particles and adsorption of the emulsifier onto the surface of the aggregate. This process is the result of electrostatic attraction between the aggregate and the emulsifier caused by the surface charge on the aggregate and the charge of the functional head group of the emulsifier. In this process free emulsifier in the water phase of the emulsion will be attracted first, because it is much more mobile than the emulsifier adsorbed to the bitumen droplet. Three possible breaking mechanisms are shown in Figure 15.

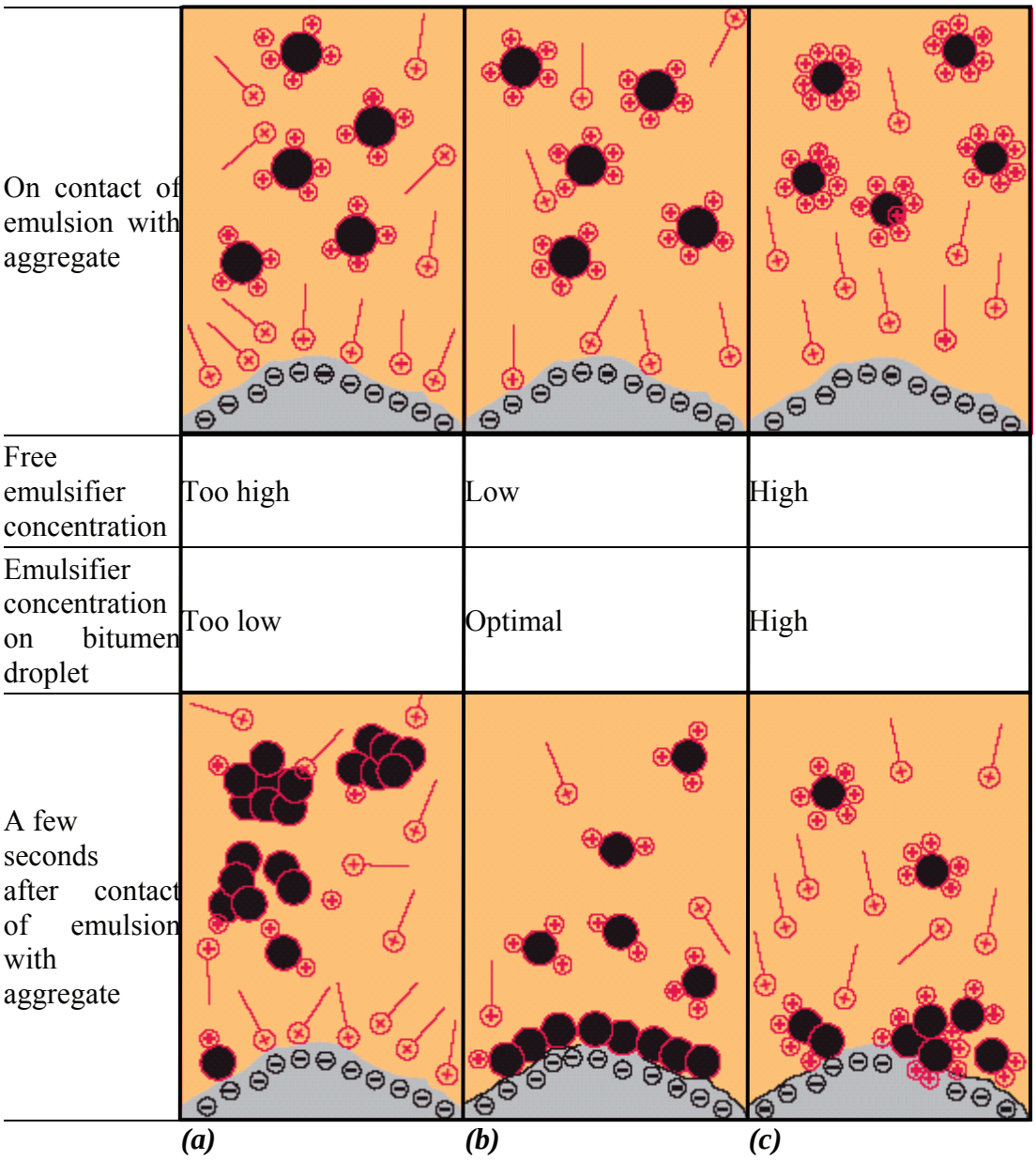


Figure 15: Different breaking mechanism of bitumen emulsion (example of cationic emulsion on 'acid' aggregate) (GPB, 2006)

The mechanism shown in Figure 15 (a) would typically be observed with a poorly formulated bitumen emulsion. Poor adsorption of the emulsifier to the bitumen droplets result in a too low concentration of emulsifier on the bitumen droplet and a too high concentration of free emulsifier. The free emulsifier is very quickly attracted to the aggregate surface and the bitumen droplets coalesce without being adhered to the aggregate surface.

The mechanism shown in Figure 15 (b) would typically be observed with a rapid setting spray type or pre-mix type emulsions. The low concentration of free emulsifier in the water phase ensures that the negative surface charge of the aggregate remains sufficient to attract the positively charged bitumen droplets. The bitumen droplets rapidly coalesce on the aggregate surface and a good adhesive bond is obtained between the bitumen and the aggregate.

The mechanism shown in Figure 15 (c) would typically be observed with a slow set or stable-mix type emulsion used in cold mixes (plant or in situ recycled), slurries and soil stabilisation. The free emulsifiers are quickly adsorbed on the aggregate surface, which reduces the surface charge of the aggregate. Due to the lipophilic tails of the emulsifier absorbed onto the aggregate surface, the aggregate becomes oil-loving. Sufficient emulsifier remains on the bitumen droplets to prevent quick coalescence of the bitumen droplets away from the aggregate surface. This results in a slow breaking rate of the bitumen onto the aggregate surface as the water evaporates. The adhesion eventually obtained between the bitumen and aggregate is good.

2.2.2.5 The role of cement in the breaking of bitumen emulsion

Cement consists mainly of tricalcium silicate, $Ca_3SiO_5$ (≡ $C_3S$), and dicalcium silicate, $Ca_2SiO_4$ (≡ $C_2S$). The hydration of cement takes places as follows:

$$\underset{\text{tricalcium silicate}}{2\,C_3S} + \underset{\text{water}}{7\,H_20} \rightarrow \underset{\text{cement gel}}{C_3S_2H_3} + \underset{\text{calcium hydroxide}}{3\,CH}$$

$$\underset{\text{dicalcium silicate}}{2\,C_2S} + \underset{\text{water}}{5\,H_20} \rightarrow \underset{\text{cement gel}}{C_3S_2H_3} + \underset{\text{calcium hydroxide}}{CH}$$

$C_3S_2H_3$ is the abbreviated notation for calcium silicate hydrate ($3CaO{\cdot}2SiO_2{\cdot}4H_2O$), also referred to as cement gel or paste. CH is the notation for calcium hydroxide, $Ca(OH)_2$, also referred to as hydrated lime. Both of the above reactions generate heat.

The cement gel crystallizes or sets into an interlocking matrix causing a cementing action. The calcium hydroxide that comes free during the hydration of the calcium silicates is partly soluble and ionised. The calcium ion and ionised hydroxide become freely available:

$$Ca(OH)2 \rightarrow Ca^{2+}\,(aq) + 2\,OH^{-}\,(aq)$$

The pH can rise to over 12 because of the release of alkaline hydroxide ($OH^-$). The hydroxide influences the behaviour of cationic emulsifiers, while the calcium ion typically influences anionic emulsions.

The negatively charged hydroxide concentrates around the positively charged cationic bitumen droplets and it (a) neutralises the free acid and (b) converts the amine hydrochloride ($R\text{-}NH_3^+Cl^-$) emulsifier to insoluble amine ($R\text{-}NH_2$). It thereby destroys the charge of the cationic soap:

| $R-NH_3^+$ | + | $OH^-$ | → | $R\text{-}NH_2$ | + | $H_20$ |
|---|---|---|---|---|---|---|
| *cationic soap* | | *hydroxide* | | *amine* | | *water* |

The bitumen droplets in the rapid setting (spray type) and medium setting (pre-mix type) cationic emulsions now start to coalesce due to a lack of repulsion. The slow setting (stable-mix type) emulsions do not coagulate, even though the cationic charge is neutralised. The emulsifiers used for these types of emulsions have such long and complex hydrocarbon chain tails that when they are adsorbed to the circumference of the bitumen droplet they create a "hairy" layer around the bitumen droplet. This layer creates a barrier between the bitumen droplets and prevents close approach of bitumen droplets and thus coalescence. This resistance to coalescence is called steric repulsion. This steric repulsion causes that slow setting emulsion only break due to evaporation or absorption of the water phase.

In spray and premix grade anionic emulsion, which are based on the alkali soaps of fatty acids, the free $Ca^{2+}$ ion enters into a reaction with the anionic soap $R\text{-}COO^-$ radical:

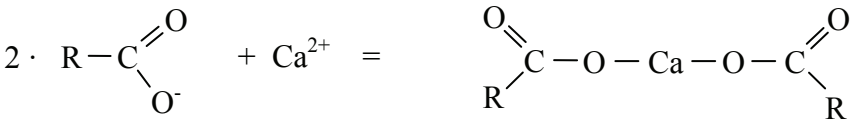

*anionic soap based on fatty acid* *calcium* *insoluble calcium soap of fatty acids*

The product of this reaction is insoluble and precipitates, which results in immediate breakdown or coalescence of the emulsion.

In stable anionic grade emulsions, which are based on alkali soaps of wood resin derivatives, the free $Ca^{2+}$ ion also enters into a reaction with the soap. Some precipitation of the soap occurs, but the complex soap also contains other functional groups that continue to stabilise the bitumen droplets. Also here it is possible that steric repulsion occurs between the bitumen droplets as a result of the complex branched nature of the resin molecule.

### *2.2.3 Foamed bitumen*

2.2.3.1 Early work by Dr. Ladis Csanyi, "the inventor" of foamed bitumen

Foamed bitumen, basically as it is used nowadays, and its potential as a binder in road building applications were discovered during the 1950's. This is approximately 50 years after the first bitumen emulsions were produced. Dr. Ladis Csanyi, Professor in Charge of Bituminous Research Laboratory of the Iowa State College, performed pioneering work in the development of the foamed bitumen technology. His discoveries were the result of logically progressing studies and a combination of practical and innovative thinking.

One of the main drivers of Csanyi's studies was the scarcity of road materials suitable for highway purposes in Iowa State. The Iowa Highway Research Board therefore undertook to develop means of using local materials. Loess and soft limestones were the local materials abundant in Iowa State. Csanyi (1955) therefore studied the treatment of loess, fine sands and soft limestones with liquid binders during the early 1950's. He developed a "mortar theory" in which the fines fraction of the mineral aggregate forms a mastic with the bituminous binder. This mastic was used to bond the coarser particles of the ungraded aggregate (various sands and agricultural limestone).

In this study, Csanyi (1955) considered three known techniques in introducing the bituminous binder into the asphalt mix:

- Bitumen emulsion;
- "Steam mix"; and
- Atomising of bitumen, also called the "impact process".

As mentioned in Section 2.2.2, only two types of anionic bitumen emulsions were available at the time (*i.e.* a spray type and a pre-mix type emulsion). Cationic emulsions were first produced around the same time as Csanyi developed his mortar theory and stable-mix type anionic emulsions only during the late 1950's. It is the latter that is of importance as it is very likely that Csanyi did not work with stable-mix type emulsions. The high fines content in Csanyi's mixes would cause the bitumen emulsions at his disposal to break very quickly. This fact was acknowledged by Csanyi and he noted that "special emulsions that could resist this action" should be used (Csanyi and Fung, 1955). It is most likely that therefore Csanyi did not consider the use of bitumen emulsion further.

Csanyi furthermore suspected that emulsion water would cause problems in combination with the high clay content in the loess. He reported a "balling" problem when bitumen emulsions were used. However, it is more likely that this problem was caused by the type of emulsion used (rapid breaking of the emulsion due to high fines content and the resulting extremely high surface area) and the mineralogy and particle charge of the fines fractions, than by the emulsion water. This is further substantiated by the fact that in his later studies he introduced high moisture contents into the same mixes (with high clay content), which then did not pose a problem.

In Appendix A it is mentioned that the soil classification used at the time, based on grain size, may be misleading. The high "clay" contents reported by Csanyi are more likely to refer to the high content of "clay size" particles, than to particles that bear a resemblance to the chemical properties of clay.

Regardless whether the balling problem was caused by the type of emulsion or the combination of emulsion water and high clay (fines) content, the option of using bitumen emulsion was put aside because of the balling problem. Csanyi therefore continued with studying the use of "steam mix" and the "impact process". This avenue eventually led him to the development of the foamed bitumen technology. It could therefore be hypothesized that would Csanyi at the time had to his disposal more advanced bitumen emulsions that would worked well in combination with the aggregates he used, as were available less than a decade later, he would probably not have developed the foamed bitumen technology.

The "steam mix" technology consists of achieving a reduction in the viscosity of the bitumen by the introduction of steam into the bitumen to produce a "temporary bitumen emulsion". When fine spray nozzles are used and no emulsifying agent this temporary emulsion breaks rapidly. Although the water vapour introduced into the mix by the steam was not considered to create a problem with the loess, some balling was encountered (this is a further indication that the balling problem is bitumen related and not water related, as discussed above). Because there was no assurance that a consistent mortar mix could be produced using the "steam mix" technology, this option was also put aside (Csanyi and Fung, 1955).

The attention was subsequently turned to the "impact process". This process was patented and developed by Dr. Albert Sommer (1879 – 1968). It is interesting to note that Sommer was General Director of the *Trinidat Deutsche Öl- und Asphalt AG*. In 1925 this company was a founding company of *COLAS Kaltasphalt GmbH*, which specialised in the production of bitumen emulsion.

The impact process is based on the concept that the liquid binder is reduced to very small particles or to a condition of (mist) spray. This is achieved by pumping the liquid binder under pressure through an atomising nozzle. The binder is heated to approximately 165ºC and the pressure applied is up to 17 bar. The nozzle is placed over the mixer (in the top of a closed mixing chamber). The aggregate is thrown up with force into the cloud of atomised binder. A twin-shaft pugmill mixer can be used. The mineral dust is also heated to approximately 160ºC. Using this method a uniformly distributed bitumen film covering the aggregate particles is achieved (Csanyi and Fung, 1955).

Using the impact process, Csanyi was able to successfully produce a bituminous mortar from mineral dust and loess. The binder content of the mortar alone was about 23%. This was a technological advance, because at the time this was not possible using the standard hot mix asphalt or bitumen emulsion technology. Csanyi also showed that this mortar could successfully be used to bind uniformly graded sands. On mixing the binder rich mortar with sand, the binder content of the total mixture would reduce to between 6% and 7%. In 1953 test sections were constructed

adopting this bituminous mortar theory and using only local materials readily available such as fine sands, blown sand, loess and limestone (Csanyi and Fung, 1955).

An important recommendation that resulted from Csanyi's work on bituminous mortars was to investigate other means of applying thin films of binders in the preparation of the mortar. The driver of this further investigation was to overcome certain drawbacks of the impact process such as the high speed of mixing, casting of the aggregate and the high pumping pressures required in order to atomise the binder. It was during this "quest" that Csanyi developed the foamed bitumen technology.

At the time when Csyani was looking to improve on the impact process, foams were found extensively in normal day's practices. Examples were in foods, drinks, detergents, toiletries, cosmetics and the likes. Even bitumen was known to be able to foam, long before it was put to practical use. Foaming of bitumen was however for long an undesirable event that accidentally took place when bitumen containing water was heated, or especially when at the time that steam was still used to heat the bitumen in hot mix asphalt plants, a leak in the steam coil occurred. Csanyi (1959) reports that:

> *"under these conditions the bitumen expands tremendously and bubbles and froths out of the tank, flowing like water, permeating every nook and cranny, penetrating deeply into the ground and adhering tenaciously to anything it covers."*

Csanyi considered making use of controlled foaming of bitumen in his quest to improve the mixing technology of bituminous mortars, having observed the uncontrolled foaming bitumen phenomena, combined with his experiences with the steam mix and impact process concept. In order to control the foaming, Csanyi developed a nozzle, in which small quantities of saturated steam were injected into the heated bitumen. Basically this was a combination of the "steam mix" and the atomising process.

Although Csanyi experimented with different methods to produce foam, which included water, air, gases, foaming agents and steam, the latter was chosen as it proved to be the simplest, most effective and efficient (Csanyi, 1959). The operating pressures in the nozzle were 3.5 bar for the heated bitumen and up to 4.8 bar for the steam. At these magnitudes of pressures the need for high pressure piping, required for the atomising process, was eliminated (Csanyi, 1957). The bitumen was heated to approximately 140ºC (Csanyi, 1959). The nozzle developed by Csanyi and patented by the Iowa State College Research Foundation is shown in Figure 16.

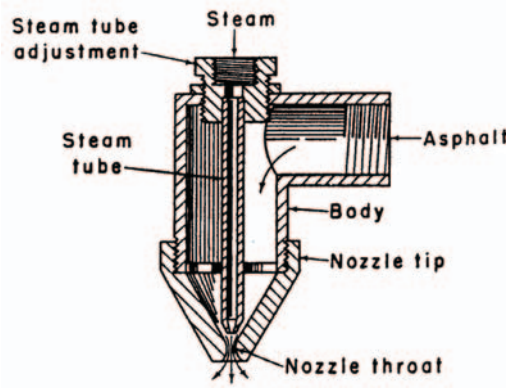


Figure 16: The first foamed bitumen ("asphalt" in the annotations is "bitumen") nozzle developed by Csanyi (1957)

With this nozzle configuration Csanyi was able to produce two types of foamed bitumen:

- discrete foam; and
- concentrated foam.

The discrete foam consists of separate individual small bubbles. Concentrated foam on the other hand is a continuous mass of jointed bubbles emitted from the nozzle. In producing the foamed bitumen mixes Csanyi used the same pug mill mixer and materials as from his previous study (Csanyi, 1955). The pug mil mixer however, was operated at a lower speed to bring the aggregate in contact only with the foam, without the need for any impact (Csanyi, 1957).

The first tests consisted of producing mixes with discrete foam. In this process the sand and fine aggregates had to be heated to about 175ºC – 200ºC, while the dust fraction was added at room temperature. When using concentrated foam, the temperature of the fine aggregates could be reduced to approximately 140ºC (Csanyi, 1957).

Csanyi also studied the effect of the aggregate temperature. He prepared mixes with aggregates ranging in temperature from 70ºC to 150ºC. Csanyi found that when the aggregate temperature exceeds 95ºC, a good distribution of the binder and coating of the aggregate was achieved. Below 95ºC however, the fine aggregate is fully coated, but the larger particles are partially coated (Csanyi,1959).

Csanyi also identified that his foamed bitumen had a potential to be used in soil stabilisation. The perceived problem he encountered was the fact that soil is moist and damp. Also, he had found that up to 8% of moisture was required to break up unprocessed lumps of loess. Tests with moist aggregate at ambient temperatures showed that satisfactory mixes could be obtained, with partial coating of the coarser aggregates. In fact, he found that in order to produce satisfactory mixes at ambient temperature, a certain minimum amount of water is required. Csanyi provided the following reasons for the fact that moisture is required in foamed bitumen soil stabilisation (Csanyi, 1957):

- it softens up lumps of clayey materials and heavy soil fractions;
- it assists in the uniform distribution of the material;
- it suspends the fine particles in a water medium;
- it provides "channels of moisture" in the mix through which the foamed bitumen can travel to coat all mineral particles during the mixing.

In addition to the above factors identified by Csanyi, moisture may also be required for compaction purposes.

Csanyi (1959) concluded that cold mixes can be made using cold wet aggregate and foamed bitumen. The need to cure foamed bitumen cold mixes was also immediately identified. Also it was found that the specimens gained strength and stability as moisture evaporates and retain a higher stiffness once dried. During 1956 a small test section (about 3 tons of foamed bitumen cold mix) was constructed using fine sand and raw loess. This test section performed well (Csanyi, 1957).

The next logical step was to investigate the potential to use foamed bitumen for in-place soil stabilisation. In-place mixing (breaking up, pulverising, adding binder and mixing) was already in use for soil stabilisation with lime. A standard pulvi-mixer (pulveriser and mixer) was modified to enable foamed bitumen stabilisation. The pulvi-mixer used was a basic model tractor-type vehicle, with a rotary drum for pulverising and mixing covered by a hood, attached to the back of the tractor. The modifications consisted of attaching a steam boiler at the front of the tractor and a spray bar with nozzles at the assembly hood, together with piping, fittings and controls. A bitumen heater kettle was towed on a trailer alongside the tractor.

A section of nearly 100 metres of an 8 metre wide street was successfully stabilised using the in-place foamed bitumen stabilisation during 1956. The material stabilised was similar as the soil that Csanyi stabilised in the laboratory as described above. About 6% of foamed bitumen was added in successive passes. Multiple passes were required due to limitations of the equipment. Only about 1% of binder could be added per pass. A week after construction a slurry seal was applied on the top of the stabilised section. The test section performed well during the first four months of service (Csanyi, 1957). No reports on the performance of the test section after the first four months were found.

The performance of the smallish test section constructed in 1956 was such that is was decided to undertake larger road tests during 1957. These tests consisted of extension of the first test section by about 250 metres and stabilisation of just over 800 metres of a gravel county road. After just over a year, the street extension section performed well, while the stabilised gravel county road showed some distress due to subgrade failures. Based on his research and pilot projects, Csanyi (1960) summarised the following advantages of foamed bitumen stabilisation over conventional soil stabilisation methods (cement, lime and bitumen emulsion):

- A wider range of soils, including more marginal materials, can be stabilised;
- The aeration phase during the soils stabilising process can be eliminated;

- The foamed bitumen stabilised base can be compacted, sealed immediately and opened for traffic sooner; and
- Any grade of asphalt desired can be used.

2.2.3.2 The Mobil patent on foamed bitumen

Although Csanyi published positive and promising results, the use of foamed bitumen up to 1965 was not widespread. Acott (1980) provides a very comprehensive bibliography, probably the most comprehensive one up to that time, of publications concerning foamed bitumen. Based on this bibliography it would appear that research and pilot projects using foamed bitumen remained small scale and limited to a few states in the USA (*inter alia* Iowa, Kansas, Arizona and New Mexico) and Canada. Most of the projects involved stabilising sand or producing sand asphalt using foamed bitumen. The foamed bitumen mixes were both used in base course as well as in surfacing layers (Csanyi, 1959; Lee, 1980).

The publications concerning foamed bitumen projects during the late 1950's and early 1960's emphasize the positive aspects of the foamed bitumen process. However, the fact that the use of foamed bitumen as an alternative binder did not receive widespread attention during the 1960's could well be the results of the fact that the method also had some disadvantages. These disadvantages are however not well documented.

The most probable disadvantages of the Csanyi process that limited the use of foamed bitumen are summarised as follows:

- The expansion ratio of the foamed bitumen that can be achieved using steam is limited (Mobil Oil Australia Ltd, 1971);
- The properties of the foamed bitumen, such as expansion and half-life time, are controlled by adjusting the pressures used (Anderson *et al.*, 1965). This is an indirect and inaccurate control of the volumetric flows;
- The quality and properties of the foamed bitumen as well as the stabilised mix were variable. This could not always be correlated with the type of bitumen or aggregate used;
- The process required availability or dedicated production of saturated steam.

Another aspect that played a role and that is not directly a disadvantage of foamed bitumen technology was that in many states in the USA, good quality aggregates and energy were cheap. This reduced the possible economic advantage of bitumen stabilised materials in comparison with the production of hot-mix asphalt.

In 1968 Mobil Oil Australia Ltd. acquired the patent right for the Csanyi process (Jenkins, 2000). Within a few years Mobil had adjusted Csanyi's process and acquired patent rights for the modified process. In the Mobil patent specification, it is stated that the commercial value of the known method (*i.e.* Csanyi's method) has been retarded because of the relatively poor and inconsistent quality of foam produced. An expansion ratio of at least 10, but generally 15 to 20, is well suited for coating and binding aggregate. With Csanyi's method using steam it is common to

obtain an expansion ratio of 2 and unlikely to achieve ratios exceeding 4 (Mobil Oil Australia Ltd, 1971).

The limited expansion ratio that can be achieved using steam is because steam is already in an expanded state. The volume of steam required to achieve a high expansion ratios is such that it is difficult and hardly practicable to incorporate it into the hot bitumen in the time generally allowed and with the equipment developed by Csanyi (Mobil Oil Australia Ltd, 1971).

Shackel et al. (1974) and Bowering and Martin (1976) both report that the Csanyi process was modified (by Mobil) so that foamed bitumen could be produced with more accurate and consistent properties. This would imply that accurate and consistent foamed bitumen properties could not be obtained using Csanyi's process.

The modification by Mobil Oil Australia Ltd of the Csanyi process mainly concerned the nozzle configuration (see Figure 17) and the use of cold water instead of steam. Given a constant flow of hot bitumen, it was necessary to vary only the quantity of water injected in order to control the foam quality. Besides providing a more precise and simpler system, the improved method required less capital outlay as it entirely eliminates the necessity for a steam generating system (Bowering and Martin, 1976).

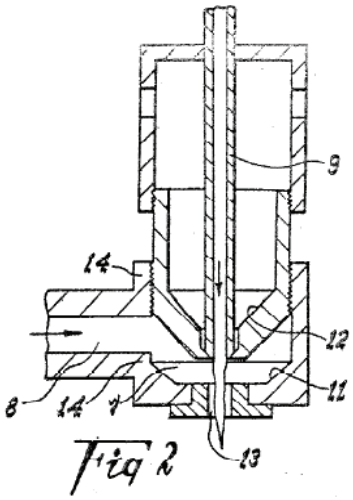


7. Mixing chamber
8. Bitumen passage
9. Water passage
11, 12. Frusto-conical opposed end surfaces
13. Discharge orifice
14. Side wall

Figure 17: Foamed bitumen nozzle modified and patented by Mobil (1971)

The principle of adding to two streams of bitumen and water together in a nozzle is still the same as in Csanyi's nozzle. The cold water (9) is injected into the hot bitumen flow (8). However, where in Csanyi's nozzle the steam and hot bitumen flow in the same direction (see Figure 16), in Mobil's nozzle the two streams transverse each other on entering the mixing chamber (7) close to the discharge orifice (13). Proper dispersion of the cold water into the hot bitumen is finalised during passage through the orifice (Mobil Oil Australia Ltd., 1971). The shape of the mixing chamber and discharge orifice, together with the operating pressures, determine the time the foaming bitumen is contained in the nozzle. This influences the foamed bitumen properties.

Lee (1980) states that one of the advantages of the Mobil process is the reduction in energy consumption compared with Csanyi's process as no saturated steam is required. This may not have been any issue at the time Csanyi developed his process. In the discussion of Lee's paper (1980), Robert Nady, Csanyi's assistant at the time of the development of his foamed bitumen process, comments that in the mid 1950's all asphalt plants had a steam jetty to keep the asphalt warm and to keep the pipe jacketing, the piping system and the pugmills all warm. Hence, when foamed asphalt mixes were produced in-plant, steam was readily available without any additional cost and energy requirement. When producing in-situ mixes, this would obviously not hold true.

The advantages presented of using cold water instead of steam to foam the bitumen as used in the Mobil process seem numerous and logical. It is therefore difficult to understand that in the process of the development of the original process, Csanyi opted to use steam, even though he had experimented using water, besides other methods. Csanyi (1959) however explained that of these methods the use of steam proved to be the simplest, most effective and efficient.

Lee (1980) reported that the Mobil patent was extended to at least 14 countries, resulting in foamed bitumen related work being undertaken in 16 countries. The Mobil process, named Foamix, was adapted to continuous mix plants, drum mixers and batch plants. The process has also been used in "travel plants" for processing in-situ material for soil stabilization. Although many miles of foamed bitumen mixtures have been produced by the Csanyi process for surface construction, mixtures produced by the Mobil process were mainly used for base and subbase construction.

It would appear that the usage of foamed bitumen in in-situ recycling operations was not without trouble. In the discussion to the paper of Shackel *et al.* (1974), Jones, Engineer at the Department of Main Roads in New South Wales, provides some practical insight in the problems that occurred with in-situ recycling at the time. He states that:

> *"the development of the travelling unit had received considerable attention in Australia and that above normal care in equipment operation and construction technique is required. Blockage of the spray bar jets (nozzles) was not infrequent and this leaves a strip of untreated or partly treated pavement behind the machine. Untreated strips can also be caused by accumulation of treated material to the interior sides of the mixer was also a common problem. ……. The use of a secondary rotary mixer and cross mixing was considered necessary with this method."*

These practical problems with in-situ recycling with foamed bitumen and the fact that Mobil had the monopoly, may be some of the reasons that during the term of Mobil's patents rights the usage of foamed bitumen was still not widespread. Projects including foamed bitumen were mainly limited to Australia, South Africa, New Zeeland, Japan and Germany. The work that has been carried out during this period is included in a comprehensive literature study by Jenkins (2000). In this study Jenkins discussed *inter alia* the bitumen requirements, aggregate properties, fluid and

temperature considerations, mixing methods, compaction and curing and evaluation of the properties of foamed bitumen mixtures.

Mobil's patent rights lapsed in 1987 (IP Australia, 2006). This opened up the market for foamed bitumen usage and stimulated further development of technology and especially the equipment.

#### 2.2.3.3 The role of improved in-situ recycling machines

A considerable contribution to the development and usage of the foamed bitumen has been provided by the developments and improvements to in-situ recycling machines. During the 1970's first hot milling machines and later also hot in-place recycling machines were developed. The development of cold in-place milling machines soon followed (Wirtgen, 2006).

After the lapse of Mobil's patent rights producers of cold in-place recycling machines could now also incorporate foamed bitumen technology in their range of machines and equipment. The development and further improvement of in-situ recyclers capable of applying foamed bitumen has contributed considerably to the more widespread use of foamed bitumen today.

Advancements in this field that lead to the increased use and quality of in-situ cold mixes are summarised as:

- Increased power rating of the recyclers (up to 500 kW for wheel mounted recyclers) allowing:
  - increased width and depth of milling;
  - milling of stronger bound layers;
- Improved milling drum and cutting tool technology;
- Flow meters and heated nozzles;
- Microprocessor controlled addition on binding agents.

#### 2.2.3.4 Foamed bitumen production

In the original process developed by Csanyi, foaming of bitumen was achieved by injecting saturated steam into the hot bitumen. As discussed in the previous sections, this was later modified to injecting small quantities of cold water into the hot bitumen. In the modern nozzles the water is injected as a fine mist spray under pressures of up to 5 bar. A schematic diagram of foamed bitumen production in a laboratory scale plant is shown in Figure 18.

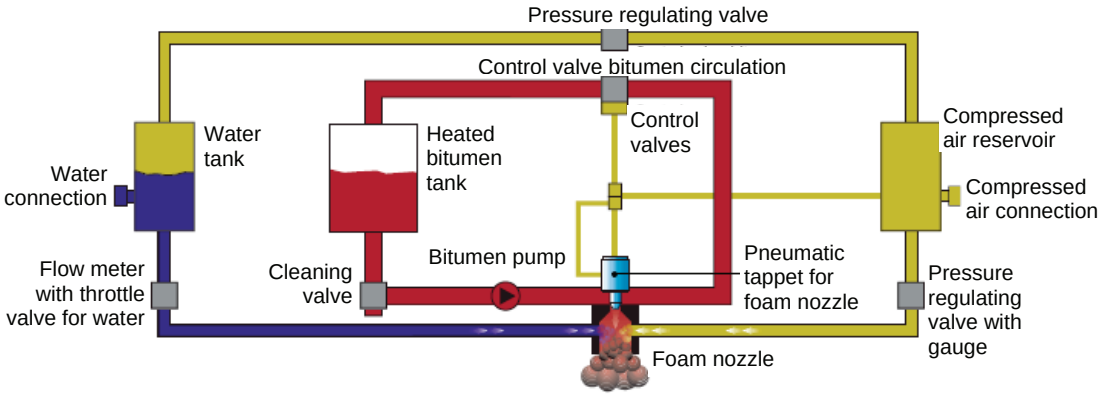


Figure 18: Schematic diagram of foamed bitumen production in a laboratory scale plant (Wirtgen, 2001)

The temperature of the bitumen (160ºC – 180ºC) exceeds the boiling point of water. Therefore the water that is injected into the hot bitumen becomes gaseous instantaneously. The transition of water from liquid to gaseous form in itself results in an increase in volume, pressure or both. Because this transition is taking place within a continuous medium, being the hot bitumen, expansion of this bitumen is the resulting action. A schematic diagram of the nozzle in which the water is injected into the bitumen is shown in Figure 19. An expansion chamber in which the bitumen foams before being released into the mixing chamber is also included in the nozzle.

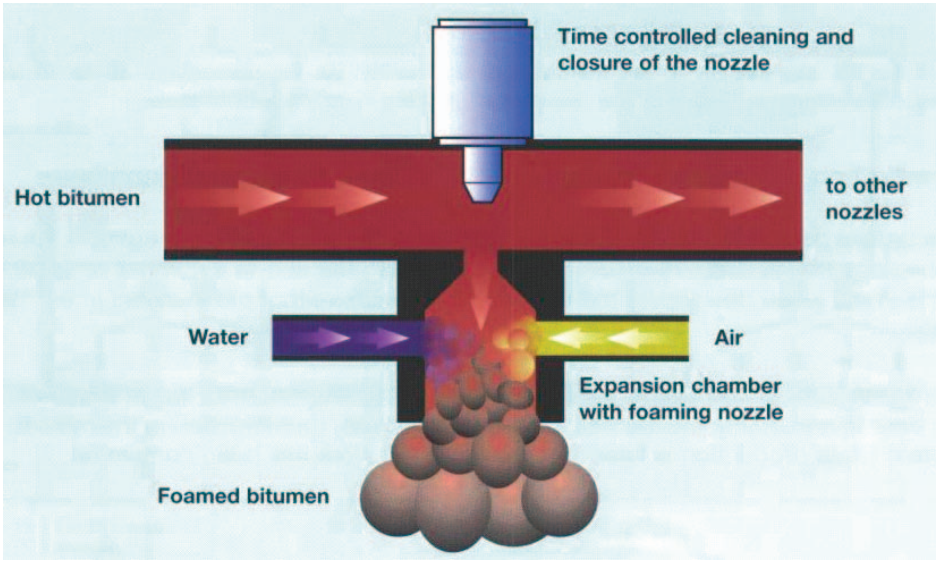


Figure 19: Schematic of nozzle for foamed bitumen production (Wirtgen, 2001)

A foamed bitumen spray bar consisting of a number of nozzles as shown above can be fitted to a standard hot-mix asphalt batch plant, or, as shown in Figure 20, to a milling drum of an in-situ recycler.

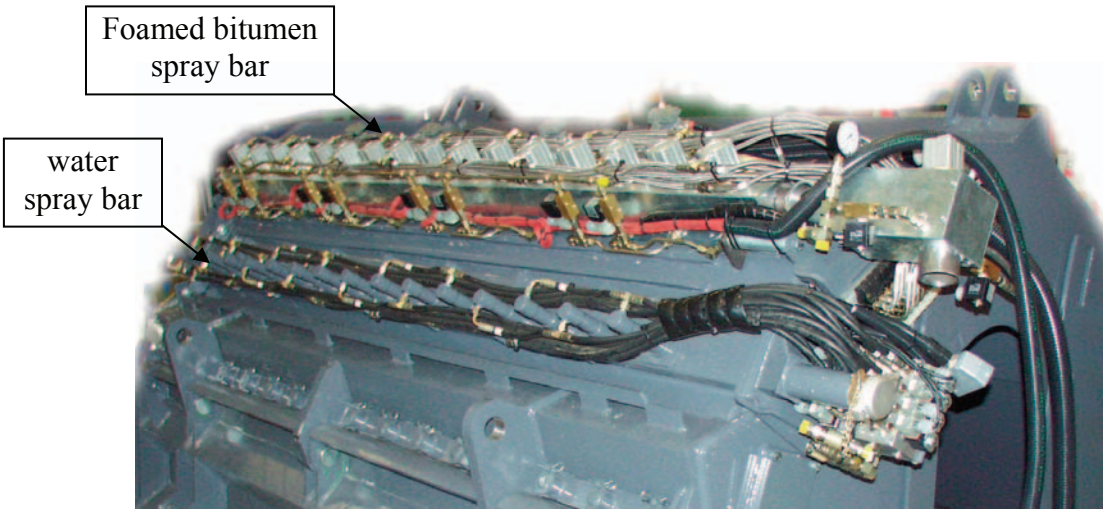


Figure 20: Foamed bitumen spray bar fitted to the milling hood of a recycling machine (Wirtgen, 2002)

2.2.3.5 Foamed bitumen technology

Foamed bitumen is traditionally characterised by two properties, *i.e.*:

- Expansion Ratio ($ER_m$); and
- Half-life time ($\tau_{½}$).

The expansion ratio is the ratio between the maximum expanded volume of the foamed bitumen and the original volume of the base bitumen (before foaming). The half-life time is defined by the period (in seconds) during which the volume of the foamed bitumen has reduced to half of its maximum expanded volume (at t = 0).

The expansion of the bitumen and the half-life time are dependent on a large number of variables, of which the most important ones are summarised below:

- The type of base bitumen;
- The temperature of the bitumen;
- The working pressures of bitumen, water and air;
- The quantity of foamant water added;
- The presence of foamants or anti-foamants;
- The configuration of the nozzle and the nozzle outlet;
- Temperature of the mixing chamber or bucket into which the foamed bitumen is sprayed.

Given a foamed bitumen production plant with standard operation procedures (therefore with the variables resulting from configurations and settings fixed), the effect of changes in the quantity of foamant water for a certain bitumen at a certain temperature can be determined. A typical dependency of the two properties $ER_m$ and $\tau_{½}$ is shown in Figure 21. It can be seen that choosing the optimum quantity of foamant water is a trade-off between $ER_m$ and $\tau_{½}$. The more foamant water, the higher the expansion ratio, but the shorter the half-life time.

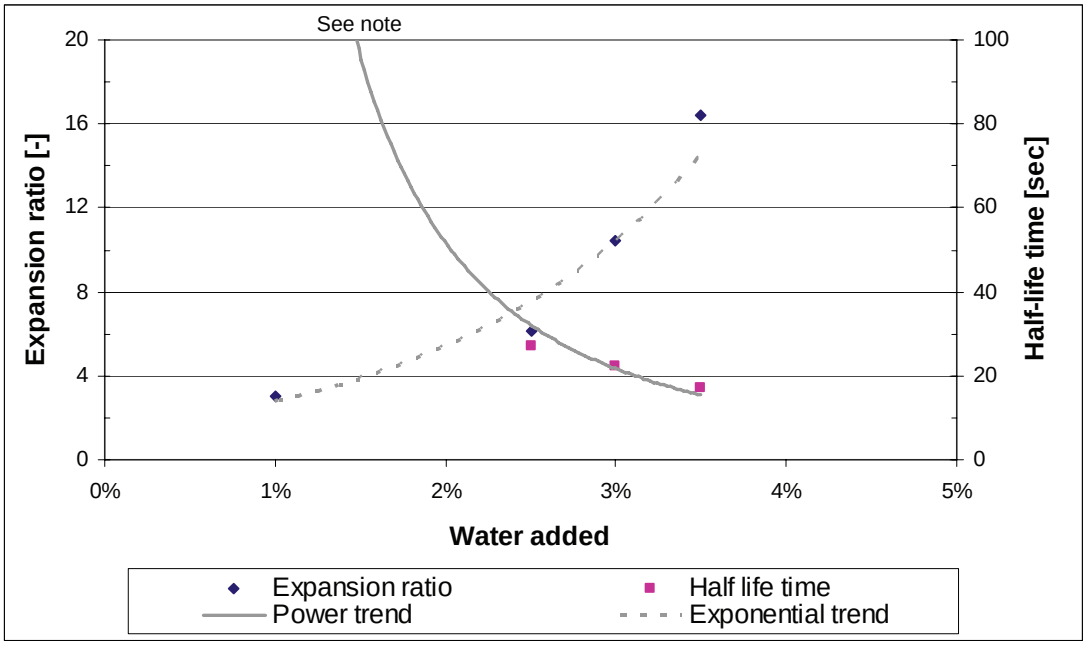


Note: $\tau_{½}$ at 1% foamant water in excess of 3 minutes is not shown on the graph

Figure 21: Foamed bitumen characteristics ($ER_m$ and $\tau_{½}$) for PG58-28 bitumen at 170ºC

Various minimum recommended combinations of expansion ratio and half-life time can be found in literature, *inter alia*:

- $ER_m \geq 10$ and $\tau_{½} \geq 12$ seconds (CSIR, 1998);
- $ER_m \geq 7$ or $\tau_{½} \geq 7$ seconds (in combination with foam index guidelines, Asphalt Academy, 2002);
- $ER_m \geq 10$ and $\tau_{½} \geq 8$ seconds (Wirtgen, 2004).

Jenkins (2000) identified that the two parameters, $ER_m$ and $\tau_{½}$, alone are not sufficient for adequate characterisation of the foamed bitumen properties or the optimised performance thereof. The two parameters define only two points on the curve that outlines the collapse of the foam with time. Jenkins defines this collapse with time as foam decay. A typical foam decay curve is shown in Figure 22. By taking into account only the two points shown [($t = 0$, $ER_m$) and ($t = \tau_{½}$, $½ER_m$)], the shape of the remainder of the curve is ignored. According to Jenkins additional parameters describing foam decay are required for more complete characterisation of the foam and the prediction of performance of foamed bitumen in mixing and coating applications.

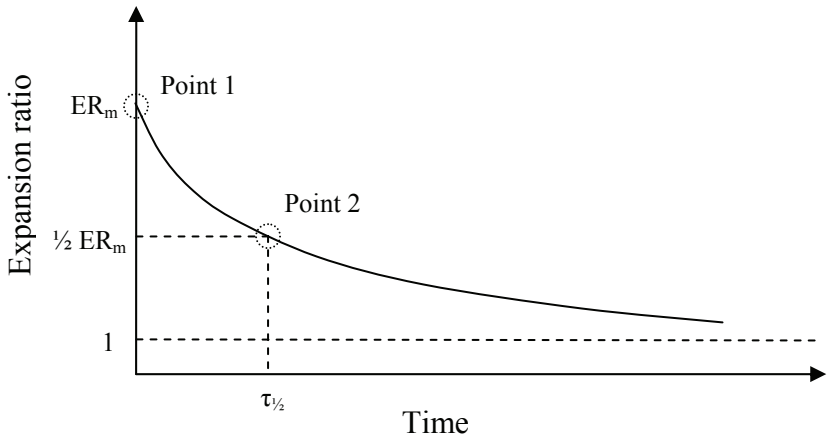


Figure 22: Typical curve outlining collapse of foam with time (foam decay, after Jenkins, 2000)

Jenkins (2000) used the area under the decay curve within specific limits for characterising and optimising foamed bitumen. He defined this area as the Foam Index. The area within the specific limits is shown in Figure 23 ($A_1 + A_2$). The Foam Index (FI) can be calculated using (Jenkins, 2000):

$$FI = A_1 + A_2 = \frac{-\tau_{1/2}}{\ln 2}\left(4 - ER_m - 4\ln\left(\frac{4}{ER_m}\right)\right) + \left(\frac{1+c}{2c}\right)\cdot ER_m \cdot t_s \qquad \text{Eq. 1}$$

where

| | | |
|---|---|---|
| $\tau_{½}$ | = | half-life time [sec] |
| $ER_m$ | = | Maximum Expansion Ratio [-] |
| $c$ | = | ratio between $ER_m$ and $ER_a$, see Figure 24 [-] |
| $t_s$ | = | spray time [sec] |

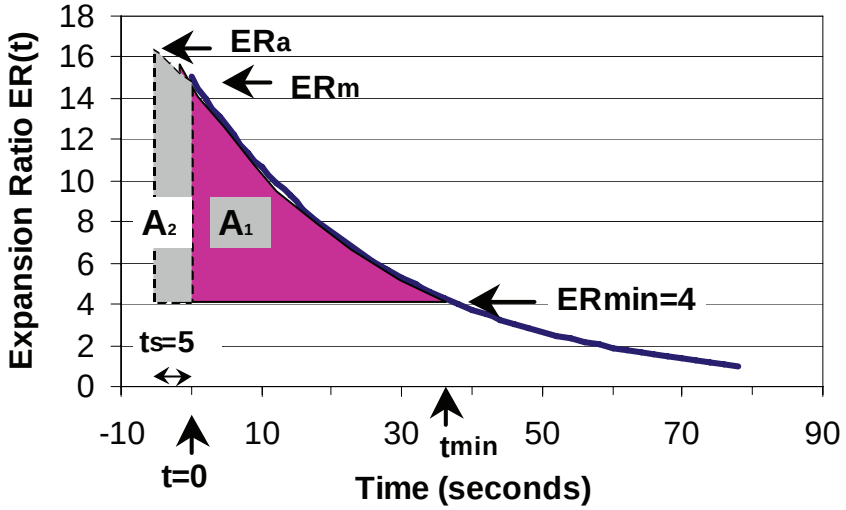

Figure 23: The Foam Index (FI) for characterising the "foamability" of bitumen for a given foamant water application rate, where FI = A1+A2 (Jenkins, 2000)

On the expansion ratio axis the area under the decay curve is limited by $ER_a$, the actual maximum expansion ratio, and $ER_{min}$, the minimum expansion ratio. $ER_a$ takes account for the fact that during the spraying of the foamed bitumen, decay already takes place. For practical reasons only $ER_m$ can be measured directly after the spraying of foamed bitumen has stopped (t = 0). Due to decay of the foamed bitumen during the spraying time $ER_a$ is larger than $ER_m$. The $ER_a$ can be determined using Figure 24 (Jenkins, 2000).

The minimum expansion ratio, $ER_{min}$, is defined as the expansion ratio at which the viscosity of the foamed bitumen is at the upper limit of the bitumen viscosity range that is recommended for adequate mixing and coating of mineral aggregate. Jenkins has found that to stay within the suitable viscosity range of bitumen for mixing a minimum value of 4 needs to be maintained for $ER_{min}$ (Jenkins, 2000).

On the time axis the area under the decay curve is limited by $t_s$ and $t_{min}$. $t_s$ is the spray time (t = 0 is the end of the spray time). $t_{min}$ is the time at which the expansion ratio has reduced to $ER_{min}$ (Jenkins, 2000).

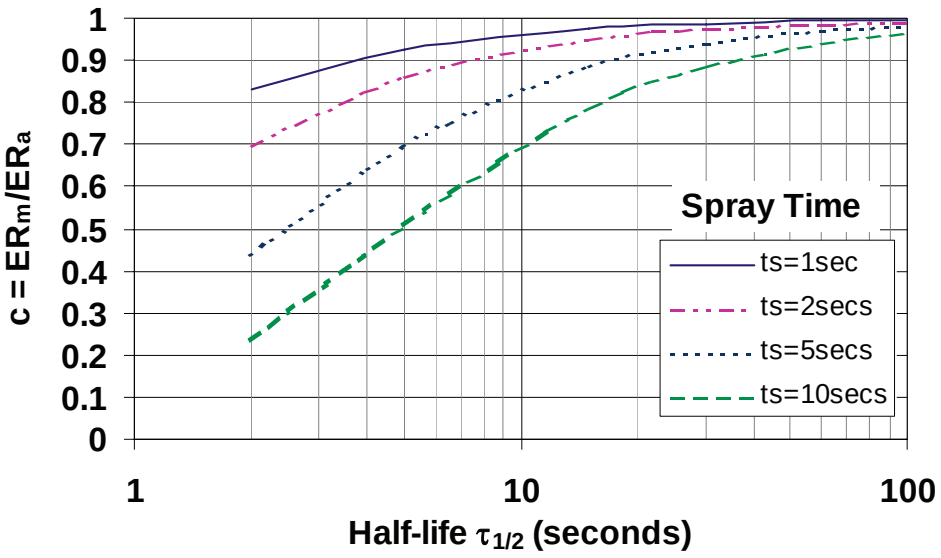


Figure 24: Ratio between $ER_m$ and $ER_a$ (c) as function of half-life time and spray time (Jenkins, 2000)

Iso-lines of the Foam Index can be plotted in the expansion ratio versus half-life time plane. This is shown in Figure 25. The zone in which the foamed bitumen is located will indicate its suitability for use in foamed bitumen mixes. Depending on the aggregate temperature, minimum foam indices are recommended in Table 4 (Asphalt Academy, 2002).

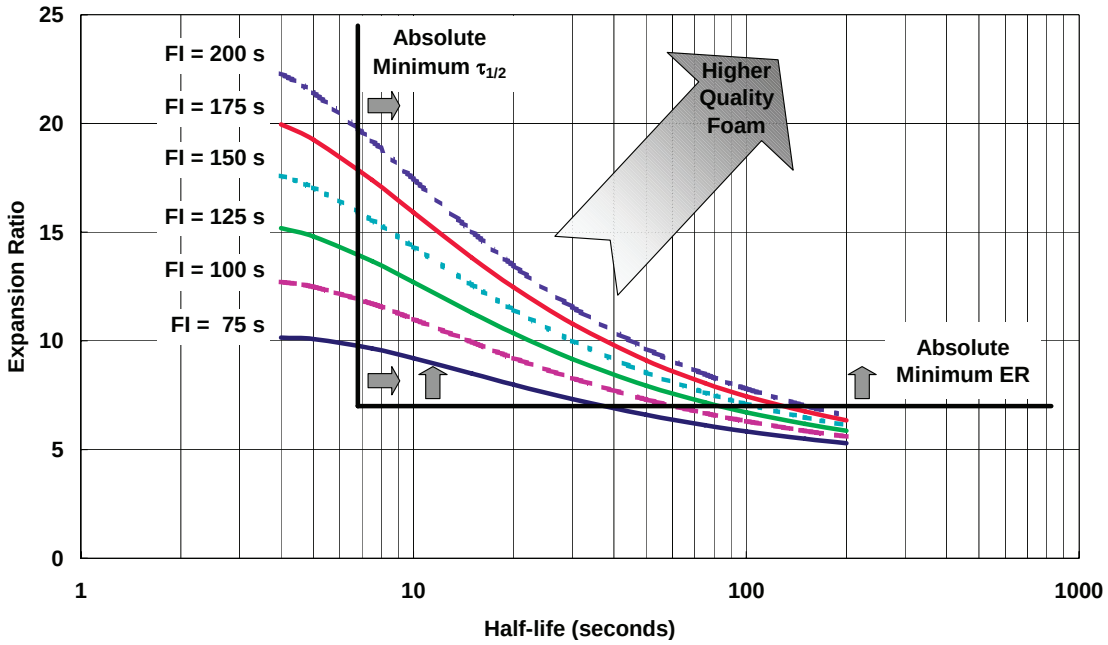


Figure 25: Ranking of Foamed Bitumen Suitability on the Basis of the Foaming Characteristics (Asphalt Academy, 2002)

Table 4: Classification of the Suitability of Foamed Bitumen for Cold Mixes (Asphalt Academy, 2002)

| Foam Index (seconds) | Aggregate at 15 °C | Aggregate at 25 °C |
|---|---|---|
| < 75 | Unsuitable | Unsuitable |
| 75 – 100 | Very Poor | Poor |
| 100 – 125 | Poor | Moderate |
| 125 – 175 | Moderate | Good |
| 175 – 200 | Good | Very Good |
| > 200 | Very Good | Very Good |

## 2.3 Bitumen Stabilised Materials (BSM's) in Southern Africa

### *2.3.1 Overview of guideline documents*

Treatment of granular material with bitumen emulsion has been used in pavement construction in Southern Africa since the 1960's. The initial development of foamed bitumen took place during the same period (late 1950's by Csanyi), but because of patent rights, the use of the foamed bitumen was limited to a small group of countries. After the expiration of the patent rights in the 1990's, the use and further development of foamed bitumen technology accelerated (Jenkins, 2000).

Throughout the years a number of guidelines have been developed by various institutions in South Africa. The publishing of these guidelines was generally prompted by pioneer work and developments that took place in the pavement

construction industry. An overview of BSM guidelines as published in South Africa is provided in Table 5. It can be seen that because of the limited application of foamed bitumen prior to the 1990's, no guidelines for the use of foamed bitumen were developed earlier on.

Table 5: Overview of BSM guidelines published

| Published | Bitumen emulsion | Foamed bitumen |
|---|---|---|
| 1972 | TRH 7: The use of bitumen emulsions in construction and maintenance of roads | |
| 1993 | SABITA manual 14: GEMS - The design and use of granular emulsion mixes | |
| 1999 | SABITA manual 21: ETB, the design and use of emulsion-treated bases | |
| 2002 | | TG 2: The design and use of foamed bitumen treated materials |

The first document, THR7 : The Use of Bitumen Emulsion in Construction and Maintenance of Roads (Department of Transport, 1972), provided little guidance in terms of stabilisation and/or cold-mix design. It incorporated general aspects of the use of bitumen emulsions in all fields of pavement construction, including seals, tack and prime coats, bitumen treatment and recycling. For the possible use of bitumen emulsion in soil stabilisation (reduction of plasticity index (PI) and increase of shear strength) reference was made to the knowledge and experience that existed in the industry at the time. The THR7 did, however, provide some general practical guidelines for the reuse of existing base layers treated with bitumen emulsion.

During the 1970's and 1980's the popularity of bitumen emulsion treatment of granular pavement layers increased and the term ETB's was established. Following APT using the HVS on pavements incorporating such ETB layers, SABITA published the GEMS manual in 1993. This manual dealt with the design and use of granular emulsion mixes. It made a clear distinction between stabilisation and modification. Stabilisation was defined as addition of bitumen emulsion with the residual binder content exceeding 1.5% by mass with the purpose to produce a structural layer with an 'asphalt type' of material. Modification was defined as generally less than 1.5% residual binder content by mass being added with the objective to improve the properties of substandard material (SABITA, 1993). The latter was the more popular application in Southern Africa during that time period.

The SABITA GEMS manual was the first of its kind to introduce laboratory test procedures, mix design procedures, evaluation criteria and structural design guidelines for granular bitumen emulsion mixes in South Africa.

While the GEMS manual was still fairly new, SABITA embarked on a follow-up research programme to address certain shortcomings that were already identified in the GEMS manual. The main objective was to provide updated and extended

guidelines on structural design, mix design, constructability and economic guidelines to broaden the range of the application of ETB's. An ETB would typically have a residual binder content of 1.5% by mass or less. Therefore it would according to the GEMS manual be classified as a modified granular emulsion mix. The mix design and structural design guidelines for such a modified granular emulsion mix were not appropriate for an ETB material. This resulted in the publishing of SABITA's ETB manual (Manual 21) in 1999.

Prior to the publishing of the Asphalt Academy's TG2 Interim Guideline for foamed bitumen treatment in 2002, designers in Southern Africa mainly 'borrowed' from the available guidelines for bitumen emulsions, international foamed bitumen guidelines, as well as hot-mix asphalt design guidelines. TG2 introduced laboratory test procedures, mix design procedures, evaluation criteria and structural design guidelines for foamed bitumen treated materials in South Africa. The guideline was launched as an interim guideline with the intention to update the manual once further research results (on different types and qualities of parent material and more bitumen : cement ratios) became available.

### *2.3.2 Grading considerations*

Guidelines for optimum grading are provided by *inter alia* Akeroyd and Hicks (1988), SABITA (1993), Jenkins (2000) and Asphalt Academy (2002). These guidelines are based on the principle that a material performs best with a grading approaching the maximum density curve (Nijboer curve with n = 0.45). In addition the parent material of BSM's should comply with the grading of the specified parent material class (see Appendix A). In this regard it should be noted that the grading after recycling, in case of CIPR, may differ from the grading of the parent material prior to the recycling operation. The former is to be used for design purposes.

It is noted that when using foamed bitumen the filler content (< 0.075 mm fraction) has an important effect on the behaviour of the mix. A certain amount of fines is required in order to ensure optimum dispersion of the foamed bitumen mastic in the mix (Jenkins, 2000). A minimum filler content of 5% and up to 20% is considered "ideal" while up to 35% may be suitable. Less than 5% filler is considered "unsuitable" (Akeroyd and Hicks, 1988). This is a key difference with bitumen emulsion mixes, which do perform well with low filler contents. High filler contents in bitumen emulsion mixes may lead to early breaking of the emulsion and "balling" (Ebels, 1998)

### *2.3.3 Curing*

Curing is the process of reduction of the moisture content in the BSM with time. During mixing and compaction this moisture content is near the optimum moisture content for compaction. In the field curing continues typically up to 6 – 18 months. With the reduction of moisture in the mix the strength and stiffness increase. The field curing times are too long for laboratory mix design purposes. When specimens are to be tested at equilibrium field moisture content, the laboratory curing process needs to be accelerated.

A plethora of different curing procedures have been developed globally and locally for accelerated laboratory conditioning after compaction of specimens (Jenkins *et al.*, 2006). As shortcomings were recognised, adjustments were made and so the protocols evolved. Some of the more recent methods, pertinent to Southern Africa, are summarised below:

Table 6: Overview of curing methods with discussion of shortcomings

| Curing method | Shortcoming |
|---|---|
| • The GEMS Manual (Sabita, 1993) proposed a curing method requiring 3 days at 60ºC in an oven (unsealed) | Final moisture content of specimen <1% which does not represent field moistures (equilibrium moisture content, EMC) |
| • The ETB Manual (Sabita, 1999) made provision for the influence of active fillers by curing at non-elevated temperatures. Where cement was included in emulsion mixes, a 7 day ambient temperature cure was proposed whilst for no cement, a 28 day ambient temperature cure was recommended | Commercial mix designs are protracted by the curing, resulting in time delays. |
| • The TG2 Guideline (Asphalt Academy, 2002) introduced the sealing of the specimen in a plastic bag and placement in an oven at 40 ºC for 72 hours. Although the guideline was developed for foamed bitumen, the curing procedures could also be directly applied to bitumen emulsion mixes | Sealing of the specimens retains too much moisture in the mixture, about EMC, thus resulting in conservatively low strength and stiffness. |
| • Houston and Long (2004) proposed a curing procedure for foamed mixes of 24 hours at ambient (25ºC) unsealed followed by 48 hours of sealed curing in an oven at 40ºC | Whilst this protocol more closely simulates EMC values observed in the road, it does not account for relative humidity i.e. climatic influences of the area, something which European procedures aim to simulate. In addition, it does not provide any evidence that the BSM stiffness in the laboratory represents that which is experienced in the field. |
| • Kekwick (2005) proposed that the material stiffness be included in curing procedures. His conceptual approach is a good one and suggests that stiffness be interpreted from the tangent modulus from a stress-strain response measured in a modified CBR-type compression test (rather than ITS or UCS testing currently being used). Kekwick suggests that the curing time (at ambient temperature) that yields laboratory stiffness comparable to the resilient modulus used in the mechanistic design, be established. An acceptable curing period would imply that a reasonable design modulus has been selected for the cold mix in question | Commercial mix designs are protracted by the curing, resulting in time delays. In addition, the modified CBR-type test requires further R&D. |
| • Malubila (2005) re-evaluated the prediction models for equilibrium moisture content (EMC) of foamed mixes based on material properties (OMC and BC) and climate, by carrying out field tests on pavements incorporating these materials across South Africa and one case in Zambia | Although Malubila's work provided more robust prediction models for EMC, he identified that Houston and Long's procedure of 2004 and a similar one produced at University of Stellenbosch (Jenkins *et al.*, 2006) were most representative, with the deficiencies already listed, being applicable. |

Research is currently underway at the Stellenbosch University to track the in situ moisture and stiffness trends of BSM's incorporating bitumen emulsion or foamed bitumen binders. Parallel to this, laboratory testing is carried out to identify a representative and yet simple (if possible) accelerated curing protocol that simulates field trend realistically (Moloto, to be published 2008). This is shown conceptually in Figure 26.

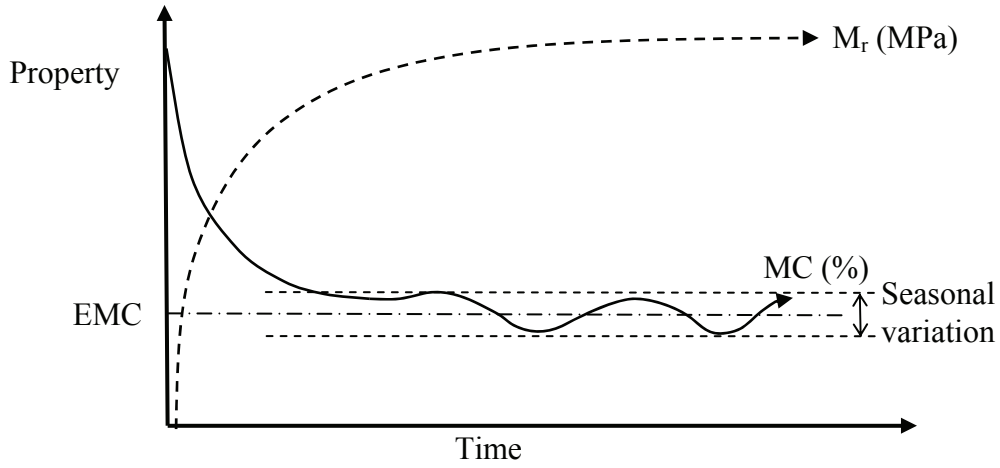


Figure 26: Conceptual change in material properties through curing (Ebels and Jenkins, 2007)

### *2.3.4 Mix design tests*

The mix design tests suggested by the several manuals discussed in the previous section are summarised in Table 7. When the type of mix design tests are evaluated, one has to consider that the residual binder contents of the mixes that are used in practice in Southern Africa are generally low. It can be seen that the laboratory mix design tests for these types of mixes used during past ten years are typically soil mechanics tests (CBR and UCS) used for soil stabilisation design (especially cement stabilisation).

Emulsion mixes with higher residual binder contents would typically be covered under the mix design procedure for stabilised GEMS. To date this guideline has not been superseded and thus according to the most recent published South African guideline on emulsion mixes (SABITA, 1993) these mixes are to be treated as 'hot-mix asphalt type' mixes. The design for these leans heavily on the Marshall mix design method. This method has a number of drawbacks and has in HMA mix design lost popularity in favour of 'Superpave' and performance graded mix design methodologies. One could argue that because of recent developments in HMA mix design, the Marshall mix design era is nearing its end. The same would also apply in the field of cold-mix design methods for mixes with high residual binder contents. The Marshall design method would therefore not be the most suitable method for modified GEMS.

Table 7: Summary of development of laboratory mix design tests

| Published | Manual | Mix design test | | Specimen size (diameter) |
|---|---|---|---|---|
| 1972 | TRH 7 | - | | - |
| 1993 | GEMS manual | Modified GEMS: | CBR<br>UCS | 150mm |
| | | Stabilised GEMS: | Marshall<br>ITT<br>ITS | 100mm |
| 1999 | ETB manual | CBR<br>UCS | | 150mm |
| 2002 | TG 2 guideline | UCS<br>ITS | | 150mm |

Prior to the publishing of the TG2 guideline, the Marshall method was also popular for the design of foamed bitumen mixes. However, with the publishing of TG2 (Asphalt Academy, 2002) a mix design philosophy that considers properties such as stiffness and flexibility was introduced. In this mix design methodology the stiffness is tested by means of UCS testing and the flexibility (elasticity) by means of ITS testing. These tests would apply even when the residual bitumen contents are relatively low. A foamed bitumen treated mix can, according to the specifications given in the TG2 guideline, be rated in one of four categories as follows, from best to worst:

- FB1: material with high stiffness and high tensile strength;
- FB2: material with high stiffness, low tensile strength;
- FB3: material with low stiffness and high tensile strength;
- FB4: material with low stiffness and low tensile strength.

Table 8: TG2 Foamed bitumen treated material classification (Aphalt Academy, 2002)

| UCS at 25ºC [kPa] | ITS (dry) at 25ºC [kPa] | |
|---|---|---|
| | 100 – 300 | 300 – 500 |
| 700 – 1400 | FB4 | FB3 |
| 1400 – 2000 | FB2 | FB1 |

The TG2 guideline was specifically developed for foamed bitumen treated materials, but the methodology would be applicable to bitumen emulsion treated materials as well. This methodology would therefore supersede the mix design approach for bitumen emulsion described in the two SABITA manuals. Extensive research including APT on emulsion BSM pavements has also been undertaken by the CSIR

during recent years. Although draft guidelines incorporating this mix design philosophy for emulsion mixes were compiled, these were never published. Liebenberg and Visser also did some research in this field and they proposed a mechanistic structural design procedure according to the same philosophy as the TG2 guideline did for foamed bitumen treated materials (Liebenberg and Visser, 2004). The mix design tests for emulsion-treated granular material proposed by Liebenberg and Visser are also UCS and ITS tests. The specifications for the four categories of mix quality were slightly adjusted in terms of UCS values from the foamed bitumen treated materials.

Table 9: Proposed bitumen emulsion treated material classification (Liebenberg and Visser, 2004)

| UCS at 25ºC [kPa] | ITS (dry) at 25ºC [kPa] | |
|---|---|---|
| | 100 – 300 | 300 – 500 |
| 750 – 1200 | ET4 | ET3 |
| 1200 – 2000 | ET2 | ET1 |

### *2.3.5 BSM design philosophy*

Pavement design in South Africa during the past decades has revolved around the South African Mechanistic Design Method (SAMDM), which was first developed during the late 1970's and refined throughout the 1980's and 1990's. Theyse *et al.* (1996) and Theyse and Muthen (2000) provided updates on this method, which incorporates granular, hot-mix asphalt and cemented materials. However, BSM's were never considered at the time.

For granular materials distress through cumulative permanent deformation and inadequate stability were considered to be the dominant behavioural mechanisms. The shear strength of granular materials is thus the most important material property in the design process. For the structural design for cemented materials a phased approach was developed in the SAMDM. Effective fatigue and crushing are considered the dominant behavioural mechanisms in the first phase during which the stiffness of the cemented materials reduces. In the second phase the cemented material is considered to behave equivalent to granular material with the associated behavioural mechanisms. The material property used in the analysis of effective fatigue is the strain-at-break from static beam flexure, whilst the crushing failure mechanism is evaluated using UCS.

Table 10: Material properties used as input for structural design

| Material type | Phase I | Phase II |
|---|---|---|
| Granular | Shear strength | |
| Cemented | Strain-at-break & UCS | Shear strength |

In the project level design process, the shear strength properties, strain-at-break and UCS values are seldom tested and designers rely on tabulated values once the material class has been established. Hence, the material property input in the

structural design relies heavily on the classification of the granular material (G-codes) and cemented materials (C-codes), as per TRH14 (CSRA, 1985) as discussed in Appendix A.

The ETB Manual states that the behaviour of emulsion-treated material resembles that of lightly cemented material, with a similar deterioration pattern, but on a different time scale. The reduction of stiffness of ETB is believed to take place over a longer time span. The structural design in the ETB manual is however based on a catalogue of standard pavement structures, with two ETB material classes, i.e. E1 and E2. The material properties that govern this classification are CBR and UCS.

The TG2 Guideline introduces pavement life phases for foamed bitumen treated materials that is very similar to those for cemented materials, *i.e.* an effective fatigue phase and an equivalent granular phase. The TG2 Guideline also provides a catalogue of standard pavement structures, with four foamed bitumen treated material (FBTM) classes, *i.e.* FB1 – FB4. The material properties that govern this classification are ITS and UCS.

Besides the catalogue of pavement structures, the TG2 Guideline also provides designers with a mechanistic-empirical procedure for the pavement design. The analysis of the effective fatigue phase is very similar to that of cemented materials and tabulated values for the strain-at-break are provided based on the FBT material classes. On a project design level, strain-at-break properties of FBT material are not measured and hence, designers rely on these tabulated values.

For the equivalent granular phase the TG2 Guideline provides a slightly different approach as used for cemented materials in the SAMDM. The structural capacity of this phase is not only given as a function of the shear strength properties (as is the case for cemented materials), but is linked to permanent deformation, which is given as a function of density, plastic strain, shear strength properties and cement : bitumen ratio. The transfer functions provided in the TG2 Guideline are based on a limited number of HVS tests and have proved to be conservative.

It can thus be concluded that, although the design guidelines are based on more fundamental material tests, such as the tri-axial tests and four-point beam test, the mix design tests on a project level are still relatively unsophisticated tests such asCBR and UCS (ETB) and ITS and UCS (FBTM).

### *2.3.6 Shortcomings of the existing design methods*

Residual binder contents of BSM's seldom exceed 3% by mass in South Africa. BSM's have increased cohesion compared to granular materials and do show some time and temperature dependent behaviour. The visco-elastic behaviour of BSM's can however not be compared with that of hot-mix asphalt. This is illustrated by Figure 27, but is further discussed in Chapters 6 and 8.

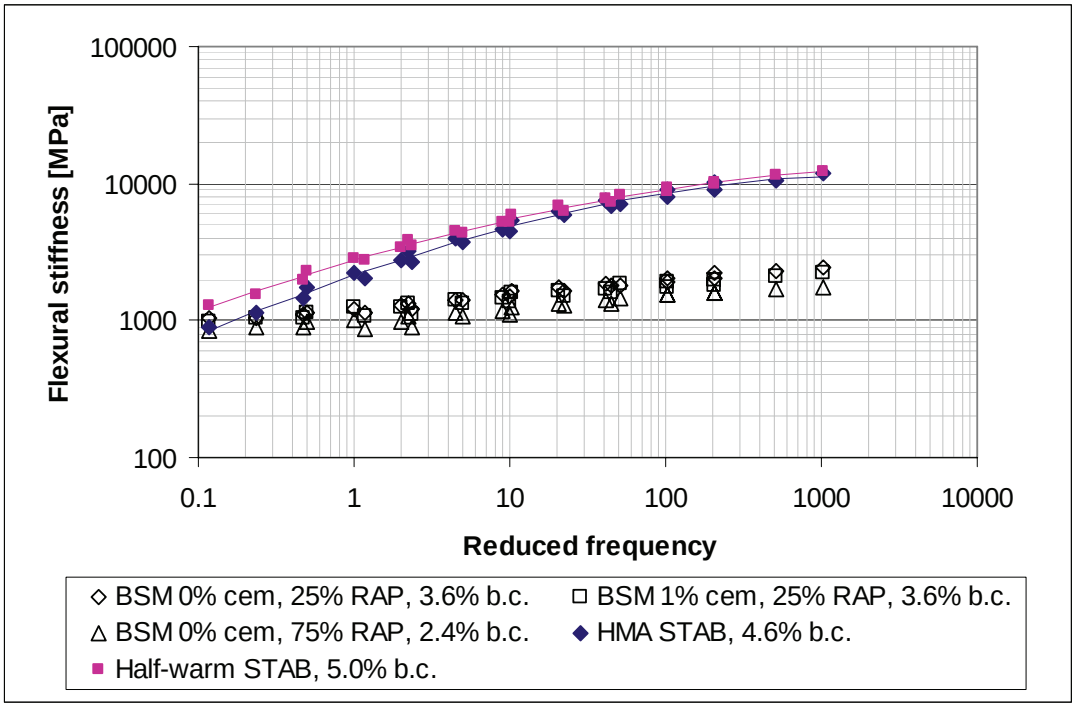


Figure 27: Master curves of BSM (foam), Half-Warm and HMA ($T_{ref}$ = 20ºC)

In this study it was found that the testing temperature for four-point beam testing of BSM's needs to be reduced to 5ºC in order to develop flexural bending induced cracking. At higher temperatures cracking at the supports due to shear failure is dominant. This is discussed in more detail in Chapter 4.

The above shows that with the relatively low residual binder contents commonly used in South Africa and with in-service base temperatures generally in excess of 15ºC, BSM's do not behave like HMA type materials. Hence, failure due to fatigue cracking is also not believed to be a dominant mechanism for BSM's.

Twagira *et al.* (2006) found that great care needs to be given to the preparation of BSM beam test specimens. Unless a very strict and sound specimen preparation protocol is followed, the results of four-point beam testing may become unreliable, especially for monotonic strain-at-break tests. The flexural beam strain-at-break was found not to be a good parameter to normalize fatigue test results and the strain-at-break test would require further development before it can be considered in the characterisation of flexibility properties in terms of fatigue resistance of BSM. Twagira *et al.* (2006) and Ebels and Jenkins (2007) recommended not to use flexural beam strain-at-break properties as a mix design parameter for BSM's. This is opposing what was recommended by Long and Theyse (2004), who are of the opinion that it should be relatively easy to determine the strain-at-break in a monotonic four-point beam test in standard laboratories and that this can be widely adopted in practice.

Ebels *et al.* (2005) discussed the appropriateness of a two-phase approach to describe the general behaviour of BSM pavements as outlined in the TG2 Guideline. The fact

that fatigue distress only develops with time and that the bulk of permanent deformation (excluding tertiary flow) takes place in the early life of a pavement is not in support of this two phase approach. A conceptual stiffness model as shown in Figure 28 was proposed. The stiffness reduction as correctly identified during accelerated pavement testing and adopted as general behaviour in the TG2 Guideline is also shown in this figure. Contrary to the TG2 model, the proposed stiffness development model as shown in Figure 28 takes into account an initial increase in stiffness due to curing and possibly densification. This initial increase in stiffness which may typically take 6 – 18 months has been observed in a number of LTPP BSM pavements. This is further discussed in Chapter 8.

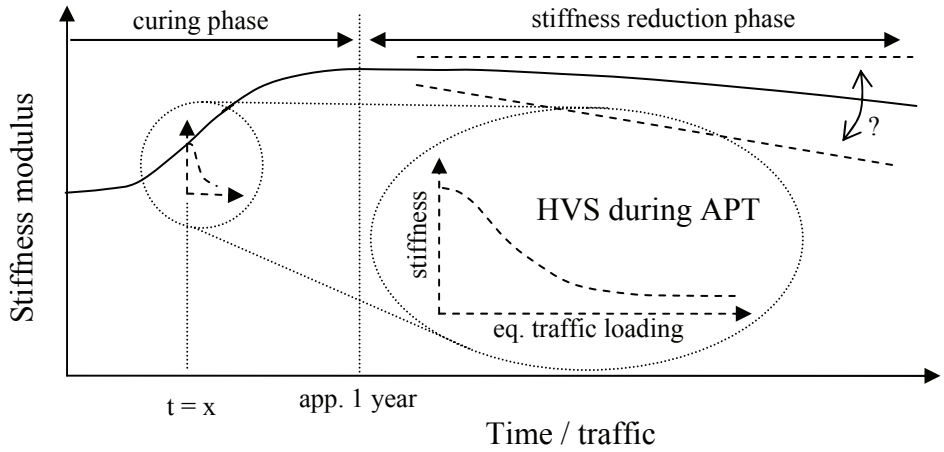


Figure 28: Conceptual stiffness development during the service life of bitumen stabilised material (Ebels et al., 2005)

If the above conceptual stiffness development is correct, it could be argued that the stiffness development during the service life differs significantly from the measured stiffness reduction during APT. This being the case, it could be deducted that structural design models that are based on the rapid stiffness reduction identified during APT are not correct and that fatigue resulting in rapid stiffness reduction either does not occur during the early stages of the service life or is overshadowed by the effect of curing. In such cases it may be concluded that stiffness reduction as a failure mechanism of BSM's is currently over-emphasised and that the design of BSM should focus more on shear strength and permanent deformation.

As such, the mix design of BSM should also reflect material properties that are related to shear strength and permanent deformation. In this regard there are a number of laboratory tests that could be used to determine the shear strength properties and permanent deformation behaviour, including:

- Static and dynamic creep test;
- Tri-axial test;
- Hveem stabilometer; and
- Leutner shear test

Since the 1960's researcher have successfully used the tri-axial test to related fundamental shear properties of material and the permanent deformation behaviour to the performance of these materials in the pavement structure (see Chapter 3). As early as 1974 Shackel *et al.* (1974) found good correlation between tri-axial testing (monotonic and dynamic) of BSM's and the permanent deformation of these materials in the pavement.

The advantage of tri-axial testing is that it is also capable of determining the stress-dependent behaviour, *i.e.* the material response at different levels of confinement. In this regard the tri-axial test is believed to have potential to provide fundamental material properties that should be included in the mix design process.

The current use of the UCS and ITS tests for mix design purposes has certain limitations:

- The UCS test is much like a tri-axial test with zero confinement. The most significant difference is the specimen geometry, *i.e.* the height : diameter ratio. In the UCS tests this ratio is 0.85, which is considered too low to provide reliable shear strength parameters. A ratio in the order to 2.0 is preferred in order to eliminate edge effect (additional confinement due to friction at the specimen-loading plates interface);
- The ITS test is considered to be a "simple test", *i.e.* it can be performed with relative ease. It is generally accepted that the interpretation of the results of "simple tests" is often more complex than the results of "complex tests". The ITS (splitting) tests is a prime example of this, because the internal stress distribution in this test is extremely complicated. There exists no direct relation between the applied force and the stress at the centre of the specimen (Erkens, 2002, pp. 29);
- Interpretation of ITS results is under the assumption that plane stress is achieved. This assumption is an approximation of the real stress state and becomes less correct with thicker specimens. A minimum ratio of diameter : thickness of 4.0 is recommended. Hence, with a specimen diameter of 150 mm, as per TG2, the maximum thickness of specimens for ITS testing should not exceed 37.5 mm. The thickness prescribed in the TG2 Manual is 95 mm, i.e. a ratio of 1.6. A state of approximate plane stress will thus not be achieved in the ITS test and the test is more of a compressive test than a tension test. This is confirmed by the fact that various researchers (Houston and Long, 2004; Bondietti *et al.*, 2004) have, after the introduction of the USC-ITS based classification system, found linear relationships between the UCS and ITS test results. It would be an improvement to the current TG2 ITS testing method to reduce the thickness of the specimens.

Because of the above it has been found difficult to obtain close relations of the test results with fundamental and performance related material properties. Therefore the ITS test in its current form is deemed unsuitable for specification testing of BSM's. This is also related to issues of loading rate and temperature, variability in test results and the visco-elastic behaviour of BSM's. It is however believed that the ITS test can in its current form be used as an indicator test.

Other researchers have carried out work to improve the ITS test or have used finite element models (FEM) to assist in the interpretation of the ITS test results. Information available in this regard is all focussed on HMA and similar work for BSM would require robust material models that describe the visco-elastic behaviour of BSM (which is different to HMA), actual ITS testing and FEM modelling of BSM materials. This is outside the scope of this study, but the identification of the visco-elastic behaviour of BSM's by means of Burgers Model parameters, as discussed further on in this study, is a step in this direction.

Issue relating to the specimen geometry (height : diameter (h/D) ratio) in case of the UCS test and the effect of friction between the loading plates and the specimen in case of low h//D ratios can in some cases be overcome by applying friction reduction. Erkens (2002) successfully developed a friction reduction system consisting of a highly plastic interlayer between the specimen and the loading plates of foil in combination with soft soap in combination with HMA specimens.

It needs to be noted though that with HMA specimens the cut top and bottom face of the specimen provide a very smooth and "rigid" suface that works well in combination with the highly plastic friction reducing interface layer. The top and bottom face of BSM specimens, even when cut, render a much more textured surface than is the case for HMA. Preliminary testing with friction reduction by Jenkins (pers. comm.) indicated that the typically rough and textured surface of BSM specimens protrudes into and damages the highly plastic interlayer, thereby limiting the friction reducing effect. Applying friction reduction has therefore generally been unsuccessful in a uniaxial compression test of BSM's due to the granular nature of the material.

Furthermore, applying a system of friction reduction requires considerable attention to detail. This may not be a problem in a research environment or a well equipped laboratory with highly skilled personnel, but it becomes a limiting factor when commercial laboratories, especially those with generally lower skilled testing operators, need to include a friction reduction system in a uniaxial compression test. With the current status quo it is therefore recommended that additional work be carried into developing a robust and easy to apply friction reduction system before it is introduced for UCS testing of BSM materials.

## 2.4 Importance of parameters other than the experimental variables

### *2.4.1 Parameters not tested in this study*

Limitations to the extent that only a few experimental variables are tested in this study were discussed in the Introduction to this dissertation. Some important other aspects that could not be included in the experimental matrix and their possible effect on the properties and behaviour of BSM's are discussed in this section. These aspects include:

- Compaction;

- Grading;
- Binder content; and
- Curing.

### *2.4.2 Compaction*

Compaction was not considered an experimental variable in this study. All specimens tested were compacted to the target density of 98% of Modified AASHTO Density, which was a requirement of the sponsor of the research. This is a relatively low density specification by South African standards, where crushed stone base layers are normally compacted to 86% or 88% of bulk relative density of the stone and gravel base layers up to 102% of Modified AASHTO Density. For BSM materials a relative density requirement in terms of Modified AASHTO Density is often specified with a minimum of 102%.

Compaction of soils has been used for as long as mankind had the need to improve the properties of the soil. Properties such as strength and bearing capacity increase with compaction, while the compressibility and permeability reduce (Ebels *et al.*, 2004). This would also apply to bound and stabilised granular materials. Increasing the compaction of a material has proven to be one of the most cost-effective and easiest methods of improving the properties of the compacted material.

Examples of improved material response at higher density levels are plentiful in literature. The effect of compaction on the bearing capacity of a crushed stone material is *e.g.* shown in Figure 29.

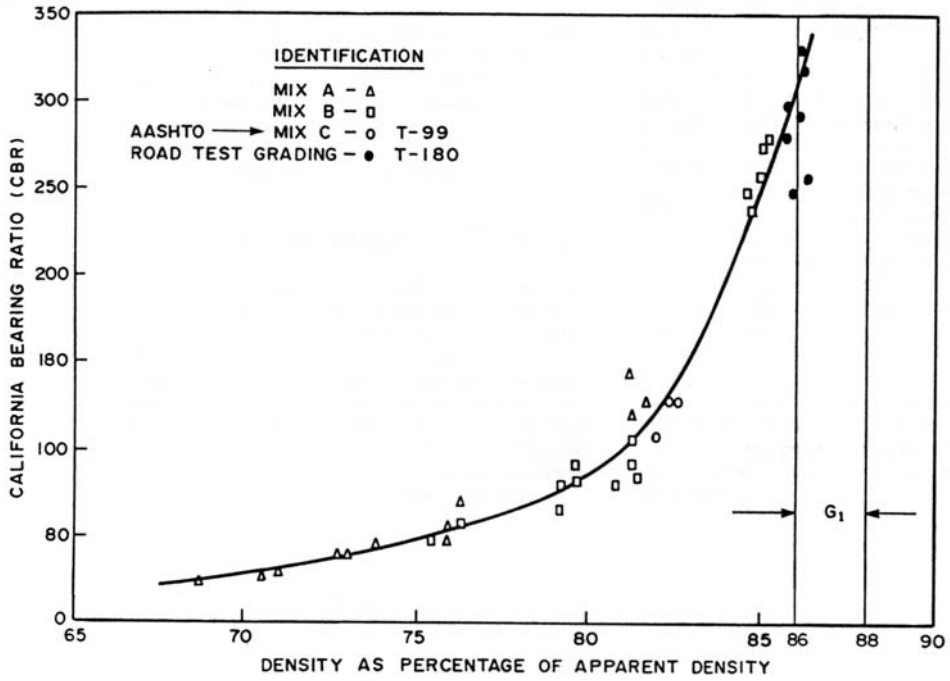


Figure 29: CBR vs. density of G1 crushed stone (Semmelink, 1988)

One of the main findings of van Niekerk's work (2002) was that the degree of compaction ranks as the most important factor influencing mechanical behaviour of unbound and hydraulically bound granular materials. He stated that it improves the shear strength, the resilient response and "has by far the largest effect" on the permanent deformation behaviour.

Although density was not varied on this study, it can safely be assumed that the material properties and behaviour of BSM's as presented in this study would improve at higher levels of compactions. Furthermore, the response of pavements incorporating BSM's would improve when the density of the BSM's increases. Vertical deflections would reduce significantly due to better load spreading ability and shear failure would occur only at higher load levels. This would improve the load carrying capacity of the pavement and therefore impact on the structural design.

This is illustrated by the transfer functions for permanent deformation provided in the TG2 Guideline for foamed BSM's, in which the relative density is the most important variable. This transfer function for a 90% reliability level (South African Road Category B) is shown in Equation 2.

$$N_{PD} = \frac{1}{30} \cdot 10^{[-1.95+11.938\,RD+0.0726\,PS-1.628\,SR+0.691(cem/bit)]} \qquad 2$$

whereby

| | | | |
|---|---|---|---|
| | $N_{PD}$ | = | Structural capacity [No. of load repetitions] |
| | $RD$ | = | Relative density [%-Apparent Density] |
| | $PS$ | = | Plastic strain in the layer [%] |
| | $SR$ | = | Deviator Stress Ratio |
| | $cem/bit$ | = | ratio of cement and bitumen contents |

For the laboratory compaction of test specimens for mix design purposes the methods used for compaction of BSM's emerged from an HMA approach to these materials. In Europe and the USA these materials were perceived to be hot-mix asphalt equivalent cold-mixes and Marshall Compaction was adopted as the preferred laboratory compaction method. In developing countries such as Australia and South Africa, the BSM's were perceived as "modified, slightly bituminous granular materials" and a shift to Modified AASHTO compaction was adopted (as outlined in the TG2 Guideline, Asphalt Academy, 2002).

Problems encountered with the Marshall and Modified AASHTO Compaction methods when used on BSM's in Southern Africa included *inter alia* (Ebels and Jenkins, 2007):

- *Lack of simulation of the kneading effect* of rollers and particle orientation achieved in the layers in the field. Especially Marshall Compaction resulted in specimens with coarse outside texture due to the vertical hammering action not allowing mortar to occupy the voids between large aggregate on the annulus

- *Variability in target densities* achieved on site for quality control purposes. This is due to variation in material type and grading along the length of a rehabilitation project.
- *Delamination* of specimens produced using Mod AASHTO Compaction. The individual layers of BSM split during ITS tests, for example, yielding unrepresentative results.

During recent years various institutions in South Africa have used other forms of compaction such as vibratory and gyratory compaction for BSM's. The test specimens for this study were compacted using a gyratory compactor (tri-axial testing) and a vibratory roller (slab compaction for four-point beam fabrication) These methods have intrinsic disadvantages for commercial application in mix designs, such as cost, moisture damage to equipment (gyratory) and variability of results.

Vibratory compaction is however considered to have the best potential to simulate field compaction. Reducing the variability of results can be achieved using a vibratory hammer in a fixed mechanical set-up with a constant dead weight surcharge, without the variable interference of an operator. Therefore refusal density using vibratory compaction is considered to be the method of laboratory compaction identified as having great potential for BSM's. Refusal density compaction has been effectively used for HMA in the UK and other countries and also for BSM's (British Standards, 2004).

The refusal density of a BSM depends on the applied compaction energy. Variables of the compaction energy are mass, frequency and amplitude. Modern compaction equipment has on-board sensors that indicate when refusal density is achieved. Specifying refusal density in the field is however not possible without specifying the type of roller (mass) and roller setting (frequency and amplitude) and a bench-mark for subgrade support. Further research into these variables in relation to the laboratory refusal density using a vibratory hammer is required.

### *2.4.3 Grading*

The grading of the BSM's was also not considered a variable in this study. The mixes were also not blended to achieve an optimum design grading. Instead, the grading of the materials received, i.e. the crushed rock and RAP, was accurately determined, which formed the basis of the target grading. The experimental blends were constituted according to this grading. This target grading was consistently obtained by fractionating the materials received and reconstituting them accurately according to mass.

Guidelines for optimum grading are discussed in Section 2.3.2. The key difference between bitumen emulsion mixes and foamed bitumen mixes in terms of filler content (foamed bitumen mixes require a certain minimum amount of filler and high filler contents may still be suitable, while emulsion mixes perform well with low filler contents and high filler contents may be problematic) is believed to be confirmed by the shear strength testing in this study. For the mixes with a low filler

content (75M-0, 3.0% < 0.075 mm) the cohesion of the mixes with bitumen emulsion is higher than that of the mixes with foamed bitumen. The opposite was observed for the mixes with a higher filler content (75C-0, 7.1% < 0.075 mm). For the mix annotations refer to Chapter 4.

Although not tested here, it can be expected that mixes with a more continuous grading closer to the maximum density curve perform better than the mixes with a more discontinuous (gap or semi-gap grading). This would be the case for both foamed bitumen and bitumen emulsion mixes.

The testing conducted for this study confirms that increasing the filler content improves the shear strength when stabilising with foamed bitumen. It is however difficult to predict based on grading alone which type of binder, *i.e.* foamed bitumen or bitumen emulsion, performs better. Comparative testing is therefore recommended when performing a BSM mix design.

### *2.4.4 Binder content*

Although the binder content was not an experimental variable in this study, not all mixes were tested at the same binder content. The mixes with a higher percentage of RAP (*i.e.* 75 % in case of the high RAP mixes used in this study) were stabilised using a lower residual binder content (2.4% vs. 3.6% for the mixes with 25 % RAP). The binder content of the mixes with a high percentage of RAP was chosen lower because the existing bitumen present in the RAP. The binder contents adopted in this study were chosen arbitrarily in consultation with the sponsor of the research. It is believed that similar mix properties may be achieved with the lower binder content for mixes with a high percentage of RAP for reasons stated in Section 2.2.1.

As also mentioned in Section 2.2.1 the RAP aggregate in a BSM should be regarded as “black rock” and the existing bitumen in the RAP has little “binding” effect of its own.

In evaluating the results of the mixes with high and low percentages of RAP it needs to be kept in mind that the binder contents of these mixes differ. It is therefore difficult to conclude with confidence if the difference in performance is the effect of the percentage of RAP or the binder content.

The range of practical binder contents in BSM’s for application in CIPR is fairly limited. Minimum flow rates and particularly pumping pressures that need to be maintained in the recycling machine result in minimum application rates in the order of 1.5 % (lower application rates down to 1.0% have been achieved successfully in cases where the standard nozzles have been replaced with smaller nozzles in order to maintain sufficient pressure). It is particularly with thinner layers (100 – 150 mm) and low binder contents that the minimum application rate becomes critical. With bitumen emulsion the minimum application rate results in a minimum residual binder content in the order of 1.0 % (35 – 40 % of the application is emulsion water). For emulsions the application rate could be further reduced by using a diluted emulsion,

however, at such low residual binder contents the effect of the bitumen is more as compaction aid and improvement to moisture susceptibility then as stabilising agent.

At the upper application range of bitumen emulsion the amount of water in the mix plays a role. Depending on the in-situ moisture content, high application rates of bitumen emulsion may lead to BSM's after CIPR with over-optimum moisture contents. For foamed bitumen and otherwise also for bitumen emulsion, the upper limit of application rates is more based on economics. High residual binder contents are expensive and results in the use of BSM being less favourable from an economical perspective. Practically, binder contents in excess of 3 % are seldom used for BSM's in Southern Africa.

Within the practical binder content range of 1.5% - 3.0%, the following effects on material properties and behaviour as tested in this study is to be expected:

Table 11: Effect of increasing binder content on material properties

| Material property or behaviour | Effect |
|---|---|
| Cohesion | increase |
| Friction angle | decrease |
| Shear strength | variable |
| Stiffness | variable |
| Time-temperature dependency | increase |
| Permanent deformation resistance | variable |
| Strain-at-break | increase |
| Fatigue life | increase |

It can furthermore be expected that the durability of BSM's improves with increasing binder contents. This durability, which may exhibit itself *inter alia* in improved moisture susceptibility, improved resistance to erosion and reduced permeability, could be an important BSM property that currently receives little attention in the mix design.

### *2.4.5 Curing*

The curing protocol followed in this study is discussed in Chapter 4 and in more detail specified in Appendix D. Save for the step of changing after the first 24 hours the plastic bag used to seal the specimen, the curing procedure is identical to the one developed by Houston and Long (2004). It was found in this study that the reduction in the moisture content of the specimens in the last 24 hours of the curing process is very limited. It would therefore make little difference if the bag is changed after 24 of the 48 hours at 40ºC sealed in a plastic bag or not. The process of changing the bag after 24 hours is cumbersome and unpractical. This step could therefore be omitted, which effectively means that the protocol as developed by Houston and Long is recommended.

There is however a number of factors that are not taken into account in this recommend curing protocol or the protocol adopted in this study. These are:

- The effect of the relative humidity during curing;
- The type of oven used (ventilated *vs.* non-ventilated, this would have an effect on the first bulleted factor above);
- The stiffness development during curing.

It is postulated here that it is not as much the temperature, but more the relative humidity at time of curing that influences the rate of moisture reduction in the specimens. It is therefore proposed that this parameter is monitored (or specified) in combination with the curing temperature. Also, the draft of air over the specimens has a considerable effect on the evaporation rate of moisture out of the specimens. This aspect requires further attention.

Eventually it is the strength and stiffness of the laboratory specimens at time of testing that should be comparable to the strength and stiffness of the mix in the field. This strength and stiffness is influenced by the moisture content in the laboratory specimens as well as the curing time in case active fillers are used (*i.e.* cement or lime). This is along the lines of the proposal by Kekwick (2005). It would imply that the curing time could be variable and that the stiffness of the specimens needs to be monitored during curing. It would also require knowledge of the expected field stiffness of the BSM laboratory mix, which in itself is a challenge.

A final consideration with regard to curing is the type of curing term that is critical. This may be a short-term cure to simulate the BSM properties immediately after construction and opening to traffic and up to a week's time, a medium-term cure to simulate the properties up to a month after construction and a long-term cure to simulate the BSM properties at equilibrium moisture content (EMC). The time required in the field to achieve this EMC is variable and can in some cases last up to 18 months. The field strength and stiffness of the BSM continuously increases during this time.

The curing protocol adopted in this study aims to simulate a long-term cure to arrive at the EMC. Often short-term curing properties are not critical in practice. When, however, immediate opening to heavy traffic and high traffic volumes is required short-term curing properties may become critical and should be verified.

## 2.5 The advantages of Cold In-Place Recycling

### *2.5.1 Introduction*

The use of BSM's in Cold In-Place Recycling (CIPR) has become increasingly popular in Southern Africa since the early 1990's because it has distinct advantages over conventional construction methods using newly procured construction materials (Ebels *et al.*, 2005). These advantages of CIPR can be categorised as:

- Environmental;
- Economical; and
- Logistical.

Because the CIPR process recycles and improves the properties of existing materials, the need for new natural materials is reduced in comparison with conventional construction methods. This is an advantage in a time where natural resources are becoming scarcer and costlier to exploit. CIPR is thus a more sustainable construction method.

The exploitation of natural resources to obtain road building materials is regarded as a mining activity under the National Legislation. It therefore needs to comply with the new regulations that were promulgated under the new Minerals and Petroleum Resources Development Act during 2004. Applying CIPR technology instead of using new materials may reduce the requirements and the application process for authorisation of such mining activity. It may even not be necessary to undertake any mining activity at all on certain projects when CIPR technology is used.

Recently, July 2006, new regulations dealing with environmental management came into effect. These new regulations have a direct impact on the requirements for planning, design and execution of road infrastructure projects. These new regulations place more emphasis of identifying alternatives with a reduced environmental impact for the proposed activity. From this perspective, CIPR should provide an advantage over conventional construction methods because it is an environmentally friendlier method. The environmental advantages of CIPR discussed here are mainly discussed in light of the South African national environmental legislation.

Some of the economic aspects are demonstrated by means of a limited economical analysis on project that was out on tender in the Western Cape recently (2006) and which called for both ETB patching and CIPR. In this analysis a comparison is made between CIPR and ETB patching as alternative methods of base layer repair.

Many other economical advantages are also associated with the CIPR process but are believed to be outside the scope of this study to discuss them here. On that same note the logistical aspects are also not discussed here.

### *2.5.2 South African environmental legislation*

The South African legislation that deals with the environment is discussed comprehensively in Appendix B. Attention is given to this legislation here because of the fact that some of it is fairly new legislation and therefore relatively unknown by practitioners. The legislation also has a significant impact on the road building industry, and more specific the use of cold bituminous mixtures, as it promotes the use of more environmental-friendly techniques such as CIPR. It is therefore of utmost importance to the design engineer to have a sound knowledge of the legal framework of the environment he is operating in.

The following South African legislation that is of relevance to the use of BSM and CIPR in light of their environmental advantages is discussed in this study:

- The Constitution of the Republic of South Africa;

- The Environmental Conservation Act of 1989;
- The National Environmental Management (NEM) Act of 1998; and
- The Mineral and Petroleum Resources Development (MPRD) Act of 2002.

Regulations and Notices in terms of the NEM Act were recently promulgated (2006). Also the MPRD Act came into effect recently (2004). In order to be able to understand the legislative framework and context of the NEM Act and MPRD Act, relevant sections of the Constitution of the Republic of South Africa and the Environmental Conservation Act of 1989 are also discussed.

According to the South African Constitution everyone has the right to have the environment protected through reasonable legislative and other measures that, amongst others, secure ecologically sustainable development and use of natural resources. CIPR is a more sustainable construction method than using new natural materials to achieve the same technical objective. It saves scarce natural resources and reduces the impact on the environment. Using CIPR would thus be in accordance with the philosophy of the Constitution.

New regulations and notices dealing with environmental impact assessments (EIA) under the National Environmental Management Act of 1998 came into effect on 3 July 2006. With this, the Environment Conservation Act of 1989 is no longer of importance in terms of determining the environmental impacts of activities that may be detrimental to the environment. This role has completely been taken over by the National Environmental Management Act.

What is important in the new regulations is that a lot more emphasis has been placed on identifying and assessing alternatives. This is important for CIPR, because it is an alternative technology that can be used to meet the same general purpose as conventional construction methods. At the same time, the environmental impacts of CIPR are less than those of construction with new materials.

The Mineral and Petroleum Resources Development (MPRD) Act of 2002 came into effect on 1 May 2004. It replaces the Minerals Act of 1991. Quarries and borrow pits as commonly used for road building purposes also fall under the definition of a mining area in the MPRD Act. Removing material from quarries and borrow pits is therefore a mining activity. As such the person undertaking the activity needs to comply with the requirements of the MPRD Act. The act makes distinction between a mining permit and a mining right, depending on the scale of the activity. This distinction is important, because the application process for each have different requirements in terms of environmental assessment. The application process for a mining permit and more so for a mining right can be involved, costly and time consuming. It can therefore be a real advantage if one does not require new natural material for the rehabilitation of a road. This could be achieved by adopting the CIPR process.

### *2.5.3 Some economic considerations*

CIPR in South Africa is mainly used to produce a layer that functions as a base layer in the pavement structure. It is mainly the materials of the top part of the existing pavement structure that are recycled. It is an alternative construction method for removing the existing top part and replace it with new material using conventional construction methods. Alternatively a new base layer using new materials and conventional construction methods could be added on top of the existing pavement. An economic analysis comparing CIPR with these two possible alternatives is difficult because the costs of the alternatives are very dependent on site specific factors such as the proximity of the closest material source and the quality thereof. Also, the structural capacity and the design life of the pavement structure rehabilitated with CIPR and conventional construction methods are not necessarily the same. This makes it difficult to make a fair economic comparison of the different construction methods.

The economical analysis given in this section is limited to comparing ETB base patching with CIPR. To this end the rates recently tendered (2006) for a Western Cape provincial reseal / special maintenance contract have been used to compare the cost of base patching and CIPR using bitumen emulsion. The rates tendered by six different contractors, labelled A through to F, were used to determine an inclusive square metre price for patching and CIPR. The scheduled items in the Bill of Quantities that were used to determine the patching rate per square metre are:

- Sawing asphalt (40mm)
- Excavating asphalt (40mm) and crushed stone / gravel base (200mm)
- Compaction of floor excavation and backfilling with ETB (200mm)
- Stockpiling of excavated material
- Prime (0.6 l/m$^2$ diluted emulsion) and tack coat (0.5 l/m$^2$)
- Asphalt surfacing (40mm) in patches

The scheduled items in the Bill of Quantities that were used to determine the CIPR rate per square metre are:

- CIPR (240 mm = 40 mm asphalt + 200 mm base)
- Stabilising agents bitumen emulsion (3.0%) and cement (1.5%)
- Removing and stockpiling bulked material incl. overhaul (restricted + 1 km ordinary)
- Providing milling machine on site and transport it once on site over more than 1 km
- Prime (0.6 l/m$^2$ diluted emulsion) and tack coat (0.5 l/m$^2$)
- Asphalt overlay (40mm)

Preliminary and general items, traffic accommodation, *etc*. are not included in this comparison as they are deemed to be more or less the same for the two operations. There is however a difference in establishment costs of a CIPR team compared to a patching team and this mainly revolves around transportation costs of plant to site. The main items of plant required for the two operations are shown in Table 12. The difference in transportation cost of these items of plants is estimated at R 55.00 / km

(based on 2007 rates). This would mean that the difference in establishment costs of plant on a site 500 km away from the contractor's yard is approximately R 55,000. The difference in operational costs of the plant required once established on site is accounted for in the rates of the items of work as listed above and do not play a role in the establishment costs.

Table 12: Main items of plant required

| Equipment | CIPR | Patching |
|---|---|---|
| CIPR machine | ✓ | |
| Padfoot roller | ✓ | |
| Smooth drum roller | ✓ | |
| Pneumatic tired roller | ✓ | |
| Grader | ✓ | |
| Watercart 1 | ✓ | ✓ |
| Watercart 2 | ✓ | |
| Static tank for on-site emulsion storage | ✓ | ✓ |
| TLB | | ✓ |

The amount of patching the contractors priced for in this particular tender was approximately 1,000 $m^2$. The extent of the CIPR is approximately 73,000 $m^2$. (The total amount of patching is limited compared to the CIPR because the project analysed was already divided into sections with many failures where CIPR would be more economical and into sections with fewer failures where CIPR was not cost effective.) The small area of patching in comparison to CIPR may have led to higher rates tendered for the patching work items. This however would make the comparison of the economical advantage of CIPR more conservative. Table 13 shows the square metre rates (including all items as listed above). The rates are graphically compared in Figure 30.

Table 13: Patching and CIPR rates per square metre

| Contractor | A | B | C | D | E | F |
|---|---|---|---|---|---|---|
| Patching [R/$m^2$] | 389.23 | 457.26 | 394.91 | 174.21 | 285.26 | 334.06 |
| CIPR [R/$m^2$] | 124.24 | 124.87 | 138.61 | 146.58 | 148.35 | 139.44 |
| ratio CIPR : patching | 0.32 | 0.27 | 0.35 | 0.84 | 0.52 | 0.42 |

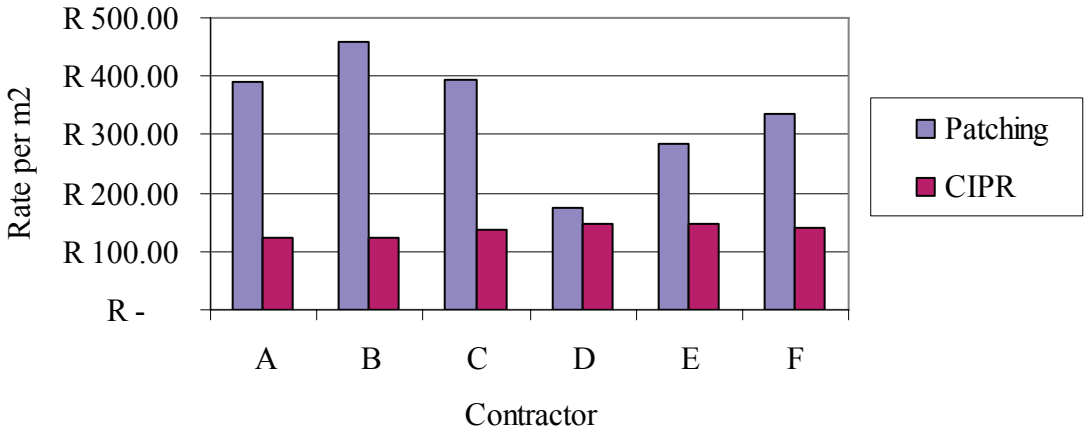


Figure 30: Graphical comparison of patching and CIPR rates

It can be seen that the price of patching varies considerably. Contract D has the lowest rate of R174.21/$m^2$. The highest rate is R457.26/$m^2$, tendered by Contractor B. The rate for CIPR is more constant and varies between R124.24/$m^2$ and R148.35/$m^2$. It can be seen that per square metre CIPR is much cheaper than base patching. The average difference between the square metre rates of CIPR and patching is R 202.14. When this is compared with the R 55,000.00 difference in establishment cost of the major plant items, it can be deduced that this difference in establishment costs is equal to an area of 272 $m^2$ to be patched. When the total size of a project is considerable, as in the example worked out here where the total area of CIPR is approximately 73,000 $m^2$, this difference in establishment cost may become insignificant.

One needs to take into account that patching can be carried out selectively on only those places that require base repair. The CIPR process is a more continuous process. It requires a certain length of road to be recycled in order for it to become effective. In this regard the ratio between the rates of CIPR and patching as given in Table 13 are of interest. This ratio indicates the break-even point in terms of cost. For example, if Contractor E is doing the work, CIPR is about half of the price of patching. Therefore, with the same amount of money, approximately twice a much recycling can be done than patching in terms of area. In other words, if the total area to be patched on a certain section of road exceeds 52% of the total area, it is cheaper to CIPR the entire section of road than to patch selectively (the figure of 52% of area applies to the example of Contractor E only). This would be the break even point in terms of cost.

It can be seen that the break-even point in terms of cost for the contractors as shown in Figure 30 varies between 27% and 84%. This is a wide range and it could be the result of different pricing strategies of the contractors that tendered. It needs to be said that Contractor D is a specialist maintenance contractor. This may be the reason for the low rate for patching, which skews the break-even point ratio. In general it can be concluded that break-even point in terms of cost varies between 30% and 50% (ratio rates CIPR : patching).

The advantage of CIPR is that not only the areas most in need of repair are attended to, but also the areas in between. A patching operation generally results in a more variable base quality along the length and over the width of the road. With CIPR, on the contrary, much less variability in terms of construction quality and base material after completion is obtained. A base layer that is less variable in quality and consists of more homogenous material has more value to the road owner. In addition, CIPR would result in a finished product that would typically have a longer design life than when localised base repair by means of patching is used. The break-even point in terms of value to the road authority therefore lies below the break-even point in terms of cost as discussed above. The difference in total cost is a premium that the road owner pays for less base quality variability and more material homogeneity. The amount of premium is difficult to quantify and would be project and authority specific. A graphical comparison between the total costs of patching and CIPR is given in Figure 31. The break-even point for cost is also indicated. The quality / consistency factor with the resulting premium for the road owner is conceptually drawn in Figure 31.

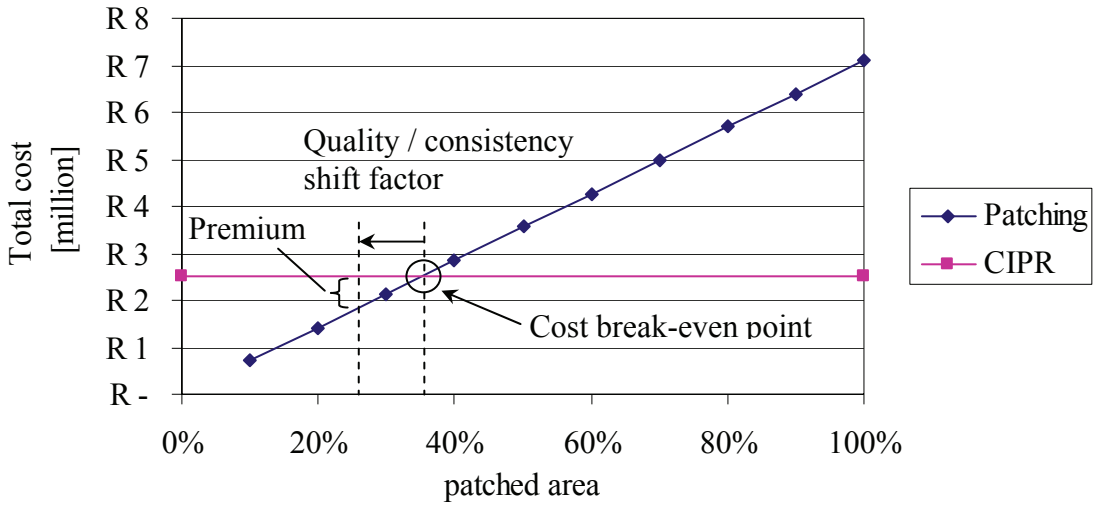


Figure 31: Total cost comparison patching and recycling Contractor C

Taking into account the shift for quality and consistency, the break-even point in terms of value to the road owner could vary from an area to be patched of 20% up to 40% of the total section of road being considered for repair. That means that if as little as 20% of a sizeable portion of road would require base repairs, CIPR of the whole portion could be a more cost-effective measure than patching the failed areas within that portion. When the area that requires base repair exceeds 40% of the total area, local base repair by means of patching should not be considered. In such cases CIPR should be the preferred and most economical measure.

The example worked out here is of a limited nature and based on one project only. Systematically building a database comparing project specific tendered rates for patching and CIPR would give more insight and make the economic comparison more reliable.

## References


Acott, S.M., *The Stabilisation of a Sand by Foamed Bitumen – A Laboratory and Field Performance Study*, Thesis for the degree of Master of Science in Engineering, University of Natal, South Africa, 1980

Ackeroyd F. M. L. and Hicks, B. J., *Foamed bitumen road recycling*, Highways, London, UK, January 1988

Akzo Nobel, *Bitumen Emulsion Plants – In-line Plants*, www.asphalt-akzonobel.com/equipment/bep/bep.htm, accessed 14 November 2006

Akzo Nobel, *Bitumen Emulsion*, Technical Bulletin, Akzo Nobel Asphalt Applications Stockholm, Sweden, 2000. Downloaded from: http://www.surface.akzonobel.com/asphalt_russian/publications/tb/tb.htm

Akzo Nobel, *Microemulsions*, Technical Bulletin 1, Akzo Nobel Surface Chemistry AB Stenungsund, Sweden, 2001

Akzo Nobel, *Product Overview Surfactants Europe*, Akzo Nobel Surface Chemistry AB, Stenungsund, Sweden, April 2005

Anderson, K. O., Haas, R. C. G. and La Plante, A. D., *Tri-axial Shear Strength Characteristics of some Sand-asphalt Mixtures*, Highway Research Record 91, Washington DC, USA, 1965

Asphalt Academy, *The design and use of foamed bitumen treated materials*. Interim Technical Guideline No. 2, Pretoria, South Africa, 2002.

Baumgardner, G. L., *Asphalt Emulsion Manufacturing Today and Tomorrow*, Asphalt Emulsion Technology, Transportation Research Circular E-C102, Transportation Research Board, Washington DC, USA, August 2006, pp. 16-25

Bondietti, M., Murphy, D., Jenkins, K. and Burger, R., *Research on the stabilisation of two different materials using bitumen emulsion and cement,* Proceedings of the 8th Conference on Asphalt Pavements for Southern Africa, Sun City, South Africa, 2004

Bowering, R. H. and Martin, C. L., Foamed bitumen – Production and Application of Mixtures – Evaluation and Performance of Pavement, Proceedings of Association of Asphalt Paving Technologists, Vol. 45, New Orleans, USA, 1976

British Standards, *Manual of Contract Documents for Highway Works*, Volume 1 Specification for Highway Works. Series 900 Road Pavements – Bituminous Bound Materials, 2004

Csanyi, L. H. and Fung, H. P., *Mortar Theory for Use of Ungraded Aggregates in Bituminous Mixes*, Bulletin No. 109, Highway Research Board, Washington D.C., USA, 1955

Csanyi, L. H., *Foamed Asphalt in Bituminous Paving Mixtures*, Bulletin No. 160, Vol. 10, Highway Research Board, Washington D.C., USA, 1957

Csanyi, L. H., *Foamed Asphalt*, Technical Bulletin Vol. 240, American Road Builders' Association, USA, 1959

CSIR – Council for Scientific and Industrial Research, *Foamed Asphalt Mixes – Mix Design Procedure*, Contract Report CR-98/077, SABITA and CSIR Transportek, Pretoria, South Africa, 1998

CSIR – Council for Scientific and Industrial Research, *Standard Methods of Testing Road Construction Materials*, Technical Methods for Highways No. 1, second edition, National Institute for Transport and Road Research, Pretoria, South Africa, 1986

CSRA – Committee of State Road Authorities, *Guidelines for road construction materials*, Technical Recommendations for Highways (TRH) 14, Department of Transport, Pretoria, South Africa, 1985

Department of Transport, *TRH 7: The use of bitumen emulsion in construction and maintenance of roads*. Pretoria, South Africa, 1972

Ebels, L. J., *Bitumen stabilised paving blocks*, MSc. Eng thesis Delft University of Technology, the Netherlands, 1998

Ebels, L. J., Lorio, R. and van der Merwe, C. J., *The importance of compaction from a historical perspective*, Proceedings of the 23rd South African Transport Conference, Pretoria, South Africa, 2004

Ebels, L. J., Jenkins, K. J. and Collings, D., *Cold mix (bitumen stabilisation) technology in Southern Africa into the 21st Century*, International Symposium on Pavement Recycling, São Paulo, Brazil, 2005

Ebels, L. J. and Jenkins, K. J., *Mix design of bitumen stabilised materials : Best practice and considerations for classification*, Proceedings of the 9th Conference on Asphalt Pavements for Southern Africa, Gaborone, Botswana, 2007

Erkens, S. M. J. G, *Asphalt Concrete Response (ACRe) – Determination, modelling and prediction*. PhD dissertation Delft University, the Netherlands, 2002

GPB – Groupement Professionel des Bitumes, *Évolutions et nouveaux defies (in French)*, Bitume Info No. 13, Groupement Professionel des Bitumes, Paris, France, September 2006

Houston, M. and Long, F., *Correlations between different ITS and UCS test protocols for foamed bitumen treated materials,* Proceedings of the 8th Conference on Asphalt Pavements for Southern Africa, Sun City, South Africa, 2004

IP Australia, Personal communication by the author with IP Australia, Canberra, Australia, 2006

James, A., *Overview of Asphalt Emulsions*, Asphalt Emulsion Technology, Transportation Research Circular E-C102, Transportation Research Board, Washington DC, USA, August 2006, pp. 1-15

Jenkins, K. J., *Mix design considerations for cold and half-warm bituminous mixes with emphasis on foamed bitumen*. PhD dissertation University of Stellenbosch, South Africa, 2000

Jenkins, K. J., Ebels, L. J. and Mathaniya E. T., *Updating Bituminous Stabilised Materials Guidelines: Mix Design Inception Study*, SABITA and Gauteng Department of Transport, Roads and Public Works. Pretoria, South Africa, 2006

Kekwick, S. V., *Best Practice: Bitumen-Emulsion and Foamed Bitumen Materials Laboratory Processing*. Proceedings 24th South African Transport Conference, Pretoria, 2005

Le Corroler, A., The Use of Bitumen Emulsion in Europe, www.eapa.org/START/positionprs_publications/papers/bitumen.htm, 2005

Lessueur, D. and Potti, J. J., *Cold-mix design: A rational approach based on the current understanding of the breaking of bituminous emulsions*, Paper 199 3rd Eurasphalt and Eurobitume Congress, Vienna, Austria, 2004

Liebenberg, J. J. E and Visser, A. T. *Towards a mechanistic structural design procedure for emulsion-treated base layers*. Journal of the South African Institution of Civil Engineering, Vol 46 (3), 2004, pages 2 – 8, paper 554.

Long, F. and Theyse, H., *Mechanistic-empirical structural design models for foamed and emulsified bitumen treated materials*, Proceedings of the 8th Conference on Asphalt Pavements for Southern Africa, Sun City, South Africa, 2004

Louw, K., *Comparison between stabilising agents – foam / bitumen emulsion*, slide show presentation for Society of Asphalt Technology Seminar, Cape Town South Africa, 26 August 2004

Louw, K., Personal communication, 2 November 2006

Louw, K., Spence, K. and Kuun, P., *The Use of Bitumen Emulsions as a Cost Effective Solution for Constructing Seals during Winter*, 8th Conference on Asphalt Pavements for Southern Africa (CAPSA), Sun City, South Africa, 2004

Malubila, S. M., *Curing of foamed bitumen mixes*. M.Eng thesis Stellenbosch University, South Africa, 2005

Mobil Oil Australia Ltd., *Method and Apparatus for Producing Foamed Materials*, Patent Specification 24, 857/71, Commonwealth of Australia, 1971

Moloto, P., *Curing of bitumen stabilised materials*, MSc. Eng thesis Stellenbosch University, South Africa, to be published 2008

Mom, G. P. A., *Inter-artifactual Technology Transfer: Road Building Technology in the Netherlands and the Competition between Brick, Macadam, Asphalt and Concrete*, History and Technology, Vol. 20 No.1, Taylor and Francis, Oxford, United Kingdom, March 2004, pp. 75-96

SABITA. *Manual 14: GEMS – The design and use of granular emulsion mixes*. Roggebaai, South Africa, 1993.

SABITA. *Manual 21: ETB – The design and use of emulsion-treated bases*. Roggebaai, South Africa, 1999

ScanRoad (now Akzo Nobel Surface Chemistry), *Bitumen Emulsions*, Technical Bulletin 2, May 1983

Shackel, B., Makiuchi, K. and Derbyshire, J. R., The Response of Foamed Bitumen Stabilised Soil to Repeated Triaxial Loading, paper No. A23, 7th ARRB Conference, Volume 7, Part 7, Australia, 1974

Semmelink, C.J., *Compaction, Course notes Road Infrastructure Course*, South Africa, 1988

Theyse, H. L.., De Beer, M. and Rust, F. C., *Overview of the South African Mechanistic Pavement Design Method*, Transportation Research Record No. 1539, Transportation Research Board, Washington DC, USA, 1996. pp 6 – 32

Theyse, H. L. and Muthen M, *Pavement analysis and design software (PADS) based on the South African Mechanistic-Empirical Design Method*. South African Transport Convention, Pretoria, South Africa, 2000

Twagira, M. E., Jenkins, K. J. and Ebels, L. J., *Characterisation of Fatigue Performance of Selected Cold Bituminous Mixes***.** Proceedings of the 10th International Conference on Asphalt Pavements. Quebec City, Canada, 2006.

VBW Asfalt, *Bitumenemulsie in de Wegenbouw (in Dutch)*, VBW Asfalt, Breukelen, the Netherlands, 2003

Voskuilen, J. L. M., Mangnus, S., van de Ven, M. F. C., van Wieringen, J. B. M. and Bolk H. J. N. A., *Experiences with half-warm foamed bitumen treatment process in the Netherlands*. Proceedings of the 8th Conference on Asphalt Pavements for Southern Africa, Sun City, South Africa, 2004

Wirtgen GmbH, 1st Wirtgen Recycling Days, PC Compact Disc, Windhagen, Germany, 2002

Wirtgen GmbH, *Laboratory-scale foamed bitumen plant WLB10*, Information brochure No. 54-12 EN-06/01, Windhagen, Germany, 2001

Wirtgen GmbH, *Cold Recycling Manual*, 2nd edition published by Wirtgen GmbH, Windhagen, Germany, 2004

Wirtgen GmbH, *Our Company's History*, www.wirtgen.com/en/ewgmbh/ehist.html, last accessed 14 December 2006

# 3 MATERIAL PROPERTIES AND BEHAVIOURAL MODELS

## 3.1 Introduction

For the understanding of a material it is necessary to have some knowledge of the intrinsic properties of such. These properties can both be physical, *e.g.* density and coefficient of thermal expansion, as well as mechanical, *e.g.* behaviour of material when subjected to loading. This study mainly focuses on the latter.

Material can be categorised according to comparable structure and properties, but also based on functionality. Five main groups can be distinguished when categorising based on structure and properties (Askeland and Phulé, 2006):

1. Metals and alloys;
2. Ceramics and glasses;
3. Polymers;
4. Semiconductors; and
5. Composite materials.

In terms of functional aspects, the following categories can be used (Askeland and Phulé, 2006):

1. Mechanical (including functional and structural);
2. Biological;
3. Electrical;
4. Magnetic; and
5. Optical

The Bitumen Stabilised Materials (BSM's) studied here are composite materials that fulfil a structural function. In the case of road building materials general mechanical requirements to ensure a comfortable and safe ride for the road user include longitudinal and transverse eveness and no or limited permanent deformation. BSM's used in the pavement structure should also comply with these requirements. Other functional aspects that are of importance to materials that are used in the surfacing layer of road pavements, *i.e.* skid resistance and noise generation, do not apply to BSM's, because BSM's as discussed in this study are generally used in base layer applications. The main composites are aggregate, an inorganic crystalline material, and bitumen, an organic material. These two components are also composites themselves. The aggregate used here is a blend of different types of rock, active filler (cement) and recycled asphalt pavement (RAP) material. The bitumen is a complex chemical mixture of molecules of a predominantly hydrocarbon nature (Shell, 1990) and contains both solid and oily medium.

The mechanical properties of a material include, but are not limited to, strength, modulus of elasticity, elasticity, plasticity and elongation. These properties can be determined in a direct tension test (ASTM E8 in case of steel), but also by means of a compression test. It is common in pavement engineering to determine the material properties in a compression test. The direct tension test is nevertheless discussed here, because the ideology is similar to the compression test and the direct tension test is more frequently used to illustrate the material properties in the field of mechanics of materials.

The definitions of the fundamental term "stress", as most commonly used in mechanics of materials, and an introduction to normal stress and shear stress are included in Appendix C. The discussion in this appendix focuses on normal and shear stress and principal stresses and planes. Methods and formulas to derive the stress diagram and the Mohr diagram are also provided.

Discussion of the engineering stress-strain diagram, and the properties that can be derived from it, is included in the first section of this chapter, while the chapter ends with the discussion of a number of material properties and behaviour that are of specific interest for BSM's. These include:

- Shear properties;
- Resilient modulus;
- Permanent deformation behaviour;
- Strain-at-break;
- Flexural stiffness; and
- Fatigue behaviour.

Compressive and tensile strength properties are covered elsewhere, *i.e.* these material properties are not a focal point of this study. For each of the above properties or characteristic behaviour a review of the available models to describe the respective properties or behaviour is provided. Some of these models will be used in the subsequent chapters of this study to analyse and describe the experimental data from tests carried out on the BSM's that are subject of this study.

## 3.2 Material engineering properties

As mentioned in the introduction to this chapter, the most commonly used mechanical properties are derived from a standard tension test. This test is a displacement controlled test whereby a specimen is forced to gradually deform with a constant rate of displacement. The force required to impose this displacement is measured. By dividing with the loading area this force can be converted into a stress.

The stress is calculated using the original cross-sectional area of the unstressed specimen. During a tension or compression tests necking and barrelling respectively occurs which influences the cross-sectional area of the test specimen. The stress calculated using the original cross-sectional area at the beginning of a test differs

therefore from the "true stress" in the specimen as the specimen deforms. It is however difficult to approximate this "true stress" as it would require sophisticated measurements of the change in cross-sectional area as the test progresses. For all practical purposes the original cross-sectional area is therefore used and the stress derived in this manner is called the "engineering stress".

The strain can be derived from the incremental increase in length of the specimen as ratio per unit length. When the values of the stress versus the corresponding strain are plotted against each other a stress-strain diagram is obtained. A typical example of such a stress-strain diagram for a tension test is shown in Figure 32. Although steel is not a common road building material, it is used here because it is a good example to define the several limits and strengths that can be derived from a stress-strain diagram.

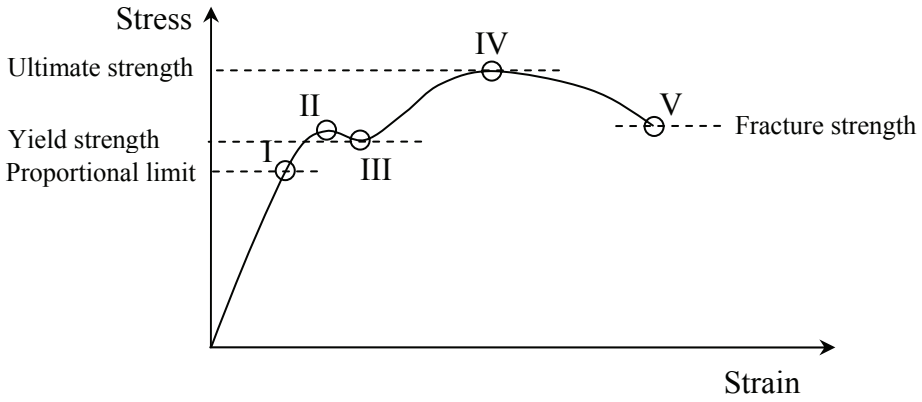


Figure 32: Typical tension stress-strain diagram of steel

A number of points of interest can be identified on the stress-strain curve. These are indicated with the Roman symbols in Figure 32. The stress and strain are proportional up to Point I, which is at the end of the first straight-line part of the curve. The stress corresponding with Point I is also called the proportional limit.

In order to determine the elastic limit, a specimen would need to be subjected to a large number of loading cycles with small increments in the loading magnitude. After every unloading cycle it then needs to be checked whether all strain has been recovered until such time that a plastic strain (permanent) starts to develop. The elastic limit is defined as the lowest stress at which plastic strain starts to develop. For many materials the elastic limit is approximately equal to the proportional limit, with only the latter being determined for practical reasons.

After Point I the strain starts to increase more rapidly than the stress until at Point II the strain increases while there is no further increase in stress. This point is called the yield point. A yield point is defined as a stress, short of the ultimate stress, at which the material undergoes a marked increase in strain, without any significant increase in stress. Point III is therefore also a yield point. Points II and III are referred to as upper and lower yield point respectively. The position of the upper yield point

depends on the speed of testing, the shape of the section and the form of the specimen. The lower yield strength is usually considered to be a true characteristic of the material and is referred to simply as the yield strength (Park and Paulay, 1975)

When, as shown in Figure 32, a material is stressed beyond its yield point, strain-hardening takes place. Hereby the stress increases again with the strain until the ultimate strength is reached at Point IV. This is the highest stress that the material can withstand. In case of a tensile test the tensile strength is defined as the ultimate strength.

When deformation is continued beyond the ultimate strength, the stress at the corresponding strain will decrease until, in case of a tensile test, the specimen breaks. This is indicated by Point V. The fracture strength of a material subjected to tensile is defined as the stress at which fracture occurs (ordinate of Point V).

The stress-strain diagram shown in Figure 32 is a typical diagram of a tension test (*e.g.* steel). A similar stress-strain diagram can be derived from a compression test. Materials such a concrete are often subjected to compressive tests. A typical example of a stress-strain diagram of a compressive test on concrete is shown in Figure 33.

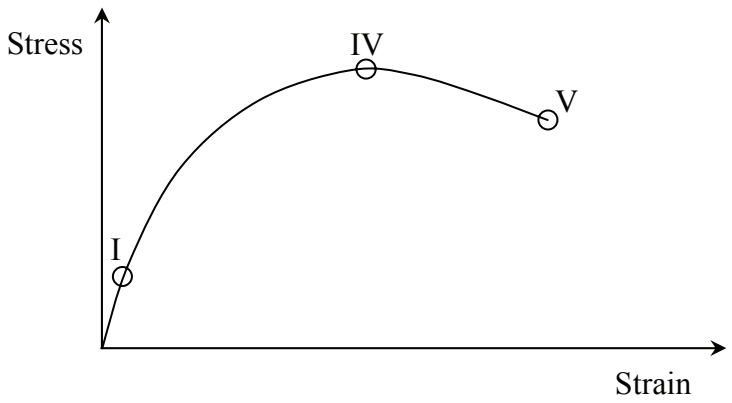


Figure 33: Typical compressive stress-strain diagram of concrete

The first linear part of the stress-strain curve is shorter and the proportional limit less clearly identifiable compared to the tensile stress-strain diagram. Furthermore, a yield point is not present. The maximum compressive strength is equal to the ultimate strength as defined by Point IV.

Road building materials such as asphalt concrete, stabilised materials and also compacted granular materials are often subjected to compressive testing and not to direct tension tests. In such cases similar behaviour as shown in Figure 33 can be expected.

Standard material characteristics of interest that can be derived from a stress-strain diagram include:

- Modulus of Elasticity or Young's Modulus;
- Yield and Ultimate Strength;

- Elastic vs. plastic behaviour;
- Ductile vs. brittle behaviour.

The Modulus of Elasticity, also known as Young's Modulus, is the ratio between stress and strain and is equal to the slope of the first straight line part of the stress-strain curve. It is therefore equal to the slope of the line from the origin of the stress-strain diagram through Point I. The Modulus of Elasticity is a measure of the stiffness of the material.

The Yield Strength has a significant meaning for engineering purposes. Yielding material may be deemed as failing because strains may increase significantly without any significant further increase in stress. The yield strength of a material is therefore often used for design purposes. However, this mostly applies to materials subjected to tensile stresses. A yield point does not occur in materials subjected to compression (see Figure 33). In this case the ultimate strength or maximum compressive stress is of most importance and used for design purposes.

The term "elasticity" as used in Modulus of Elasticity can be confusing. Elasticity refers to the ability of a material to deform when loaded and to return to its original shape when unloaded. Materials with a relatively low stiffness (low Modulus of Elasticity) can still exhibit a high degree of elasticity. Plasticity, on the other hand, is the ability of a material to deform when loaded and to retain this deformation when unloaded.

Elastic deformation takes place approximately up to the proportional limit. Thereafter plastic deformation occurs. The degree of elasticity or plasticity of a material can be judged from the shape of the stress-strain curve.

There is a difference between plastic and viscous deformation. In order for plastic deformation to occur, the proportional limit needs to be exceeded first. Deformation in viscous material occurs regardless of how small the load is. Viscous behaviour is time- and temperature-dependent. Plastic deformation is irreversible and so is pure viscous deformation. Delayed viscous deformation, however, is reversible and a certain relaxation time applies (visco-elastic material).

Ductility is the ability of a material to deform plastically prior to fracture under tensile stress. Malleability is the ability of a material to deform plastically prior to fracture under compressive stress. Materials that behave ductile under tensile stress often also behave malleable under compressive stress. Brittleness is the absence of ductility and malleability (Arges and Palmer, 1963).

There is no distinct boundary between ductile and brittle behaviour. The terms are relative and some degree of engineering judgement is required. Ductility or brittleness gives information on how failure is reached. Ductile behaviour implies that extensive plastic deformation takes place before failure occurs. The extent of the failure (or micro-fracture) increases progressively as the deformation or loading increases. Brittle behaviour, on the other hand shows relatively little plastic deformation before failure. When behaving brittle, failure (or cracking) propagates

rapidly without significant increase in deformation or loading. There is no "warning" that failure is imminent. Examples of ductile and brittle behaviour are given in Figure 34. It can be seen that the area under the stress-strain curve (dissipated energy) is much higher in the case of ductile curve compared to the brittle curve. The amount of dissipated energy is a measure for the toughness of the material.

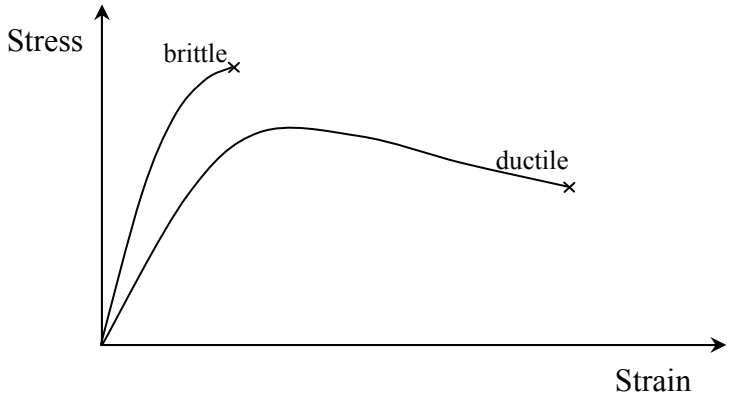


Figure 34: Typical examples of ductile vs. brittle behaviour

## 3.3 Models for material properties and characteristic behaviour

### *3.3.1 Shear parameters*

The shear parameters of a material, *i.e.* cohesion $C$ and angle of internal friction $\varphi$, can be determined in a monotonic tri-axial test. A monotonic tri-axial test consists of a series of failure tests on comparable specimens, but over a range of different confinement pressures ($\sigma_3$). For each test a plot of the load development (required force) versus the induced displacement is made. The applied failure load is defined as the maximum applied load. This failure load is converted to applied failure stress ($\sigma_{a,f}$) by dividing by the cross-sectional area of the specimen. This stress would be the ultimate strength as defined in Section3.2. The major principal stress ($\sigma_1$) is defined as the applied failure stress plus the confinement pressure and the stress as a result of the dead weight of the top loading plate and piston ($\sigma_{dw}$):

$$\sigma_1 = \sigma_{a,f} + \sigma_3 + \sigma_{dw} \qquad \text{Eq. 3}$$

The relation between the major principal stress at failure ($\sigma_{1,f}$) and the confinement stress ($\sigma_3$) is described by:

$$\sigma_{1,f} = A \cdot \sigma_3 + B \qquad \text{Eq. 4}$$

where

$$A = \frac{1+\sin\varphi}{1-\sin\varphi}, \quad B = \frac{2 \cdot C \cdot \cos\varphi}{1-\sin\varphi} \qquad \text{Eq. 5}$$

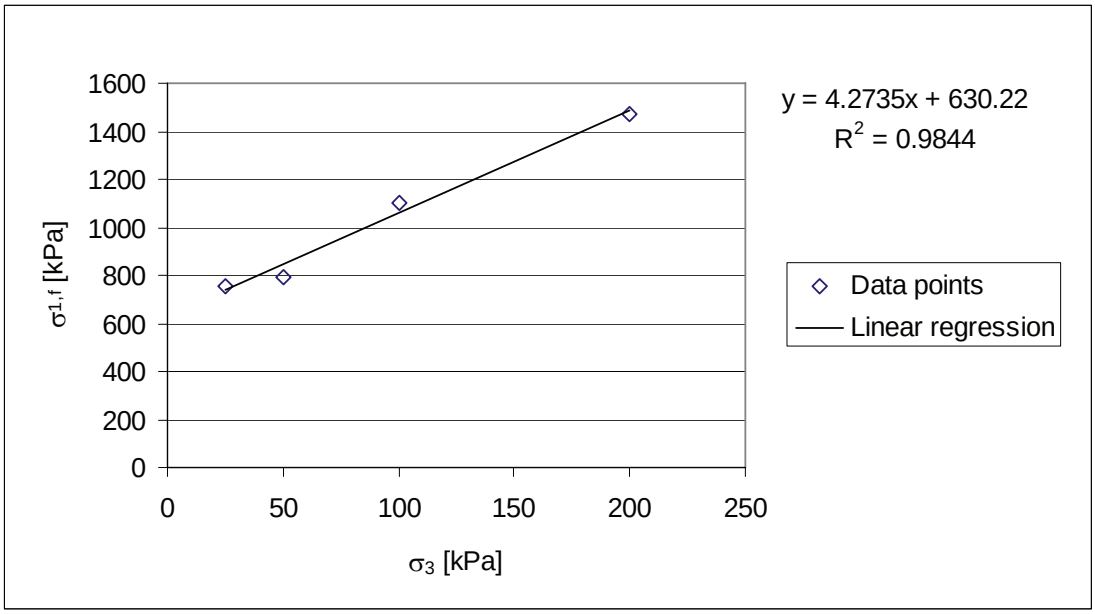


Figure 35: Example of relationship between the major principal stress at failure ($\sigma_{1,f}$) and the confinement stress ($\sigma_3$), mix A-75C-0

Linear regression analysis of the measurement data (array of [$\sigma_{1,f}$ , $\sigma_3$]) results in values for the factors A and B and subsequently solutions for the cohesion ($C$) and the angle of internal friction ($\varphi$).

Coulomb's failure criterion for shear is shown in Equation 6. In the Mohr diagram this represents a straight line that envelopes the Mohr circles. This is shown in Figure 36. In this diagram the cohesion $C$ is the value at which the failure line intersects the ordinate, while $\varphi$ indicates the slope of the failure line. The combination of the Mohr circles and Coulomb's failure line in a stress diagram is commonly referred to a Mohr-Coulomb diagram.

$$\tau_{\max} = \varphi \cdot \sigma + C \qquad \text{Eq. 6}$$

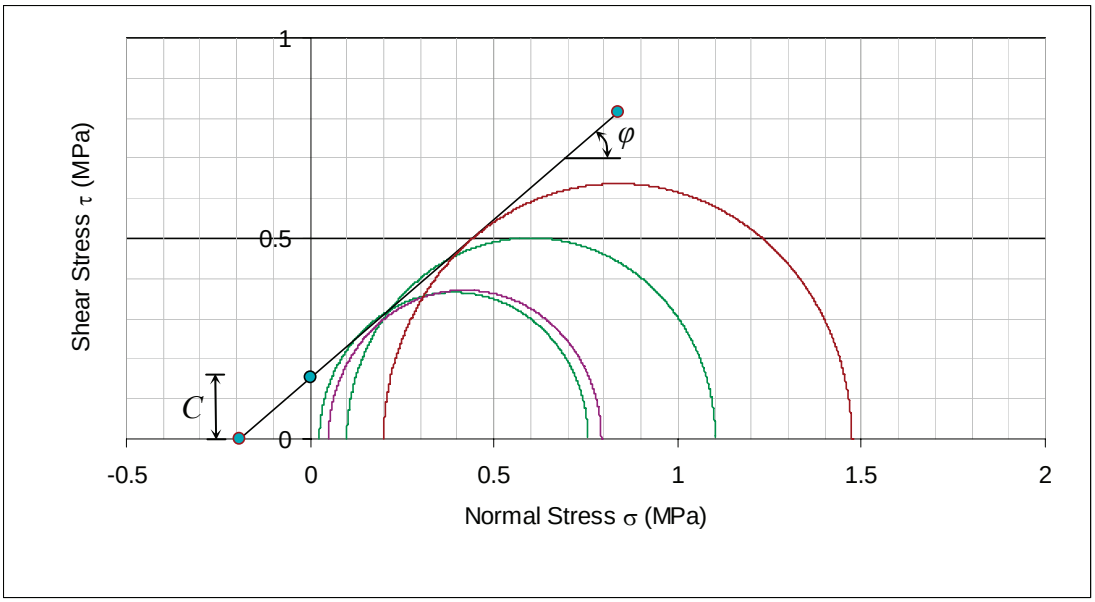


Figure 36: Example of Coulomb's failure criterion enveloping the Mohr circles, mix A-75C-0

As shown above, in the determination of the shear parameters, *i.e.* cohesion and friction angle, only the maximum stress at failure ($\sigma_{max}$) for a given confining stress ($\sigma_3$) is taken into consideration. Other information that can possibly be extracted from the monotonic tri-axial test is often ignored.

This possible other information from the engineering stress-strain diagram could include tangent and secant moduli and strain-at-failure. These parameters will also be explored in this study. The tangent modulus ($E_{tan}$) is defined here as slope of the tangent at the linear part of the stress-strain diagram or where the steepest slope occurs. The tangent modulus is approximately similar to the Modulus of Elasticity as defined in Section 3.2.

The secant modulus ($E_{sec}$) is defined here as the slope of the line drawn from the origin of the stress-strain diagram to the point on the curve where the maximum stress occurs. In this study the applied stress ($\sigma_a$) will be used in the determination of the secant modulus and not the major principal stress ($\sigma_a + \sigma_3$). The strain-at-failure ($\varepsilon_f$) is defined here as the strain at which the maximum stress occurs. The respective parameters are shown in the schematic stress-strain diagram in Figure 37.

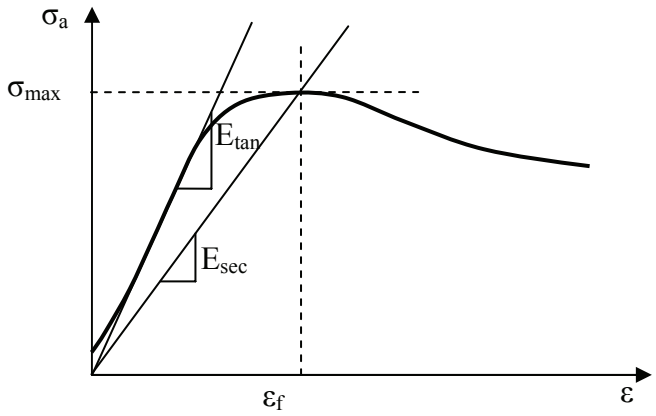


Figure 37: Stress-strain diagram defining tangent and secant modulus, maximum stress and strain-at-failure

### *3.3.2 Resilient modulus*

From research carried out during the 1960's, Hicks and Monismith (1971) summarised that the resilient response of granular materials under short-duration dynamic loading is significantly influenced by:

- Stress levels (confining pressures);
- Degree of saturation;
- Dry density;
- Fines content (percentage passing 0.075mm sieve); and
- Aggregate properties (density, type, particle angularity, particle texture)

Hicks and Monismith (1971) concluded that the resilient response of untreated granular materials is most significantly affected by the stress level and can therefore be related to the confining pressure, $\sigma_3$, or to the bulk stress, $\theta = \sigma_1 + \sigma_2 + \sigma_3$, as follows, for as long as shear failure does not occur:

$$M_r = k_1 \sigma_3^{k_2} \qquad \text{Eq. 7}$$

or

$$M_r = k_3 \theta^{k_4} \qquad \text{Eq. 8}$$

where $M_r$ = Resilient modulus [MPa]
$\sigma_3$ = Confinement pressure [kPa]
$\theta$ = Bulk stress = $\sigma_1 + \sigma_2 + \sigma_3$ [kPa]
$k_1$, $k_3$ = model coefficients [MPa]
$k_2$, $k_4$ = model coefficients [-]

The model shown in Equation 7 is used model for fine-grained soils, while the the model as shown in Equation 8 has been widely accepted to describe the stress-

dependent behaviour of a granular material, amongst others for its simplicity. The latter is often referred to as the $M_r$-$\theta$ model. On a log-log scale this model represents a linear function, whereby the $k_1$-value is a measure of the intersection with the y-axis, while the $k_2$-value indicates the slope of the line. The $M_r$-$\theta$ model as shown in Equation 8 will be used for analysis of the resilient modulus test results in this study.

It is however not uncommon for a material to exhibit the following phenomena concurrently:

- An increase in resilient modulus (stiffening) with increasing confinement ($\sigma_3$) at a constant deviator stress ($\sigma_d$); and
- A decrease in resilient modulus (softening) with increasing deviator stress ($\sigma_d$) at a constant confinement ($\sigma_3$).

Both abovementioned changes in the stress conditions result in an increase of the bulk stress $\theta$. The $M_r$-$\theta$ model can describe overall stiffening (positive $k_4$-value) or overall softening (negative $k_4$-value), but not stiffening due to increase in $\sigma_3$ and softening due to increase in $\sigma_d$ at the same time. Also, the $M_r$-$\theta$ model predicts an ever-increasing stiffness with increasing levels of bulk stress. The $M_r$-$\theta$ model is therefore fundamentally incorrect. It is however capable of accurately describing the stress-dependent behaviour of certain materials under certain stress conditions.

May and Witczak (1981) found that the shear modulus of a granular material is not only dependent on the stress state but also on the level of shear strain. When the shear modulus is substituted for the resilient modulus using Poisson's ratio, a similar dependency exists for the resilient modulus. This effect is neglected in Equations 7 and 8. Uzan (1985) concluded that these equations are therefore only valid in the range of low strain values and suggested the following extensions:

$$M_r = k_1 \sigma_3^{k_2} \varepsilon_a^{k_5} \qquad \text{for} \qquad \varepsilon_a > 10^{-5} \qquad \text{Eq. 9}$$

or

$$M_r = k_1 \sigma_3^{k_2} \sigma_d^{k_6} \qquad \text{for} \qquad \sigma_d > 0.1\sigma_3 \qquad \text{Eq. 10}$$

where $\varepsilon_a$ = axial strain [-]
$\sigma_d$ = deviator stress ($\sigma_1 - \sigma_3$) [kPa]
$k_5$, $k_6$ = model coefficients [-]
*other symbols same as Equation 8*

Uzan (1985) concluded that Equation 10 appeared to be in good agreement with all aspects of granular material behaviour. Uzan *et al.* (1992) added that Equation 10 is valid for both granular and fine-grained materials. It is therefore also referred to as "the universal model". As the material changes from granular to fine-grained, the $k_2$-value approaches zero, the model degenerates into the model shown in Equation 7.

Whereas the $M_r$-$\theta$ model cannot describe stiffening due to increase in $\sigma_3$ and softening due to increase in $\sigma_d$ at the same time, the universal model (Equation 17) is capable of concurrently describing the opposite effects the confinement stress and deviator stress may have on the resilient modulus. The universal model is therefore physically more correct than the $M_r$-$\theta$ model.

It is however also common for granular materials to show stress-stiffening with increasing deviator stresses at a constant confinement pressure until a maximum stiffness is reached at a certain deviator stress. An increase in load levels beyond this deviator stress results in stress softening again. The universal model is not capable of, at a constant confinement stress, describing such initial stress-stiffening up until a certain deviator stress level and subsequent stress-softening beyond this deviator stress level.

In order to be able to describe both stress-stiffening and stress-softening at a constant confinement stress, van Niekerk (2002) adjusted the power-law relation between the resilient modulus and the deviator stress, as shown in Equation 10, to a parabolic relation as follows:

$$M_r = k_1 \sigma_3^{k_2} \cdot \left(k_7 (S.R.)^2 + k_8 (S.R.) + k_9\right) \qquad \text{Eq. 11}$$

where
$S.R.$ = stress ratio ($\sigma_d/\sigma_{d,f}$) [-]
$\sigma_{d,f}$ = deviator stress at failure [kPa]
$k_7$, $k_8$, $k_9$ = model coefficient [-]
*other symbols same as in Equations 8 and 10*

A negative value of the $k_7$-coefficient would result in a parabola with a local maximum, which is capable of describing initial stress stiffening and subsequent stress softening. The opposite, a positive value of the $k_7$-coefficient, would result in a parabola with a local minimum, i.e. initial stress softening and subsequent stress stiffening.

One has to be careful when predicting resilient modulus values outside the experimental range of deviator stress values. Unrealistic resilient modulus values may be predicted if the quadratic part of the parabola ($k_7(S.R.)^2$) becomes dominant and a small increase in deviator stress may result in a large increase or decrease in the resilient modulus. This is illustrated by an example shown in Figure 38.

The experimental data in Figure 38 shows stress softening with increasing deviator stress levels. When the parabolic model is fitted to the data a good fit is obtained, but unrealistic resilient modulus values are predicted for deviator stresses outside the experimental range.

Various researchers, amongst others Jenkins (2000) and van Niekerk (2002) have shown that the resilient modulus models developed for granular material can also be used to describe the stress-dependency of stabilised granular materials.

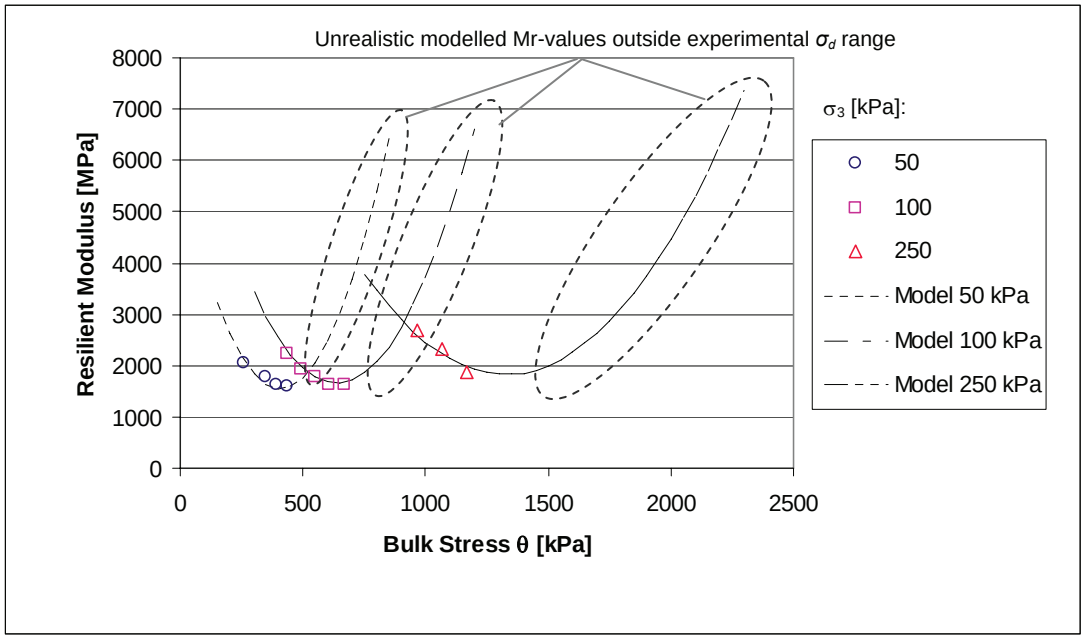


Figure 38: Measured resilient modulus of a foamed bitumen stabilised material with fitted the parabolic model of Equation 11 (Jenkins and Ebels, 2004)

### *3.3.3 Permanent deformation*

3.3.3.1 Historic developments

During the AASHO Road Test in Ottawa, Illinois, which was carried out from 1956 through to 1961, the question arose how to simulate the behaviour of the crushed stone and gravel bases in the laboratory. In 1960 a laboratory test program was devised in which the base materials from the AASHO Road Tests were subjected to repeated load tri-axial testing (Haynes and Yoder, 1962). This is one of the earlier references to the permanent deformation tri-axial test. During their experiments the relative compaction of the approximately 100 mm diameter (4 in.) specimens was kept constant and the moisture contents of the specimens were varied. Haynes and Yoder found that the permanent deformation increases with increasing levels of saturation. The tests were continued to 100,000 load repetitions or 25 mm permanent deformation, whichever came first. A rest period was included in the loading cycle. The absolute permanent deformation results were plotted against the number of load cycles on a log-normal scale. The permanent axial deformation was not analysed in terms of strain. Also, the permanent deformation behaviour was not modelled.

In 1972 Barksdale reported that up until that stage very few studies had been made of unstabilised base course material using the repeated load tri-axial test. Barksdale tested a variety of base materials including sand, crushed stone and soil-aggregate mixtures. The specimens tested were approximately 150 mm in diameter and 300 mm high (6 in. and 12 in. respectively), expect for the sand specimens, which were smaller in size. The triangular load pulse had a duration of 0.1 sec followed by a 1.9 sec rest period. The permanent deformation tests were continued up to 100,000 load

repetitions. The cumulative plastic strain was plotted against the number of load repetitions on a log-normal scale.

Barksdale (1972) analysed the permanent deformation behaviour in relation to the applied deviator stress. He identified a stable secondary phase for lower applied stress levels and the existence of a flow point and a tertiary flow phase as the deviator stress increases beyond a critical value.

During the 1970's the Belgian Road Research Centre carried out work in the field of permanent deformation of hot-mix asphalt mixes using the repeated load tri-axial test. The primary goal of this study was to develop a general deformation law that takes account of the physical conditions characterising the permanent deformation test. The HMA specimens were 320 mm high and approximately 159 mm in diameter. The applied deviator stress levels, loading frequency, temperature and constant confinement pressure were all varied during the study (Francken, 1977).

Francken (1977) plotted the permanent axial strain against the loading time on a log-log scale and found that the permanent deformation behaviour of HMA mixes could be adequately described by a loading time dependent creep curve as follows:

$$\varepsilon_p(t) = A \cdot t^B + C \cdot \left(e^{D \cdot t} - 1\right) \qquad \text{Eq. 12}$$

where $\varepsilon_p(t)$ = permanent deformation (axial strain)
$t$ = loading time
$A, B, C, D$ = model parameters

In the above Francken model the permanent deformation can be related to the number of applied load cycles by substituting the loading time variable with the number of applied load cycles taking account of the loading frequency.

$$N = \frac{\omega t}{2\pi} \qquad \text{Eq. 13}$$

$$\sigma_v = \sigma_0 + \sigma_1 \sin \omega t \qquad \text{Eq. 14}$$

where N = number of applied load cycles
$\omega$ = angular frequency [rad.]
$\sigma_v$ = applied vertical stress
$\sigma_0$ = static component of vertical stress
$\sigma_1$ = amplitude (dynamic component) of vertical stress

As did Barksdale (1972), Francken (1977) identified threshold stress combinations ($[\sigma_v , \sigma_3]$) below which the creep curve is nearly linear and the relationship between permanent axial strain and loading time is reduced to (coefficient C = 0):

$$\varepsilon_p(t) = A \cdot t^B \qquad \text{Eq. 15}$$

When the stress ([$\sigma_v$ , $\sigma_3$]) exceeds certain limits the rate of strain ($d\varepsilon/dt$ or $d\varepsilon/dN$) increases in the final part of the test. The second term in Equation 12 appears in this case ($C \neq 0$). The exponential shape is characteristic of an irrecoverable failure of the material in the tertiary flow phase.

Huurman (1997) researched the development of permanent strain in typical Dutch sands (eight different types) and granular base course material (four different types) used in concrete block pavements using the repeated load tri-axial test. Huurman used two different specimen sizes, *i.e.* 200 mm high, 101.6 mm in diameter and 800 mm high, 400 mm in diameter. The permanent deformation tests were continued up to 1,000,000 load repetitions or 10% permanent axial strain, whichever came first. The loading was applied in the form of a half-sine shaped wave with a frequency of 1 Hz (0.5 sec load pulse, 0.5 sec rest period). Only the applied deviator stress levels were varied (four different levels) during the permanent deformation study.

Huurman found that the reduced Francken model ($C = 0$) for permanent deformation of HMA mixes also applies to the permanent deformation behaviour of sand. When analysing the behaviour of granular base course materials, it was found that for certain applied stress conditions $C \neq 0$ and that tertiary flow occurs. Huurman substituted however the loading time in Equation 12 with the number of applied load cycles as described above, following which Equation 12 can be re-written as:

$$\varepsilon_p = A \cdot \left( \frac{N}{1000} \right)^B + C \cdot \left( e^{D \cdot \frac{N}{1000}} - 1 \right) \qquad \text{Eq. 16}$$

Huurman (1997) stated that the model parameters A, B, C and D are a function of the applied stresses and that this stress dependency can be described by:

$$A = a_1 \cdot \left( \frac{\sigma_1}{\sigma_{1,f}} \right)^{a_2} \quad ; \quad B = b_1 \cdot \left( \frac{\sigma_1}{\sigma_{1,f}} \right)^{b_2}$$

$$C = c_1 \cdot \left( \frac{\sigma_1}{\sigma_{1,f}} \right)^{c_2} \quad \text{and} \quad D = d_1 \cdot \left( \frac{\sigma_1}{\sigma_{1,f}} \right)^{d_2} \qquad \text{Eq. 17}$$

where $\sigma_1$ = major principal stress
$\sigma_{1,f}$ = major principal stress at failure
$a_1, a_2, \ldots, d_2$ = model coefficients

The model coefficients $a_1, a_2, \ldots, d_2$ as determined by Huurman can be used in the prediction of permanent strain in a pavement structure modelled using finite element methods. Huurman developed a rutting performance model to this extent.

The fundamental mechanical behaviour of unbound and lightly bound base and sub-base materials (mixed granulate) as commonly used in the Netherlands was further investigated by van Niekerk (2002). The repeated load tri-axial test was used to investigate the behaviour of the mix granulate in a very similar fashion as Huurman (1997) did. The specimens tested by van Niekerk were 600 mm high and 300 mm in diameter. Each type of mix material was tested at four different applied stress levels, all with a constant confinement pressure of 12 kPa. The tests were continued to 1,000,000 load repetitions or 10% permanent axial strain, whichever came first. The continuous haversine load (no rest period) was applied at 5 Hz.

Van Niekerk used a similar model to describe the permanent deformation as Huurman (1997) did, save for the fact he replaced the principal stress ratio ($\sigma_1/\sigma_{1,f}$) as used in Equation 17 with a deviator stress ratio ($\sigma_d/\sigma_{d,f}$). The advantage hereof is that the deviator stress ratio is not influenced by the confinement pressure levels, while the principal stress ratio is. At decreasing friction angles $\varphi$, this difference becomes more evident (Jenkins, 2000). A material subjected to two different stress levels can have a significantly different principal stress ratio, but relatively to it shear capacity be in a similar stress state. In such a scenario the deviator stress ratio of the two different stress levels would be the same.

During his research, Van Niekerk tested the permanent deformation behaviour of mixed granulate whereby he varied the grading and relative density of the specimens. A limited investigation was also performed on a mix granulate that was hydraulically bound with 10% blast furnace slag. For these mixes he determined the model coefficients $a_1$, $a_2$, ..., $d_2$ as used in Equation 17. Van Niekerk (2002) showed that these model coefficients can be used in the prediction of rutting in a pavement structure analysed with a finite element program.

In his study of foamed bitumen stabilised material Jenkins (2000) also investigated the permanent deformation behaviour using the repeated load tri-axial test. Jenkins tested both approximately 250 mm high, 150 mm diameter specimen as well as 600 mm high, 300 mm diameter specimens. The latter were tested in the same set-up and under the same conditions as described for the work done by Van Niekerk (2002). The smaller specimens were loaded with a haversine wave (no rest period) with a frequency of 2 Hz and a constant confinement pressure of 50 kPa. The tests were continued to 1,000,000 load repetitions or 4% permanent axial strain (10% in case of the larger specimens).

Jenkins (2000) determined the model coefficients $a_1$, $a_2$, ..., $d_2$ as used in Equation 17. He showed that these model coefficients can be used in the prediction of rutting in a pavement structure analysed with a finite element program.

#### 3.3.3.2 General formula for permanent deformation curves

The formula which describes the permanent deformation behaviour as shown in Equation 16 is referred to in this study as the General Permanent Deformation Law.
The first term of this model describes the linear part (on a log-log scale) of the permanent deformation curve and is characterised by the parameters A and B. The

second term in Equation 16 describes the tertiary flow part and is characterised by the parameters C and D. To illustrate the effect of these four model parameters (A to D) a series of graphs is shown in Figure 39 to Figure 42, whereby in each of them only one parameter is changed. The default values for the four parameters used in the graphs below are A = 0.2 ; B = 0.3 ; C = 0.1 and D = 0.001. The permanent deformation curve described by these default coefficients is shown in bold the graphs below. It will be shown further on that the chosen default parameter values are realistic and more or less average values found for the BSM mixes tested in this research.

The scale of the axes of the graphs in Figure 39 to Figure 42 has been extended beyond realistic values (*i.e.* beyond $10^6$ load repetitions) in order to be able to clearly demonstrate the effect of the various coefficients. Realistic values of permanent strain are limited to about 5 %, while values of *N* should not be extended much beyond $10^6$ (none of the tests described in this study were extended beyond $10^6$ load repetitions).

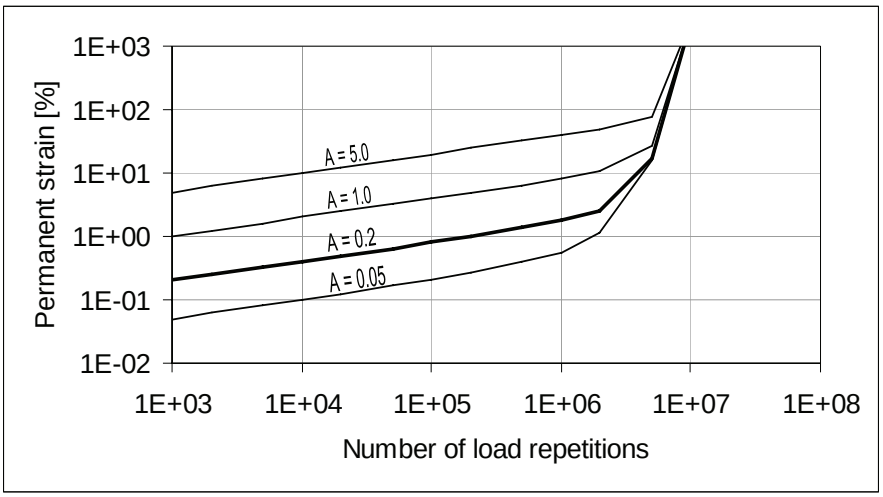


Figure 39: The effect of changing model parameter A on the PD curve

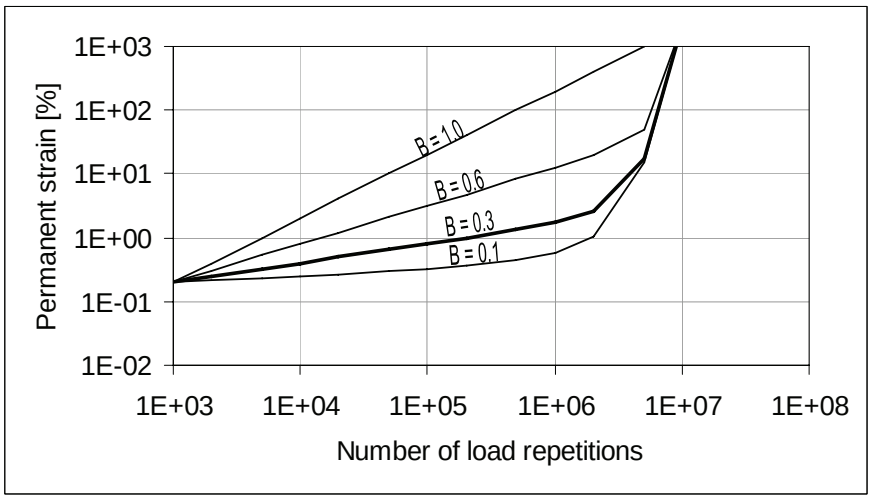


Figure 40: The effect of changing model parameter B on the PD curve

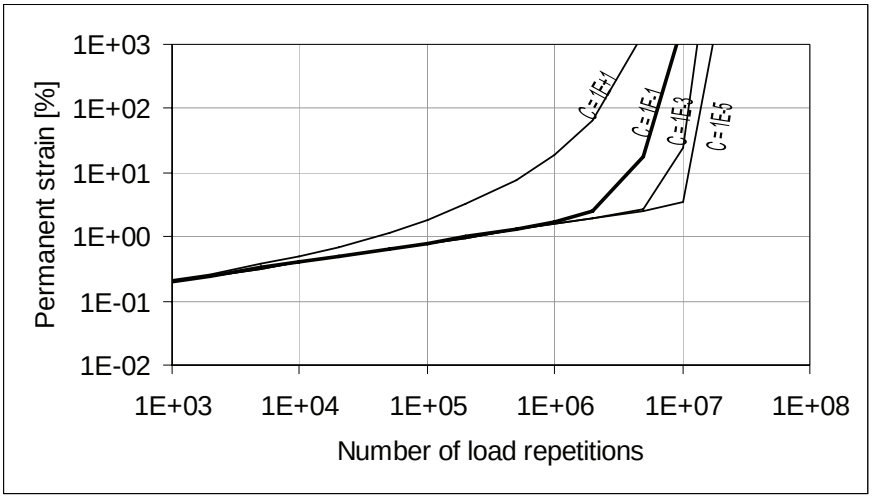


Figure 41: The effect of changing model parameter C on the PD curve

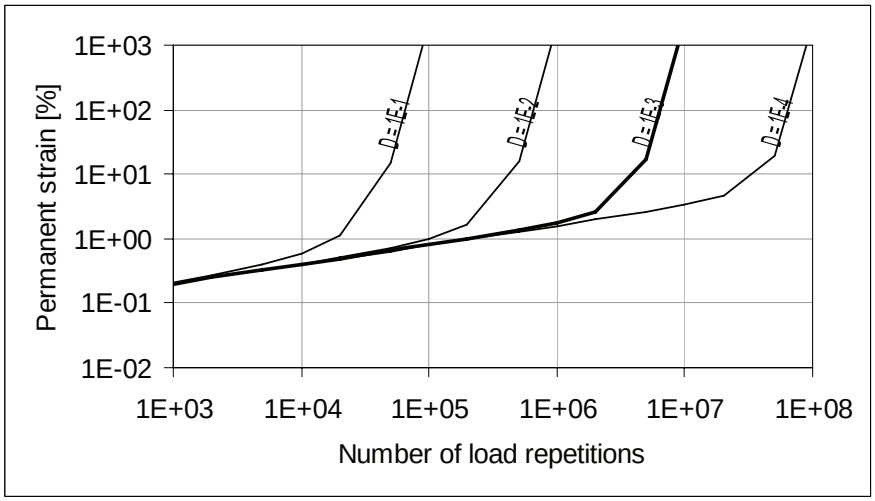


Figure 42: The effect of changing model parameter D on the PD curve

In Figure 39 it can be seen that model parameter A does not influence the shape of the PD curve, but only the vertical positioning thereof. The value of model parameter A is equal to the permanent strain at N = 1000. This is the initial strain as defined in Chapter 3. Model parameter B determines the slope of the linear part (on log-log scale) of the PD curve. It can also be seen from Figure 40 that a lower B parameter "brings forward" the flow point, which defines the initiation of the tertiary flow phase. The flow point occurs where the slope of the linear part is equal to the tangent of the tertiary flow part.

Model parameter C determines the "abruptness" of the transition from the linear phase to the tertiary flow phase, whereby a lower value for the C parameter results in a more abrupt transition. The asymptotic limit whereby $\varepsilon(N) \rightarrow \infty$ is not influenced by the C parameter. This asymptotic limit is only influenced by model parameter D. A higher D parameter "brings forward" this limit. This limit exists for as long as $C \neq 0$ and even for very small values for C and D tertiary flow will eventually set in, albeit far beyond N values that have any relevance to pavement engineering.

3.3.3.3 Stress dependency of model parameters

Huurman (1997) stated that the model parameters A, B, C and D are a function of the applied stresses and that this stress dependency can be described by Equation 17. Jenkins (2000) and van Niekerk (2002) found the deviator stress ratio and not the major principal stress ratio to be a fundamental performance parameter and adjusted stress dependency of the model parameter *X* as follows:

$$X = x_1 \left( \frac{\sigma_d}{\sigma_{d,f}} \right)^{x_2} \qquad \text{Eq. 18}$$

In this equation $x_1$ is called "the multiplier", while $x_2$ is called "the exponent". To illustrate the effect of change in the model parameter *X* as a results of changing model coefficients $a_1, a_2, b_1, \ldots, d_2$ two graphs are shown in Figure 43 and Figure 44 respectively. In Figure 43 the exponent (model coefficient $x_2 = a_2, b_2, c_2$ or $d_2$) is kept constant at a value of 2, while multiplier (model coefficient $x_1 = a_1, b_1, c_1$ or $d_1$) is varied. In Figure 44 the multiplier is kept constant at a value of 5, while the exponent is varied.

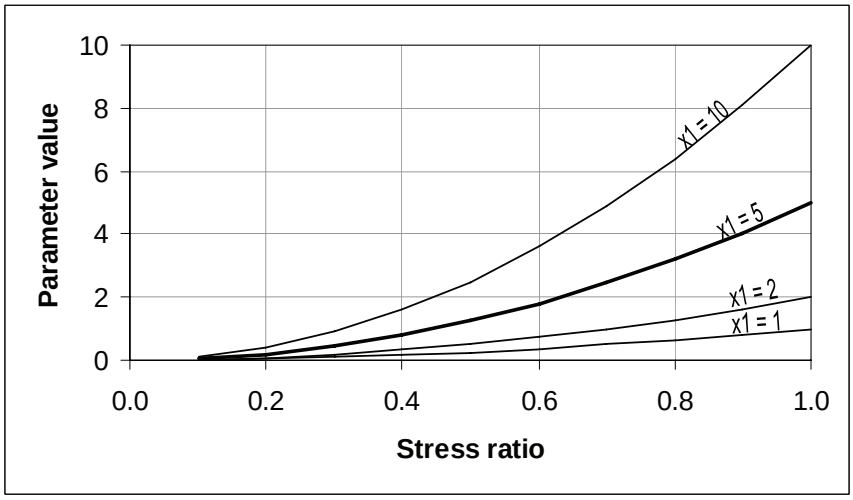


Figure 43: The effect of changing the multiplier $x_1$ on the model parameter *X*

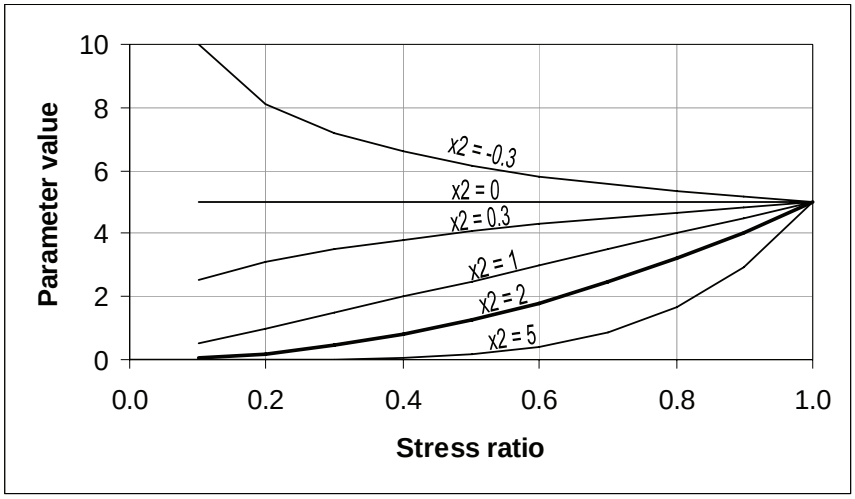


Figure 44: The effect of changing the exponent $x_2$ on the model parameter $X$

In general terms the exponent determines the shape and slope of the stress dependency curve. The effect hereof for increasing stress ratios is either increased ($x_1 > 1$), decreased ($x_1 < 1$) or remains the same ($x_1 = 1$). For a constant multiplier, the parameter value $X$ for different exponent values converges at a stress ratio of 1.0 (see Figure 44). At a stress ratio of 1.0, the parameter value (X = A, B, C or D) is equal to the value of the multiplier. This is illustrated by Figure 43.

Five cases of values for the exponent $x_2$ are discussed below. These cases are all shown in Figure 44.

- $x_2 = 0$
- $x_2 = 1$
- $0 < x_2 < 1$
- $x_2 > 1$
- $x_2 < 0$

In the case of $x_2 = 0$, no stress dependency exists and the value model parameter $X$ will be entirely determined by the value of the multiplier (and is the same for all stress ratios).

In the case of $x_2 = 1$, a linear relationship between the stress ratio and the model parameter $X$ exists. In this relationship the value of the model parameter is 0 when the stress ratio is 0 (hypothetical case) and increases proportionally to the value of the multiplier at a stress ratio of 1.0.

In the case of $0 < x_2 < 1$, a hyperbolic relation between the stress ratio and the model parameter $X$ exists. For exponent values close to zero a high stress dependency exist for low stress ratios and this stress dependency reduces for increasing stress ratios. At stress ratios close to one a near linear stress dependency exists for exponent values close to zero. This typical behaviour is relaxed for increasing exponent values tending towards a linear stress dependency for exponent values approaching one.

For the case of $x_2 > 1$ an exponential relation between the stress ratio and the model parameter $X$ exists. The exponential effect in the stress dependency is limited for exponent values close to one and the stress dependency is near linear. The exponential effect increases however with increasing values of $x_2$.

For the case of $x_2 < 0$ a hyperbolic relation between the stress ratio and the model parameter $X$ exist. The general slope of the stress dependency curve is however decreasing from very high values at low stress ratios towards a model parameter value equal to the multiplier value at a stress ratio of one. The model parameter value for very low stress ratios approaches infinity in case $x_2 < 0$.

3.3.3.4 Initial strain and initial strain rate

Further to the above model coefficients, parameters that can be used to describe or are able to predict the permanent deformation behaviour during an early stage of the permanent deformation test are discussed in this study. The initial permanent strain and the initial strain rate as is shown in Figure 45 were explored to this objective. The initial value of the strain and strain rate is defined here as the respective values after 1000 load repetitions (N = 1000). Furthermore, relations between the strain rate and the permanent axial strain are sought that would indicate asymptotic permanent axial strain, tertiary flow, or failure ($\varepsilon_p > 4$ %) without tertiary flow.

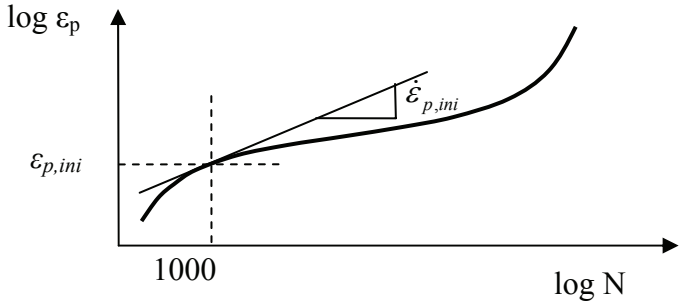


Figure 45: Definition of initial strain and initial strain rate

### *3.3.4 Bending beam strain-at-break*

Strain-at-break as a material property was first introduced in South Africa by Freeme during the 1970's for cement and lime treated materials. These materials develop significant cementation and behave in a semi-brittle manner. They crack under tension or flexure. The initiation of cracking under traffic or the so-called effective fatigue life of cement stabilised materials is believed to be directly related to the strain-at-break property of these materials as shown by (Maree and Freeme, 1981):

$$N_f = 10^{9.1\left(1-\frac{\varepsilon_s}{\varepsilon_b}\right)} \qquad \text{Eq. 19}$$

where $N_f$ = number of load repetitions at strain $\varepsilon_s$ to crack initiation
$\varepsilon_s$ = applied strain

εb = strain-at-break

Typical strain-at-break values for different categories of cement treated materials (C1-C4) were recommended by Otte (1978) as shown in Table 14. The transfer function shown in Equation 19 and the typical strain-at-break values were adopted in the South African Mechanistic Pavement Design Method during the 1970's and 1980's. The transfer functions were updated by Theyse *et al.* (1995). The recommended strain-at-break values shown in Table 14, however, are still in use for design purposes today, some 30 years after they were determined.

Table 14: Recommended strain-at-break values for standard cement treated materials (Otte, 1978)

| Cement treated material class | Strain-at-break [με] |
|---|---|
| C1 | 145 |
| C2 | 120 |
| C3 | 125 |
| C4 | 145 |

The TG2 Guideline (Asphalt Academy, 2002) introduced pavement life phases for foamed-bitumen stabilised materials very similar to those for cement stabilised materials adopted in the South African Mechanistic Design Method. These phases consist of an initial effective fatigue phase and a second equivalent granular phase. During the former the effective stiffness of the stabilised material reduces as a result of crack initiation and propagation. During the latter phase the behavioural state of the stabilised material has reduced from pure cemented behaviour to equivalent granular behaviour.

In the TG2 Guideline the strain-at-break is adopted as parameter controlling the effective fatigue life (first phase) comparable to the relation for cement stabilised materials as shown in Equation 19:

$$N_f = 10^{\left(A - 0.708\frac{\varepsilon_s}{\varepsilon_b}\right)} \qquad \text{Eq. 20}$$

where $N_f$ = number of load repetitions at strain $\varepsilon_s$ to crack initiation
$A$ = coefficient depending on confidence level
$\varepsilon_s$ = applied strain
$\varepsilon_b$ = strain-at-break

Typical strain-at-break values for different categories of foamed-bitumen stabilised materials were recommended (Asphalt Academy, 2002):

Table 15: Recommended strain-at-break values for foamed bitumen stabilised materials

| Foamed-bitumen stabilised material class | Strain-at-break [με] |
|---|---|
| FB1 | not determined |
| FB2 | 172 |
| FB3 | 490 |
| FB4 | not determined |

Liebenberg and Visser (2004) adopted a similar methodology for bitumen emulsion stabilised materials:

$$N_f = 10^{A-1.2775\left(\frac{\varepsilon_s}{\varepsilon_b}\right)} \quad \text{Eq. 21}$$

Where $N_f$ = number of load repetitions at strain $\varepsilon_s$ to crack initiation
$A$ = coefficient depending on confidence level
$\varepsilon_s$ = applied strain
$\varepsilon_b$ = strain-at-break

Typical strain-at-break values for different categories of bitumen emulsion stabilised materials were recommended (Liebenberg and Visser, 2004):

Table 16: Recommended strain-at-break values for bitumen emulsion stabilised materials

| Bitumen emulsion stabilised material class | Strain-at-break [με] |
|---|---|
| ET1 | 230 |
| ET2 | 145 |
| ET3 | not determined |
| ET4 | not determined |

The transfer function and the typical strain-at-break values proposed by Liebenberg and Visser (2004) were however never implemented as "best design practice" in South Africa, pending the updating of the TG2 Guideline. This updated guideline for BSM's is to include both foamed-bitumen and bitumen emulsion stabilised materials.

Prior to the strain-at-break testing published by Twagira (2006) and Twagira *et al.* (2006), which is also discussed in this study, the only research in South Africa relating to strain-at-break properties of BSM's was conducted at the CSIR, Pretoria. The strain-at-break is defined as the strain corresponding to the ultimate strength derived from the engineering stress-strain diagram. An example of such a curve is given in Figure 46.

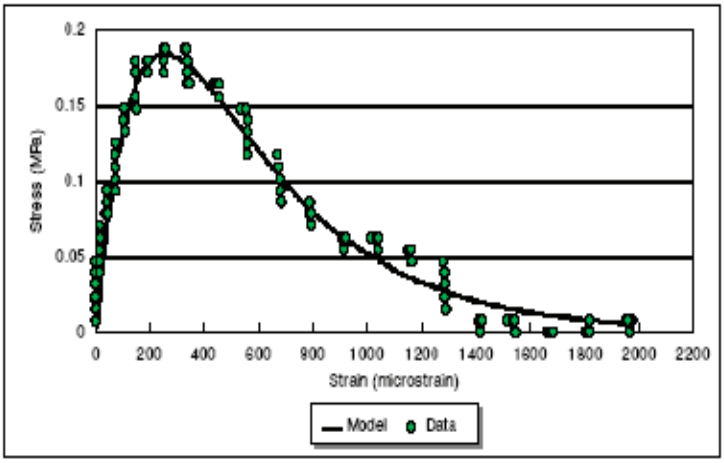


Figure 46: Example of stress–strain diagram from bending beam strain-at-break test (Theyse, 2000)

Twagira (2006) concluded that the strain-at-break does not accurately reflect fatigue properties of the BSM's tested. It can therefore not be used independently in a mix design process to characterise fatigue performance of BSM's.

### *3.3.5 Flexural stiffness master curves*

The typical flexural stiffness master curve for hot-mix asphalt shows resemblance with an S-shaped curve. Pellinen (1998) and Medani and Huurman (2003) have shown that a sigmoidal model can describe the S-curve shape of the master curve. This model is described by (Medani and Huurman, 2003):

$$\log S_{mix} = \log S_{\min} + \left(\log S_{\max} - \log S_{\min}\right) \cdot S \qquad \text{Eq. 22}$$

and

$$S = 1 - e^{-\left(\frac{10+\log f_{red}}{\beta}\right)^{\gamma}} \qquad \text{Eq. 23}$$

where $S_{mix}$ = Mix stiffness [MPa]
$f_{red}$ = reduced frequency [Hz]
$S_{min}$ = Minimum stiffness [MPa]
$S_{max}$ = Maximum stiffness [MPa]
$\beta, \gamma$ = shape parameters

The parameters $\beta$ and $\gamma$ define the shape of the S-curve, while $S_{min}$ and $S_{max}$ are the lower and upper asymptotic limits respectively of the stiffness curve. An idealised S-curve is shown in Figure 47.

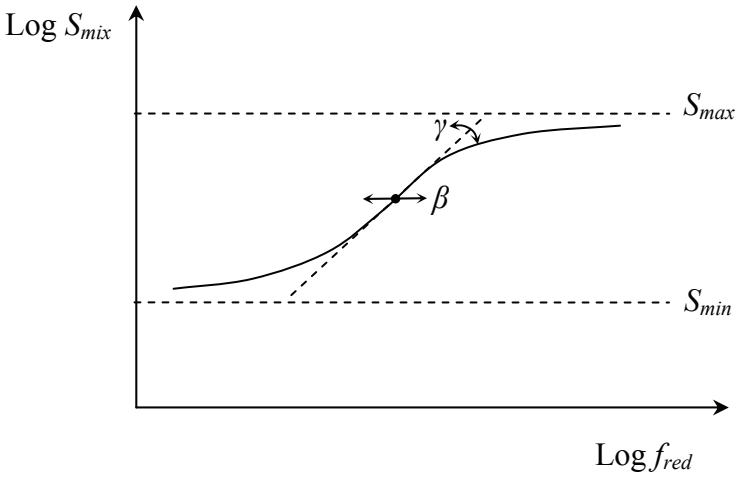


Figure 47: Idealised S-curve for hot-mix asphalt stiffness master curve

The typical shape of the master curves of the BSM tested in this study appears to differ from a typical master curves for hot-mix asphalt. This difference can mainly be found in the fact that the master curve of the BSM mixes are much flatter in general and that the slope of the curve is more constant over the range of reduced frequencies.

The master curves developed for BSM's in this study therefore have a much more linear appearance (on double-log scale). It is therefore that modelling by means of a power function results in a fairly good fit to the experimental data:

$$S_i = a \cdot f_{red}{}^{n} \qquad \text{Eq. 24}$$

or

$$\log S_i = \log a + n \cdot \log f_{red} \qquad \text{Eq. 25}$$

where $S_i$ = Stiffness after 100 load cycles [MPa]
$f_{red}$ = reduced frequency [Hz]
$a, n$ = model coefficients

The reduced frequency of both Equations 23 and 24 is obtained by applying a shift factor based on the principle of time-temperature correspondence. The shift factor is calculated in this study using the Arrhenius type equation and is described by:

$$\log f_{red} - \log f = \log \alpha_T = C\left(\frac{1}{T} - \frac{1}{T_{ref}}\right) \qquad \text{Eq. 26}$$

where $f_{red}$ = reduced frequency [Hz]
$f$ = test frequency [Hz]

| | | |
|---|---|---|
| $\alpha_T$ | = | shift factor |
| $C$ | = | log$e$·ΔH/R [K] |
| $T$ | = | test temperature [K] |
| $T_{ref}$ | = | reference temperature [K] |
| $\Delta H$ | = | activation energy [J/mol] |
| $R$ | = | gas constant, 8.314 [J/(mol·K)] |

Francken and Clauwaert (1988) determined that a $C$ constant of 10290 yielded a good fit of the master curve for the HMA mixes they had tested. This value for C was also adopted in this study, as it too yielded good fits for the BSM master curves. A constant value for $C$ assumes however that the activation energy is independent of the temperature. Sayegh (1967) found, however, that this activation energy can reduce by some 60 % with an increase of 60 ºK in temperature from 253 ºK. Investigations into this thermodynamic aspect were however not a focal point in this study and therefore a constant activation energy is assumed here.

### *3.3.6 Visco-elastic response*

A pure elastic material can be characterised by a spring with a certain spring stiffness and obeys Hooke's Law:

$$\sigma = E\varepsilon \qquad \text{Eq. 27}$$

where

| | | |
|---|---|---|
| $\sigma$ | = | stress |
| $\varepsilon$ | = | strain |
| $E$ | = | Modulus of Elasticity or Young's Modulus |

A pure viscous material is characterised by a dashpot with a certain viscosity and obeys Newton's Law:

$$\sigma = \lambda \frac{\partial \varepsilon}{\partial t} \qquad \text{Eq. 28}$$

where

| | | |
|---|---|---|
| $\lambda$ | = | viscosity |
| $t$ | = | time |

Several mechanical models consisting of combinations of springs and dashpots have been developed to describe visco-elastic behaviour of a material, *inter alia*:

- Maxwell Model
- Kelvin-Voigt Model (delayed elastic)
- Burgers Model
- Generalised Model

The Maxwell Model is a combination of a spring and a dashpot in series, while the Kelvin-Voigt Model is a parallel combination of a spring and dashpot. Burgers Model is a combination of Maxwell and Kelvin-Voigt models in series. The creep

compliance *J(t)* of the Burgers Model consists of three parts, *i.e.* an instantaneous elastic part, a viscous part and a retarded elastic part:

$$J(t) = \frac{\varepsilon(t)}{\sigma} = \frac{1}{E_0} + \frac{t}{\lambda_0} + \frac{1}{E_1}\left(1 - e^{-\frac{E_1 t}{\lambda_1}}\right) \qquad \text{Eq. 29}$$

The Burgers Model represents the behaviour of a visco-elastic material well. It is however quantitatively not sufficient to cover the long period of time over which retarded strain takes place. For this a number of Kelvin-Voigt Models in series may be required, which is called the Generalised Model (Huang, 1993). The above listed models are shown in Figure 48.

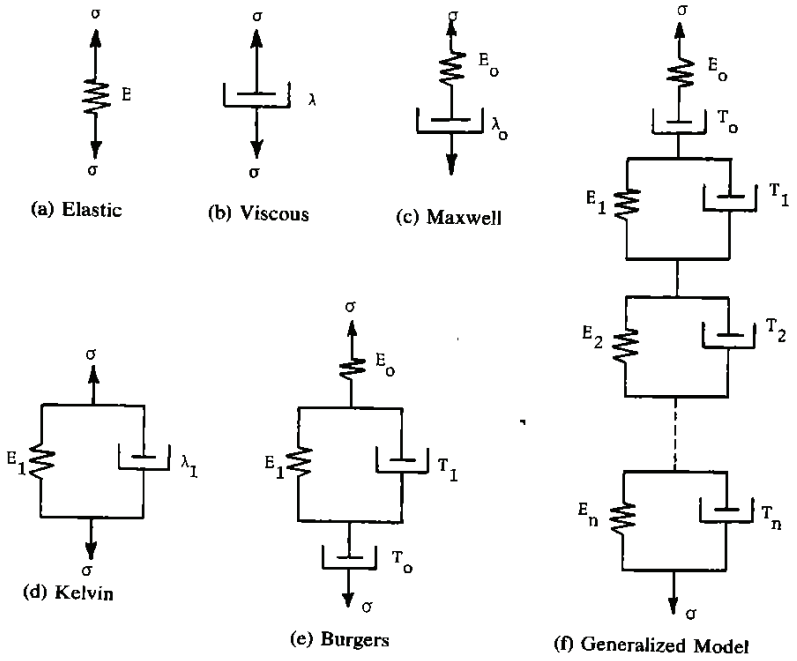


Figure 48: Mechanical models for visco-elastic materials (Huang, 1993)

The complex stiffness modulus $E^*$ of a material is a vector that can be resolved in an elastic (real) component, $E'$, and an viscous (imaginary) component, $E''$:

$$\left|E^*\right| = \sqrt{E'^2 + E''^2} \qquad \text{Eq. 30}$$

The elastic component is also called the Storage Modulus, while the viscous component is called the Loss Modulus. The direction of the complex modulus vector is described by the phase angle $\delta$ (see Figure 49). Pure elastic behaviour would be characterised by a phase angle of 0º, while pure viscous behaviour would be characterised by a phase angle of 90º.

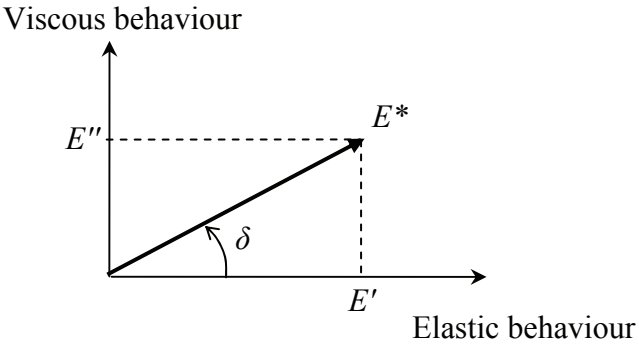


Figure 49: Vectorial characterisation of complex stiffness modulus

Therefore, the Storage Modulus is equal to:

$$E' = |E^*| \cdot \cos\delta \qquad \text{Eq. 31}$$

and the Loss Modulus is equal to:

$$E'' = |E^*| \cdot \sin\delta \qquad \text{Eq. 32}$$

From Equations 31 and 32 it can be derived that the phase angle can be determined as:

$$\delta = \arctan\left(\frac{E''}{E'}\right) \qquad \text{Eq. 33}$$

The phase angle characterises the lag of the responsive stress behind the induced strain in case of displacement controlled testing. This is shown in Figure 50.

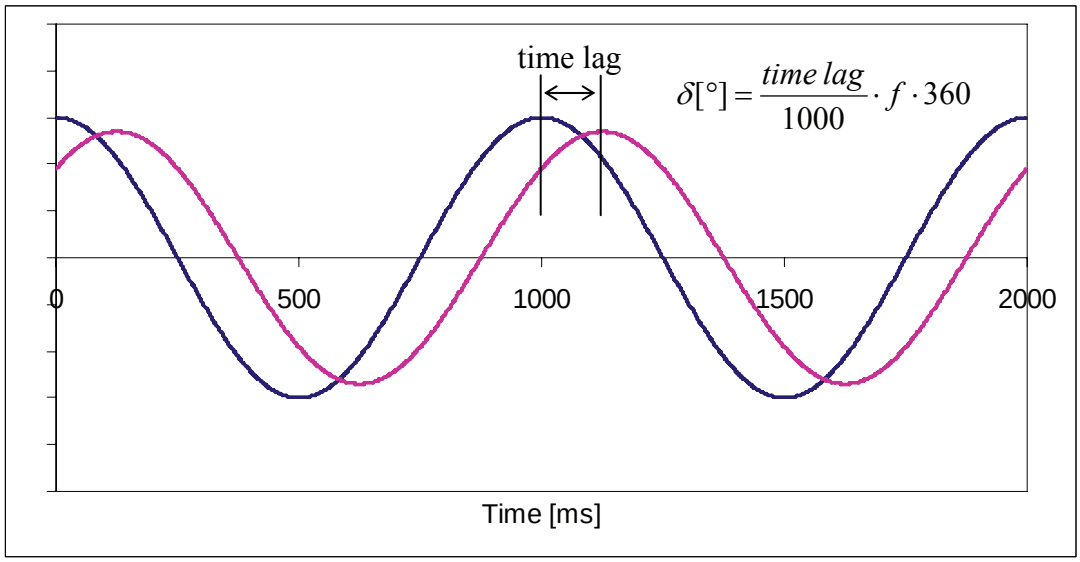


Figure 50: Phase angle between load and response

With the four-point beam flexural stiffness testing (temperature and frequency sweep testing) the complex stiffness and the phase angle are obtained as variables dependent on the frequency and temperature. Experimental data is shown in Figure 51. The time-temperature superposition as discussed in 3.3.5 for the flexural stiffness is also used here.

Non-linear regression methods can be used to obtain solutions for the Burgers Model coefficients $E_0$, $E_1$, $\lambda_0$ and $\lambda_1$ when the models for complex stiffness (Equation 30) and phase angle (Equation 33) are fitted to the experimental data ($E^*$ and $\delta$).

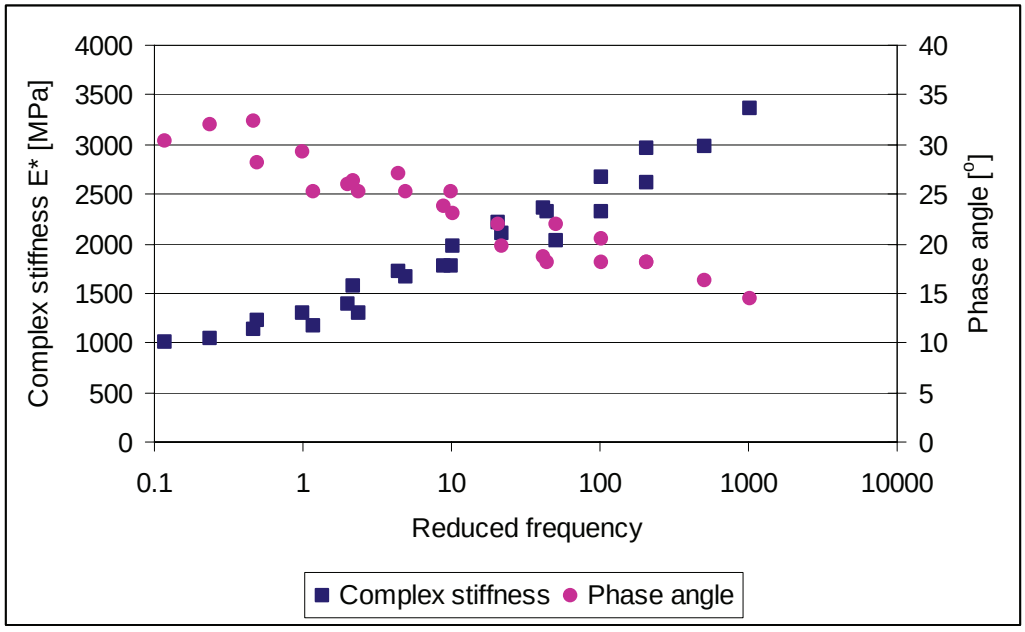


Figure 51: Example of frequency dependency of complex stiffness and phase angle (mix A-75C-0, beam E5)

The time-temperature dependency in the characterisation of a material can be eliminated when the phase angle is plotted against the complex stiffness. This is the so-called Black Diagram. This diagram is useful to characterise and compare the rheological behaviour of mixes, as it is unique for a certain mix.

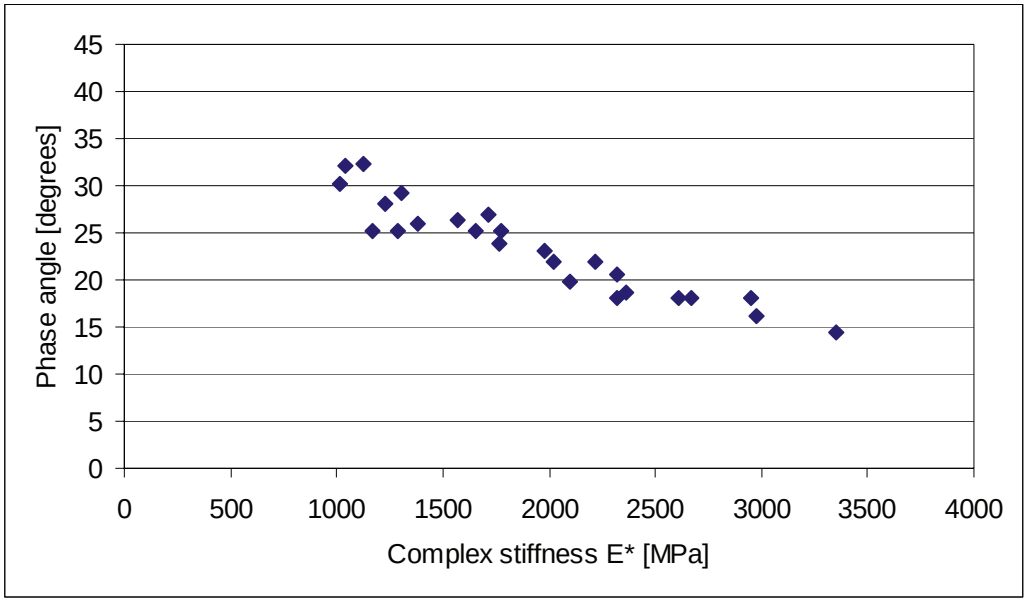


Figure 52: Example of a Black Diagram (mix A-75C-0, beam E5)

### *3.3.7 Fatigue behaviour*

3.3.7.1 Wöhler approach

When a material is subjected to repetitive loading, the stiffness of the material reduces as a result of cumulative damage on a micro-scale (cracking, crack growth and crack propagation). Failure of a material is often defined as the number of load repetitions, $N_f$, whereby the stiffness of the material has reduced to 50% of the initial stiffness $S_{ini}$. This is illustrated by Figure 53.

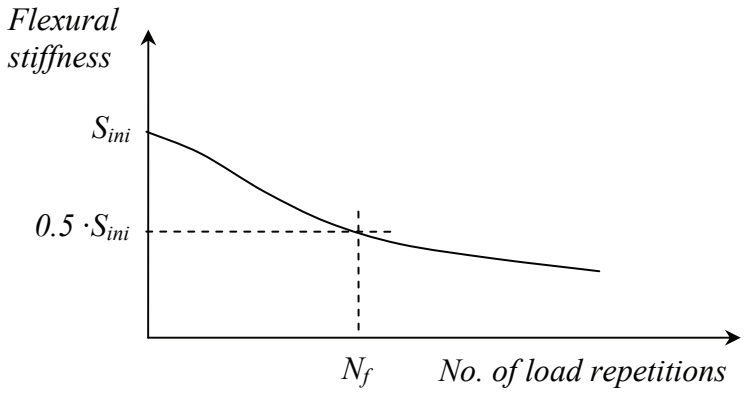


Figure 53: Conceptual stiffness reduction during repetitive loading

When fatigue tests are carried out at different load levels, a series of curves similar to the one shown in Figure 53 is found, with for each load level a different number of load repetitions to failure, $N_f$. When the number of load repetitions to failure and the corresponding load levels are plotted against each other, a so-called fatigue line is obtained.

Traditionally the fatigue of a material is characterised by an S-N curve, also called Wöhler-curve. This curve depicts the number of load repetitions to failure corresponding to a certain cyclic loading stress. The S-N curve is generally drawn on a log-normal scale, due to the large range of number of load repetitions and the more rapid reduction in stiffness at the lower number of load repetitions. The S-N curves imply that at increased loading magnitude, the number of allowable load repetitions to failure become less (see Figure 54).

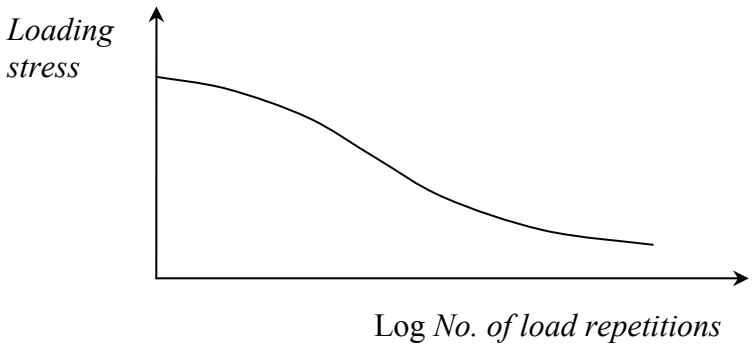


Figure 54: Conceptual S-N (Wöhler) curve for fatigue characterisation

Because the time- and temperature-dependent stiffness of hot-mix asphalt, fatigue tests on hot-mix asphalt specimens at a constant cyclic loading stress, but at different temperature and / or different loading frequency would results in a series of parallel S-N curves. Pell and Cooper (1975) found that when the fatigue test results are plotted using the strain instead of the stress, the results of the tests at different temperature and frequency coincide to form one fatigue line. When plotted on a double-log scale this line approximates a linear relationship that can be described by:

$$N_f = a \cdot \varepsilon^{-n} \qquad \text{Eq. 34}$$

or

$$\log N_f = \log a - n \log \varepsilon_t \qquad \text{Eq. 35}$$

where $N_f$ = the number of load repetitions to failure
$\varepsilon_t$ = applied strain level [micron]
$a, n$ = model coefficients

The fatigue relationship as shown in Equations 34 and 35 based on the Wöhler approach are used for the analysis of the fatigue results in this study.

3.3.7.2 Dissipated energy approach

An alternative fatigue characterisation approach to the Wöhler approach is the dissipated energy approach. The dissipated energy per unit volume within one load cycle can be described by (Van Dijk, 1975):

$$W_0 = \pi \cdot \sigma_0 \cdot \varepsilon_0 \cdot \sin \delta_0 \qquad \text{Eq. 36}$$

where $W_0$ = dissipated energy per unit volume per cycle [joule/m$^3$]
$\sigma_0$ = stress amplitude [N/m$^2$]
$\varepsilon_0$ = strain amplitude [m/m]
$\delta_0$ = phase angle between stress and strain wave [rad]

In the case of strain-controlled fatigue testing (constant strain level throughout the fatigue test), the stress amplitude will decrease as a result of a lowering stiffness modulus as the fatigue test progresses. The phase angle between the stress and strain wave also changes as the fatigue test progresses. To determine the total dissipated energy per unit volume the stress function and the strain function need to be integrated. This can be achieved by divding the time scales of these functions into fixed intervals. The dissipated energy $W_i$ in such intervals can then be calculated by using mean values for the stress, strain and phase angle (van Dijk, 1975):

$$W_i = \pi \cdot N_i \cdot \bar{\sigma}_i \cdot \bar{\varepsilon}_i \cdot \sin \bar{\delta}_i \qquad \text{Eq. 37}$$

where $N_i$ = number of cycles in interval [-]
$\bar{\sigma}_i$ = mean stress amplitude [N/m$^2$]
$\bar{\varepsilon}_i$ = mean strain amplitude [m/m]
$\bar{\delta}_i$ = mean phase angle [rad]

The total dissipated energy $W_{fat}$ is then determined by summation (van Dijk, 1975):

$$W_{fat} = \sum_{i=1}^{n} W_i \qquad \text{Eq. 38}$$

Van Dijk (1975) found that a unique relationship exists between the number of load repetitions to failure (N) and the total dissipated energy per unit volume to that number of load repetitions, which can be described by:

$$W_{fat} = A \cdot N^z \qquad \text{Eq. 39}$$

where $N$ = number of load repetitions to failure [-]
$A$ = model coefficient [joule/m$^3$]
$z$ = model coefficient [-]

As can be seen in the above equations, the dissipated energy is a function of *inter alia* the phase angle. The version of the user interface software used for the four-

point beam fatigue testing in this study (UTM21 V1.05) gave at times erroneous and unreliable phase angle outputs (this is discussed in more detail in Chapter 4). Hence, the dissipated energy calculations by this version of the software are also deemed to be not reliable. Therefore, the dissipated energy approach is not used to analyse the fatigue test results in this study.

## References


Arges, K. P. and Palmer, A. E., *Mechanics of Materials*, published by McGraw-Hil, USA, 1963

Askeland, D. R. and Phulé, P. P., *The Science and Engineering of Materials*, fifth edition published by Thomson, Toronto, Canada, 2006

Asphalt Academy, *The design and use of foamed bitumen treated materials*, Interim Technical Guideline No. 2, Pretoria, South Africa, 2002.

Barksdale, R. D., *Laboratory Evaluation of Rutting in Base Course Materials*, 3rd International Conference on the Structural Design of Asphalt Pavements, London, England, 1972

Francken, L., Permanent Deformation Law of Bituminous Road Mixes in Repeated Triaxial Compression, 4th International Conference on the Structural Design of Asphalt Pavements, Ann Arbor, Michigan, USA, 1977.

Francken, L. and Clauwaert, C. *Characterisation and structural assessment of bound materials for flexible road structures,* 6th International Conference on the Structural Design of Asphalt Pavements, Ann Arbor, Michigan, USA, 1988

Haynes, J. H. and Yoder, E. J., *Effects of Repeated Loading on Gravel and Crushed Stone Base Course Materials*, Highway Research Record No. 39, Highway Research Board, Washington, USA, 1962.

Hicks, R. G. and Monismith, C. L., *Factors influencing the resilient response of granular materials*, Highway Research Record No. 345, Highway Research Board, Washington DC, USA, 1971

Huang, Y. H., *Pavement Analysis and Design*, published by Prentice Hall, Englewood Cliff, New Jersey, USA, 1993

Huurman, H., Permanent Deformation in Concrete Block Pavements, PhD Dissertation Delft University of Technology, the Netherlands, 1997.

Jenkins, K. J. and Ebels, L. J., *Rehabilitation of a section of Victoria Road Llandudno : Special materials investigation : Addendum dynamic triaxial testing*, ITT Report 3/2003, Stellenbosch University, South Africa, 2003

Jenkins, K. J., *Mix design considerations for cold and half-warm bituminous mixes with emphasis on foamed bitumen.* PhD dissertation University of Stellenbosch, South Africa, 2000.

Liebenberg, J. L. L. and Visser, A. T., *Towards a mechanistic structural design procedure for emulsion treated base layers*, Paper 554, Journal of the South African Institution of Civil Engineering, Vol. 46 (3), 2004.

Maree, J. H. and Freeme, C. R., *The mechanistic design method used to evaluate the pavement structures in the catalogue of the draft TRH4 1980*, Technical Report RP/2/81, National Institute for Transport and Road Research, CSIR, Pretoria, South Africa, 1981.

May, R. W. and Witczak, M. W., *Effective Granular Modulus to Model Pavement Responses*, Transportation Research Record 810, Transportation Research Board, Washington DC, USA, 1981

Medani, T. O. and Huurman, M., *Constructing the stiffness master curves for asphaltic mixes,* Report 7-01-127-3, Delft University of Technology, The Netherlands, 2003

Otte, E., A structural design procedure for cement-treated layers in pavements. PhD dissertation University of Pretoria, South Africa, 1978.

Park, R. and Paulay, T., *Reinforced Concrete Structures*, published by John Wiley & Sons, USA, 1975

Pell, P. S. and Cooper, K. E., The effect of testing and mix variables on the fatigue performance of bituminous materials. Volume 44 of the Proceeding of the Association of Asphalt Paving Technologists, 1975.

Pellinen, T., *The Assessment of Validity of Using Different Shifting Equations to Construct a Master Curve of HMA*, University of Maryland, Department of Civil Engineering at College Park, MD, USA, 1998

Shell Bitumen U.K., *The Shell Bitumen Handbook*, United Kingdom, 1990

Sayegh, G., *Viscoelastic Properties of Bituminous Mixtures*. Proceedings of the 2nd International Conference on Structural Design of Asphalt Pavements, Ann Arbor, MI, USA, 1967

Theyse, H. L., De Beer, M., Prozzi, J. and Semmelink, C. J., *TRH4 Revision 1995, Phase I: Updating the Transfer Functions for the South African Mechanistic Design Method*, National Service Contract NSC24/1, Division for Roads and Transport Technology, CSIR, Pretoria, South Africa, 1995.

Theyse, H. L., *Laboratory design models for materials suited for labour-intensive construction*, Contract Report CR-99/038 Volume I: Report, Transportek, CSIR, Pretoria, South Africa, 2000

Twagira, M. E., *Characterisation of Fatigue Performance of Selected Cold Bituminous Mixes*. M.Sc. Thesis University of Stellenbosch, South Africa, 2006.

Twagira, M. E., Jenkins, K. J. and Ebels L. J., *Characterisation of Fatigue Performance of Selected Cold Bituminous Mixes*. Proceedings of the 10th International Conference on Asphalt Pavements, Quebec City, Canada, 2006

Uzan, J., *Characterization of Granular Material*, Transportation Research Record 1022, Transportation Research Board, Washington DC, USA, 1985

Uzan, J., Witczak, M. W., Scullion, T. and Lytton R. L., *Development and validation of realistic pavement response models*, Proceedings of the 7th International Conference on Asphalt Pavements, Nottingham, UK, 1992

Van Dijk, W., *Practical fatigue characterization of bituminous mixes*, Journal of the Association of Asphalt Paving Technologists, Vol. 44, Phoenix, USA, 1975

Van Niekerk, A. A., *Mechanical Behavior and Performance of Granular Bases and Sub-bases in Pavements*, PhD Dissertation Delft University of Technology, the Netherlands, 2002

# 4 MATERIALS, TESTING SCHEDULE AND METHODOLOGY

## 4.1 Introduction

The bitumen stabilised material (BSM) mixes that are subject of this study were produced using two sources of mineral aggregate, *viz*:

- Crushed limestone; and
- Reclaimed Asphalt Pavement (RAP) millings.

Between 2004 and 2006 the Stellenbosch University has been carrying out a research project for a client in the United States. This project forms an integral part of this study. Both of the above listed mineral aggregates were therefore sourced in the United States and subsequently shipped to South Africa.

The RAP was milled from a surface layer of a US highway. The recovered binder content was between 5.3 % and 5.6 %. The penetration value at 25 ºC of the recovered binder was determined as 19 (x 0.1 mm). No details of the type and age of the surfacing mix and the type of aggregate used are known.

The crushed limestone rock was sourced from a commercial quarry in the Terre Haute district, Indiana (USA). The limestone is a non-plastic material and has a CBR-value of 105 % at 98 % Modified AASHTO Density (determined according to Methods A3 and A8 respectively of the South African Standard Methods of Testing Road Construction Materials, TMH 1 [CSIR, 1986]).

The bitumen emulsion and the base bitumen for the production of the foamed bitumen were also imported from the United States. The only material that was sourced locally in South Africa was the cement that was used as active filler.

This chapter begins with a discussion of the materials used to produce the BSM mixes, providing some background on the material properties and characteristics. This is followed by a description of the type and number of mixes tested. Although most detail on the procedures followed to produce the mixes and the specimens is provided in the Appendices to this study, this chapter includes a summary of the most pertinent issues relating to the mix and specimen preparation.

The experimental testing described in this study is mainly focussed on two types of testing, *i.e.*, tri-axial testing and four-point beam testing. The types of tri-axial and four-point beam testing equipment used during the study are briefly discussed in this chapter. The most important aspects relating to test conditions and methods are also provided.

Additional four-point beam testing was carried out in order to investigate the appropriate testing temperature for the testing of BSM's. Due to the different characteristics of BSM compared with hot-mix asphalt (HMA) failure due to shear in the beam ends at the clamps may become critical with the former instead of failure due to bending in the middle section of the beam.

The four-point beam testing apparatus used in this study was commissioned shortly before the experimental phase of this study commenced. This chapter closes off with some detail on correlation testing with another four-point beam testing apparatus in a laboratory in the United States.

## 4.2 Materials

### *4.2.1 Mineral aggregate*

4.2.1.1 Grading

The mineral aggregates that were used in this study (virgin crushed limestone, RAP millings) were shipped from the United States to South Africa. These materials were subjected to sieve analysis according to TMH1 method B4 (CSIR, 1986).

For testing purposes, all particles with a size larger than 19.0mm were scalped off. For the RAP material the fraction larger than 19.0 mm was in the order of approximately 10 % (oversize material), whereas for the limestone, almost all material passed through the 19.0 mm sieve. The washed grading curves of the crushed limestone and RAP millings are provided in Table 17 below. The grading curves are shown in Figure 55.

Scalping material off has the disadvantage that the grading used for the laboratory testing is not the same as the grading in the field, however, consistency of results took priority over representativity of field mixes. Especially with the small specimen dimension for four-point beam testing, *i.e.* 63.5 mm x 50.0 mm (width x height), including larger particles in the mix may cause significant variation in test results.

Table 17: Washed sieve analysis of aggregates used (percentage passing)

| Sieve size [mm] | Crushed rock (limestone) | | RAP Millings | |
|---|---|---|---|---|
| | average | st.dev. | average | st.dev. |
| 19.0 | 100 | 0.0 | 100 | 0.0 |
| 13.2 | 86.0 | 4.6 | 91.1 | 2.2 |
| 9.5 | 72.5 | 8.5 | 77.5 | 2.5 |
| 4.75 | 52.3 | 9.3 | 51.9 | 1.6 |
| 2.00 | 39.6 | 7.6 | 30.5 | 1.5 |
| 1.18 | 32.4 | 6.3 | 19.9 | 1.4 |
| 0.600 | 27.2 | 5.4 | 8.8 | 0.7 |
| 0.425 | 24.6 | 5.1 | 5.3 | 0.4 |
| 0.300 | 21.6 | 4.7 | 3.4 | 0.3 |
| 0.150 | 14.4 | 3.1 | 1.5 | 0.1 |
| 0.075 | 9.2 | 2.0 | 0.9 | 0.1 |

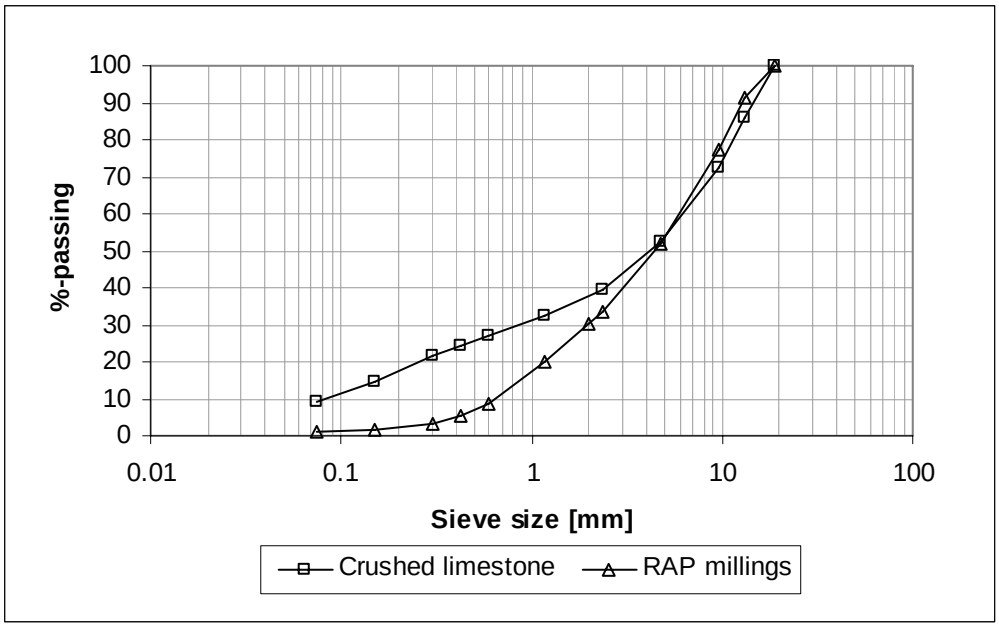


Figure 55: Grading curve RAP material as received

The RAP was manually separated into the following five fractions using large (1.2 m x 1.5 m) suspended screens:

Table 18: Fraction particle sizes manual fractionation

| Fraction | Greater than | Smaller than |
|---|---|---|
| 1 | 19.0 mm | - |
| 2 | 12.2 mm | 19.0 mm |
| 3 | 4.75 mm | 12.2 mm |
| 4 | 2.20 mm | 4.75 mm |
| 5 | - | 2.20 mm |

The limestone was separated into four fractions with the smallest particle size fraction being < 4.75 mm particles. This fraction was not further divided using the large screens because of the high fines content of this fraction. Using the large screens in the open air would have resulted in a high loss of fines.

The smallest particle size fractions (< 2.20 mm in case of RAP and < 4.75 mm in case of limestone) were taken for further fractionation in the laboratory using 600 mm diameter vibrating sieves with standard mesh sizes (2.36, 1.18, 0.600, 0.300, 0.150, 0.075).

Two blends of virgin crushed limestone and RAP millings have been tested in this research. These two blends were chosen in order to study the effect of BSM's with a high and a low percentage of RAP. The proportions of mineral aggregate in these two blends were:

- 75 % (m/m) crushed limestone rock + 25% (m/m) RAP millings. This blend is labelled 75C;
- 25 % (m/m) crushed limestone rock + 75% (m/m) RAP millings. This blend is labelled 75M.

The 75C blend (75% crushed rock + 25% RAP) consisted of two sub-blends, *i.e.* one with 1% active filler (cement) and one without active filler:

- 75% crushed rock + 25% RAP without cement; labelled 75C-0;
- 75% crushed rock + 25% RAP + 1.0 % cement; labelled 75C-1;

The blend with 75% RAP was only tested without active filler added. It is therefore also referred to as 75M-0.

The usage of 75% RAP in BSM's is an extreme case (lower percentages are normally used) but it was included in the testing matrix here to study the effect of high percentages of RAP in BSM's. When recycling with high percentages of RAP consideration should also be given to other economical and sustainability aspects, which may favour the re-use of RAP in an HMA instead of in a BSM application.

The grading of the blends follows out of the washed grading curves of the crushed limestone and RAP millings and is summarised in Table 19 and Figure 56 below.

The grading changes slightly (mainly the percentage passing 0.075 mm sieve) from the 75C-0 blend compared to the 75C-1 blends because only 1.0 % active filler (<0.075 mm) is added to the blend. It can be seen in Figure 57 that all three mixes classify as sand skeleton mixes. The blends were reconstituted according to mass percentages from the fractions discussed above. This ensured that the grading of the mixes and specimens was consistent throughout the study.

Table 19: Target grading curves

| Sieve size [mm] | 75C-0<br>75% crushed limestone<br>25% RAP millings<br>no active filler | 75C-1<br>75% crushed limestone<br>25% RAP millings<br>1% active filler | 75M-0<br>25% crushed limestone<br>75% RAP millings<br>no active filler |
|---|---|---|---|
| 19.0 | 100 | 100 | 100 |
| 13.2 | 87.3 | 87.4 | 89.8 |
| 9.5 | 73.7 | 74.0 | 76.3 |
| 4.75 | 52.2 | 52.7 | 52.0 |
| 2.36 | 38.0 | 38.7 | 34.9 |
| 1.18 | 29.3 | 30.0 | 23.0 |
| 0.600 | 22.6 | 23.3 | 13.4 |
| 0.425 | 19.8 | 20.6 | 10.1 |
| 0.300 | 17.1 | 17.9 | 7.9 |
| 0.150 | 11.2 | 12.0 | 4.7 |
| 0.075 | 7.1 | 8.1 | 3.0 |

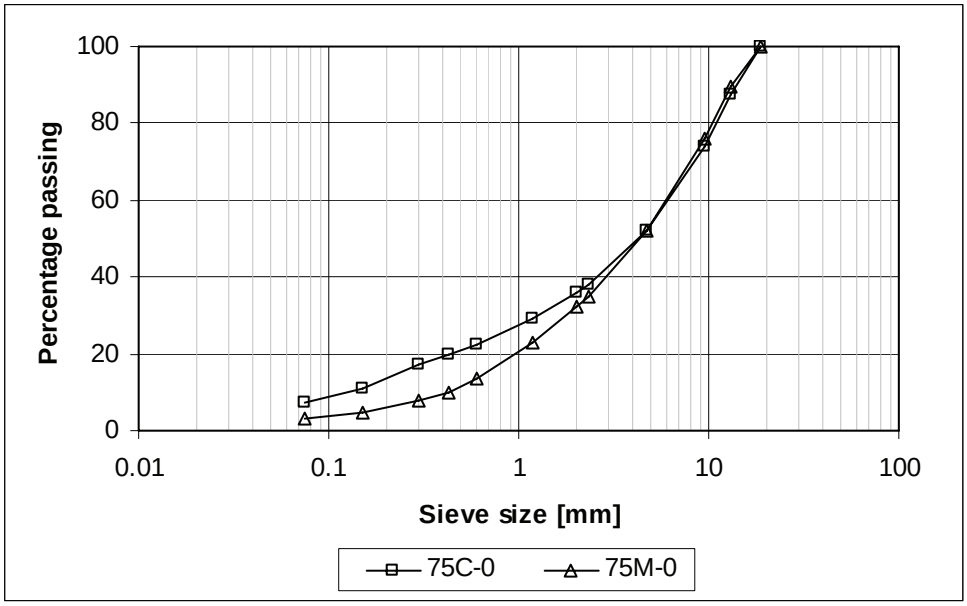


Figure 56: Grading curves of 75C-0 and 75M-0 blends

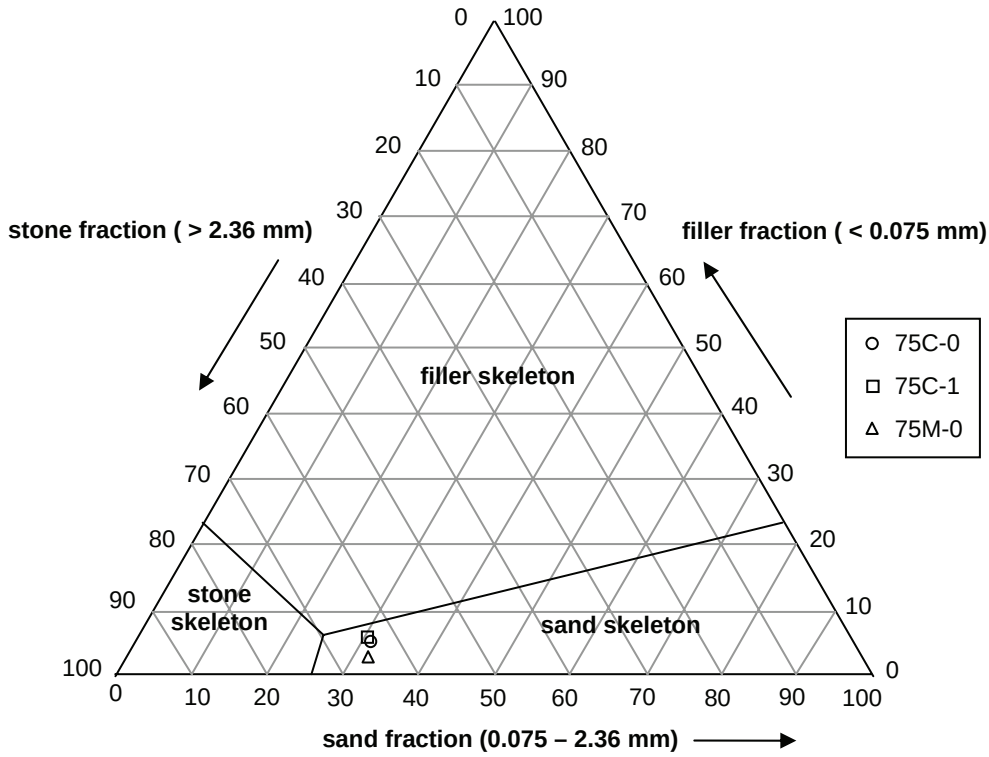


Figure 57: Classification of mixes according to type of mineral skeleton

4.2.1.2 Maximum dry density and optimum moisture content

The two blends, *i.e.* 75C and 75M were subjected to maximum dry density tests and optimum moisture content determination according to THM1 Methods A7 (CSIR, 1986). Density – moisture content curves were compiled for modified AASHTO compaction as well as for standard Proctor compaction. Difference in level of compaction exists between the several international standards. In Table 20 below some of the details of the THM1 tests are listed and the Proctor compaction according to TMH1 is compared with the Proctor compaction according to ASTM. As can be seen the total applied compactive energy using the South African standard (TMH1) in case of standard Proctor compaction is higher than that of the ASTM standard.

Table 20: Details of Modified AASHTO and Standard Proctor compaction

| Description | Mod AASHTO (TMH1) | Proctor (TMH1) | Proctor (ASTM) |
|---|---|---|---|
| Mass hammer [kg] | 4.536 | 2.495 | 2.495 |
| Drop height [mm] | 457.2 | 304.8 | 304.8 |
| No. of layers [-] | 5 | 3 | 3 |
| No. of blows [-] | 55 | 55 | 25 |
| Total no. of blows [-] | 275 | 165 | 75 |
| Total compaction energy [J] | 5595 | 1231 | 560 |

The density – moisture content curves as determined for the 75C blend are shown in Figure 58 below. The modified AASHTO curve shows a well defined optimum at 7.6% moisture with a maximum dry density of 2105 kg/m$^3$. The low density data point at 8% moisture appears to be an outlier. For the lower compaction energy (Proctor) the curve is less well defined and the high density values at approximately 10% moisture are not a true reflection of the material behaviour. It was visually established that at these high moisture contents the material appears wet and is over the optimum moisture content. It appears as if the optimum moisture content for the Proctor compaction is only slightly higher than for the Modified AASHTO compaction and approximately 8%. The Proctor maximum dry density is approximately 100 kg/m$^3$ lower than the Modified AASHTO maximum dry density.

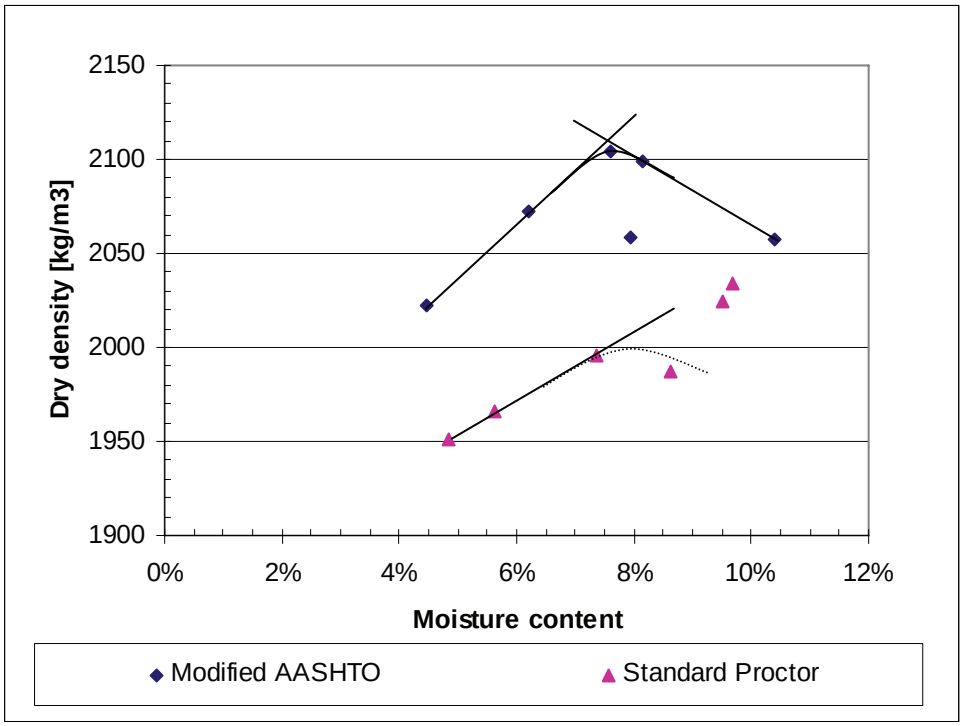


Figure 58: Density - moisture content relation 75C blend

The results for the 75M blend show more scatter than the 75C blend, as can been seen in Figure 59. This is believed to be inherent to the type of material. The 75M blend is non-cohesive, coarser than the 75C blend. The optimum moisture content for Modified AASHTO compaction was determined to be 5.2% with a maximum dry density of 1930 kg/m$^3$. The optimum moisture content for the standard Proctor compaction is 7.0% with a considerable lower maximum dry density of 1800 kg/m$^3$.

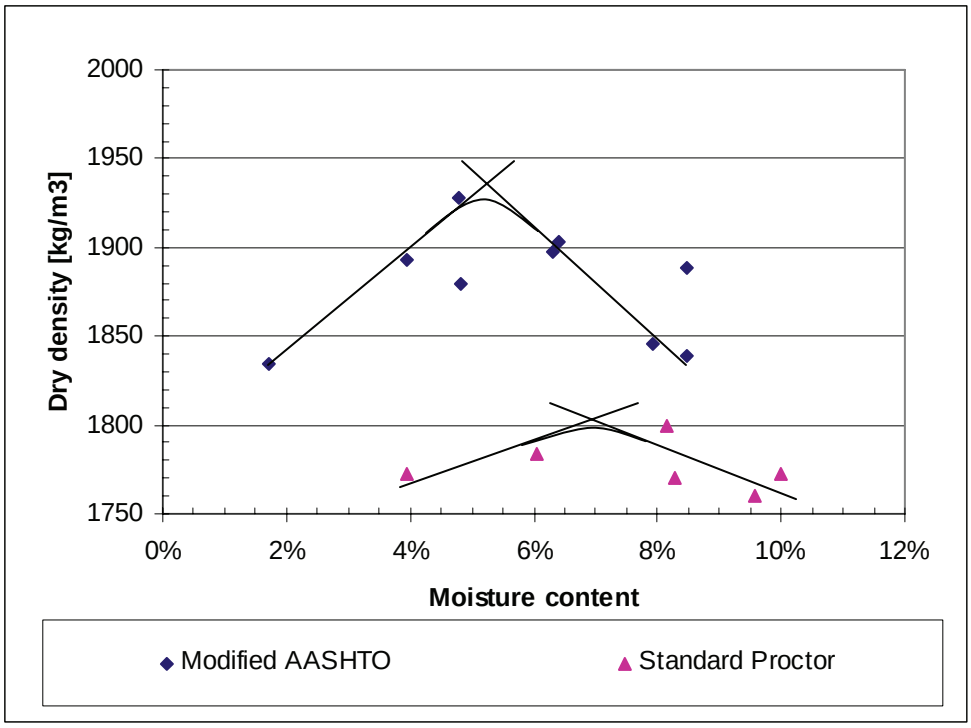


Figure 59: Density - moisture content relation 75M blend

The Modified AASHTO and Standard Proctor maximum dry densities and the moisture contents at which they occur are summarised in Table 21.

Table 21: Summary of maximum dry densities and optimum moisture contents

| Blend | Compaction | M.D.D. [kg/m$^3$] | O.M.C [%] |
|---|---|---|---|
| 75C-0 | Mod AASHTO | 2105 | 7.6 |
| | Standard Proctor | 2000 | 8.0 |
| 75M-0 | Mod AASHTO | 1930 | 5.2 |
| | Standard Proctor | 1800 | 7.0 |

It can be seen that for both blends the reduction in compaction energy results in a decrease in maximum dry density and increase in the optimum moisture contents. This is a general behaviour for granular materials.

For the compaction of test specimens a density level of 98% of Modified AASHTO density was aimed for. In case of the 75C blend this would be a target dry density of 2063 kg/m$^3$ and for the 75M blend 1896 kg/m$^3$.

### *4.2.2 Bituminous binder*

4.2.2.1 Bitumen emulsion

Two types of bitumen emulsions were used in this study, labelled A and B respectively. Both emulsion A and B were shipped from the United States to South Africa. Care was taken that during transport (air freight) the emulsions were not damaged by exposure to low temperatures. Emulsion A is an emulsion specially formulated to be used for in-situ recycling operations. The nature of bitumen emulsion A and what the specific formulation entails are subject to intellectual property rights and cannot be disclosed here. Emulsion A is a cationic emulsion with a bitumen content of 65%. Emulsion B is a standard available CSS-65, which is used as a reference emulsion.

Some settlement occurred during transport and the emulsion was in an initial stage of flocculation. Two methods were considered to bring all the bitumen droplets in a state of full suspension again, i.e. re-milling the emulsion using a bench-top colloid mill and stirring by hand after heating to between 60ºC and 70ºC. The emulsions were subjected to particle size analysis to investigate the effect of these two methods. It was found that the average particle size of the re-milled samples was in the order of 20 micron, while the samples that were only stirred by hand had an average particle size of 10 micron (see Figure 60). Based hereon it was decided not to re-mill the emulsions received. Instead, all emulsions used for the production of the BSM's were heated to between 60ºC and 70ºC and manually stirred one or two days prior to their use.

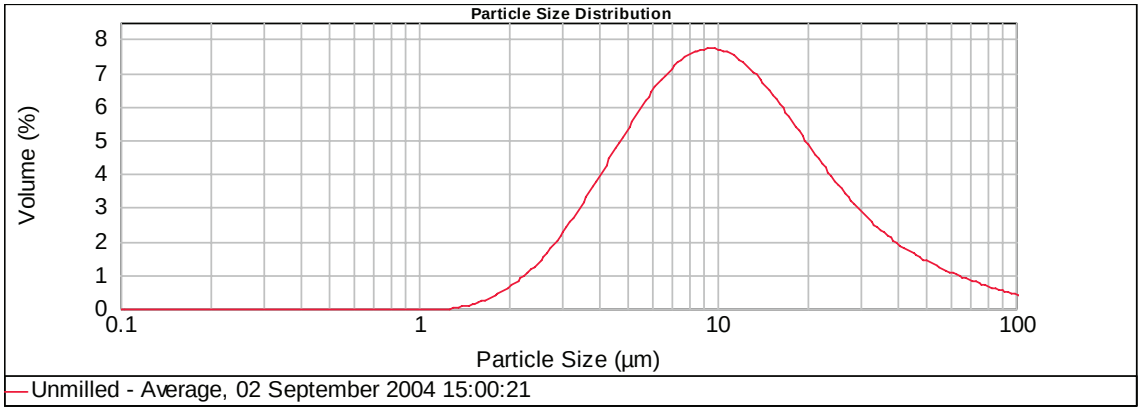


Figure 60: Typical particle size distribution after reheating and stirring only

4.2.2.2 Foamed bitumen

PG 58 – 28 bitumen was also shipped from the United States to South Africa to be used as binder in the foamed bitumen mixes. No binder tests were undertaken on the bitumen received and it was assumed that the binder received was according to specification. A PG 58 – 28 bitumen would be equivalent to a 80/100 penetration grade bitumen according to the South African specifications.

For the production of the foamed bitumen a Wirtgen WLB-10 laboratory foam plant was used. The temperature of the bitumen during all foamed bitumen testing and mix

production was kept constant at 170ºC. Before foamed bitumen mix production the foaming properties of the bitumen were determined at different levels of foamant water as mass percentage of the bitumen. The expansion ratio and half-life time of the foamed bitumen are shown in Figure 61 below.

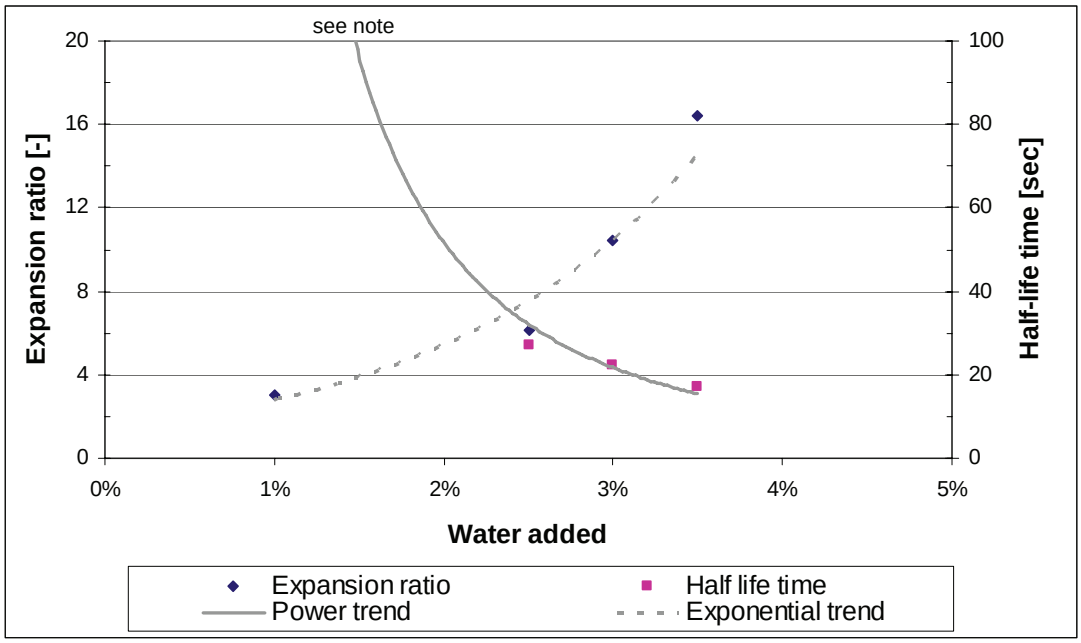


Note: The half-life time of the foamed bitumen at a foamant water level of 1% was in excess of 3 minutes and is not shown on the graph in order to be able to show the data at the lower scale values

Figure 61: Foaming properties of PG 58 - 28 bitumen

It was decided to produce all foamed bitumen with 3.0% foamant water. The half-life time of the foamed bitumen produced with 3.0% foamant water is in excess of 20 seconds and the expansion ratio in excess of 10.

A half-life time of 20 seconds in combination with an expansion ratio of 10 would result in a Foam Index of 125. The TG2 Manual (Asphalt Academy, 2002) provides a guideline for the suitability of foamed bitumen according to their Foam Index. In case of a minimum aggregate temperature of 25ºC, a Foam Index of 125 would indicate a good suitability.

It is noted that the values of 10 for expansion ratio and 20 seconds for half-life time were maintained as minimum values during the production of the foamed bitumen mixes. The variation of the foam quality was however limited and expansion ratio's did not exceed 12, while half-life times in excess of 30 seconds were seldom recorded. During the winter periods the aggregate was pre-heated to approximately 25 ºC in a draft oven to ensure consistent mix quality throughout the study period.

### *4.2.3 Active filler*

Cement was added as active filler to the 75C-1 blend. The cement was locally purchased and is a Surebuild$^{TM}$ , 42.5 CEM II – B/M (L/S) according to the South African specification (SABS EN 197 and SABS 1491). The cement used during all phases of the project came from the same batch and was kept sealed in plastic containers during storage. The cement falls in the strength class 42.5N, which means an early strength (after 2 days) in excess of 10 MPa and a standard strength (after 28 days) between 42.5 MPa and 62.5 MPa. Opposed to "CEM I" type cement, which is an ordinary Portland cement with a maximum of 5% of minor additional constituents, the "CEM II" type cement is a Portland-composite cement. The annotation "B/M" indicates that besides clinker, which makes up 65% – 79% of the cement, it contains 21% - 35% of other main constituents and 0% - 5% of minor additional constituents. The 21% – 35% of other main constituents may be a mixture of blast-furnace slag, silica fume, pozzolana, fly ash, burnt shale or limestone. In the case of the Surebuild$^{TM}$ cement used in this study, the other main constituents are limestone and slag (blast-furnace), which is indicated by the addition "(L/S)".

## 4.3 Mixes and testing schedules

The experimental matrix of this study was developed to test the influence of the following variables:

- The proportion of RAP in the mix (high or low);
- The effect of the use of active filler (1% cement compared to no active filler);
- The type of binder (two types of bitumen emulsion and one foamed bitumen).

As discussed above the aggregate blend with a high percentage of RAP was only tested without any active filler. The binder content was not varied in this study and the following residual binder contents were used:

- 3.6% for the 75C mixes; and
- 2.4% for the 75M mixes

These binder contents were chosen to represent typical binder contents as used in full-depth recycling in the United States. For the mixes with a high percentage of RAP a lower binder content (*i.e.* 2.4% i.o. 3.6%) was selected because of the existing binder already present in the RAP aggregate. The chosen binder contents are believed to represent typical binder contents not only in the United States, but in many other countries where CIPR is carried out.

The lower binder content for the mixes with a high percentage of RAP was chosen because of *inter alia* the difference in grading of the two blends. The fact that the RAP particles already have a film of old bitumen also plays a role. The old bitumen film may perhaps not have a "glueing" effect, but it reduces absorption of fresh bitumen and results in a greater affinity between the fresh bitumen and the RAP particles than what would be the case for virgin rock.

The density at which the specimens were tested was also not varied. The target density for the compaction of the specimens was 98% of Modified AASHTO Density.

This resulted in a total of three different aggregate blends combined with three different binders. Hence, a total of nine different mixes. These nine mixes tested are summarised in Table 22 below:

Table 22: Mix names and composition

| No. | Name | Binder | Aggregate blend | Res. binder | Cement |
|---|---|---|---|---|---|
| 1 | A-75C-0 | Emulsion | 75% limestone – 25% RAP | 3.6% | 0% |
| 2 | A-75C-1 | | 75% limestone – 25% RAP | 3.6% | 1% |
| 3 | A-75M-0 | | 25% limestone – 75% RAP | 2.4% | 0% |
| 4 | B-75C-0 | Emulsion | 75% limestone – 25% RAP | 3.6% | 0% |
| 5 | B-75C-1 | | 75% limestone – 25% RAP | 3.6% | 1% |
| 6 | B-75M-0 | | 25% limestone – 75% RAP | 2.4% | 0% |
| 7 | C-75C-0 | Foamed bitumen | 75% limestone – 25% RAP | 3.6% | 0% |
| 8 | C-75C-1 | | 75% limestone – 25% RAP | 3.6% | 1% |
| 9 | C-75M-0 | | 25% limestone – 75% RAP | 2.4% | 0% |

The mix properties that were tested included strength, stiffness and behaviour under repeated loading. The strength of the mixes was determined in monotonic destructive tests, while the stiffness was determined in non-destructive dynamic testing (short loading duration). The behaviour under repeated loading was evaluated by subjecting specimens to long duration dynamic testing.

The abovementioned properties were determined both in compressive mode and in bending mode. The tri-axial test was selected to test the material properties in the compressive mode, while the four-point bending beam test was used for the bending mode testing. An overview of the testing modes and the test outputs is given in Table 23.

Table 23: Overview of testing modes and outputs

| Testing Mode | Test output | |
|---|---|---|
| | Compression (tri-axial) | Bending (four-point beam) |
| Monotonic testing to failure | Shear parameters | Strain-at-break |
| Short duration dynamic testing | Resilient modulus | Flexural stiffness |
| Long duration dynamic testing | Permanent deformation behaviour | Fatigue behaviour |

The number of specimens tested per mix for each of the tests shown in Table 23 is given in Table 24.

Table 24: Number of tests to be conducted

| Testing Mode | Number of specimens tested per mix | |
|---|---|---|
| | Tri-axial | Four-point beam |
| Monotonic testing to failure | 4 | 3 |
| Short duration dynamic testing | 2 | 12 |
| Long duration dynamic testing | 4 | 2 |

## 4.4 Mixing and specimen preparation

It can be deducted by combining Table 23 and Table 24 that a total of 90 tri-axial specimens were produced and tested, while in the four-point beam mode a total of 153 beam specimens was tested. The specimen preparation consisted of the step listed below:

- Weighing out and blending the mineral aggregate;
- Mixing with compaction water, active filler (if required) and bitumen;
- Compaction of specimens;
- Curing of the specimens;
- Installation of instrumentation (if required).

Both for the tri-axial and four-point beam testing the specimen preparation is discussed in more detail in Appendix D.

The BSM mixes prepared for the tri-axial specimens and all foamed bitumen mixes were mixed in a twin-shaft pugmill mixer. The emulsion mixes prepared for the four-point beam specimens were mixed in a vertical shaft drum mixer due to limited availability of the pugmill mixer and in order to meet the required production rate. The mixers used are shown in Figure 62. No difference in mixing quality was visually observed when comparing the two types of mixers.

Figure 62: Twin-shaft puggmill mixer (left) and vertical shaft drum mixer (right)

The tri-axial test specimens were compacted using a gyratory compactor to the target density of 98% of Modified AASHTO density. The specimens were 150mm in diameter and approximately 130 mm in height. Gyratory compaction is known to result in density gradients in the specimens when compacting HMA and this is expected to apply to BSM's as well. The use of gyratory compaction was however a requirement in this study. Investigating possible density gradients was not a focal point of this study, but it has been identified to form part of a follow-up research project taking place in 2008.

Two gyratoy specimens of 130 mm in height were placed one on top of the other to form one tri-axial specimen of the desired height. Specimens with perfectly parallel top and bottom faces, both perpendicular to the axis of the cylinder, were obtained with the gyratory compaction. The stacking of specimens was required because it was not possible to produce one specimen of the required height in the gyratory compactor. The vertical stress at the interface between the two specimens is many times higher than the shear stress in the plane of the interface and friction at the interface ensures that the two specimens behave as one uniform specimen.. This was confirmed by visual observation during and after the testing, *i.e.*:

- The same barrelling effect was observed for the stacked specimens as for one high specimen;
- The angle of the shear plane was in the order of 45º and continued through the interface of the two stacked specimens;
- The two specimens were difficult to separate after testing (see Figure 63) and a hammer and chisel were used to achieve separation;
- The interface after separation was rough whereby the large particles at face of the one specimen protrude into the opposite face of the other sepecimen.

Figure 63: Stacked specimens adhering to each other after testing

BSM slabs were produced for the production of the beam specimens for the four-point beam testing. The beams were cut out of these slabs, which were thicker than the required beam height. Therefore all faces of the beams were cut. The slabs were compacted using a vibrating steel drum roller as shown in Figure 64. The saw cutter with a 1.5 mm wide continuous rim diamond blade is also shown in this figure.

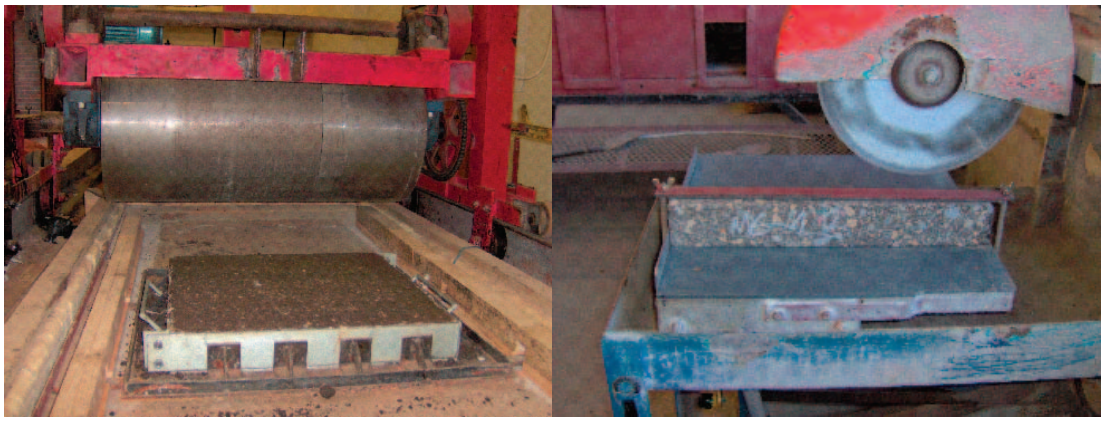

Figure 64: Vibratory steel drum roller and saw cutter used for beam production

For practical reasons and because of the different surface area to volume ratio the tri-axial specimens and the beam specimens were subjected to a different curing protocol. The protocol used for the curing of the tri-axial specimens is similar to a curing protocol proposed by Houston and Long (2004) and consists of:

- Extraction of the specimens from the mould immediately after compaction and placement on a base plate;
- 20 hours curing at 30 ºC, unsealed; followed by
- 48 hours curing at 40 ºC, sealed in plastic bag, whereby the bag is replaced with a new (dry) one after 24 hours.

Because the slabs are too bulky and heavy to easily handle and seal in plastic bags and because it was not possible to immediately remove the slabs from the moulds, the following curing protocol was used for the curing of the beam specimens:

- 72 hours curing at 40 ºC in the mould (top uncovered);
- After the first 24 hours removing the side frames of the mould (specimen remains on base plate).

The mixing-compaction-curing-testing cycle was carried out in batches one mix at the time. The time lag between end-of-curing and testing was kept as constant as practically possible and was specifically well controlled for the monotonic and resilient modulus tri-axial testing. Due to the longer duration of the tri-axial permanent deformation and four-point beam fatigue testing difference in this time lag of a number of days, but never exceeding one week, was inevitable.

No instrumentation was installed on the specimens, except for the resilient modulus testing. For this tests three on-specimen LVDT's were attached to the specimen using special clamps and a cement paste. The three LVDT's were positioned at 120º angles around the circumference to measure the displacement over the middle 80mm of the specimen. This is shown in Figure 65.

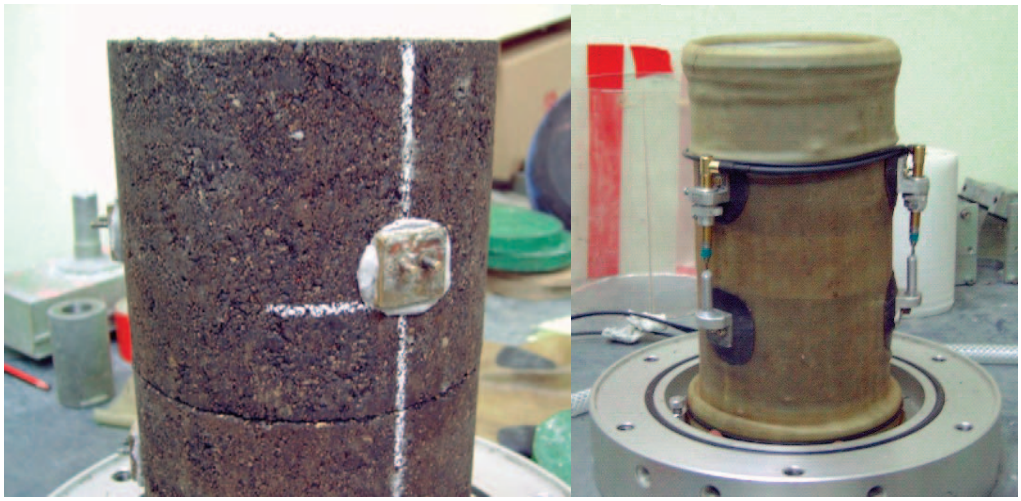

Figure 65: Tri-axial specimen for resilient modulus testing with clamps (left) and on-specimen LVDT's (right)

Details of all the specimens prepared pertaining to density levels and moisture content during testing are elaborately discussed by Jenkins and Ebels (2006). A summary is given in Table 25 – Table 27.

Table 25: Average moisture content of all tested specimens per mix and type of testing (absolute [%] / relative to O.M.C [%])

| Mix | Triaxial testing | | | Four-point beam testing | | |
|---|---|---|---|---|---|---|
| | $C$ and $\phi$ | $M_r$ | $N$ - $\varepsilon_p$ | $\varepsilon_b$ | $S_i$ | $N$ - $\varepsilon_t$ |
| A-75C-0 | 3.42 / 45 | 2.99 / 39 | 3.45 / 45 | not rec. | 0.70 / 9 | 0.76 / 10 |
| A-75C-1 | 3.25 / 43 | 3.44 / 45 | 3.84 / 51 | not rec. | 1.12 / 15 | 1.26 / 17 |
| A-75M-0 | 2.68 / 52 | 2.61 / 50 | 2.09 / 40 | not rec. | not rec. | not rec. |
| B-75C-0 | 4.60 / 61 | 3.17 / 42 | 2.78 / 37 | 0.6 / 8 | 0.4 / 5 | 1.2 / 16 |
| B-75C-1 | 3.45 / 45 | 3.21 / 42 | 3.08 / 41 | not rec. | not rec. | 0.8 / 11 |
| B-75M-0 | 2.84 / 55 | 2.54 / 49 | 2.16 / 42 | 1.2 / 16 | 1.2 / 16 | 1.1 / 14 |
| C-75C-0 | 2.17 / 29 | 3.44 / 45 | 2.69 / 36 | 0.4 / 5 | 0.4 / 5 | not rec. |
| C-75C-1 | 2.73 / 36 | 3.58 / 47 | 2.89 / 38 | 0.7 / 9 | 0.7 / 9 | 0.5 / 7 |
| C-75M-0 | 2.08 / 40 | 2.89 / 36 | 1.28 / 25 | 0.6 / 8 | 0.9 / 13 | 0.8 / 11 |

Table 26: Average bulk dry density of all tested specimens per mix and for tri-axial testing (absolute [kg/m$^3$] / relative to 100% Modified AASHTO density [%])

| Mix | Triaxial testing | | |
|---|---|---|---|
| | $C$ and $\phi$ | $M_r$ | $N$ - $\varepsilon_p$ |
| A-75C-0 | 2065 / 98.1 | 2090 / 99.2 | 2104 / 100.0 |
| A-75C-1 | 2096 / 99.6 | 2093 / 99.4 | 2091 / 99.3 |
| A-75M-0 | 2010 / 104.1 | 1996 / 103.4 | 1998 / 103.5 |
| B-75C-0 | 2095 / 99.5 | 2071 / 98.4 | 2149 / 102.1 |
| B-75C-1 | 2094 / 99.5 | 2072 / 98.4 | 2085 / 99.0 |
| B-75M-0 | 2025 / 104.9 | 2001 / 103.7 | 2043 / 105.9 |
| C-75C-0 | 2059 / 97.8 | 2041 / 97.0 | 2112 / 100.3 |
| C-75C-1 | 2097 / 99.6 | 2029 / 96.4 | 2106 / 100.0 |
| C-75M-0 | 1933 / 100.2 | 2007 / 104.0 | 2027 / 105.0 |

Table 27: Average bulk dry density of all tested specimens per mix and for four-point beam testing (absolute [kg/m$^3$] / relative to 100% Modified AASHTO density [%])

| Mix | Four-point beam testing | | |
|---|---|---|---|
| | $\varepsilon_b$ | $S_i$ | $N$ - $\varepsilon_t$ |
| A-75C-0 | not recorded | 2157 / 102.4 | 2168 / 103.0 |
| A-75C-1 | 2197 / 104.4 | 2167 / 102.9 | 2167 / 102.9 |
| A-75M-0 | not recorded | 1986 / 102.9 | not recorded |
| B-75C-0 | 2240 / 106.4 | 2332 / 110.8 | 2286 / 109.0 |
| B-75C-1 | 2224 / 105.7 | 2212 / 105.1 | 2219 / 105.4 |
| B-75M-0 | 2128 / 110.3 | 2153 / 111.6 | 2140 / 110.9 |
| C-75C-0 | 2052 / 97.5 | 2087 / 99.1 | not recorded |
| C-75C-1 | 2060 / 97.8 | 2101 / 99.8 | 2058 / 97.7 |
| C-75M-0 | 2009 / 104.1 | 2053 / 106.3 | 1998 / 103.5 |

## 4.5 Tri-axial testing

### *4.5.1 Hydraulic testing system*

The tri-axial testing was carried out on a hydraulic testing system (MTS 810, Model 318.10). This testing system is a closed loop servo-hydraulic testing press system. The system uses a MTS model 506.03 hydraulic power unit with a high pressure supply of approximately 70,000 kPa. It has a 10 metric tons actuator with 80 mm stroke (up and down). The MTS is operated and controlled by an MTS Controller 407.

The test data (load and displacement) of the monotonic and short duration dynamic tri-axial tests was captured by a computer program separately and independently from the control system while the tests are in progress. The test data of the long duration dynamic tri-axial tests was manually captured and read off from the MTS Controller 407.

The load and displacement test data of the load cell and MTS LVDT are amplified by the MTS controller to a +/- 10.0 V scale. The displacement data of the on-specimen LVDT's was amplified to a +/- 10.0 V scale by separate external amplifiers. The analogue voltage data was converted to digital data using a 12 bit A/D converter and captured by the computer in binary format. The fact that the converter uses 12 bits results in a counts scale of +/- 2048 (-2048 is -10.0 V and +2048 is +10.0 V). The data is captured using a Pascal written program and stores the data on the computer in ASCI format. This data file was further analysed using a spreadsheet programme.

The measuring range of the load cell and the MTS LVDT can be adjusted to suit the testing range. This is done by increasing or decreasing the gain for either of the measuring devices. Increasing the gain results in a smaller measuring range and therefore a higher accuracy.

For the monotonic tri-axial testing the load cell gain was set to measure over the full capacity (98.1 kN), while the LVDT gain was set to measure over 50 % of the full range (80mm). Because high loads are not required for resilient modulus and permanent deformation testing, the gain setting for the load cell was increased by a factor 5, which effectively reduces the measuring range of the load cell to +/- 19.6 kN.

The accuracy of the MTS build-in LVDT is not sufficient for resilient modulus testing. Therefore, to measure the dynamic displacements during testing, three LDVT's with a range of +/- 2.0mm, were fitted to the specimens, equally distributed around the circumference, to measure the displacements over the middle 80 mm of the specimen only. By doing so, side effects, such a displacement / movement of the loading plates, internal displacements of the tri-axial cell and edge effects of the specimens are excluded from the measured displacements. The manner in which the on-specimen LVDT's used were fitted to the specimens is discussed in Appendix D.

Although the accuracy of the MTS build-in LVDT is also not sufficient to measure the elastic strains during the permanent deformation testing, it is suitable to measure the accumulated plastic deformation.

The measuring scale setting of the load cell and MTS LVDT for the three types of tri-axial testing are summarised in Table 28.

Table 28: Scale settings of load cell and MTS LVDT for tri-axial testing

| Testing Mode | Range settings | |
|---|---|---|
| | Load cell | MTS LVDT |
| Monotonic testing to failure | 100% = +/- 98.1 kN | 50% = +/- 40 mm |
| Short duration dynamic testing | 20% = +/- 19.6 kN | not applicable |
| Long duration dynamic testing | 20% = +/- 19.6 kN | 10% = +/- 8 mm |

A triaxial cell manufactured by Wykeham-Farrance of the United Kingdom was used for the tri-axial tests. The pressure rating of this cell is 1,700 kPa. Samples with a maximum diameter of 150 mm can be accommodated. The maximum sample height in the cell is 280 mm, however, for practical reasons sample heights were being limited to between 250 m and 260 mm.

As discussed in Chapter 2, no friction reduction between the specimen and the loading plates was applied in this study due to the problems of this system associated with the granular nature of the specimens. The friction between the specimen and loading plate was however kept as constant as possible by thoroughly cleaning the loading plates after each tests and ensuring the same conditions at the start of every new test.

The MTS system is situated in a climate chamber where the temperature can be controlled between 0 ºC and 60 ºC. All tri-axial tests were however conducted at 25 ºC. This is believed to be a representative temperature for BSM's in base layers in South Africa. Investigations by Moloto (to be published 2008) have shown that during the coldest month (July) the base temperature varies between 10 and 20 ºC, while during November (summer) temperatures between 20 and 35 ºC were found.


Figure 66: Tri-axial cell (left), control unit (middle) and MTS 810 in climate chamber (right)

### *4.5.2 Monotonic tri-axial test – shear parameters*

All tri-axial testing of the specimens commenced within 48 – 72 hours after completion of the curing. This delay was kept constant for all mixes. The monotonic tri-axial test is a fairly short test and all specimens were tested on the same day.

The monotonic tri-axial tests were carried out at 25 °C and the specimens were overnight conditioned at this temperature. The test is performed with a controlled constant strain rate of 2.6 % per minute. For a typical height of 260 mm this results in 6.76 mm per minute. This strain rate has in the past been used for numerous monotonic tri-axial tests in South Africa and in order to eliminate any possible variables in the comparison of the results of this study with that of other studies, the same strain rate was adopted here.

Confinement pressure was provided by regulating the air pressure in the tri-axial cell. A set of four monotonic tri-axial tests were carried out over a range of confinement pressures. The confinement pressures at which the tests were carried out were:

- 25 kPa;
- 50 kPa;
- 100 kPa; and
- 200 kPa.

Due to limitations of the on-specimen instrumentation, radial expension could not be measured during the tri-axial testing. Therefore the effect of dilatation could not be accounted for.

The type of failure observed in the BSM specimens is somewhere between that what is typical for HMA and granular materials. HMA specimens generally show a distinct and well defined shear plane. The BSM specimens failed in a shear “band”, having the same angle of approximately 45º with the vertical axis. Shear failure of BSM specimens does however not result in complete disintegration, which is typical for granular specimens.

Immediately after completion of a set of monotonic tests (one series with four different confinement pressures) the tested specimens were broken up and a sample for the determination of the moisture content was taken from the middle of the specimens.

### *4.5.3 Dynamic tri-axial test – resilient modulus*

Two dynamic tri-axial tests were done for each of the nine mixes. Due to the nature of the test preparation, these two tests cannot be performed on the same day. They were therefore performed on two consecutive days. In doing so the delay between completion of curing and testing was kept constant as much as practically possible.

The dynamic tri-axial tests were also carried out at 25 ºC. The deformation in the specimen was measured by an external system of on-specimen LVDT’s and amplifiers. The loading consisted of a continuous haversine load with a pre-load of

20 kPa applied with frequency of 2 Hz. No rest period was included in the loading. The resilient modulus determined in this study is therefore an instantaneous resilient modulus.

During the dynamic tri-axial test the response of the specimen to different levels of loading at a range of confinement pressures is measured. These confinement pressures are the same as used during the monotonic testing. The load level during the dynamic tri-axial test is described by the deviator stress ratio. This is the ratio between the applied deviator stress and the deviator stress at failure:

$$Stress\ Ratio\ (S.R.) = \frac{\sigma_{d,a}}{\sigma_{d,f}} \qquad \text{Eq. 40}$$

where $\sigma_{d,a}$ = applied deviator stress
$\sigma_{d,f}$ = deviator stress at failure

The latter is derived from the cohesion and friction angle as determined by the monotonic tri-axial testing. The confinement pressures and deviator stress ratios at which the resilient moduli are determined are summarised in Table 29.

Care was taken not to overstress the specimens at the lower confinement pressures and therefore the resilient modulus testing at the 25 kPa and 50 kPa confinement pressure was limited to deviator stress ratios of up to 0.30 and 0.35 respectively. Only when the permanent deformation in the specimen was limited, resilient moduli data could be sampled at the high deviator stress ratios of 0.50 and 0.60 at 200 kPa confinement pressure.

Table 29: Confinement pressures and deviator stress ratio's

| Confinement pressure | 25 kPa | 50 kPa | 100 kPa | 200 kPa |
|---|---|---|---|---|
| Deviator stress ratio | 0.10 | 0.15 | 0.15 | 0.15 |
| | 0.15 | 0.20 | 0.20 | 0.20 |
| | 0.20 | 0.25 | 0.25 | 0.25 |
| | 0.25 | 0.30 | 0.30 | 0.30 |
| | 0.30 | 0.35 | 0.35 | 0.40 |
| | | | 0.40 | 0.50 |
| | | | | 0.60 |

Before the actual sampling of test data, the specimen was subjected to 10,000 conditioning cycles at the lowest confinement pressure (25 kPa) and at a deviator stress ratio of 0.30. There are indications that the stiffness of previously unloaded BSM specimens reduces during the initial stages of loading and that the stiffness stabilises after a certain number of initial load repetitions. The number of conditioning cycles used in this study was chosen high to ensure that all initial stiffness reduction and settlement had taken place. The number of 10,000 may be too high for production testing and could possibly be reduced. This would however require further testing and investigation.

The load and displacement data was sampled at a frequency of 1000 Hz for a duration of 5 seconds. Prior to the data sampling the specimen was subjected to 120 load cycles at each deviator stress ratio.

For each test a plot of the load signal and the displacement signal of each of the three on-specimen LVDT's was made. The sampling duration of 5 seconds results in the data of 10 cycles being captured. For each cycle the amplitude of the load signal and for each of the three displacement signals can be determined by calculating the difference between the minimum and the maximum value during one cycle. A typical plot of a loading cycle is shown in Figure 67.

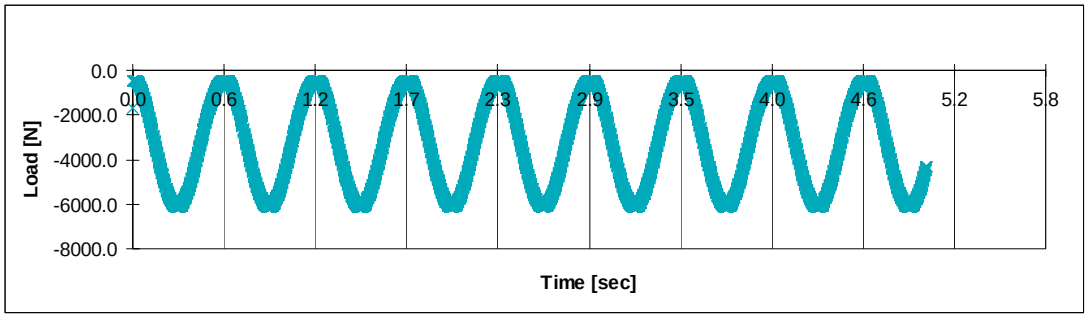


Figure 67: Load signal B-75C-0, 100 kPa and deviator stress ratio of 0.15

The signal from the three on-specimen LVDT's had in some cases a considerable amount of 'noise', which necessitated filtering, while 'spikes' also occurred in the signals of some of the LVDT's. Examples of the noise on the signal and spikes are shown in Figure 68 and Figure 69 respectively. The noise and spikes on the signal occurred consistently throughout all tests and are not test or specimen related. The noise and spikes did not influence the loading of the specimens, nor the actual deformation. The cycles that contained spikes were not included in the analysis and determination of the resilient modulus and do therefore not influence the results.

The filtering of the LVDT signal was done by comparing the measured value with a predicted value obtained by straight line extrapolation of the preceding 10 measured values. The degree of filtering was per test adjusted until a visibly acceptable signal was obtained (on a larger scale than the one shown in Figure 68).

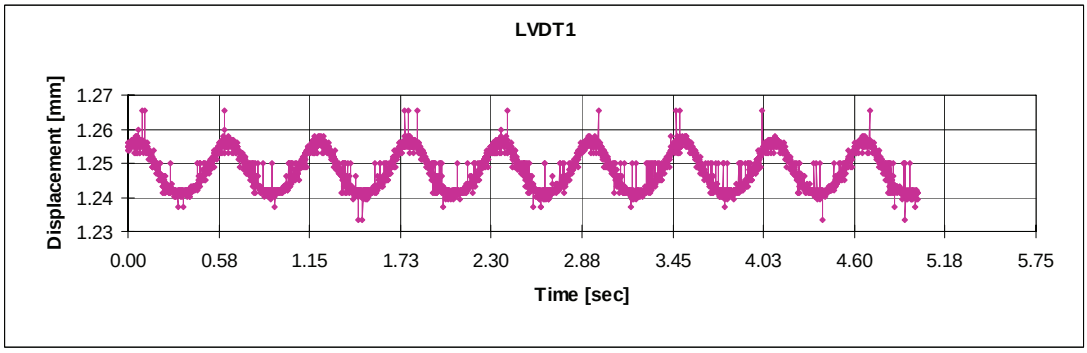


Figure 68: LVDT1 signal B-75C-1 with noise, 100 kPa and stress ratio of 0.20

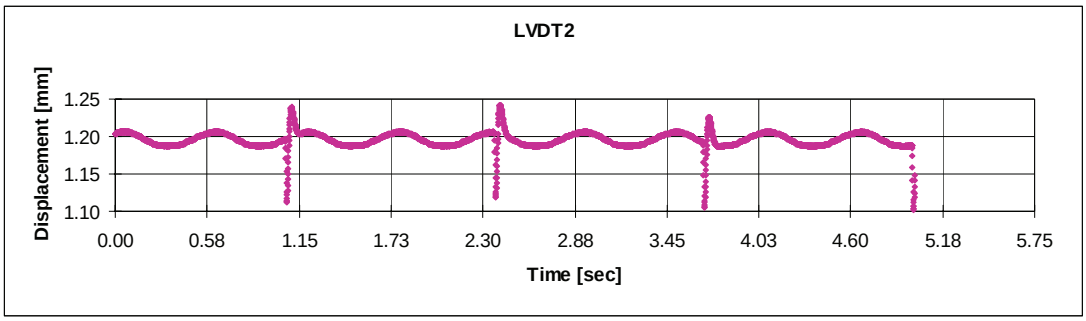


Figure 69: LVDT2 signal B-75C-1 with spikes, 100 kPa and stress ratio of 0.20

For each analysed cycles a resilient modulus was determined by:

$$M_r = \frac{\sigma_{corr}}{\varepsilon_a} \qquad \text{Eq. 41}$$

with

$$\sigma_{corr} = \sigma \cdot (1 - \varepsilon_a) \qquad \text{Eq. 42}$$

where $\sigma_{corr}$ = corrected stress [MPa]
$\varepsilon_a$ = average axial strain measured by the three LVDT's [m/m]

Equation 42 was proposed by Maree (1979) to approximate the influence of radial expansion in the absence of measured radial expansion data and the corrected stress was used here in the calculation of the resilient modulus. The radial expansion of the specimen during testing effectively reduces the stress as a result of an increased area. The resilient modulus reported is the average of the resilient moduli for each of the sampled and analysed cycles.

### *4.5.4 Repeated load tri-axial test – permanent deformation*

4.5.4.1 Test conditions and measurements

As for the first two types of tri-axial tests, the permanent deformation tests were also started within 48 to 72 hours after completion of the curing process. However, these tri-axial tests are of long duration, whereby, depending on the performance of the specimen, a test can last up to one million load repetitions or 6 days. Typically all four tests on one mix can be completed in 10 – 14 days. The permanent deformation test runs continuously around the clock until failure of the specimens occurs.

The permanent deformation tests were also performed at 25ºC. The load signal is the same as with the resilient modulus testing, *i.e.* a haversine load with a pre-load of 20 kPa applied at a frequency of 2 Hz. The confinement pressure for all permanent deformation testing was kept constant at 50 kPa. This is in line with previous research carried out. The confinement pressure was not a variable in this study. The

effect of varying confinement pressure has been identified as an area that requires further investigation.

Due to geometric limitations of the tri-axial test set-up at the Stellenbosch University (SU) is was not possible to test at higher frequencies because of dynamic effects. In the SU set-up not the loading piston is moved up and down from the top against the reaction of a fixed tri-axial cell, but the tri-axial cell is moved up and down from the bottom against the reaction of the fixed loading piston. This is because the actuator is situated below the tri-axial cell. The permanent deformation tests were continued to either 4% total plastic strain or 1 million load repetitions, whichever came first.

For each mix, four permanent deformation tests were performed, each at a different deviator stress ratio. The deviator stress ratios at which the tests were performed were determined as the series of tests progressed. The objective of the testing was, *inter alia*, to determine which deviator stress ratio is the critical stress ratio.

Specimens subjected to a stress ratio higher than the critical stress ratio will show an accelerating rate of plastic strain accumulation towards the end of the test. Specimens subjected to a stress ratio lower than the critical stress ratio typically shows an ever decreasing rate of plastic strain accumulation resulting in a stable condition until the end of the test (1 million load repetitions).

Typically, the applied stress ratios were chosen to first obtain a test result at a stress ratio well above and one well below the critical stress ratio. The stress ratios for the two remaining tests were chosen approximately around the critical stress ratio.

The total plastic strain was recorded manually by reading off the MTS actuator position at the start of the test and after certain intervals of load repetitions. In order to be able to read off the actuator position during a running test, the cyclic loading was interrupted, whereby the loading applied to the specimen returns to a constant load equal to the dynamic load, but with zero amplitude. This load level was the same each and every time the cyclic loading was interrupted in order to take a reading.

In the early stages of a permanent deformation test the measurement intervals were short, but as the rate of permanent deformation accumulation decreases, these intervals were increased. Typically measurements were taken at 0, 20, 50, 100, 200, 500, 1 000, 2 000, 5 000, 10 000, 20 000, 50 000, 100 000 load repetitions and thereafter twice a day. When it was observed that a specimen started to fail (increase in rate of permanent deformation) the intervals were again shortened.

The displacement after 20 load repetitions was taken as zero-reference ($u_0$) to allow for setting in of the specimen, base and loading plate. The accumulated plastic strain after a certain number of load repetitions is calculated as:

$$\varepsilon_i = \frac{u_i - u_0}{h} \qquad \text{Eq. 43}$$

where $\varepsilon_i$ = plastic strain after $i$ load repetitions
$u_i$ = actuator displacement after $i$ load repetitions [mm]
$h$ = height of the specimen [mm].

4.5.4.2 Method for determining of model parameters and coefficients

A combination of both linear and non-linear regression was used to determine the model parameters A, B, C and D. The procedure as discussed below was followed.

1. Plot the PD curve on a log-log scale;
2. Cancel out to a large extent the effect of the primary bedding-in phase by only evaluating the data from N = 1,000 onwards;
3. Determine the flow point (N = $N_{flow\ point}$). This is where the slope of the PD curve is minimal. The flow point marks the transition from linear to non-linear behaviour and was determined as the number of load repetitions with the lowest strain accumulation rate;
4. Perform a linear regression on the data between N = 1,000 and N = $N_{flow\ point}$, which yields the model parameters A and B;
5. Determine the residual value of $C \cdot \left( e^{D \cdot \frac{N}{1000}} - 1 \right) = \varepsilon_p - A \cdot \left( \frac{N}{1000} \right)^B$. An example of this residual value is given in Figure 70;
6. Perform a non-linear regression on this residual over the full data range (N = 1,000 to N = $N_f$), which yields the model parameters C and D. A Matlab procedure was developed to perform this non-linear regression

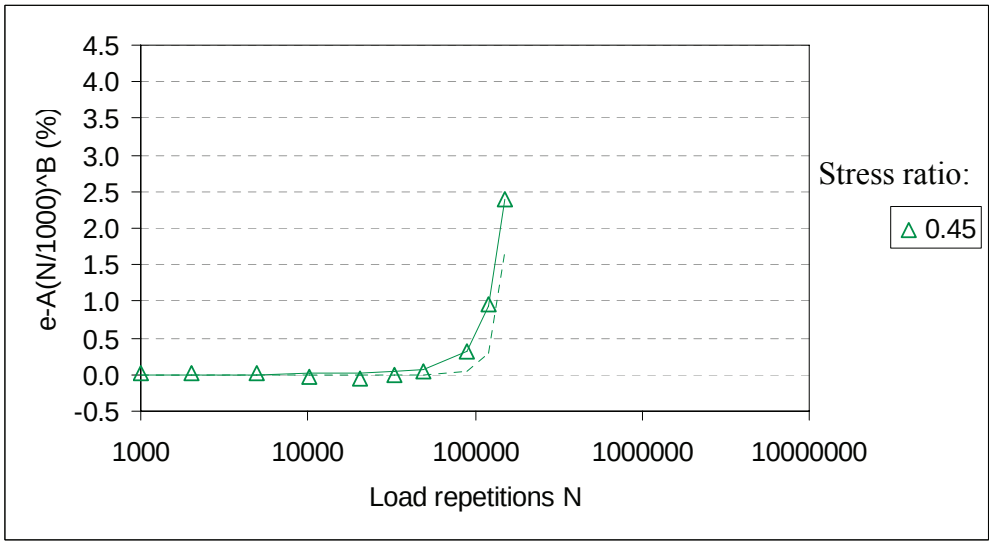


Figure 70: Example of residual value C · (exp(D·N/1000)-1), mix A-75C-1

The above procedure yields the model parameters A, B, C and D for each PD curve. The stress dependency of each mix can be illustrated by plotting the values of the model coefficients against the different deviator stress ratio used for that particular mix. An example of this stress dependency is given in Figure 71. For each of the nine

mixes tested this stress dependency can be quantified by determining the model coefficients $a_1$, $a_2$, $b_1$, …, $d_2$ of the General Permanent Deformation Law (see Chapter 3) using non-linear regression. It was however found that the stress dependency of the two emulsion mixes (Emulsion A and Emulsion B) form part of the same trend in stress dependency. This is also illustrated by Figure 71, but better by Figure 72.

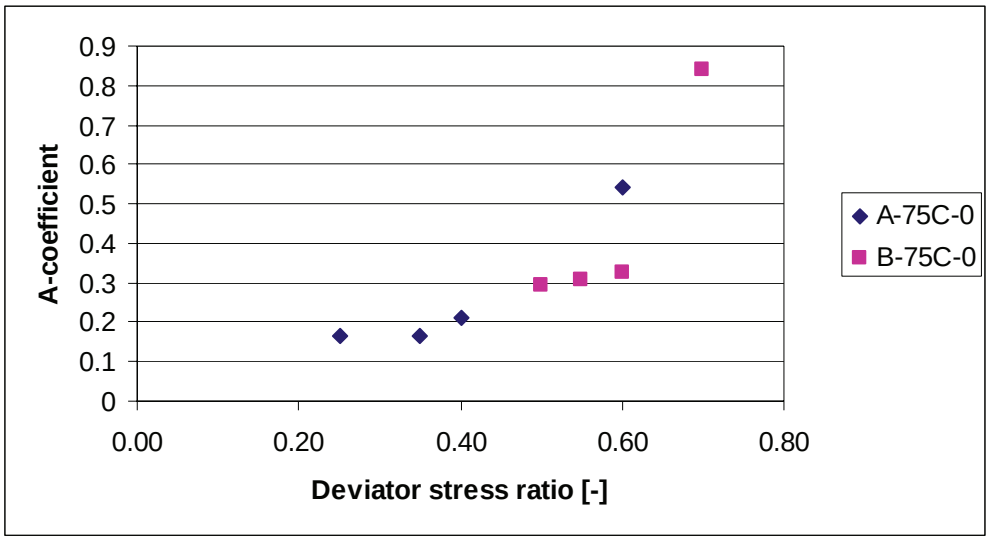


Figure 71: Stress dependency of model parameter A for mixes A- and B-75C-0

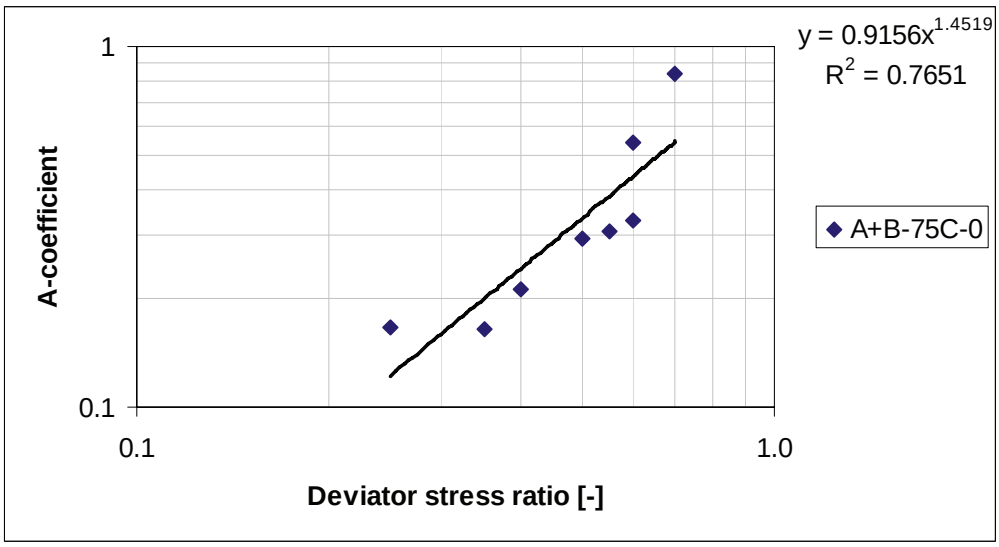


Figure 72: Combined trend in stress dependency of model parameter A for mixes A- and B-75C-0 (log-log scale)

## 4.6 Four-point beam testing

### *4.6.1 Four-point beam testing apparatus*

The four-point beam testing apparatus used for all four-point bending beam testing was the Beam Fatigue Apparatus (BFA) manufactured and supplied by IPC Global, Australia. The apparatus is designed to perform the AASHTO Standard T321 beam fatigue test.

The BFA consists of a stand-alone testing unit that incorporates a testing rig, a 5 kN actuator, an actuator LVDT with a span of 5 mm and an on-specimen LVDT with a span of 1.0 mm. The BFA also has a closed-loop feedback system and the actuator is operated by a pneumatic servo-valve (operating pressure approximately 700 kPa). The BFA is controlled and operated through a CDAS (control and data acquisition system). The user interface is provided in the form of UTM software on a personal computer. The load cell and the LVDT's have in-line amplifiers and are calibrated during manufacturing. Their settings can therefore not be adjusted by the user. The data storage takes place by the UTM software.

The BFA is located in a climate chamber where the temperature can be controlled between 0 ºC and 50 ºC. Both the monotonic and the long duration dynamic loading four-point beam tests were carried out at 5 ºC. For the short duration dynamic loading the temperature was varied.

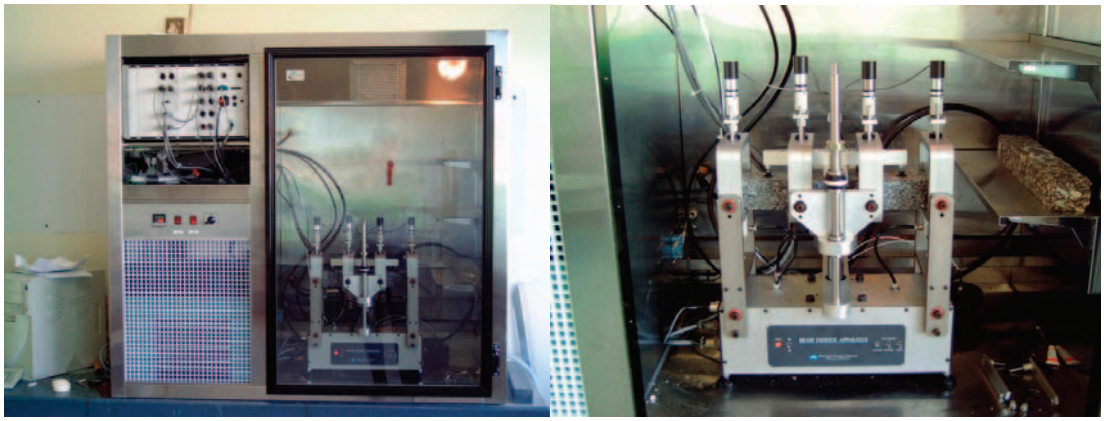

Figure 73: Climate chamber with CDAS (left) and beam fatigue apparatus (right)

The need for clean and dry air to be used for testing became evident when tests were conducted at low temperatures (5 ºC). The moisture vapour in the air supply condensed against the cold metal mechanical part of the servo valve. Permanent damage to the pneumatic servo valve occurred as a result of this condensation as well as due to shortcomings in the design of the seal between the mechanical and electrical part of the servo valve.

### *4.6.2 Monotonic four-point beam test – strain-at-break*

The BFA was developed with the aim of performing the fatigue test (long duration dynamic loading). This requires only sinusoidal loading. Similar dynamic loading is also applied during the bending beam stiffness determination (master curves), during

which frequency-temperature sweep tests are performed. Both these tests, *i.e.* short and long duration dynamic loading for stiffness and fatigue behaviour respectively, can be performed using the standard UTM software (UTM21) that is supplied with the BFA.

The strain-at-break test however, makes use of a monotonic or ramp load. The UTM21 V1.05 software does not cater for this type of loading or test. However, by using the UTM12 software as user interface and adjusting the testing rig slightly, monotonic ramp loading tests could be performed in the BFA set-up. This adjustment consisted of adding 5mm spacers to the reaction frame clamping system, which lifted the level of the beam by 5mm. This created sufficient span (10mm) to perform a downward monotonic ramp loading failure test.

The strain-at-break four-point beam tests were conducted at 5 ºC and a loading rate of 1.0 mm/min (0.0167 mm/sec). This loading rate was chosen in order to obtain results that would be comparable to strain-at-break testing that has been carried out in South Africa previously by the CSIR. A detailed description of the test method and test protocol is given by Twagira (2006).

The measurement data from the strain-at-break test which is captured using the UTM12 software requires additional formatting of the captured data using a spreadsheet program. The data file created by the UTM12 software is in a format that can only be read by the UTM12 software itself. It can however be exported to a comma separated values file (.csv) that in turn can be imported into a spreadsheet program for further processing.

Of the two LVDT's fitted on the IPC four-point beam apparatus, *i.e.* the on-specimen and actuator LVDT's, only the actuator LVDT has sufficient span (+/- 5.0 mm) to capture data. The on-specimen LVDT with a span of +/- 0.5 mm goes out of range during the strain a break test and loses contact with the specimen. The actuator LVDT data is therefore used to determine the strain-at-break. However, the formula to calculate the strain from the displacement requires input from the on-specimen LVDT. It is therefore necessary to convert the actuator LVDT readings into equivalent on-specimen LVDT readings and use these converted values to determine the strain.

The displacement of the on-specimen LVDT and actuator LVDT can be plotted against each other and a straight line correlation in the form of $y = ax + b$ can be determined for that part of the deformation where the on-specimen LVDT is measuring in range. This is done for every single test and because of the influence of the specimen geometry, the correlation values $a$ and $b$ vary slightly per test. For the conversion of the actuator displacement to the on-specimen LVDT displacement the following factors $a$ and $b$ were used:

Table 30: Conversion factors actuator LVDT to on-specimen LVDT

| Aggregate Blend | Binder type | | | | | | | | |
|---|---|---|---|---|---|---|---|---|---|
| | A | | | B | | | C | | |
| | beam | a | b | beam | a | b | beam | A | b |
| 75C-0 | F1 | 0.2880 | 0.0102 | C1 | 0.5674 | 0.0010 | C2 | 0.5875 | 0.0084 |
| | F2 | 0.5695 | 0.0109 | C5 | 0.5934 | -0.0102 | C5 | 0.5938 | 0.0035 |
| | F3 | 0.5444 | 0.0118 | C6 | 0.6042 | -0.0026 | C6 | 0.6573 | 0.0064 |
| 75C-1 | D1 | 0.5645 | 0.0062 | D1 | 0.6156 | -0.0145 | C1 | 0.5490 | -0.0039 |
| | D2 | 0.3462 | 0.0162 | D3 | 0.7214 | -0.0243 | C3 | 0.7070 | -0.0211 |
| | D3 | 0.5678 | -0.0019 | D4 | 0.5693 | 0.0063 | C5 | 0.5380 | -0.0020 |
| | - | - | - | - | - | - | C6 | 0.5915 | -0.0037 |
| 75M-0 | Y5 | 0.6194 | -0.0021 | C1 | 0.5807 | -0.0057 | B1 | 0.6131 | -0.0037 |
| | Z2 | 0.5990 | 0.0029 | C2 | 0.6117 | -0.0112 | B2 | 0.6084 | -0.0182 |
| | Z3 | 0.6044 | 0.0076 | C5 | 0.7236 | -0.0363 | B3 | 0.5780 | -0.0018 |
| | - | - | - | C6 | 0.6340 | -0.0135 | - | - | - |

The strain-at-break ($\varepsilon_b$) is subsequently determined using the following formula (IPC, 2003):

$$\varepsilon_b = \frac{12 \times (a \cdot \delta_c + b) \times h \times 10^6}{3 \times G_o^{\,2} - 4 \times G_i^{\,2}} \qquad \text{Eq. 44}$$

where
$\varepsilon_b$ = strain-at-break [με]
$a,b$ = conversion factor shown in Table 30
$\delta_c$ = peak deflection at centre of the beam [mm]
$h$ = average height of the beam [mm]
$G_o$ = distance between the outer clamps (355.5 mm)
$G_i$ = distance between the inner clamps (118.5 mm)

This formula for the calculation of the strain is based on linear elastic theory. The actual strain may differ slightly from this.

The applied force is plotted against the actuator displacement. The applied failure load is taken as the peak load during the test. Because the recorded load is not a continuous smooth curve, but rather a band of measurement values with some variation and scatter, the visually determined average peak load is taken as the applied failure load. The actuator displacement ($\delta_c$) at which the peak loading occurs is visually determined and used to determine the strain-at-break.

The peak load measured during the strain-at-break test can be converted to maximum tensile stress $\sigma_t$ at the bottom of the beam (in the middle of the beam) using the following formula (IPC, 2003):

$$\sigma_t = \frac{G_o \times P}{w \times h^2} \times 10^6 \qquad \text{Eq. 45}$$

where
$\sigma_t$ = maximum tensile stress [kPa]
$G_o$ = distance between the outer clamps (355.5 mm)
$P$ = peak load [kN]
$w$ = average beam width [mm]
$h$ = average height of the beam [mm]

### *4.6.3 Dynamic testing – haversine vs. sinusoidal loading*

All dynamic four-point beam testing discussed in this study was carried out using a displacement controlled haversine loading wave. The haversine wave loading is the standard loading form prescribed in the AASHTO Standard T321 (formerly AASHTO TP8) based on work carried out for the Strategic Highway Research Program (SHRP). Haversine loading was adopted in this study because it was a requirement in the research project carried out by the Stellenbosch University for a United States client, a project which forms an integral part of this study.

There is general debate amongst researchers about the fact whether truly haversine loading can be applied to visco-elastic materials in a beam fatigue test. At the beginning of a displacement controlled beam fatigue test on hot-mix asphalt both the displacement and load signal are of a haversine shape. Pronk and Erkens (2001) however, stated that after only a few load cycles (within the first five on the material they tested), the load signal would change into a pure sinusoidal signal, while the displacement signal would retain its haversine shape.

They believe this to be the result of viscous deformation of the material or accumulation of residual strains occurring in the beam. As a result of this the shape of the beam (and the neutral axis) changes thereby from straight prior to loading to slightly bent during the running of the test. Consequently, the peak-to-peak strain of the sinusoidal displacement signal of the bent beam after a few load cycles would be equal to half the peak-to-peak strain of the specified haversine displacement signal of the straight beam at the beginning of the fatigue test.

Pronk and Erkens (2001) concluded that it is not possible to subject a beam of visco-elastic material to dynamic loading of a pure haversine shape. After only a few load repetitions a new equilibrium would be reached whereby the load signal has changed into a pure sinusoidal shape and whereby the peak-to-peak strain of the displacement signal has reduced to half the value of the specified strain amplitude.

They carried out a limited number of beam fatigue experiments, comparing specified sinusoidal loading with specified haversine loading of double the amplitude. In theory these two types of specified loading shapes should yield the same results. For the one mix tested (ACRE) this was experimentally found to be true. For another mix however (half-warm STAB), a better fatigue resistance was found when tested using a haversine loading signal. The experimental results of Pronk and Erkens were thus to a certain extent inconclusive and appear to be related to the type of material tested.

It is postulated here that materials with a high degree of visco-elasticity would be more prone to creep of the neutral axis occurring during fatigue testing than more pure elastic materials. The experimental testing of Pronk and Erkens (2001) was carried out at a temperature of 20ºC. At this temperature the response of hot-mix asphalt is more viscous than at lower temperatures. It would have been possible that they would have found larger differences between sinusoidal loading and haversine loading of twice the amplitude had the experimental testing been carried out at a lower temperature, *i.e.* with less viscous deformation of the beam.

The beam fatigue testing in this study was carried out a 5ºC, which would result in a less visco-elastic response of the material and a larger difference between sinusoidal loading and haversine loading of twice the amplitude. Over and above that, it is shown later on in this study that the viscous part of the stiffness (loss modulus) of the BSM mixes tested here is less than for hot-mix asphalt. This would result in a longer creep time of the neutral axis and even larger differences between sinusoidal loading and haversine loading of twice the amplitude compared to hot-mix asphalt.

The strain levels reported in this study are the specified strain amplitudes for a haversine loading signal. A limited evaluation of the load response during displacement controlled fatigue testing shows that creep of the neutral axis does occur in the BSM beam specimens. This evaluation consisted of analysing the maximum upward and downward force required to induce the haversine displacement for selected beam fatigue tests. If no viscous deformation of the neutral axis occurs and the load signal remains a haversine shape, the required downward force would be in excess of the required upward force. In case during the test the shape of the neutral axis does change from straight to slightly curved, and the loading signal changes to a pure sinusoidal signal, the downward force should be similar to the upward force.

There are indications that the load response of the BSM mixes tested in this study changes from haversine to sinusoidal during fatigue. Unlike HMA materials, where a change from haversine loading to sinusoidal loading takes place almost immediately, it takes longer for BSM materials to reach a new equilibrium. This is illustrated by Figure 74, in which it can be seen that after 10 load cycles the downward force is higher than the upward force and that the magnitudes of the downward and upward forces change relatively to each other. A new equilibrium is reached after approximately 100 load repetitions. The difference between the downward and upward force might have been larger during the first 10 load cycles, but unfortunately no data was sampled before the $10^{th}$ load repetition. The equilibrium that is reached is typical of a sinusoidal load response. The constant difference between the upward and downward force is believed to be the results of the dead weight of the beam and that part of the testing rig that moves up and down with the beam during testing.

This behaviour was observed for all fatigue tests analysed, but the rate of change from a haversine load shape to a sinusoidal load shape differs per mix and per applied strain level. This is illustrated by Figure 75, which is the same mix as shown in Figure 74, save for the fact that 1% of cement was added to the mix. This mix has

a stiffer and more elastic response. It can be seen that a new equilibrium is only reached after close to 10,000 load repetitions.

Unfortunately no experiments could be carried out whereby beams of the same mix would be subjected to both sinusoidal loading and haversine loading of twice the amplitude in order to establish a relation between the responses to these two different loading types. The fact that this relation would differ per mix and per strain level would require a comprehensive experiment.

It is therefore at this stage not possible to make any quantitative judgement on what the performance of the mixes, tested in this study with haversine loading specified, would be in case they would have been loaded with a specified sinusoidal load shape. It would however be incorrect to assume that the fatigue performance of the mixes tested with haversine loading specified would be equal to the performance with sinusoidal loading with half the strain amplitude. Due to the time required for the loading signal to change from haversine to sinusoidal (eg. see Figure 75), this would result in an underestimation of the actual fatigue life of the material.

It is however evident that a shift from haversine to sinusoidal loading is taking place when BSM beams are subjected to a four-point beam bending test (as shown in Figure 74 and Figure 75). Following this, it can be concluded that the actual applied strain reduces as the fatigue test progresses. Therefore, the fatigue lives as reported in this study are an overestimation of the actual fatigue performance of the material at the specified haversine strain levels. The fatigue lives as reported in this study should therefore be associated with a lower strain level that is somewhere between the initially applied haversine strain and the eventual sinusoidal strain at the end of the test, *i.e.* 50% of the initially applied haversine strain, The reduction from the specified haversine strain to the lower actual strain depends on the type of mix as well as the specified test strain level.

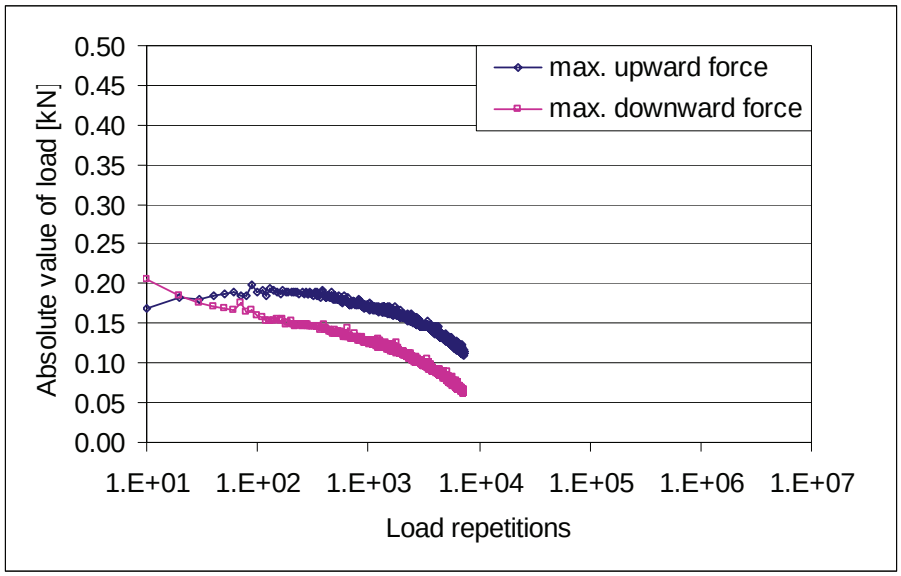


Figure 74: Maximum forces during beam fatigue testing (Mix A-75C-0, 5ºC, 10 Hz, specified haversine displacement of 370 με)

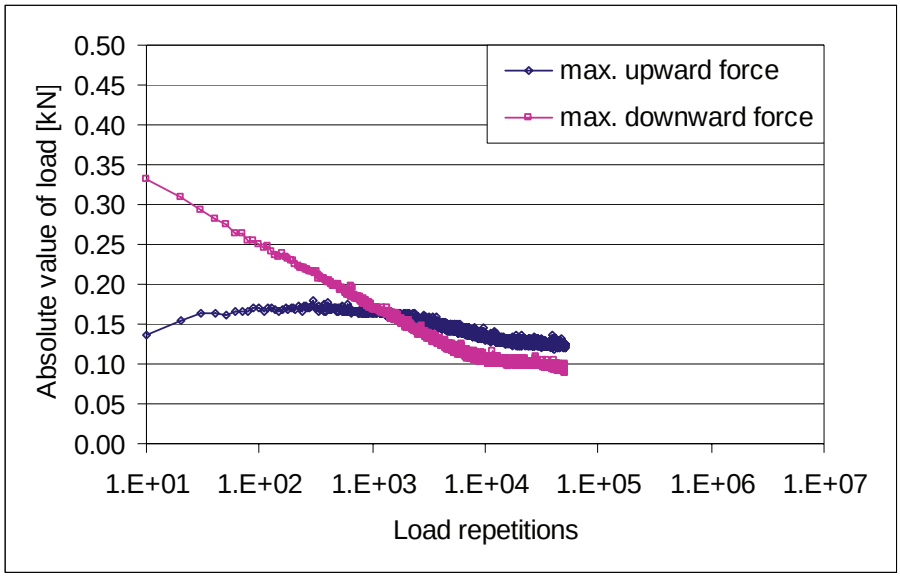


Figure 75: Maximum forces during beam fatigue testing (Mix A-75C-1, 5ºC, 10 Hz, specified haversine displacement of 400 με)

In order to prevent similar problems with future four-point beam testing of materials that exhibit visco-elastic behaviour it is recommended to only apply sinusoidal loading. Haversine type loading should not be considered for these types of materials.

### *4.6.4 Dynamic four-point beam test – stiffness master curves*

The frequency-temperature sweep testing in order to develop a master curve is a standard dynamic test of short duration in the BFA set-up.

The loading consist of a displacement controlled haversine wave at a strain level of 70 micron. The type of loading selected for the flexural stiffness master curve testing was the same type of loading as used for the fatigue testing, with the latter being the prescribed loading type in ASTM T321. The frequency-temperature sweep is performed according to the matrix shown in Table 31. The numbers in the cells of the matrix indicate the order in which the tests are performed. The frequency sweeps were performed at each of the five temperatures, starting with the highest frequency and lowest temperature. The load duration was 300 cycles. The UTM21 beam fatigue program was used to control the test and capture the data.

Table 31: Order of testing temperature-frequency sweep

| Temperature [ºC] | Frequency [Hz] | | | | |
|---|---|---|---|---|---|
| | 0.5 | 1.0 | 2.0 | 5.0 | 10.0 |
| 5 | 5th | 4th | 3rd | 2nd | 1st |
| 10 | 10th | 9th | 8th | 7th | 6th |
| 15 | 15th | 14th | 13th | 12th | 11th |
| 20 | 20th | 19th | 18th | 17th | 16th |
| 25 | 25th | 24th | 23rd | 22nd | 21st |

Prior to the first frequency sweep, the specimen were conditioned overnight at 5 ºC. The frequency-sweep tests at one temperature are performed with approximately 5 minutes relaxation time between the frequencies. After the temperature was raised by 5 ºC, the specimen was left to adjust to the new increased temperature for approximately 5 hours. The total temperature-frequency sweep test on one beam specimen therefore takes 2 to 3 days.

In the UTM21 software, the flexural stiffness after 50 load cycles is automatically recorded. However, because of the variation in stiffness per load cycle, an average flexural stiffness after 50 load cycles was determined based on a regression analysis of the first 300 cycles. This was done by exporting the measurement data to a comma separated values (.csv) file and import it into a spreadsheet program. The stiffness was then plotted against the number of load repetitions and a power-function in the form of $S_i = a\ x_i^{\ b}$ was fitted to the data, where $S_i$ is the flexural stiffness after $i$-number of load repetitions and $a$ and $b$ and model coefficients.

The obtained stiffness measurements were averaged for the two repeat tests for each temperature and frequency combinations. When the series of stiffness per temperature are plotted against the frequency a number of more or less parallel curves are obtained as shown in Figure 76.

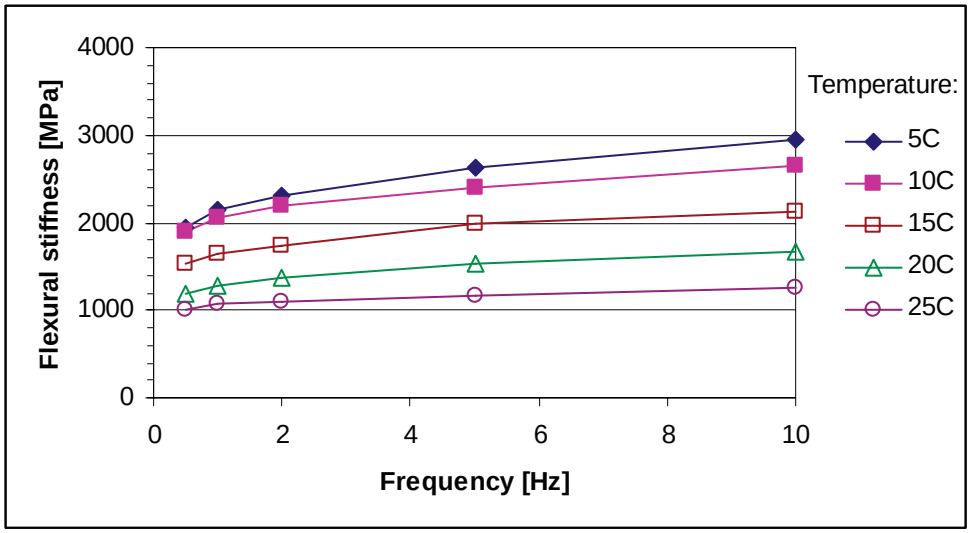


Figure 76: Example of flexural stiffness curves per temperature (A-75C-0)

The curves in the above figure were shifted horizontally to form an isotherm. In this study the 20 ºC isotherm is used and the Arrhenius type equation was used to reduce the frequency as described in Chapter 3.

### *4.6.5 Phase angle determination*

As mentioned previously, the UTM21 V1.05 software was used as user interface for the four-point beam testing. The phase angle output as calculated by this version of the software was however erroneous and unreliable. This is illustrated by Figure 77, which shows the highly variable and even negative phase angles. The latter is physically impossible.

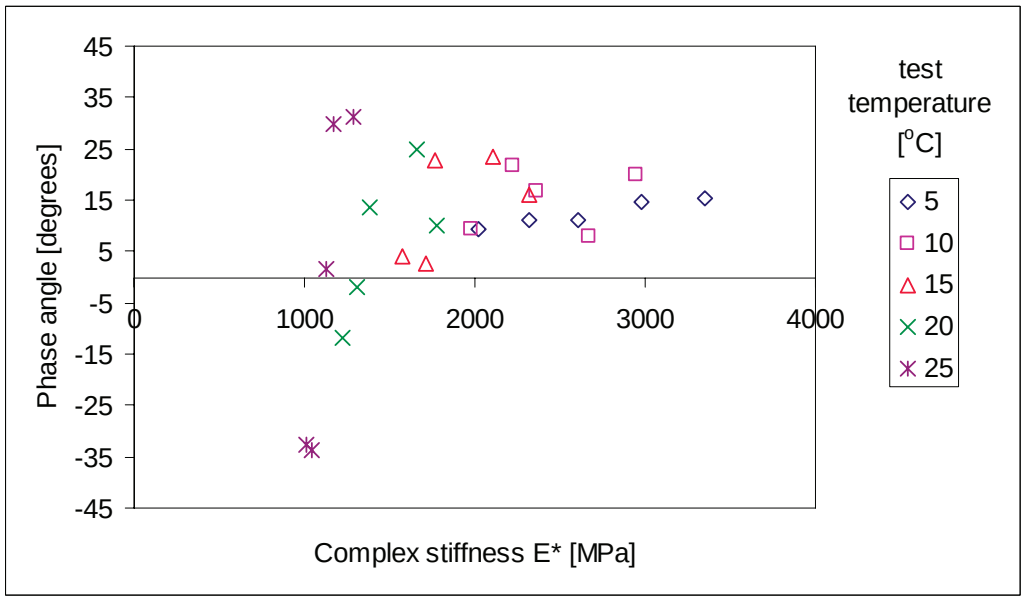


Figure 77: Incorrect phase angle output of the UTM21 V1.05 software (A-75C-0 beam E5)

Two alternative methods were explored to determine the phase angle, *viz*:

- Reading off the time lag between zero-crossings of the load and displacement signal of a single load cycle from the UTM21 generated plot (see Figure 78);
- Exporting the load and displacement data of a single loading cycle to a spreadsheet application and fit sinusoidal curves to the data, from which the peak-to-peak time lag can be calculated (see Figure 79).

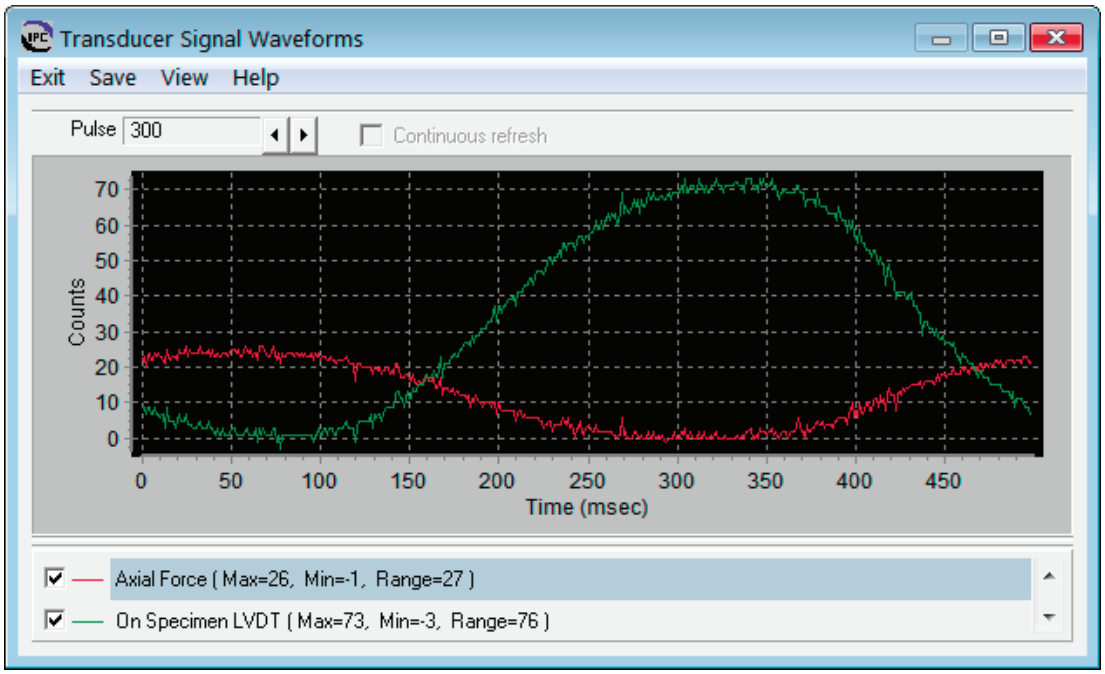


Figure 78: UTM21 load and displacement signal waveforms (C-75C-1, 5ºC, tested at 2 Hz)

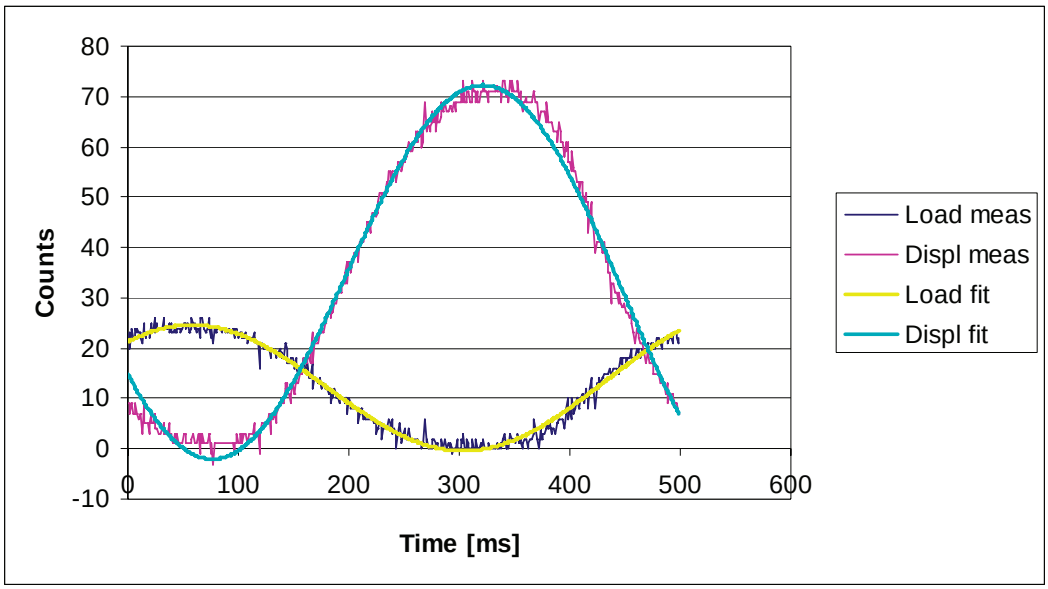


Figure 79: Load and displacement signal waveforms with curve fits (C-75C-1, 5ºC, 2 Hz)

The curve fitting method was followed here for the determination of the phase angle. The sinusoidal curves that were fitted are of the equation:

$$Y_i = A_0 + A_1 t_i + A_2 \cos(\omega_o t_i) + B_2 \sin(\omega_0 t_i) + e_i \qquad \text{Eq. 46}$$

where $t_i$ = time at data point i
$\omega_0$ = angular frequency
$e_i$ = error at data point i
$A_0, A_1, A_2, B_2$ = model coefficients

The model coefficients were optimised by minimising the sum of the squared residuals.

### *4.6.6 Dynamic four-point beam test – fatigue*

4.6.6.1 Test conditions and methodology

The BFA and the UTM21 software are specifically designed to undertake the long duration dynamic testing in order to determine the fatigue life of a specimen.

The fatigue tests were performed at 5 ºC. It was found during the initial stages of the project that fatigue testing of cold mix beams tested at higher temperatures lead to shear failure between the inner and outer clamping points at the beam ends rather than flexural failure at the bottom of the beam in the centre. This is more elaborately discussed in the next section. The loading consisted of a displacement controlled haversine wave with a frequency of 10 Hz.

Approximately twelve beams per BSM mix type were tested at different strain levels ranging between 100 micron and 500 micron. The strain levels for the various tests were chosen in such a manner, that the maximum test duration at the lowest strain level is approximately 1 million load repetitions. Care was taken to ensure a more or less equal spread of strain levels over the full range.

The beams were typically conditioned overnight at 5 ºC with a minimum of 30 minutes relaxation time once the beams were inserted into the testing rig and clamped with zero deflection.

The initial flexural stiffness of the beam was determined in the same manner as described in Section 4.6.4. The fatigue tests were continued sufficiently beyond the 50 % reduction in flexural stiffness in order to allow for variations between the derived initial flexural stiffness and the initial flexural stiffness recorded by the UTM21 software.

The UTM21 software automatically produces a plot of the flexural stiffness versus the number of load repetitions. The number of load repetitions to failure $N_f$ is visually read off from this plot. This is done for each and every beam at all the strain levels tested. By doing so an array of strain and number of load repetitions to failure

combinations per mix is obtained. The fatigue line for a particular mix is determined by fitting a power function to the array of data as discussed in Chapter 3.

4.6.6.2 Investigation into test temperature for fatigue testing

The fatigue testing of the BSM mixes discussed in this study started off with a testing temperature of 20 ºC, following AASHTO Standard T321. During testing of the first mix it was discovered that some of the beams failed in shear mode at the beam ends between the inner and outer clamps, instead of failing in bending mode in the middle of the beam between the two inner clamps. This would indicate that the resistance to transverse forces is less than the resistance to bending moment. A simplified illustration of the transverse forces and bending moment diagrams is given in Figure 80.

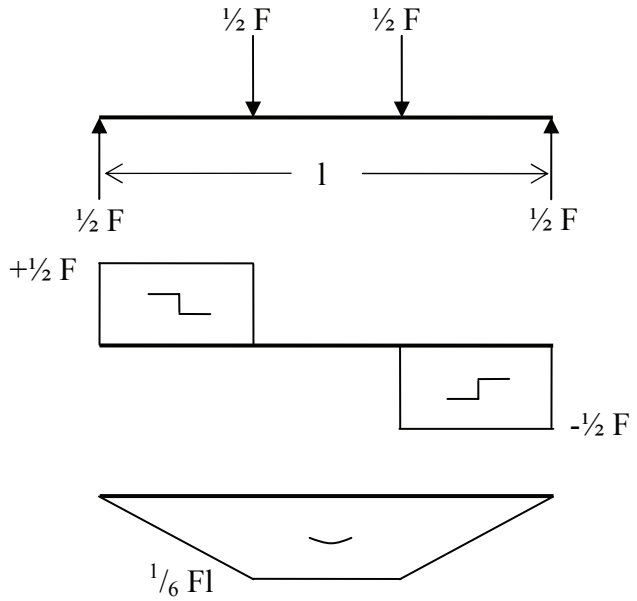


Figure 80: Simplified transverse forces and bending momenten diagram of four-point beam test

An illustration of the cracking that was observed at both ends of the beam between the inner and outer clamps is shown in Figure 81.

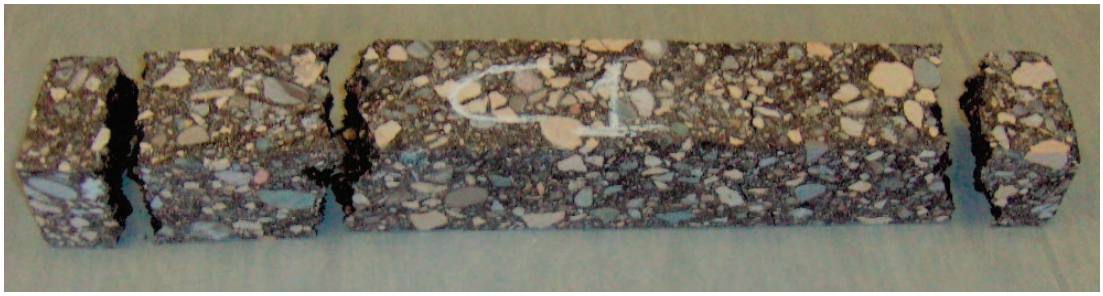

Figure 81: Cracking as a result of transverse forces at the beam ends instead of cracking in the middle as a results of bending moment (A-75C-0, 20 ºC)

Due to the relatively lower binder stiffness at 20 ºC, the mix stiffness is also lower compared to those obtained at lower temperatures. It was believed that the mix stiffness would be low to such an extent that not bending in the middle, but shear failure on either end of the beam would become critical. By lowering the test temperature, the binder stiffness increases and hence also the mix stiffness. In such case shear failure would become less likely and bending failure more likely.

A limited experiment was carried out whereby fatigue tests were conducted at three different temperatures, *i.e.* 20 ºC, 10 ºC and 5 ºC. It was found that at 10 ºC less beams failed due to shear at the beam ends than at 20 ºC, but still a considerable number of the beams tested at 10 ºC did fail due to shear and the beam ends. At first the test temperature was reduced to 10 ºC. However, some of the beams still failed in shear mode rather than bending mode as can be seen in Figure 82. Subsequently the testing temperature was further reduced to 5 ºC at which predominantly failure due to bending in the middle of the beam was observed (Jenkins and Ebels, 2006).

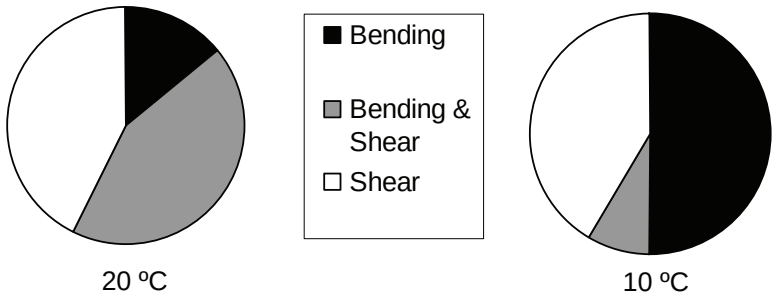


Figure 82: Influence of test temperature on type of failure during fatigue testing

4.6.6.3 Correlation testing beam fatigue apparatus

The BFA apparatus used for the four-point beam testing discussed in this study was commissioned at the Stellenbosch University during February 2004. A limited correlation study was carried out in order to ensure the reliability of the test results obtained. This correlation study is more elaborately discussed by Jenkins and Ebels (2006), but a summary is provided here.

Duplicate specimens of a sand asphalt mix were produced by SemMaterials L.P. in the United States. One set of beams was tested on fatigue in SemMaterials' laboratory in Wichita (USA), while a duplicate set of nine beams was shipped to the Stellenbosch University. Both set of beams were tested under similar laboratory conditions in Wichita and Stellenbosch. The testing methodology followed by both laboratories was similar to the methodology as discussed in Section 4.6.6.1. The testing temperature was 5 ºC and the haversine controlled displacement wave was applied a 10 Hz. Both set of beams had similar air void contents. The results of the correlation testing are shown in Figure 83.

It can be seen that on the face of it the two data sets compare well, except for the results of beam 6C tested by the SU. The outlying result of Beam 6C could be due to damage that may have occurred during transport (some of the beams had deformed during transport from the USA to Stellenbosch), however, this could not be verified. A repeat test on another beam but at the same strain level (300 microstrain) provided a results much more in line with the other test data.

Due to the capacity limitations of the four-point beam apparatus at the Stellenbosch University, which is a pneumatic operated system, strains in excess of 400 microstrain could not be tested given the test conditions (5 ºC and 10 Hz). This is contrary to the machine used by SemMaterials, which is a hydraulically operated machine.

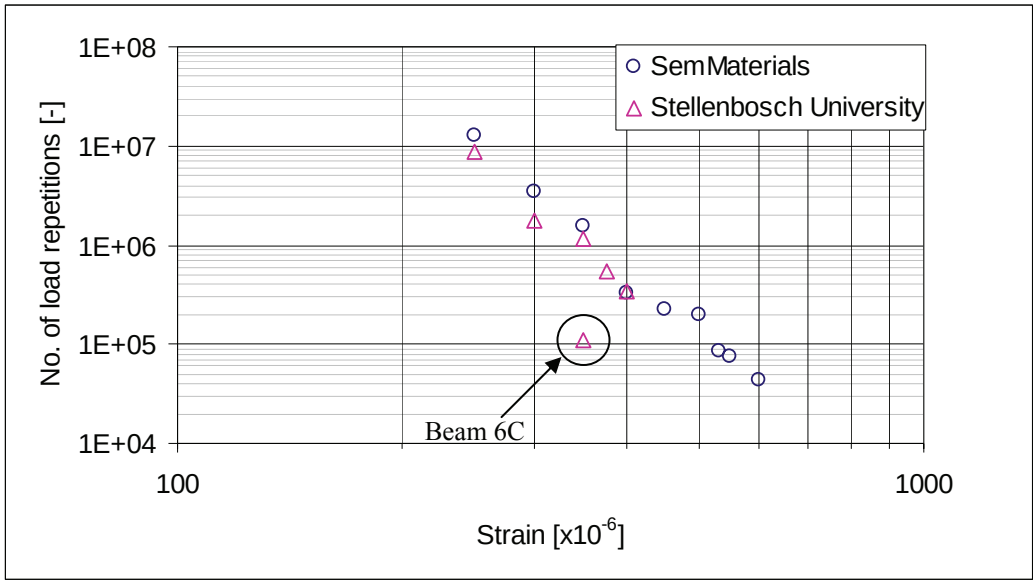


Figure 83: Fatigue results of correlation testing sand asphalt mix at SemMaterials and Stellenbosch University

The initial stiffness of the two data sets was also comparable. It is noted however that the initial stiffness of the set as measured by the SemMaterials' four-point beam apparatus was consistently slightly lower than that measured by the SU's four-point beam apparatus (average of 11,332 MPa versus 12,450 MPa). Furthermore the variation in the initial stiffness of the SemMaterials set is lower than that of the SU set (standard deviation of 278 MPa versus 663 MPa). It is believed that this difference could be inherent to the two different test and measurement set-ups. It is also believed that such a difference in initial stiffness (*i.e.* systematic error of less than 10%) would not result in greater differences in fatigue life.

When a fatigue line function in the form of $N = a\ \varepsilon^{-n}$ is fitted to the two data sets, the following model coefficients are obtained:

Table 32: Model coefficients from correlation testing (strain in μm/m)

| Laboratory | a | n | $R^2$ |
|---|---|---|---|
| SemMaterials | $2.32 \times 10^{22}$ | 6.39 | 0.983 |
| Stellenbosch University | $3.78 \times 10^{22}$ | 6.54 | 0.970 |

The results of the correlation testing show that the fatigue results of the same mix tested on two different four-point beam testing machines are comparable. This gives confidence that the results obtained by the new test set-up commissioned in 2004 at the Stellenbosch University are reliable.

## References

Asphalt Academy, *The Design and Use of Foamed Bitumen Treated Materials*. Interim Technical Guideline No. 2, Pretoria, South Africa, 2002.

CSIR - Council for Scientific and Industrial Research, *Standard Methods of Testing Road Construction Materials,* Technical Methods for Highways No. 1, 2nd edition, Pretoria, South Africa, 1986

Houston, M. and Long, F., Correlations between different ITS and UCS test protocols for foamed bitumen treated materials. Proceedings of the 8th Conference on Asphalt Pavements for Southern Africa, Sun City, South Africa, 2004

IPC Global, *UTM21 Beam Fatigue Test V1.05*, User Manual, Boronia, Australia, 2003

Jenkins, K. J. and Ebels, L. J., *Performance models of bitumen emulsion treated materials*, Final Report, Institute for Transport Technology, Stellenbosch University, South Africa, 2006

Maree, J. H., *Die laboratoriumbepaling van die elastiese parameters, die skuifparameters en die gedrag onder herhaalde belasting van klipslagkroonlaagmateriale: toetsmetodes en apparaatbeskrywing*, Technical Report RP11/78 (in Afrikaans), National Institute for Transport and Road Research, CSIR, Pretoria, South Africa, 1979

Moloto, P., *Curing of bitumen stabilised materials*, MSc. Eng thesis Stellenbosch University, South Africa, to be published 2008

Pronk A. C. and Erkens, S. M. J. G., *A note on fatigue bending test using a haversine loading, Road Materials and Pavement Design*, Volume 2 Issue 4/2001, Hermes Science Publications, France, 2001

Twagira, E. M., *Characterisation of Fatigue Performance of Selected Cold Bituminous Mixes*, MSc. Eng. Thesis, Stellenbosch University, South Africa, 2006.

# 5 MATERIALS TESTING RESULTS

## 5.1 Introduction

The preceding Chapters 3 and 4 provided background information on the material properties and behaviour that are investigated in this study as well as on the testing methodology and conditions. In this chapter the test results are presented. Discussion and interpretation of the test results, as well as the modelling of the material properties and behaviour is subject of the following chapters.

The test results presented in this chapter comprise:

- Shear parameters
- Resilient modulus
- Permanent deformation behaviour
- Bending beam strain-at-break
- Flexural stiffness
- Fatigue behaviour

## 5.2 Monotonic tri-axial test - shear parameters

A typical example of an engineering stress-strain diagram derived from a monotonic tri-axial test is shown in Figure 84 below. The shape of the curves in the stress-strain diagram is identical to the shape of the curves in the force-strain diagram. These force-strain diagrams for all mixes are included in Appendix E.

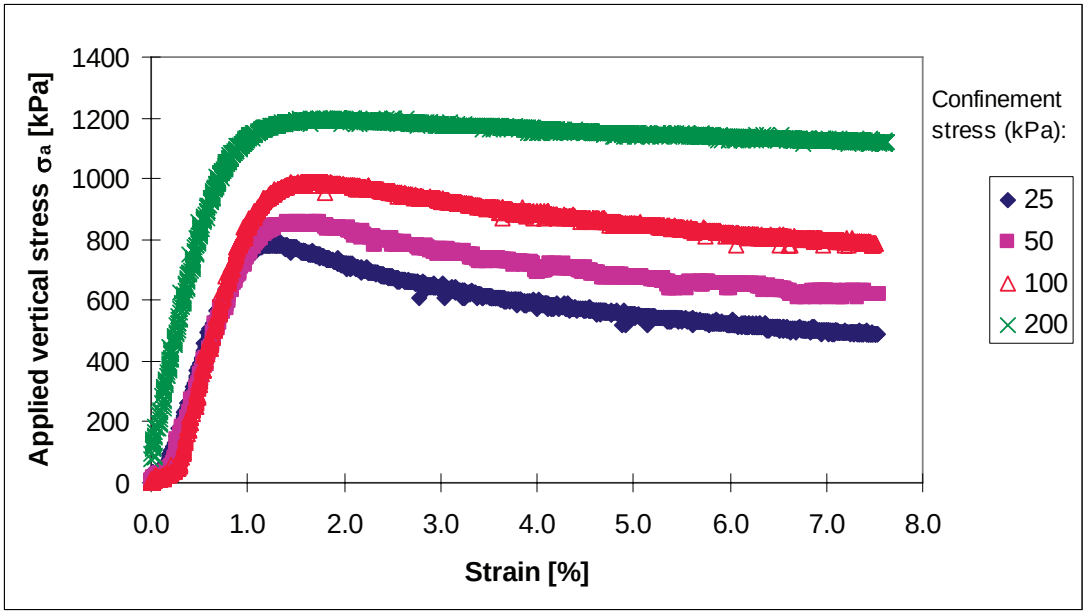


Figure 84: Stress-strain diagram for mix B-75M-0

The cohesion and angle of internal friction determined according to the methodology discussed in Chapter 3 are summarised in Table 33.

Table 33: Summary of cohesion and angle of internal friction (25ºC)

| Mix | Cohesion C [kPa] | Angle of internal friction φ [º] | Coefficient of variance ($R^2$) |
|---|---|---|---|
| A-75C-0 | 152 | 38.4 | 0.98 |
| A-75C-1 | 387 | 29.7 | 0.97 |
| A-75M-0 | 195 | 33.8 | 0.99 |
| B-75C-0 | 142 | 43.7 | 0.95 |
| B-75C-1 | 397 | 33.8 | 1.00 |
| B-75M-0 | 206 | 32.2 | 1.00 |
| C-75C-0 | 184 | 41.0 | 0.99 |
| C-75C-1 | 390 | 30.0 | 0.90 |
| C-75M-0 | 136 | 34.0 | 0.98 |

In general, good coefficients of variance ($R^2$-values) were obtained for the linear regression analyses to obtain the Mohr-Coulomb failure envelope lines. This indicates that the ultimate strength results obtained at the different confinement pressures are in line with each other. All $R^2$-values are in excess of 0.95, except for mix C-75C-1, for which an $R^2$-value of 0.90 was obtained.

For two mixes however, where it was observed that one of the four Mohr-Coulomb circles was far from the failure envelope of the other three circles, the failure envelope line is based on those three circles only. These two mixes were C-75C-0 and C-75C-1. Including the fourth Mohr-Coulomb circle in the analysis results in a cohesion 170 kPa and friction angle of 41.0º ($R^2$ = 0.89) for mix C-75C-0 and a cohesion of 429 kPa and friction angle of 27.1º ($R^2$ = 0.89) for mix C-75C-1.

It is noted that due to inadvertent circumstances all foamed bitumen mixes (C-mixes) and mix A-75M-0 were tested at confinement pressures of 40 kPa and 60 kPa instead of 25 kPa and 50 kPa respectively. This should however not influence the accuracy of the determined failure envelope lines. Mohr-circles derived from the measured combinations of $\sigma_{1,f}$ and $\sigma_3$, as well as the failure envelope line according to the $C$ and $\varphi$ determined can be drawn in the Mohr-Coulomb diagram as discussed in Chapter 3. An example thereof is shown in Figure 85. The Mohr-Coulomb diagrams for all mixes are also included in Appendix E.

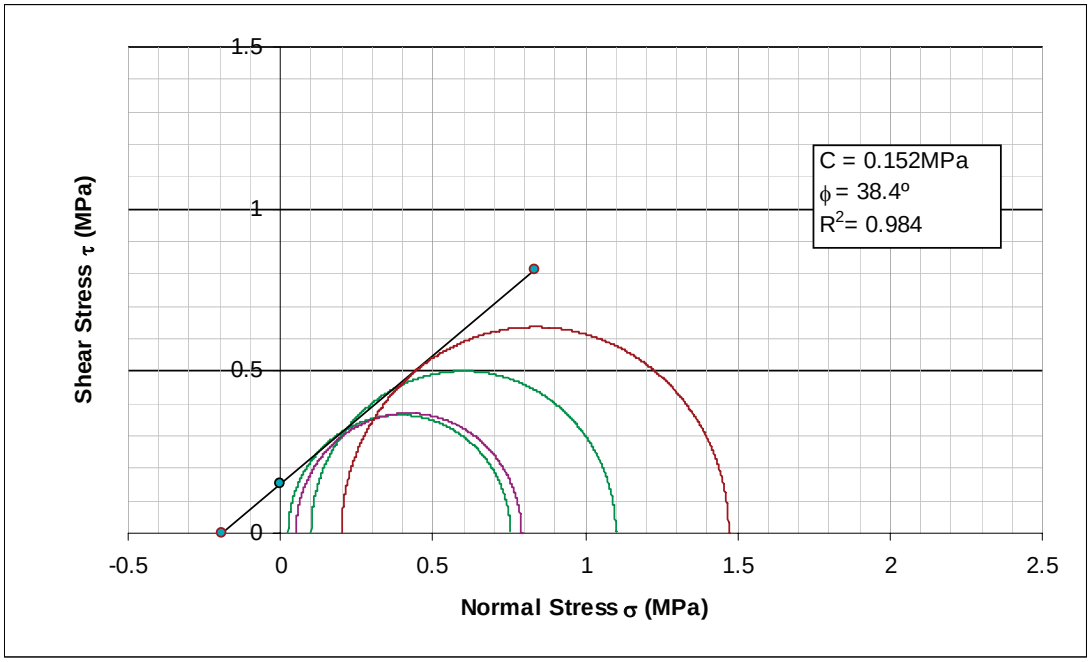


Figure 85: Mohr-Coulomb diagram for A-75C-0

## 5.3 Dynamic tri-axial test - resilient modulus

The resilient modulus for each of the deviator stress ratios at the four confinement pressures was calculated following the methodology as discussed in Chapter 4. When the resilient modulus is plotted against the bulk stress, plots as shown in Figure 86 and Figure 87 are typically obtained. In the example of Figure 86 it can be seen that there is a good correlation between the experimental data and the $M_r$-θ model. This was however not found for all mixes as illustrated by the example in Figure 87. The $M_r$-$\theta$ plots for all the mixes are included in Appendix F.

The two repeat tests for each mix compare fairly well and also the trends in the repeat tests (constant stiffness, stress stiffening or stress softening) are consistent. This gives confidence that the results obtained are reliable.

The results of all nine mixes are summarised in Figure 88 to Figure 90. In these figures the average of the repeat tests are shown. The resilient modulus per target deviator stress ratio and per confinement pressure is included in tabular format in Appendix F. For some of the tests the actual deviator stress ratio differs marginally from the target ratio, but only the target ratios are shown in the tables in Appendix F in order to reduce the complexity. The difference between the target stress ratio and the actual applied stress ratio never exceeded 0.02 in absolute terms

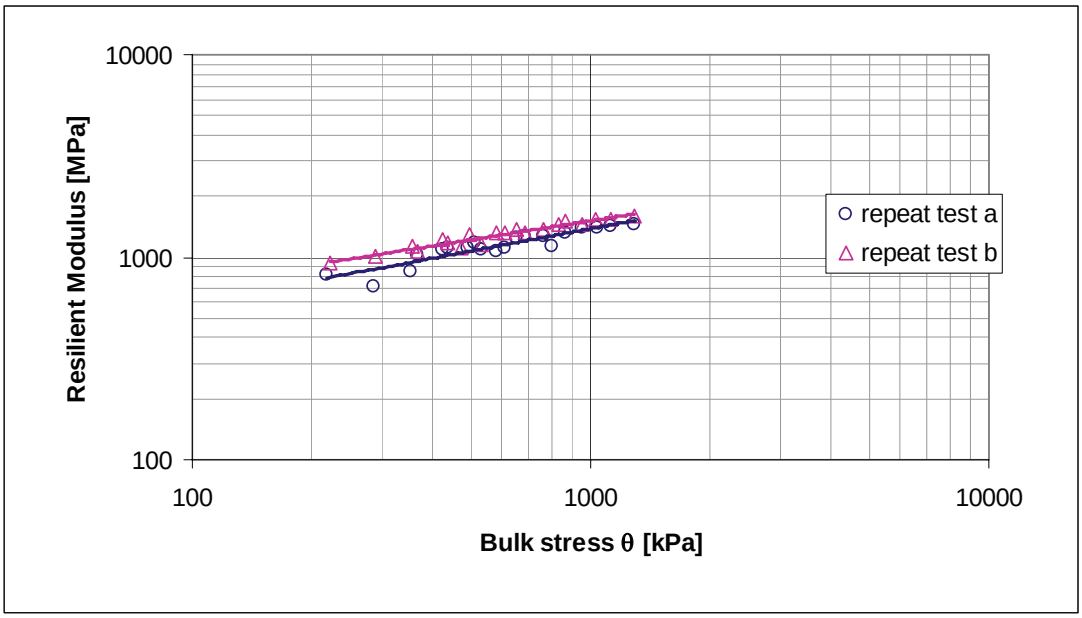


Figure 86: Example of good Mr-θ model fit (mix A-75C-1)

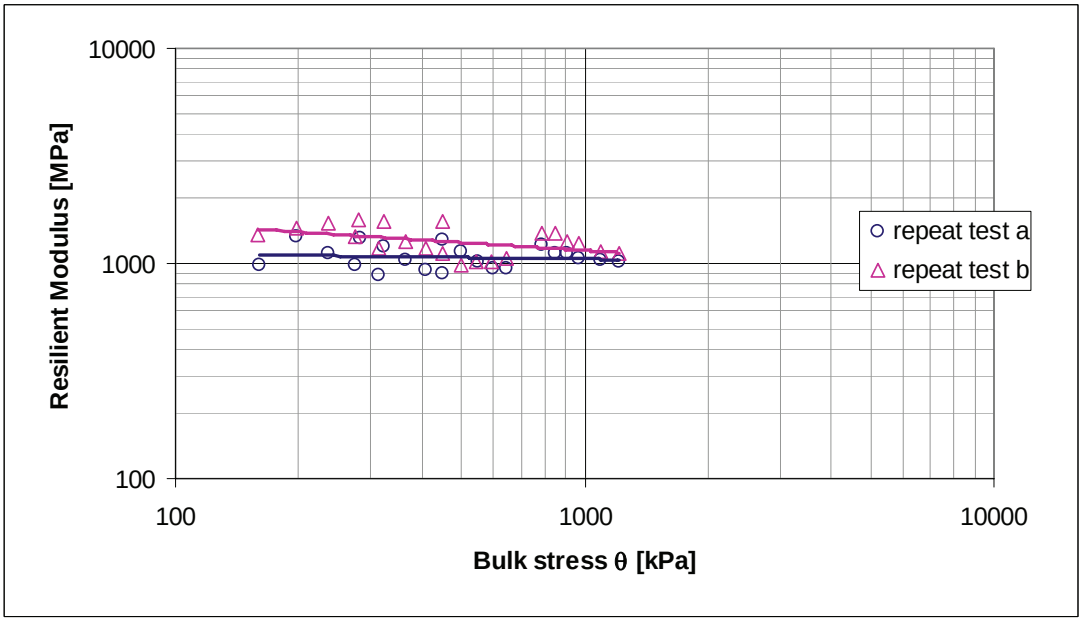


Figure 87: Example of poor Mr-θ model fit (mix A-75M-0)

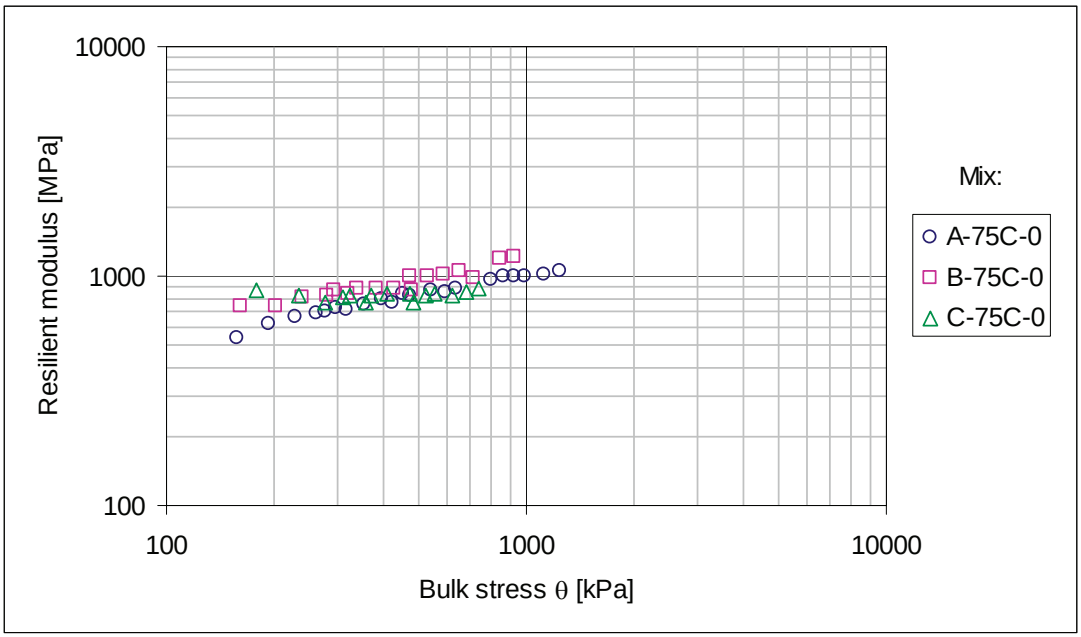


Figure 88: Resilient Modulus per binder type for aggregate blend 75C-0 (2 Hz and 25ºC)

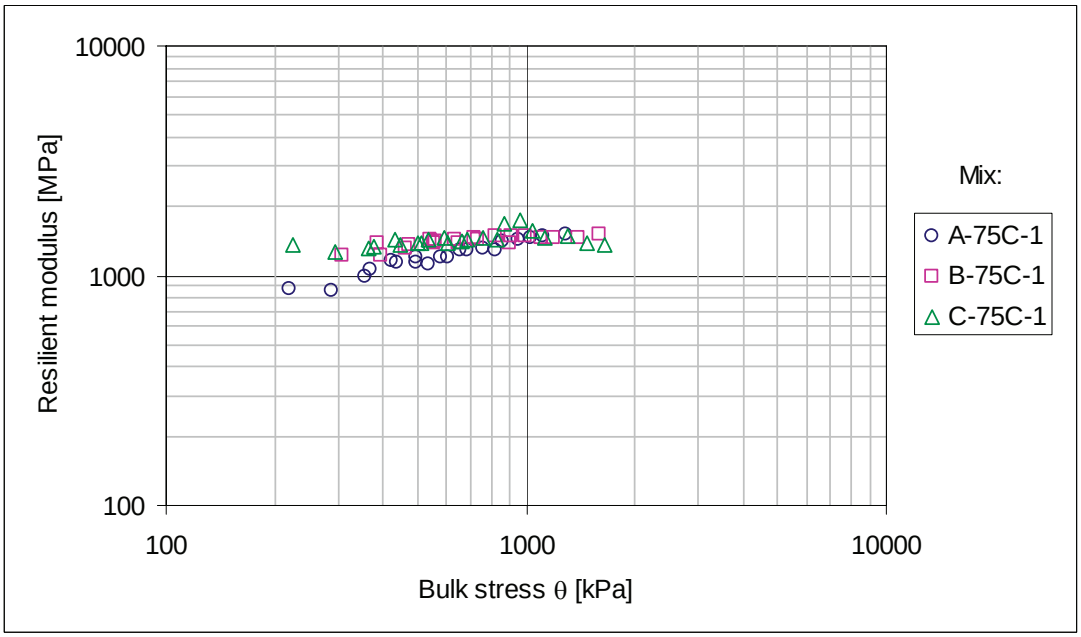


Figure 89: Resilient Modulus per binder type for aggregate blend 75C-1 (2 Hz and 25ºC)

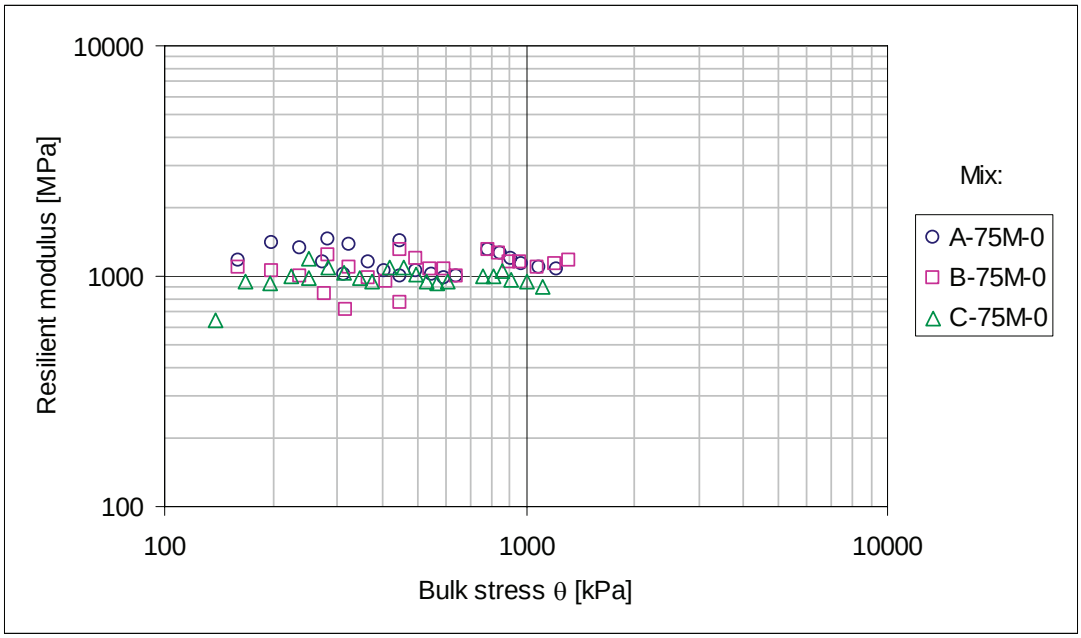


Figure 90: Resilient Modulus per binder type for aggregate blend 75M-0 (2 Hz and 25ºC)

## 5.4 Repeated load tri-axial test - permanent deformation

The permanent deformation accumulation curves are shown in Figure 91 to Figure 99. The plots are shown on a double log scale. These plots may sometimes be deceiving because what appears to be nearly identical on double log scale can be quite different on normal scale. It is therefore recommended that the plots shown below are used in combination with plots on normal scale. The latter are not shown here but are included in Appendix G. The numerical data as recorded manually during the test is also included in this appendix.

Not all mixes were subjected to the same range of loading. The nine mixes were subjected to at least four different stress ratio's, with the objective to determine the critical stress ratio, as discussed in Chapter 4.

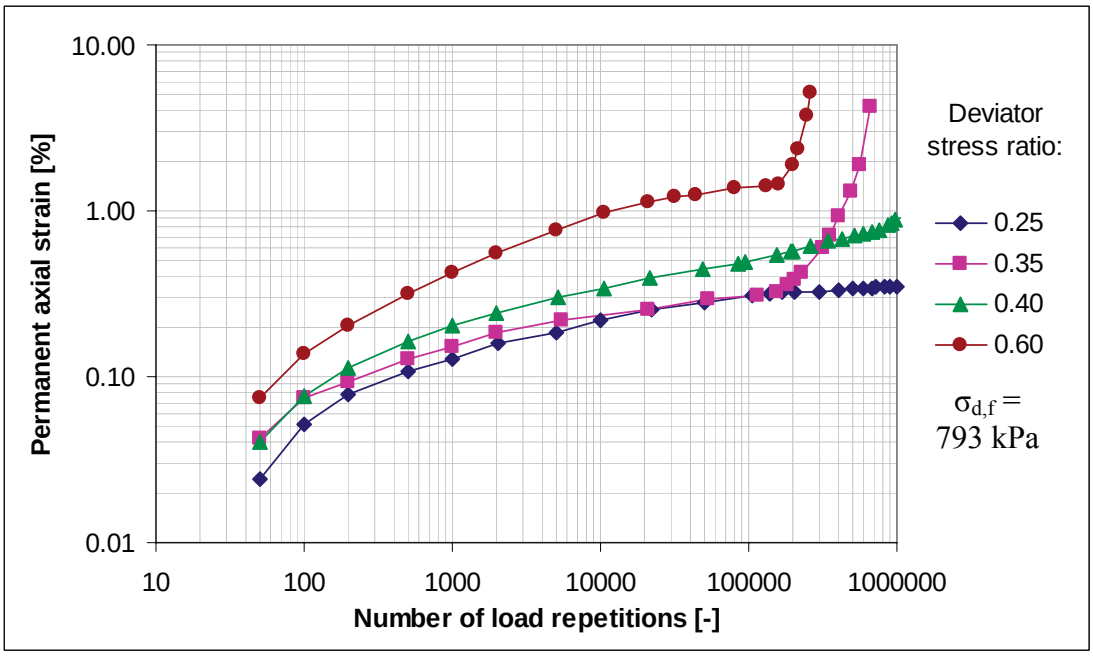


Figure 91: Permanent deformation curves Mix A-75C-0 ($\sigma_3$ = 50 kPa, T = 25ºC)

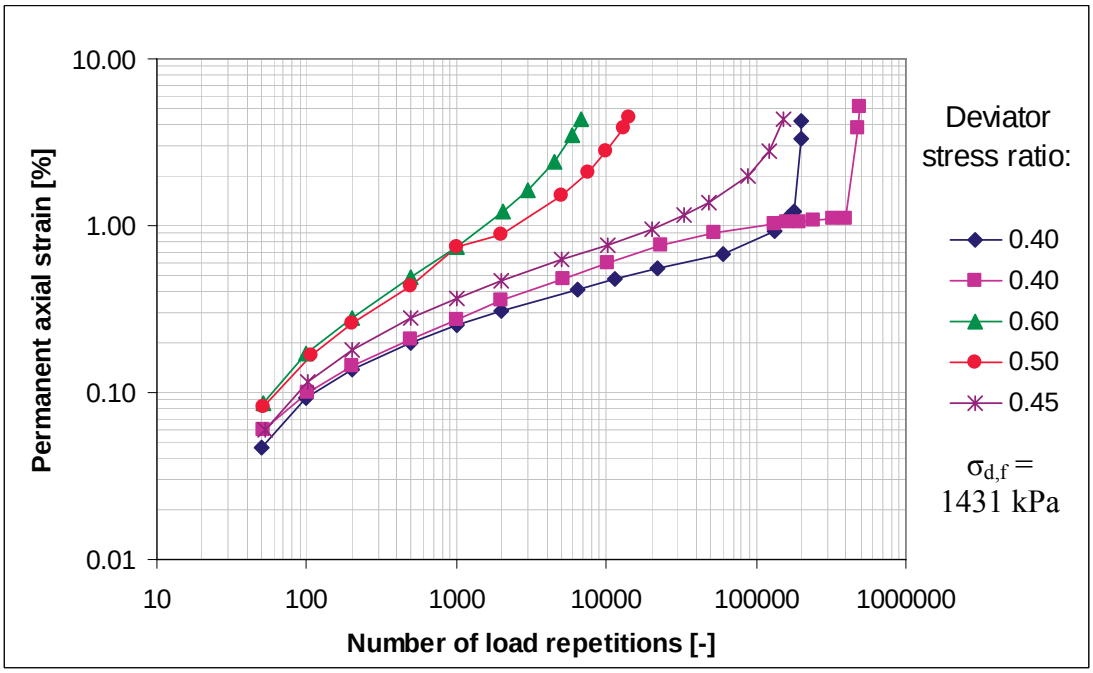


Figure 92: Permanent deformation curves Mix A-75C-1 ($\sigma_3$ = 50 kPa, T = 25ºC)

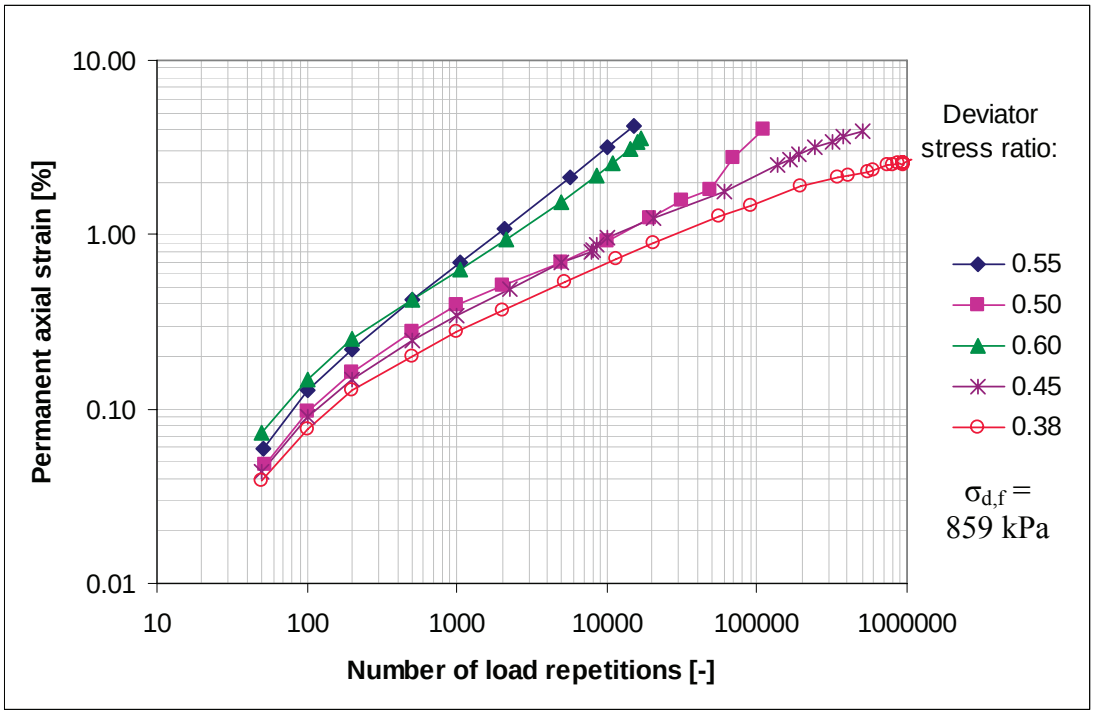


Figure 93: Permanent deformation curves Mix A-75M-0 ($\sigma_3$ = 50 kPa, T = 25ºC)

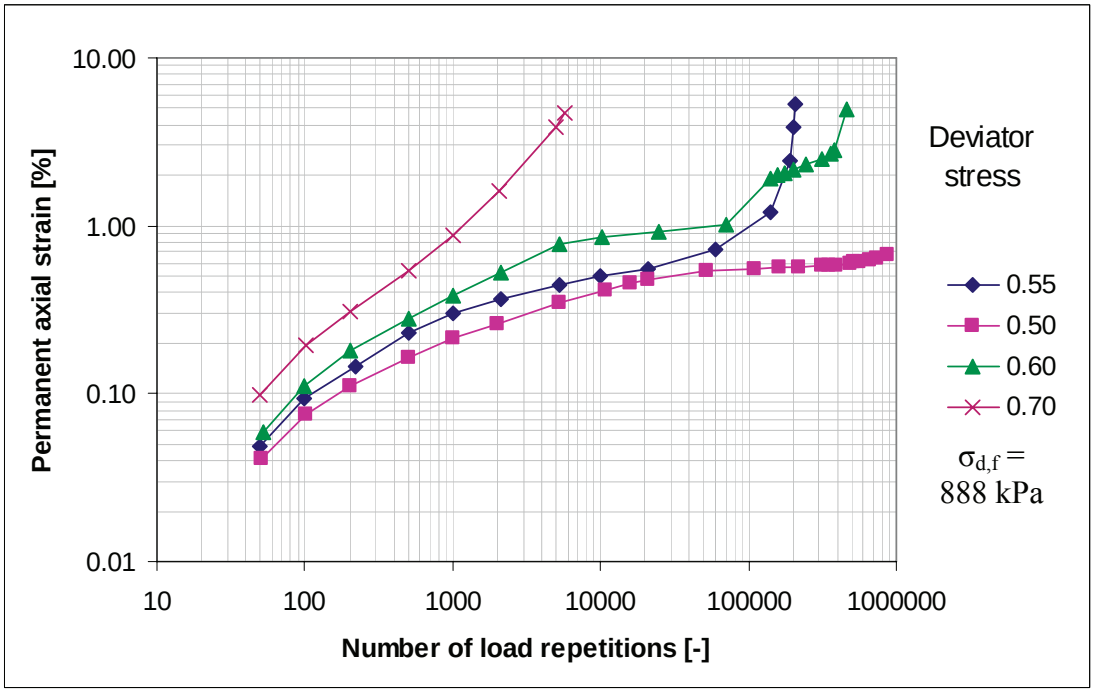


Figure 94: Permanent deformation curves Mix B-75C-0 ($\sigma_3$ = 50 kPa, T = 25ºC)

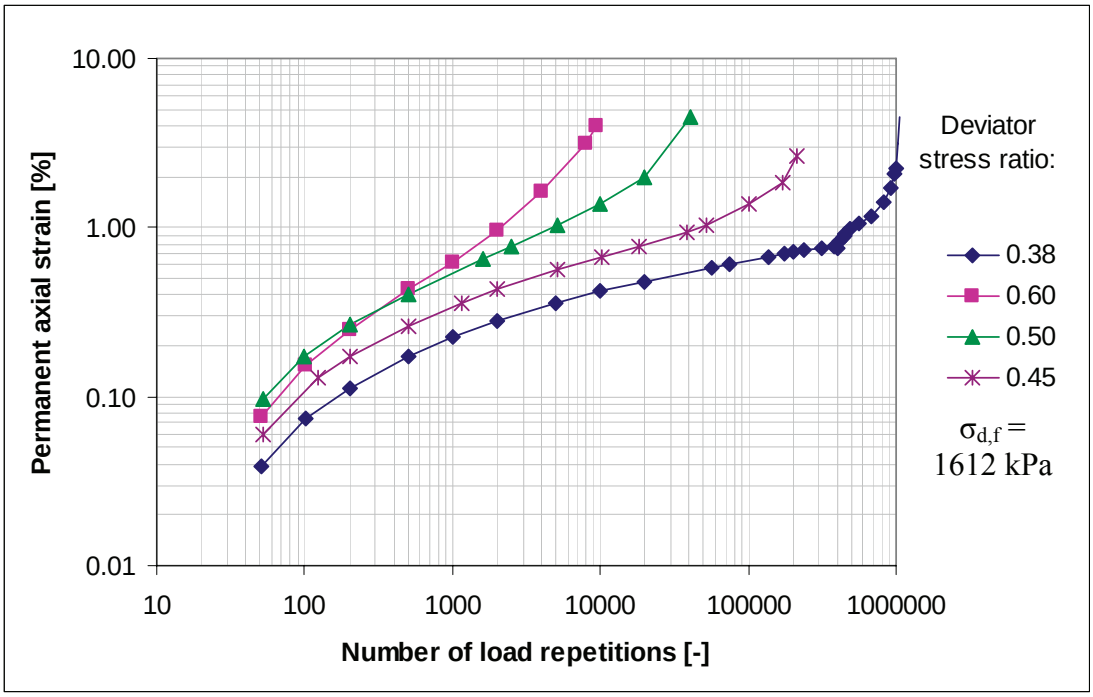


Figure 95: Permanent deformation curves Mix B-75C-1 ($\sigma_3$ = 50 kPa, T = 25ºC)

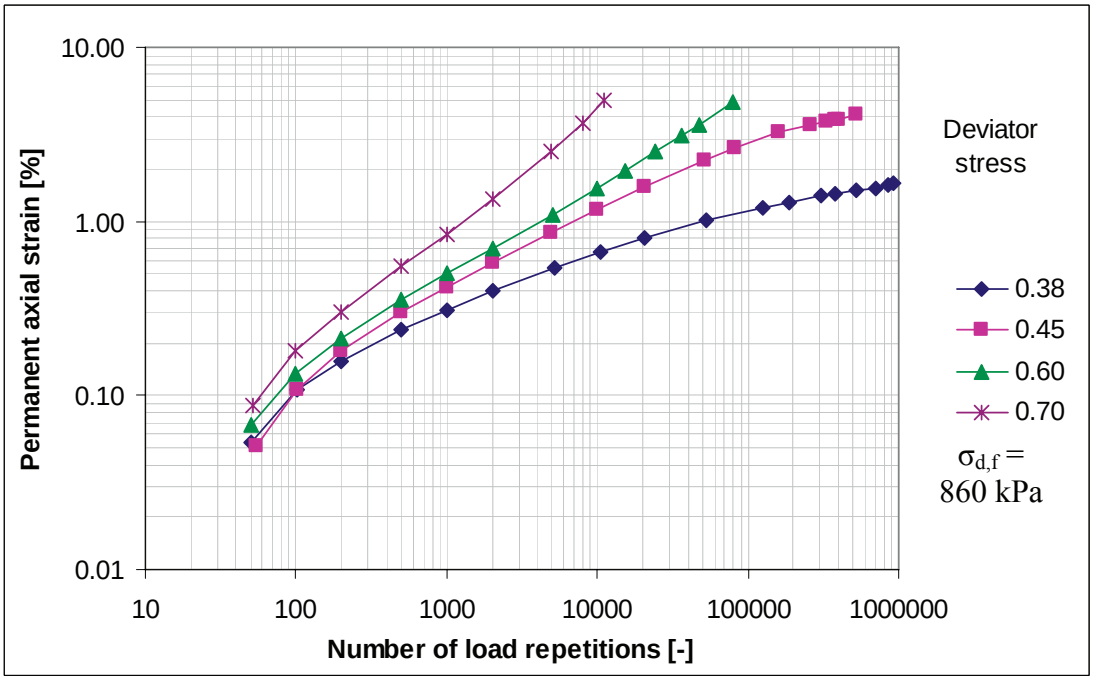


Figure 96: Permanent deformation curves Mix B-75M-0 ($\sigma_3$ = 50 kPa, T = 25ºC)

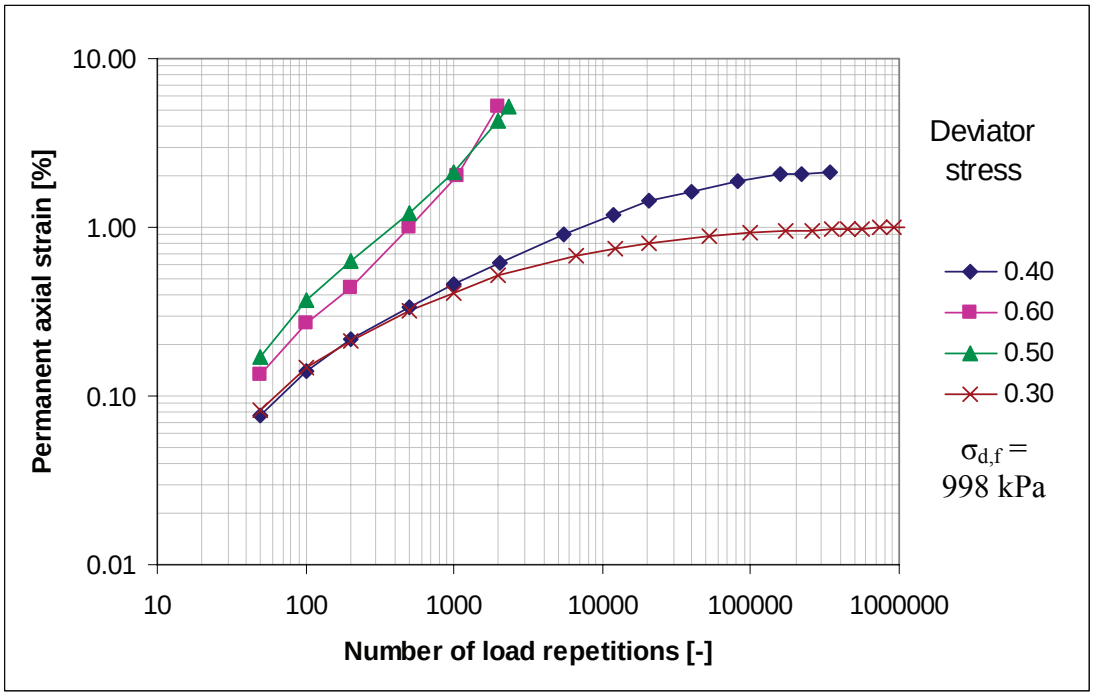


Figure 97: Permanent deformation curves Mix C-75C-0 ($\sigma_3$ = 50 kPa, T = 25ºC)

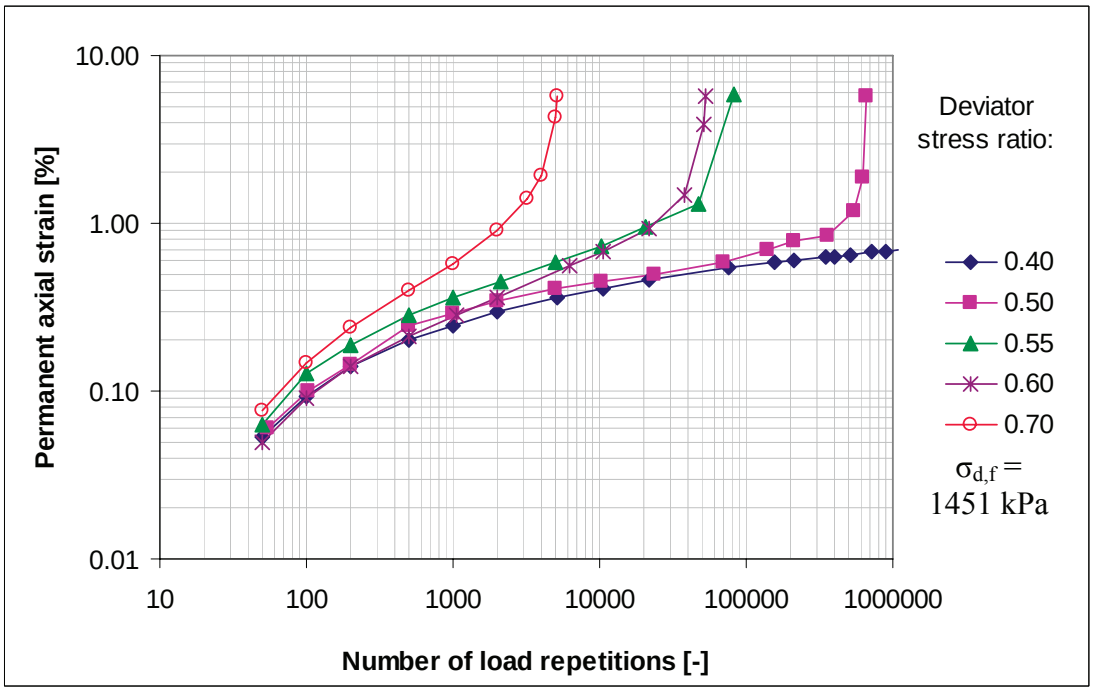


Figure 98: Permanent deformation curves Mix C-75C-1 ($\sigma_3$ = 50 kPa, T = 25ºC)

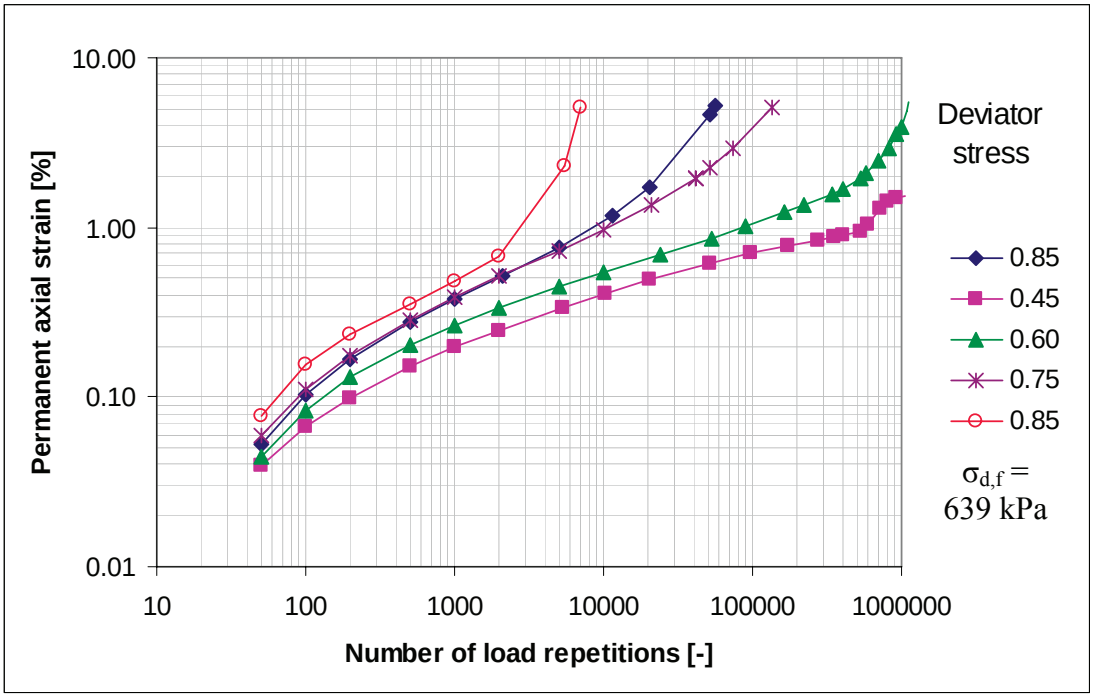


Figure 99: Permanent deformation curves Mix C-75M-0 ($\sigma_3$ = 50 kPa, T = 25ºC)

## 5.5 Monotonic four-point beam test - strain-at-break

For each of the nine mixes three beams were tested for strain-at-break. The peak stress and strain at which peak stress occurs are summarised in Table 34. The detailed test results are included in Appendix H.

The results shown are based on linear-elastic theory and calculated using formulas as discussed in the previous chapters. Since the BSM's tested behave visco-elastic, which is confirmed by the Burgers Model parameters as shown further on in Chapter 6, the true material behaviour is not linear-elastic. The "true" strain-at-break can therefore be expected to deviate from the reported values. To determine this "true" strain additional testing with strain gauges attached to the specimens and FEM modelling would be required, which falls outside the scope of this study.

It is noted that the material response also depends on the loading time and temperature. The applied displacement rate of 1.0 mm/min is fairly low and it can be expected that at higher loading rates, the strain-at-break increases. The test temperature is also fairly low, but at higher temperature the strain-at-break can be expected to decrease.

Table 34: Strain-at-break results per aggregate blend and per binder type (displacement rate 1.0 mm/min at 5ºC)

| Aggregate Blend | Binder type | | | | | | | | |
|---|---|---|---|---|---|---|---|---|---|
| | A | | | B | | | C | | |
| | beam | peak stress at break [kPa] | strain at break [%] | beam | peak stress at break [kPa] | strain at break [%] | beam | peak stress at break [kPa] | strain at break [%] |
| 75C-0 | F1 | 106 | 0.20 | C1 | 419 | 0.16 | C2 | 342 | 0.13 |
| | F2 | 151 | 0.29 | C5 | 262 | 0.22 | C5 | 412 | 0.17 |
| | F3 | 171 | 0.33 | C6 | 499 | 0.17 | C6 | 339 | 0.19 |
| 75C-1 | D1 | 190 | 0.21 | D1 | 344 | 0.11 | C1 | 536[1] | 0.29 |
| | D2 | 77[1] | 0.39[1] | D3 | 244[1] | 0.08[1] | C3 | 353 | 0.12[1] |
| | D3 | 248 | 0.23 | D4 | 344 | 0.12 | C5 | 353 | 0.24 |
| | - | - | - | - | - | - | C6 | 272 | 0.20 |
| 75M-0 | Y5 | 220 | 0.19[1] | C1 | 715 | 0.15[1] | B1 | 236 | 0.10 |
| | Z2 | 209 | 0.34 | C2[1] | 364 | 0.09 | B2 | 294 | 0.12 |
| | Z3 | 166 | 0.38 | C5 | 380 | 0.08 | B3 | 266 | 0.14 |
| | - | - | - | C6 | 427 | 0.10 | - | - | - |

Notes: 1) See comments in Table 35

The results shown in the table above are the results of all the beams tested. However, during the testing of some of the beams, or the interpretation of the results thereof, some anomalies were observed. Comments on these anomalies are summarised in Table 35.

Table 35: Comments on some of the beams tested for strain-at-break

| Mix | Beam | Comment |
|---|---|---|
| A-75C-1 | D2 | The peak loading is substantially lower than the other two beams tested for this mix. At the same time, the displacement at which peak loading occurs is much higher. This makes that the results of this beam fall out of line with the other two beam results obtained |
| A-75M-0 | Y5 | The peak loading of Beam Y5 is more or less in line with the results of the other two beams. The displacement at which peak loading occurs is however a lot less. This makes that the strain-at-break value for beam Y5 is much lower than that of the other two beams |
| B-75C-0 | C5 | The peak loading of Beam C5 is substantially lower than that of the other two beams. At the same time the displacement at which peak loading occurs is much higher. This makes that the results of this beam fall out of line with the other two beam results obtained |
| B-75C-1 | D3 | The first part of the stress-strain path is the same for all three beams, but Beam D3 fails substantially earlier than the other two beams |
| B-75M-0 | C1 | Beam C1 has a significantly higher peak load and higher displacement at which peak load occurs compared to the other three beams tested for this mix |
| | C2 | There is a kink in the stress path of Beam C2. It appears to have failed, but then a sudden rise in loading occurs again |
| C-75C-1 | C3 | The peak loading of Beam C3 is comparable to that measured for beam C5 and C6 of the same mix. The displacement at which it occurs is however much less. This makes that the strain-at-break of Beam C3 falls out of line compared with Beams C5 and C6 |
| | C1 | The stress path shows a similar kink as for Beam C2 of Mix B-75M-0. Peak loading occurs after this kink and is significantly higher than for the other three beams tested for this mix. |

It was judged that only the results of Beam Y5 of Mix A-75M-0 and Beam C1 of Mix B-75M-0 can be considered outliers and are not representative for the mix. The results of the other beams mentioned in Table 35 are somewhat different than that of the other beams of the same mix, however, not too such an extent that they can be regarded as being not representative of the mix. Therefore, these results have been included in the analysis of the mixes.

The average strain-at-break values per mix and the statistical parameters are summarised in Table 36.

Table 36: Summary of strain-at-break results (%-strain) per mix

| Aggregate Blend | Binder type | | | | | | | | |
|---|---|---|---|---|---|---|---|---|---|
| | A | | | B | | | C | | |
| | ave. [%] | st.dev. [%] | C.O.V. [%] | ave. [%] | st.dev. [%] | C.O.V. [%] | ave. [%] | st.dev. [%] | C.O.V. [%] |
| 75C-0 | 0.27 | 0.06 | 25 | 0.18 | 0.03 | 19 | 0.16 | 0.03 | 20 |
| 75C-1 | 0.22 | 0.01 | 4 | 0.10 | 0.02 | 22 | 0.21 | 0.07 | 34 |
| 75M-0 | 0.30 | 0.10 | 34 | 0.09 | 0.01 | 13 | 0.12 | 0.02 | 17 |

## 5.6 Dynamic four-point beam test – stiffness master curves and phase angles

The master curves determined in the manner discussed in Chapter 3 are shown in Figure 100 to Figure 102. The detailed flexural stiffness results are included in Appendix I. For a selected number of beams the phase angles have also been determined in the manner discussed in Chapter 3. These are shown in Table 37. The detailed test results are included in Appendix I.

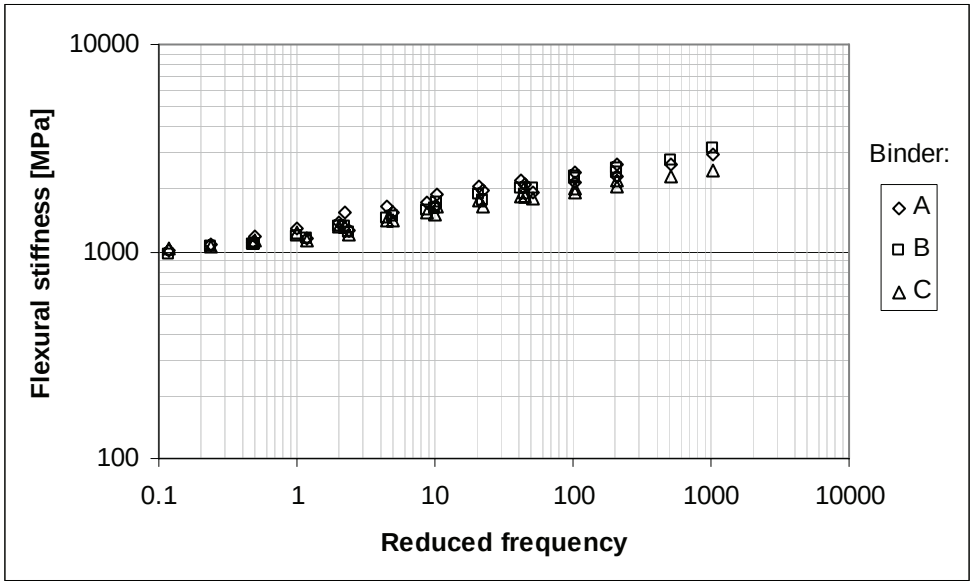


Figure 100: Master curves per binder type for aggregate blend 75C-0 ($T_{ref}$ = 20ºC)

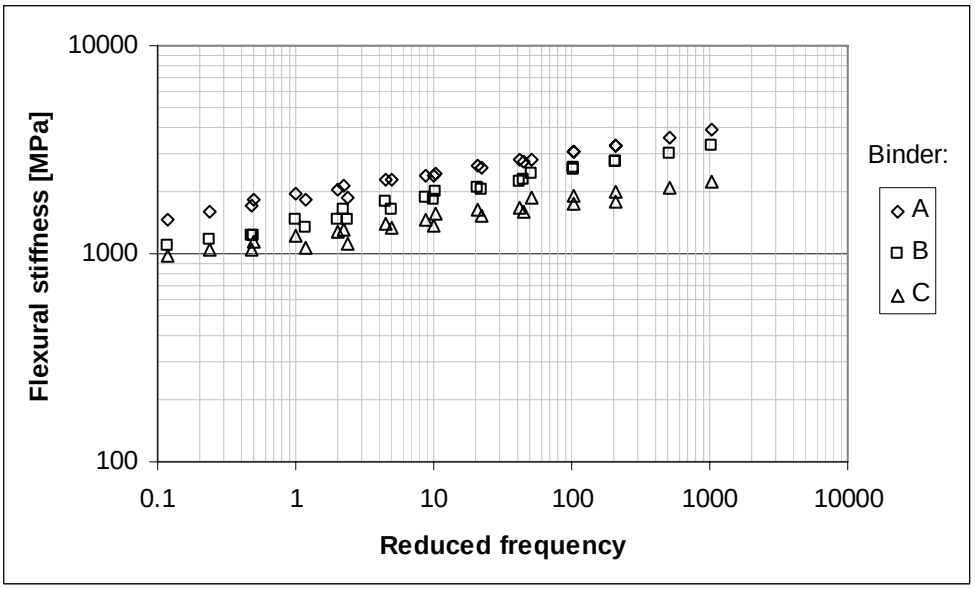


Figure 101: Master curves per binder type for aggregate blend 75C-1 ($T_{ref}$ = 20ºC)

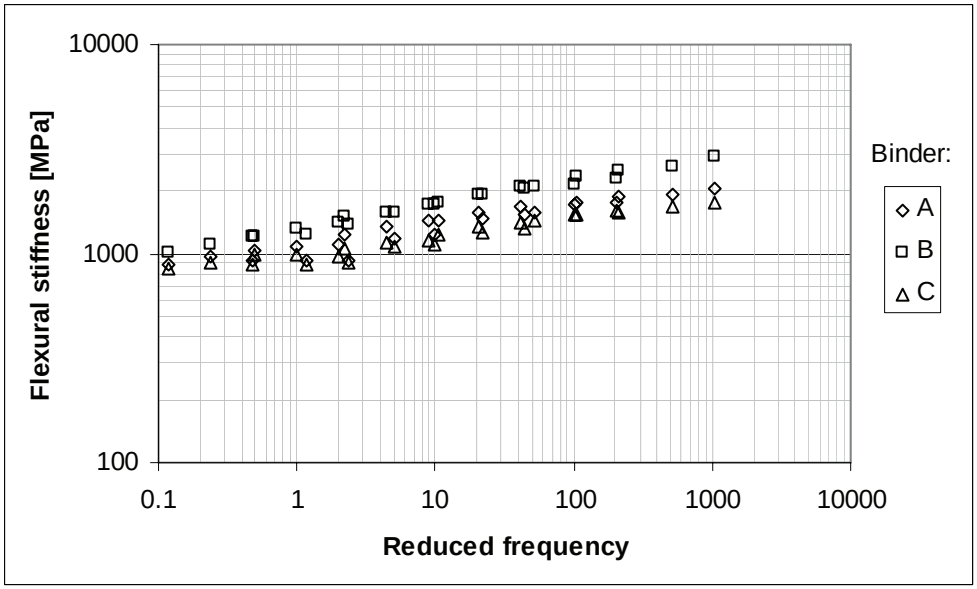


Figure 102: Master curves per binder type for aggregate blend 75M-0 ($T_{ref}$ = 20ºC)

Table 37: Phase angles for selected beams

| Test temperature [ºC] | Frequency [Hz] | Phase angle per aggregate blend and binder [º] | | | | | | |
|---|---|---|---|---|---|---|---|---|
| | | 75C-0 | | | 75C-1 | | 75M-0 | |
| | | A Beam E5 | B Beam D3 | C Beam E6 | A Beam C2 | C Beam C4 | A Beam C5 | C Beam C3 |
| 5 | 0.5 | 22.0 | 20.9 | 18.0 | 13.3 | | 19.8 | 19.4 |
| | 1 | 20.5 | 18.7 | 16.9 | 12.2 | 13.3 | 19.4 | 19.8 |
| | 2 | 18.0 | 16.6 | 17.3 | 11.5 | 12.2 | 17.3 | 18.7 |
| | 5 | 16.2 | 14.4 | 16.2 | 10.8 | 10.8 | 14.4 | 16.2 |
| | 10 | 14.4 | 18.0 | 14.4 | 10.8 | 14.4 | 14.4 | 18.0 |
| 10 | 0.5 | 23.0 | 23.0 | 20.2 | 16.2 | 15.1 | 21.6 | 23.8 |
| | 1 | 22.0 | 21.6 | 20.2 | 15.1 | 15.1 | 15.1 | 24.1 |
| | 2 | 18.7 | 20.2 | 18.7 | 14.4 | 13.7 | 20.2 | 20.9 |
| | 5 | 18.0 | 19.8 | 18.0 | 14.4 | 12.6 | 19.8 | 18.0 |
| | 10 | 18.0 | 18.0 | 18.0 | 14.4 | 10.8 | 18.0 | 21.6 |
| 15 | 0.5 | 26.3 | 27.0 | 25.6 | 16.2 | 16.9 | 25.6 | 25.2 |
| | 1 | 27.0 | 27.0 | 23.0 | 16.6 | 19.1 | 25.2 | 24.5 |
| | 2 | 23.8 | 23.8 | 20.2 | 15.8 | 16.6 | 23.0 | 22.3 |
| | 5 | 19.8 | 21.6 | 19.8 | 14.4 | 16.2 | 19.8 | 23.4 |
| | 10 | 18.0 | 21.6 | 18.0 | 18.0 | 14.4 | 18.0 | 21.6 |
| 20 | 0.5 | 28.1 | 28.8 | 25.6 | 19.1 | 20.5 | 27.4 | 25.2 |
| | 1 | 29.2 | 30.2 | 26.3 | 18.7 | 18.7 | 28.1 | 26.6 |
| | 2 | 25.9 | 25.9 | 25.2 | 18.0 | 18.0 | 28.8 | 23.8 |
| | 5 | 25.2 | 27.0 | 23.4 | 16.2 | 18.0 | 25.2 | 21.6 |
| | 10 | 25.2 | 25.2 | 21.6 | 18.0 | 14.4 | 21.6 | 28.8 |
| 25 | 0.5 | 30.2 | 28.1 | 27.0 | 20.5 | 21.2 | 27.4 | 25.9 |
| | 1 | 32.0 | 30.2 | 27.7 | 20.9 | 22.0 | 32.4 | 26.6 |
| | 2 | 32.4 | 28.8 | 28.1 | 19.4 | 23.0 | 31.0 | 24.5 |
| | 5 | 25.2 | 27.0 | 23.4 | 19.8 | 19.8 | 25.2 | 23.4 |
| | 10 | 25.2 | 25.2 | 21.6 | 18.0 | 21.6 | 28.8 | 21.6 |

## 5.7 Dynamic four-point beam test – fatigue

Following the investigation into the optimum test temperature for fatigue testing discussed in Chapter 4, the actual fatigue testing as part of this study was conducted at 5 ºC. Due to the fact that a large number of beams produced with the A-emulsion were tested at 10 ºC and 20 ºC, only a limited number of beams of the aggregate blend 75C-0 and 75M-0 produced with the A-emulsion were tested at 5 ºC. For all

other mixes at least 12 beams were tested per mix over the full range of strain levels. The results per beam are included in Appendix J.

A number of the beam fatigue tests were aborted before the 50% reduction in stiffness was reached. This was done because of time constraints, while some of the fatigue tests at low strain levels lasted for many days without reaching the 50% reduction in stiffness failure criteria (Twagira, 2006). The details of the beam fatigue tests that were aborted prematurely and the results that were obtained by extrapolation are summarised in Table 38. The extrapolation procedure was checked by extrapolating tests that actually had run for the full length. Hereby only the data up to approximately 300,000 load repetitions before the end of these tests was considered. It would appear that in extrapolating there is a tendency to underestimate the number of load repetitions to failure by about 10% to 20%.

The results of the beam fatigue test and the fatigue lines are plotted on double log scale. These plots are shown in Figure 103 to Figure 105. It should be noted that, as explained in Section 4.6.3, the fatigue performance at the reported strain levels are unconservative and an over-estimation of the actual fatigue performance of the material. The fatigue lives as reported should be associated with strain levels that are anything between 0 % and 50 % lower than the reported strain levels, depending on the type of mix and specified strain levels.

Table 38: Summary of extrapolated fatigue results (all mixes, 10Hz, 5ºC)

| Aggregate blend | Beam specimen | Strain level [με] | Actual duration of test [load reps.] | Extrapolated no. of load repetitions to failure [-] | %-initial stiffness at abortion of test [%] |
|---|---|---|---|---|---|
| B-75C-1 | B2 | 300 | 46 210 | 88 200 | 63[1] |
| | B6 | 250 | 266 490 | 560 000 | 57 |
| | B5 | 200 | 104 260 | 172 000 | 56 |
| | C3 | 140 | 2 174 340 | 2 400 000 | 52 |
| | C5 | 120 | 1 558 680 | 1 700 000 | 57 |
| B-75M-0 | A5 | 180 | 753 730 | 1 260 000 | 56 |
| | B3 | 150 | 1 310 770 | 2 630 000 | 65[1] |
| C-75C-0 | B5 | 250 | 2 096 640 | 3 420 000 | 62[1] |
| | A6 | 200 | 545 520 | 1 620 000 | 71[1] |
| | A5 | 180 | 873 570 | 3 600 000 | 66[1] |
| C-75C-1 | B1 | 230 | 155 470 | 822 000 | 81[1] |
| | B6 | 180 | 4 935 000 | 5 680 000 | 56 |
| C-75M-0 | C1 | 280 | 182 000 | 194 177 | 51 |
| | A5 | 200 | 1 672 300 | 1 850 000 | 52 |
| | B6 | 180 | 2 374 900 | 3 520 000 | 59[1] |

Note: 1) These extrapolations are regarded less reliable due to the fact that the extent of the forward extrapolation is considerable and that the stiffness at abortion of the tests was still far from the 50% failure stiffness. The other extrapolation in the table are regarded as reliable indications of the true fatigue life of the tested beam

The extrapolations that were regarded as unreliable, as indicated in Table 38 have been excluded from the graphs, fatigue lines and further analyses.

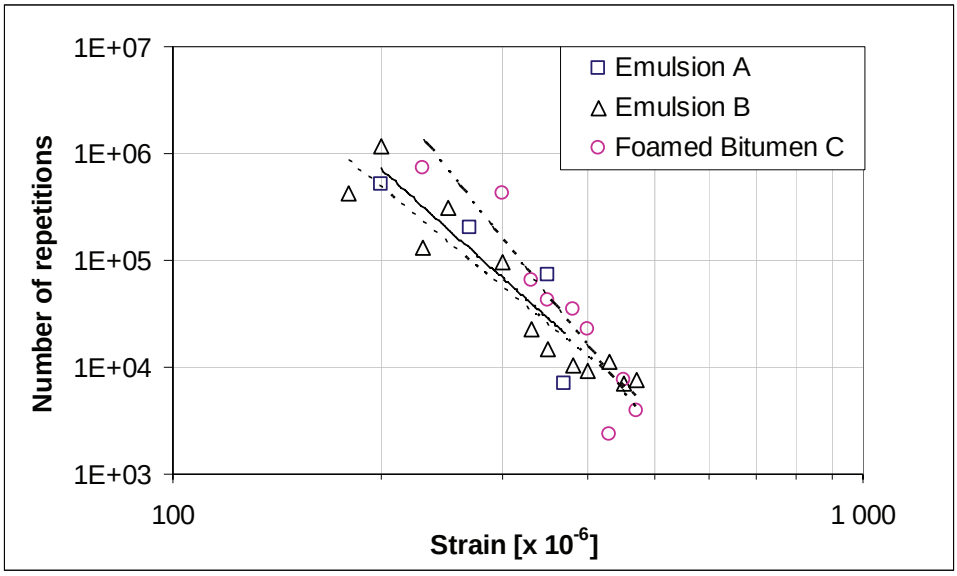


Figure 103: Fatigue lines for aggregate blends 75C-0 (10Hz and 5ºC). Note the reduction in strain that applies as discussed in Section 4.6.3

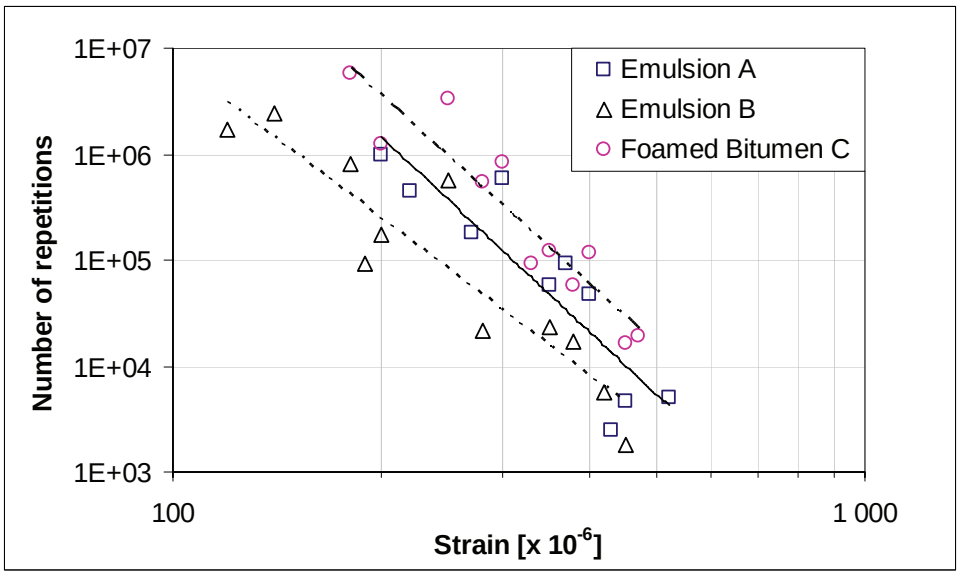


Figure 104: Fatigue lines for aggregate blends 75C-1 (10Hz and 5ºC). Note the reduction in strain that applies as discussed in Section 4.6.3

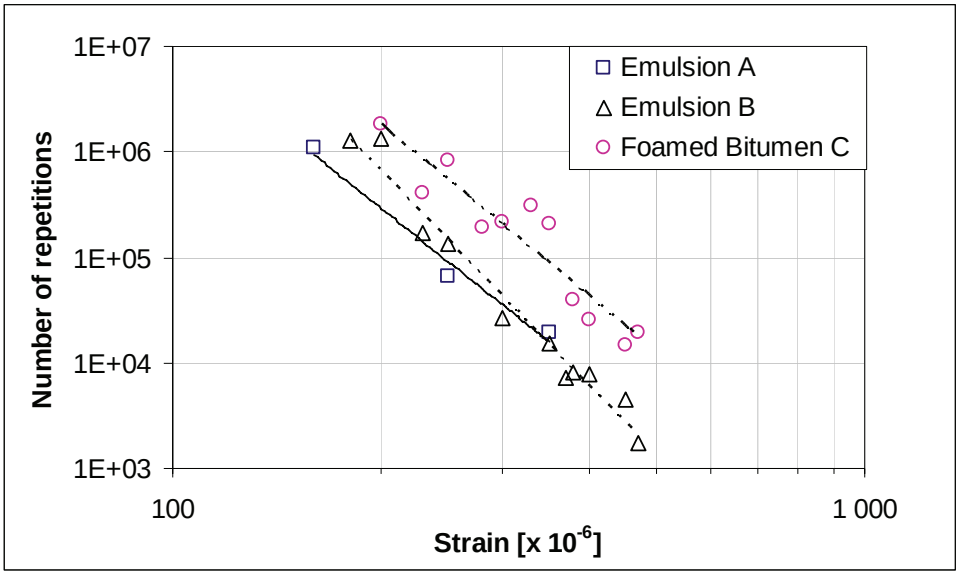


Figure 105: Fatigue lines for aggregate blends 75M-0 (10Hz and 5ºC). Note the reduction in strain that applies as discussed in Section 4.6.3

## References

Twagira, M. E., *Characterisation of Fatigue Performance of Selected Cold Bituminous Mixes*. M.Sc. Thesis University of Stellenbosch, South Africa, 2006

# 6 INTERPRETATION AND MODELLING OF MATERIAL PROPERTIES AND BEHAVIOUR

## 6.1 Introduction

In this Chapter the test results as presented in the previous chapter will be discussed and interpreted. Also will the models for material properties and behaviour as presented in Chapter 3 be applied to the experimental data. For each of the material properties the effect of the experimental variables will be discussed. These variables were discussed in Chapter 4 and can be summarised as:

- Increasing the proportion of RAP in the mix from 25% to 75%;
- Adding 1% of cement as active filler to the mixes; and
- Varying the type of binder, i.e. Emulsion A, Emulsion B and Foamed Bitumen C.

The influence of volumetric composition, such a difference in void content, binder content and compaction were factored out as much as possible. This was ensured by following consistent mixing and specimen preparation protocols. Therefore, when analysing the results in this chapter, only analyses in terms of the above listed experimental variables are made.

First the results of the tri-axial testing will be discussed, which include shear parameters, resilient modulus and permanent deformation behaviour. This chapter concludes with the discussion the of the results of the four-point beam testing, *i.e.* strain-at-break, flexural stiffness and fatigue behaviour.

## 6.2 Tri-axial testing

### *6.2.1 Shear parameters*

The failure envelope as defined in a Mohr-Coulomb diagram is characterised by the cohesion $C$ and the friction angle $\varphi$ and it represents a straight line. This was shown in Section 3.3.1. It is however generally recognised that when low applied compressive stresses or when cohesive material is subjected to small tensile stresses the failure envelope of the Mohr-Coulomb circles is non-linear (Theyse, 2006). When however the confinement pressures are sufficiently high, the Mohr-Coulomb failure line remains sufficiently accurate for material modelling purposes (Jenkins *et al.*, 2007).

The monotonic tri-axial test results as presented in the previous chapter are compared graphically in Figure 106. Typical shear parameters for crushed stone and natural gravel as used in South Africa are provided in Section 8.5.1 for comparison.

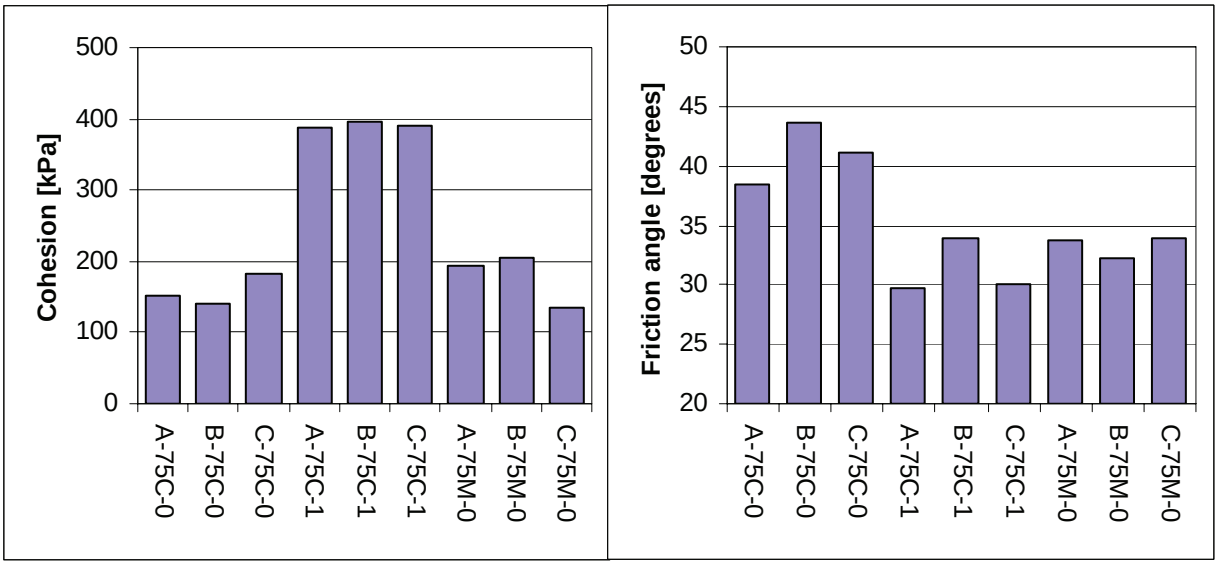


Figure 106: Cohesion and friction angle grouped per mix type

6.2.1.1 Cohesion

From Figure 106 it can be seen that there is little difference between the cohesion values of the same aggregate blends treated with either Emulsion A or Emulsion B. When treated with foamed bitumen however, slight differences compared to the emulsion treated blends are observed. For the aggregate blend with 75% crushed rock and no cement (75C-0), the cohesion of the mix treated with Foamed Bitumen C is slightly higher than that of the two emulsion mixes. For the aggregate blend with 75% RAP (75M-0) however, the cohesion of the foamed bitumen mix is slightly lower compared to the two bitumen emulsion mixes. When 1% of cement is added to blend with 75% crushed rock (75C-1) the differences in cohesion reduce and the results for both the bitumen emulsion and the foamed bitumen mixes is comparable.

It can also be seen that the addition of cement as active filler, even in small quantities (1%), has a significant effect on the cohesion, which increases from approximately 150 kPa to 390 kPa for the two emulsion mixes. The cohesion of the foamed bitumen treated mixes increases to a similar level (390 kPa) when 1.0% of cement is added. It would appear that the difference in cohesion for the aggregate blends without active filler as a result of the use of a different type of binder is masked by the addition of active filler.

It can be seen that the effect of increasing the proportion of RAP in the mix also depends on the type of binder used (compare mixes 75C-0 and 75M-0). In case of the two bitumen emulsions the cohesion increases from approximately 150 kPa to 200 kPa. When foamed bitumen is used the opposite occurs. The cohesion decreases from 184 kPa to 136 kPa. The difference in behaviour between the bitumen emulsion and the foamed bitumen for the 75% crushed rock blend and 75% RAP blend may be caused by the percentage of fines present in these mixes. It is known that foamed bitumen (compared to bitumen emulsion) requires a higher fines content to perform

at its best. There are substantial more fines is present in the 75% crushed rock mixes than in the 75% RAP mixes.

The effects of the experimental variables as discussed in Chapter 3, *i.e.* increasing the percentage of RAP, adding 1% cement and varying the type of binder, are summarised in Table 39.

Table 39: Effect of experimental variables on cohesion

| Experimental variable | Emulsion mixes | Foamed bitumen mixes |
|---|---|---|
| Increasing %-RAP | increase | decrease |
| Adding 1% cement | increase | increase |
| Type of binder | Emulsion A ≈ Emulsion B<br>emulsion < foam in combination with 75C-0<br>emulsion ≈ foam in combination with 75C-1<br>emulsion > foam in combination with 75M | |

6.2.1.2 Angle of internal friction

The angle of internal friction for the 75C-0 mixes ranges between 38.4º and 43.7º, while for the 75C-1 mixes the range is between 29.7º and 32.2º and for the 75M-0 mixes between 32.2º and 34.0º.

There is not a clearly discernable trend in the effect of the type of binder on the friction angle. For the mixes with 75% crushed rock (*i.e.* 75C-0 and 75C-1) the use of emulsion B results in a higher friction angle compared to when emulsion A is used. The friction angle of the mixes with foamed bitumen is in between the mixes with emulsion. For the mixes with 75% RAP the use of Emulsion B results in a slightly lower friction angle compared to when Emulsion A is used. There is little difference between the use of emulsion A and Foamed Bitumen C.

When the percentage of RAP in the mix is increased the friction angle reduces. This was observed for all three binder types. The friction angle also reduces when 1% of cement is added. The reduction of the friction angle is more significant in case 1% cement is added than when the percentage of RAP is increased.

The angle of internal friction is believed to be mostly dependent on aggregate properties such as grading and angularity of particles. There should therefore be little difference between the angles of internal friction for the 75% crushed rock blend with and without active filler, because the grading and particle angularity is approximately the same. However, the test results show a significant reduction from approximately 40º to approximately 30º. This is believed to be the result of the influence of the cohesion. The cohesion and friction angle are not entirely independent of each other since there is some sort of a balancing effect with the friction angle reducing when the cohesion increases significantly as a result of chemical stabilisation for the same material. Jenkins (2000) even reported friction angles of as low as 0º for crushed stone foamed bitumen mixes to which 1.5 to 2.0%

cement was added. The cohesion in these cases were reported as high as between 800 and 1100 kPa.

The effects of the experimental variables on the friction angle are summarised in Table 40.

Table 40: Effect of experimental variables on friction angle

| Experimental variable | Emulsion mixes | Foamed bitumen mixes |
|---|---|---|
| Increasing %-RAP | decrease | decrease |
| Adding 1% cement | decrease | decrease |
| Type of binder | Emulsion B > Foam C > Emulsion A for 75C mixes<br>Emulsion B < Emulsion A ≈ Foam C for 75M mixes | |

6.2.1.3 Maximum shear stress

The cohesion and friction angle cannot be evaluated and compared in isolation. What is of importance when comparing the performance of several mixes is the maximum shear stress that a material can withstand. This is dependent on both the cohesion and the friction angle. For each binder type, the effect of increasing the percentage of RAP and adding 1 % cement on the shear stress is shown in Figure 107, Figure 108 and Figure 109.

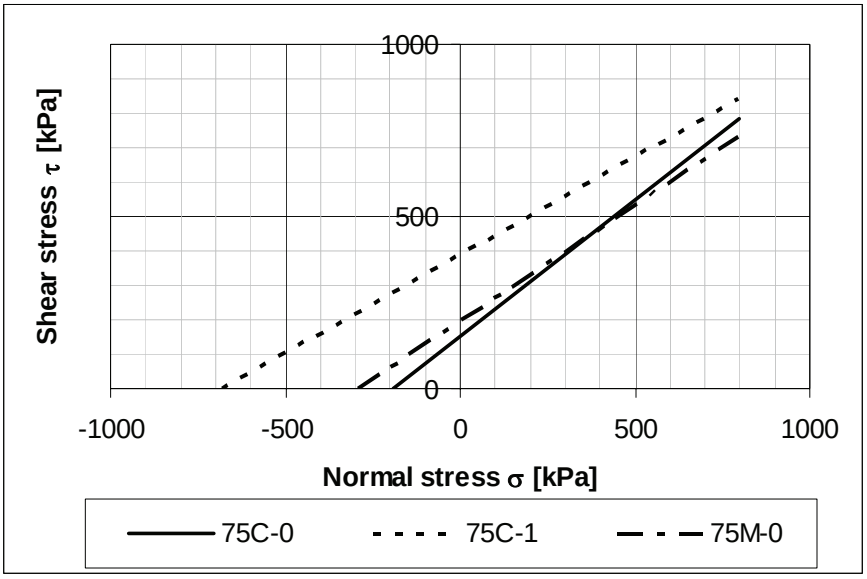


Figure 107: Maximum shear stress for mixes with Bitumen Emulsion A

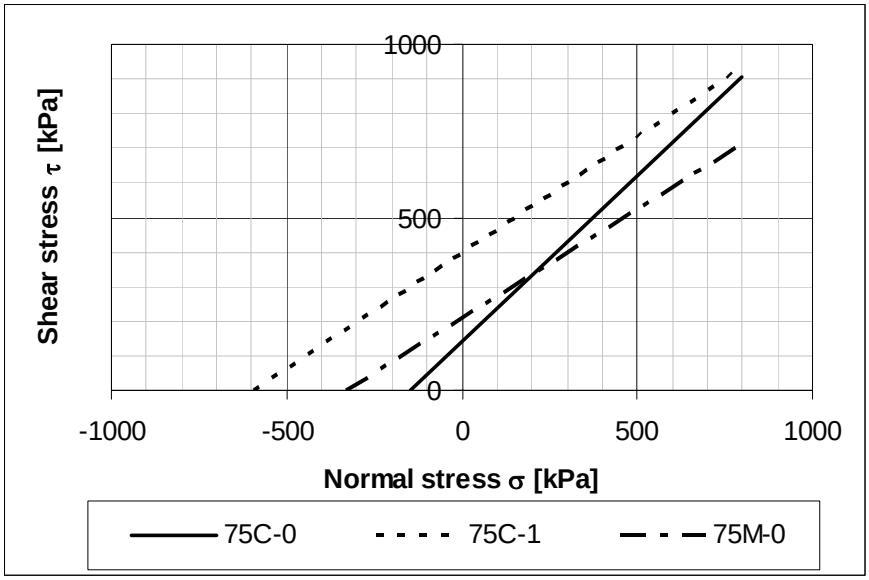


Figure 108: Maximum shear stress for mixes with Bitumen Emulsion B

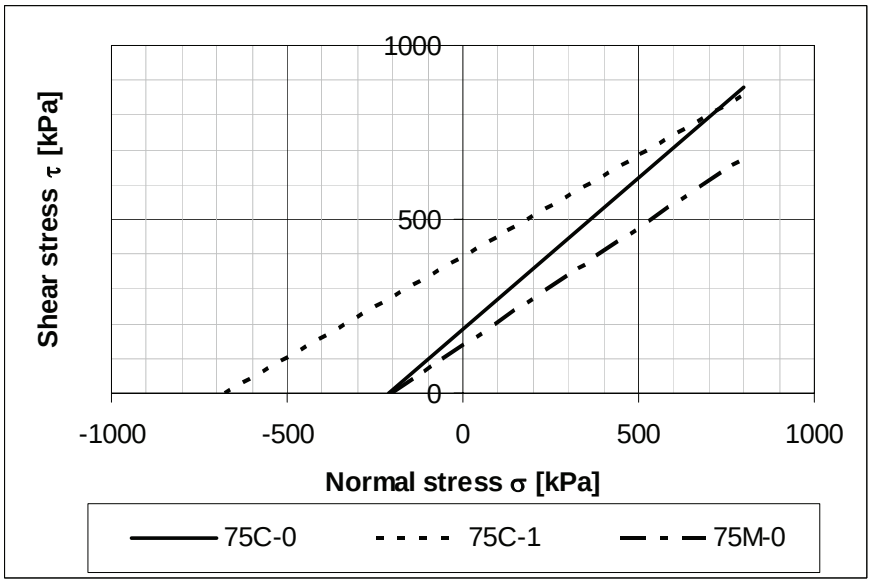


Figure 109: Maximum shear stress for mixes with Foamed Bitumen C

The effects of the experimental variables on the maximum shear stress are summarised in Table 41.

Table 41: Effect of experimental variables on maximum shear stress

| Experimental variable | Emulsion mixes | Foamed bitumen mixes |
|---|---|---|
| Increasing %-RAP | increase at low stress<br>decrease at high stress<br>(more pronounced for Em. B) | decrease |
| Adding 1% cement | increase | increase |
| Type of binder | emulsion A ≈ emulsion B ≈ foam C for 75C-0 mixes<br>(A slightly lower at high stresses)<br>emulsion A ≈ emulsion B ≈ foam C for 75C-1 mixes<br>(B slightly higher at high stresses)<br>emulsion A ≈ emulsion B > foam C for 75M mixes | |

6.2.1.4 Estimated compressive and tensile strength from Coulomb failure line

The Coulomb failure line in the Mohr Diagram can be used to estimate a compressive strength (case with $\sigma_3 = 0$) and a tensile strength ( case with $\sigma_1 = 0$). These two cases are shown in Figure 110.

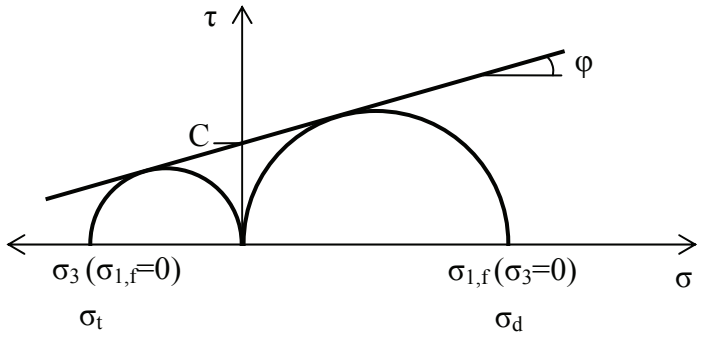


$$\sigma_{1,f} = \frac{1+\sin\varphi}{1-\sin\varphi}\sigma_3 + \frac{2 \cdot C \cdot \cos\varphi}{1-\sin\varphi}$$

Figure 110: Compressive and tensile strength in Mohr-Coulomb Diagram

The compressive and tensile strength that can be estimated in this manner are summarised in Table 42 and graphically shown in Figure 110.

Table 42: Estimated compressive and tensile strength from monotonic tri-axial testing (Mohr-Coulomb Diagram)

| Mix | Estimated compressive strength [kPa] | Estimated tensile strength [kPa] |
|---|---|---|
| A-75C-0 | 630 | 147 |
| A-75C-1 | 664 | 121 |
| A-75M-0 | 747 | 155 |
| B-75C-0 | 1333 | 449 |
| B-75C-1 | 1487 | 423 |
| B-75M-0 | 1403 | 525 |
| C-75C-0 | 732 | 209 |
| C-75C-1 | 748 | 228 |
| C-75M-0 | 512 | 145 |

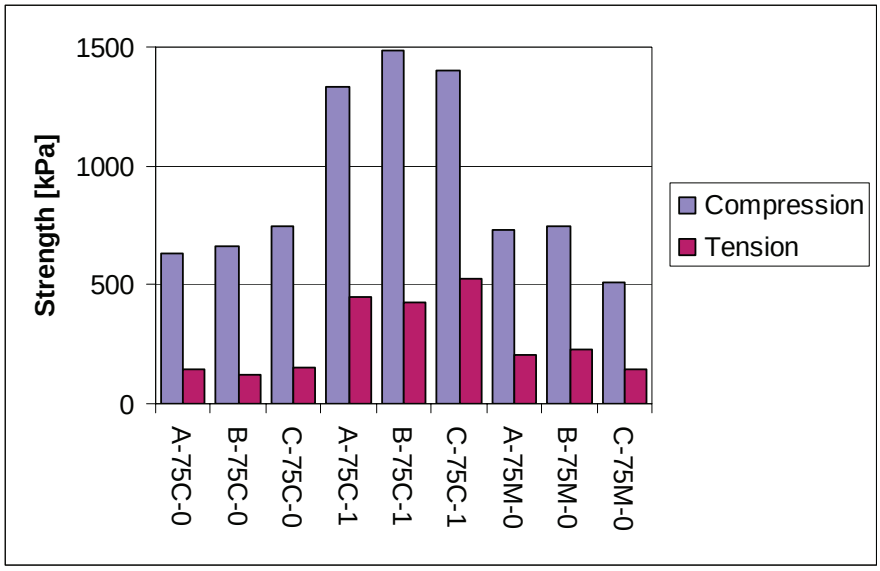


Figure 111: Estimated compressive and tensile strength from monotonic tri-axial testing (Mohr-Coulomb Diagram)

It can clearly be seen that the effect of the experimental variables and trends as discussed for the shear strength in the previous section also apply to the estimated compressive and tensile strength. When adding 1% of cement, both the compressive and tensile stresses increase significantly. When increasing the percentage of RAP in the mix, the tendency for the bitumen emulsion mixes is to increase in strength, while for the foamed bitumen mixes there is a decreasing trend.

6.2.1.5 Strain-at-failure

As discussed in Chapter 3, the strain-at-failure, $\varepsilon_f$, during the monotonic tri-axial test is a parameter that could possibly provide some additional inside in the material

characterisation. The strain-at-failure at each of the four confinement pressures for all nine mixes tested is summarised in Figure 112. Looking at the confinement pressure only, there is a trend that the strain-at-failure increases with increasing confinement pressure. This would indicate that the strain-at-failure is stress-dependent parameter. This stress dependency becomes more evident when the strain-at-failure is plotted against the Bulk Stress $\theta$. These plots are shown in Figure 113.

It can be seen that the strain-at-failure $\varepsilon_f$ ranges from 1.0 % at the lowest confinement pressure to 2.5 % at the highest confinement pressure. The strain-at-failure is most stress-dependent for the 75C-0 mixes, regardless of the type of binder used. When 1.0 % cement is added as active filler to the mix (75C-1 mixes), $\varepsilon_f$ becomes much less stress-dependent and ranges from 1.2 % to 1.7 %. It is only with the mixes that have a high percentage of RAP (75M-0) that a clear difference between the two bitumen emulsion binders and the foamed bitumen binder can be observed. The foamed bitumen mix (C-75M-0) has a higher strain-at-failure than the two bitumen emulsion mixes.

Shear failure for any of the mixes and at any of the confinement pressures only occurs when the strain is in excess of 1.0 %. It would appear that this strain level could be regarded as a threshold limit, below which shear failure does not occur under monotonic loading.

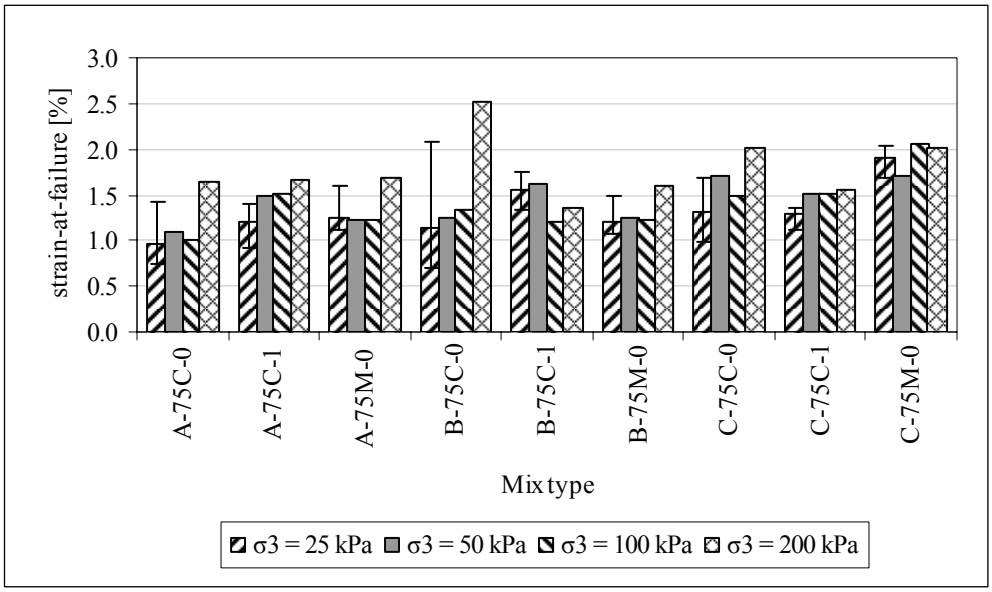


Figure 112: Strain-at-failure per mix and confinement pressure

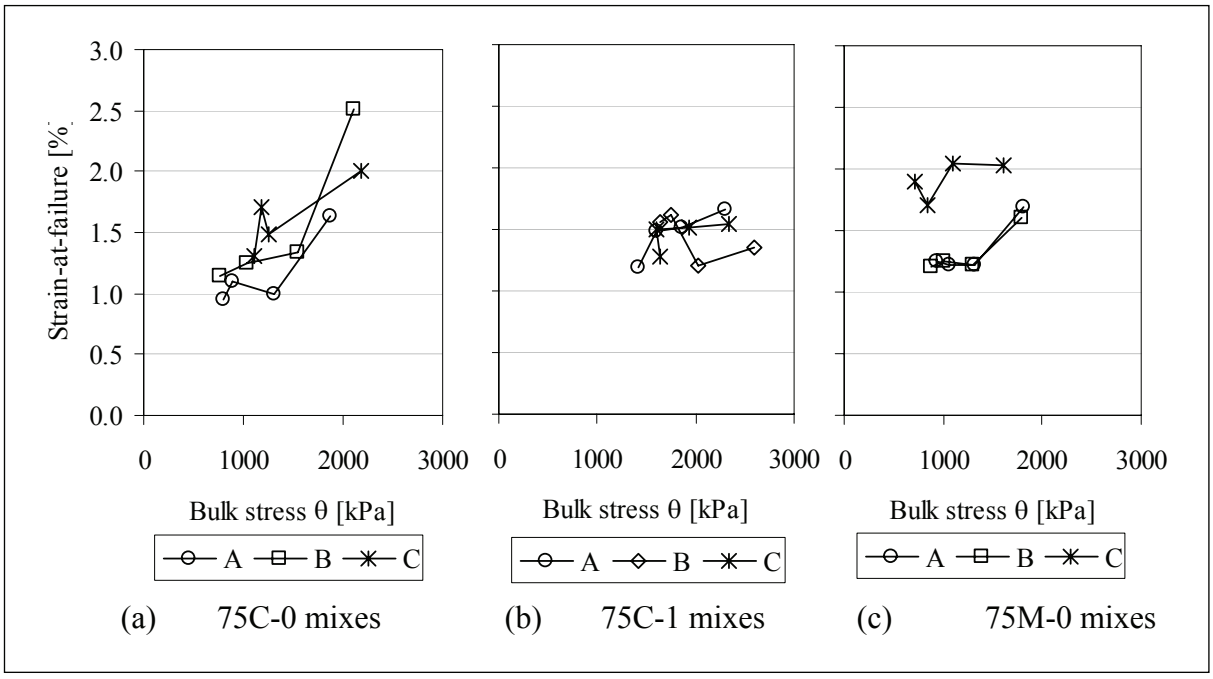


Figure 113: Strain-at-failure vs. bulk stress for each of the three aggregate blends

6.2.1.6 Tangent modulus

The tangent modulus, $E_{tan}$, as defined Chapter 3, is another material property that may be derived from the monotonic tri-axial test. The tangent modulus of all nine mixes is summarised in Figure 114. It can be seen that the tangent modulus generally varies between 50 MPa and 200 MPa. As the tangent modulus is determined from the linear part of the stress-strain diagram, it should provide an indication of the elastic stiffness modulus of the material.

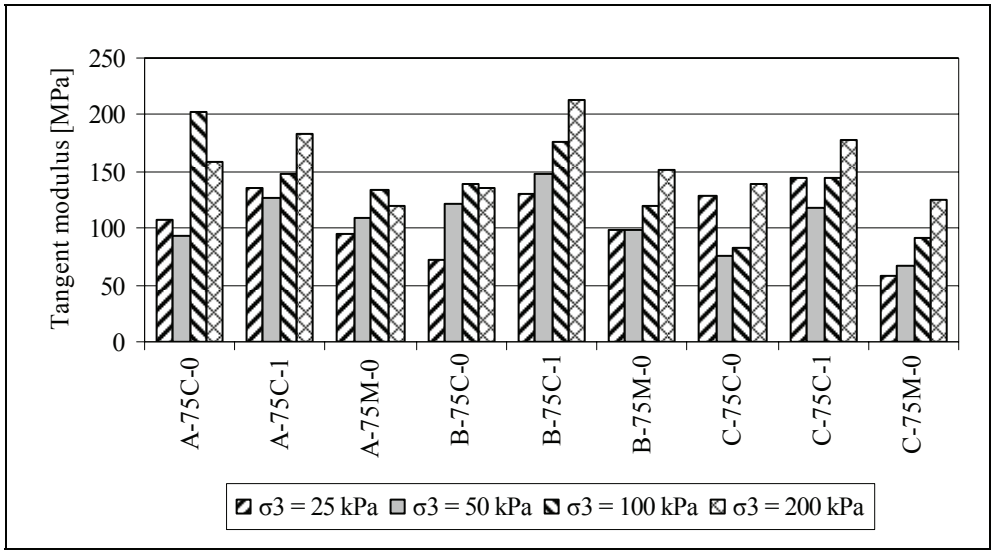


Figure 114: Tangent modulus per mix and confinement pressure

The tangent modulus also shows a stress dependent behaviour, although for some mixes (*eg.* A-75C-0, C-75C-0 and C-75C-1) this trend is less consistent. When comparing the three different blends per binder, the blends with 1 % cement (75C-1) show without exception the highest tangent modulus. The tangent moduli for these three 75C-1 mixes are comparable. There is also a tendency that when comparing the three different blends per binder, the blend with 75 % RAP (75M-0) shows the lowest tangent modulus. Finally, it can clearly be seen that the C-75M-0 mix provides the lowest tangent moduli of all nine mixes.

The tangent modulus is an order of magnitude lower than the resilient modulus as determined in the dynamic tri-axial test. In comparing the tangent moduli and the resilient moduli, one should keep in mind that the loading rate during the monotonic tri-axial test is also an order of magnitude lower than in the dynamic resilient modulus tri-axial test. The latter is carried out at a loading frequency of 10 Hz. The strains observed during the resilient modulus tests in combination with a loading frequency of 10 Hz result in loading rates in the order of 1.0 % strain/sec for the dynamic tests. The strain rate for the monotonic tests is 0.1 % strain/sec. The significant difference in loading rates could be one of the major factors that result in the differences observed.

Furthermore, it needs to be kept in mind that there is a systematic error between the tangent modulus as derived from the monotonic tri-axial test and the resilient modulus derived from the dynamic tri-axial test. This results from the different manner in which displacements are measured (actuator LVDT *vs.* on-specimen LVDT's).

#### 6.2.1.7 Secant modulus

Finally, the secant modulus, $E_{sec}$, also defined in Chapter 3, has been determined here. The secant modulus for each of the nine mixes is shown in Figure 115. As opposed to the two parameters discussed above ($\varepsilon_f$ and $E_{tan}$), the secant modulus shows no clear stress dependency. This can be explained by the fact that both the maximum stress and the strain-at-failure increase with increasing bulk stress. As both parameters have a similar but opposite effect on the secant modulus, the net effect is little change to the secant modulus. There would also appear to be less variation between the nine mixes when evaluating the secant modulus. This parameter, the secant modulus, is therefore regarded as not having the potential to evaluate mixes qualitatively nor quantitatively.

Nevertheless, the secant modulus does show that the blends with active filler have the highest stiffness per binder. Also, the C-75M-0 mix shows the lowest secant modulus, as it did for the tangent modulus. This is in line with the other type of tests discussed in this study.

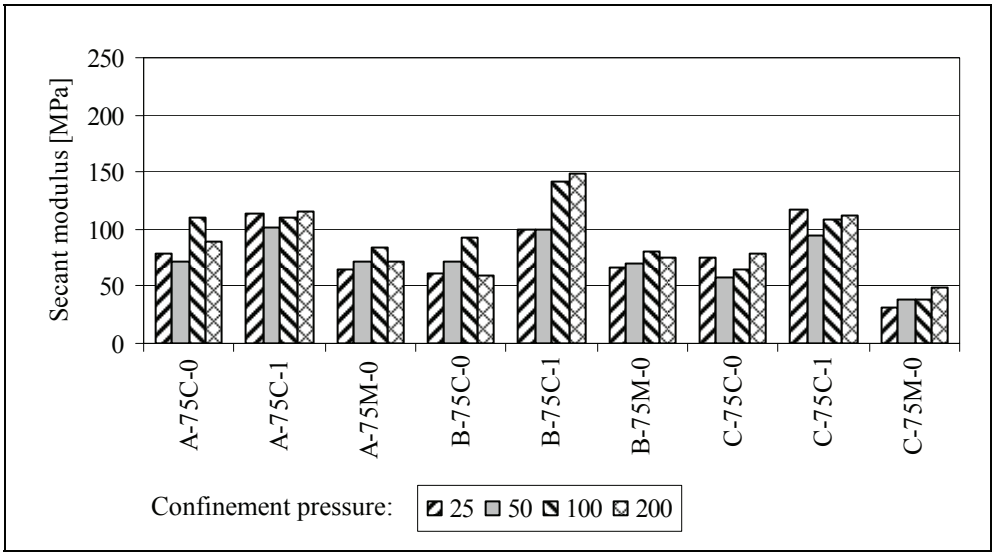


Figure 115: Secant modulus per mix and confinement pressure

### *6.2.2 Resilient modulus*

As discussed in Chapter 3, one of the most common models to describe the stress dependent behaviour of a material is the so-called $M_r$-$\theta$ model. A summary of the model coefficients $k_1$ and $k_2$ is given in Table 43. It can be seen from this table that not all mixes show a $M_r$-$\theta$ relation with a good fit ($R^2$-value). It would appear that this is related to the aggregated blend used. The mixes with 75% crushed rock (75C-0) show the best coefficient of correlation. This is especially so for the mixes with either of the two emulsions (Binder A and B). The repeat test on Mix C-75C-0 (test *c*) also shows a good fit. Although the $R^2$-value of C-75C-0 (test *a*) is low, it can be seen (see Appendix F) that visually the test results do not oppose the $M_r$-$\theta$ model.

For the mixes with 75% crushed rock and 1% active filler the model fits slightly less good. Nevertheless, for Binder A the $R^2$-values are still very good. With Binder B there is still an increase noticeable with increasing bulk stress at a constant confinement pressure. However, as the bulk stress increases due to an increase in confinement pressure, the stiffness behaviour starts to deviate from the typical $M_r$-$\theta$ model behaviour. For the mixes with Binder C, the results show a reduction in stiffness as the bulk stress increases (stress softening) at a constant confinement pressure. This is most pronounced for the highest confinement pressure. This behaviour cannot be appropriately modelled by the $M_r$-$\theta$ model.

The stress softening effect with increasing bulk stress at a constant confinement pressure becomes a more regular pattern in case of the mixes with 75% RAP (75M-0). It can be seen that for none of the mixes with 75% RAP the correlation with the $M_r$-$\theta$ model is good. In order to be able to describe the observed behaviour of these mixes a parabolic model developed by van Niekerk as discussed in Chapter 3 should be explored.

Table 43: Model coefficients $k_1$ and $k_2$ ($M_r$-$\theta$ model)

| Aggregate blend | Binder | Repeat test | $k_1$ [MPa] | $k_2$ [-] | $R^2$ |
|---|---|---|---|---|---|
| 75C-0 | A | a | 124.53 | 0.3008 | 0.907 |
| | | b | 134.34 | 0.2957 | 0.975 |
| | B | a* | - | - | - |
| | | b* | 241.52 | 0.1641 | 0.669 |
| | | c | 132.79 | 0.3639 | 0.904 |
| | C | a | 744.29 | 0.0269 | 0.034 |
| | | b** | - | - | - |
| | | c | 287.2 | 0.165 | 0.378 |
| 75C-1 | A | a | 109.09 | 0.3676 | 0.843 |
| | | b | 193.73 | 0.2958 | 0.930 |
| | B | a | 1314.2 | -0.0042 | 0.001 |
| | | b | 427.4 | 0.1926 | 0.812 |
| | C | a | 997.04 | 0.0663 | 0.205 |
| | | b | 752.38 | 0.0879 | 0.308 |
| 75M-0 | A | a | 1238.6 | -0.0241 | 0.013 |
| | | b | 2805.9 | -0.1305 | 0.257 |
| | B | a | 1525.4 | -0.0526 | 0.106 |
| | | b | 200.51 | 0.2529 | 0.175 |
| | C | a | 974.29 | 0.0101 | 0.002 |
| | | b | 623.37 | 0.0656 | 0.147 |

Notes * : Some of the LDVT's out of range or unreliable during the test
** : Specimen failed during conditioning

The effect of the experimental variables on the resilient modulus is somewhat difficult to discern because of the variability between some of the repeat tests and the variation in the test result of a single test.The general trends are however summarised in Table 44.

Table 44: Effect of experimental variables on resilient modulus

| Experimental variable | Emulsion mixes | Foamed bitumen mixes |
|---|---|---|
| Increasing %-RAP | increase at low bulk stress, no effect at high end of bulk stress tested | small increase |
| Adding 1% cement | increase | increase |
| Type of binder | 75C-0: C > B > A, similar at high $\theta$<br>75C-1: A ≈ B ≈ C (A slightly lower at low $\theta$)<br>75M-0: A ≈ B > C (A slightly lower at low $\theta$) | |

The resilient modulus of the 75C-0 mixes ranges from approximately 600 MPa at the lower bulk stresses to about 1200 MPa at the high end of the bulk stresses tested. The largest differences between the different binders occur at the lower bulk stresses, where Emulsion A has the lowest resilient modulus and Foamed Bitumen C the highest.

Adding 1% cement as active filler to the mix results in a significant increase in the resilient modulus of all the mixes (compare 75C-0 mixes with 75C-1 mixes). The resilient modulus for the 75C-1 mixes ranges from approximately 900 MPa at the lower bulk stresses to about 1500 MPa at the higher bulk stresses. There is no significant difference between the different binders used.

Increasing the percentage of RAP in the mix results in an increase in the resilient modulus, particularly at the lower bulk stresses. Because the mixes with a high percentage of RAP are less "stress stiffening" the difference at the higher bulk stresses is smaller. The resilient modulus of the 75M-0 mixes is more dependent on the applied deviator stress than on the bulk stress. Increasing the applied deviator stress leads to a reduction in resilient modulus. There is also no significant difference between the different binders used.

### *6.2.3 Permanent deformation*

6.2.3.1 Phases of permanent deformation

Permanent deformation is believed to occur in three phases. During the first phase the accumulation of permanent deformation takes initially place at a fast rate. This can mainly be attributed to bedding-in, seating of the loading plates and initial permanent strain due to densification. The deformation during this initial phase follows a hyperbolic curve. It can be seen that most of the deformation takes place in the first 20,000 load repetitions. Afterwards the rate of deformation starts to reduce. The first phase can last up to 200,000 load repetitions or even more depending on the type of mix and the applied loading. An extreme case was observed for the both emulsion mixes (A and B) with the 75M-0 aggregate composition where the 4 % plastic strain limit was reached after approximately 500,000 load repetitions at a

stress ratio of 0.45, but where the permanent deformation accumulation was still following the trend of the initial phase.

The second phase is characterised by a constant rate of deformation. The accumulation of permanent deformation is more or less linear with respect to load repetitions. The third phase is one of accelerated accumulation of permanent deformation due to tertiary flow. During the third phase the material may be considered to be failing in shear under repeated loading. The third phase starts at the so-called flow-point, which is the number of load repetitions at which the strain accumulation rate is minimal. Up until the flow point the rate of strain accumulation reduces, while after the flow point the rate of strain accumulation accelerates.

The number of load repetitions at which the flow point occurs cannot easily be predicted, as tertiary flow may initiate quite unexpectedly. For some of the tests conducted this transition took place after a number of load repetitions varying from 100,000 to 500,000 following a second phase with a stable and low rate of permanent deformation accumulation.

6.2.3.2 Critical deviator stress ratios

Previous researchers, as discussed in Chapter 3, already identified the existence of a critical stress ratio. When a material is repeatedly loaded above this critical deviator stress ratio the permanent deformation behaviour includes a third phase as described above. Repeated loading below this critical stress ratios results in a ongoing stable second phase behaviour.

The critical deviator stress ratios as identified for the mixes tested here are summarised in Table 45 below:

Table 45: Range of critical deviator stress ratio summarised per mix composition and binder type ($\sigma_3$ = 50 kPa, 25 ºC and 2 Hz)

| Mix composition | Emulsion A | Emulsion B | Foamed Bitumen C |
|---|---|---|---|
| 75C-0 | 0.30 – 0.40 | 0.50 – 0.60 | 0.40 – 0.50 |
| 75C-1 | < 0.40 | < 0.45 | 0.40 – 0.50 |
| 75M-0 | 0.45 – 0.50 | 0.45 – 0.60 | 0.45 – 0.60 |

The addition of 1% active filler (cement) to the 75C mixes results in similar first and second phases of permanent deformation accumulation, but a much more abrupt third phase. While the mixes without active filler exhibit a gradual acceleration in the accumulation of permanent deformation, the mixes with active filler fail relatively quickly after the second phase. This effect is most pronounced for Bitumen Emulsion A and Foamed Bitumen C.

From the results presented in Chapter 5 it can be seen that the initial plastic strain for the mixes with 75M-0 mixes (75% RAP) is higher than for the 75C-0 mixes. Furthermore the rate of accumulation of permanent deformation during the secondary phase is also higher for the 75M-0 mixes. This is however compensated

by the fact the 75M-0 mixes can withstand higher levels of plastic strain before tertiary flow initiates. This may indicate that mixes with a high percentage of RAP have initially less resistance to permanent deformation, but are tougher at high plastic strain levels. The former may be caused by the fact that the friction angle of the 75M-0 mixes is much lower than the 75C-0 mixes. The latter may be the result of the higher cohesion and the interaction between the newly added binder and the binder already present in the RAP material. Based on this one could state that the 75M-0 material is a more ductile material than the 75C-0 material, even though the residual binder added is lower (2.4% versus 3.6%). Furthermore, it can be seen from Table 45 that the critical stress ratio for the 75M-0 mixes (all binders) is the highest of the three types of mix composition. This critical stress ratio is fairly constant over the range of binders tested and can be as high as 0.60. The effects of the experimental variables on the critical deviator stress ratio are summarised in Table 46.

Table 46: Effect of experimental variables on critical deviator stress ratio

| Experimental variable | Emulsion mixes | Foamed bitumen mixes |
|---|---|---|
| Increasing %-RAP | increase | increase |
| Adding 1% cement | decrease | no effect |
| Type of binder | B ≈ C > A<br>(B slightly higher than C for mixes 75C-0) | |

The influence of the stress ratios on the number of load repetitions to reach a certain strain level is summarised in Figure 116 and Figure 117 for 1 % and 4 % plastic strain respectively. For a 200 mm thick pavement layer 1 % strain equates to a total deformation of 2 mm at the top of the layer. For 4 % strain this is 8 mm at the top of the layer.

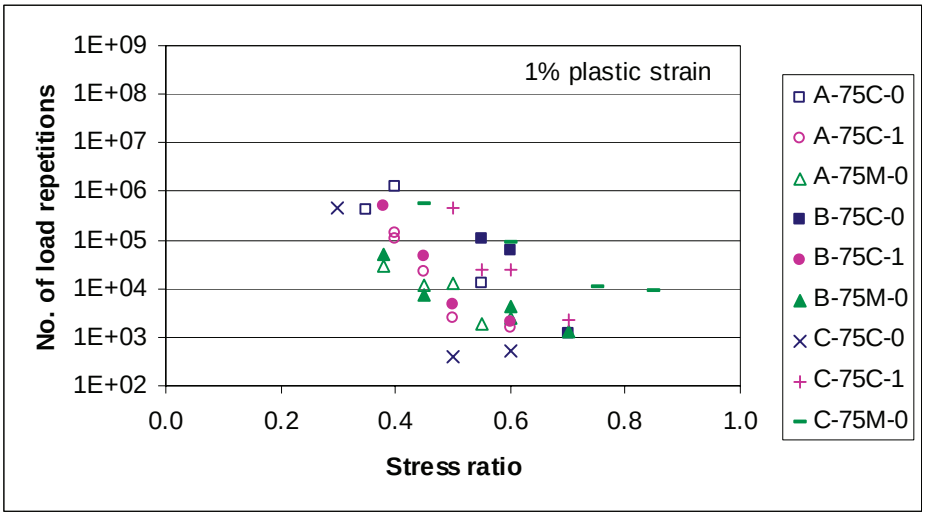


Figure 116: Influence of deviator stress ratio on permanent deformation to achieve 1% plastic strain

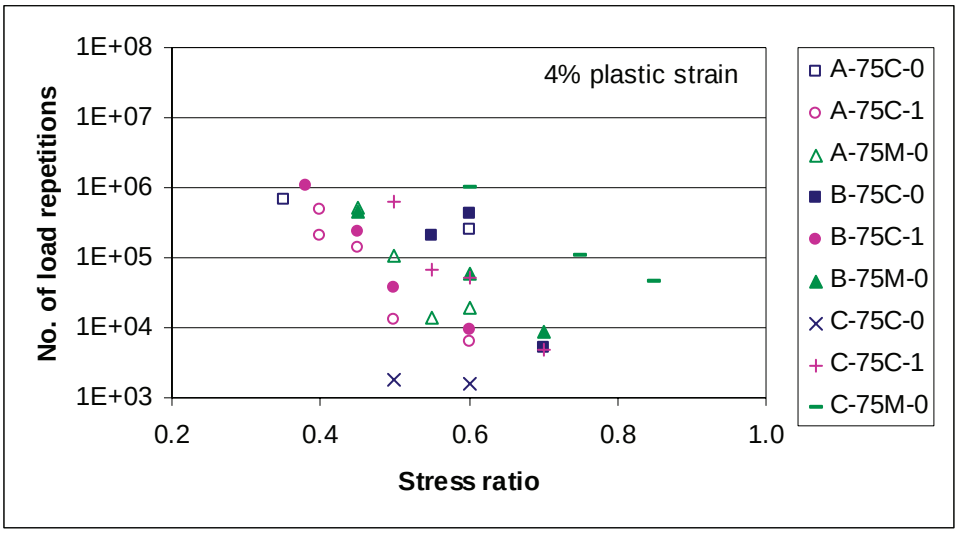


Figure 117: Influence of deviator stress ratio on permanent deformation to achieve 4% plastic strain

The mixes with active filler seem to be more sensitive to the stress ratio. With all binders, the reduction in allowable number of load repetitions with increasing stress ratio is higher for the mixes with active filler than for the mixes without active filler. This is most clearly demonstrated by comparing mix A-75C-0 and A-75C-1 (Figure 117). The same effect can also be seen in Table 45, where the critical stress ratio range is generally lowest for the 75C-1 mix for each binder type. The critical stress ratio for cemented mixes appears not to exceed 0.45.

At the high stress ratios, Emulsion A and B perform similarly, while at the lower stress ratios emulsion B seems to perform slightly better. This is the case for all three aggregate blends. At the same time, the range of critical stress ratio for the mixes with Emulsion B are higher than for the mixes with Emulsion A. This is most pronounced for the 75C-0 mix. This may indicate that Emulsion B performs slightly better than Emulsion A.

The difference in performance between bitumen emulsion and foamed bitumen is not unequivocal and seems to be dependant on the mix composition. For the 75C-0 mixes the bitumen emulsions clearly perform better, while for the 75M-0 mixes the opposite is true. In fact the C-75M-0 mix performs the best of all in terms of resistance to permanent deformation. For the mixes with active filler (75C-1) the foamed bitumen performs more or less the same as both bitumen emulsions. This may indicate that foamed bitumen works better in combination with a high percentage of RAP than with a high percentage of virgin aggregate. This is contrary to the performance of this mix in terms of maximum shear stress (see Figure 109).

#### 6.2.3.3 Permanent deformation curves and model coefficients

As discussed in Chapter 4, it was found that the stress dependency of the Model Parameter A, B, C and D of the two types of bitumen emulsions that were used, followed the same trend. It was therefore decided to combine the data of the two

bitumen emulsion mixes and develop one model permanent deformation curve that, depending on the type of blend used, describes the permanent deformation behaviour of the bitumen emulsion mixes (Emulsion A and Emulsion B). The number of model permanent deformation curves is hereby reduced from nine to six, *i.e.* three bitumen emulsion model curve sets (A+B-x-x) and three foamed bitumen model curve sets (C-x-x). These three sets for each binder type consist of one set for the aggregate blend with 75% crushed rock and no active filler (75C-0), one for the aggregate blend with 75% crushed rock and 1% active filler (75C-1) and one set for the aggregate blend with 75% RAP and no active filler (75M-0). The model coefficients $a_1$, $a_2$, $b_1$, …, $d_2$ as discussed in Chapter 3 are summarised in Table 47.

Table 47: Model coefficients of PD curves according to type of binder (bitumen emulsion or foamed bitumen) and type of aggregate blend

| Mix | Model coefficients | | | | | | | |
|---|---|---|---|---|---|---|---|---|
| | $a_1$ | $a_2$ | $b_1$ | $b_2$ | $c_1$ | $c_2$ | $d_1$ | $d_2$ |
| A+B-75C-0 | 0.92 | 1.45 | 0.66 | 1.47 | $1.9\cdot10^{-7}$ | -12.14 | $7.9\cdot10^{0}$ | 8.72 |
| C-75C-0 | 6.16 | 2.07 | 14.54 | 4.27 | $2.1\cdot10^{-3}$ | -8.41 | $1.3\cdot10^{-3}$ | 10.72 |
| A+B-75C-1 | 2.53 | 2.39 | 2.31 | 2.47 | $4.9\cdot10^{2}$ | 18.09 | $3.3\cdot10^{1}$ | 7.81 |
| C-75C-1 | 0.59 | 0.90 | 2.29 | 3.30 | $7.3\cdot10^{-2}$ | 11.18 | $1.5\cdot10^{2}$ | 12.66 |
| A+B-75M-0 | 0.83 | 0.75 | 1.74 | 2.05 | - | - | - | - |
| C-75M-0 | 0.43 | 1.00 | 0.60 | 1.04 | $1.0\cdot10^{-1}$ | 2.61 | $2.4\cdot10^{-1}$ | 7.80 |

Note: E = Emulsion A + Emulsion B combined, and F = Foamed Bitumen C.

Because no tertiary flow was observed for the A+B-75M-0 mixes, no values for the model parameter C and D could be determined.The stress dependency of the model parameter A, B, C and D as numerically expressed by the model coefficients shown in Table 47, is graphically shown in Figure 118 - Figure 121 respectively.

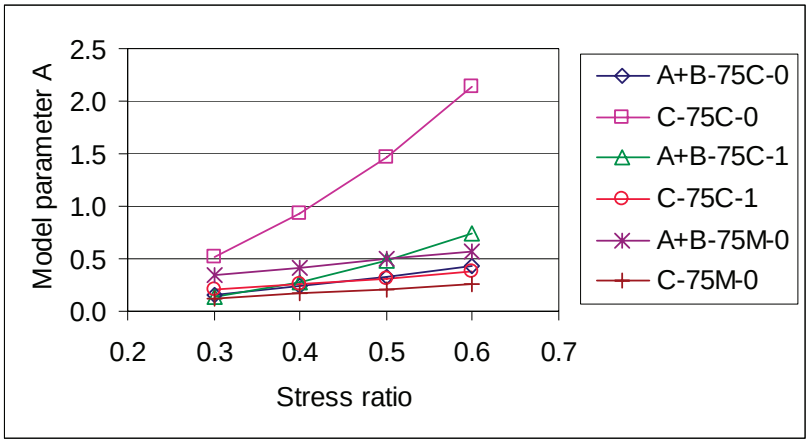


Figure 118: Stress dependency of model parameter A

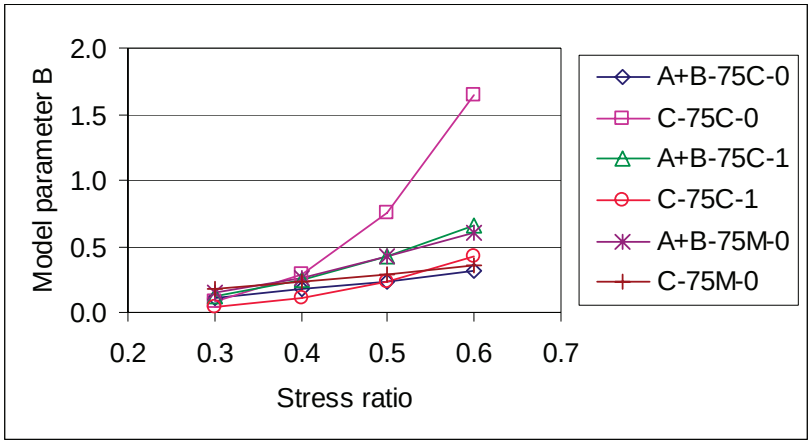


Figure 119: Stress dependency of model parameter B

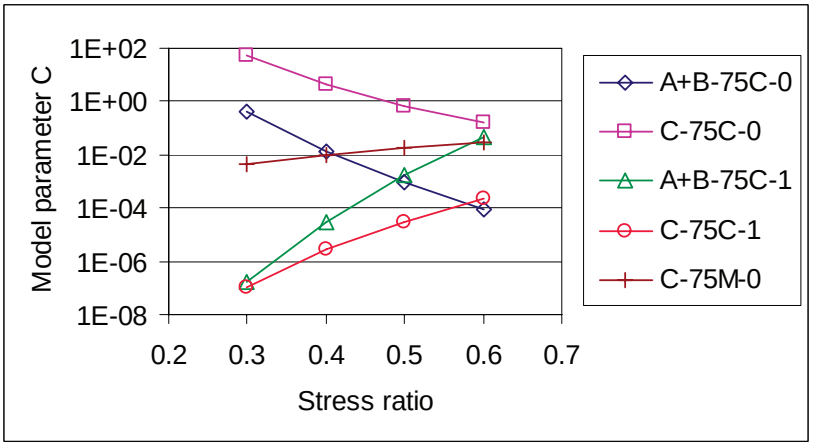


Figure 120: Stress dependency of model parameter C

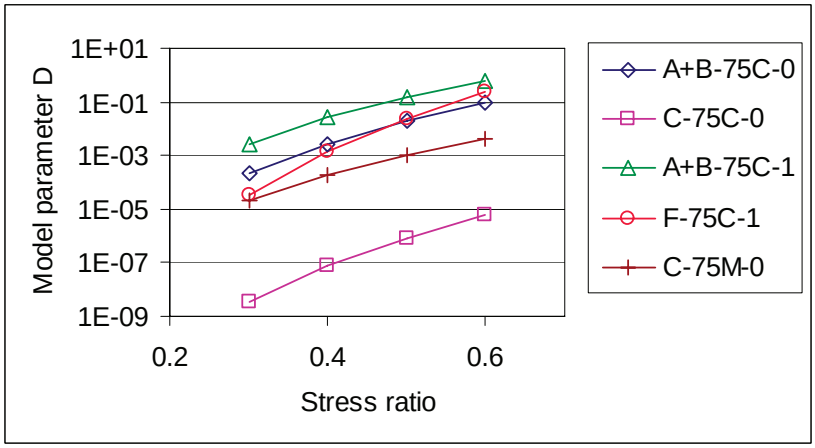


Figure 121: Stress dependency of model parameter D

With the model coefficients summarised in Table 47 model fits such as those shown in Figure 122 and Figure 123 are obtained. The model fits of all nine mixes are shown in Appendix G. The model fit shown in Figure 122 is a typical example of the PD behaviour of a BSM material with active filler. A well defined flow point and

tertiary flow phase can clearly be distinguished for all stress ratio's tested. The model fit shown in Figure 123 is a typical example of a BSM material with a high percentage of RAP and stabilised with bitumen emulsion. No tertiary flow can be distinguished.

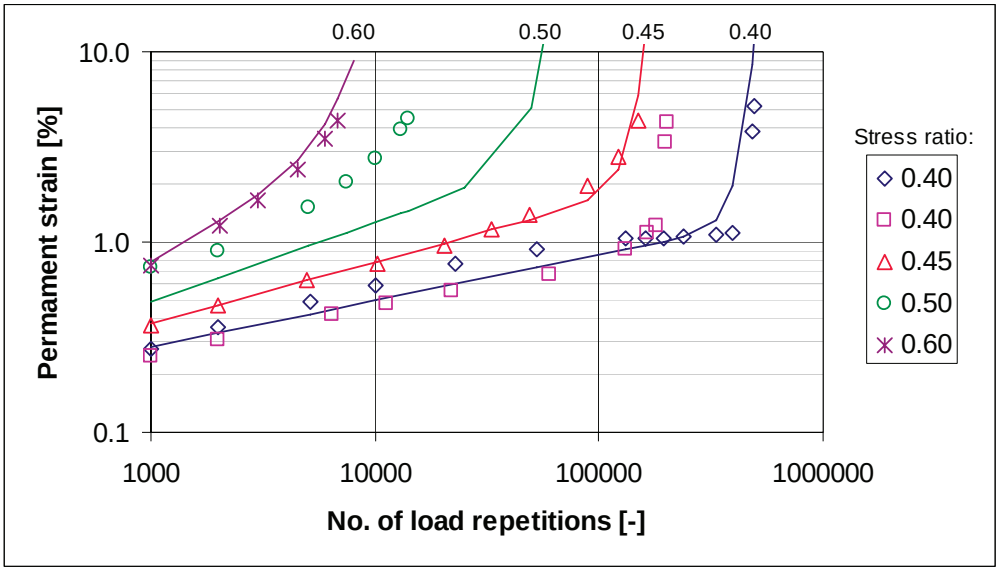


Figure 122: PD curves A-75C-1; experimental data and model fits

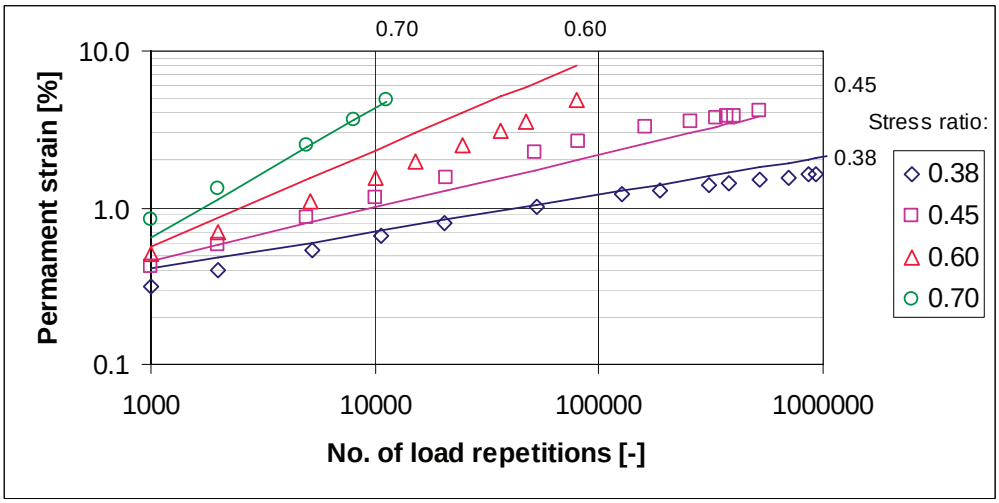


Figure 123: PD curves B-75M-0; experimental data and model fits

6.2.3.4 Discussion of model coefficients

Model parameters A and B describe the linear part of the permanent deformation curve up to the flow point. From Table 47 it can be seen that, except for mixes C-75C-0 and A+B-75C-1, the exponent $a_2$ for model parameter A is close to one. This indicates a near linear stress dependency for most of the mixes. Even for the mixes C-75C-0 and A+B -75C-1 the stress dependency of model parameter A is not distinct exponential ($a_2$ exponent of 2.07 and 2.39 respectively). It can thus be concluded that the stress dependency of model parameter A, which is a measure of the initial

permanent axial strain at 1000 load repetitions, is near linear. The slope of this stress dependency curve is determined by the multiplier $a_1$ (when $a_2$ is close to one). The two mixes C-75C-0 and A+B -75C-1 also have the largest multiplier values, *i.e.* 6.16 and 2.53 respectively, while the multiplier values of model parameter A for the other mixes are all below one.

Based on the above it can be concluded that mixes C-75C-0 and A+B -75C-1 show the highest stress dependency. Due to the large multiplier for mix C-75C-0, this mix has the highest values for model parameter A. This means that this mix shows the largest initial permanent strains (after 1000 load repetitions). Due to the combination of higher multiplier and higher exponent value for mix A+B -75C-1, the values of model parameter A for this mix is only higher than for the other mixes at the higher stress ratios (S.R. > 0.5).

It should be noted that with a high percentage of virgin crushed rock the foamed BSM shows the highest initial permanent strain, while with a high percentage of RAP the foamed BSM shows the lowest initial permanent strain. It is also noteworthy that for the mixes with 1% of cement as active filler added, the foamed BSM shows lower initial permanent strains (model parameter A) than the emulsion BSM.

Model parameter B is a measure of the slope of the linear part of the PD curve. This parameter is determined by the multiplier $b_1$ and exponent $b_2$. Model parameter B is generally more stress dependent than model parameter A and the stress dependency curves have more of an exponential shape (only two of the six mixes, i.e. A+B -75C-0 and C-75M-0) have exponent values below 2 for the B model parameter). This is most pronounced for mix C-75C-0. Also the multipliers $b_1$ are generally higher (only two of the six mixes, i.e. A+B -75C-0 and C-75M-0) have multipliers values below one for the B model parameter). The multiplier of mix C-75C-0 is with a value of 14.5 the highest.

The initial permanent strain and the slope of the PD curve need to be interpreted in conjunction with each other. A low initial permanent strain does not mean a lot when the slope of the linear part of the PD curve is very high. Also, a high initial permanent strain is not necessarily a problem when the slope of the PD curve is very low.

Model parameters C and D determine the tertiary flow part of the PD curve. Model parameter C is a measure of the abruptness with which tertiary flow occurs, while model parameter D determines the flow point. Although the occurrence of tertiary flow is mainly governed by the model parameter D, both model parameters C and D need to be evaluated in conjunction. The abruptness of tertiary flow (low C parameter) is irrelevant if it only sets in after a very high number of load repetitions (low D parameter). Similarly, tertiary flow setting in very gently is meaningless if the flow point occurs early.

The smaller the value for model parameter C, the more abrupt tertiary flow sets in. The shape of the stress dependency curve of this parameter is again determined by

the exponent, *i.e.* coefficient $c_2$. Negative $c_2$ coefficients were found for the mixes with a high crushed rock percentage and no active filler, *i.e.* mixes A+B -75C-0 and C-75C-0. This means that the abruptness with which tertiary flow occurs increases with increasing stress ratios. For the two mixes with a high percentage of RAP and no active filler, *i.e.* mixes A+B -75C-1 and C-75C-1 high positive values for the $c_2$ coefficients. This would indicate that the abruptness with which tertiary flow occurs decreases for increasing stress ratios. For mix C-75C-1 however this effect is largely nullified by the low multiplier value for this mix.

The stress dependency of model parameter C is the least for mix C-75M-0 (low $c_1$ coefficient and $c_2$ coefficient close to 1). No tertiary flow was observed during the experiments for mix A+B -75M-0.

.The higher the value of this model parameter D the earlier the flow point occurs. When the value of model parameter D is less than $10^{-3}$ the flow point only occurs after 1 million load repetitions, which is outside the experimental range of applied load repetitions. Model parameter D of Mix C-75C-1 has a low multiplier value of $1.3 \times 10^{-3}$, which results in such low model parameter values for this mix that tertiary flow does not occur during the first 1 million load repetitions over the full range stress ratios.

For all mixes the model parameter D shows a strongly exponential stress dependency (high $d_2$ exponents ranging from 7 to 13). The two mixes with active filler, *i.e.* A+B-75C-1 and C-75C-1, have the highest D parameter values and also the strongest stress dependency (high $d_1$ multiplier values). This means that the mixes with active filler are more susceptible to tertiary flow at increasing stress ratios.

By evaluating the three most important model parameters, *i.e.* A, B and D, in conjunction, six scenarios of material behaviour were identified. These are shown in the flow chart in Figure 124. It can be seen that in case all three parameters have low values, stable behaviour without failure is the most likely scenario. When only the D-parameter is high, the behaviour will initially be stable, possibly with tertiary flow later on. High values of parameter B, regardless of the other parameters, are likely to results in failure. When only the A-parameter is high, failure is possible, but difficult to predict with confidence. In combination with a high D-parameter, early failure with tertiary flow is likely to occur.

The extent to which the model parameters are dependent on each other is difficult to determine, based on the limited number of variables that have been tested in this study. It is recommended that this dependency and especially the relation between compositional factors and the model parameters be studied further.

Initial indications are, however, that there is a strong correlation between parameter A and B, which is shown by the good correlation between the initial permanent strain and initial permanent strain rate as discussed in the next section

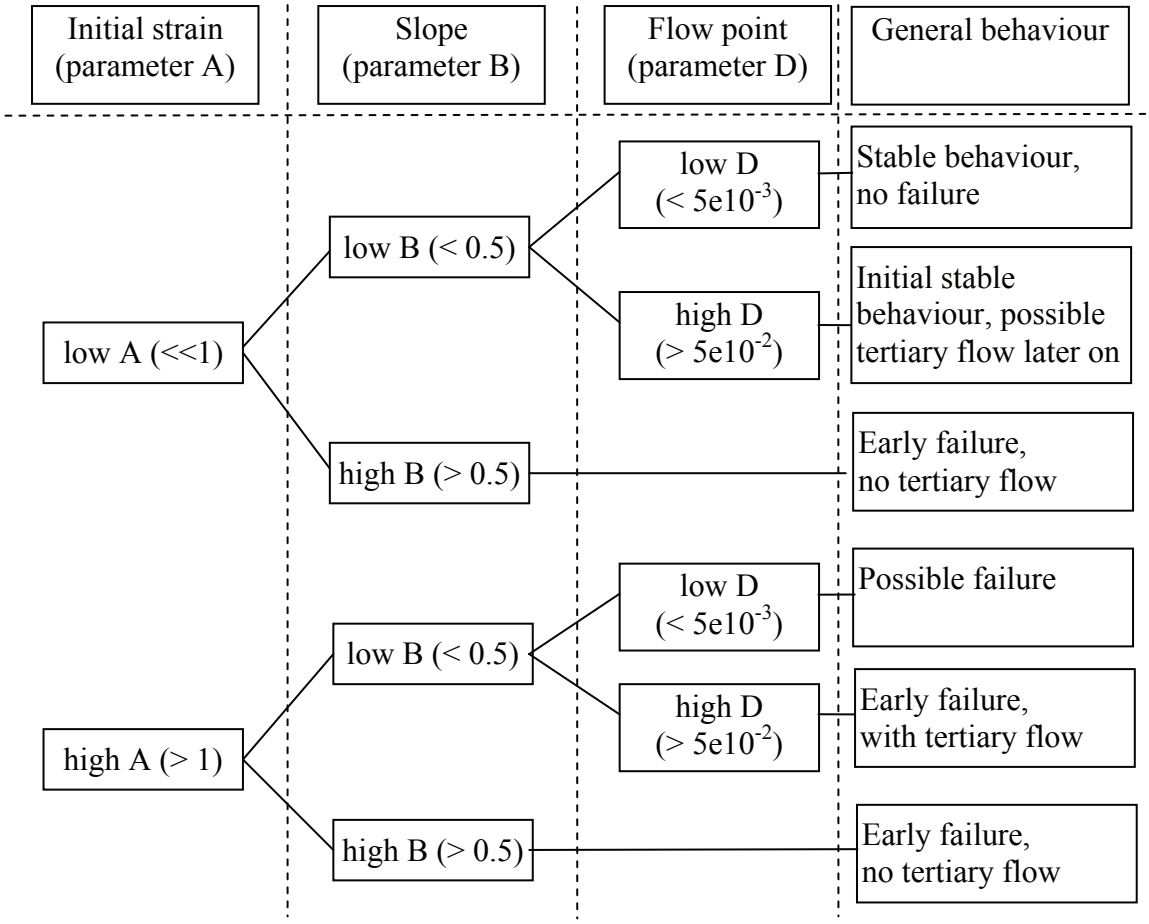


Note: The coefficient values provided are approximate values and are indicative only

Figure 124: Material behaviour scenario flow chart

The effect of the experimental variables on the permanent deformation behaviour is discussed by evaluating the model parameter A, B and D and using the scenario flow chart shown in Figure 124.

Increasing the percentage of RAP in the mix has different consequences for the bitumen emulsion mixes compared to the foamed bitumen mixes. First of all the initial strain reduces significantly for the foamed bitumen mixes and the Model Parameter A changes from high to low. At the same time the slope of the linear part of the permanent deformation curve also reduces, which changes the Model Parameter B from high (especially at higher deviator stress ratios) to low. Model Parameter D increases from low to intermediate levels in case the percentage of RAP is increased in the foamed bitumen mixes. This all results in the general behaviour being initially more stable and an increase in the number of load repetitions to failure.

Increasing the percentage of RAP in the emulsion mixes the results in an increase in the initial strain and in the slope of the linear part of the permanent deformation

curve (Model Parameters A and B respectively). Model Parameter D is fairly high for the emulsion mixes with low percentages of RAP and could not be determined for the emulsion mixes with a high percentage of RAP, because no flow points were observed. This means that the increase in the percentage of RAP results in a change in general behaviour from initial stable with possibly tertiary flow later on to earlier failure without tertiary flow. Generally, this means a reduction in the number of load repetitions to failure.

Also the effect of adding 1% cement as active filler to the mixes has a different effect for the bitumen emulsion compared to foamed bitumen. For foamed bitumen it reduces the initial strain significantly, although not as much with increasing the percentage of RAP. Model Parameter A changes from high to low. The slope of the linear part (Model Parameter B) also changes from high to low. Model Parameter D changes from low to high when 1% cement is added to the foamed bitumen mixes. This changes the general behaviour of the foamed bitumen mixes from likely early failure without tertiary flow (at the higher stress ratios) to being initially more stable, but with the risk of tertiary flow later on. The number of load repetitions to failure increase by the addition of 1% cement to the foamed bitumen mixes.

For the emulsion mixes adding 1% cement as active filler results in an small increase in both the initial strain and the slope of the linear part (increase in Model Parameters A and B). In addition there is a slight increase in Model Parameter D, which increases the risk of tertiary flow earlier on. This results in less stable initial behaviour and a higher risk of tertiary flow (at equivalent deviator stress ratios, not at equivalent absolute load levels).

6.2.3.5 Initial permanent strain and strain rate

Figure 125 shows the initial strain rate vs. the initial permanent axial strain as defined in Chapter 3 for all mixes at all deviator stress ratios. There is an excellent correlation between these two parameters. A good fit is obtained when a linear relation is fitted to this experimental data ($R^2 = 0.988$), however, such linear relation would be physically incorrect as it does not intercept with the origin. Therefore an exponential relation was chosen, for which the model coefficients and the coefficient of determination are shown in Figure 125.

It can be learnt from Figure 125 that, because all experimental data plots on one line, the relation between the initial strain and initial strain rate is independent of the type of mix and load level. The magnitude, however, of both parameters may be dependent on the type of mix and load level. The good correlation can be explained by the fact that when the initial permanent strain is high, the initial strain rate also needs to be high in order to achieve this high permanent strain and *vice versa.* The initial strain and initial strain rate are therefore interchangeable as performance parameters during the primary deformation phase only. Although the two data points at approximately 2% permanent strain (C-75C-0 mix) would appear to be outliers, it does illustrate how strong the relation between initial strain and initial strain rate is and how independent of specimen and material parameters.

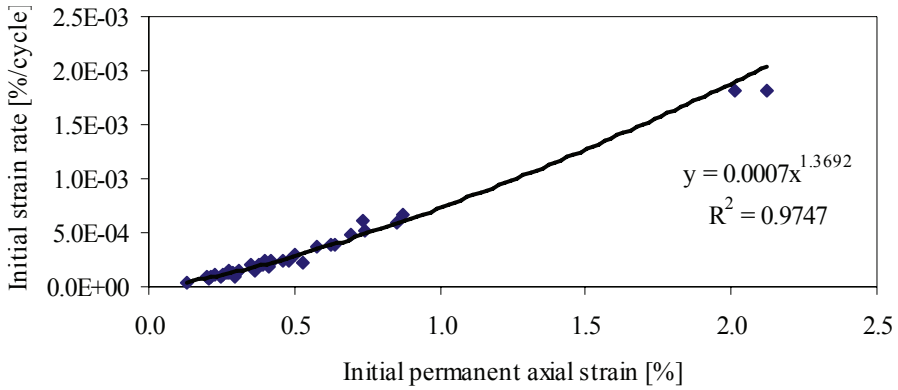


Figure 125: Initial strain rate vs. initial permanent axial strain (all mixes, $\sigma_3$ = 50 kPa, 25 ºC and 2 Hz)

The good correlation between the initial strain and initial strain rate also confirms that at N = 1000, the permanent strain accumulation is still in the primary phase of deformation. Once the stable secondary phase of deformation would be reached equal strain rates and different strain levels would be recorded for the same mix. More interesting is the relation between the loading and the initial permanent axial strain. In Figure 126 - Figure 128 the initial permanent strain is shown as a function of the major principal stress.

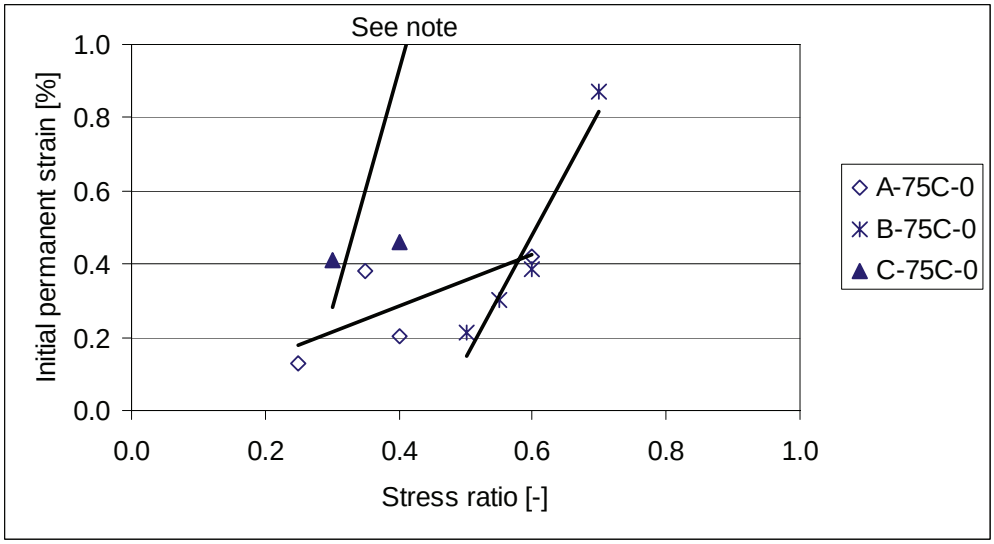


Note: The two data points of mix C-75C-0 at ± 2% permanent strain are not shown on this plot in order to enable same scale comparison with Figure 127 and Figure 128.

Figure 126: Initial permanent strain vs. major principal stress for the 75C-0 mixes ($\sigma_3$ = 50 kPa, 25 ºC and 2 Hz)

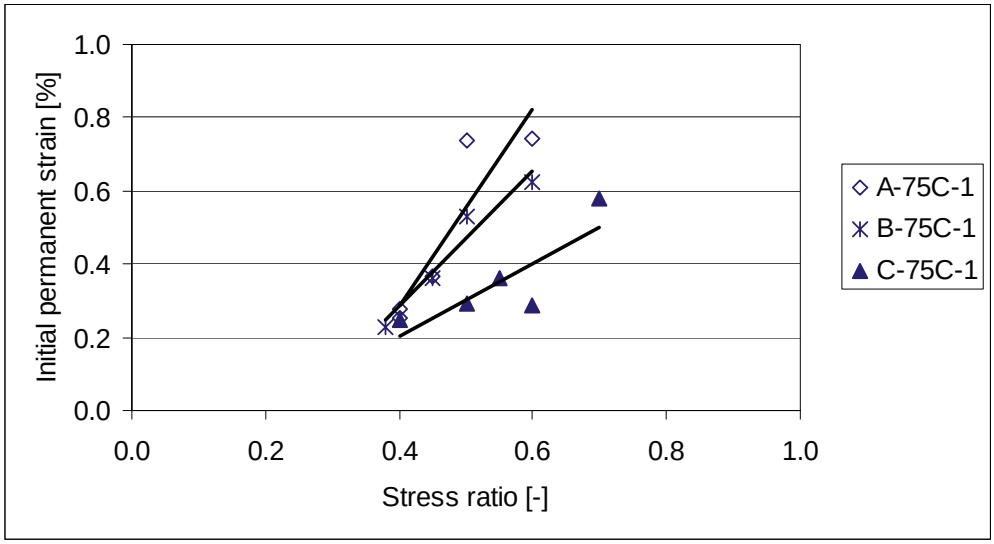


Figure 127: Initial permanent strain vs. major principal stress for the 75C-1 mixes ($\sigma_3$ = 50 kPa, 25 ºC and 2 Hz)

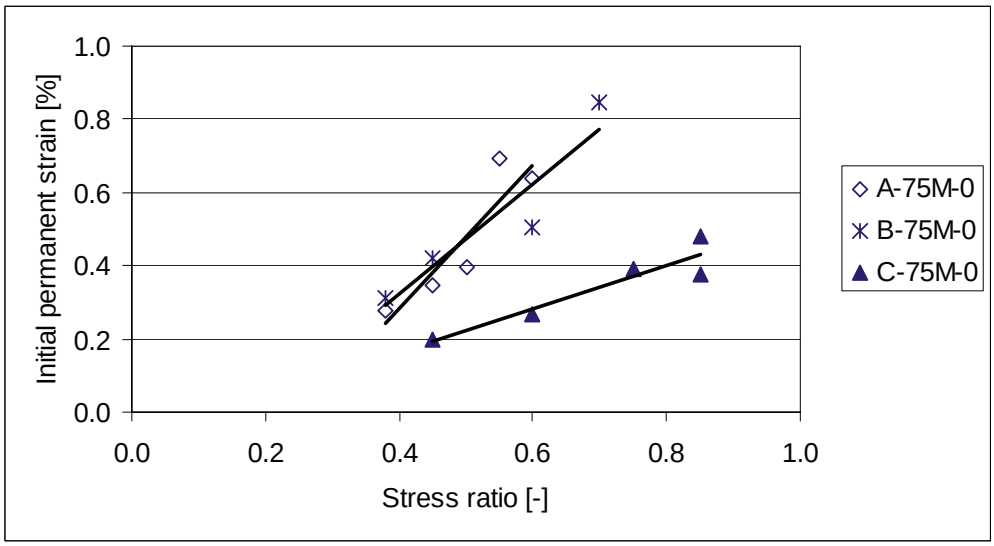


Figure 128: Initial permanent strain vs. major principal stress for the 75M-0 mixes ($\sigma_3$ = 50 kPa, 25 ºC and 2 Hz)

6.2.3.6 Correlation between permanent strain and strain rate

Three basic mechanisms were observed during the repeated load tri-axial testing:

- (a) failure due to tertiary flow;
- (b) failure due to high permanent axial strain; and
- (c) no failure with a stable strain rate after 1,000,000 load repetitions.

Tertiary flow initiates at the so-called flow point. The flow point is defined as the number of load repetitions at which there is a minimum in the strain rate. For all mixes tested and all loading levels, the combinations of strain rate and permanent

strain for these three basic mechanisms are plotted in Figure 129. The combinations of strain rate and permanent strain for each of the three basic mechanisms plot in a distinct and unique zone on the plot in Figure 129 [zone (a) – (c)]. A fourth area, zone (d), exists, but this area, which combines a high permanent strain in excess of 4%, with a low strain rate, is unlikely to contain any experimental data.

The boundary between zone (a) and zone (c) demarcates the threshold between likely failure due to tertiary flow [zone (a)] and steady state or even asymptotic permanent deformation behaviour [zone (c)]. This threshold is described by the function given in Equations 47 and 48.

$$\dot{\varepsilon} = 4 \cdot 10^{-8} e^{1.7533 \cdot \varepsilon} \quad for \quad \varepsilon \leq 2.0\,\% \qquad \text{Eq. 47}$$

and

$$\dot{\varepsilon} = 1 \cdot 10^{-6} \quad for \quad \varepsilon > 2.0\% \qquad \text{Eq. 48}$$

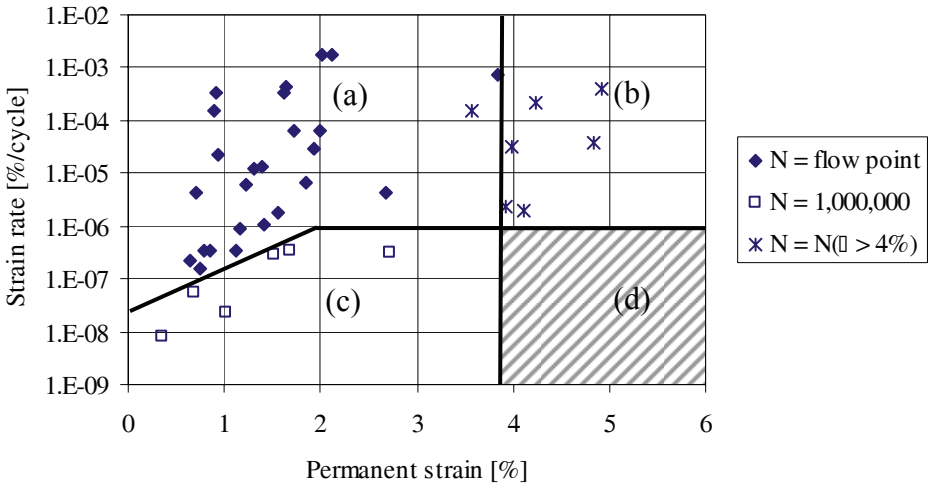


Figure 129: Strain rate vs. permanent strain at the end of repeated load tri-axial test ($\sigma_3$ = 50 kPa, 25 ºC and 2 Hz)

The only two mixes, of the nine tested, that do not show a flow point are the two bitumen emulsion mixes in combination with the 75% RAP millings blends (A&B-75M-0 mixes). Most of the specimens tested of these two mixes fall into zone (b) (failure due to high permanent strain) or, when the loading is sufficiently low, into zone (c) (no failure after 1,000,000 load repetitions). All the mixes with active filler (75C-1), except mix C-75C-1 at the lowest loading level, show flow points and fail due to tertiary flow. These mixes fall into zone (a). All the data points that fall into the zone (c) were loaded at levels below the critical stress ratio range as shown in Table 45.

## 6.3 Four-point beam testing

### *6.3.1 Strain-at-break*

6.3.1.1 Discussion of strain-at-break results

The strain-at-break results are presented in Chapter 5. These results are summarised in a bar chart in Figure 130. The range of values for all the beams of the relevant mix is also shown in this chart. The average strain-at-break values per mix vary roughly between 0.1% and 0.4%. It can be seen that Emulsion A provides the highest strain-at-break for all the mixes tested

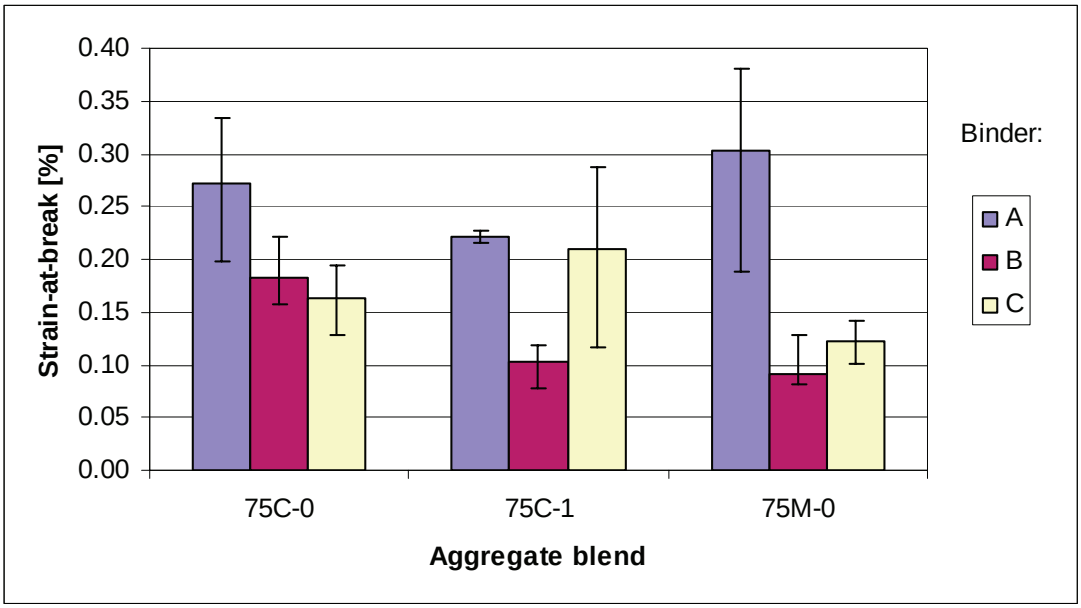


Figure 130: Average strain-at-break and range per aggregate blend and binder type (displacement rate 1.0mm/min at 5ºC)

For the aggregate blends with 75% crushed rock and no active filler (75C-0) there is little difference between Emulsion B and Foamed Bitumen C. For the other two aggregate blends (75% crushed rock with 1% active filler (75C-1) and 75% RAP, 75M-0) the strain-at-break for the mixes with Foamed Bitumen C is higher than for the mixes with Emulsion B. For the aggregate blend with 75% crushed rock with 1% active filler (75C-1) the strain-at-break values for the mixes treated with Foamed Bitumen C are similar to that of Emulsion A.

For combinations of Emulsion A and the different aggregate blends tested, the aggregate blend with 75% RAP shows the highest average strain-at-break with 0.30%. The aggregate blend with 75% crushed rock and 1% cement added shows with 0.22% the lowest average strain-at-break value. This lower strain-at-break value could be caused by the fact that 1% of cement was added to the mix, which would result in more rigid behaviour of the beam. The increase in stiffness (rigidity) by adding cement is confirmed by the frequency-temperature sweep testing of the mixes with Emulsion A. It can clearly be seen that the stiffness increases by adding

1% cement in combination with Emulsion A. It can also be seen that the aggregate blend with 75% RAP, which had the highest strain-at-break has the lowest stiffness.

Treatment with Emulsion B results in the aggregate blend with 75% crushed rock and no active filler showing the highest average strain-at-break of 0.18%. The aggregate blend with 75% RAP has the lowest average strain-at-break values of the three mixes with Emulsion B (0.09%). This average strain-at-break result is at the same time the lowest result of all nine mixes. Of the three binders, Emulsion B shows the least variation in average strain-at-break values over the three aggregate blends. The same holds true for the stiffness of these three mixes as measured during the frequency-temperature sweeps.

Treatment with Foamed Bitumen C tends to result in similar strain-at-break values than with Emulsion B, except for the 75% crushed rock blend with 1% active filler. For the latter aggregate blend, treatment with Foamed Bitumen C results in significantly higher strain-at-break results than treatment with Emulsion B. It is furthermore interesting to note that for the mixes treated with Foamed Bitumen C, the aggregate blend with 75% crushed rock with 1% active filler produces the highest average strain-at-break value (0.21%). This is in contrast to what was discussed for Emulsion A in the previous paragraph. In line with this is however that the addition of 1% of active filler to the mixes treated with Foamed Bitumen C, did not result in an increase in the stiffness of the mixes during the frequency-temperature sweep testing. Of the three mixes treated with Foamed Bitumen C, the aggregate blend with 75% RAP has the lowest average strain-at-break value (0.12%).

There is no consistent trend in the performance of the aggregate blends if one compares the results per binder. For Emulsion A, the 75% RAP blend performs the best, for Emulsion B the 75% crushed rock blend without active filler and for Foamed Bitumen C the 75% crushed rock blend with active filler. The one thing that is consistent is the fact that the addition of 1% active filler to the 75% crushed rock blends, results in a reduction of the strain-at-break values for both emulsions tested. In summary, the effects of the experimental variables on the strain-at-break are shown in Table 48.

Table 48: Effect of experimental variables on the strain-at-break

| Experimental variable | Emulsion mixes | Foamed bitumen mixes |
|---|---|---|
| Increasing %-RAP | Em. A: increase<br>Em. B: decrease | decrease |
| Adding 1% cement | decrease | increase |
| Type of binder | Generally A > B ≈ C<br>C performing relatively better with 75C-1 | |

These differences in strain-at-break values do not fully concur with the findings in fatigue performances of these mixes. Where emulsion A consistently provides the

highest strain-at-break values, mixes with emulsion A do not have the highest fatigue life.

6.3.1.2 Comparison of tensile strength from tri-axial and four-point beam tests

The peak stress, as determined from the strain-at-break testing, is reported in Chapter 5. In Section 6.2.1.4 the tensile strength as estimated from the monotonic tri-axial testing was determined. These two tensile strengths are summarised in Table 49 and graphically compared in Figure 131.

Table 49: Summary of tensile strengths from tri-axial test and four-point beam tests

| Mix | Estimated from monotonic tri-axial [kPa] | monotonic four-point beam [kPa] |
|---|---|---|
| A-75C-0 | 147 | 143 |
| A-75C-1 | 121 | 171 |
| A-75M-0 | 155 | 188 |
| B-75C-0 | 449 | 393 |
| B-75C-1 | 423 | 310 |
| B-75M-0 | 525 | 390 |
| C-75C-0 | 209 | 364 |
| C-75C-1 | 228 | 379 |
| C-75M-0 | 145 | 265 |

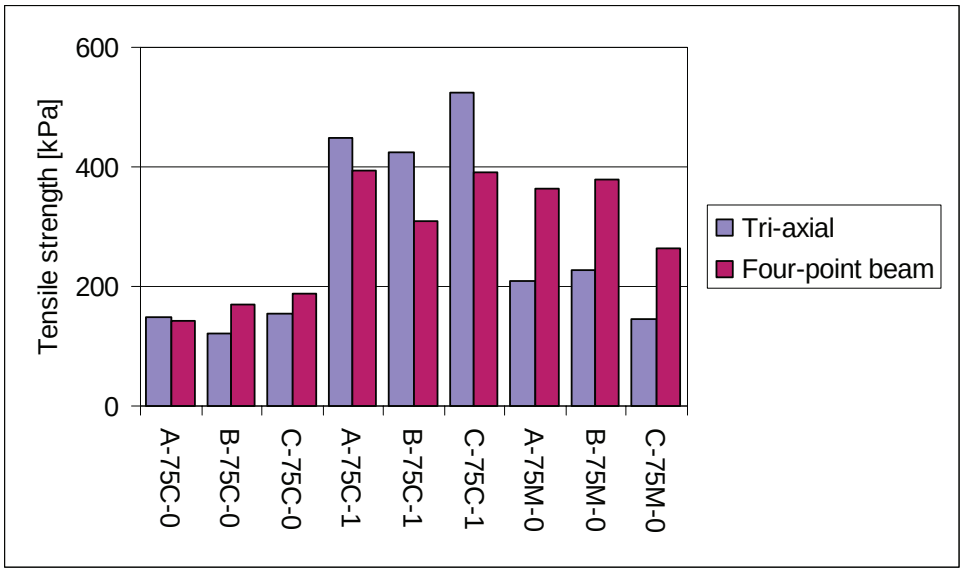


Figure 131: Comparison of tensile strengths from tri-axial test and four-point beam tests

It can be seen that the two tensile strengths compare generally well for the 75C mixes (both without and with 1% cement) but that for the 75M-0 mixes (75% RAP), the tensile strength determined from the monotonic strain-at-break tests is considerably higher than the tensile strength estimated from the monotonic tri-axial test.

It should be noted that for both tensile strengths the non-linear behaviour of the material and the test conditions (such as loading rate and temperature) and geometry play a role. The four-point beam strain-at-break testing was carried out at 5 ºC, while the monotonic tri-axial testing was carried out at 25 ºC. Also, the strain-at-break testing was carried out at a relatively low loading rate (1.0 mm/min). Increasing this rate would results in higher strengths.

In order to establish a reliable relation between tri-axial and four-point beam testing additional testing and non-linear modelling of the respective tests would be required.

### *6.3.2 Flexural Stiffness*

6.3.2.1 Master curves

The power function discussed in Chapter 3 has been fitted to the experimental data. In this case the experimental data is the average of the results from the two beam specimens tested per mix. The model coefficients and R-squared values are given in Table 50.

Table 50: Model coefficients for estimation the stiffness modulus ($T_{ref}$ = 20ºC)

| Mix type | a | n | $R^2$ |
|---|---|---|---|
| A-75C-0 | 1283.0 | 0.1247 | 0.96 |
| A-75C-1 | 1871.5 | 0.1081 | 0.99 |
| A-75M-0 | 1057.4 | 0.1022 | 0.91 |
| B-75C-0 | 1200.0 | 0.1333 | 0.99 |
| B-75C-1 | 1387.1 | 0.1292 | 0.99 |
| B-75M-0 | 1291.4 | 0.1193 | 0.99 |
| C-75C-0 | 1211.6 | 0.1044 | 0.99 |
| C-75C-1 | 1172.8 | 0.0926 | 0.94 |
| C-75M-0 | 967.7 | 0.0901 | 0.94 |

Although this power-law model would appear to result in a good fit, the experimental data is certainly not a straight line. The master curves obtained for the cold mixes tested still have some resemblance with an S-curve type of master curve (sigmoidal modal), albeit much flatter and more stretched than typically for HMA.

The flexural stiffness of the BSM mixes studied shows a dependency on temperature and rate of loading. By increasing the loading rate and keeping the temperature constant, the stiffness increases. By increasing the temperature of the mixes the stiffness modulus of the mixes reduces. This is consistent with the behaviour of HMA, however the slope of the master curve for BSM's is significantly flatter than

for HMA. Jenkins (2000) found an n-value of 0.293 for a standard HMA mix. This is much higher than the n-values shown in Table 50, which indicates that the dependency of cold mixes on the loading and the temperature is less than for HMA mixes.

Ranking in terms of flexural stiffness when the mixes are compared per aggregate blend indicates that for every aggregate blend the mixes treated with foamed bitumen have the lowest stiffness. For the 75% crushed rock blend without active filler Binder A and B provide comparable stiffness. For the 75% crushed rock blend with active filler Emulsion A provides the highest stiffness, while for the 75% RAP blend Emulsion B provides the highest stiffness.

The addition of active filler results in an increase of flexural stiffness when bitumen emulsions are used. This is most pronounced for Emulsion A. The addition of active filler makes little difference to the flexural stiffness when foamed bitumen is used. In fact, the stiffness of the 75C mix with active filler tends to be slightly lower than the 75C mix without active filler in case foamed bitumen is used. For all three binders the blends with 75% RAP result in the lowest stiffness.

In summary, the effects of the experimental variables on the flexural stiffness are shown in Table 51.

Table 51: Effect of experimental variables on the flexural stiffness

| Experimental variable | Emulsion mixes | Foamed bitumen mixes |
|---|---|---|
| Increasing %-RAP | Emulsion A: decrease<br>Emulsion B: no effect | decrease |
| Adding 1% cement | increase<br>(only slight for Emulsion B) | no effect |
| Type of binder | Difficult to discern an overall trend<br>75C-0: A ≈ B > C<br>75C-1: A > B > C<br>75M-0: B > A > C | |

6.3.2.2 Phase angles and visco-elastic behaviour

*Black Diagrams*

An investigation into the phase angle between the induced loading and delayed response of the four-point beam specimens was carried out. This was only done for a limited number of beams due to the fact that the phase angle as determined by the UTM software (UTM21 V1.05) was unreliable and most of the times erroneous. The calculations therefore had to be done manually as discussed in Chapter 4. Sufficient mixes were however investigated in order to be able to evaluate the effect of the experimental variables. These are evaluated by comparing plots of the phase angle against the complex stiffness in a Black Diagram.

The effect of the increase in the percentage of RAP in the mix (from 25% to 75%) and the effect of the presence of cement as active filler can be seen in Figure 132 for the emulsion mixes and in Figure 133 for the foamed bitumen mixes. The effect of the type of binder can be seen in Figure 134, Figure 135 and Figure 136 for the 75C-0, 75C-1 and 75M-0 mixes respectively.

It can be seen from Figure 132 and Figure 133 that an increase in the percentage of RAP in the mix reduces the phase angle in case of the emulsion mixes. Hence, the material behaves more elastic. For the foamed bitumen there is only a slight decrease in the phase angle when the percentage RAP in the mix is increased. This decrease is however not significant enough to be conclusive.

It can furthermore be seen that in the case of the emulsion mixes the phase angle becomes more sensitive to the complex stiffness (*i.e.* more time- and temperature-dependent) when the percentage of RAP in the mix is increased. This is indicated by the steeper slope of the curve in the Black Diagram, which means that at a lower complex stiffness (*i.e.* longer loading times or higher temperatures) the material behaves more viscous, while at a higher complex stiffness the material behaves more elastic. An increase of the percentage of RAP in the foamed bitumen mixes does not result in more time- and temperature-dependent behaviour of the mix (slope of the curve in the Black Diagram remains the same).

The use of 1% of cement in the mix as active filler reduces of the phase angle for both emulsion and foamed bitumen mixes. This means that the material response becomes more elastic.

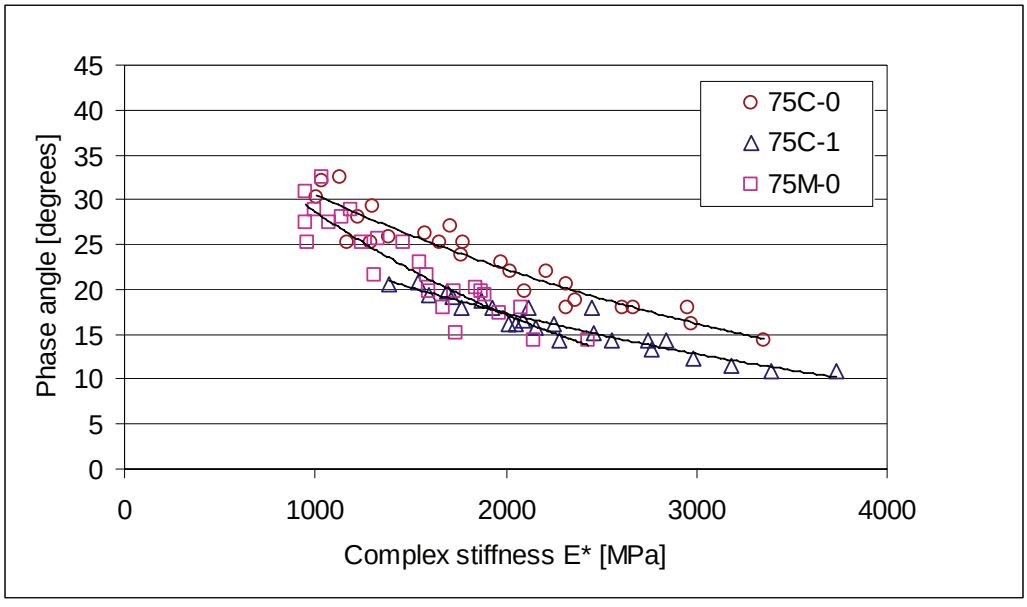


Figure 132: The effect of the %-RAP and presence of active filler in the emulsion mixes (Emulsion A only)

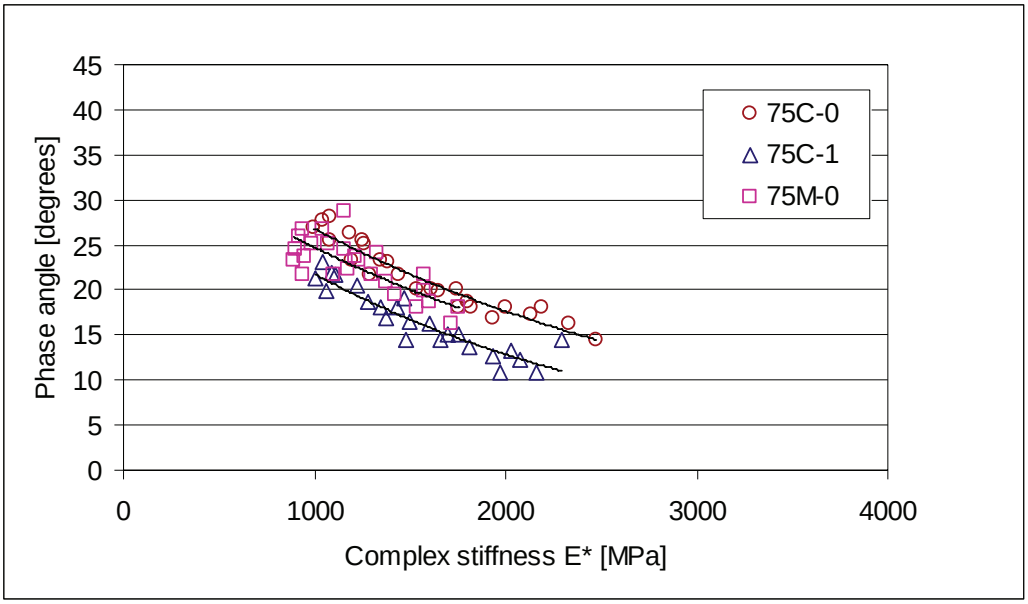


Figure 133: The effect of the %-RAP and presence of active filler in the Foamed Bitumen C mixes

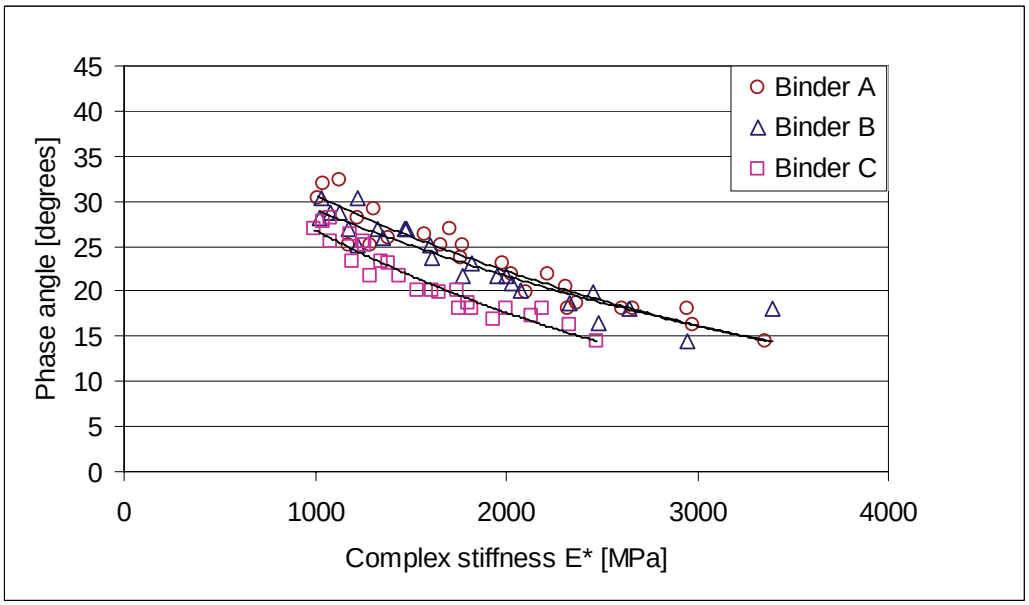


Figure 134: The effect of the type of binder for the 75C-0 mixes

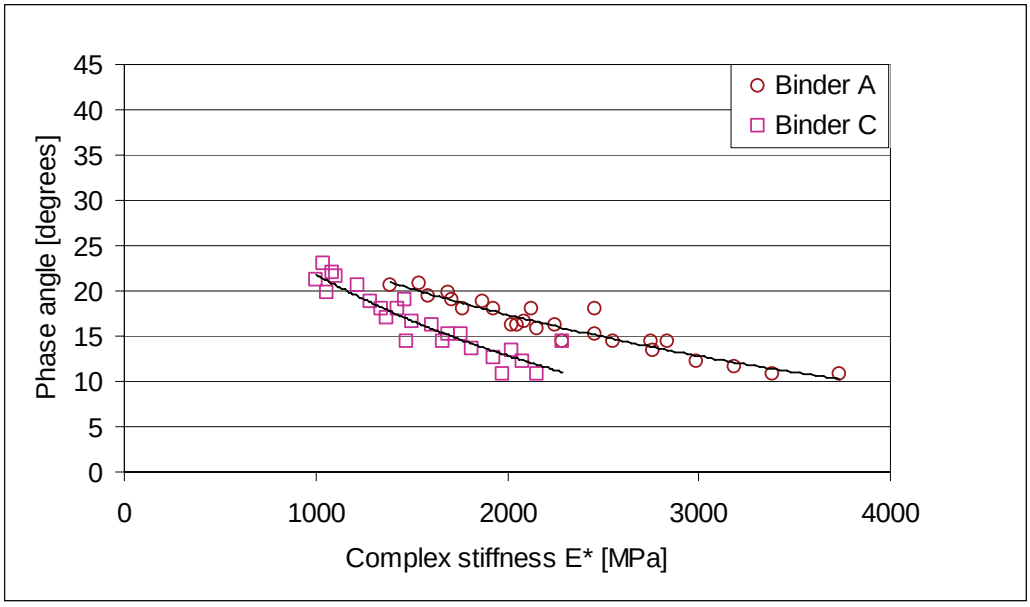


Figure 135: The effect of the type of binder for the 75C-1 mixes

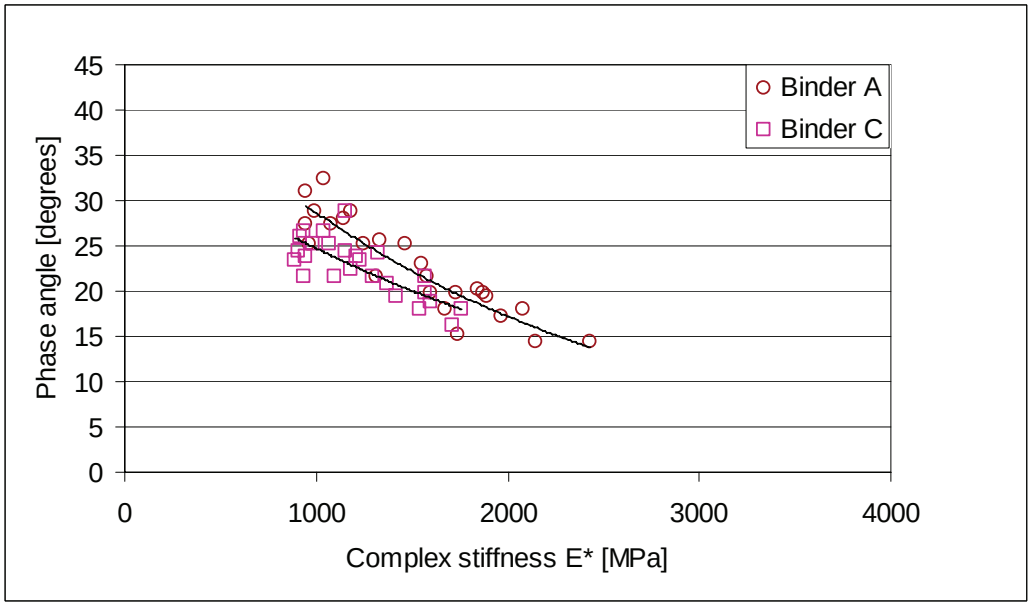


Figure 136: The effect of the type of binder for the 75M-0 mixes

From Figure 134 it can be concluded that there is little difference between the behaviour of the two bitumen emulsion mixes (Emulsion A *vs.* Emulsion B). There is however a consistent trend that the use of foamed bitumen results in lower phase angles, and therefore more elastic behaviour, compared to the use of bitumen emulsion (see Figure 134 – Figure 136).

The effects of the experimental variables on the visco-elastic behaviour are summarised in shown in Table 52.

Table 52: Effect of experimental variables on the visco-elastic behaviour

| Experimental variable | Emulsion mixes | Foamed bitumen mixes |
|---|---|---|
| Increasing %-RAP | more elastic<br>more time/temp. dependent | no significant effect |
| Adding 1% cement | more elastic | more elastic |
| Type of binder | Emulsion A ≈ Emulsion B<br>Foam more elastic than emulsion | |

*Burgers Model Parameters*

As discussed in Chapter 3, various mechanical models are available to describe the visco-elastic behaviour of a material. One of these models is the Burgers Model, consisting of a spring, a dashpot and a parallel combination of a spring and a dashpot all in series. The Burgers Models is characterised by the spring stiffness $E_0$ and $E_1$ and dashpot damping coefficients $\lambda_0$ and $\lambda_1$ (as discussed in Chapter 3).

The combinations of complex stiffness and phase angle at known temperature and loading frequency were used to determine Burgers Model Parameters using the following programs:

- Deburoad (version 2000s), a module of Veroad (Hopman, 2000)
- Burger's Fit Model (Pronk, 2007)

"Deburoad" is a Pascal-written code, while "Burger's Model Fit" is a spreadsheet making use of the Excel Solver function. A limited investigation comparing the output of both programs showed that the order of magnitude of the model parameters determined by both programs is comparable, but that the "Burger's Fit Model" showed a slightly better fit of the calculated phase angles to the measured phase angles. For this reason, "Burger's Fit Model" was used to determine the Burgers Model Parameters.

It is noted that none of the programs were able to converge at a solution that resulted in a near perfect fit of the phase angles. Especially the measured phase angles at the lowest and highest frequencies (0.5 and 10 Hz) proved to be difficult to model. It was also not possible to apply the time-temperature superposition principle as this resulted in very low and very high reduced frequencies for which no converging solution could be obtained. Therefore the Burger's Model Parameters were determined at the actual testing frequencies for each of the testing temperatures. The results for the tests at 20 ºC are shown in Table 53. The complete set of results is shown in Appendix K. The typical effect of the temperature on the Burgers Model Parameters is shown in Figure 137 for mix A-75C-0. The graphs for the other mixes are included in Appendix K.

Table 53: Burgers Model Parameters at 20ºC

| Parameter | A-75C-0 | A-75C-1 | A-75M-0 | B-75C-0 | C-75C-0 | C-75C-1 | C-75M-0 |
|---|---|---|---|---|---|---|---|
| $E_0$ [MPa] | 2342 | 2665 | 1809 | 2192 | 1981 | 1883 | 1320 |
| $E_1$ [MPa] | 2911 | 5324 | 2912 | 2806 | 2751 | 3953 | 3491 |
| $\lambda_1$ [MPa/s] | 161 | 258 | 123 | 141 | 143 | 173 | 114 |
| $\lambda_0$ [MPa/s] | 640 | 1291 | 562 | 572 | 604 | 888 | 629 |

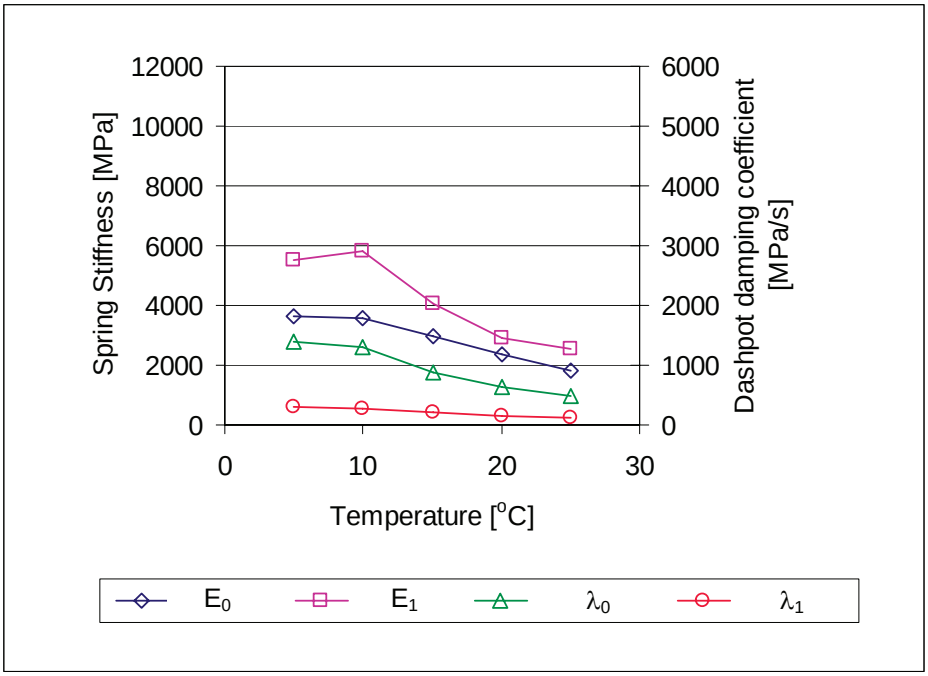


Figure 137: Effect of testing temperature on the Burgers Model Parameters (mix A-75C-0)

From Figure 137 it can be seen that increasing the temperature results in a reduction of both spring stiffness values and both dashpot damping coefficients.

Increasing the percentage of RAP in the mix has a different effect on the bitumen emulsion mixes compared to the foamed bitumen mixes. From Table 53 it can be seen that for the mix with Emulsion A (A-75C-0 *vs.* A-75M-0) increasing the percentage of RAP results in the reduction in the spring stiffness $E_0$ (more elastic deformation), a slight reduction in the dashpot damping coefficient $\lambda_0$ (more viscous deformation) and a slight reduction in the dashpot damping coefficient $\lambda_1$ while $E_1$ remains constant (less delayed elastic deformation).

For the mix with foamed bitumen (C-75C-0 *vs.* C-75M-0), increasing the percentage of RAP results in a significant reduction the in the spring stiffness $E_0$ (more elastic deformation). The dashpot damping coefficient $\lambda_0$ remains more or less the same and there is a significant increase in the $E_1$ spring stiffness while $\lambda_1$ reduces slightly (less delayed elastic deformation) with an increase in the percentage of RAP.

The effect of adding 1% of cement to the mix with 75% crushed rock (75C-0 *vs.* 75C-1) also has a different effect in combination with bitumen emulsion or foamed bitumen. For Emulsion A it can be seen that all parameters increase. This means generally a stiffer response. The increase is most significant for $E_1$ and $\lambda_1$ (less delayed elastic deformation) and $\lambda_0$ (less viscous deformation). This means that adding 1% cement results in a much stiffer and more elastic response in combination with bitumen emulsion.

For the mixes with foamed bitumen similar, but less significant, changes are observed, while there is even a slight reduction in spring stiffness $E_0$. There would be less viscous and delayed elastic deformation, but slightly more elastic deformation). Overall the response would be stiffer, but not as much as for the bitumen emulsion mixes.

There is little difference between Emulsion A and Emulsion B. However, there is a difference between foamed bitumen and bitumen emulsion. Some of this has been explained above. For the mixes with 75% crushed rock (75C-0 and 75C-1) the Burger Model Parameters are generally lower for the foamed bitumen mixes, while relatively to each other, these parameters remain the same. This would mean a generally stiffer response of the bitumen emulsion mixes.

For the mixes with 75% RAP, the $E_0$ spring stiffness is lower for the foamed bitumen mixes compared to the bitumen emulsion mixes, while the $E_1$ spring stiffness is higher. The two dashpot coefficients are comparable for the foamed bitumen and bitumen emulsion mixes. This would mean more elastic deformation in the foamed bitumen mixes, of which the delayed elastic component is less.

The effect of the testing frequency on the Burgers Model Parameters was also determined, however, only at 20 ºC. This was done by dividing the measurement data at 20 ºC into three sets of three subsequent frequencies, *i.e.* set 1 : 0,5 – 1 – 2 Hz, set 2 : 1 – 2 – 5 Hz and set 3 : 2 – 5 – 10 Hz. For each of these sets Burger Parameters were fitted to the experimental data points at the three frequencies and assigned to the middle frequency, *i.e.* 1, 2 and 5 Hz for the three respective sets of three subsequent frequencies. The frequency-dependency of the Burgers Model Paramters is obtained in this manner. An example of this frequency-dependency is shown in Figure 138.

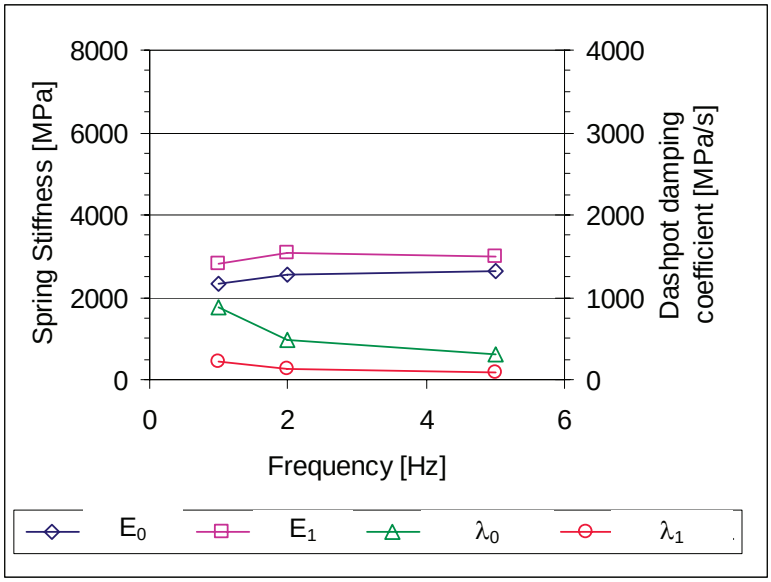


Figure 138: Frequency-dependency of Burgers Model Parameters at 20 ºC (mix A-75C-0)

The pure viscous component of deformation of the BSM mixes is characterised by the serial dashpot with damping coefficient $\lambda_0$. When the trend for the frequency-dependency of $\lambda_0$ is extrapolated to a frequency of 0, an estimation of the zero-shear viscosity is obtained. For this extrapolation a linear function has been fitted to the $\lambda_0$ curve:

$$\lambda_0 = a \cdot f + \lambda_{ZS} \qquad \text{Eq. 49}$$

where $\lambda_{ZS}$ = zero-shear viscosity [MPa/s]
$f$ = frequency [Hz]
$a$ = model coefficient

The zero-shear viscosity of the mixes for which Burger Model Parameters were determined is shown in Figure 139.

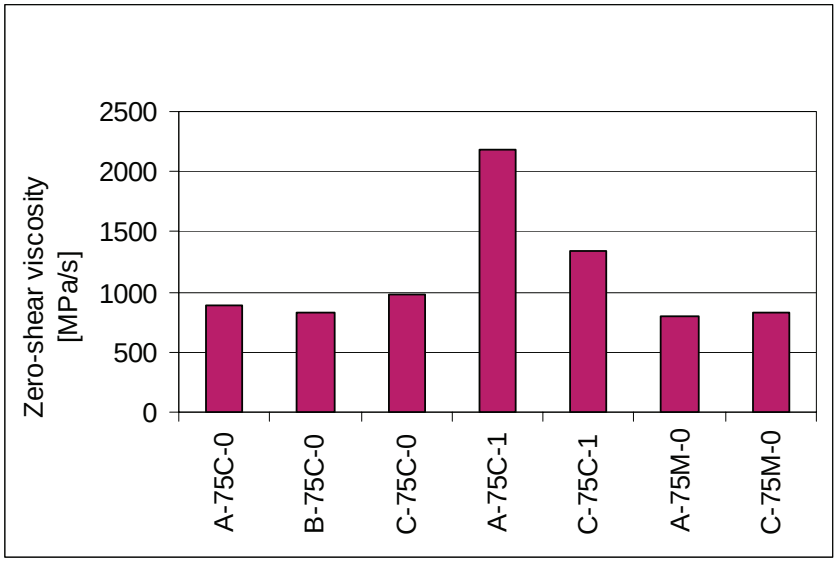


Figure 139: Zero-shear viscosity of selected BSM mixes at 20 ºC

It can be seen from Figure 139 that the pure viscous part of deformation of the 75C-0 mixes is fairly constant. The effect of adding 1 % of cement can clearly be seen and results in an increase in zero-shear viscosity (less viscous deformation). This is more the case with Emulsion A than with Foamed Bitumen C. Increasing the percentage of RAP in the mix has little effect on the zero-shear viscosity, both in case of the BSM with emulsion (A-75M-0) and foamed bitumen (C-75M-0).

### *6.3.3 Fatigue behaviour*

6.3.3.1 Fatigue lines

The plots with the fatigue lines of the mixes tested are presented in Chapter 5. The fatigue line model that can be fitted to the experimental data was discussed in Chapter 3 and the mathematical formula is repeated here:

$$\log N_f = \log a - n \log \varepsilon_t \qquad \text{Eq. 50}$$

where $N_f$ = the number of load repetitions to failure
$\varepsilon_t$ = applied strain level [micron]
$a, n$ = model coefficients

The model coefficients *log a* and *n* of the mixes tested are shown in Table 54. As mentioned in the previous chapter, some of the extrapolations of fatigue test results are regarded more reliable than others (see Chapter 5). However, the fatigue line model coefficients based on the fatigue data series without the "less reliable" extrapolated results differ only slightly from the ones shown in Table 54. This means that the effect of the extrapolations as carried out on some of the fatigue test results is not significant and that the values provided in Table 54 can be used with confidence.

Table 54: Model coefficients fatigue lines (10 Hz, 5 ºC)

| Aggregate blend | Binder A | | | Binder B | | | Binder C | | |
|---|---|---|---|---|---|---|---|---|---|
| | log a | n | $R^2$ | log a | n | $R^2$ | log a | n | $R^2$ |
| 75C-0 | 19.2 | 5.8 | 0.77 | 17.9 | 5.3 | 0.91 | 25.3 | 8.1 | 0.89 |
| 75C-1 | 20.2 | 6.1 | 0.80 | 16.8 | 4.9 | 0.86 | 20.15 | 5.9 | 0.87 |
| 75M-0 | 17.5 | 5.2 | 0.98 | 21.4 | 6.8 | 0.97 | 18.7 | 5.4 | 0.88 |

All the mixes show that fatigue life increases as tensile strain decreases. This behaviour is linear on log-log scale. At face value the fatigue lines for most of the mixes appear to be more or less parallel. The slope of the fatigue line is described by the value of the model coefficient *n* as shown in Table 54. From this table it can be seen that the slopes of the fatigue lines vary between 4.9 and 8.1. These slopes are comparable to HMA mixtures. Mix B-75C-1 has the flattest fatigue line (n = 4.9), while mix C-75C-0 has the steepest fatigue line (n = 8.1). The n-value indicates the sensitivity of the number of load repetitions to failure to the applied strain level. The steeper the line, the more sensitive is the mix to changes in applied strain levels.

It is noted that the results for some of the mixes consist of only a limited data sample. The sample size of mix A-75C-0 is four and of mix A-75M-0 three. It has been mentioned in Chapter 4 that this was the result of the fact that a large number of slabs and beams that were prepared with Emulsion and were tested at 20 ºC and 10 ºC as discussed in Chapter 4. The need to reduce the test temperature was only identified after many tests had already been completed. The small sample size does however reduce the reliability of the fatigue line for these two mixes.

It can be seen from the figures presented in Chapter 5 that for the 75% crushed rock blend without active filler, there is little difference between the fatigue results of the mixes treated with Emulsion A and B. The mix treated with Emulsion A performs marginally better than the mix treated with Emulsion B. The mix treated with Foamed Bitumen (C-75C-0) performs significantly better than the two emulsion treated mixes at the lower strain regimes. This mix is however much more sensitive to the applied strain (proof of which is the steep slope of the fatigue line as mentioned above). At the highest strain levels tested the two emulsion mixes perform similar to the foamed bitumen mix.

The addition of 1% of active filler to the 75% crushed rock blend leads to reduction in the slope of the fatigue line in case of Emulsion B and Foamed Bitumen C. This effect is most pronounced for the latter with the *n*-value reducing from 8.1 to 5.7. At the same time, in the case of Foamed Bitumen C, the performance of the 75% crushed rock blend with and without active filler at the lower strain regime is comparable (C-75C-0 *versus* C-75C-1). This means that the addition of active filler, in case foamed bitumen is used, improves the overall fatigue performance, especially at the higher strain regimes. The addition of active filler in case Bitumen Emulsion B is used only reduces the slope of the fatigue line marginally (*n*-value from 5.3 to 4.9). However, the overall fatigue performance if the mix with active filler (B-75C-1) is slightly below that of the mix without active filler (B-75C-0). This is most

pronounced at the lower strain regime. There is very little difference in the slope of the fatigue line in the case of Emulsion A (*n*-value of 5.8 and 6.1 for mix A-75C-0 and A-75C-1 respectively). This is the only of the three binders where the slope of the fatigue line increases by the addition of active filler. However, the increase is too marginal to draw any conclusions from it. The overall fatigue performance (over the full strain range) of the 75% crushed rock blend treated with Emulsion A is improved by adding 1% of active filler. Of the three binders tested, the 75% aggregate blend with 1% active filler treated with Foamed Bitumen C performs the best in terms of fatigue. The mix treated with Emulsion A performs better than the mix treated with Emulsion B.

For the 75% RAP aggregate blend, the fatigue lines of the mixes treated with emulsion A and foamed bitumen C have a comparable slope. The slope of the fatigue line of the mix treated with Emulsion B is slightly steeper (*n*-values of 5.2 and 5.4 for mix A-75M-0 and C-75M-0 respectively; *n*-value of 6.8 for mix B-75M-0). The mix treated with Emulsion B performs marginally better than the mix treated with Emulsion A in the lower strain regime. However, because of the slightly higher sensitivity to strain of the mix with Emulsion B, there is no difference in fatigue performance at the higher strain regime. The mix treated with Foamed Bitumen C performs better in terms of fatigue over the full range of strains tested.

In the case of Emulsion A, the mix with 75% RAP shows a lower performance in terms of fatigue compared to the 75% crushed rock mixes (with and without active filler). In case of Emulsion B, there is very little difference between the three aggregate blends tests in terms of fatigue performance. In case of Foamed Bitumen C there is little difference between the three aggregate blends at the lower strain regime. Due to the increased sensitivity to strain, fatigue performance of the 75% crushed rock blend without active filler is slightly less at the higher strain regime. The 75% crushed rock blend with 1% active filler performs marginally better than the 75% RAP blend over the full range of strains tested.

In summary, the effects of the experimental variables on the fatigue behaviour are summarised in Table 55.

Table 55: Effect of experimental variables on the fatigue behaviour

| Experimental variable | Emulsion mixes | Foamed bitumen mixes |
|---|---|---|
| Increasing %-RAP | Emulsion A: decrease<br>Emulsion B: no significant effect, but higher *n*-value | lower *n*-value resulting in increase at high strain |
| Adding 1% cement | Emulsion A: increase<br>Emulsion B: decrease | lower *n*-value resulting in increase at high strain |
| Type of binder | 75C-0: C > A ≈ B, C higher *n*-value<br>75C-1: C > A > B<br>75M-0: C > A ≈ B, B higher *n*-value | |

6.3.3.2 The effect of the initial stiffness

At face value, one could conclude from the discussion of the fatigue performance of the mixes studied that the foamed bitumen mixes appear to provide higher fatigue lives than the mixes with either Emulsion A or B. It must be noted, however, that the initial stiffness of the beams of mixes treated with either of the two emulsions is substantially higher than the beams of the foamed bitumen treated mixes. Subsequently the failure stiffness of the beams of the foamed bitumen treated mixes is also much lower. In all cases the failure stiffness of the emulsion mixes beams is at comparable levels to the initial stiffness of the foamed bitumen mixes beams. This is illustrated by Table 56 and Figure 140. The implication is that, in terms of fatigue lives, the mixes treated with Emulsion A or B are considered to have reached a terminal condition, while still having a higher stiffness than beams of mixes treated with Foamed Bitumen C that have not "failed" yet. This phenomenon is conceptually illustrated in Figure 141. In this figure it can be seen that the initial stiffness of the emulsion mix ($S_{i,E}$) is higher than the initial stiffness of the foamed bitumen mix ($S_{i,F}$). Consequently, the defined "failure" stiffness of the emulsion mix ($S_{f,E}$) is also higher than that of the foamed bitumen mix ($S_{f,F}$), since this is defined as 50% of the initial stiffness. When the stiffness reduction curve of the foamed bitumen mix is shifted horizontally to the right, it lines up with the stiffness reduction curve of the emulsion mix. One could argue that at equal stiffness, the fatigue behaviour of the two mixes is comparable. However, the number of load repetitions to failure for the emulsion mix ($N_{f,E}$) is significantly less than for the foamed bitumen mix ($N_{f,F}$).

Furthermore, one should take into account that in a pavement structure, granular layers treated with Emulsion A or B would provide better support than layers treated with Foamed Bitumen C. Because of the higher intrinsic stiffness of the emulsion mixes, they would be subjected to lower strain levels at equal loading. This could in turn then possibly result in higher in-service fatigue lives instead of lower. Also, because of the higher stiffness of emulsion treated layers, the subgrade would be better protected due to better load spreading. Also, the overlying layers would be subjected to lower strains because of the better support the emulsion treated layer is providing compared to foamed bitumen treated layers.

Table 56: Average initial stiffness ($S_i$) and failure stiffness ($S_f$) of the beams

| Type of binder | Aggregate blend | | | | | |
|---|---|---|---|---|---|---|
| | 75C-0 | | 75C-1 | | 75M-0 | |
| | $S_i$ [MPa] | $S_f$ [MPa] | $S_i$ [MPa] | $S_f$ [MPa] | $S_i$ [MPa] | $S_f$ [MPa] |
| A | 2377 | 1189 | 2746 | 1373 | 1612 | 806 |
| B | 2521 | 1261 | 2119 | 1059 | 3809 | 1904 |
| C | 1590 | 795 | 1592 | 796 | 1045 | 522 |

It can be seen that the intial stiffness values during the fatigue testing are generally lower than the flexural stiffness values obtained during the master curve testing. This is likely to be the result of the fact that the master curve testing was conducted at a

lower strain level of 70 micron. This is an indicated that the flexural stiffness of the BSM depends on the stress / strain level applied.

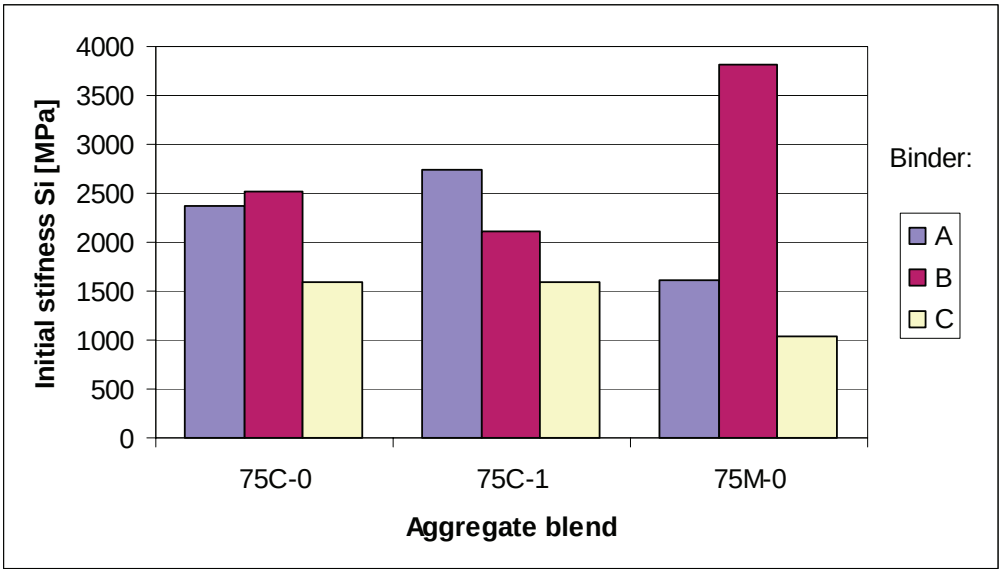


Figure 140: Average initial stiffness ($S_i$) per mix

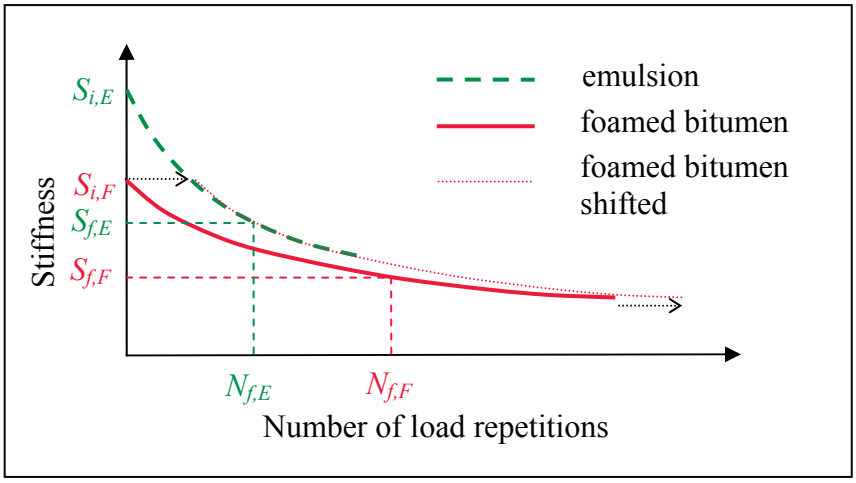


Figure 141: Conceptual difference between stiffness reduction curves of the emulsion and foamed bitumen treated mixes

## References

Hopman, P. C., VEROAD, Koac-NPC, Apeldoorn, the Netherlands, 2000

Jenkins, K. J., Long, F. M. and Ebels, L. J., *Foamed bitumen mixes = shear performance?*, International Journal of Pavement Engineering, Vol. 8, No. 2, June 2007

Jenkins, K. J., *Mix design considerations for cold and half-warm bituminous mixes with emphasis on foamed bitumen.* PhD dissertation University of Stellenbosch, South Africa, 2000.

Pronk, A. C., Burger's Fit Model, Delft University of Technology, the Netherlands, 2007

Theyse, H. L., *The suction pressure, yield strength and effective stress of partially saturated unbound granular pavement layers*, Proceedings of the 10th International Conference on Asphalt Pavements, Quebec City, Canada, 2006

Van Niekerk, A. A., *Mechanical Behavior and Performance of Granular Bases and Sub-bases in Pavements*, PhD Dissertation Delft University of Technology, the Netherlands, 2002

# 7 PAVEMENT MODELLING

## 7.1 Introduction

Structural design and modelling of pavements is a complex aspect of pavement engineering that over the past has been studied by many researchers and this will continue to be the case for considerable time in the future. The modelling of pavements incorporating BSM's, and to be more precise, to estimate the stresses and strains at critical positions in the pavement structure and especially in the BSM layer, was not a focal point of this study.

Nevertheless a chapter of this dissertation is dedicated to this topic because it is an important aspect practiced by engineers in day-to-day business of optimising mix composition and pavement dimensioning for rehabilitation design or new construction. This chapter aims to demonstrate how the experimentally determined material properties and behaviour of the BSM's, as discussed in the previous chapters, link to pavement modelling. This objective is achieved by working out a limited number of practical examples using stress and strain analysis methods that are readily available to the practitioner.

It is noted that the material properties and behaviour as determined in this study are only valid for the test conditions that were adopted, *i.e.* temperature, loading frequency, *etc*. Care was taken to select typical and representative test conditions. The actual conditions in the pavement structure may however differ from these chosen laboratory conditions. The examples worked out in this chapter are therefore hypothetical and serve the purpose of illustrating how the material properties determined in this study may assist in the pavement modelling. They are not intended to accurately estimate the structural capacity of the modelled pavement structure. Important laboratory test conditions have been identified and a follow-up study to investigate their effect is being set up.

The linear-elastic multi-layer program BISAR (Shell, 1998) and the non-linear-elastic multi-layer program KENLAYER (Huang, 1993) are used to this extent. The use of multi-layer programs has certain limitations in the estimation of the pavement response. More advanced methods such as finite element methods are required to more accurately estimate the pavement response. The use of such advanced methods is however outside the scope of this study. Some of the limitations of multi-layer programs are discussed in this chapter. Critical aspects in the analysis of pavements by means of these methods are also discussed.

In the first section of this Chapter the effect of using non-linear-elastic calculations compared to linear-elastic calculations in order to determine the response of a pavement structure in terms of stresses and strains is evaluated. To this end a typical pavement structure incorporating a BSM base layer is modelled.

The non-linear behaviour of BSM's is accounted for by adopting the $M_r$-$\theta$ model, as discussed in the previous chapters, as an estimate for the compressive stiffness, whereby the BSM base layer is divided into sub-layers. It will be shown in this Chapter that both with linear-elastic and non-linear-elastic calculations, progressively increasing tensile stresses are calculated towards the bottom of the BSM base layer. When these tensile stresses are sufficiently high, the bulk stress becomes negative. For the sub-layer to which this applies a stress-dependent compressive stiffness ($M_r$-$\theta$) can therefore not be determined. Instead, a stress-dependent tensile stiffness would need to be assigned to these lower base sub-layers.

Such a tensile stiffness would be lower than the compressive stiffness because of the anisotropy of the BSM material. Little *et al.* (2007) have found that in a tri-axial test and for granular and cement stabilised base materials the stiffness in the horizontal direction (tension) is at optimum moisture content approximately 50 % lower than the stiffness in vertical direction (compression). This principle can also be expected to apply to BSM's.

However, due to limitations of the test set-up and instrumentation of the tri-axial test used in this study, displacements and loads in the horizontal directions could not be measured. Subsequently, the anisotropic behaviour and a tensile stiffness of the BSM's tested could not be determined in this study. This would require more complex tests such a spring box or a "true" tri-axial test. A model, in which the base layer is divided into sub-layers with a compressive stiffness assigned to the upper base sub-layers and tensile stiffness assigned to the lower base sub-layers, could therefore not be developed here. Such complex material behaviour ideally requires a finite element approach and is difficult to model using linear-elastic or non-linear-elastic multi-layer software.

The bending stiffness of BSM's, as determined in this study using the four-point beam apparatus, is higher than the compressive stiffness ($\underline{M_r}$-$\underline{\theta}$) at low bulk stresses. It would therefore also be considerably higher than the tensile stiffness of the materials. The bending stiffness as determined in this study can therefore not be used to model the stiffness of the lower sub-layers of the BSM base layer.

After the comparison of the linear-elastic and non-linear-elastic calculations in this Chapter, a sensitivity analysis has been carried out to determine the effect of changes to the typical pavement structure on the pavement response. These changes include varying the subgrade support, BSM layer thickness and BSM layer stiffness.

The Chapter ends with a brief illustration of how the experimentally determined material properties and behaviour can be used in thickness design of the BSM base layer. This example is of a hypothetical nature, but it does demonstrate that the different properties experimentally determined here for different mixes lead to significant differences in design thickness.

## 7.2 Linear-elastic *vs.* non-linear-elastic multi-layer calculations

### *7.2.1 Introduction*

In Chapter 6 it was shown that the behaviour of the mixes tested here is non-linear. Their resilient modulus depends on the stress state, *i.e.* the bulk stress $\theta$. The $M_r$-$\theta$ model can be used to predict the resilient modulus in case the principal stresses are known. Because these principal stresses themselves depend on the resilient modulus, an iterative process should be followed to converge at a solution for the resilient modulus. This iterative process can be done manually, but this quickly becomes a laborious process.

The computer program KENLAYER (Huang, 1993) is an elastic multi-layer program that is able to derive a solution for the resilient modulus of non-linear layers using such an iterative process. The $M_r$-$\theta$ model as described in Chapter 3 is adopted in KENLAYER and the user input consists of values for the $k_1$ and $k_2$ coefficients of this model.

It was shown in Chapter 6 that of the three aggregate blends tested, the resilient modulus of the two blends with 75% crushed rock (75C-0 and 75C-1) are best described by the $M_r$-$\theta$ model. The resilient modulus of the mixes with 75% RAP (75M-0) cannot be predicted well using the $M_r$-$\theta$ model. Therefore, pavement structures with two typical mixes with 75% crushed rock were subjected to an analysis of stresses and strains using the program KENLAYER. To this end the mixes with bitumen emulsion A were selected, *i.e.* A-75C-0 and A-75C-1. The following model coefficients were used:

Table 57: $M_r$-$\theta$ model coefficients used in KENLAYER

| Mix | $M_r$-$\theta$ model coefficients | |
|---|---|---|
| | $k_1$ [MPa] | $k_2$ [-] |
| A-75C-0 | 130 | 0.30 |
| A-75C-1 | 150 | 0.33 |

The problem analysed consists of a layered continuous halfspace. The pavement structure model consists of a simple structure with a 40 mm asphalt wearing course with a stiffness of 5000 MPa, a 200 mm BSM base layer with varying stiffness and a subgrade with a stiffness of 200 MPa. A single wheel load of 45 kN and a tyre pressure of 700 kPa was used, which is modelled as a circular loading area with a radius of 143 mm and a uniform contact pressure equal to the tyre pressure. This is shown in Figure 142.

The asphalt thickness of 40 mm is typical for use in South Africa. The stiffness of 5000 MPa is taken from the range of values suggested by Freeme and tabulated in the South African Mechanistic Design Method (SAMDM, Theyse *et al.*, 1996). The thickness of 200 mm for the BSM layer is a typical layer thickness often used in in-situ recycling operations in South Africa. The effect of varying the above assumed values is discussed further on in this chapter.

In terms of analysing the stresses in the two horizontal directions in the pavement structure, the problem becomes symmetric by using a single wheel load instead of a dual wheel load. The current legal axle load in South Africa is 9 ton, which equates to approximately a 45 kN super single wheel load. The dual wheel configuration is still widely in use in South Africa, however, modelling with a super single wheel load is easier because of the symmetry. When modelling with a dual wheel configuration one has to, for each layer, determine the critical horizontal position, *i.e.* under the centre of one wheel or in the middle between the two wheels. When using a super single the critical horizontal position is always under the centre of the wheel, that is to say when assuming a uniform contact pressure over the loading area. This assumption may also be made because non-uniform load distribution does not influence the stress condition deeper in the pavement, but only close to the surface. Using a super single wheel also leads to a slightly more conservative estimate, because the stresses under single wheel loading are generally slightly higher than under dual wheel loading.

For reasons of simplicity it was chosen to model the support of the layers underlying the BSM base layer by a single subgrade layer. In practice a number of layers with different stiffness values would be supporting the base layer, *i.e.* a subbase layer, one or more selected subgrade layers and the in-situ subgrade. Because no in-depth analysis of the stresses and strains in these sub-layers is carried out here, it is replaced by a single subgrade layer with an equivalent stiffness. The effect of variations in the support of these sub-layers is discussed further on in this chapter.

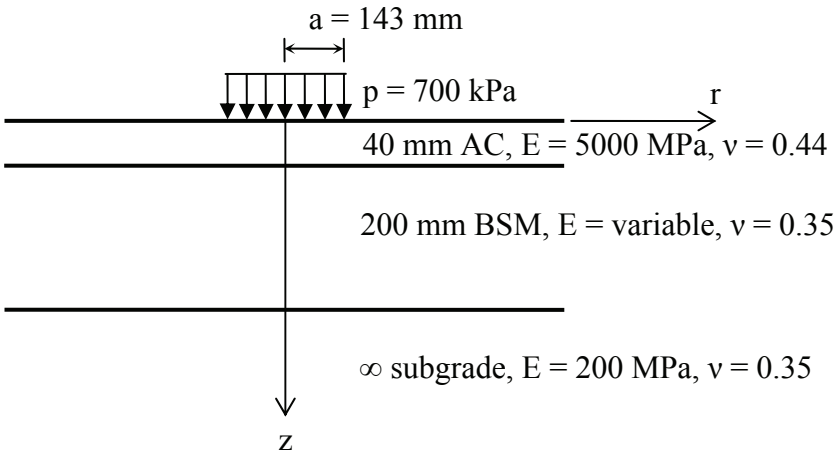


Figure 142: Pavement structure used for modelling with KENLAYER

### *7.2.2 KENLAYER example*

7.2.2.1 Stresses and strains

The stiffness of the BSM base layer was modelled in KENLAYER as non-linear. To this end the BSM base layer was subdivided into 4 layers of 50 mm each. The resilient response model coefficient assigned to each of these layers is summarised in

Table 57. A seeding value of 1000 MPa was assigned to the BSM sub-layers with a minimum limit for the stiffness of 0 MPa.

In the calculation of the bulk stress in non-linear layers KENLAYER also takes into account the geostatic stresses as a results of the weight of the overlaying material. Therefore, the unit weights of the materials also need to be specified. The unit weights as shown in Table 58 were used. The default value of 0.6 was used for the $k_o$ coefficient for static earth pressures.

Table 58: Unit weights used for calculation of geostatic stresses

| Material | Unit weight [kg/m$^3$] |
|---|---|
| Asphalt | 2400 |
| BSM | 2200 |
| Subgrade | 2000 |

Stresses and strains in the BSM base layer as shown in Figure 143 and Figure 144 were calculated by KENLAYER. The default sign convention used in KENLAYER ("+" for compression and "-" for tension) is not followed here. Instead, compressive stresses and strains are denoted negative and tensile stresses and strains positive.

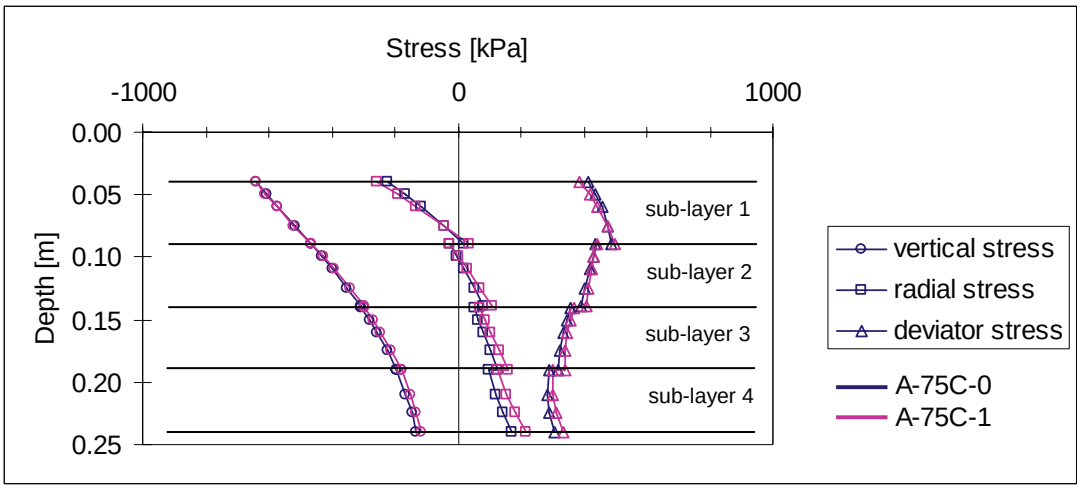


Figure 143: KENLAYER computed stresses in BSM layer

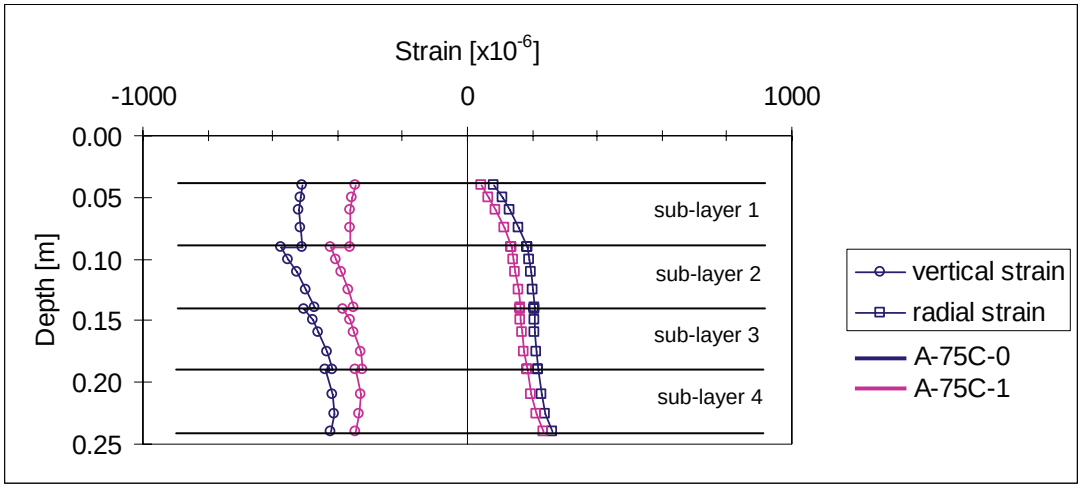


Figure 144: KENLAYER computed strains in BSM layer

It can be seen that there is very little difference in stress between the two mixes, which is to be expected. There are however significant differences in strain, especially the radial strains. Because of the higher stiffness of the A-75C-1 mix, the strains in the BSM layer of this material are lower.

The effect of dividing the 200 mm base layer into sub-layers of 50 mm each can clearly be seen in the radial stress and vertical strain. This is the result of differential stiffness of the sub-layers. Caution is required when analysing the stresses and strains over the depth of the layer when it is divided in sub-layers. If the analysis points do not include the top and bottom of each of the sub-layers (selecting a point 1 mm away from the interface is recommended when using KENLAYER), it is possible to not identify the step-wise shape of the radial stress and vertical strain curves. One needs to understand though, that these steps are the result of mathematical modelling and that in the real pavement structure these steps do not occur.

#### 7.2.2.2 Shifting of principal stresses

It should be noted that in any elastic multi-layer program significant tensile stresses are calculated. The $M_r$-$\theta$ model used here to predict the stiffness of the BSM layer was originally developed for granular materials. Most granular materials cannot take any significant tension. Therefore, in order to avoid a negative bulk stress $\theta$ and subsequently imaginary predicted $M_r$ values, the stresses as calculated by elastic multi-layer programs need to be modified (Huang, 1993). In case tensile minor principal stresses ($\sigma_3$) are computed, these are set to 0 while maintaining the same deviator stress. This means that the major principle stress ($\sigma_1$) is shifted further into compression. This type of adjustment of shifting the principal stresses is also adopted in the SAMDM (Theyse *et al.*, 1996). The effect of this shifting of principal stresses on the bulk stress is shown in Figure 145.

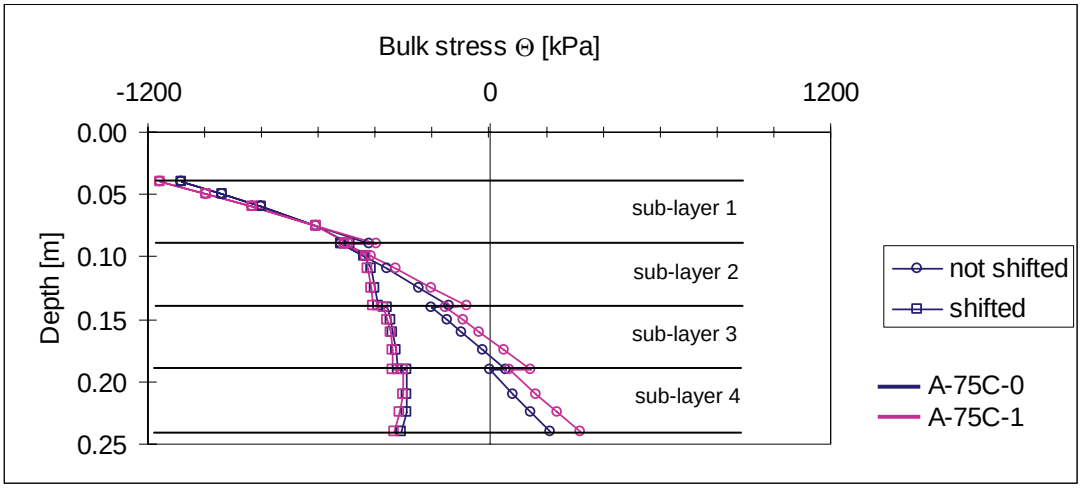


Figure 145: The effect of shifting the principal stresses in case of tensile minor principal stresses in the bulk stress θ.

It is generally accepted by researchers that the shifting of the principal stress is theoretically not correct. However, when the shifting is not performed, the $M_r$-$\theta$ model cannot be used, because no real solution exist for $\theta^{k_2}$ when $\theta$ is negative and while $k_2$ is smaller than 1 (this situation exists in sub-layer 4, see Figure 145). The negative bulk stress shown in Figure 145 would mean the $M_r$ is negative in sub-layer 4, which is physically impossible. Also in sub-layer 3, where the bulk stress is very low when the principal stresses are not shifted, this would lead to unrealistically low $M_r$ values. This is shown in Figure 146. Although shifting of the principal stresses is theoretically not correct, there is no alternative when using the $M_r$-$\theta$ model.

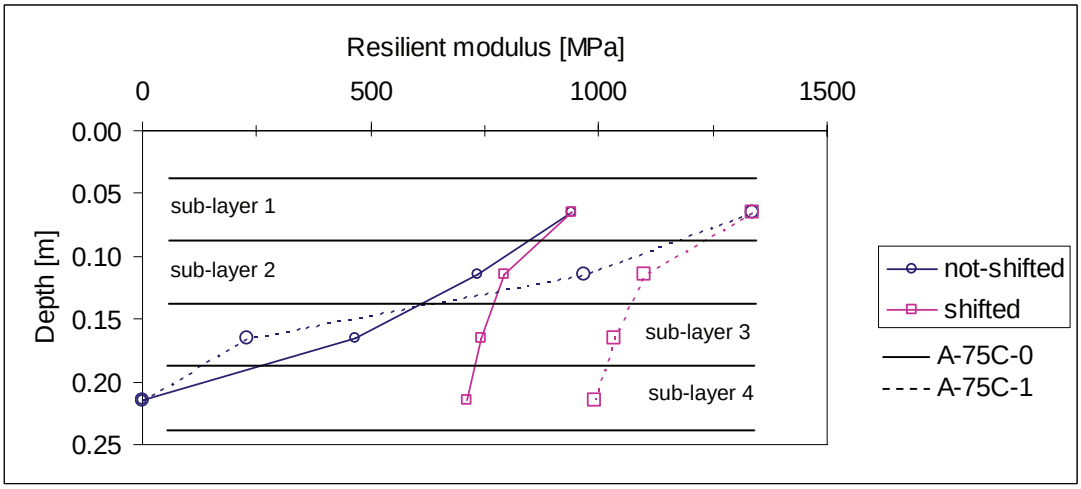


Figure 146: Comparison of $M_r$ at mid-depth of the sub-layers based on the $M_r$-θ model when the principal stress are not-shifted and shifted (geostatic stress not taken into account)

7.2.2.3 Dividing non-linear layer into sub-layers

In the above example the base layer was divided into 4 sub-layers. Increasing the number of sub-layers does not reduce the horizontal tensile stresses that are calculated in the base layer. This is illustrated by Figure 147, in which it is shown that the stress condition calculated in the BSM base layer when divided into 4 sub-layers is practically the same as when the base layer is divided into 10 sub-layers.

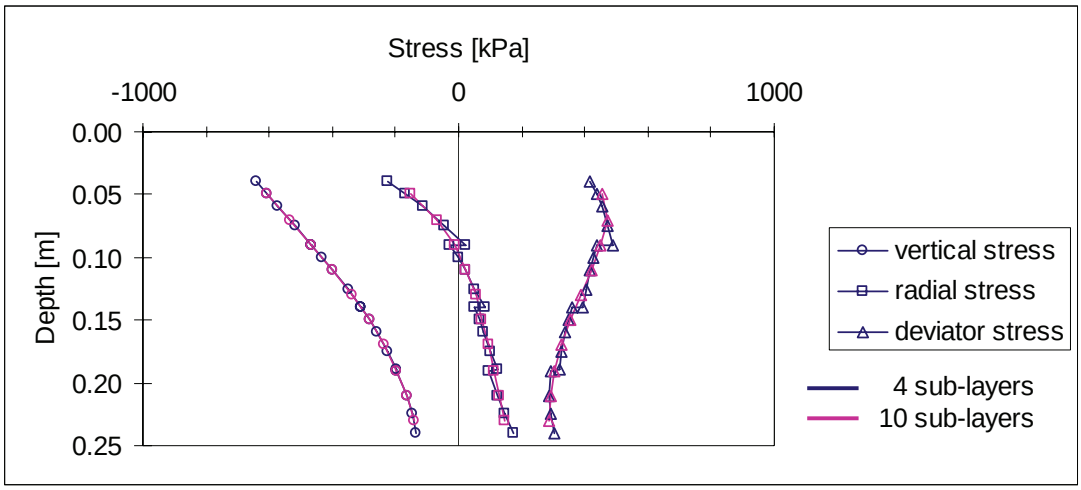


Figure 147: KENLAYER computed stresses in A-75C-0 BSM layer divided into 4 and 10 sub-layers

Consequently, there is also no difference in the development of the resilient modulus, based on the $M_r$-$\theta$ model, over the height of the base layer. This is shown in Figure 148. It can thus be concluded that, when analysing a non-linear layer, dividing this layer into more than 4 sub-layers does not increase the accuracy of the estimation of the stresses and strains using KENLAYER, nor does it reduce the tensile stresses that are calculated over a large part of the BSM base layer.

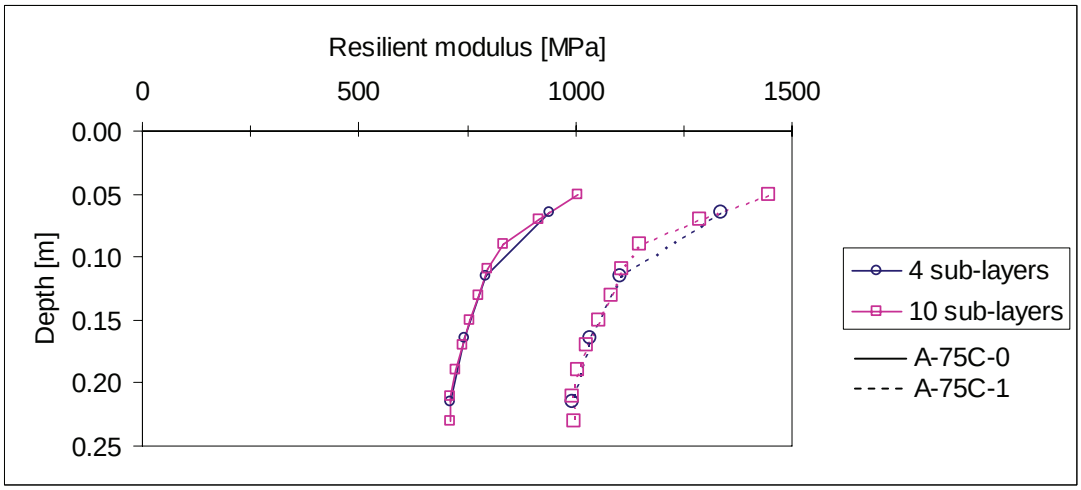


Figure 148: Comparison of $M_r$ at mid-depth of sub-layers based on $M_r$-$\theta$ model (geostatic stresses not taken into account)

7.2.2.4 Stress-dependent stiffness

With the bulk stresses as shown in Figure 145, and taking into account the geostatic stresses, resilient moduli as shown in Table 59 are calculated by KENLAYER for the four sub-layers of the BSM base layer.

Table 59: Resilient moduli predicted by KENLAYER using the $M_r$-$\theta$ model in an iterative process (including effect of geostatic stresses)

| BSM sub-layer | Resilient modulus [MPa] | |
|---|---|---|
| | A-75C-0 | A-75C-1 |
| 40 – 90 | 948 | 1345 |
| 90 – 140 | 780 | 1068 |
| 140 – 190 | 686 | 914 |
| 190 – 240 | 603 | 781 |

It can be seen that the stiffness of the BSM material reduces towards the bottom of the layer. This is as a result of decreasing levels of lateral confinement. The computed stiffness reduces with 36% and 41% for mix A-75C-0 and A-75C-1 respectively. Also, the mix with 1% cement as active filler (A-75C-1) clearly shows a higher resilient modulus compared to the mix without cement (A-75C-0).

The resilient moduli computed here, which are based on the stress state in the pavement structure modelled as shown in Figure 142, are much in line with the resilient moduli determined experimentally in this study. This gives confidence that the model coefficients $k_1$ and $k_2$ determined experimentally can be applied in the elastic multi-layer program as used in this example.

### *7.2.3 Comparison of BSM layer divided into sub-layers with differential stiffness values vs. undivided BSM layer with single stiffness value*

7.2.3.1 Comparison of stresses and strains

In the previous paragraph it was shown that KENLAYER is a powerful tool to derive an appropriate stiffness for layers consisting of a non-linear-elastic material. In the worked out example an appropriate resilient modulus for the BSM, which depends on the stress state present in that layer, was derived by KENLAYER in an automated iterative process using the $M_r$-$\theta$ model.

The BSM layer in the example was divided into four sub-layers each with an increasing stiffness towards the top of the layer where the compressive horizontal stresses increase. Once the stiffness of each of these sub-layers has been determined, the stresses and strains that KENLAYER calculates for the pavement structure are based on linear-elastic theory. It could therefore be postulated that, once the correct stiffness is assigned to the non-linear BSM layer, the stress and strain output of KENLAYER should be comparable to that of any other linear-elastic multi-layer program.

The only difference would be that in KENLAYER the BSM layer is divided into sub-layers with different stiffness values, while with any other linear-elastic multi-layer program the BSM layer is an undivided layer with a single stiffness value. (Such a subdivision with different stiffness values assigned to the different sub-layers is also possible with other linear-elastic multi-layer programs, but determining the correct stiffness values for each of these sub-layers quickly becomes a laborious manual iterative process.)

An example has been worked out here in order to compare a BSM layer divided into sub-layers with each a different stiffness value with an undivided BSM layer with a single stiffness. For the former the examples worked out in the previous section using KENLAYER are used, while for the latter the linear-elastic multi-layer program BISAR 3.0 (Shell, 1998) is used. The stiffness values for the BSM sub-layers as used in KENLAYER are shown in Table 59. For the undivided BSM layer in BISAR a stiffness of 700 MPa was used for the A-75C-0 mix and a stiffness of 1100 MPa for the A-75C-1 mix. This is more or less the average of the sub-layer stiffness values. The pavement structure and loading used for the modelling remains the same as shown in Figure 142.

The stresses calculated for the divided base layer system (KENLAYER) and the undivided base layer system (BISAR) for both the A-75C-0 and the A-75C-1 materials are shown in Figure 149 and Figure 150 respectively. The strains calculated are shown in Figure 151 and Figure 152.

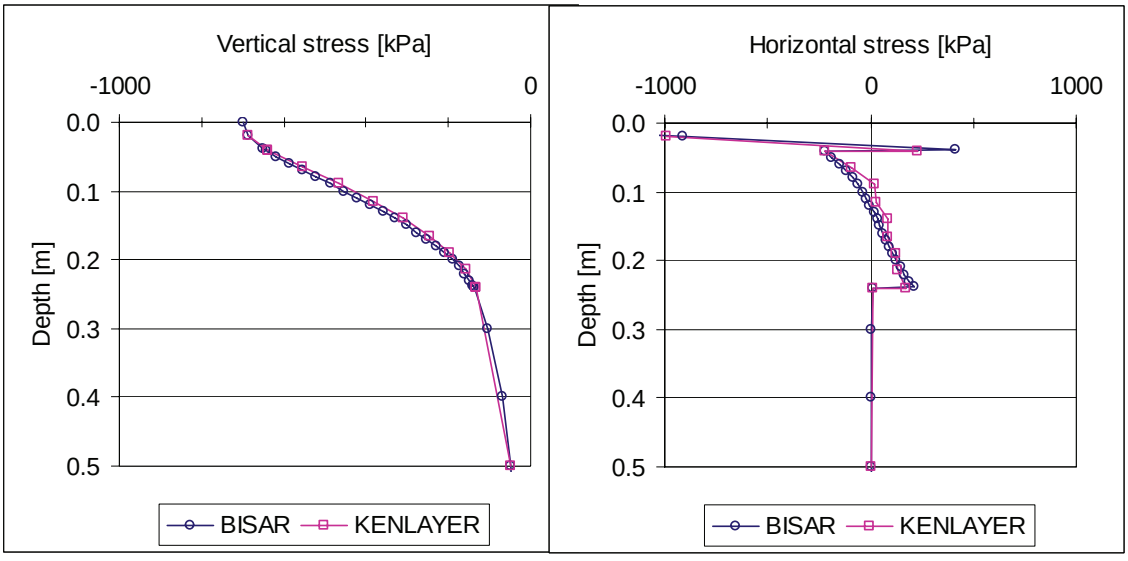


Figure 149: Comparison of stress calculated by KENLAYER (divided BSM layer) and BISAR (undivided BSM layer) for the A-75C-0 mix

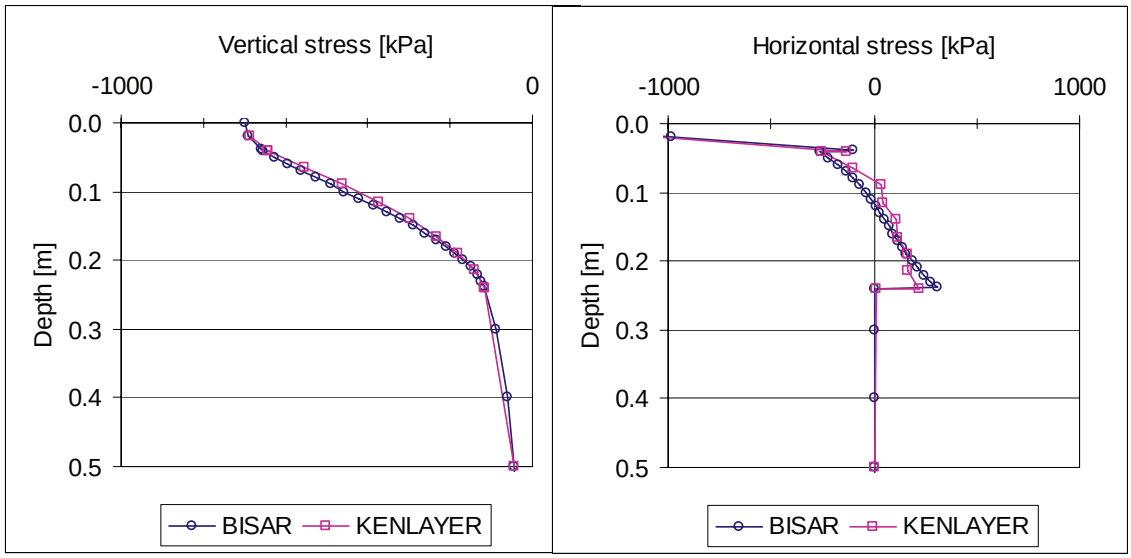


Figure 150: Comparison of stress calculated by KENLAYER (divided BSM layer) and BISAR (undivided BSM layer) for the A-75C-1 mix

It can be seen from Figure 149 and Figure 150 that there is hardly any difference in the vertical stresses calculated in the pavement structure with a BSM layer divided into sub-layers with different stiffness values (KENLAYER) compared to an undivided BSM layer with a single stiffness value (BISAR). There is however a significant difference in the horizontal stress. In the pavement structure modelled with a single BSM layer the horizontal stress gradient is more or less constant over the height of the layer. In the pavement modelled with a sub-divided BSM layer the horizontal stress gradient changes with depth from the one sub-layer to the next.

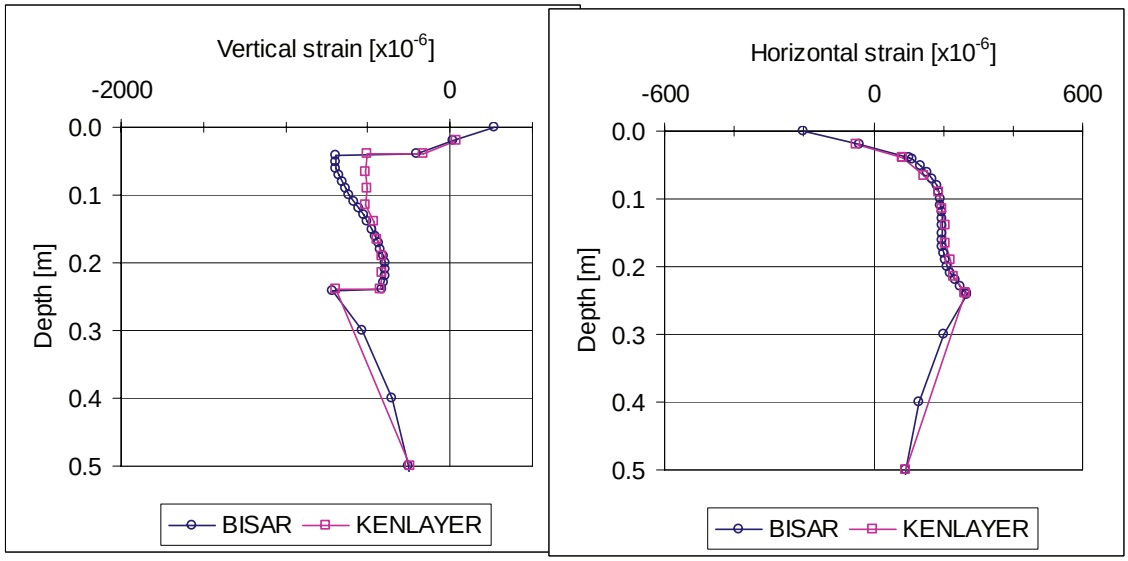


Figure 151: Comparison of strain calculated by KENLAYER (divided BSM layer) and BISAR (undivided BSM layer) for A-75C-0 mix

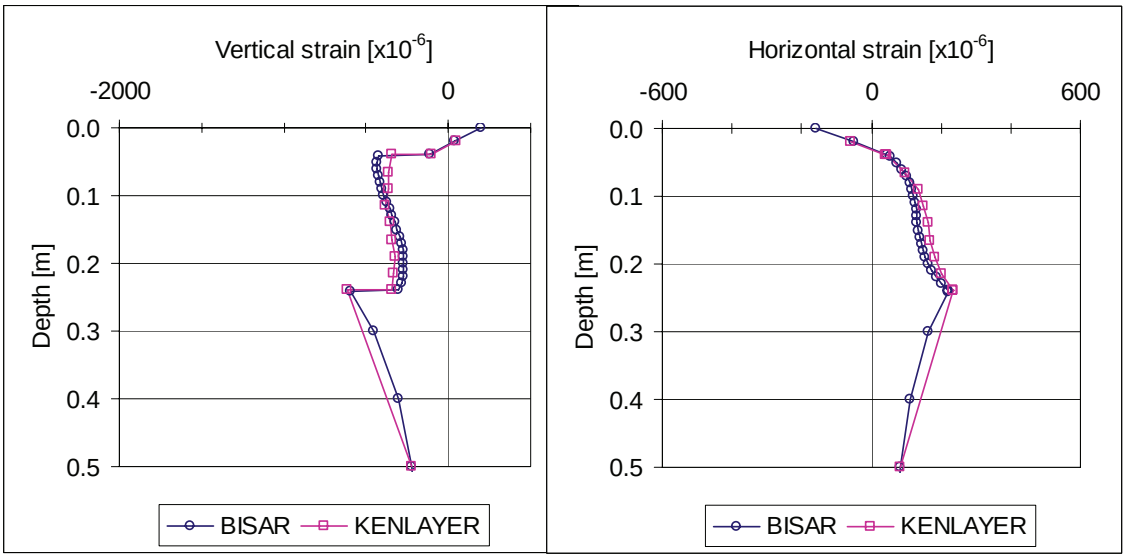


Figure 152: Comparison of strain calculated by KENLAYER (divided BSM layer) and BISAR (undivided BSM layer) for A-75C-1

The horizontal strains calculated in the pavement structure also do not show significant differences when modelled with either a BSM layer divided into sub-layers or a single BSM layer. The vertical strain however does show variation. When modelled with a sub-divided BSM layer (KENLAYER) the vertical strain is more constant over the depth of the layer. When the base layer is modelled as a single layer (BISAR) the vertical strain decreases with increasing depth.

The following points are of particular interest when analysing stresses and strains in the pavement structure with the objective to determine the structural capacity:

- Horizontal tensile stress at the bottom of the asphalt surfacing layer;
- Principal stresses in the BSM layer;
- Horizontal strain at the bottom of the BSM layer;
- Vertical strain on top of the subgrade.

It is not recommended here to use the vertical strain on top of the subgrade as a design parameter, because the subgrade also behaves non-linearly. Using a $M_r$-$\theta$ approach or evaluating the deviator stresses in the subgrade (layers) are alternative options. It is however not the purpose here to evaluate the stress condition in the layers below the BSM base layer and the vertical strain on top of the subgrade is used here merely as a measure of the load spreading capability of the BSM base layer. For this purpose the vertical strain on top of the subgrade is deemed to be an appropriate indicator.

For mechanistic analyses of granular pavement layers (or layers of a material for which shear failure is the critical failure mode) the principal stresses at mid-depth of the layer is often used (Theyse *et al.*, 1996). More recent mechanistic modelling of BSM materials (Long and Theyse, 2004) analyses the principal stresses at several depths in the layer, *i.e.* ¼ from the top, at mid-depth and ¼ from the bottom. The

difference in magnitude of the stresses and strains at these various points are summarised in Table 60 together with the pavement response at the other points of interest.

Table 60: Comparison of stresses and strains in pavement modelled with a divided BSM base layer and an undivided BSM base layer

| Analysis point | A-75C-0 | | A-75C-1 | |
|---|---|---|---|---|
| | divided | undivided | divided | undivided |
| $\varepsilon_h$ bottom asphalt [$10^{-6}$] | 82 | 103 | 42 | 46 |
| $\sigma_1$ / $\sigma_3$ (z = 90 mm) [kPa] | -465 / 22 | -487 / -61 | -463 / 35 | -492 / -68 |
| $\sigma_1$ / $\sigma_3$ (z = 140 mm) [kPa] | -308 / 84 | -329 / 32 | -297 / 111 | -321 / 52 |
| $\sigma_1$ / $\sigma_3$ (z = 190 mm) [kPa] | -195 / 126 | -208 / 110 | -180 / 163 | -187 / 160 |
| $\varepsilon_h$ bottom BSM [$10^{-6}$] | 264 | 266 | 234 | 218 |
| $\varepsilon_v$ top subgrade [$10^{-6}$] | -696 | -716 | -618 | -593 |

The effect of dividing the base layer into sub-layers on the stresses and strains at each of these analysis points is discussed in the following sections.

7.2.3.2 Effect on horizontal strain in bottom asphalt

At face value the difference to the horizontal strain at the bottom of the asphalt layer is not substantial. However, the small differences could make quite a difference on a log-scale when transfer functions for asphalt fatigue are used. To illustrate this the transfer function for fatigue of continuously graded thin asphalt wearing courses of the South African Mechanistic Pavement Design Method (Theyse and Muthen, 2000), using a 90% reliability (Category B road) is used. In case of the 82 microstrain tension at the bottom of the asphalt layer (A-75C-0 base layer), crack initiation is predicted to occur after 46 million load repetitions, while for 103 microstrain tension this would be after 14 million load repetitions. Although the predicted fatigue lives are arguably unrealistically high (at these high number of load repetitions as a results of low applied strains other functional aspect become more critical than fatigue), it does illustrate that a seemingly small difference (21 microstrain) results in a factor 3 difference in the predicted fatigue life.

It can therefore be concluded that using non-linear-elastic calculations (*e.g.* KENLAYER) to determine the stresses and strains in the pavement structure can result in large differences in the predicted structural capacity of the thin asphalt wearing course.

7.2.3.3 Effect on principal stresses in BSM layer

The principal stresses at various points in the base layer are used to calculate the deviator stress and deviator stress ratio. As discussed in the previous paragraph, these analysis points are chosen at ¼ from the top of the layer, at mid-depth and ¼ from the bottom of the layer. The most critical stress ratio is subsequently used for design purposes.

It may however not be sufficient to evaluate the stress conditions at these three analysis points, because of the step-wise function of the horizontal stress with depth. For this reason the deviator stress ($\sigma_d = \sigma_1 - \sigma_3$) and the deviator stress at failure, $\sigma_{d,f}$, at a large number of points over the depth of the base layer have been evaluated here, including points just above and below the interface of the respective sub-layers. This is shown in Figure 153 for mix A-75C-0 and Figure 154 for mix A-75C-1. The deviator stress at failure is based on the shear parameters of the two respective mixes.

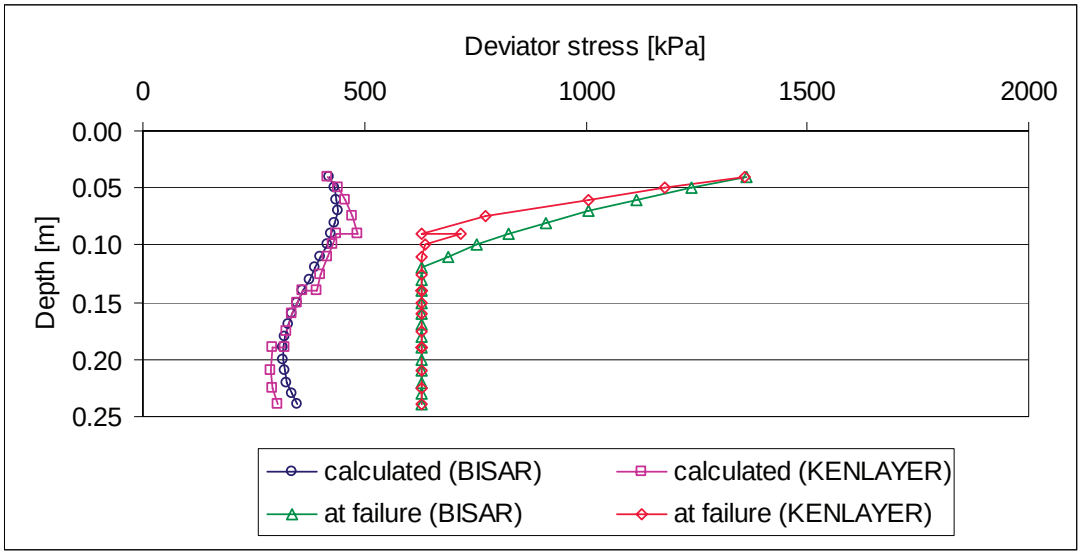


Figure 153: Mix A-75C-0: Comparison of deviator stress in the pavement structure (calculated) and deviator stress at failure determined with KENLAYER (divided BSM layer) and BISAR (undivided BSM layer)

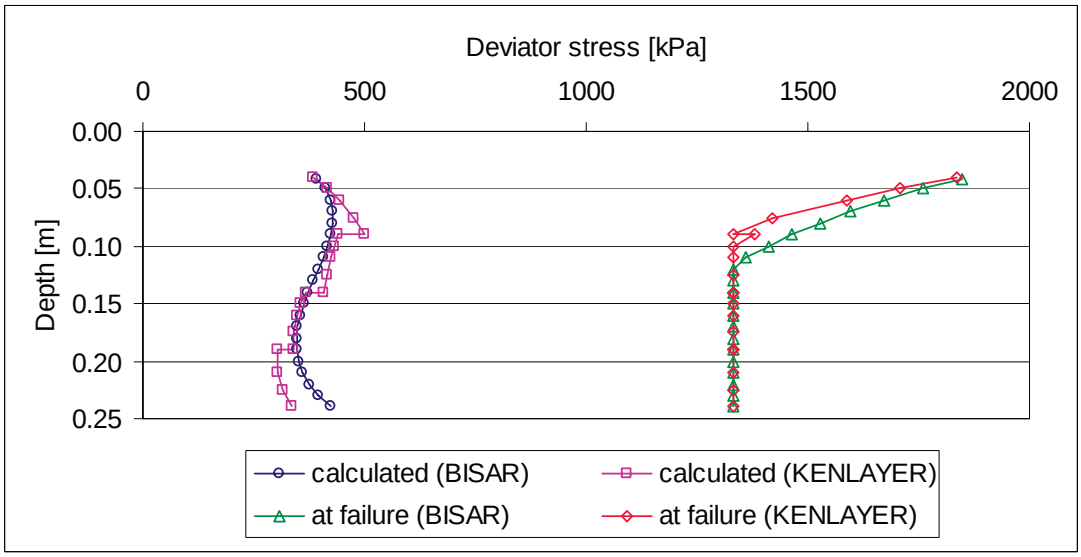


Figure 154: Mix A-75C-1: Comparison of deviator stress in the pavement structure (calculated) and deviator stress at failure determined with KENLAYER (divided BSM layer) and BISAR (undivided BSM layer)

There are some significant differences in the stress state of the BSM layer when it is analysed divided in sub-layers compared to when it is analysed as an undivided layer. It can be seen that these differences occur mainly at the bottom of the uppermost sub-layer (both deviator stress and deviator stress at failure) and in the lowest sub-layer (deviator stress only).

In the upper part of the BSM base layer, the deviator stress at failure differs. This is the result of the fact that the horizontal stresses differ significantly in the divided layer model compared to the undivided layer model. This was already shown in Figure 149 and Figure 150. From the top of the base layer downwards, the compressive horizontal stresses change to tensile horizontal stresses more rapidly in the divided layer model compared to the undivided layer model. The effect hereof is twofold. Firstly it causes in a more rapid increase in deviator stresses (see Figure 153). Secondly, the calculated major principal stress at failure, $\sigma_{1,f} = A \cdot \sigma_3 + B$, and subsequently the deviator stress at failure, $\sigma_{d,f}$, reduces more rapidly because of the diminishing first term ($A \cdot \sigma_3$, see Figure 154).

The shifting of the principal stresses when horizontal tensile stresses develop (as discussed in Section 7.2.1 $\sigma_3$ is then set to zero) starts higher up in the BMS base layer in the divided layer model compared to the undivided layer model (see Figure 153 and Figure 154). This results in differences in the deviator stress at failure at this depth range between the two models. Once $\sigma_3 \leq 0$ in both the divided and undivided base layer model there is no difference in the major principal stress at failure, hence also not in the deviator stress at failure. The calculation of the major principal stress at failure, $\sigma_{1,f} = A \cdot \sigma_3 + B$, is then reduced to $\sigma_{1,f} = B$ (when $\sigma_3 \leq 0$), and the B term is independent of the stress state.

The effect on the deviator stress ratio is thus a "double" increase in the divided layer model compared to the undivided layer model, *i.e.* $\sigma_d$ increases while $\sigma_{d,f}$ decreases, for a long as $\sigma_3 > 0$. This is shown in Figure 155 and Figure 156.

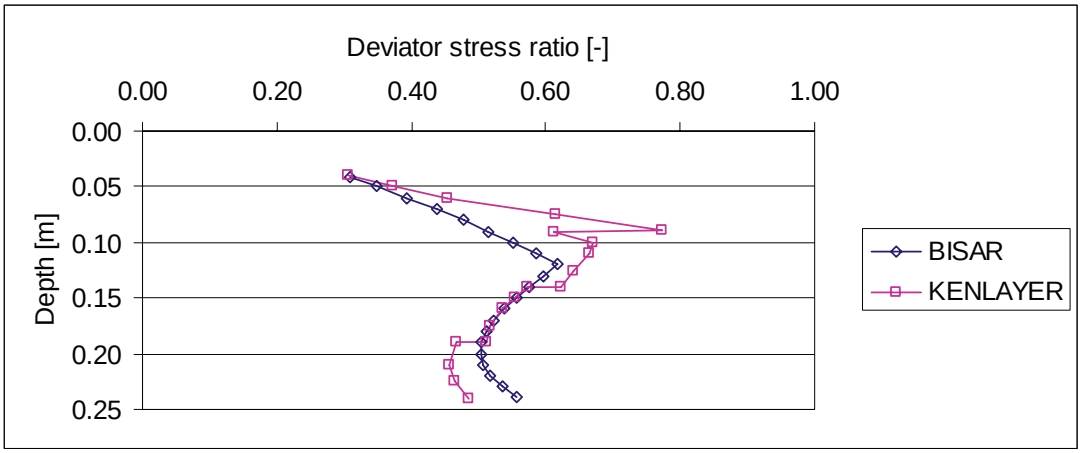


Figure 155: Mix A-75C-0: Comparison of deviator stress ratio for KENLAYER (divided BSM layer) and BISAR (undivided BSM layer)

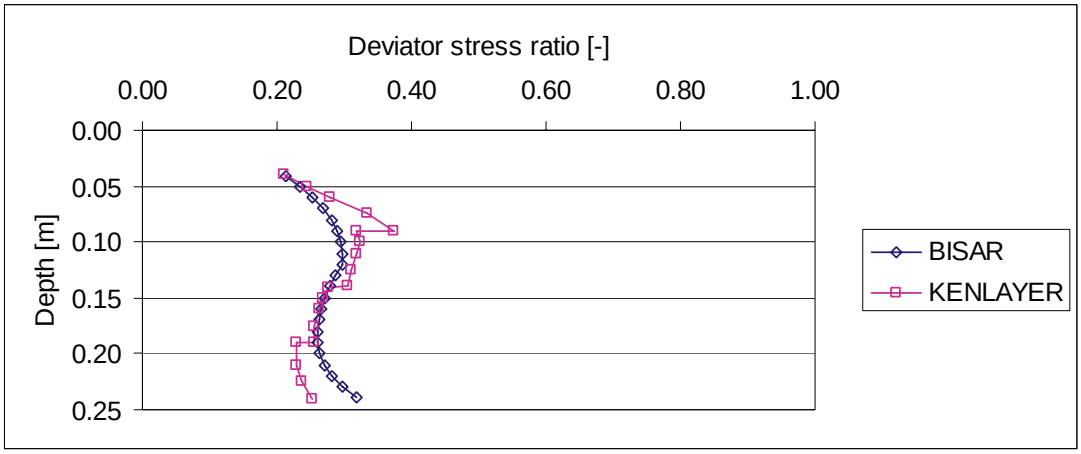


Figure 156: Mix A-75C-1: Comparison of deviator stress ratio for KENLAYER (divided BSM layer) and BISAR (undivided BSM layer)

It can be seen that the most significant differences in deviator stress ratio occur at the bottom of the uppermost sub-layer and in the lowest sub-layer. The magnitude of the critical deviator stress ratio for design purposes as well as the depth at which it occurs is therefore also affected when the pavement is analysed using the non-linear divided base layer system or the linear undivided base layer model.

In the divided base layer model (KENLAYER) the critical deviator stress ratio occurs at the bottom of the uppermost layer, approximately at the point where the calculated minor principal stress changes from compression to tension. The location of the critical stress ratio is independent of whether a stiffer (A-75C-1) or softer (A-75C-0) base layer material is used. In the undivided base layer system (BISAR), the critical stress ratio may occur at the bottom of the base layer in case of stiff layers (A-75C-1, see Figure 155) or approximately at the point where the calculated minor principal stress changes from compression to tension when softer layers are used (A-75C-0, see Figure 156).

#### 7.2.3.4 Selecting the critical deviator stress ratio

The general shape of the deviator stress ratio curves calculated with KENLAYER as shown in Figure 155 and Figure 156 is likely to be a better representation of the stress state in the pavement structure than the shape of the curves calculated with BISAR. This is because the stress dependent behaviour of the base layer material is to a certain extent accounted for in the KENLAYER calculations.

The local maximum in this curve at the bottom of the uppermost base sub-layer in the KENLAYER calculation is however an overestimation of the actual stress state in the pavement structure. This is because the stresses in the sub-layers itself are calculated linear-elastically in KENLAYER. For the same reason the horizontal stresses at the bottom of the undivided base layer (BISAR) is also an overestimation of the actual stress state at this position.

It would therefore appear that the critical deviator stress ratio approximately occurs at the depth in the base layer at which the calculated minor principal stress ($\sigma_3$) changes from compression to tension. These points differ slightly between the KENLAYER and BISAR calculations (see Figure 153 and Figure 154). The magnitude of the corresponding deviator stress ratios also differ. The KENLAYER calculations are likely to be closer to the actual stress state due to the non-linearity used in the calculations. The so-obtained critical stress ratio is slightly higher than when linear-elastic calculations are used (BISAR) and the point at which is occurs is higher up in the layer.

One needs to take care not to select the deviator stress ratio at the bottom of the uppermost sub-layer for the critical stress ratio, as this likely to be an overestimation.

#### 7.2.3.5 Effect on horizontal strain in bottom BSM layer

As can be seen from Table 60, there are only small differences in the horizontal tensile strain at the bottom the BSM layer between using the divided layer model and the undivided layer model (1% difference for the A-75C-0 mix and 7% for the A-75C-1 mix). These small differences identified here between using linear-elastic and non-linear-elastic modelling are unlikely to significantly influence the accuracy of any structural capacity predictions based on the this criterion.

The horizontal strain in the bottom of the BSM layer is chosen here to demonstrate any possible differences between non-linear-elastic and linear-elastic methods. Qualitative comments on the applicability of this criterion in relation to the fatigue life of the BSM layer for structural design are provided in Chapter 8.

#### 7.2.3.6 Effect on vertical strain on top subgrade

As for the horizontal strain at the bottom of the BSM layer, there are also only small differences in the vertical strain on top of the subgrade (3% for the A-75C-0 mix and 4% for the A-75C-1 mix). The agreement between the non-linear and linear modelling approach in the effect on the vertical strain on top of the subgrade can also be seen in Figure 151 and Figure 152.

As mentioned in 7.2.1, the layers below the base layers are simplified in the examples worked out here and modelled as a single subgrade layer. An in-depth analysis of the stresses and strains in the several sub-layers that may exist (subbase layer, selected subgrade layer, *etc*.) is therefore not provided here. It can however be concluded that there are no significant differences between the non-linear and linear modelling approach because the vertical stress on top of the subgrade, which is a measure of the load spreading of the upper layers, is near identical (see Figure 149 and Figure 150). There are likely to be significant differences when layers below the base layer are also modelled non-linearly.

### *7.2.4 Conclusions*

It can be concluded that using the non-linear-elastic approach for the modelling of the BSM base layer in lieu of a linear-elastic approach, can lead to improved

understanding of the stresses and strains that develop in the BSM layer. The stress-dependant stiffness of the BSM layer increases towards the top of the layer, where the lateral pressures are higher and the support provided by the lower part of the same layer is better. This results in differences compared to linear-elastic modelling. These differences may impact on the stresses and strains of the overlying layer (asphalt wearing course) and of the BSM layer itself. It appears to have little effect on the stress and strains in the lower layers.

The TG2 Guideline and Long and Theyse (2004) propose that for BSM materials, the most critical stress ratio determined for three positions in the layer needs to be selected for further analysis. It is shown here that this critical deviator stress ratio can differ considerably between a non-linear-elastic and linear elastic analysis. In the examples worked out above it is shown that using the non-linear approach (*e.g.* KENLAYER) and dividing the BSM layer into four sub-layers, each with a unique stiffness, results in higher stress ratios. These are believed to be a better estimate than the ones obtained by linear-elastic calculations (*e.g.* with BISAR).

The current guidelines propose that the deviator stress ratios be determined at three depths in the BSM layer, *i.e.* ¼ from the top, at mid-depth and ¼ from the bottom, and that the most critical one be selected. It is shown here that the position of the critical deviator stress ratio occurs at such a depth in the layer where the minor principal stress $\sigma_3$ (before being shifted) changes from compression to tension. This stress ratio may be higher than at any one of the three depths discussed above.

It therefore recommended here to use a non-linear approach for the analysis of stresses and strains in the pavement structure. This is relatively easy and a widely available computer program such as KENLAYER is a useful tool. It would require non-linear material coefficients, which are provided in this study. It is noted though that for BSM with a high percentage of RAP the $M_r$-$\theta$ model does not apply and care should be taken calculating with these types of BSM's.

It needs to be well understood though that stresses and strains calculated using a non-linear approach cannot be used as input for any transfer function that has been developed and calibrated using linear-elastic computer programs. Also, if such a transfer function uses a fixed analysis depth in the pavement layer, such as mid-depth, stresses calculated at any other depth in the layer can also not be used as input for these transfer functions.

It is recommend that the transfer functions that have been developed using linear-elastic multi-layer programs and for mid-depth or any other fixed depth analysis points, *i.e.* in the SAMDM (Theyse and Muthen, 2000) and by Long and Theyse (2004) for BSM's, be re-validated and re-calibrated using non-linear analysis methods.

## 7.3 Effect of changes in pavement structure

### *7.3.1 Introduction*

The pavement structure used in the example of the previous paragraphs and as shown in Figure 142 was selected because it represents a typical BSM pavement structure that is commonly used in South Africa. It has a typical subgrade stiffness (200 MPa), typical BSM base layer thickness (200 mm) and representative stiffness values were used for the BSM layer. In order to obtain a feel for the effect of changes in these typical values on the stresses and strains in the pavement structure, calculations using BISAR were made whereby each of these typical values is changed one at the time. The following ranges of values were used:

Table 61: Range of values used for parameter study

| Parameter | Range of values used |
|---|---|
| Subgrade stiffness [MPa] | 50, 200 and 400 |
| BSM base layer thickness [mm] | 150, 200 and 250 |
| BSM base layer stiffness [MPa] | 700, 1100 and 1500 |

The parameter values shown in the table above are believed to represent the practical range of these parameters in the BSM pavement structure. The same analysis points as shown in Table 60 are also used here, *i.e.*:

- Horizontal tensile stress at the bottom of the asphalt surfacing layer;
- Principal stresses in the BSM layer;
- Horizontal strain at the bottom of the BSM layer;
- Vertical strain on top of the subgrade.

### *7.3.2 Horizontal strain bottom asphalt*

The effect of changes in the subgrade stiffness, BSM base layer thickness and base layer stiffness on the horizontal strain at the bottom of the asphalt layer is summarised in Figure 157. It can be seen that the BSM layer stiffness has the largest effect on the horizontal strain at the bottom of the asphalt layer. These strains increase with decreasing BSM layer stiffness. The latter results in decreasing support to the overlying asphalt layer.

It is noted that the horizontal strain at the bottom of the asphalt layer increases with increasing subgrade support. This is contrary to what one intuitively would expect. The effect becomes however less pronounced with decreasing BSM layer thickness and decreasing BSM layer stiffness

Of the three parameters investigated, the thickness of the BSM layer has the smallest effect on the horizontal strain at the bottom of the asphalt layer, especially when the subgrade support is not very low. It can be seen that both with increasing BSM layer stiffness as well as with increasing subgrade stiffness, the difference in the horizontal strain at the bottom of the asphalt layer is minimal. The layer thickness becomes more critical at lower base layer stiffness and lower subgrade stiffness.

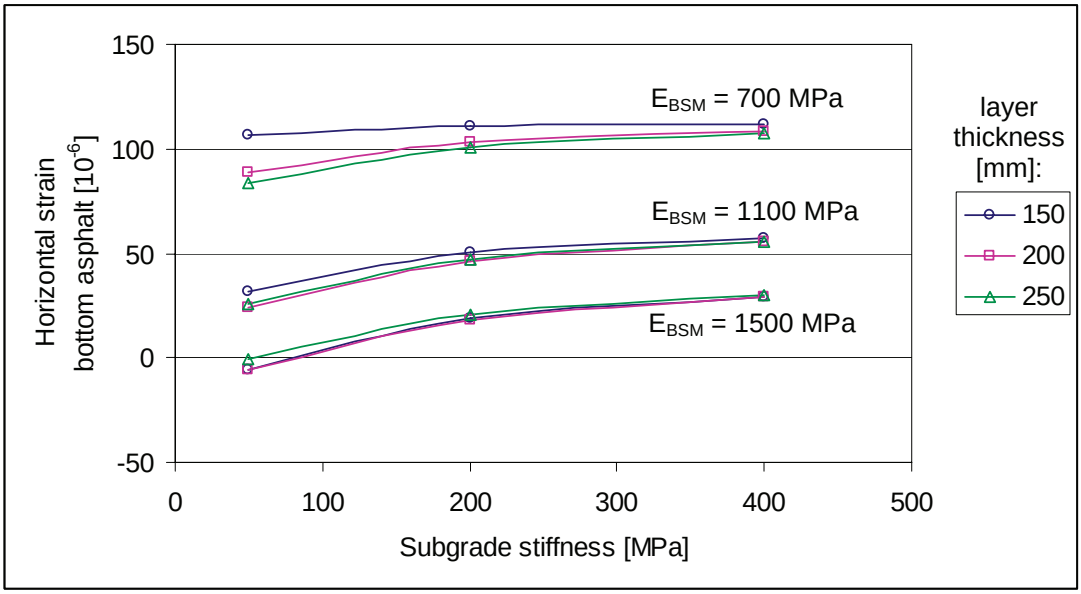


Figure 157: Effect of changing pavement structure parameters on horizontal strain in the bottom of the asphalt layer

### *7.3.3 Horizontal strain bottom BSM layer*

The effect of changes in the subgrade stiffness, BSM base layer thickness and base layer stiffness on the horizontal strain at the bottom of the BSM layer is summarised in Figure 158. It can be seen, that contrary to the effect on the horizontal strain at the bottom of asphalt layer, the thickness of the BSM layer has a significant effect on the strain at the bottom of the base layer itself. The strain reduces with increasing layer thickness. The effect is significant because in the formula for the Moment of Inertia the thickness of the layer is cubed ($I \approx 1/12 \cdot b \cdot h^3$)

The horizontal strain at the bottom of the BSM layer also reduces significantly with increasing subgrade stiffness. The effect hereof is more pronounced for the strain at the bottom of the BSM layer than for the strain at the bottom of the asphalt layer.

Lastly, the stiffness of the BSM layer itself also has an effect on the horizontal strain at the bottom of the layer. The strains decrease with increasing BSM layer stiffness. This effect of the BSM layer stiffness on the BSM horizontal strain is however less significant than the effect on the asphalt horizontal strain.

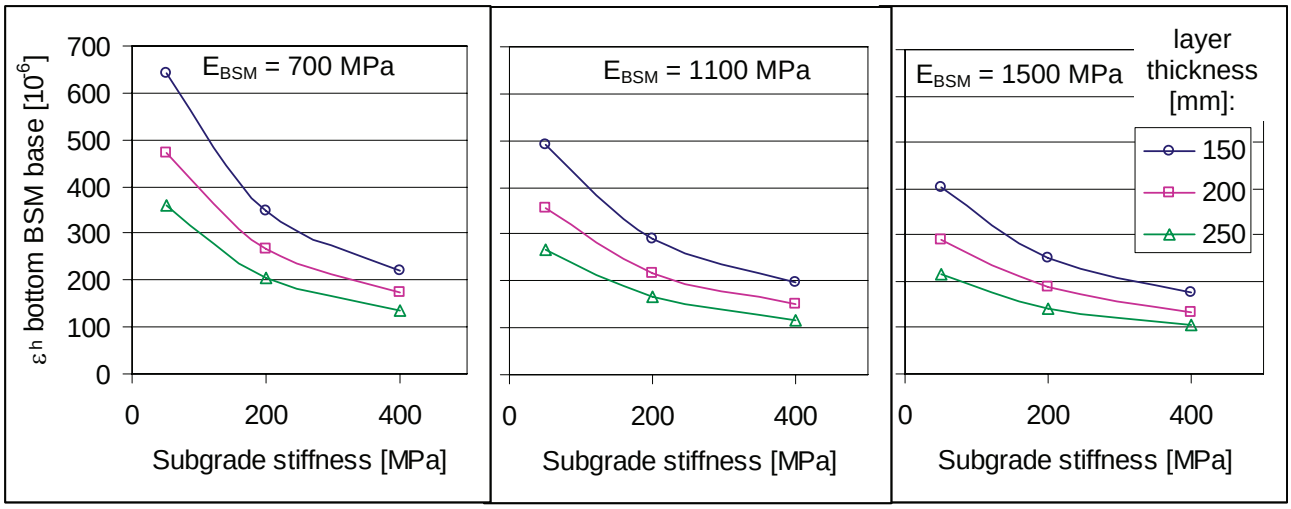


Figure 158: Effect of changing pavement structure parameters on horizontal strain in the bottom of the BSM base layer

### *7.3.4 Principal stresses in BSM layer*

In Section 7.2.3.4 it was postulated that the critical deviator stress ratio occurs at such a depth in the layer where the minor principal stress ($\sigma_3$) changes from compression to tension. Therefore this depth is used to compare the principal stresses in the evaluation of the effect of changes in the pavement structure (subgrade stiffness, BSM layer stiffness and BSM layer thickness). This depth is rounded off to the nearest 10 mm. The deviator stresses are compared, which are more or less equal to the major principal stresses because $\sigma_3$ is approximately zero. It is not possible to compare the deviator stress ratios, because the material parameters $C$ and $\varphi$ are not known in this hypothetical example. These parameters would differ substantially for the materials with different stiffness moduli.

It can be seen from Figure 159 that the deviator stress is most dependent on the layer thickness and subgrade stiffness. Increasing the layer thickness reduces the deviator stress. Increasing the subgrade support also reduces the deviator stress. The effect of the latter is reduced when the BSM layer is stiffer and thinner. It can also be seen that the BSM stiffness has a limited effect on the deviator stress in the BSM layer.

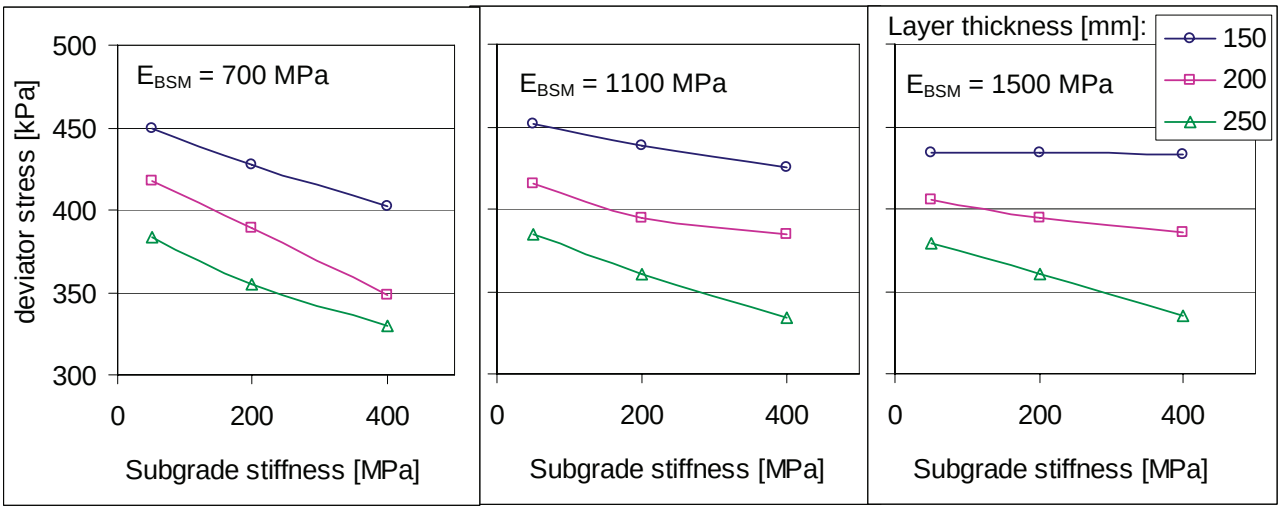


Figure 159: Effect of changing pavement structure parameters on the deviator stress ratio at a depth in the BSM base layer where $\sigma_3$ is approximately equal to zero

### *7.3.5 Vertical strain top subgrade*

The vertical strain at the top of the subgrade is mainly influenced by the stiffness of the subgrade itself. A lower subgrade stiffness results in higher vertical strains. Furthermore, the vertical strain at the top of the subgrade is significantly affected by the BSM base layer thickness. When the layer thickness decreases, the strain at the top of the subgrade increases. This is because of the increased load spreading by the BSM layer at increasing BSM base layer thickness.

Increasing the stiffness of the BSM base layer also increases the load spreading by the BSM layer and therefore reduces the vertical strain on top of the subgrade. The effect hereof is however less significant than the effect of the layer thickness.

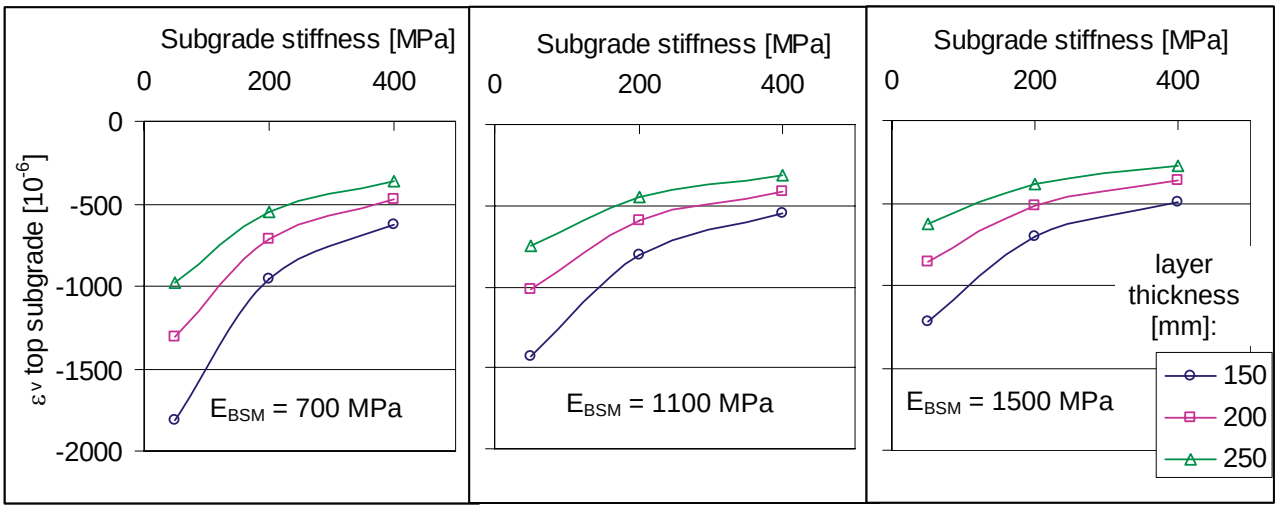


Figure 160: Effect of changing pavement structure parameters on the vertical strain on top of the subgrade

### *7.3.6 Conclusions*

The subgrade stiffness in the modelled pavement structure is an important parameter because it has a significant effect on the horizontal strain at the bottom of the BSM layer, the principal stresses in this layer and the vertical strain on top of the subgrade. An increased subgrade stiffness has a positive effect on these pavement responses. The subgrade stiffness has a more limited effect on the horizontal strain at the bottom of the asphalt surfacing and contrary to what one would expect, this strain increases with increasing subgrade support (in the specific pavement structure as modelled in the example).

The BSM base layer thickness also has a considerable effect on the horizontal strain at the bottom of the BSM layer, the principal stresses in this layer and the vertical strain on top of the subgrade. Increasing the thickness of the BSM base layer has a positive effect on these pavement responses. The effect of the BSM base layer thickness on the horizontal strain at the bottom of the asphalt surfacing layer is limited.

The stiffness of the BSM layer has a considerable effect on the horizontal strain at the bottom of the asphalt surfacing and the horizontal strain at the bottom of the BSM layer itself. An increased stiffness reduces these strains. The stiffness has a small effect on the deviator stress in the BSM layer and the vertical strain on top of the subgrade. Increasing the BSM layer stiffness reduces these pavement responses.

When designing by means of pavement modelling it is very important to work with correct input data. As concluded above the subgrade stiffness has a significant effect on design criterions used for the performance prediction of the BSM layer. Therefore, a concerted effort needs to be made to determine the correct subgrade stiffness used as input for the design process, especially when this subgrade stiffness is low (higher sensitivity). The layer thickness of the BSM layer can be fairly accurately controlled during construction. The variation between the layer thickness used during the design process and the actual layer thickness is thus a function of the construction quality.

Similarly, when determining the structural capacity of an asphalt surfacing overlying a BSM base course, the stiffness value of the BSM layer has a significant effect, while the influence of the subgrade stiffness diminishes. In such cases utmost care should be taken to obtain the correct stiffness of the BSM as input parameter of the pavement modelling. The findings of this study may assist in this regard.

## 7.4 Thickness design

A limited example has been worked out to compare the two mixes, *i.e.* A-75C-0 and A-75C-1 in terms of thickness design. An arbitrary design life of 1 million load repetitions is used. The purpose of this exercise is merely to demonstrate the difference in performance of the two mixes using the material properties and behaviour of these mixes as determined in this study. The results are purely

hypothetical and have no real meaning in terms of actual structural design life, because none of the models and transfer functions determined in this study have been validated or calibrated with known field performance. Both fatigue of the BSM layer and permanent deformation of the layer are evaluated. The validity of fatigue of BSM's as a structural design criterion is questioned in Chapter 8, but it has been included here to illustrate differences in performance of the two mixes.

The critical stress ratios for permanent deformation were presented in Chapter 6 and the maximum critical stress ratio for both mixes is approximately 0.35. Based on the assumption that the maximum deviator stress ratio occurs when $\sigma_3 = 0$, the maximum allowable deviator stress corresponding to a deviator stress ratio of 0.35 can be calculated. This is also shown in Table 62.

The coefficients governing the fatigue lines for these mixes were also presented in Chapter 6. These coefficients can be used to calculate the maximum strain the material can withstand in order to achieve a fatigue life of 1 million load repetitions. This strain would occur at the bottom of the BSM layer and is shown in Table 62.

Table 62: Fatigue and permanent deformation criteria for 1 million load repetitions (maximum allowable tensile strain and deviator stress)

| Mix | fatigue (5 ºC, 10 Hz) | | | permanent deformation (25 ºC, 2 Hz) | | |
|---|---|---|---|---|---|---|
| | log a | n | $\varepsilon_t$ | S.R. | $\sigma_{d,f}$ [1] | $\sigma_d$ |
| A-75C-0 | 19.2 | 5.8 | 127 | 0.35 | 629 | 220 |
| A-75C-1 | 20.2 | 6.1 | 146 | 0.35 | 1333 | 467 |

Note 1: The deviator stress at failure is based on the shear parameter $C$ and $\varphi$ for $\sigma_3 = 0$

The mixes A-75C-0 and A-75C-1 have a stiffness of approximately 700 MPa and 1100 MPa respectively, as discussed in Section 7.2.2. Two subgrade stiffness moduli are used in this example of BSM layer thickness design, *i.e.* 200 MPa and 400 MPa.

For the determination of the thickness of the BSM layer to satisfy the permanent deformation criteria the left graph in Figure 159 can be used for the A-75C-0 mix while the middle graph in the same figure can be used for the A-75C-1 mix. It can be seen that thickness required for having a maximum deviator stress as low as 220 kPa the A-75C-0 BSM base layer thickness needs to be much in excess of 250 mm.

It was found performing some BISAR calculations that the thickness of the A-75C-0 BSM layer needs to be in the order of 600 – 650 mm in order to have maximum deviator stresses of approximately 220 kPa, regardless whether the subgrade support is 200 MPa or 400 MPa. Since this a thickness that is not a realistic base layer thickness, it can be concluded that with the stiffness properties of the A-75C-0 material, the permanent deformation criteria of a maximum deviator stress ratio of 0.35 cannot be satisfied in the pavement structure modelled in this example.

Table 63: Minimum thickness to satisfy permanent deformation criteria (1 million load repetitions)

| Mix | Subgrade support | |
|---|---|---|
| | 200 MPa | 400 MPa |
| A-75C-0 | - [1] | - [1] |
| A-75C-1 | 120 mm | 100 mm |

Notes: 1) Unrealistic thick base layer required

The linear-elastic multi-layer program BISAR was used in iterative process to derive at the minimum required thickness of the base layer in order to satisfy the maximum allowable tensile strain at the bottom of the layer. These minimum thickness values are:

Table 64: Minimum thickness to satisfy fatigue criteria (1 million load repetitions)

| Mix | Subgrade support | |
|---|---|---|
| | 200 MPa | 400 MPa |
| A-75C-0 | 358 mm | 279 mm |
| A-75C-1 | 265 mm | 208 mm |

In this limited example of thickness design it is shown that the material properties and behaviour of BSM as experimentally determined in this study lead to vastly different requirements for the pavement dimensioning. The material properties used included shear parameters and resilient modulus and the experimentally determined behaviour includes fatigue and permanent deformation.

Again it is stressed that the example worked out here is purely hypothetical, because the experimentally determined laboratory behaviour has not yet been validated or calibrated to field performance of the BSM's.

## References

Asphalt Academy, *The design and use of foamed bitumen treated materials*, Interim Technical Guideline No. 2, Pretoria, South Africa, 2002

Huang, Y. H., *Pavement Analysis and Design*, published by Prentice Hall, Englewood Cliff, New Jersey, USA, 1993

Little, D. N.. Masad, E. and Salehi Ashtiani, *Characterization of anisotropic base materials with high fines content*, Proceedings of the 1st Conference on Advanced Characterisation of Pavement and Soil Engineering Materials, Athens, Greece, 2007

Long, F. and Theyse, H., *Mechanistic-empirical structural design models for foamed and emulsified bitumen treated materials*, Proceedings of the 8th Conference on Asphalt Pavements for Southern Africa, Sun City, South Africa, 2004

Shell Global Solutions, *BISAR 3.0 Software and User Manual*, CD-ROM, Shell International Oil Products B.V., Bitumen Business Group, Amsterdam, the Netherlands, 1998

Theyse, H. L. and Muthen M, Pavement analysis and design software (PADS) based on the South African Mechanistic-Empirical Design Method. South African Transport Convention, Pretoria, South Africa, 2000

Theyse, H. L., De Beer, M. and Rust, F. C., *Overview of the South African Mechanistic Pavement Design Method*, Transportation Research Record No. 1539, Transportation Research Board, Washington DC, USA, 1996. pp 6 – 32

# 8 SYNTHESIS

## 8.1 Introduction

The BSM properties and behaviour are discussed per test and in isolation in Chapter 6. In this chapter the properties and behaviour is summarised, whereby links are provided in terms of the trends between the different tests and in terms of the effect of the experimental variables.

The performance of the BSM's tested in this study are in this Chapter also compared to that of HMA and granular materials, as it is to be expected that the performance of BSM's ranks somewhere in between these two.

This Chapter ends with design consideration when using BSM's. These are focussed on mix design and structural design. The discussion of key aspects of the mix design and structural design aims to provide guidelines and recommendations for improving current practice.

Throughout the Chapter reference is made to the literature study results of Chapters 2 and 3 and where required additional literature has been cited. Also in the discussion of the performance of BSM's as tested in this study Chapter 6 is frequently referenced. Some repetition of results and findings from these three chapters is required to ensure the readability of this Chapter, but this is kept to a minimum.

## 8.2 BSM material properties

### *8.2.1 Strength*

8.2.1.1 Shear strength

During this study two strength properties of BSM's were determined, *i.e.* shear strength by means of tri-axial testing and strain-at-break by means of four-point beam testing. The shear strength is governed by two shear parameters, *i.e.* cohesion and angle of internal friction. These two parameters can be evaluated in isolation, which is to a certain extent meaningful and this was done in Chapter 6. It is however the overall performance in terms of the shear strength of a material that is of importance. Hence the two shear parameters needs to be evaluated in conjunction.

It was consistently found that when active filler is added to the mix in the form of cement, even in a low dosage of 1% by mass, as used in this study, the shear strength improves significantly. The increased cohesion is the shear parameter causing the shear strength to improve, even while there is a reduction in the angle of internal friction. This reduced friction angle minimises the difference in shear strength between mixes with and without active filler at higher confinement levels (higher $\sigma_3$). It was however shown in Chapter 7 that in the pavement structure the deviator stress ratio at a depth in the layer where the confinement levels are minimal is critical ($\sigma_3$

close to zero). This would make the cohesion a more important shear parameter when design for shear strength than the angle internal friction.

It also became evident that the cohesion is binder dependent, while the angle of internal friction is more dependent on the type of aggregate blend used. The binder dependency of the cohesion is masked by the addition of active filler, in case which the different binders perform similar. When the percentage of RAP in the mix is low there is also little difference between the different types of binder in terms of shear strength. Only when high percentages of RAP are used the shear strength of the bitumen emulsion mixes is higher than that of the foamed bitumen mixes. This is mainly caused by the lack of fines in the high RAP blend tested in this study.

When the percentage of RAP is increased the shear strength in case bitumen emulsion is used increases at low confinement levels. This is because of increased cohesion. However, because the angles of internal friction reduce with increasing percentages of RAP, the "advantage" of a higher cohesion is fairly quickly compensated for and the overall shear strength is lower at higher confinement levels. Increasing the percentage of RAP in foamed bitumen mixes results in an overall decrease in shear strength because both the cohesion and the angle of internal friction reduce.

8.2.1.2 Strain-at-break (bending)

The strain-at-break results generally show a high variability in the test results obtained per mix. This makes it somewhat difficult to establish the effect of changes in the experimental variables. Compared with the shear strength there are however a number of important differences. First of all there is consistently a better performance of Emulsion A compared to Emulsion B. For the shear strength testing there was no significant difference. Secondly, the increased cohesion, as determined by the shear strength testing, does not result in higher strain-at-break values. This may be explained by the fact that the addition of active filler results in a stiffer, but more brittle mix, hence a higher cohesion, but lower strain-at-break.

The effect of the percentage of RAP in the mix on the strain-at-break is inconclusive. For Emulsion A it results in an increase (this was also found for the shear strength), while for Emulsion B and Foam C there is a reduction (with Emulsion B the shear strength increased with higher percentages of RAP). In terms of shear strength, there was no difference in the performance of the two bitumen emulsions.

It is believed that the high variability in the strain-at-break results is a result of the influence of the quality of the beam specimens. Four-point beam testing requires a consistent and high quality of specimens. Due to the nature of BSM's and the saw cutting required to manufacture the beams this is sometimes difficult to achieve. This is more the case for foamed bitumen mixes, which have a more partial coating of the aggregate particles and a coarser appearance compared to bitumen emulsion mixes. This is shown in Figure 161. Local imperfections in the faces of the beam specimen, especially those situated at the bottom of the beam in the middle section that is strained the most, may critically influence the test performance. This may be an

'unfair' disadvantage of foamed bitumen mixes in four-point beam testing. Nevertheless, the fatigue performance of foamed bitumen mixes was better than that of the bitumen emulsion mixes. The influence of the specimen quality is believed to be larger for ultimate strength testing, such as the strain-at-break test, than for dynamic testing, which are performed at lower load levels.

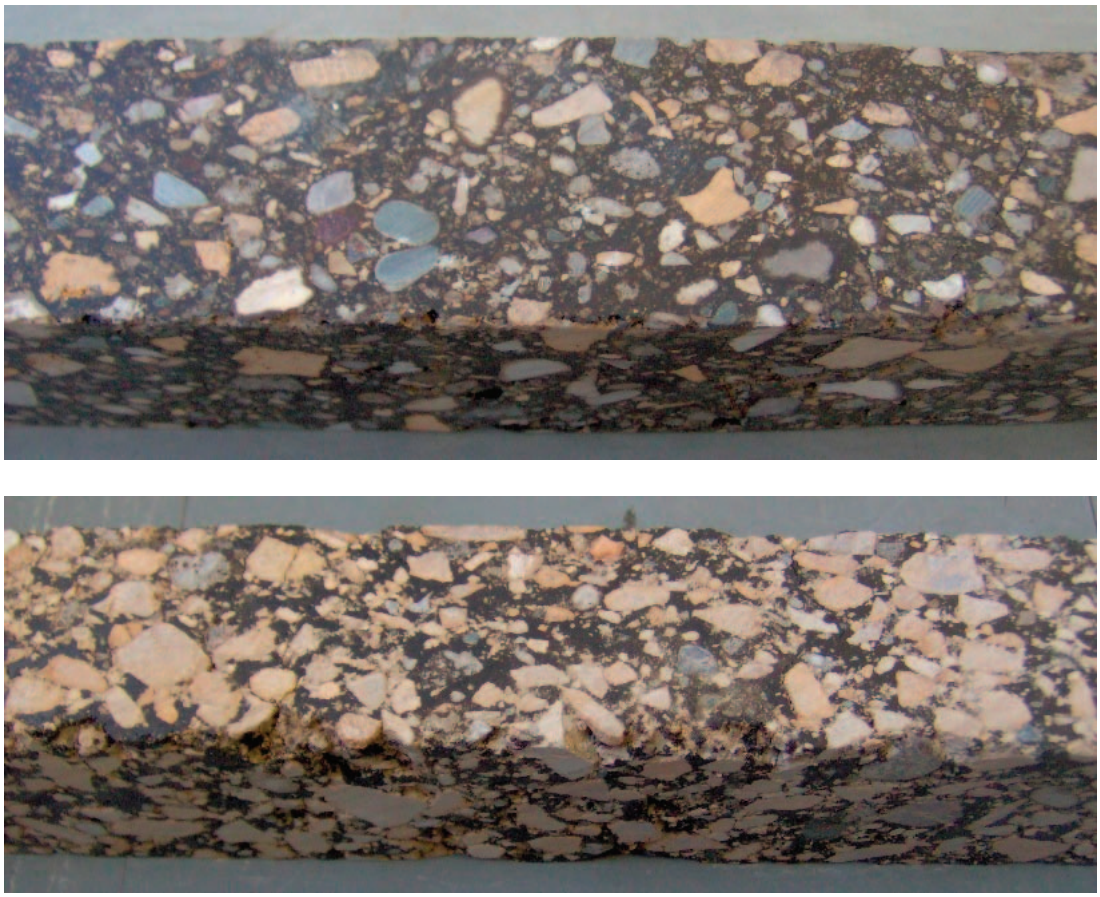

Figure 161: Four-point beam specimens; mix 75C-0 with bitumen emulsion (top) and foamed bitumen (bottom), both beams contain 3.6% residual binder

The level of sophistication required for the production of BSM beam specimens to be used for four-point beam testing may be a limiting factor in the practical application of BSM four-point beam testing. However, also in a research environment strict protocols need to be followed consistently during the specimen preparation. This is something that was ensured during this study.

When comparing the strain-at-break results obtained in this study with those of other studies, one also needs to consider if comparable specimen preparation procedures were followed. Any differences in the specimen preparation procedures may limit the fair comparison of the results.

An example of this is provided here by comparing the strain-at-break results of this study with results of similar mixes tested at the Council for Scientific and Industrial Research (CSIR) in South Africa. Over the years a large number of strain-at-break

tests on BSM's have been carried out at the CSIR. An extract from the strain-at-break database of BSM's tested at the CSIR and Stellenbosch University is shown in Figure 162.

Due to some differences in the mix composition it is difficult to compare these results in great detail, but the results shown are for selected mixes with more or less similar mix composition treated with either bitumen emulsion or foamed bitumen. The specimen preparation procedure, however, differs significantly between the CSIR and Stellenbosch University. From Figure 162 it can clearly be seen that the results of strain-at-break tests at the two institutions vary significantly. Although the trend of increasing strain-at-break with increasing binder content is the same, the strain-at-break results measured at the Stellenbosch University are systematically higher than those measured at the CSIR. This systematic difference is believed to be mainly caused by differences in the quality of the beam specimens as a result of different specimen preparation protocols.

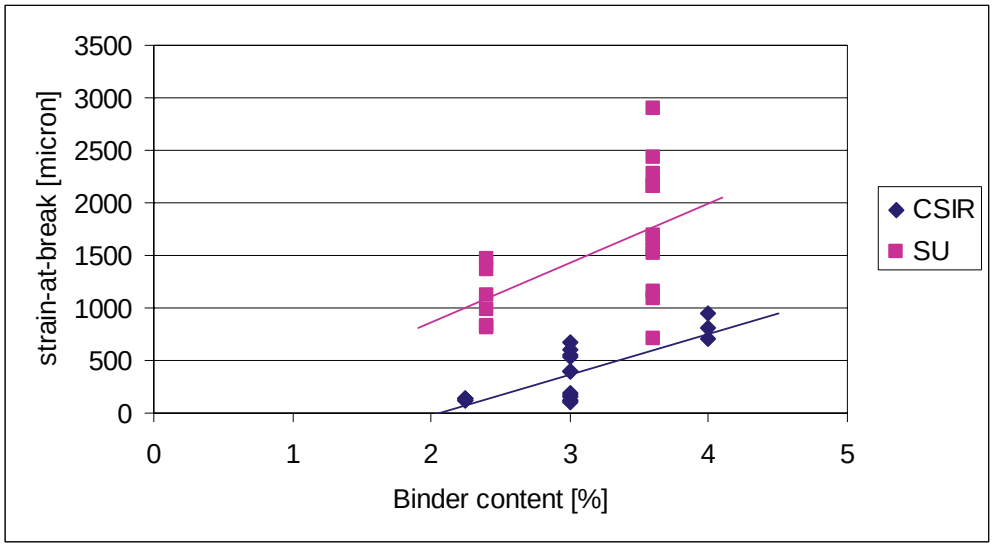


Figure 162: Extract from strain-at-break database for BMS's with 2 – 4 % residual binder and 0 – 1 % active filler tested at the CSIR and Stellenbosch University (SU)

When comparing the results obtained in this study with the recommended strain-at-break values for the different categories of foamed-bitumen (Asphalt Academy, 2002) and bitumen emulsion stabilised materials (Liebenberg and Visser, 2004) as summarised in Section 3.3.4, it can be seen that the strain-at-break values found for BSM in this study are much higher than the current recommended values for design purposes. For foamed-bitumen these recommended strain-at-break values are 172 and 490 micron for material classes FB2 and FB3 respectively, while for bitumen emulsion these values are 230 and 145 micron for material classes ET1 and ET2 respectively.

It is recommended here to generally treat BSM four-point beam strain-at-break results with caution. When comparing strain-at-break results, any possible

differences in specimen preparation protocols may easily be overlooked. It has been shown above that such inconsistencies may lead to systematic differences. Even when specimen preparation protocols are consistently followed and generally good quality beam specimens are obtained, as in this study, the variation in the beam quality that still occured may have lead to variation in the strain-at-break results.

The importance of a consistent and robust specimen preparation protocol, combined with the fact that even when this is applied the variations in the monotonic four-point beam testing are considerable, are limiting factors of the applicability of the strain-at-break property of BSM's in mix design or structural design.

It is believed that theses issues are less of a limiting factor for dynamic four-point beam testing (flexural stiffness and fatigue), during which the beam specimens are generally loaded well below the ultimate failure load (contrary to the monotonic four-point beam test). It has been shown in this study that especially the dynamic four-point beam properties of BSM materials could successfully be established.

Although it is outside the scope of this study and has not been verified here, it is likely that the same limitations on the applicability of the strain-at-break property of BSM's also apply to cement stabilised materials. Nevertheless, the strain-at-break of cement stabilised materials is an important parameter in the structural design of pavements incorporating such materials. It is recommended that caution similar to that required for dealing with BSM strain-at-break results, also applies for cemented materials

### *8.2.2 Stiffness*

8.2.2.1 Resilient modulus

Two stiffness properties of BSM's were determined, *i.e.* the resilient modulus by means of tri-axial testing and flexural stiffness by means of dynamic four-point beam testing. In addition a tangent modulus was derived from the engineering stress-strain diagrams obtained by shear strength testing. With the resilient modulus testing the stress-dependency of the BSM's was determined, while with the flexural stiffness testing the time- and temperature-dependency was tested.

It was found that the 75C-0 and 75C-1 mixes are stress dependent to the extent that the resilient modulus increases with increasing levels of confinement and increasing levels of bulk stress. This behaviour is regardless of the type of binder used and can adequately be estimated with using the $M_r$-$\theta$ model. The 75M-0 mixes, with a high percentage of RAP, were also found to be stress dependent, but the behaviour is different to the mixes with a low percentage of RAP. The resilient modulus of the 75M-0 mixes is fairly independent of the bulk stress but reduces with increasing applied deviator stress levels. This behaviour is also regardless of the type of binder used and the $M_r$-$\theta$ model cannot be applied.

The stress-dependent behaviour of the 75M-0 mixes can be explained by trends observed in the shear strength of these mixes. At low stress conditions the higher

cohesion of the 75M-0 mixes results in a stiffer resilient response. The lower friction angles of the 75M-0 mixes indicates that there is less particle interlock and once the load levels (applied deviator stress) have reached a certain threshold limit, particle reorientation takes places, which leads to increased deformation and a softer resilient response.

The resilient modulus of BSM's increases significantly and to comparable levels when active filler is added to the mix in the form of cement, even at a low dosage of 1% by mass, as used in this study. This increase is regardless of the type of binder used. This increase in stiffness can also be explained by the shear strength. As discussed in the previous section, the shear strength of BSM's increases significantly when active filler is used and this results in a stiffer resilient response.

The effect of increasing the percentage of RAP in BSM's depends on the type of binder used. In case of foamed bitumen there is a slight increase in the resilient modulus. This increase is not in line with the shear strength testing, which for the foamed bitumen reduced with increasing the percentage of RAP. In case of bitumen emulsion there was no significant difference in resilient modulus at the higher bulk stress, while for Emulsion A there was a slight increase in resilient modulus at the lower bulk stresses. These differences are however too small to conclusively determine the effect, if any, of the percentage of RAP in the mix on the magnitude of the resilient modulus. This is notwithstanding the fact that it can be concluded that the percentage of RAP influence the stress-dependency of the resilient modulus.

There is a general relation between the shear strength and resilient modulus, whereby the resilient modulus increases with increasing cohesion and the BSM's show less stress stiffening with lower angles of internal friction.

#### 8.2.2.2 Tangent modulus

The tangent stiffness is determined from monotonic tri-axial testing. Differences in loading conditions, particularly the speed of loading, edge effects and the inclusion of any possible deformation in between the specimen, end plates and tri-axial cell or piston in the monotonic test result in a lower stiffness being measured for the tangent modulus compared to the resilient modulus. There is approximately a factor of 10 difference between the two stiffness values.

The tangent modulus is capable of measuring stress dependent behaviour (tangent modulus increases with increasing confinement pressure) and rank mixes relatively to each other, *e.g.* it shows the influence of active filler and the percentage of RAP in the mix. The trends are however less distinct and consistent as with resilient modulus testing.

It is at this stage not recommended to use the tangent modulus to characterise stiffness of BSM's and one should be careful when ranking BSM's based on the tangent modulus.

8.2.2.3 Flexural stiffness

BSM's are time- and temperature-dependent, which is shown by the four-point beam flexural stiffness testing. The flexural stiffness increases if the loading rate is increased (higher testing frequencies) and if the testing temperature is lowered. This trend in time- and temperature-dependency is similar to hot-mix asphalt, however, the dependency on loading time and temperature is much less for BSM's than for hot-mix asphalt. This is illustrated by Figure 163. The master curves for the half-warm STAB (STAB is Dutch hot-mix asphalt mixture with crushed stone as mineral aggregate and mainly used for base layers) and HMA STAB were determined by Jenkins (2000).

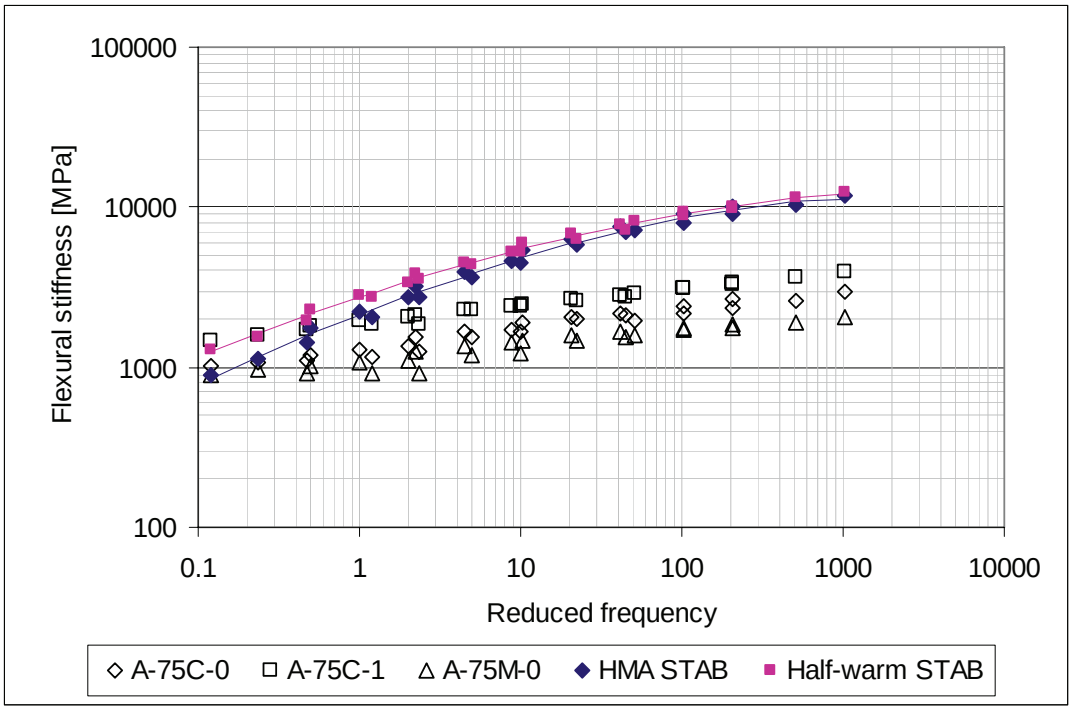


Figure 163: Comparison of time- and temperature dependency between BSM, half-warm asphalt and hot-mix asphalt (20ºC isotherm)

At low reduced frequencies (long loading time and high temperature) the flexural stiffness of BSM's is comparable to that of the STAB shown in Figure 163, while at high reduced frequencies (short loading time and low temperature) the flexural stiffness of STAB is significantly higher than that of BSM's.

The flexural stiffness is also influenced by the percentage of RAP in the mix, the use of active filler and the type of binder. The trends observed in the flexural stiffness when adding 1% cement as active filler differs from the trends in the resilient modulus. Adding 1% cement to the mix does only result in a significant increase in the flexural stiffness for Emulsion A. There is no significant effect for Emulsion B and Foamed Bitumen C (whereas it does for the shear strength and resilient modulus).

Increasing the percentage of RAP in the mix generally reduces the flexural stiffness for Emulsion A and Foamed Bitumen C. This is in agreement with the trends observed for the shear strength and resilient modulus. The effect is however not significant for Emulsion B.

8.2.2.4 Comparing resilient modulus and flexural stiffness

It is difficult to compare the resilient modulus and the flexural stiffness as one needs to consider the difference between the type of loading (compression *vs.* bending), in specimen geometry and confinement conditions. The resilient modulus was tested at 2 Hz and 25 ºC, but over a range of confinement pressures and deviator stress ratios. The flexural stiffness testing was conducted over a range of loading frequencies and temperatures. The flexural stiffness values at 2 Hz and 25 ºC are selected for comparison and are shown in Table 65.

Table 65: Bending stiffness (4PB) of BSM's tested at 2 Hz and 25ºC

| Binder | 75C-0 | 75C-1 | 75M-0 |
|---|---|---|---|
| Emulsion A | 1101 | 1693 | 929 |
| Emulsion B | 1084 | 1218 | 1198 |
| Foam C | 1107 | 1049 | 896 |

Although the mechanism of the tri-axial test and the four-point beam tests are different (hence the type of stiffness, *i.e.* compression *vs.* bending), the magnitude of the flexural stiffness at comparable temperature and loading frequency appears to be of the same order as the range of resilient modulus values (discussed in Chapter 6). This would indicate that the resilient modulus values obtained by tri-axial testing can be used as a rough estimate for the bending stiffness, with the latter being used in structural design calculations.

## 8.3 BSM material behaviour

### *8.3.1 Permanent deformation*

It is clearly demonstrated by the permanent deformation testing that the accumulation of permanent axial strain consists of three phases, *i.e.* a primary bedding-in phase, a secondary phase with a constant rate of strain accumulation and a tertiary phase with accelerating flow. Tertiary flow is initiated at the so-called flow-point and irreversibly leads to failure. The flow point is defined as the point on the permanent deformation curve with the minimum rate of strain accumulation. This three-phased concept of permanent deformation behaviour had already been identified by other researcher and applies not only to BSM's.

The general law of permanent deformation as originally developed by Francken (1977) for hot-mix asphalt material, slightly adjusted by Huurman (1997) for granular materials and later by Jenkins (2000) and van Niekerk (2002) for foamed bitumen stabilised material and granular material respectively also applies to the BSM's tested here. In this general law the permanent deformation is dependent on

the applied number of load repetitions and four model parameters, *i.e.* A, B, C and D. These model parameters are dependent on the deviator stress ratio ($\sigma_{d,a}$ / $\sigma_{d,f}$)

In order to accurately determine the permanent deformation behaviour, the testing needs to be of sufficient duration. In this study a test duration of 1 million load repetitions was adopted. Depending on the material characteristics and load levels (deviator stress ratio) one of three mechanisms may occur. These mechanisms were discussed in Chapter 6, but are for ease of reference repeated here:

- (a) failure due to tertiary flow (with flow point);
- (b) failure due to high permanent axial strain (without flow point); and
- (c) no failure with a stable strain rate after 1,000,000 load repetitions.

If, for any reason, a permanent deformation tests is stopped during the second phase with a seemingly "endless" stable behaviour, the key question is: "is a flow point, hence tertiary flow, imminent?" and if so "when is it reached?". It is found in this study that a flow point may occur rather unexpectedly after seemingly stable secondary phase, particularly if 1% cement is added to the BSM. In some instances flow points occurred between 100,000 and 500,000 load repetitions.

The bulk of the tri-axial permanent deformation testing, if not all, on foamed bitumen stabilised materials in the development of the structural design models adopted in the TG2 Guideline were aborted after 50,000 load repetitions. The permanent deformation curve up to this point is generally of a hyperbolic shape. When extrapolating the permanent deformation curve beyond the tested number of load repetitions, there is the possibility that the performance of the material is overestimated because a flow point is not accounted for. This is conceptually shown by Figure 164

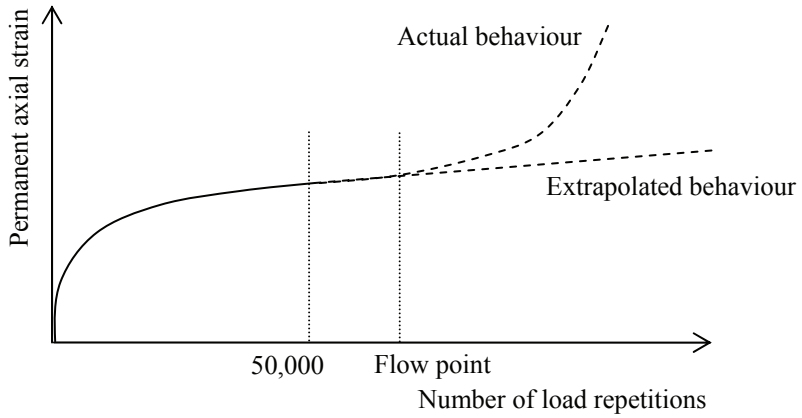


Figure 164: Possible overestimation of permanent deformation performance by extrapolation of data obtained with a short actual test duration

Jenkins *et al.* (2007) identified a "zone of concern" for unconservatively high estimations of the allowable number of load repetitions to reach a certain plastic strain level. The zone of concern is for stress ratios in excess of the critical stress ratios determined in this study. The estimations of the allowable number of load

repetitions were obtained by extrapolation of short duration test results. An example of such an unconservative estimation is the data labelled P243 in Figure 165. The results of the 75C-1 mixes of this study, which are actual results of long duration permanent deformation tests, are also shown in Figure 165. The test results obtained in this study confirm the "zone of concern" and that it is unlikely to obtain high numbers of load repetitions to achieve 4 % plastic strain at stress ratios in excess of the critical stress ratio.

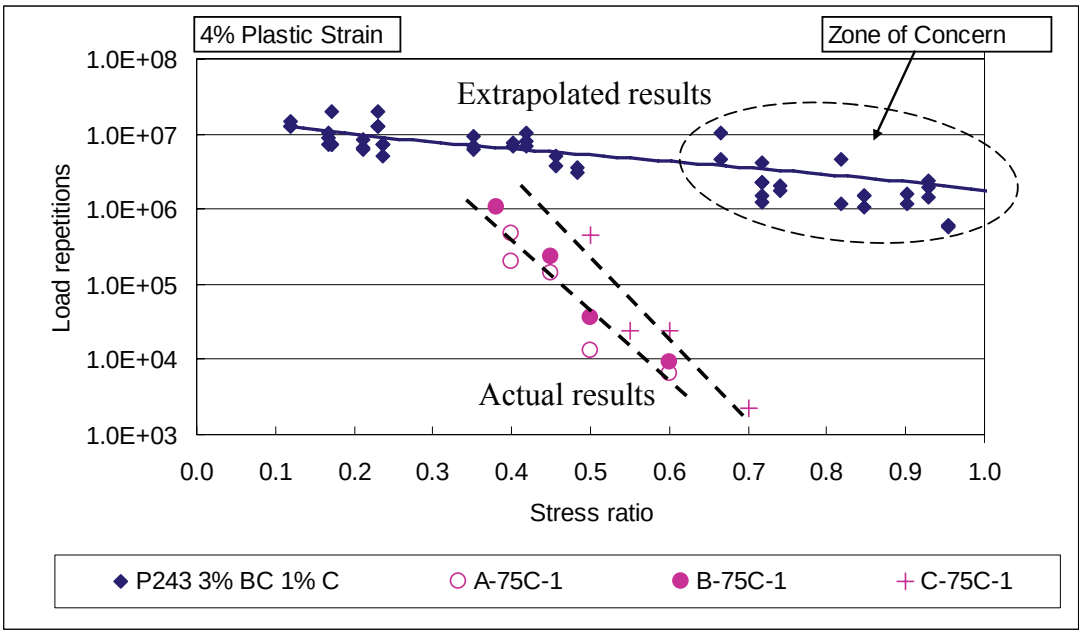


Figure 165: Influence of deviator stress ratio on number of load repetitions to achieve 4 % plastic strain

The testing conducted for this study showed that it is possible to predict, to a certain extent, the basic mechanism of permanent deformation behaviour listed as (a), (b) and (c) above by evaluating the flow path during a permanent deformation test. Such flow paths describe the development of the strain rate as a function of the accumulated permanent strain. An example is given in Figure 166. A local minimum in the flow path demarcates the flow point. In Chapter 6 a threshold function of the strain rate as function of the permanent axial strain was developed. If at any time during the permanent deformation test the strain rate falls below this threshold, a flow point, hence tertiary flow is unlikely to occur during the remainder of the test. Plotting the flow path as the permanent deformation tests progresses is a useful tool to estimate the basic mechanism of permanent deformation.

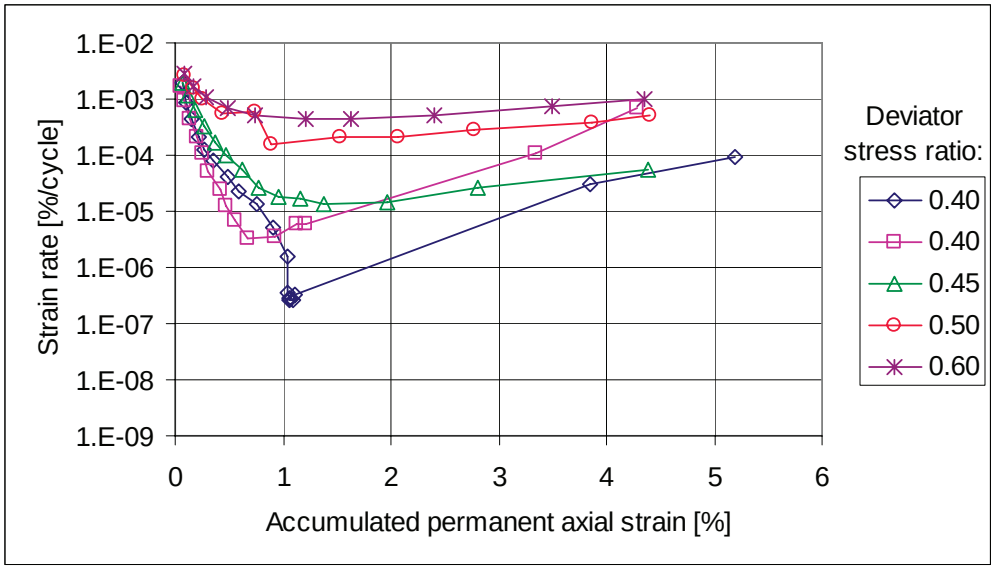


Figure 166: Permanent deformation flow paths for mix A-75C-1

The effect of the experimental variables on the permanent deformation behaviour was discussed in Chapter 6. The flow chart developed for the material behaviour scenarios is useful in this regard. One of the main observations was that the performance of the foamed bitumen mixes with a low percentage of RAP and without active filler (mix 75C-0) is poor compared to the other mixes. Increasing the percentage of RAP or adding active filler improves this behaviour.

In Chapter 6 the initial permanent strain and the initial permanent strain rate were also discussed for the mixes tested. These parameters are defined in Chapter 3 as the permanent strain and strain rate respectively after 1,000 load repetitions. Generally good correlations exist between these two parameters and the Model Parameter A and B respectively. This renders these two parameters, that can be obtained early on during the permanent deformation tests (after 1,000 load repetitions), very useful to estimate the Model Parameters A and B using the correlations shown in Figure 167.

With an estimate for Model Parameters A and B in hand, the permanent deformation behaviour of the emulsion mixes with a high percentage of RAP (E-75M-0) can be estimated as no tertiary flow was observed for these mixes. For the other mixes it is only the Model Parameter D that is required to estimate the permanent deformation behaviour. For the stress ratios below the critical stress ratio this is not even required because the second term in the general permanent deformation law diminishes for lower stress ratios and tertiary flow does not occur.

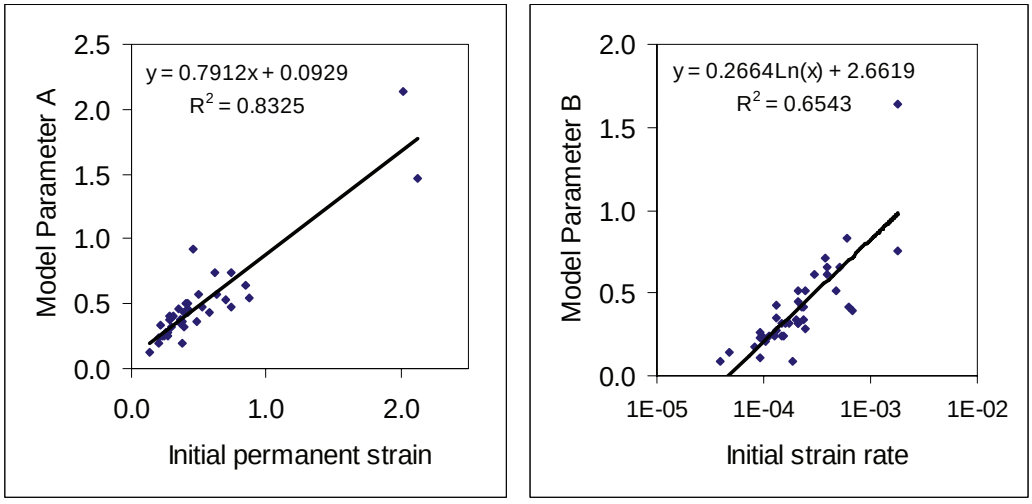


Figure 167: Correlation between the initial permanent strain and initial strain rate derived from the permanent deformation test and Model Parameters A and B respectively

### *8.3.2 Fatigue*

The fatigue behaviour, the fatigue line parameters and the influence of the experimental variables is in detail discussed in Chapter 6. It is noteworthy that the slopes of the fatigue lines (*n*-values) are generally between 5 and 6. Mix C-75C-0 with an *n*-value of 8.1 is an exception. This higher n-value is partly compensated for by a higher *log(a)*-value (intercept of the fatigue line) but it renders this mix less favourable at higher strain levels. This is in line with other tests, which show that the performance of foamed bitumen increases with increasing levels of RAP and addition of active filler.

It should also be noted that the fatigue performance of the foamed bitumen mixes is generally higher than for the bitumen emulsion mixes. The influence of the initial stiffness of the beams is discussed in Chapter 6 and the relatively good laboratory fatigue performance of the foamed bitumen should also be evaluated in light of the performance in the pavement structure, where the foamed bitumen mixes may be subjected to higher strains because of a lower intrinsic stiffness.

There are no clear trends or identifiable links between the strain-at-break, flexural stiffness properties of the BSM's tested and the fatigue performance of these mixes. This is, in general terms, on the one side caused by the variability in the test results within one mix and on the other hand by the relatively similar performance of the mixes tested. This was observed for each of the three types of four-point beam testing carried out.

## 8.4 The role of active filler

More often than not BSM's are in practice produced in combination with active filler. Both cement and lime are used to this end. The active filler can serve the following purposes (Ebels and Jenkins, 2007):

- Catalyst for breaking bitumen emulsion;
- modifier (reduction of PI);
- anti-stripping agent;
- stabilising agent (early strength and cementitious bonds); and
- dispersive agent for foamed bitumen.

The catalyst function has elaborately been discussed in Chapter 2. Brown and Needham (2000) also found the improved rate of emulsion coalescence after compaction by the addition of small doses of active filler (lime or cement) to improve key properties of BSM's. The function of modifier and anti-stripping agent are not a focal point of this study and are discussed elsewhere.

Brown and Needham (2000) also found that cement hydration and enhancement of the binder viscosity lead to improvements in the key BSM properties. Addition of non-active filler did not result in any of these improvements. Similar findings from research in South Africa were reported by Hodgkinson and Visser (2004).

Although the mechanism relating to the active filler have not been researched in detail in this study, there is strong evidence that the addition of active filler, even in a low dosage of 1% cement, leads to improvements in the properties of BSM's. The following significant improvements were found:

- Increase in the cohesion resulting in a superior shear strength;
- Increase in the resilient modulus;
- Increase in the flexural stiffness in case of bitumen emulsions;
- More elastic visco-elastic behaviour; and
- Increase in the fatigue life in case of Emulsion A.

For a few properties the performance reduced by the addition of 1% cement. These are:

- Reduction in the angle of internal friction;
- Reduction in the critical deviator stress ratios for permanent deformation in case of the emulsion mixes; and
- Reduction in the strain-at-break in case of the emulsion mixes.

The reduction in the angle of internal friction is compensated for by the more significant increase in cohesion and the resultant effect on the shear strength is still and overall increase.

The reduction in critical deviator stress ratio is only a slight reduction, but in addition the permanent deformation behaviour becomes more sensitive to changes in the

deviator stress ratio in the range close to the critical stress ratio. The critical stress ratio is however a relative concept. The higher shear strength as a result of the addition of active filler, results in a significantly higher deviator stress at failure and even with a lower stress ratio, the absolute level of deviator stress that can be applied is significantly higher for mixes with active filler compared to mixeswithout active filler. This is clearly demonstrated in the BSM layer thickness design example in Chapter 7.

It is therefore recommended to by default add small quantities of active filler to BSM's. The addition of active filler should be limited to 2%. Addition in excess of this would lead to more cemented, brittle behaviour of BSM similar to cement stabilised materials with associated disadvantages.

## 8.5 BSM in relation to hot-mix asphalt and unbound granular materials

### *8.5.1 Shear strength*

Shear testing conducted by Jenkins (2000) showed that the friction angle of untreated graded crushed rock is higher than for the same material treated with foamed bitumen. The friction angle reduces with increasing binder contents. The cohesion of granular material is generally below 100 kPa and thus lower than that of BSM's. Jenkins *et al.* (2007) concluded that the cohesion of foamed bitumen stabilised materials increases more as a result of the active filler then of the bituminous binder. This was found to be the case for different type of parent materials, i.e. crushed rock, a blend of sand and Calcrete and Ferricrete. The overall the shear strength of granular material is improved by the bitumen stabilisation, especially if active filler is used.

The SAMDM (Theyse *et al.*, 1996) provides typical angles of internal friction and cohesion values for crushed stone and natural gravel in the form of a $\varphi$-term and a $C$-term, whereby the $\varphi$-term is equal to $K \cdot A$ and the $C$-term equal to $K \cdot B$. In these formulas $K$ is a coefficient that takes into account the moisture regime and the $A$ and $B$ terms are from the formula $\sigma_{1,f} = A \cdot \sigma_3 + B$. These $\varphi$-terms and $C$-terms can be converted mathematically to the angle of internal friction and the cohesion. These typical values are shown in Table 66.

Table 66: Typical shear parameters for crushed stone and natural gravel used in the South African Mechanistic Design Method (based on Theyse *et al.*, 1996)

| Material class (Refer App. A) | Friction angle $\varphi$ [º] | Cohesion $C$ [kPa] |
|---|---|---|
| G1 | 52.7 | 50 |
| G2 | 49.1 | 44 |
| G3 | 46.7 | 40 |
| G4 | 43.8 | 37 |
| G5 | 37.6 | 33 |
| G6 | 29.2 | 32 |

It can be seen that the shear parameters determined for BSM's compare favourably with these typical values, especially when lateral confinement stresses ($\sigma_3$) are small or in tension. This is also illustrated by Figure 168.

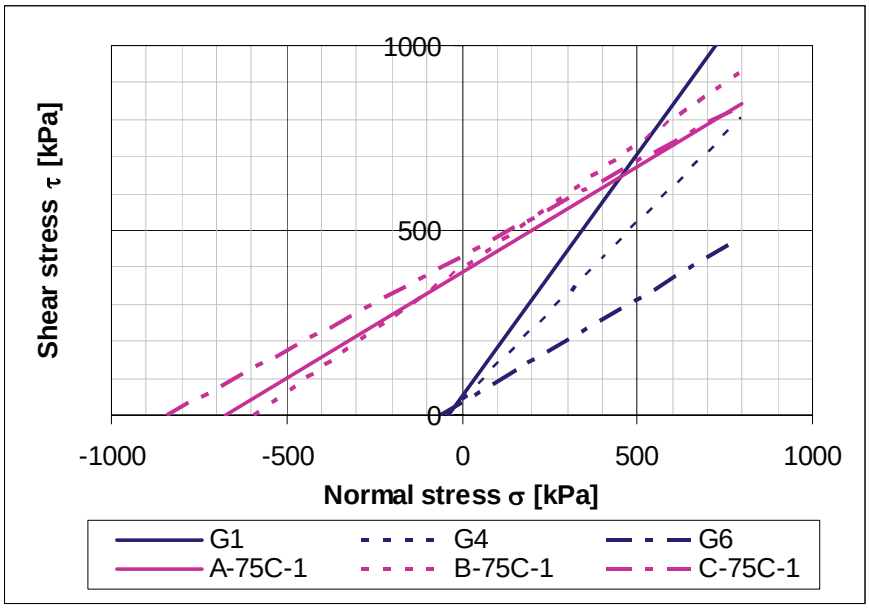


Figure 168: Typical shear strength of granular material (G1, G4 and G6) compared with selected BSM's

### *8.5.2 Resilient Modulus*

Very roughly, the resilient modulus values for BSM's determined in this study vary from 600 MPa to 1500 MPa depending on the type of mix and stress conditions. In the SAMDM there are also typical values provided for the resilient modulus of granular materials. These are shown in Table 67. The stress dependent behaviour is to a certain extent accounted for by differentiating the resilient modulus for a stiff support provided by a cement sub-layer and a softer support provided by a granular sub-layer. It can be seen that the resilient modulus of BSM's as determined in this study is significantly higher than typical values for crushed stone and natural gravel.

Table 67: Typical resilient modulus values for crushed stone and natural gravel (dry condition) used in the South African Mechanistic Design Method (Theyse *et al.*, 1996)

| Material class (Refer App. A) | On stiff (cemented) support [MPa] | On granular support [MPa] |
|---|---|---|
| G1 | 450 | 300 |
| G2 | 400 | 250 |
| G3 | 350 | 230 |
| G4 | 300 | 225 |
| G5 | 250 | 200 |
| G6 | 200 | 150 |

Huang (1993) provides typical values for the $k_1$ and $k_2$ constants of the $M_r$-$\theta$ model for granular materials. These are for comparison shown in Table 68. The BSM's tested in this study have less stress dependency with lower $k_2$ exponent values (maximum of 0.37), but with higher $k_1$ multiplier values (in excess of 100 MPa). Hence the BSM's also have a significantly higher resilient modulus than the typical values for unbound materials provided by Huang.

Table 68: Typical values for the $k_1$ and $k_2$ constants of the $M_r$-$\theta$ model (Huang, 1993)

| Material type | $k_1$ [MPa] | $k_2$ [-] |
|---|---|---|
| Crushed stone | 49.7 | 0.45 |
| Sand-aggregate blend | 29.9 | 0.59 |
| Sand-gravel | 30.8 | 0.53 |

### *8.5.3 Permanent deformation behaviour*

As mentioned in the previous sections, Huurman (1997), Jenkins (2000) and van Niekerk (2002) have undertaken similar permanent deformation testing save for the fact that different materials were used. Huurman and van Niekerk tested a mixture of crushed concrete and masonry, while Jenkins tested foamed bitumen stabilised materials. All determined model coefficients similar to those presented in Chapter 6, *i.e.* $a_1$, $a_2$, …, $d_2$.

In this section the model coefficients describing the permanent deformation behaviour as determined by Huurman, Jenkins and van Niekerk for their materials are compared with those determined for some of the BSM's in this study. For ease of comparison the model parameters A, B, C and D are compared instead of the model coefficients $a_1$, $a_2$, …, $d_2$. The model parameters A, B, C and D were calculated at a deviator stress ratio of 0.40 and are shown in Table 69. Huurman used the principal stress ratio instead of the deviator stress ratio to analyse the permanent deformation behaviour of his materials. The deviator stress ratio of 0.40 has been converted to a principal stress ratio to allow the use of the model coefficients determined by Huurman.

The materials tested by Huurman (1997) included granular crushed concrete / masonry base course material (according to the Dutch specification for 0/40 base course materials). The two materials discussed here were sampled from the Max Havelaarweg and Pascalweg respectively in Rotterdam, the Netherlands. Both materials have a continuous grading, whereby the Max Havelaarweg material is finer than the Pascalweg material. The two materials have comparable cohesion as determined in the monotonic tri-axial test (approximately 70 kPa), but the Pascalweg material has a higher friction angle than the Max Havelaarweg material (51º *vs.* 44º).

The materials tested by van Niekerk (2002) also included granular crushed concrete / masonry base course material. These materials were sampled at the crusher and reconstituted in the lab. A jaw crusher (annotation: -J-) was used to crush the

concrete and masonry. The mixes discussed here consisted of 65% concrete and 35% masonry (annotation: -65). The two materials differ in grading, whereby the AL-material follows the Average of the Limits of the grading envelope. The CO-materials also has a COntinuous grading, but has more fine and less coarse material than the AL-material. The CO-J-65 material has a cohesion of 30 kPa and a friction angle of 43º. The AL-J-65 material has a higher cohesion of 48 kPa and a comparable friction angle of 45º

Jenkins (2000) tested a range of materials stabilised with foamed bitumen. In the analysis of the permanent deformation behaviour he made distinction between mixes in which cement was used as active filler and mixes without any active filler. The parent material consisted of crushed rock with a continuous grading. Various mass percentages of foamed bitumen were used to stabilise the material, ranging from 1.0 % to 4.0 %. When cement was added as active filler, the mass percentage cement ranged from 1.0 % to 2.0%.

The model coefficients of Jenkins' mixes shown below describe the average permanent deformation behaviour of the two categories of foamed bitumen stabilised materials, *i.e.* with and without active filler. The cohesion of the mixes without active filler was approximately 160 kPa with a friction angle of approximately 45º. For the mixes with active filler Jenkins reported high cohesions of up to 1100 kPa and a friction angle of 0º.

Table 69 : Comparison of parameters describing permanent deformation of different materials under the same stress condition (deviator stress ratio of 0.40)

| Researcher | Reference | A | B | C | D |
|---|---|---|---|---|---|
| Huurman | M. Havelaar | 0.098 | 0.301 | 3.80E-03 | 1.92E-02 |
| | Pascal | 0.097 | 1.490 | 1.61E+00 | 9.22E-02 |
| v. Niekerk | CO-J-65 | 0.381 | 0.094 | 2.09E-04 | 5.12E-03 |
| | AL-J-65 | 0.105 | 0.292 | 7.00E-03 | 3.82E-03 |
| Jenkins | Foam mix without cement | 0.204 | 0.136 | 0.00E+00 | 0.00E+00 |
| | Foam mix with cement | 0.154 | 0.144 | 0.00E+00 | 0.00E+00 |
| Ebels | E-75C-0 | 0.244 | 0.172 | 1.29E-02 | 2.68E-03 |
| | E-75C-1 | 0.283 | 0.240 | 3.10E-05 | 2.57E-02 |
| | F-75C-1 | 0.259 | 0.111 | 2.60E-06 | 1.37E-03 |

The model parameters shown in Table 69 describe a permanent deformation behaviour that is graphically shown in Figure 169.

It can be seen that the modelled behaviour of the foamed bitumen mix F-75C-1 tested in this study compares well with modelled behaviour determined by Jenkins (2000) for the "foam mix with cement" save for the fact that the modelled permanent deformation of the F-75C-1 mix is slightly higher than Jenkins' foam mix. It is noted though that Jenkins modelled his mixes without tertiary flow (Model Parameter C

and D equal to zero) even though some of his mixes showed tertiary flow. This is a difference that will show up at the higher deviator stress ratios (the comparison was done for a deviator stress ration of 0.4) at which Jenkins' model will over-estimate the performance of foamed bitumen mixes.

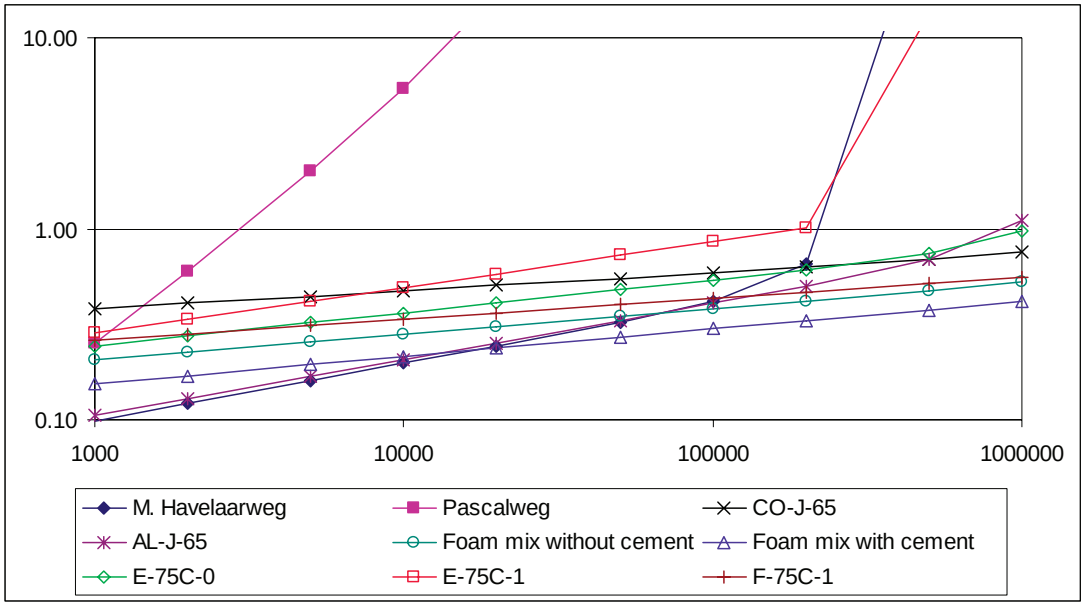


Figure 169: Comparison of permanent deformation behaviour of different materials under the same stress condition (deviator stress ratio of 0.40)

The materials modelled by van Niekerk (2000) for the unbound mix granulate also show very similar behaviour, save for the fact that tertiary flow is not predicted during the first 1 million load repetitions. Huurman's materials, unbound mixed granulate similar to van Niekerk's materials, show more varying behaviour. The one materials, *i.e.* Pascalweg quickly goes to failure due to a high B model parameter. This is mainly a function of the intrinsic properties of this mix.

In general it can be concluded that the permanent deformation model based on the general permanent deformation law developed by Francken (1977) adopted in this study yields comparable model coefficients compared to similar and other (in some cases unbound) materials studied by other researchers. Again it needs to be borne in mind that the behaviour shown is based on a relative parameter, *i.e.* the stress ratio. This means that it is quite possible for the materials to behave different from each other under similar loading conditions in the pavements structure due to differences in absolute deviator stress levels and intrinsic properties such as shear parameters, stiffness and maximum principal stress at failure.

### *8.5.4 Flexural stiffness*

The flexural stiffness of BSM's in comparison to HMA was already shown in Figure 163. In this figure it was shown that BSM's have a lower stiffness than HMA. The difference reduces however at higher temperatures. This is because at higher

temperatures the stiffness of the bitumen reduces to such an extent that the stiffness is of the asphalt mix is mainly provided by the aggregate skeleton. Typical stiffness values for HMA provided by Theyse et al. (1996) range from 300 MPa to 6,000 MPa for a depth range of 50 – 150 mm, depending on the condition of the mixture and the temperature. Hence it can be concluded that the BSM's tested here generally have a lower stiffness than HMA typically has.

### *8.5.5 Visco-elastic behaviour*

The visco-elastic behaviour of the BSM is characterised in Chapter 6 by means of the phase angle between strain and stress, determined from strain-controlled four-point beam testing. The phase angle $\delta$ is a measure for the loss modulus $E''$, which is the viscous component of the complex modulus $E^*$ ($E'' = E^* \cdot \sin \delta$). The relation between the phase angle and the complex modulus is unique for a material, which is shown in a Black Diagram. Van Dijk (1975) provided a summary shown in Figure 170 of a number of Black Diagram curves typical for hot-mix asphalt as determined by other researchers, combined with data determined by himself. The area of the Black Space into which the BSM's plot, based on the phase angles and complex stiffness modulus determined in this study, is also show in this figure.

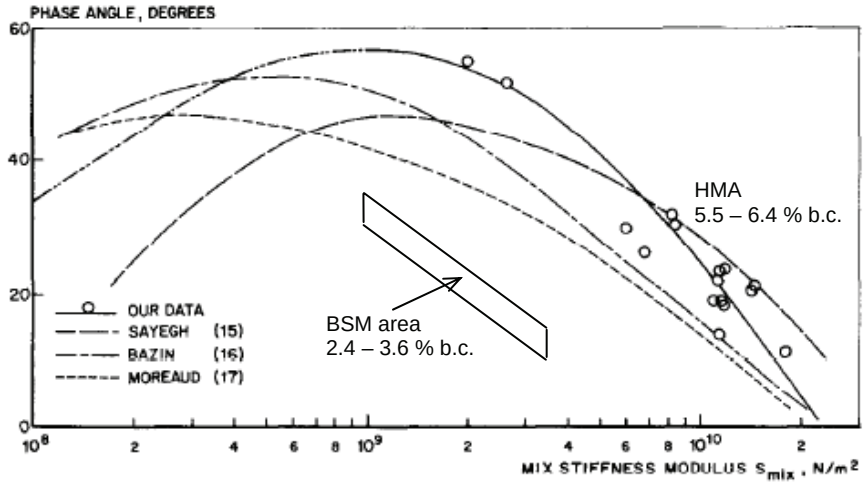


Figure 170: Black Diagram showing the relations between phase angle and complex stiffness of HMA summarised by van Dijk (1975)

It can be seen that area in the Black Space into which BSM's fall is outside the range typical for HMA. At comparable complex stiffness values, the phase angles of the BSM's are much lower than that of HMA. Lower phase angles translate into less viscous, more elastic behaviour.

Based on the above, as well as the differences between BSM and HMA in terms of the flexural stiffness master curves it can be concluded that the BSM tested in this study have different visco-elastic behaviour to HMA. The lower phase angles measured translate in a more elastic behaviour in BSM's, which is also less dependent on loading time and temperature.

The behaviour of BSM's is however more viscous and more time- and temperature-dependent than granular materials, which behave (when loaded below the elastic limit) elastically and have little to no time- and temperature-dependent stiffness behaviour.

### *8.5.6 Fatigue*

The fatigue performance of the BSM's tested in this study varies depending on the type of aggregate blend and binder. This is elaborately discussed in Chapter 6. The area into which the BSM fatigue lines plot is shown in Figure 171. It should be noted that the area indicated encapsulates all the fatigue line, but the individual fatigue lines may have different slopes and the upper and lower boundary is not necessarily described by the one fatigue line. Two HMA mixes are also shown in this figure. Both these HMA mixes were tested in the same test set-up and with similar test conditions. The one HMA mix is the sand-asphalt mix used for the correlation testing as discussed in Chapter 4 and the other mix is a BRASO mix. This is a Bitumen Rubber Asphalt mix with a Semi-Open grading (Jenkins and Twagira, 2007)

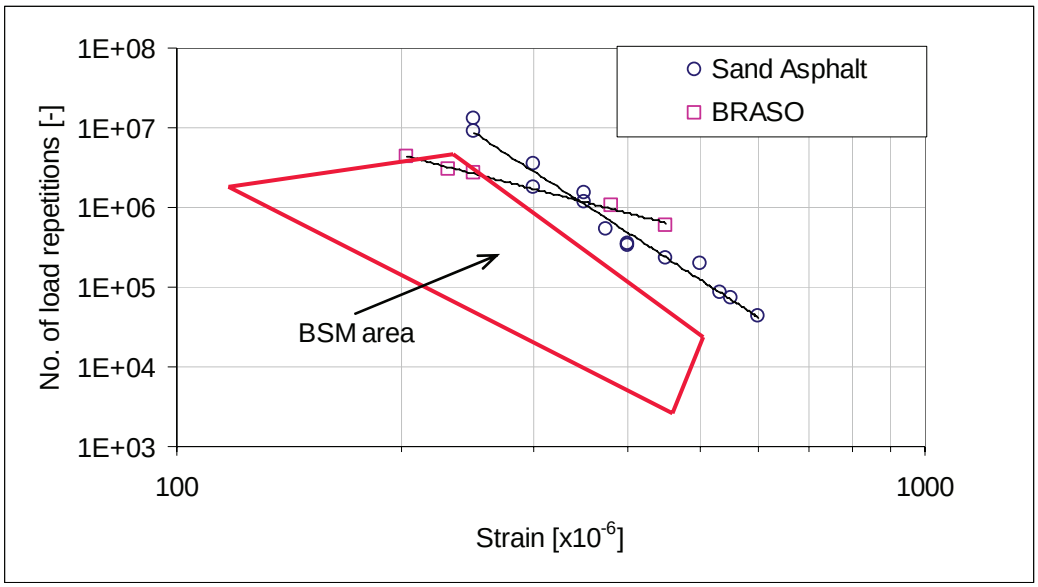


Figure 171: Comparison of fatigue life of BSM with selected HMA mixes (10 Hz, 5ºC)

It can be seen that the fatigue life of BSM's, especially at higher strain levels, is significantly lower than that of HMA. At the lower boundary of the BSM area the difference can be in the order of two decades (factor $10^2$). In the best case scenario, the fatigue life approaches that of HMA at strain levels around 200 micron, but again it needs to be borne in mind that the flexural stiffness of the BSM and HMA materials differs considerably.

## 8.6 Design considerations when using BSM's

### *8.6.1 Mix design*

Currently the latest published South African guidelines on mix design of BSM's are the ETB Manual (SABITA, 1999) in case of bitumen emulsion and the TG2 Guideline (Asphalt Academy, 2002) in case of foamed bitumen. The concepts presented in the TG2 Guidelines were an improvement to those presented in the ETB Manual and would also apply to emulsion BSM's. After the publishing of the TG2 Guideline work was carried out to bring the guidelines for emulsion BSM's in line with the TG2 Guideline, but this was never published in anticipation of one unified BSM Guideline incorporating both foamed bitumen and bitumen emulsion.

The ETB Manual may be considered outdated and for the mix design of emulsion BSM's it would recommendable to rather follow the concepts of the TG2 Guideline (UCS and ITS testing for mix design) instead of adhering to the UCS and CBR testing, curing protocol and material classification of the ETB Manual. In addition there is an international Cold Recycling Manual (Wirtgen, 2004) which one could use, but the mix design concepts in this manual are to a large extent based on the TG2 Guideline.

There are certain drawbacks to the use of UCS and ITS testing, which are discussed in Chapter 2. These tests can however still fulfil a useful role in the mix design process and should not be discarded in it entirety. In a comprehensive BSM mix design there are many variables that need to be tested. These include (Ebels and Jenkins, 2007):

- Aggregate grading;
- Blend proportions RAP and granular aggregate;
- The use of active filler;
- The use of cement or lime as active filler;
- Moisture susceptibility;
- Type of binder;
- Binder content.

A two-phase approach to the mix design of BSM's is proposed, *i.e.* preliminary investigations in the first phase and testing of more fundamental properties in the second phase. It is proposed that the UCS and ITS tests still be used as indicator tests during the first phase of the mix design process. The UCS test is believed to a suitable indicator to aid in the optimisation of the grading and aggregate blend. The retained tensile strength (TSR = ratio of wet and dry ITS) is believed to be a suitable indicator to highlight the effect of active filler and to determine the possibly different effects of cement and lime. It also identifies the moisture susceptibility of the mix.

In case of definite incompatibility of a certain combination of aggregate and bitumen emulsion, this would also show up by these indicator tests. A feel for the optimum binder content may also be developed during this first phase of mix design testing.

The outcome of the first phase of indicator testing is a reduced matrix of test variables, which are to be considered during the second phase. Typically this reduction results in:

- One or two optimal grading curves and / or blend proportions;
- One type of active filler (or no active filler at all);
- Only compatible combinations of binder and aggregate;
- Two binder contents around the optimum binder content;

The first phase of mix design testing can currently be carried out at a number of commercial laboratories in South Africa and does not require sophisticated research-level testing. The mix design testing should however not stop here, as is currently the practice in South Africa. Testing of the more fundamental BSM properties such as shear strength and stiffness and the permanent deformation behaviour is required for optimal decision making and mix design, as well as to obtain input parameters for the structural design of pavements incorporating BSM's.

It is shown in this study that the shear strength is an important parameter that can be used to rank and classify BSM materials and to evaluate the influence of changes in the mix design parameters (bitumen and active filler contents and aggregate blends). The shear parameters (cohesion and angle of internal friction) are also indicators of the resilient modulus of BSM's.

Knowledge of the stiffness and ultimate strength of a BSM, in combination with information obtained from the permanent deformation tests (critical stress ratios and permanent deformation behaviour) is required for the structural design of BSM pavements.

### *8.6.2 Structural design*

8.6.2.1 Temperature regime in base layers

There is limited information available on the temperature regime in base layers in Southern Africa. It is however unlikely that it is similar to the testing temperature at which the fatigue testing of BSM's in this study was carried out, *i.e.* 5 ºC. It is discussed in Chapter 4 that fatigue testing at higher testing temperatures was not possible, due to the fact that cracking due to shear stresses at the beam supports becomes more critical than cracking due to flexural stresses in the middle of the beam.

It is recommended that the temperature regime in BSM base layers be investigated to have better knowledge of the prevailing temperatures in such layer. Research initiatives are currently underway to address this (Moloto, to be published 2008). At the same time relationship between the test temperature and the fatigue performance of BSM should be further investigated.

8.6.2.2 BSM fatigue cracking in pavements

It has been shown in this study that BSM's exhibit a fair degree of flexural stiffness, which is confirmed by the four-point beam strain-at-break test results. The strain-at-break results are much higher than what is typically assumed for cemented materials (see Chapter 2) and also higher than what was previously found for BSM's. Flexural stiffness master curves and fatigue have also been successfully established for BSM's in a four-point beam testing mode, which is something that had not yet been done before for BSM's.

The trends in BSM flexural stiffness and fatigue are similar to those found for HMA, but all to a lesser degree. Whereas fatigue and associated cracking is a prominent failure mechanism in HMA, the question "do BSM pavements also crack as a result of BSM fatigue?" is a topical and valid one. It was however outside the scope of this study to investigate this in detail, but some comments are warranted here. Generally this topic is not well researched and documented, which is a situation that should be addressed.

Goacolou *et al.* (1997) found by means of APT testing using the LCPC's Carousel that foamed BSM's in comparison to HMA produce smaller cracks with a higher frequency of occurrence. This could be explained by the lower cohesion of BSM's and a more 'granular' behaviour than HMA.

A possible behaviour of BSM's is that fine cracks occur at micro-level, but that these cracks are not as distinct as the wider spaced and larger cracks in HMA. The finer cracks in BSM's may not propagate as one larger fatigue crack to the overlying layer, in which it would subsequently reflect through to the surface.

Jenkins (pers. comm., 2007) makes mention of larger cracks in BSM base layer that reflect through to the surface, but these are caused by severe local shearing as a results of heavy (over-)loading in combination with a weak subgrade support.

These are indications that, although BSM's exhibit material properties that can be associated with flexural fatigue, the failure mechanisms of flexural fatigue are not observed in BSM pavements. This would imply that there are other failure mechanisms, typically shear failure, that are more critical in BSM pavements than failure resulting from BSM fatigue.

8.6.2.3 BSM stiffness development in pavements

The current (design) approach to stiffness development of BSM in a pavement structure as detailed in the TG2 Guideline is discussed in Chapter 2. It is a two-phase approach with a first phase of rapid stiffness reduction associated with fatigue and a second phase of equivalent granular behaviour with shear failure being the critical failure mechanism. The correctness of this two-phased approach is questionable for the following reasons:

- Fatigue damage under real loading (not APT) develops with time, of which the effects only become significant at the end of the structural life;

- Most of the permanent deformation on the other hand takes place during the early life of a pavement, with tertiary flow possibly setting in later
- Field observations during LTPP of BSM pavements point at a stiffness increase of the BSM during the early life rather than a rapid decrease. This is the effect of curing, which is not accounted for in the current design approach.

The first two phenomena are conceptually shown in Figure 172.

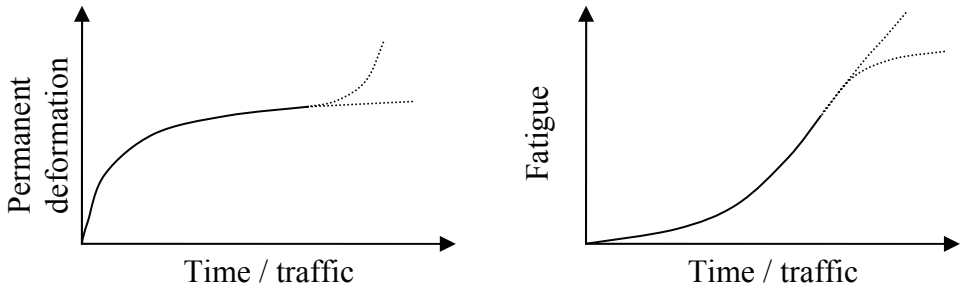


Figure 172: Generalised distress development with time or traffic (Ebels *et al.* 2005)

Several researchers (Collings et al., 2004; Overby et al., 2004; Loizos et al., 2004) in various parts of the world have found the stiffness of BSM's in the pavement to increase in the first period, *i.e.* typically 6 – 18 months, after construction. A summary of the findings of these researchers is provided by Ebels *et al.* (2005). Jooste and Long (2007) recently completed a comprehensive study of the LTPP of 30 sections in South Africa that incorporate BSM materials. They concluded that a general assessment of available deflection measurements indicates that on no section a significant increase in deflections (which would be indicative of stiffness reduction of some of the pavement layers) occurred over the monitoring period. More specific findings by Jooste and Long (2007) are listed as follows:

- N1-1 near Kraaifontein constructed in 1984: Deflections on this section increased by 200 microns at most between 1989 and 2005 with an estimated cumulative traffic loading of 12 – 16 million equivalent standard axles;
- N1-13 and N1-14, Springfontein to Trompsburg constructed in 1987: The difference between the average deflections taken in 1994 and 2006 appears to be less than 50 micron;
- N7-7 Garies to Okiep constructed in 1987: Deflections taken at various stages between 1989 and 2005 remain very stable and do not show any significant increase to suggest a significant breakdown of phase-change in any layer;
- N2-16 near Kwelera constructed around 1981: A significant increase in deflections between 1989 and 2005 is not apparent;
- N3-4 near Mooirivier constructed in 1988: No increase in deflections between 1990 and 2004 is apparent

The above is indicative of the actual stiffness development of bitumen stabilised materials in the pavement being substantially different to the two-phased stiffness development of the TG2 Guideline. It would also follow that the LTPP observations differ from APT observations on BSM pavements using HVS testing. Notwithstanding the fact the stiffness reduction phase and steady state stiffness phase are a correct representation of the behaviour of BSM's under APT loading, it does not take into account the strength and stiffness increase that take place after construction as a result of curing.

8.6.2.4 Recommendations for structural design of BSM pavements

The following observations should be taken into account when considering the structural design of BSM pavements:

- The increase in stiffness (and even a constant level of stiffness) of BSM layers in pavements during the first period after construction would indicate that damage due to fatigue, with associated stiffness loss, does not occur during the early service life of the pavement or is overshadowed by the influence of curing;
- There are indications that fatigue cracking in BSM pavements is on a different scale compared to HMA (finer cracks more frequently occurring; micro-cracking in BSM's *vs.* macro-cracking in HMA);
- The prevailing temperatures in the BSM base layers are generally higher than the fatigue testing temperature of 5 ºC; and
- Residual binder contents in BSM's are usually lower compared to HMA.

The above leads to the conclusion the effect and importance of fatigue as a structural design parameter for BSM pavements is over-estimated. It is recommended that the structural design of BSM pavements should rather focus on shear strength and permanent deformation behaviour than fatigue performance.

## References

Asphalt Academy, *The design and use of foamed bitumen treated materials*. Interim Technical Guideline No. 2, Pretoria, South Africa, 2002

Brown, S. F. and Needham, D., *A study of cement modified bitumen emulsion mixtures*, Journal of the Association of Asphalt Paving Technologists, Vol. 69, Reno, Nevada, USA, 2000.

Collings, D., Lindsay, R. and Shumnugam, R., *LTPP exercise on foamed bitumen treated base – evaluation of almost 10 years of heavy trafficking on MR 504 in Kwazulu-Natal,* Proceedings of the 8th Conference on Asphalt Pavements for Southern Africa, Sun City, South Africa, 2004

Ebels, L. J. and Jenkins, K. J., *Mix design of bitumen stabilised materials : Best practice and considerations for classification*, Proceedings of the 9th Conference on Asphalt Pavements for Southern Africa, Gaborone, Botswana, 2007

Francken, L., Permanent Deformation Law of Bituminous Road Mixes in Repeated Triaxial Compression, 4th International Conference on the Structural Design of Asphalt Pavements, Ann Arbor, Michigan, USA, 1977

Goacolou, H. , Le Bourlot, F., Brosseaud, Y., Gramsammer, J-C. and Kerzreho, J-P., *Expérimentation (deuxième partie) de la Grave-Mousse sure le manège de fatigue*, Revue Géneralé des Routes et des Aerodromes No. 754 (in French), pp 73-78, September 1997

Hodgkinson, A. and Visser, A. T., *The role of fillers and cementitious binders when recycling with foamed bitumen or bitumen emulsion*, Proceedings of the 8th Conference on Asphalt Pavements for Southern Africa, Sun City, South Africa, 2004

Houston, M. and Long, F., *Correlations between different ITS and UCS test protocols for foamed bitumen treated materials,* Proceedings of the 8th Conference on Asphalt Pavements for Southern Africa, Sun City, South Africa, 2004

Huang, Y. H., *Pavement Analysis and Design*, published by Prentice Hall, Englewood Cliff, New Jersey, USA, 1993

Huurman, H., Permanent Deformation in Concrete Block Pavements, PhD Dissertation Delft University of Technology, the Netherlands, 1997.

Jenkins, K. J. and Twagira, M. E., *Laboratory fatigue testing on modified bitumen rubber mixes – test report on four point beam tests*, ITT Report 1-2007, Institute for Transport Technology, Stellenbosch University, 2007

Jenkins, K. J., Ebels, L. J. and Mathaniya E. T., *Updating Bituminous Stabilised Materials Guidelines: Mix Design Inception Study***.** Sabita and Gauteng Department of Transport, Roads and Public Works. Pretoria, South Africa, 2006

Jenkins, K. J., Long, F. M. and Ebels, L.J., *Foamed bitumen mixes = shear performance?*, International Journal of Pavement Engineering, Vol. 8, No. 2, June 2007, pp. 85-98

Jenkins, K. J., *Mix design considerations for cold and half-warm bituminous mixes with emphasis on foamed bitumen*. PhD dissertation University of Stellenbosch, South Africa, 2000

Jooste, F. and Long, F., A knowledge based structural design method for pavements incorporating Bituminous Stabilized Materials, Draft Technical Memorandum CSIR/BE/IE/ER/2007/0004/B prepared by Modelling and Analysis Systems cc,, Cullinan, South Africa, 2007

Loizos, A., Collings, D. and Jenkins, K., *Rehabilitation of a major Greek highway by recycling / stabilising with foamed bitumen,* Bulletin paper, Proceedings of the 8th Conference on Asphalt Pavements for Southern Africa, Sun City, South Africa, 2004

Moloto, P., *Curing of bitumen stabilised materials*, MSc. Eng thesis Stellenbosch University, South Africa, to be published 2008

Overby C., Johanson, R. and Mataka, M., *Bitumen foaming: An innovative technique used on a large scale for pavement rehabilitation in Africa. Case study: Same-Himo monitored pilot project*. Proceedings of the 8th Conference on Asphalt Pavements for Southern Africa, Sun City, South Africa, 2004.

SABITA. *Manual 14: GEMS – The design and use of granular emulsion mixes*. Roggebaai, South Africa, 1993

SABITA. *Manual 21: ETB – The design and use of emulsion-treated bases*. Roggebaai, South Africa, 1999

Theyse, H. L.., De Beer, M. and Rust, F. C., *Overview of the South African Mechanistic Pavement Design Method*, Transportation Research Record No. 1539, Transportation Research Board, Washington DC, USA, 1996. pp 6 – 32

Van Dijk, W., *Practical fatigue characterization of bituminous mixes*, Journal of the Association of Asphalt Paving Technologists, Vol. 44, Phoenix, USA, 1975

Van Niekerk, A. A., *Mechanical Behavior and Performance of Granular Bases and Sub-bases in Pavements*, PhD Dissertation Delft University of Technology, the Netherlands, 2002

Wirtgen GmbH, *Cold Recycling Manual*, 2nd edition published by Wirtgen GmbH, Windhagen, Germany, 2004

# 9 CONCLUSIONS AND RECOMMENDATIONS

## 9.1 Introduction

This final Chapter deals with conclusions and recommendations that follow out of the research conducted for this study. Throughout this dissertation, and especially in Chapters 6 (material and behaviour modelling), 7 (pavement modelling) and 8 (synthesis), salient findings, conclusions and recommendations are provided. This Chapter aims to summarise these in general terms. For more details on a specific conclusion or recommendation reference is made to the relevant aforementioned chapters.

## 9.2 Conclusions

### *9.2.1 General conclusions on four-point beam testing*

For the four-point beam testing a haversine strain-controlled loading signal was used in this study. In case of HMA plastic deformation occurs after only a few load cycles at the beginning a fatigue test whereby the neutral axis of the beam shifts and the loading changes to a sinusoidal signal. This was also found to be the case for BSM's. However, due to the less viscous behaviour of BSM's it much longer before a sinusoidal equilibrium has been reached. Especially the addition of active filler to the mix increases the time required to reach the new equilibrium. For this reason it cannot be assumed that the fatigue life of BSM's in haversine mode is equal to the fatigue in sinusoidal mode with half the amplitude.

However, because during the fatigue testing there is a shift taking place from haversine to sinusoidal loading (with associated reduction in strain), the fatigue lives as reported in this study are unconservatively high and belong to an actual strain level that can be anything up to 50% smaller than the strain levels at which they are reported in this study.

Four point beam testing of BSM's needs to be carried out at sufficiently low testing temperatures. A temperature of 5 ºC was found to be suitable. Testing at higher temperature results in damage, *i.e.* shear cracking at the beam ends close to the clamps.

Correlation testing of the Stellenbosch University four-point beam apparatus (pneumatically driven) with another apparatus in a USA laboratory (hydraulically driven) using a sand-asphalt mix showed that a good correlation exists. The four-point beam apparatus at the SU, which was commissioned in 2004 as part of this study can therefore be considered to provide reliable results.

Relatively large variation was found in the four-point beam test results of BSM's, especially for monotonic strain-at-break testing. This makes it more difficult to

determine the relative performance of different type of BSM's. The beam specimen preparation protocol and attention to detail is crucial for obtaining reliable test results.

Nevertheless, flexural properties such as flexural stiffness and bending fatigue have successfully been established in this study and the general trends are in agreement with what one would expect for these mixes (*i.e.* reducing fatigue life with increasing strain and time-temperature dependent flexural stiffness, but to a lesser extent as for HMA). Increasing the strain rate during the monotonic four-point beam testing could possibly improve the repeatability of this test and reduce variation in test results.

### *9.2.2 Material properties of BSM*

The shear strength of BSM improves compared to the shear strength of the parent material as a result of the bitumen stabilisation. The addition of cement to the mix in a low dosage of 1% by mass results in a significant increase in the overall shear strength of BSM's. This is the result of increased cohesion.

The following general trends in shear strength were observed:

- The cohesion depends on the type of binder.
- The amount of fines in the mix is an important factor when using foamed bitumen.
- The angle of internal friction is more dependent on the aggregate properties, but also on the level of cohesion.
- Increasing the percentage of RAP in the BSM generally results in a reduction of the shear strength.

Relatively high strain-at-break results were found for BSM's compared to similar testing conducted elsewhere. This is likely to be the result of differences in specimen preparation protocols and beam quality. The trends in the strain-at-break test results were variable and do not relate well to the trends in flexural stiffness and fatigue performance.

The resilient modulus of BSM's tested in this study ranges, in broad terms, from 600 MPa to 1500 MPa. This ranks BSM in between granular material and HMA in terms of their typical resilient modulus values. The flexural stiffness of the BSM's is of similar magnitude as the resilient modulus.

The resilient modulus of BSM's is stress dependent. The $M_r$-$\theta$ model is able to accurately describe this stress dependent behaviour, but only in cases where the percentage of RAP in the mix is low (25% in this study). For high percentages of RAP in the mix (75% in this study) the resilient modulus is fairly independent of the Bulk Stress, but decreases significantly with increasing deviator stress levels at a constant confining pressure. This behaviour for the mixes with a high percentage of RAP cannot be described by the $M_r$-$\theta$ model.

The resilient modulus and the stress dependent behaviour of BSM are not sensitive to the type of binders tested. A significant increase in resilient modulus is however observed when 1% cement is added to the mixes.

A tangent modulus can be determined from the tri-axial shear testing. This tangent modulus is capable of demonstrating the stress dependent behaviour of BSM's. The magnitude is however a factor of 10 lower than the resilient modulus. Trends in the tangent modulus are less clear and consistent than what is the case for the resilient modulus.

The stiffness of BSM's is dependent on the loading time and temperature. This is shown by the flexural stiffness master curves of BSM's. The viscous behaviour of BSM's is however less than that of HMA. Increasing the percentage of RAP in the mix generally reduces the flexural stiffness. The flexural stiffness of foamed BSM tested in this study was generally lower than that of emulsion BSM.

### *9.2.3 Material behaviour of BSM*

Permanent deformation behaviour of BSM's consists of three-phases, *i.e.* primary bedding-in, secondary stable phase and a tertiary phase with accelerating flow to failure. The occurrence of tertiary flow depends on the applied deviator stress ratio. Critical deviator stress ratios have been determined. Adding 1% cement to the mix renders BSM's more sensitive to changes in stress ratio.

The permanent deformation behaviour can adequately be modelled using the General Permanent Deformation Law. As part of this study a method was developed using non-linear regression methods to obtain solutions for the C and D Model Parameters, which describe the second term of this deformation law. This is an improvement to similar existing models for BSM's.

A flow chart of possible permanent deformation behaviour linked to the model parameters of the permanent deformation law is provided. The initial permanent strain and the initial permanent strain rate (both after 1,000 load repetitions in a permanent deformation test) show a good correlation with the Model Parameters A and B and can be used to estimate these parameters.

The permanent deformation behaviour of foamed BSM without active filler and with low percentage of RAP in the mix ranks as the worst of the mixes tested. The fatigue performance of the foamed BSM mixes, however, is generally ranks as the best of the mixes tested. The low initial stiffness of foamed BSM during fatigue testing may however contribute to the perceived longer fatigue life.

The fatigue performance of the BSM's tested here is significantly lower than that of HMA. Compared to asphalt mixes tested under similar conditions the fatigue life of BSM can be a factor of 100 lower.

BSM's are visco-elastic, but to a lesser extent than HMA. The phase angles between load and response do not exceed 35º at the lowest complex modulus tested.

## 9.3 The influence of active filler

There is strong evidence that the addition of active filler, even in a low dosage of 1% cement, leads to improvements in the properties of BSM's. The following significant improvements were found:

- Increase in the cohesion resulting in a superior shear strength;
- Increase in the resilient modulus;
- Increase in the flexural stiffness in case of bitumen emulsions;
- More elastic visco-elastic behaviour; and
- Increase in the fatigue life in case of Emulsion A.

For a few properties the performance reduced by the addition of 1% cement. These are:

- Reduction in the angle of internal friction;
- Reduction in the critical deviator stress ratios for permanent deformation in case of the emulsion mixes; and
- Reduction in the strain-at-break in case of the emulsion mixes.

### *9.3.1 Aspects pertaining to structural design*

It was found that the method of analysis of stresses and strain in pavement for modelling purposes, *i.e.* non-linear-elastic *vs.* linear elastic, influences the outcome. *Inter alia* higher deviator stress ratios are calculated using non-linear methods.

The position of the critical deviator stress ratio in a BSM layer was found to be at the depth at which the minor principal stress changes from compression to tension (before any shifting of principal stresses is applied). This ratio may differ from the ones calculated at certain fixed depths, a concept that is adopted in some structural design methods.

Although the shifting of principal stresses during pavement modelling with multi-layer programs is theoretically incorrect, not performing such a shift is not an option because it would result in negative bulk stresses and no solution for the non-linear resilient modulus.

Accurate and reliable estimates of the stiffness modulus of the layers supporting a BSM base layer are of importance during the pavement modelling, because this parameter has a significant effect on the stress conditions in the BSM layer, especially when the support is weak. Similarly, an accurate and reliable estimate of the BSM base layer stiffness is required when evaluating strains in the overlying asphalt layer.

There are indications that shear failure in BSM is more critical than failure as a result of fatigue. The effect of curing resulting in an increase in BSM stiffness in the period after construction, *i.e.* typically 6 – 18 months, is currently ignored in structural

design models. The rapid stiffness reduction of BSM's during the first period after construction in the current structural design models is not being observed in LTPP. On the contrary, an increase in stiffness is observed in LTPP. This would indicate that stiffness reduction as a result of fatigue does not occur or is overshadowed by the effect of curing and that fatigue as a failure mechanism of BSM's is currently over-emphasized.

The critical stress ratio concept is a relative one. The critical stress ratio must be evaluated together with the stiffness and ultimate strength of the material. Two materials with similar performances in terms of stress ratio can perform substantially different from each other in the pavement structure under similar absolute levels of loading.

## 9.4 Recommendations

### *9.4.1 General recommendations*

A sinusoidal loading signal is recommended for four-point beam testing in general.

The addition by default of active filler in the order of 1 % by mass is recommended in the process of bitumen stabilisation. The percentage of active filler should however not be too high in order to prevent the stabilised material exhibiting cemented behaviour with associated disadvantages of shrinkage cracking and alike. It is recommended that this upper limit for the percentage for active filler be further investigated.

Taking into account the effect the specimen preparation methods and quality of the beam specimens have on the strain-at-break results, it is recommended not to use the strain-at-break tests as a mix design tests or the test result as an input variable for structural design of BSM's.

The tangent modulus determined from tri-axial shear testing may be used to rank mixes and evaluate certain parameter related to the mix composition, however, care is required in this regard and it is recommended not to use values of the tangent modulus to characterise the stiffness of the BSM or as input in structural design.

When performing permanent deformation tests in a research environment it is recommended to adopt a minimum test duration of 1 million load repetitions (unless failure occurs prior to this).

When thick asphalt pavements are to be recycled consideration should be given to the reuse of the RAP in HMA (or equivalent) applications. The usage of high percentages of RAP in BSM's, in the order of 75% as tested in this study, is therefore not recommended.

### *9.4.2 Recommendations related to mix design*

Although there are certain drawbacks to the use of UCS and ITS testing, these tests can still fulfil a useful role in the mix design process. It is recommended that a two-phased mix design process is followed, whereby the large number of variables that typically needs to be considered is reduced by means of UCS and ITS testing following the established protocols.

It is recommended that during the second phase of mix design the mix composition and binder contents are finalised by means of tri-axial testing. Also during this phase the fundamental properties of the mix, such as shear parameters, resilient modulus, and ideally permanent deformation characteristics, should be established.

It may for smaller projects not be necessary to go to the extent of determining fundamental material (shear) properties on a project scale, especially when the behaviour of the BSM to be used is well known from research or similar applications. However, for high profile and important projects the effort and cost to determine the fundamental properties of BSM's in a second mix design phase are deemed to be minor in relation to the possible benefits thereof and in comparison to the overall project budget.

A limiting factor regarding the determination of fundamental material properties during second phase mix design testing is the non-availability of tri-axial test equipment at commercial laboratories. The possibilities of a relatively easy and inexpensive simple tri-axial test (*e.g.* along the lines of the Texas Triaxial Test) should therefore be investigated. Even modifying the UCS test, which is the simplest of tri-axial tests (with $\sigma_3 = 0$) could be considered. In this regard the possibilities and issues relating to friction reduction when testing with BSM's should also be investigated.

It is recommended that the shear strength is used in a system to classify BSM's. It is not recommended to include any form of four-point beam testing in a BSM mix design procedure.

### *9.4.3 Recommendations related to structural design*

When embarking on pavement modelling it is of utmost importance to determine accurate and reliable values for input variables such a layer stiffness and subgrade support. It is recommended that in practice a concerted effort is made to ensure this.

It is recommended that the structural design of BSM pavements focuses on shear strength and permanent deformation behaviour rather then on fatigue performance.

## 9.5 Topics to be considered for further research

Except for the flexural stiffness testing, all laboratory tests were conducted at a fixed loading type, loading rate or frequency and testing temperature. It is recommended that further investigations be carried out that includes establishing the effects of:

- Loading rate in case of monotonic testing and in particular four-point beam strain-at-break testing;
- Confinement pressure, temperature, loading frequency and rest periods in the loading signal on the permanent deformation behaviour.

It is recommended to conduct further research to establish correlations between mix design and compositional parameters and the Model Parameters A, B, C and D of the General Permanent Deformation Law.

It is recommended that the laboratory behaviour established in this study should be validated by linking it to known performances in the field. This should be combined with efforts focussing on developing reliable transfer functions between laboratory performance and known behaviour in the field.

It is recommended to gather accurate information on temperatures regimes in BSM base layers. The development with time of the moisture content and the stiffness of BSM's should also be further investigated. This should include a range of mixes in different climatic areas (temperature and rainfall).

# APPENDIX A : ROCK AND SOIL

## 1.1 Introduction to rock and soil

Except for the bituminous binder, which is a hydro-carbon obtained by distillation of crude oil, the materials that make up a flexible pavement are predominantly granular materials. In their unprocessed from in nature these materials are called “rock” and “soil”. There is generally a common understanding of what “rock” is. Rocks are aggregates of many different grains (minerals), which are fused, cemented or bound together (Pellant, 2000; Terzaghi *et al.*, 1996). According to Weinert (1980) rock is solid, hard material which makes up the actual crust of the earth.

Soil is in the Oxford English Dictionary defined as “the upper layer of the earth in which plants grow, consisting of disintegrated rock usually with an admixture of organic remains”. This definition is of little use from an engineering perspective. According to Weinert (1980) “soil” refers to the loose, unconsolidated layer, which is derived from the break-down, i.e. weathering, of rocks. Both definitions indicate that rock changes into soil. It is because of this process that the distinction between rock and soil becomes more difficult.

Rocks are formed by geological processes. Based on the type of process according to which rocks are formed, they can be classified into three major groups:

- igneous rocks;
- sedimentary rocks; and
- metamorphic rocks.

The geological processes that result in the formation of rock and soil form part of the a genetic cycle. Deep beneath the earth’s continental crust magma exists. Magma is a viscous melt of silicates. Magma may rise towards the surface as a result of pressure differential or earth movements. On cooling the minerals in magma crystallise to form igneous rock.

All types of rocks may weather, either by mechanical disintegration or chemical decomposition to form residual soil. This residual soil may be transported under the influence of the environment, *i.e.* wind, water, gravity and biotic action (Weinert, 1980). The transported particles are deposited as sedimentary layers in lakes, deltas, dunes and on the sea bed. The deposit is classified as transported soil. Both residual and transported soils exist in Southern Africa. Transported soils or sediments may as a result of consolidation or the cementing action between the particles lithify into sedimentary rocks.

Sedimentary and igneous rocks can transform into metamorphic rocks when subjected to high pressures or temperatures (metamorphism). If the temperature (and pressure) rises sufficiently and exceeds the melting point of the minerals that make

up the rock, the rock melts and turns into magma again. This process is called anatexis and closes the genetic cycle of rocks and soils (Brink *et al.*, 1982). A graphical presentation of the genetic cycle is given in Figure 1:

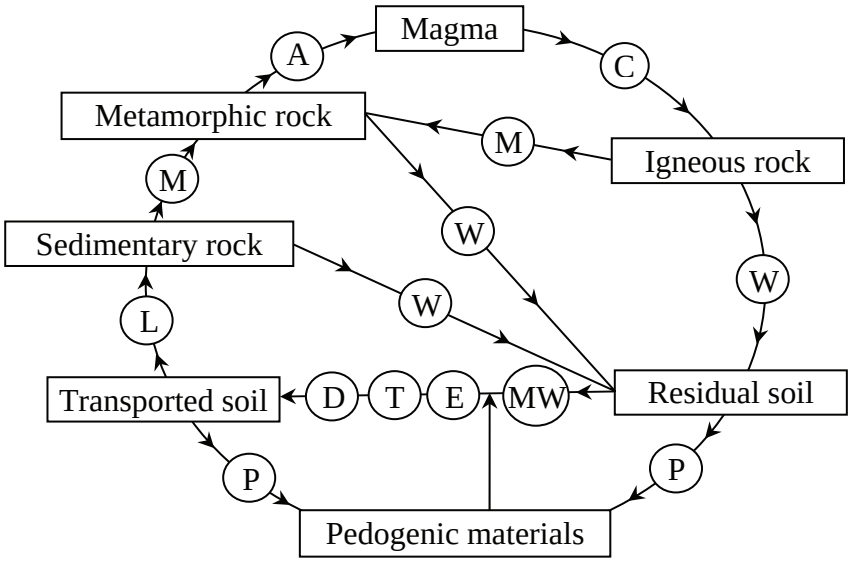


| | | | |
|---|---|---|---|
| C: | Crystallisation | A: | Anatexis |
| W: | Weathering | MW: | Mass wasting |
| P: | Pedogenesis | E: | Erosion |
| L: | Lithifaction | T: | Transportation |
| M: | Methamorphism | D: | Deposistion |

Figure 1: Genetic cycle of rock and soil (after Brink *et al.*, 1982)

Pedogenic materials, examples of which are calcrete, ferricrete, silcrete and laterite, are formed by a process called pedogenesis. During this process the soluble substances in the soil are transported by water and precipitate into a host soil. These precipitated materials cement the particles of the soil and can eventually form rock-like hardpan (Weinert, 1980).

## 1.2 Minerals

As mentioned in the previous section, rocks are aggregates of mineral particles. These minerals can either be free, uncombined elements, or element compounds particles. There are only eight elements that make up nearly 99% by mass of all rocks and soils in the earth's crust (Brink *et al.*, 1982). These are summarised in Table 1.

A large number of minerals exist. However, the majority of all minerals occur in rocks in small quantities. These minerals act as accessory minerals and not as rock-forming minerals. Of the latter, there are only a limited number and the ones with similar properties can be grouped together and regarded as one entity. Most rock-

forming minerals are silicates ($SiO_2$), others are carbonates (containing $CO_2$) or sulphur-containing minerals (Weinert, 1980). The minerals present in the magma and the way and rate at which it cools determine the composition of igneous rock. Feldspars, mica, quartz and ferromagnesians make up the bulk of the rock-forming minerals (Pellant, 2000).

Table 1: Common elements of the earth's crust (Brink *et al.*, 1982)

| Element | Symbol | Mass (%) |
|---|---|---|
| oxygen | O | 46.7 |
| silicon | Si | 27.7 |
| aluminium | Al | 8.1 |
| iron | Fe | 5.0 |
| calcium | Ca | 3.6 |
| sodium | Na | 2.8 |
| potassium | K | 2.6 |
| magnesium | Mg | 2.1 |
| | | 98.6 |

In cooling magma the minerals start to crystallise at different temperatures. This is illustrated in Figure 2. During the cooling process, the crystals may either settle and concentrate in the bottom of the magma chamber or remain suspended in the magma. When remaining suspended the crystals may transform into other minerals forming a mixture of different minerals. If crystals are separated from the magma by settling out, this transformation does not take place.

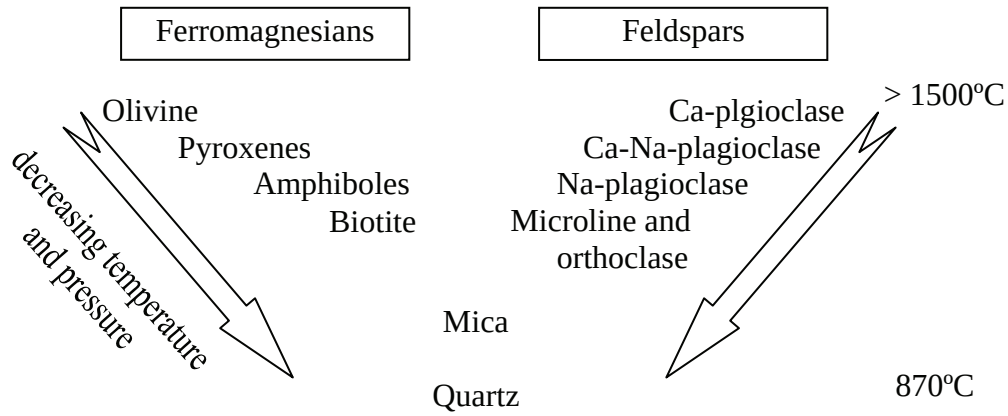


Figure 2: Order of crystallisation of minerals (after Brink *et al.*, 1982)

Quartz, mica, feldspar, pyroxene, amphibole and olivine frequently occur in igneous and some metamorphic rocks. Rocks containing these minerals are called crystalline rocks. Except for quartz, these minerals are susceptible to decompose.

Calcite, dolomite, gypsum and other sulphate salts, rock salt and clay minerals are characteristic of sedimentary rocks and certain metamorphic rocks. Metamorphic rocks also contain quartz. These minerals, except quartz, are the end product of weathering and do therefore not decompose further.

## 1.3 Rock classification

Besides the mineralogical characteristics of rocks, which are described in the previous section, the structural and textural properties are also of importance. Based on these properties the different rocks can be identified and named. Recognition guides are available to assist in this process (Pellant, 2000).

From an engineering perspective and using rock and soil as road building materials, engineering properties such a strength, texture and shape are of importance. The many rock types that are in use in Southern Africa can be divided into nine groups with similar engineering properties of interest for road construction. This grouping is mainly based on the presence or absence of quartz and the effect this has on the weathering of the rocks. The nine groups are (CSRA, 1985):

- basic crystalline rocks (a.o. basalt, dolerite and gabbro)
- acid crystalline (a.o. felsite, gneiss, granite)
- high-silica rocks (a.o. hornfels, quartzite)
- arenaceous rocks (arkose, conglomerate, gritstone, mica schist, sandstone)
- argillaceous rocks:
    a) shale, slate, mudstone; and
    b) sericite schist, phyllite
- carbonate rocks (dolomite, limestone, marble)
- diamictites (tillite and greywacke)
- metalliferous rocks (ironstone, magnesite, magnetite)
- pedogenic materials (calcrete, ferricrete, phoscrete, silcrete)

CSRA (1985) gives a brief description of these nine groups and their properties. Weinert (1980) provides an extensive discussion of the nine groups, their properties and their use in road construction.

## 1.4 Soil classification

The primary soil property that is used for classification is the grain or particle size. It is common to assign names to soils based on grain size, although this could be misleading. Common names are clay, silt, sand, gravel, cobbles and boulders. This is illustrated by Figure 3.

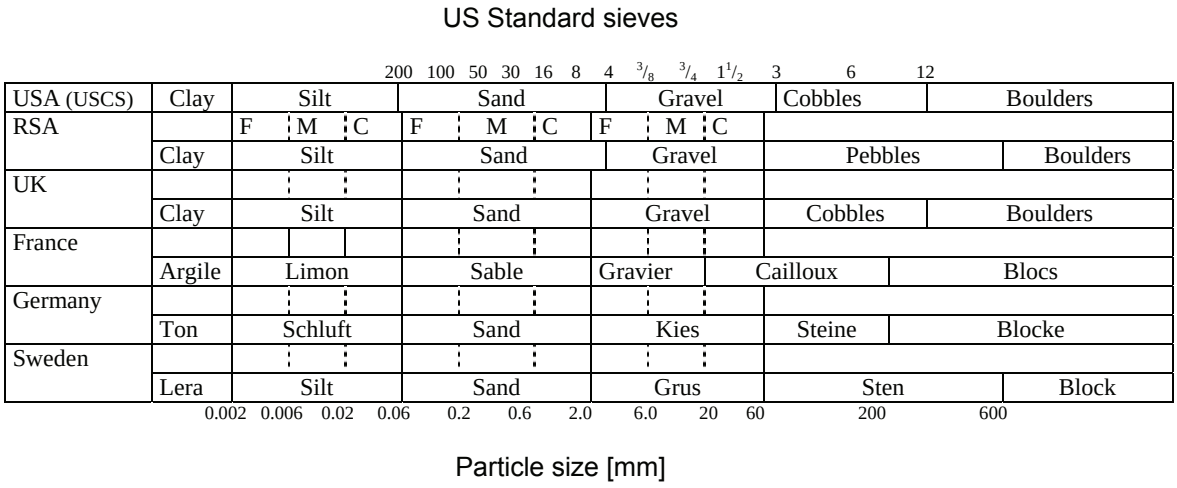


Figure 3: Grain-size classification systems used in different countries (SARF, 2004)

However, a classification based on grain size alone is not sufficient. The physical properties of the individual particles and the soil fabric are also of importance. Soil fabric refers to the spatial arrangements and orientation of the soil particles and the nature of the voids (Brink *et al.*, 1982). Albeit for agricultural purposes, Atterberg was the first to depart from grain size as the only basis for soil classification in 1908 (Casagrande, 1948). Atterberg's classification is based on soil consistency and the so-called Atterberg limits (plastic limit and liquid limit).

Early work carried out by the U.S. Bureau of Public Roads (BPR), forerunner of the Federal Highway Administration (FHWA), during the late 1920's formed the basis of the AASHTO Classification System. The BPR's classification system made use of groupings (A1 – A8) that were based on stability characteristics of soils when directly acted upon by wheel loads. The plastic and liquid limit and the linear shrinkage test, besides their particle size distribution (grading curve), were used to classify soils (Casagrande, 1948). The BPR's classification system was later modified and adopted by AASHTO (AASHTO Method 145 [AASHTO, 2000]). The groupings are now A1 – A7 (with subgroups, see Table 2) based on grading, liquid limit and the plasticity index (P.I.). For each group the suitability as subgrade material is rated. The classification system is described in ASTM D3282 "Classification of Soil and Soil-Aggregate Mixtures for Highway Construction Purposes" (ASTM International, 2003a). This classification system has been widely used and still is by road engineers nowadays, particularly in America.

Table 2: AASHTO Classification System for soils and soil-aggregate mixtures (ASTM International, 2003a)

| General Classification | Granular Materials (35% or less passing No. 200 [75µm]) | | | | | | | Silt-Clay Materials (More than 35% passing No. 200 [75µm]) | | | |
|---|---|---|---|---|---|---|---|---|---|---|---|
| Group Classification | A-1 | | A-3 | A-2 | | | | A-4 | A-5 | A-6 | A-7 |
| | A-1-a | A-1-b | | A-2-4 | A-2-5 | A-2-6 | A-2-7 | | | | A-7-5, A-7-6[1] |
| Sieve analysis, % passing: | | | | | | | | | | | |
| No. 10 (2.00mm) | 50 max | ... | ... | ... | ... | ... | ... | ... | ... | ... | ... |
| No. 40 (425µm) | 30 max | 50 max | 51 min | ... | ... | ... | ... | ... | ... | ... | ... |
| No. 200 (75µm) | 15 max | 25 max | 10 max | 35 max | 35 max | 35 max | 35 max | 36 min | 36 min | 36 min | 36 min |
| Characteristics of fraction passing No. 40 (425µm): | | | | | | | | | | | |
| Liquid Limit | ... | | ... | 40 max | 41 min | 40 max | 41 min | 40 max | 41 min | 40 max | 41 min |
| Plasticity Index | 6 max | | N.P. | 10 max | 10 max | 11 min | 11 min | 10 max | 10 max | 11 min | 11 min |
| Usual types of significant constituent materials | Stone fragments, Gravel and sand | | Fine sand | Silty or clayey gravel and sand | | | | Silty soils | | Clayey soils | |
| General rating as subgrade | Excellent to good | | | | | | | Fair to poor | | | |

[1] Plasticity Index of A-7-5 subgroup is equal to or less than Liquid Limit minus 30, Plasticity Index of A-7-6 subgroup is greater than Liquid Limit minus 30

During the Second World War, Arthur Casagrande developed an Airfield Classification System for the U.S. Engineering Department. Originally this classification system was intended for army courses on the control of soils in military construction (Casagrande, 1948). This system was later extended and adopted as Unified Soil Classification System (USCS). The system is described in ASTM D2487 "Classification of Soils for Engineering Purposes" (ASTM International, 2003b). In the USCS soils are divided into three main groups (coarse grained, fine grained and highly organic) which are further subdivided. Each group has its own symbol (*eg.* GW, SP, CL, *etc.*). Ratings to be used in pavements construction, soil characteristics and typical soil properties after compaction were assigned to each group (Brink *et al.*, 1982).

In South Africa granular materials for use in pavement structures are discussed in various documents, most importantly:

- Guidelines for Road Construction Materials, TRH14 (CSRA, 1985);
- Standard Specification for Road and Bridge Works for State Authorities (COLTO, 2000);
- Structural Design of Flexible Pavements for Interurban and Rural Roads, Draft TRH4 (COLTO, 1996).

The classification for the untreated materials is based on:

- Grading;
- Liquid Limit, Plasticity Index and Linear Shrinkage (Atterberg Limits);
- Crushing strength;
- Flakiness Index;
- Bearing strength and swell.

The crushing strength is determined by the Aggregate Crushing Value and the Fine Aggregate Crushing Test (10% FACT). These tests are described in Method B1 and B2 respectively in Technical Methods for Highways No. 1 (TMH1 [CSIR, 1986]) as well as in SABS Standard Method 841 and 842 respectively (SABS, 2004a and 2004b). The Flakiness Index is also included in TMH1 and is described in Method B3 (CSIR, 1986) and in SABS Standard Method 847 (SABS, 2004c). No ASTM or AASHTO standard exists for this test. However, British Standard 812 includes these tests.

Finally, the bearing strength and swell are determined using the California Bearing Ratio (CBR), which is described in Method A8 of TMH1, ASTM D1883 and AASHTO T193.

Based on the above properties, granular materials are divided into:

- Graded crushed stone or rock (groups G1 – G3)
- Natural gravels, including modified and processed gravel (groups G4 – G6)
- Gravel-soil (groups G7 – G10)

| SYMBOL | CODE | MATERIAL | ABBREVIATED SPECIFICATIONS |
|---|---|---|---|
|  | G1 | Graded crushed stone | Dense - graded unweathered crushed stone; Maximum size 37,5 mm; 86 - 88 % apparent relative density; Soil fines PI < 4 |
|  | G2 | Graded crushed stone | Dense - graded crushed stone; Maximum size 37,5 mm;100 - 102 % Mod. AASHTO or 85 % bulk relative density; Soil fines PI < 6 |
| 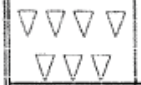 | G3 | Graded crushed stone | Dense - graded stone and soil binder; Maximum size 37,5 mm; 98 - 100 % Mod. AASHTO ; Soil fines PI < 6 |
| 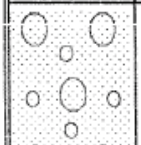 | G4 | Crushed or natural gravel | Minimum CBR = 80 % @ 98 % Mod. AASHTO; Maximum size 37,5 mm; 98 - 100 % Mod. AASHTO; PI < 6; Maximum Swell 0,2 % @ 100 % Mod. AASHTO. For calcrete PI ≤ 8 |
| 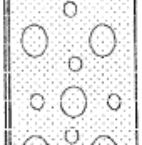 | G5 | Natural gravel | Minimum CBR = 45 % @ 95 % Mod. AASHTO; Maximum size 63 mm or 2/3 of layer thickness; Density as per prescribed layer usage; PI < 10; Maximum swell 0,5 % @ 100 % Mod. AASHTO * |
| 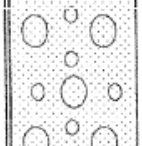 | G6 | Natural gravel | Minimum CBR = 25 % @ 95 % Mod. AASHTO; Maximum size 63 mm or 2/3 of layer thickness; Density as per prescribed layer usage; PI < 12; Maximum swell 1,0 % @ 100 % Mod. AASHTO * |
| 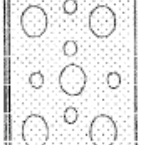 | G7 | Gravel / Soil | Minimum CBR = 15 % @ 93 % Mod. AASHTO; Maximum size 2/3 of layer thickness; Density as per prescribed layer usage; PI < 12 or 3GM** + 10; Maximum swell 1,5 % @ 100 % Mod. AASHTO *** |
| 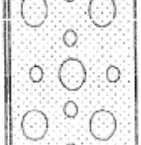 | G8 | Gravel / Soil | Minimum CBR = 10 % @ 93 % Mod. AASHTO; Maximum size 2/3 of layer thickness; Density as per prescribed layer usage; PI < 12 or 3GM** + 10; Maximum swell 1,5 % @ 100 % Mod. AASHTO *** |
| 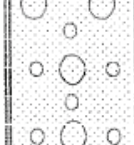 | G9 | Gravel / Soil | Minimum CBR = 7 % @ 93 % Mod. AASHTO; Maximum size 2/3 of layer thickness; Density as per prescribed layer usage; PI < 12 or 3GM** + 10; Maximum swell 1,5 % @ 100 % Mod. AASHTO *** |
| 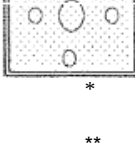 | G10 | Gravel / Soil | Minimum CBR = 3 % @ 93 % Mod. AASHTO; Maximum size 2/3 of layer thickness; Density as per prescribed layer usage; or 90% Mod. AASHTO |

* For calcrete PI ≤ 15 on condition that the Linear Shrinkage (LS) does not exceed 6%

** GM = Grading Modulus = $\frac{300-(P_{2.00mm}+P_{0.425mm}+P_{0.075mm})}{100}$, where $P_{2.00mm}$, etc. is the percentage passing through the sieve size

*** For calcrete PI ≤ on condition that the Linear Shrinkage (LS) does not exceed 7%

Figure 4: Material codes and summarised specifications (COLTO, 1996)

## References

AASHTO, *Classification of Soils and Soil-Aggregate Mixtures for Highway Construction Purposes*, American Association of State Highway Officials, Standard Specifications for Transportation Materials and Methods of Sampling and Testing, Part 1A, 2000

ASTM International, *Classification of Soils and Soil-Aggregate Mixtures for Highway Construction Purposes*, Designation 3282-93, Annual Book of ASTM Standards 2003, Section 4, Volume 04.08, West Conshohocken PA, USA, 2003a

ASTM International, *Classification of Soils for Engineering Purposes (Unified Soil Classification System*, Designation 2487-00, Annual Book of ASTM Standards 2003, Section 4, Volume 04.08, West Conshohocken PA, USA, 2003b

Brink, A.B.A., Partridge, T.C. and Williams, A.A.B., *Soil survey for engineering*, Oxford University Press, New York, USA, 1982

Casagrande, A., *Classification and Identification of Soils*, Transactions of the American Society of Civil Engineers, Vol. 113, published by the Society, New York, USA, 1948

COLTO – Committee of Land Transport Officials, *Standard Specification for Road and Bridge Works for State Authorities*, South African Institution of Civil Engineering, Halfway House, South Africa, 1998

COLTO – Committee of Land Transport Officials, *Structural Design of Flexible Pavements for Interurban and Rural Roads*, Draft Technical Recommendations for Highways No. 4, revised edition, Department of Transport, Pretoria, 1996

CSIR – Council for Scientific and Industrial Research, *Standard Methods of Testing Road Construction Materials*, Technical Methods for Highways No. 1, second edition, National Institute for Transport and Road Research, Pretoria, South Africa, 1986

CSRA – Committee of State Road Authorities, *Guidelines for road construction materials*, Technical Recommendations for Highways (TRH) 14, Department of Transport, Pretoria, South Africa, 1985

Pellant, C., *Rocks and Minerals*, Dorling Kindersley Ltd, London, United Kingdom, 2000

SABS – South African Bureau of Standards, *Aggregate Crushing Value of Coarse Aggregates*, SABS Method 841, SABS, Pretoria, South Africa, 2004a

SABS – South African Bureau of Standards, *FACT Value (10% Fines Aggregate Crushing Value) of Coarse Aggregates*, SABS Method 842, SABS, Pretoria, South Africa, 2004b

SABS – South African Bureau of Standards, *Flakiness Index of Coarse Aggregates*, SABS Method 847, SABS, Pretoria, South Africa, 2004c

South African Road Federation (SARF), *Comprehensive course on the compaction of road building materials*, Johannesburg, 2004

Terzaghi, K., Peck, R. B. and Mesri, G., *Soil Mechanics in Engineering Practice*, Third edition, John Wiley & Sons Inc., New York, USA, 1996

Weinert, H. H., *The Natural Road Construction Materials of Southern Africa*, H&R Academia Ltd, Cape Town, South Africa, 1980

This page is left blank intentionally.

# APPENDIX B: ENVIRONMENTAL LEGISLATION

## 1.1 Introduction

For the discussion of environmental aspects, one first needs to establish a common understanding of what the term "environment" means. The Oxford English Dictionary gives a number of definitions of "environment". The following are most relevant in the light this paper:

a. *(concrete)* That which environs; the objects or the region surrounding anything;
b. *(especially)* The conditions under which any person or thing lives or is developed; the sum-total of influences which modify and determine the development of life or character.

The National Environmental Management Act, Act No. 107 of 1998, provides a very similar definition of "environment" in Section 1(xi) (Government Gazette, 1998): "the surroundings in which humans exist and that are made up of:

(i) the land, water and atmosphere of the earth;
(ii) micro-organisms, plant and animal life;
(iii) any part or combination of (i) and (ii) and the interrelationships among and between them, and
(iv) the physical, chemical, aesthetic and cultural properties and conditions of the foregoing that influence human health and well-being."

The definitions given in these two references are deemed suitable for the purpose of understanding what "environment" means in the discussion of this paper that follows below.

## 1.2 The Constitution of the Republic of South Africa

The most important national legislation that deals with the environment is the Constitution of the Republic of South Africa, Act No. 108 of 1996. Section 24 of the Constitution stipulates that (Government Gazette, 1996): "Everyone has the right:

a. to an environment that is not harmful to their health or well-being; and
b. to have the environment protected, for the benefit of present and future generations, through reasonable legislative and other measures that
    (i) prevent pollution and ecological degradation;
    (ii) promote conservation; and

(iii) secure ecologically sustainable development and use of natural resources while promoting justifiable economic and social development."

For the topic of this paper it is mainly part (b) of Section 24 of the Constitution that is relevant and of interest. "Everyone has the right to have the environment protected" is a passive sentence. This implies that there is a person, in the legal sense of the word, that is protecting the environment on behalf of "everyone". It is assumed here that the State takes the leading role upon itself in this regard. Section 24(b) also indirectly implies that "everyone else" has the duty to protect the environment, so as to not infringe on the constitutional right of "everyone".

To "protect the environment" means to "preserve it intact". It can also mean to preserve it from encroachment, invasion, annoyance, or insult. To protect the environment can finally mean to keep it safe or to take care of it. The Constitution states that the protection of the environment should be achieved through "reasonable legislative and other measures". The objectives of this are given in subclauses b(i) through to b(iii) of Section 24. The last two objectives are most relevant here.

"To promote conservation" [subclause 24b(ii)] would mean to preserve the environment in its existing state from destruction or change. This is in essence a re-iteration of the foregoing in Section 24 that the environment needs to be protected. "To secure ecologically sustainable development and use of natural resources while promoting justifiable economic and social development" [subclause 24b(iii)] is probably the most relevant and at the same time practical passage i.r.t. road building practices. Key-words are "sustainable development" combined with ecological (environmental), economic and social aspects. Specific reference is also made to the use of natural resources, which is of utmost importance to the road-building industry.

CIPR is a more sustainable construction method than using new natural materials to achieve the same technical objective; increasing or extending the design life of a road pavement structure. It saves scarce natural resources and reduces the impact on the environment. This is an advantage of CIPR over conventional construction methods.

### 1.3 Sustainable development

Sustainable development can be defined as development that takes places in a manner that can be kept going or continued. According to Brundtland in his report "Our Common Future", a United Nations report published in 1987, sustainable development is a process of developing land, cities, business, communities, and so on that "meets the needs of the present without compromising the ability of future generations to meet their own needs" (United Nations, 1987). Also in this report reference is made to the environmental, economic and social aspects. The "meets the needs (…)" definition of sustainable development is probably one of the most widely adopted definitions of sustainable development.

Sustainable development received a great deal of attention in South Africa in 2002 when the World Summit on Sustainable Development was held in Johannesburg under the auspices of the United Nations. At this World Summit the second resolution comprised an elaborate "Plan of Implementation of the World Summit on Sustainable Development" (United Nations, 2002). This plan contains a specific chapter dealing with sustainable development for Africa. It is remarkable that in this chapter hardly any mention is made of infrastructural development in African countries. It is generally accepted that there are great backlogs in infrastructural developments in Africa. The eradication of these backlogs would have a great impact on the environment. Also, while the mining sector is one of the foremost industries in Africa and in the light of the fact that African countries are generally rich in terms of natural resources, it is striking that no concrete plan of action was proposed in terms of sustainable development for the mining sector and the management of Africa's natural resources at the 2002 World Summit. Also, particularly in the mining and minerals sector, the possible impacts on the environment are enormous.

Recycling of materials as a concept to reduce the current need and demand for natural resources received little attention at the 2002 World Summit on Sustainable Development.

It was however in general acknowledged at the 2002 World Summit that human activities are having an increasing impact on the environment. Managing the natural resources in a sustainable manner is essential for sustainable development. In order to achieve this strategies, policies, frameworks, programmes and alike are proposed at the Summit. It can therefore be concluded that resolutions of the 2002 World Summit on Sustainable Development are very broad-based and intended to provide more of a framework for sustainable development, than to implement practical measures to address the problem. Although it is an important document, and essential reading for obtaining the right mindset, it is of little practical use to deal with issues relating to sustainable development in the road building industry.

At the recent 60$^{th}$ Session General Assembly of the United Nations in New York during September 2005, two outcomes that are significant to the topic of this paper are highlighted here (United Nations, 2005):

1. The commitment to achieve the goal of sustainable development, through amongst other the implementation of the Johannesburg Plan of Implementation, was reaffirmed. To this end, the Assembly committed itself to undertake concrete actions and measures at all levels and to enhance international cooperation. These efforts will also promote the three components of sustainable development as interdependent and mutually reinforcing pillars. The three components are:
    a. economic development;
    b. social development, and
    c. environmental protection.
2. The Assembly promotes sustainable consumption and production patterns, with the developed countries taking the lead and all other countries benefiting from the process, as called for in the Johannesburg

> Plan of Implementation. In that context, the Assembly supports developing countries in their efforts to promote a recycling economy.

The three pillars of sustainable development form an important concept, which is also referred to as the "triple bottom-line". It is finding its way into all levels of government and management of both public and private companies. Bottom-line refers to profit in the economical sense of the word and in traditional capitalistic corporate environments this was the only and most important result that a company or institution was judged upon. The other two "bottom-line" are the social and environmental ones. The triple bottom-line concept means that making economical profit alone is not good enough these days. It combines overall sustainability with economical profit. In the process of trying to make economical profit, there is likely to be a loss to the environment. The person making economical profit or the person judging the business should take this loss into account. Although the economical bottom-line is difficult to quantify in monetary terms, it may overshadow the economical profit. Finally, in the process of making a profit, economically and environmentally, social factors are of importance as well. With social factors one should think of, the well-being of people, both those that are involved in the process as well as outsiders, poverty, health and safety, social security, *etc*.

Overall, one should strive to keep a positive balance when the economical, environmental and social aspects are all factored in. That is the crux of sustainable development. This would thus also apply to the road building industry which contributes substantially to development by providing infrastructure.

## 1.4 Environment Conservation Act

In 1982 the Environment Conservation Act, Act No. 100 of 1982, was enacted. This act was a first attempt to provide legislation that addressed conservation of the environment comprehensively. It was revised in 1989 and then called the Environment Conservation Act, Act 73 of 1989. This Act was in place until recently. The Environment Conservation Act was a framework act, based on which government could promulgate regulations to deal with specific and practical issues relating to environmental conservation. This resulted in a gazetted policy for environmental conservation in 1994. Promulgated regulations were however limited to noise control, waste management and environmental impact assessment (EIA) (Brauteseth, 2006). The latter, regulations on EAI, were:

- Regulations 1182 of 1997: List of activities for which an EIA must be carried out;
- Regulations 1183 of 1997: Procedures to be followed for amongst others:
  - Application for authorisation to undertake activity;
  - Plan of study for scoping;
  - Scoping report;
  - Plan of study for EIA;
  - EIA report.
- Regulations 1184 of 1997: Designation of competent authorities.

The National Environmental Management Act is intended to replace the Environment Conservation Act. It has done so already for Parts I and II of the Environment Conservation Act. Part I provided a policy for environmental conservation, which is replaced by the environmental management principles of the National Environmental Management Act. Part II dealt with institutional arrangements.

The part of the Environment Conservation Act that dealt with the EIA (regulations and notices issued under this act in terms of Sections 21, 22, 26 and 28) were repealed on 23 June 2006 (Government Gazette, 2006). New regulations and notices in terms EIA's under the National Environmental Management Act were promulgated on 21 April 2006. These new regulations came into effect on 3 July 2006. With this, the Environment Conservation Act is no longer of importance in terms of determining the environmental impacts of activities that may be detrimental to the environment. This role has completely been taken over by the National Environmental Management Act.

### 1.5 National Environmental Management Act

The National Environmental Management Act (NEM Act), Act No. 107 of 1998, provides a set of national environmental management principles. The act basically followed out of the Environment Conservation Act. It also provides a framework for coordination of actions and decision-making of all organs of government. The act is broad-based and is a "legislative umbrella" in terms of environmental management to which more specific legislation, such as the Mineral and Petroleum Resources Development Act of 2002, refers back. With the recent promulgation of regulations and notices, the NEM Act is now the most important piece of national legislation, besides the Constitution, that deals with the protection of the environment. The promulgations of 21 April 2006 are (Government Gazette, 2006a):

- Regulations in terms of Chapter 5 (integrated environmental management) of the NEM Act (Government Notice No. R.385 of 2006);
- List of activities and competent authorities identified in terms of Sections 24 and 24d of the NEM Act (Government Notice No. R.386 and R.387 of 2006);

The need for new regulations rose out of the fact that the regulations under the Environment Conservation Act called for a long and complex authorisation process to undertake a certain activity. The new regulations under the NEM Act are more streamlined and the process of obtaining authority should be less lengthy. For this purpose clear timeframes have been given for both the applicant and the authority. It is noted however that although the authority should "strive" to adhere to these timeframes, they cannot be forced to do so (Daneel, 2006).

Furthermore the list of activities that require environmental assessment has been revised and provides for the following categories:

- Exemption;

- Basic Impact Assessment (BIA);
- Environmental Impact Assessment (EIA).

The Listing Notices R.386 (BIA) and R.387 (EIA) identify the specific activities to which each type of assessment applies. Under the old regulations, many activities fell in an inappropriate category resulting in a high number of applications for exemption and many small activities being subject to a detailed EIA (Daneel, 2006). The process of a BIA is shorter and the requirements are less than that for an EIA.

Listing Notice R.387 (Government Gazette, 2006b) specifies that any activity on a national road or a provincial road is subject to an EIA. This EIA consists of both scoping (preliminary investigation) and environmental assessment (full investigation). Any other road with a road reserve wider than 30 metres or that caters for more than one lane of traffic in both directions also falls under this provision. All other roads, but with a road reserve wider than 6 metres and longer than 30 metres, are subject to Listing Notice R.386 (Government Gazette, 2006b). For these roads a basic impact assessment generally applies. In case the road reserve is less than 6 metres wide one can apply for exemption of authorisation for the activity.

What is important in the new regulations (Government Notice No. R.385 of 2006) is that a lot more emphasis has been placed on identifying and assessing alternatives (Daneel, 2006). The regulations define alternative as: “different means of meeting the general purpose and requirements. This may include alternative design or technology to be used”. The new regulations allow for the authority to approve a listed alternative instead of the original proposed activity or technology. This is important for CIPR, because it is an alternative technology that can be used to meet the same general purpose as conventional construction methods. At the same time, the environmental impacts of CIPR are less than those of construction with new materials.

Proper identification of alternatives, is part of compiling a basic impact assessment report or environmental impact assessment report. This would mean that, in the case that the proposed activity is construction of a base layer consisting of new material, CIPR would always have to be mentioned as an alternative. This would imply that the persons compiling such reports, namely independent environmental assessment practitioners (EAP’s), need to be aware of the alternative technology that CIPR offers.

## 1.6 Mineral and Petroleum Resources Development Act

The Mineral and Petroleum Resources Development Act (MPRD Act) in its current form was enacted in 2002 (Government Gazette, 2002) and came into effect on 1 May 2004 (Regulation No. R.527). It replaces the Minerals Act of 1991. Quarries and borrow pits as commonly used for road building purposes also fall under the definition of a mining area in the MPRD Act, although this act is mainly aimed at larger scale industrial mining. Removing material from quarries and borrow pits is

therefore a mining activity that needs to comply with the requirements of the MPRD Act.

The MPRD Act refers back to the environmental principles of the NEM Act. The act further stipulates integrated environmental management, also referring back to the NEM Act. It also states that the person undertaking a mining activity has the responsibility to remedy. This means that when the mining activity is completed, the area must be rehabilitated to its natural or predetermined state.

As far as relevant to the road building industry, the MPRD Act makes distinction between:

- Reconnaissance permission;
- Prospecting right;
- Mining permit;
- Mining right.

Reconnaissance is more applicable to liquid mining and industrial mining than to mining for road building material. Reconnaissance is defined as any operation carried out for or in connection with the search for a mineral or petroleum by geological, geophysical and photogeological surveys and includes remote sensing techniques. In some cases these types of surveys may be carried out in search for road building materials and hence permission to carry out such reconnaissance operations needs to be obtained. When permission for reconnaissance has been given no physical excavation, sampling, trenching or any prospecting or mining related excavation may be made. For this a prospecting right is required.

Defining that part of prospecting that is relevant to road building, prospecting means intentionally searching for any mineral by means of any method:

- which disturbs the surface or subsurface of the earth;
- in or on any residue stockpile or residue deposit.

This is a very general definition and almost any physical activity that is carried out on site during the preliminary phase of a project in order to identify suitable sources of road building materials can be regarded as prospecting. As such, the person undertaking the activity needs to apply for a prospecting right in terms of the MPRD Act.

Mining is defined as any operation or activity for the purpose of winning any mineral on, in or under the earth, water or any residue deposit, whether by underground or open working or otherwise. Hence, the removal of any material for the purpose of using it in the road building process from any commercial mine, quarry, borrow pit or even residue deposits is regarded as mining. The person undertaking the activity thus needs to apply for either a mining permit or mining right. A mining permit may only be issued if the mineral in question can be mined optimally within a period of two years and the mining area in question does not exceed 1.5 hectares. In all other cases one needs to apply for a mining right.

The distinction between mining permit and right is important, because the application process for each have different requirements in terms of environmental assessment. The applicant of prospecting right or a mining permit needs to submit an environmental management plan. The applicant of mining right needs to conduct an environmental impact assessment (EIA) and to submit an environmental management programme .

The environmental management plan needs to be in the standard format (forms) provided by the Department of Minerals and Energy (DME). This standard format does not require a lot of detail. The EIA in respect of a mining right is similar to the EIA discussed above under the NEM Act. The environmental management programme gives detail of, besides the environmental objectives and specific goals, the outline of the implementation programme. This programme contains, amongst others, procedures for environmental related emergencies and remediation and performance assessment of the planned monitoring and environmental management programme (Government Gazette, 2004). The assessment requirements for a mining right are thus more elaborate and time consuming and costlier than for a mining permit.

From the above it can be concluded that in case the road building activity involves some kind of removal of natural material from quarries or borrow pits to be used in the pavement construction, a fairly extensive process needs to be followed. Authorisation from the DME needs to be obtained for this “mining activity”. To obtain a mining permit instead of a mining right, the limit of 2 years is fair. The limit of 1.5 hectares is however quite low and even for small scale mining to obtain road building material, this limit is quickly exceeded. And although one could apply for exemption, the process becomes more involved, costly and time consuming. Over and above, another authority (the DME) needs to be involved in the process. It can therefore be a real advantage if one does not require new natural material for the rehabilitation of a road. This could be achieved by adopting the CIPR process.

## References

Brauteseth, N.L., *Environmental law*. www.lawinfo.org.za/general/lawinfo.asp, accessed 28 August 2006

Daneel, J., *The new EIA regulations : what they mean to you*. Address to IMESA Border Region, 17 August, East London, South Africa, 2006, not published

Government Gazette, *No. 17678*. Vol. 378, Cape Town, South Africa, 1996

Government Gazette, *No. 19519*. Vol. 401, Cape Town, South Africa, 1998

Government Gazette, *No. 23922*. Cape Town, South Africa, 2002

Government Gazette, *No. 26275*. Vol. 466, Pretoria, South Africa, 2004

Government Gazette, *No. 28753, No. 385,No. R.386 and No. R.387*. Cape Town, South Africa, 2006b, pp. 3-62, 130-145 and 165-174

Government Gazette, *No. 28938, No. R.615 and R.616*. Cape Town, South Africa, 2006a, pp. 6-7

United Nations, *2005 World Summit Outcome*, Report A/RES/60/1, New York, USA, 2005

United Nations, *Report of the World Commission on Environment and Development*, Report A/42/427, 1987

United Nations, *Report of the World Summit on Sustainable Development*, Report A/CONF.199/20, Johannesburg, South Africa, 2002

# APPENDIX C: NORMAL AND SHEAR STRESS

### *1.1.1 Stress*

1.1.1.1 Normal and shear stress

Stress can be defined as the internal force per unit area. Stress is therefore expressed in [N/mm$^2$] or [Pa]. If the external force on a member is a tensile force, the internal forces are also tensile forces and thus the stress generated a tensile stress. In case of compressive external forces, the stress generated is a compressive stress.

Two general types of stresses are considered, *i.e.* normal stress and shear stress. A normal stress acts perpendicular to a section, while shear stress acts parallel to a section. In reality however, the majority of stresses act neither exactly perpendicular nor parallel to a section, but are inclined. These inclined stresses however, can always be resolved in a normal component and a shear component.

The general type of a pure normal stress is shown in Figure 1. A member is subjected to an external force Q [see Figure 1 (a)]. The resulting internal force P in Section *abcd* with area A is equal to Q [see Figure 1 (b)]. The internal force P is distributed over Section *abcd* and for a differential area shown in Figure 1 (c) the stress σ is:

$$\sigma = \frac{dP}{dA} \qquad \text{Eq. 1}$$

In case the normal stress over Section *abcd* is uniformly distributed, it can be derived that the normal stress in Section *abcd* is:

$$\sigma = \frac{P}{A} = \frac{Q}{A} \qquad \text{Eq. 2}$$

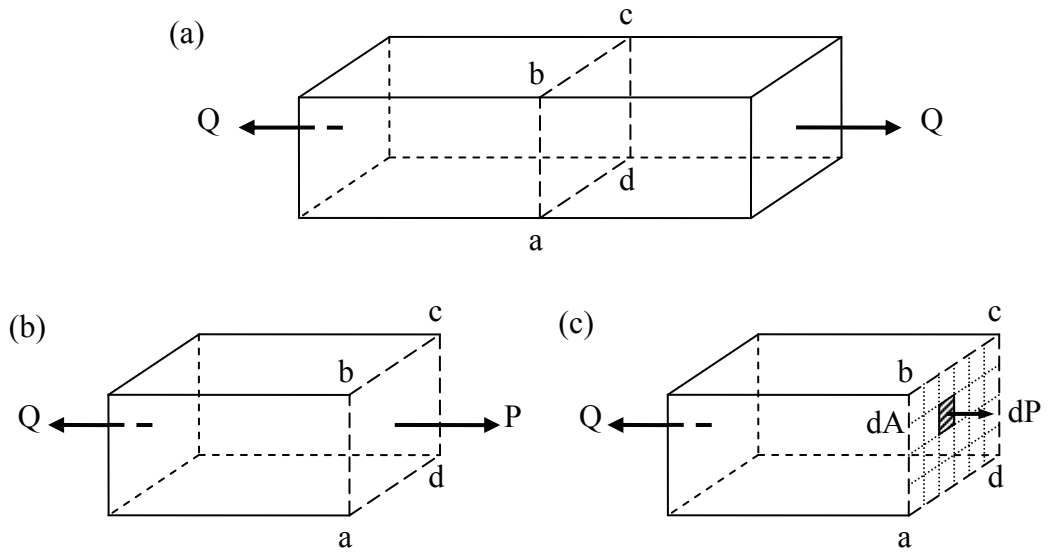


Figure 1: Analysis of tensile stress (after Arges and Palmer, 1963)

The force P is in the normal direction of plane *abcd* and so is the stress. For this particular case the stress is called *normal stress*. Uniform stress distribution, as assumed in Figure 1 above, only occurs when (Arges and Palmer, 1963):

- The section is not immediately adjacent to the point of application of a concentrated load;
- The line of action of the internal force passes through the centroid of the area of the section;
- There is no discontinuity at the section; and
- The member is made of homogeneous material.

Similar to the normal stress in Figure 1, the shear stress can be derived:

$$\tau = \frac{dP}{dA} = \frac{P}{A} = \frac{Q}{A} \qquad \text{Eq. 3}$$

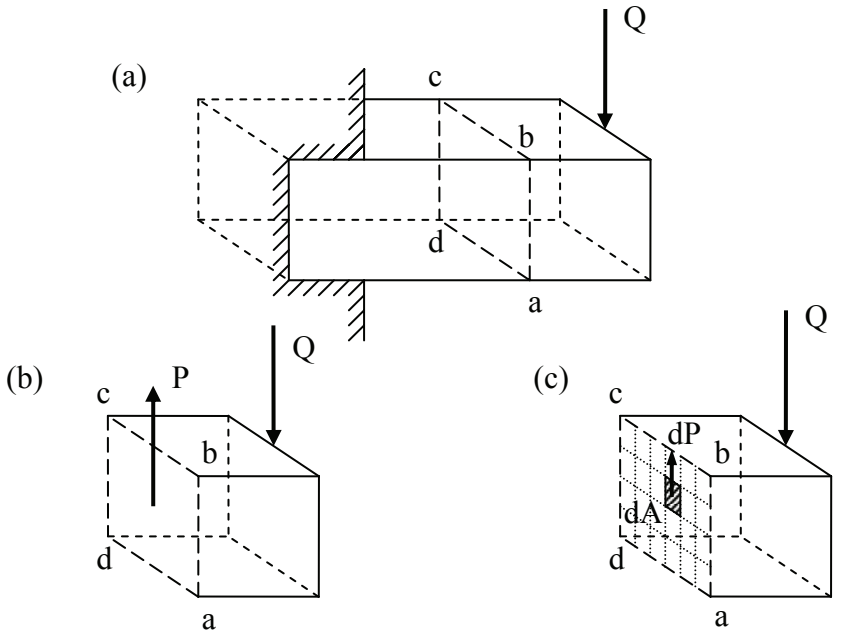


Figure 2: Analysis of shear stress (after Arges and Palmer, 1963)

1.1.1.2 Principal stresses and planes

Stresses occur in all three dimensions and in an *x*-*y*-*z* coordinate system are referred to as $\sigma_x$, $\sigma_y$, $\sigma_z$, $\tau_{xy}$, $\tau_{xz}$, $\tau_{yx}$, $\tau_{yz}$, $\tau_{zx}$ and $\tau_{zy}$. These normal and shear stressed are shown in Figure 3. The directions shown are positive. Only the stresses on the positive planes are shown. The notation followed is that *e.g.* $\tau_{xy}$ is acting in the *y*-direction on the plane of which the normal stress is in the *x*-direction.

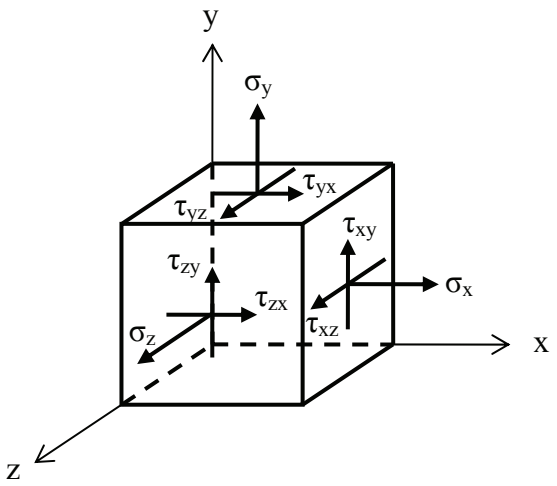


Figure 3: Definition of all normal and shear stress components required to describe the stress state at any point

It can be shown (Arges and Palmer, 1963) that the shear stress in two mutually perpendicular directions must be equal to satisfy that the sum of moments of forces acting on the free-body in equilibrium is equal to zero:

$$\tau_{xy} = \tau_{yx} \; ; \; \tau_{xz} = \tau_{zx} \text{ and } \tau_{yz} = \tau_{zy} \qquad \text{Eq. 4}$$

The stresses shown in Figure 3 are not necessarily the largest stresses that exist at that point and when the member is rotated to a new *x′-y′-z′* coordinate system the stresses shown may change in magnitude. Of interest for the analysis of the stress state at any given point, are the maximum and minimum stress that occur at the particular point and the direction of the planes on which they act. The planes on which the maximum and minimum normal stresses are acting are called the *principal planes*. The *maximum principal stress* is denoted as $\sigma_1$ and the *minimum principal stress* as $\sigma_3$. The principal stress in the third direction is denoted as $\sigma_2$, and has an intermediate value. The planes on which the maximum shear stress is acting and which have another direction as the principal planes are called *planes of maximum shear* on which the maximum shear stresses $\tau_1$, $\tau_2$ and $\tau_3$ act.

A two-dimensional state of stress occurs at any free surface which is not subjected to external loading. This two-dimensional state will be discussed further here. If the z-plane is free and unloaded it follows that $\sigma_z = \tau_{zx} = \tau_{zy} = 0$. Equilibrium requires that $\tau_{xz}$ and $\tau_{yz}$ also must be zero. The two-dimensional state of stress is thus reduced to the *x-y* plane as shown in Figure 4(a).

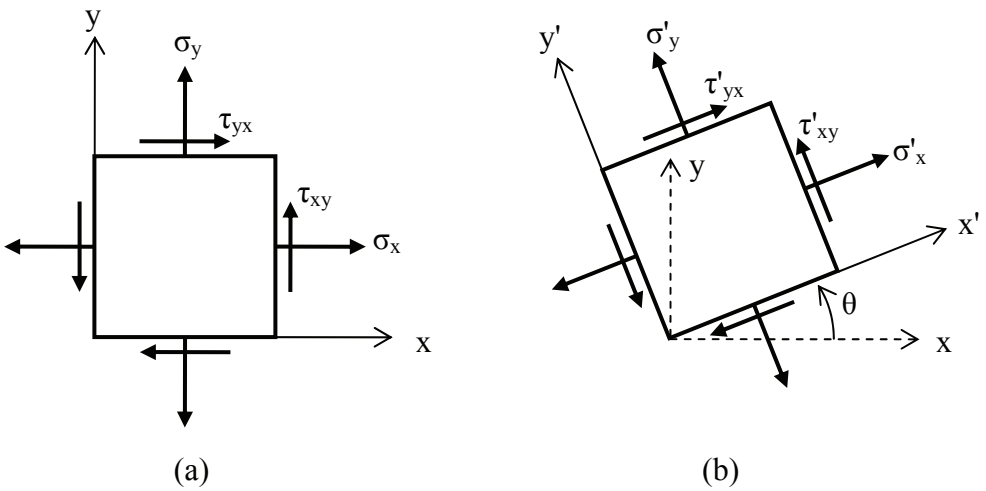


Figure 4: Plane stress in the two-dimensional state of stress (*z*-plane free and unloaded)

In order to find the principal stresses, the member shown in Figure 4(a) needs to be rotated over an angle $\theta$. This is shown in Figure 4(b). This transformation of axes does not change the stress state in the member shown. The stresses in the transformed direction can be determined by analysing the free-body diagram of a portion of the member with an oblique plane at an angle $\theta$ shown in Figure 5. Opposed to what was shown in Figure 1, the direction of the stress acting on the oblique plain is not in the normal direction and can therefore be resolved in a component in the normal direction of the oblique plane, $\sigma'_x$, and parallel to the oblique plane, $\tau'_{xy}$.

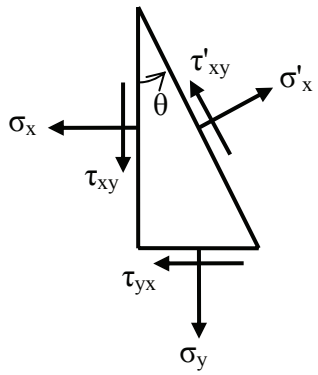


Figure 5: Free-body diagram for analysis of transformed stress state

Equilibrium of forces (note that the stresses are multiplied with the length of the respective sides of the triangle in order to obtain the forces) in *x* and *y* direction results in the following equations for $\sigma$ and $\tau$ (after Dowling, 2007):

$$\sigma'_x = \frac{\sigma_x + \sigma_y}{2} + \frac{\sigma_x - \sigma_y}{2}\cos 2\theta + \tau_{xy}\sin 2\theta \qquad \text{Eq. 5}$$

$$\tau'_{xy} = -\frac{\sigma_x - \sigma_y}{2}\sin 2\theta + \tau_{xy}\cos 2\theta \qquad \text{Eq. 6}$$

Rotation of another 90º, thus substituting $\theta$ by $\theta + 90^o$, gives the stresses on the plane in the transformed *y'*-direction. The angle $\theta$ which gives the maximum and minimum stresses, or the principal stresses, can be found by equating the derivatives $d\sigma/d\theta$ of Equation 5 and $d\tau/d\theta$ of Equation 6 to zero. Following out of the former is Equation7, while out of the latter follows Equation 8:

$$\tan 2\theta_n = \frac{2\tau_{xy}}{\sigma_x - \sigma_y} \qquad \text{Eq. 7}$$

$$\tan 2\theta_s = -\frac{\sigma_x - \sigma_y}{2\tau_{xy}} \qquad \text{Eq. 8}$$

For any given stress state, two angles $\theta_n$ can be found that satisfy Equation 7 and these two differ by 90º. This means that the orientation of the two planes on which the principal normal stresses act are perpendicular to one another. The angles $\theta_n$ can be substituted in Equation 5, which leads to the following principal normal stresses:

$$\sigma_1, \sigma_3 = \frac{\sigma_x + \sigma_y}{2} \pm \sqrt{\left(\frac{\sigma_x - \sigma_y}{2}\right)^2 + \tau_{xy}^2} \qquad \text{Eq. 9}$$

When the angles $\theta_n$ are substituted in Equation 6 it can be found that the shear stress on the principal planes is equal to zero. This particular scenario is shown in Figure 1.

The two angles $\theta_s$ that satisfy Equation 8 also differ by 90º. Substituting these angles into Equation 6 results in the maximum shear stress in the *xy*-plane and these are called the principal shear stresses. The two angles $\theta_s$ result in two mutually perpendicular planes and because of Equation 6 the shear stress on these planes are equal. Therefore, the principal shear stresses obtained by rotating $\theta_{s1}$ and $\theta_{s2}$ are both maximum shear stresses, unlike the principal normal stresses, where the maximum principal normal stress occurred on the one plane and the minimum principal normal stress on the other perpendicular plane. Substituting the angles $\theta_s$ in Equation 6 leads to the following equation for the principal shear stress:

$$\tau_{\max} = \sqrt{\left(\frac{\sigma_x - \sigma_y}{2}\right)^2 + \tau_{xy}^2} \qquad \text{Eq. 10}$$

While there is no shear stress on the planes on which the principal normal stresses act, there are normal stresses (equal in magnitude) on the principal shear planes (substituting $\theta_s$ in Equation 5):

$$\sigma_{\tau_{\max}} = \frac{\sigma_x + \sigma_y}{2} \qquad \text{Eq. 11}$$

It can be seen from Equations 7 and 8 that $tan\ 2\theta_n$ is the negative reciprocal of $tan\ 2\theta_s$. This means that $2\theta_n$ and $2\theta_s$ differ by 90º from each other and that $\theta_n$ and $\theta_s$ differ by 45º from each other. Hence, at any given point the maximum shear planes are at 45º with the principal planes.

1.1.1.3 Stress diagram and Mohr diagram

A circle is formed when the shear stress (Equation 6) is plotted against the normal stress (Equation 5) for $\theta$ ranging from 0 to 2π in a so-called stress diagram. The centre of the circle is at $\sigma_{\tau max} = (\sigma_x + \sigma_y)/2$ (Equation 11) while the radius of the circle is equal to $\tau_{\max}$ as given in Equation 10. This can be verified by letting $(\sigma_x - \sigma_y) / 2 = B$ and substituting $\sigma_{\tau max}$ and $B$ into Equation 5 and Equation 6 respectively. Subsequently squaring the two equations and adding them together leads to (after Arges and Palmer, 1963):

$$\left(\sigma - \sigma_{\tau_{\max}}\right)^2 + \tau^2 = B^2 + \sigma_{xy}^2 = \tau_{\max}^2 \qquad \text{Eq. 12}$$

This is the equation for a circle with the centre at ($\sigma = \sigma_{\tau max}$ and $\tau = 0$) and a radius of $\tau_{max}$.

The circle can also be derived graphically making use of stress vectors. The free-body diagram of Figure 5 is repeated again in Figure 6 (b) and (d). The oblique plane makes an angle θ with the vertical. The normal stress $\sigma'_x$ and shear stress $\tau'_{xy}$ are the

components of the stress vector G resolved in the transformed $x'y'$-directions. This is illustrated in Figure 6 (b). Note that $\tau'_{xy}$ is shown in the negative direction here. The stress vector G is plotted in the stress diagram shown in Figure 6 (a). In this stress diagram the normal stress is on the horizontal axis and the shear stress on the vertical axis. Stress vector G makes an angle β with the normal stress direction and is the same in both Figure 6 (a) and (b).

As shown in Figure 6 (d), stress vector G can also be resolved in components $G_x$ and $G_y$ in the $xy$-directions. These components are also plotted in Figure 6 (a), maintaining the angle θ between the $xy$ and the $x'y'$ coordinate systems. When $G_x$ and $G_y$ are projected on the normal stress axis, points $n$ and $t$ are obtained. The coordinates of point $n$ are $(\sigma_3,0)$ and of point $t$ $(\sigma_1,0)$, the minor and major principal normal stress respectively. Points $n$ and $t$ are independent of angle $\theta$ and their coordinates remain the same. This contrary to point G, being the endpoint of stress vector G, which changes with changing angles $\theta$. When $\theta$ is varied from 0 to $2\pi$ a circle as shown in Figure 6 (d) is formed. This is the same circle as described by the formula in Equation 12.

The circle plotted in the stress diagram as shown in Figure 6 (c) is not to be confused with the so-called Mohr's Circle in the Mohr diagram. Mohr's Circle is obtained by mirroring the circle in the stress diagram around the normal stress axis. The disadvantage is that the stress vector G is now not in the actual direction anymore (angle $\beta$ is also mirrored). The advantage however, is that the angle $\theta$ is in the same direction as for the transformation of the coordinate systems and that points $n$ and $t$ remain. The most important difference is that direction of lines $G''n$ and $G''t$ are the same as the directions of the normal stress and the shear stress respectively on the oblique plane as shown in Figure 6 (b) and (d).

The angles 2θn and 2θs can directly be read off from the Mohr diagram and in the right direction. This means that the orientation of the principal planes (both normal and shear) can directly be obtained graphically from the Mohr diagram.

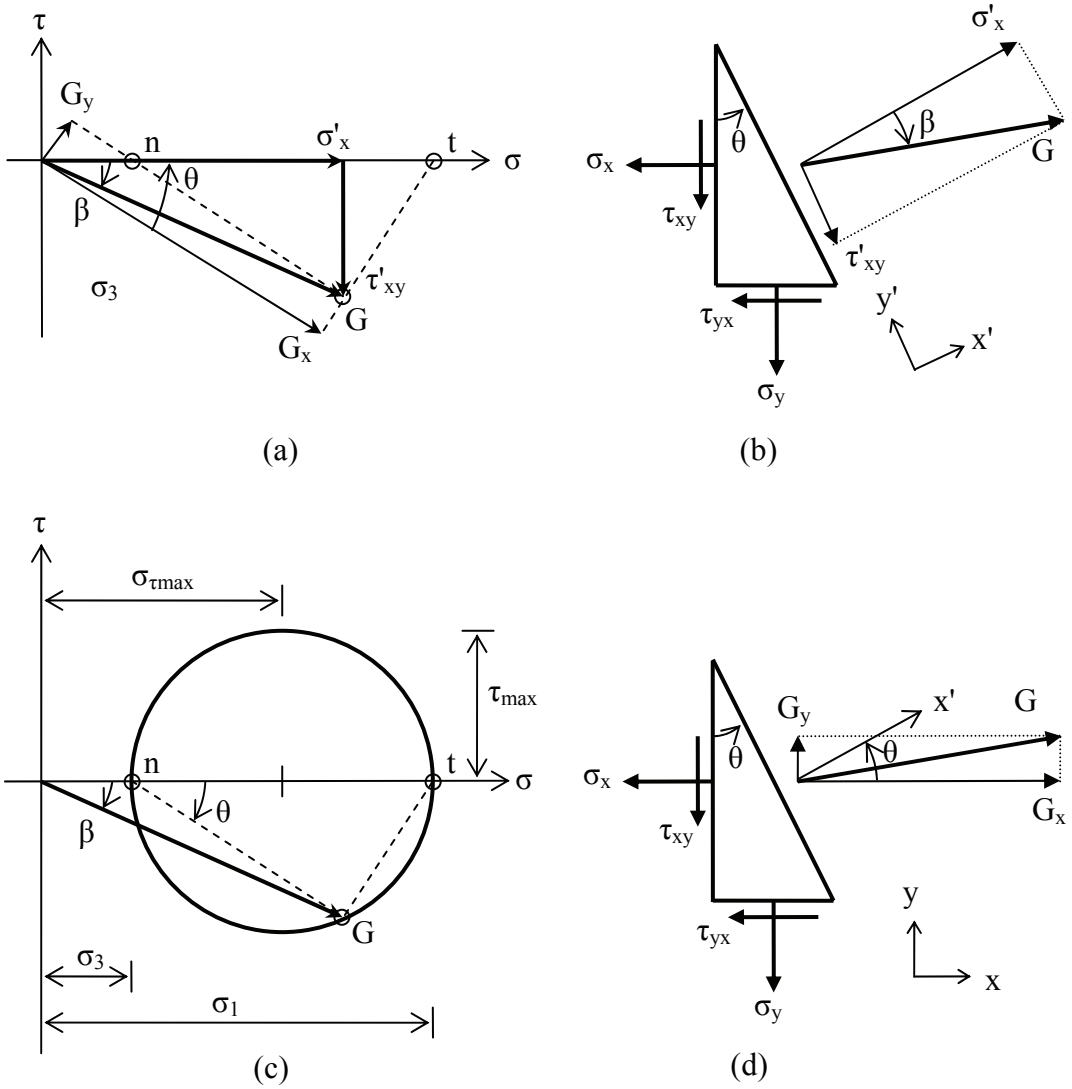


Figure 6: Stress diagram

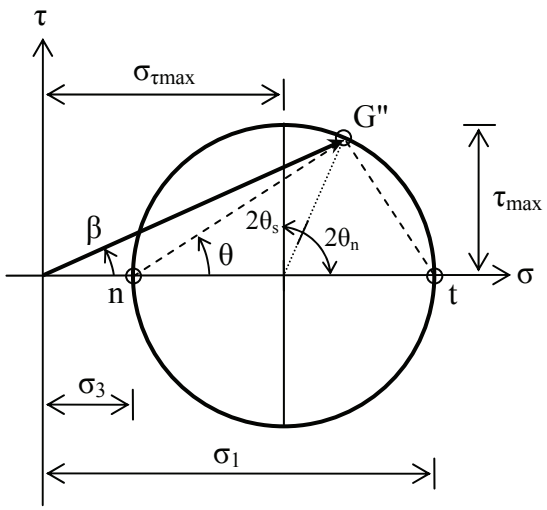


Figure 7: Mohr's diagram

In plotting Mohr's Circle, one has to take care as far as the sign (+ or -) is concerned. Because of the mirroring, some of the negative shear stresses are plotted on the positive $\tau$-axis (the negative shear stress $\tau_{xy}$ of Figure 6 (b) is plotted positive in Figure 7). The following sign convention is used when plotting Mohr's Circle; shear stresses on a member in the clockwise (CW) direction are positive and in a counter-clockwise (CCW) direction are negative.

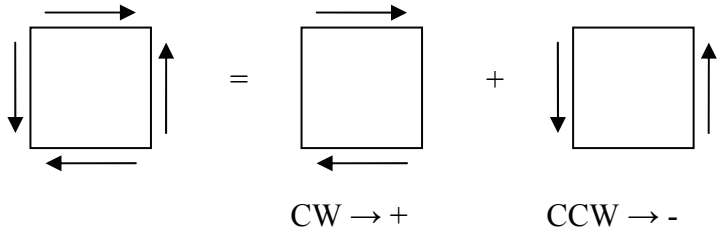


Figure 8: Shear stress sign convention for Mohr's Circle (Dowling, 2007)

## References

Arges, K. P. and Palmer, A. E., *Mechanics of Materials*, published by McGraw-Hil, USA, 1963

Dowling, N. E., *Mechanical Behavior of Materials : Engineering Methods for Deformation, Fracture and Fatigue*, third edition published by Pearson Prentice Hall, USA, 2007

This page is left blank intentionally

# APPENDIX D : SPECIMEN PREPARATION

## 1.1 Tri-axial specimens

### *1.1.1 Weighing out and blending mineral aggregate*

All coarser particle size mineral aggregate are kept in stockpiles of which the grading is known (as described in Chapter 4) and the smaller particle size mineral aggregate are sieved out in single particle size fractions.

The mineral aggregate is weighed off to form a total batch size of 50 kg. The required amount of material from each stockpile is detailed in Table 1 below. A batch size of 50 kg is chosen, as it allows to compact ten specimens (four sets of two specimen, plus one set of two spare).

Table 1: Stockpile quantities required for blending 50 kg batches

| Stockpile [mm] | 75% limestone – 25% RAP | | 25% limestone – 75% RAP | |
|---|---|---|---|---|
| | Limestone [kg] | RAP [kg] | Limestone [kg] | RAP [kg] |
| 19.0 – 12.5 | 4.620 | 1.211 | 1.540 | 3.634 |
| 4.75 – 12.5 | 13.883 | 4.754 | 4.628 | 14.261 |
| 2.36 / 2.2 – 4.75 | 5.164 | 2.999 | 1.721 | 8.996 |
| 1.18 | 2.760 | 1.156 | 0.920 | 3.469 |
| 0.600 | 2.993 | 1.403 | 0.998 | 4.208 |
| 0.300 | 3.574 | 0.686 | 1.191 | 2.059 |
| 0.150 | 2.689 | 0.199 | 0.896 | 0.596 |
| 0.075 | 1.463 | 0.076 | 0.488 | 0.229 |
| <0.075 | 0.356 | 0.016 | 0.119 | 0.049 |

The aggregate is spread on a clean concrete base and thoroughly mixed by hand. When mixed in the pugmill mixer, the maximum batch size is between 15 and 25 kg. The total batch (50kg) is therefore divided into three batches by repeatedly splitting into two equal batches using a riffler and combining the sub-batches according to the following procedure

Sub-batches a.a.b and a.a.a.b combined give a total of 19.25 kg. When sub-batches a.a.a.a.a and a.a.a.a.b are combined with a.b.a and a.b.b. respectively, sub-batches of 15.875 kg are obtained. The splitting and combining resultsin three sub-batches between 15 and 20 kg, which is appropriate for use in the pugmill mixer.

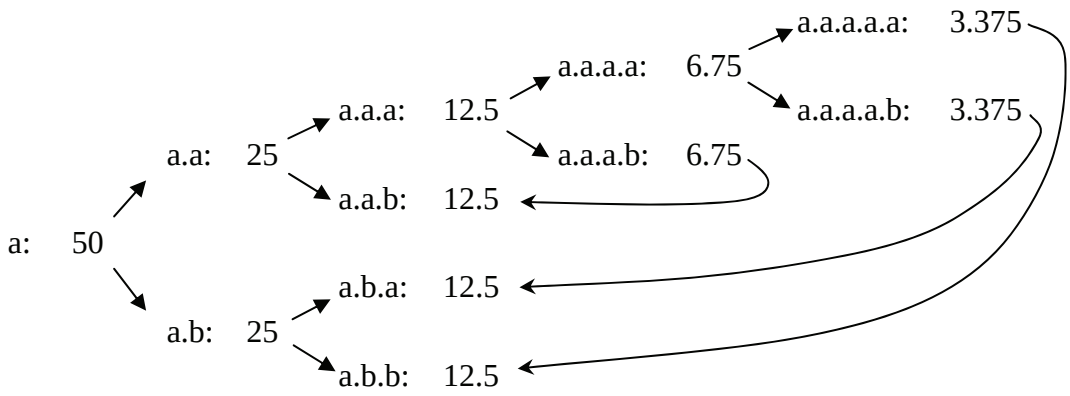


### *1.1.2 Mixing and compaction*

For the mixing of the bitumen emulsion or foamed bitumen and the mineral aggregate and for the compaction of the tri-axial specimens, the following procedure is followed:

1. The weight of the batches of mineral aggregate is determined. The mineral aggregate is kept at room temperature.
2. The hygroscopic moisture content of the mineral aggregate is assumed to be 0.75%.
3. The quantity of compaction water to be added is determined taking into account the hygroscopic moisture. In case of mixing with foamed bitumen total quantity is 70% of O.M.C. In case of mixing with bitumen emulsion, the total quantity of water is 100% of O.M.C. The compaction water added is the total quantity of water required reduced by the quantity of water in the bitumen emulsion.
4. The mineral aggregate is mixed with the compaction water in the pugmill mixer for approximately one minute or until a good dispersion of the compaction water is achieved.
5. The wetted mineral aggregate is put in plastic bags and kept sealed for three hours. For the production of foamed bitumen mixes during the winter period the mineral aggregate is conditioned at 25ºC.
6. In case of mixes that require addition of cement, the quantity of cement is determined based on the dry weight of the aggregate. The cement is mixed into the mineral aggregate after the three hours sealing period and shortly before the bitumen is mixed into the mix.
7. The quantity of bitumen required is determined based on the dry weight of the mineral aggregate or, in case of active filler being added, on the dry weight of the mineral aggregate and active filler together. The residual binder content for the 75C mixes is 3.6% and for the 75M mixes 2.4%.
8. For the production of bitumen emulsion mixes, the emulsion is poured manually into the running pugmill mixer (see Figure 1), ensuring a good distribution. The mixing is continued after adding of emulsion for approximately one minute.
9. For the production of foamed bitumen mixes use is made of a Wirtgen™ WLB-10 laboratory foamed bitumen plant. The foamed bitumen is sprayed directly into the running pugmill mixer by the WLB-10. The binder output of the WLB-10 is approximately 115 grams of bitumen per second. The mixing is continued after spraying for approximately 40 seconds.

10. Moisture content samples of each batch are taken immediately after mixing.
11. Before compaction, the mixed batches are combined and mixed by hand.
12. The compaction process is started as soon as possible after the mixing. Care is taken that the mix does not dry out.
13. The amount of material required for 150 mm Ø specimens with a height of approximately 130 mm is determined based on the target dry density of 98% of Modified AASHTO density.
14. The moulds for the gyratory compactor are filled with the required amount of material and placed in the draft oven at 40ºC for 30 minutes, in order to simulate the delays and working of the mixed material that may occur on site during construction.
15. The first three specimens are compacted to 30 gyrations with an induced angle of 1.25º and a pressure of 600 kPa. Subsequently, the remaining specimens are compacted to the average compacted height of the first three specimens, regardless of the number of gyrations (amount of material in all moulds is equal).
16. After compaction the specimen is immediately removed from the mould and enters into the curing procedure.

Figure 1: Twin-shaft pugmill mixer

### *1.1.3 Curing*

The following curing procedure has been adopted for the specimens for triaxial testing:

1. The wet mass of the specimen immediately after compaction is determined. The specimen is placed on the wooden base plate (160 mm diameter) and placed unsealed in the oven for 20 hours at 30ºC.
2. After the 20 hours the specimens are weighed, placed in a plastic bag and sealed. The specimens are put in the oven for 24 hours at 40ºC.
3. After the 24 hours the specimens are removed from the plastic bag, weighed and placed in another dry plastic bag and again sealed. The sealed specimens are put in the oven for another 24 hours at 40ºC.

4. After the last 24 hours the specimens are removed from the plastic bag and weighed. This mass is used to determine the moisture content after curing.
5. The specimens are immediately placed in a dry placed bag, which is sealed after the specimen has cooled down to room temperature (approximately one hour).
6. After curing the specimens are kept sealed in plastic bags at room temperature.

### *1.1.4 Specimen preparation*

The specimens to be tested are placed in the climate chamber the day before testing and conditioned overnight at 25ºC. The triaxial cell including the loading plates are also subjected to that same conditioning.

Two specimens with a height of approximately 125 - 130 mm height are placed one on top of the other to form one specimen with the desired height. The friction on the interface between the two specimens ensures that the two specimens behave as one uniform specimen. The bottom faces of the specimens form the interface in the middle. For a set of two, specimens with more or less equal moisture content and weight after curing are combined. The two specimens with the highest and the lowest moisture content are used as spare specimens.

The specimens for the monotonic and long duration dynamic tri-axial testing require no further preparation and just before testing the specimen is covered with a latex membrane and sealed at the top and bottom of the sample with a rubber O-ring on the base plate and load plate of the tri-axial cell.

The specimen preparation for the short duration dynamic testing (resilient modulus) is more complicated and requires installation of three on-specimen LVDT's. The installation of these LVDT's is done according to the following protocol:

1. The two specimens that make up one test specimen are put on top of each other (the specimen with the lowest specimen number was always put on top);
2. Markings are made on the specimens to identify the positions of the seating plates. An equilateral triangle is used to ensure that the on-specimen LVDT's are at radial angles of 120° relatively to each other (see Figure 2 left);
3. The seating plates are glued to the specimens using RockSet®. The cement is allowed to set overnight (see Figure 2 right);
4. The specimen is placed on the bottom loading plate;
5. The membrane is placed over the specimen and the seating plates. The studs on the seating plates are lined up with the small holes in the membrane and protrude through the membrane (see Figure 3 left);
6. The bottom clamps are placed on the lower seating plates and the LVDT clamps on the upper seating plates and all are fastened with M5.5 nuts (see Figure 3 middle);
7. By fastening the nuts, the membrane acts as a seal between the seating plate and the clamp for the holes in the membrane through which the studs protrude;
8. The LVDT's (range ±2.0mm with a output of ± 10V) are placed in the clamps and are fastened;
9. Spacers are glued between the bottom clamps and the LVDT's using quick setting epoxy (see Figure 3 right hand side).


Figure 2: Stacked specimens with markings (left) and seating plates cemented on (right)

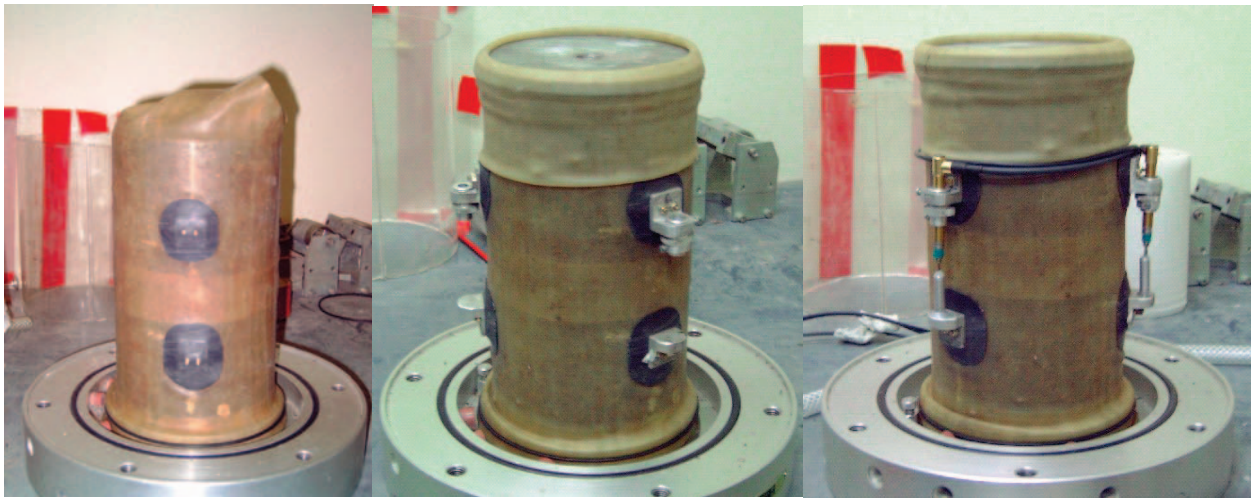

Figure 3: Specimen in membrane (left) with clamps (middle) and LVDT's fitted (right)

## 1.2 Four-point bending beam specimens

### *1.2.1 Weighing out and blending of mineral aggregate*

In principal the same procedure was followed as described in Section 1.1 above, except for the fact that the total batch size for the preparation of a slab was with approximately 29 kg less than the total batch size used for the preparation of tri-axial specimens. The batch of 29 kg was divided in two equal sub-batches using a riffler.

### *1.2.2 Mixing and compaction*

For the mixing of the bitumen emulsion or foamed bitumen and the mineral aggregate and for the compaction of the slabs the same procedure as for the tri-axial specimens is followed, save for the following:

1. For the mixing of the emulsion mixes a vertical shaft mixer is used (see Figure 4).
2. Compaction moisture of 65% of OMC is added to the mineral aggregate and mixed in for approximately 1 minute.
3. After mixing in of the binder (either bitumen emulsion or foamed bitumen) the two mixing batches are added together and mix by hand.
4. Subsequently the total batch is again divided in two by hand and placed in an oven at 40ºC for 30 minutes in order to simulate delays and working of the material on site.
5. After the 30 minutes the separated batches are added together again.
6. A mould with the dimensions of 450mm x 450mm x 62mm is used of the compaction of the slab.
7. The required amount of material for a slab is calculated based on the target dry density (98% of Mod AASHTO) and the volume of the mould. The required amount of material is then placed in the mould in two layers. Each layer is lightly tampered using a hand-tamper (see Figure 5).
8. A steel wheel roller of laboratory size (880mm wide by 450mm diameter, see Figure 6) with a compaction mass of approximately 250 kg is used to compact the slab with both static and vibration roller action. 50 to 60 roller passes are applied for the compaction of bitumen emulsion mixes and 60 to 70 for passes for foamed bitumen mixes.

Figure 4: Vertical shaft drum mixer

Figure 5: Tamping of mix in slab mould prior to roller compaction

Figure 6: Lab roller for slab compaction (static and vibration)

### *1.2.3 Curing*

The curing of the slabs is different to the curing of the tri-axial specimens, because the slabs are too bulky and heavy to easily handle and seal in plastic bags. Therefore the following procedure was used:

1. The slab, while still in the mould, is placed in an oven at 40$^{o}$C for 72hours.
2. After 24 hours the sides frames of the mould are removed and the slab remains on the base plate
3. After the 72 hours curing period the slab is left to cool at ambient temperature and sealed prior to beam cutting process.

### *1.2.4 Cutting of beams*

For the preparation of the beam specimens to be tested in the four-point beam set up a saw-cutter was used (see Figure 7). The saw-cutter table was modified in order to enable cutting of slabs 450 mm wide and 450 mm long. The saw-cutter consists of a fixed 1.5 kW electrical motor and a blade that can only be adjusted in height cutting from the top downwards. The slab to be cut is fixed on a sliding table, which is pushed through underneath the blade. Initially use was made of a 3mm thick slotted diamond blade, however it was found that spalling and chipping off of material occurred on the edges of the beams. Subsequently a 1.5 mm thick continuous rim diamond blade was used, which resulted in better quality beams. It should be emphasized that attention to detail is required in the sawing of the beams to ensure quality.

The beams were dry-cut as the addition of water during the cutting process would result in damage of the cold-mix material. A side effect of the dry cutting however was the excessive dust generation.

Figure 7: Cutting of beams at SU for four-point beam testing

A maximum of six beams can be obtained from a single slab. The beams dimensions are 63.5±5mm in width, 50±5mm in depth and 380±5mm in length. All faces of the beam are cut. Cutting is carried out in the direction of compaction. Utmost care is to be taken during the cutting of the beams to prevent chipping off of stones resulting in irregular beam faces and edges.

All beams are labelled according to mix number M1 to M9, slab number (A, B, C, etc.) and beam number (1 to 6), for instance M3-A-5 or M8-D-2.

### *1.2.5 Specimen preparation*

Unlike for the tri-axial testing, the beam specimens to be used for the BFA testing do not require any further preparations.

# APPENDIX E: SHEAR TESTING RESULTS

**Mix A-75C-0**

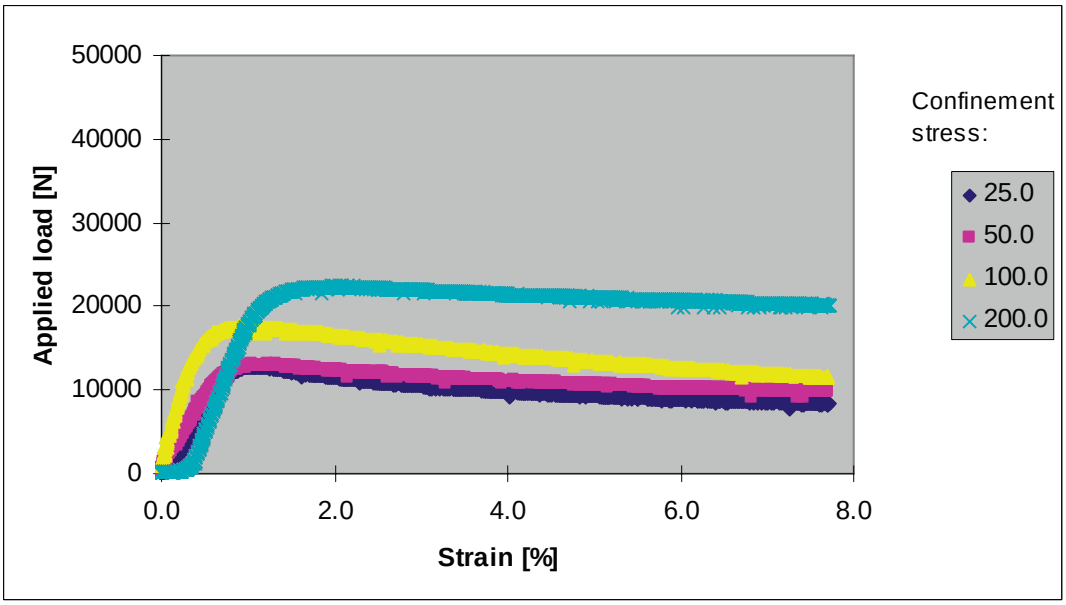


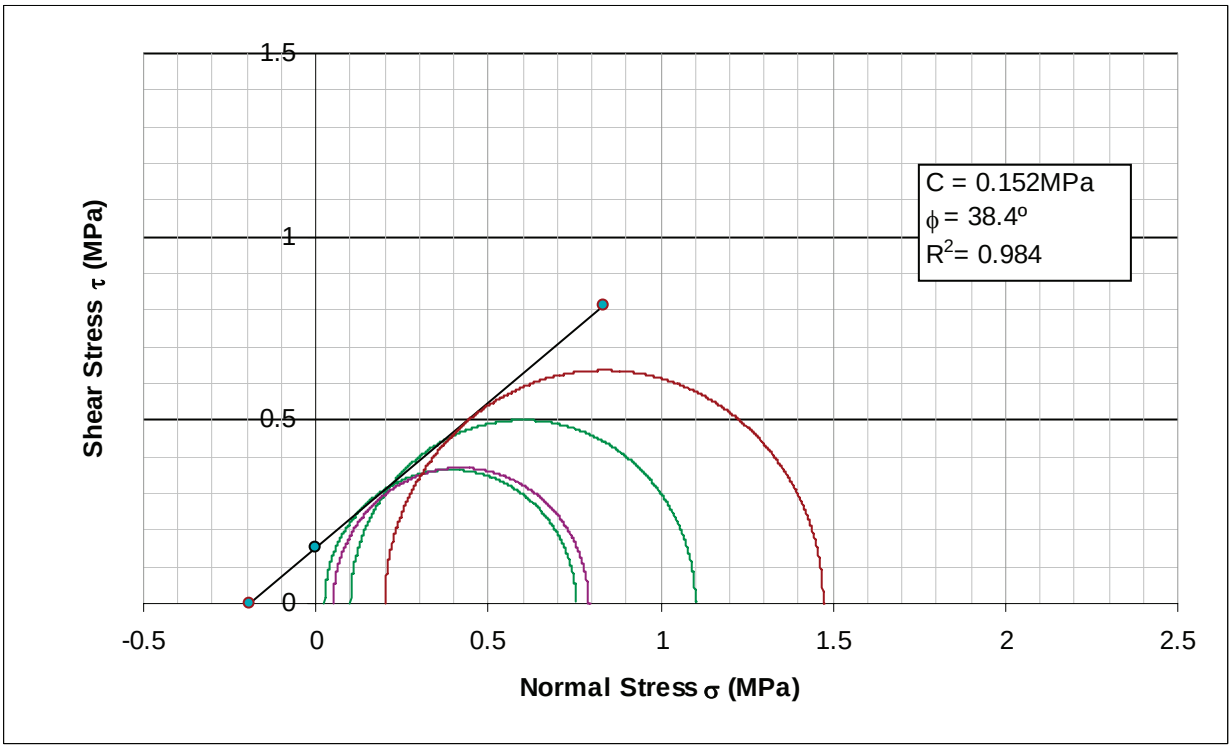

**Mix A-75C-1**

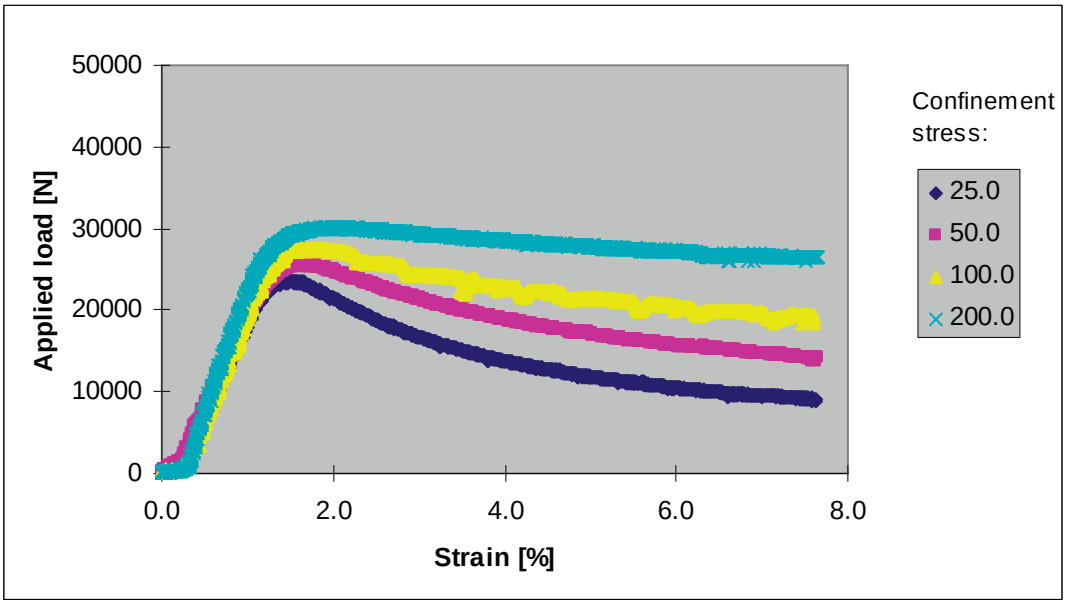
50000
40000
30000
20000
10000
0
Applied load [N]
0.0
2.0
4.0
6.0
8.0
Strain [%]
Confinement stress:
25.0
50.0
100.0
200.0

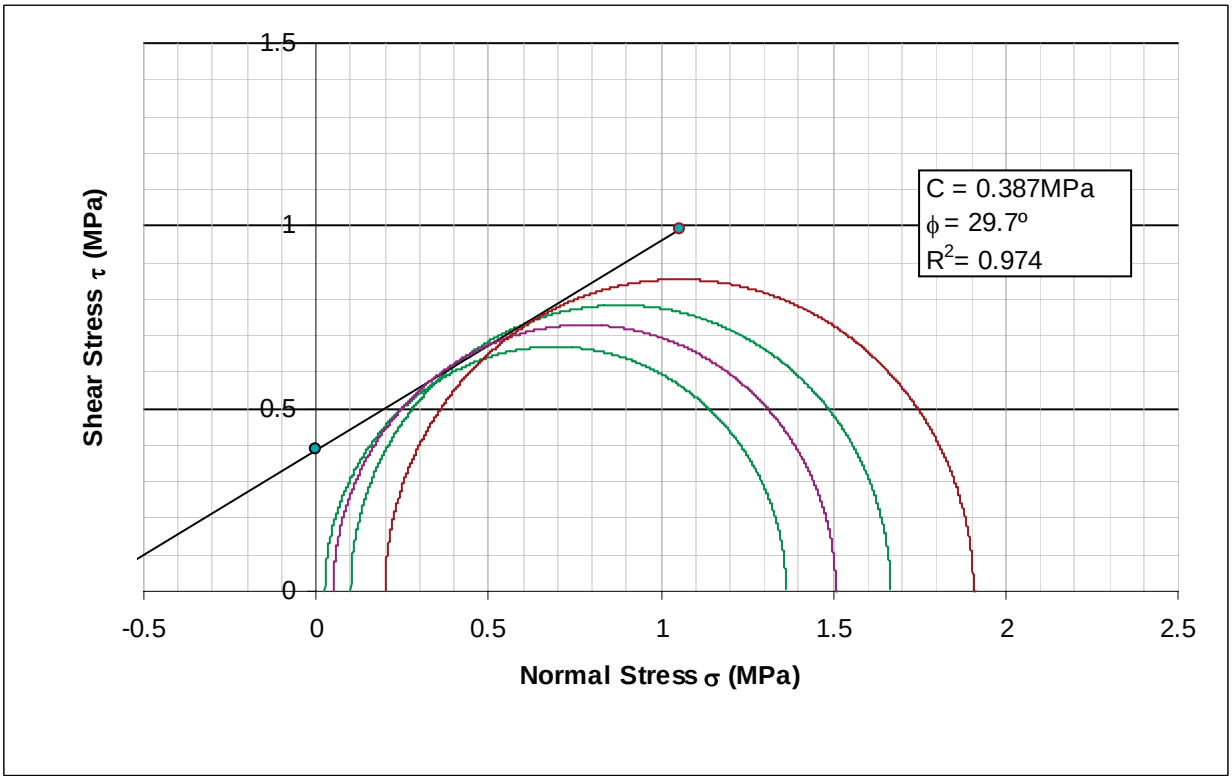
1.5
1
0.5
0
Shear Stress τ (MPa)
-0.5
0
0.5
1
1.5
2
2.5
Normal Stress σ (MPa)
C = 0.387MPa
ϕ = 29.7º
R2= 0.974

**Mix A-75M-0**

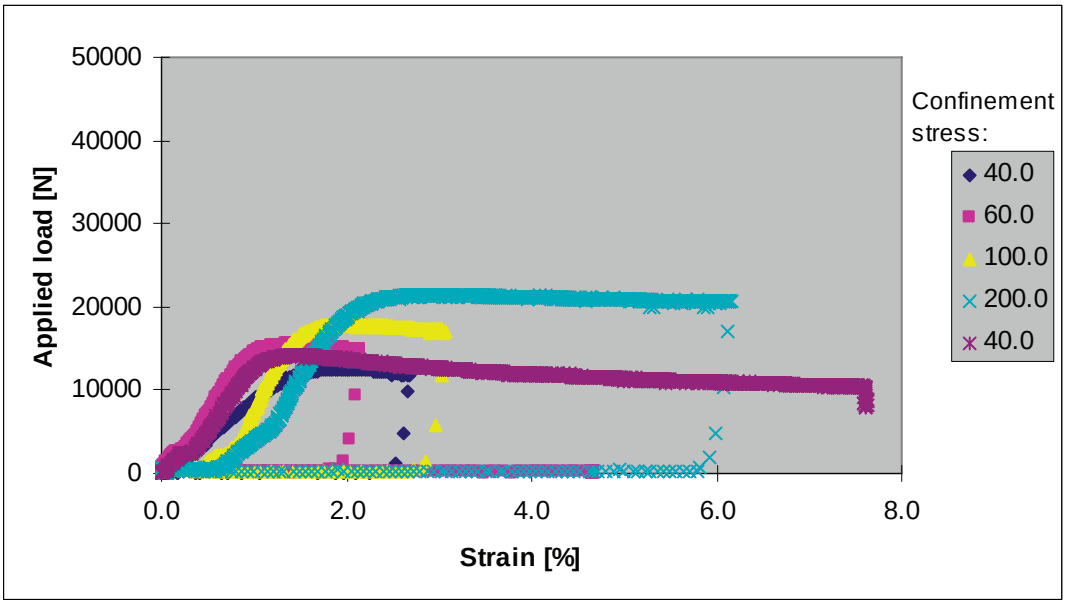
50000
40000
30000
20000
10000
0
Applied load [N]
0.0
2.0
4.0
6.0
8.0
Strain [%]
Confinement stress:
40.0
60.0
100.0
200.0
40.0

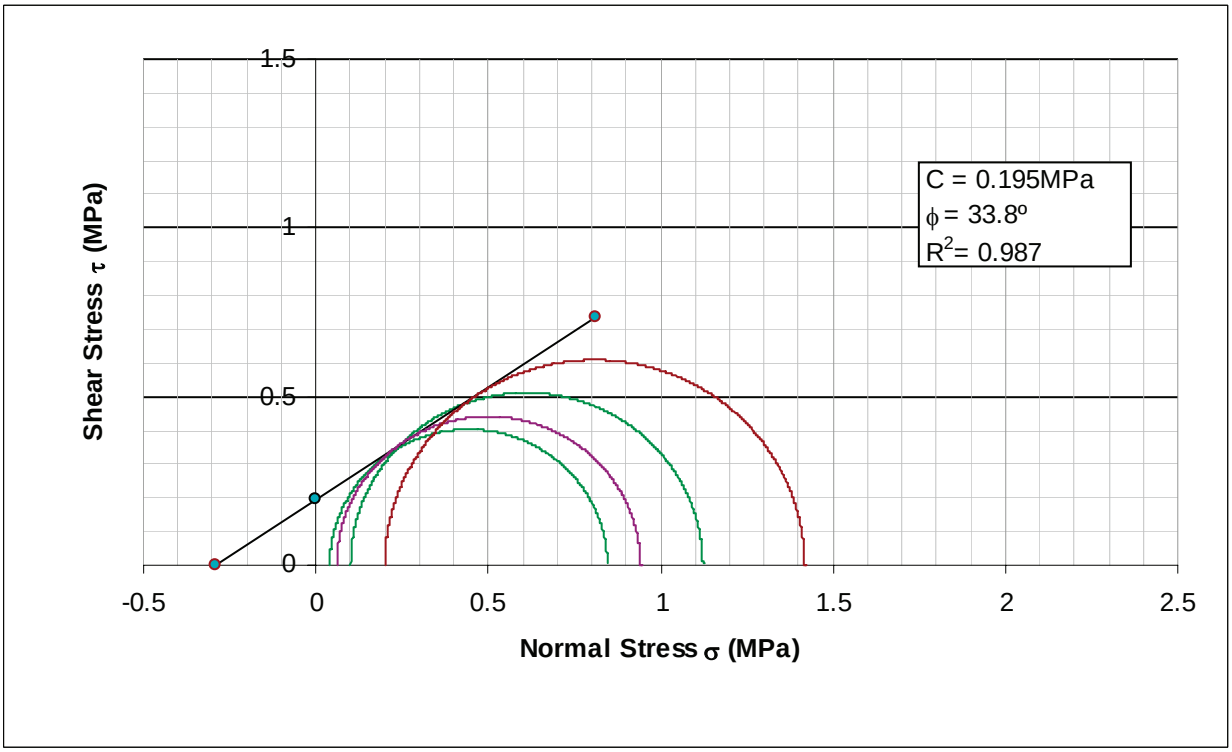
1.5
1
0.5
0
Shear Stress τ (MPa)
-0.5
0
0.5
1
1.5
2
2.5
Normal Stress σ (MPa)
C = 0.195MPa
ϕ = 33.8º
R2= 0.987

**Mix B-75C-0**

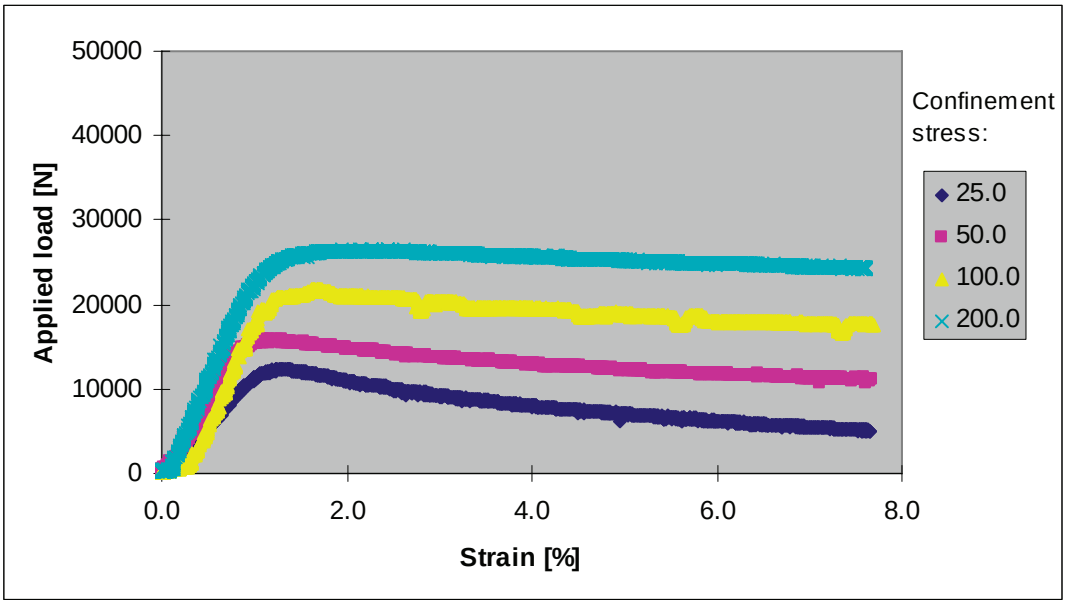
50000
40000
30000
20000
10000
0
Applied load [N]
0.0
2.0
4.0
6.0
8.0
Strain [%]
Confinement stress:
25.0
50.0
100.0
200.0

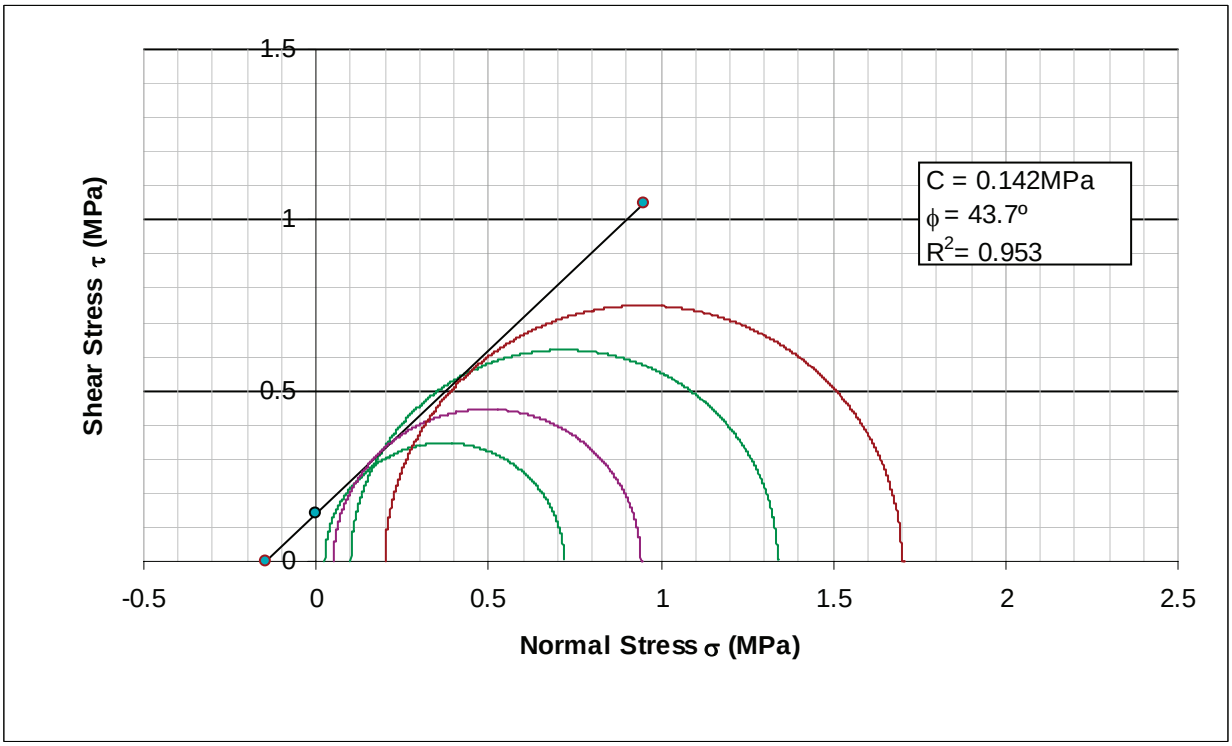
1.5
1
0.5
0
Shear Stress τ (MPa)
-0.5
0
0.5
1
1.5
2
2.5
Normal Stress σ (MPa)
C = 0.142MPa
ϕ = 43.7º
R2= 0.953

**Mix B-75C-1**

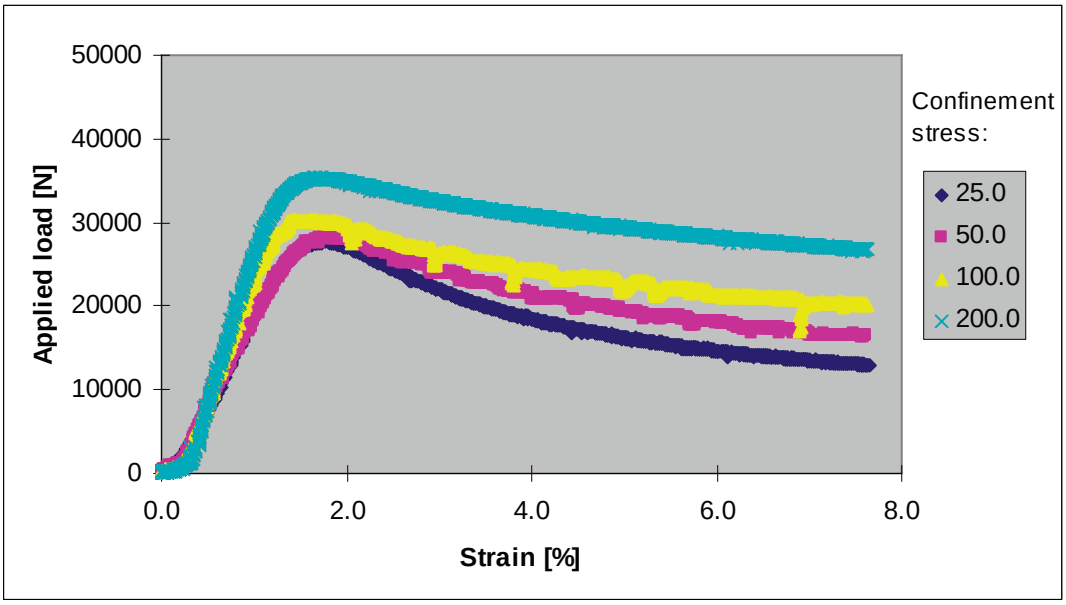
50000
40000
30000
20000
10000
0
Applied load [N]
0.0
2.0
4.0
6.0
8.0
Strain [%]
Confinement stress:
25.0
50.0
100.0
200.0

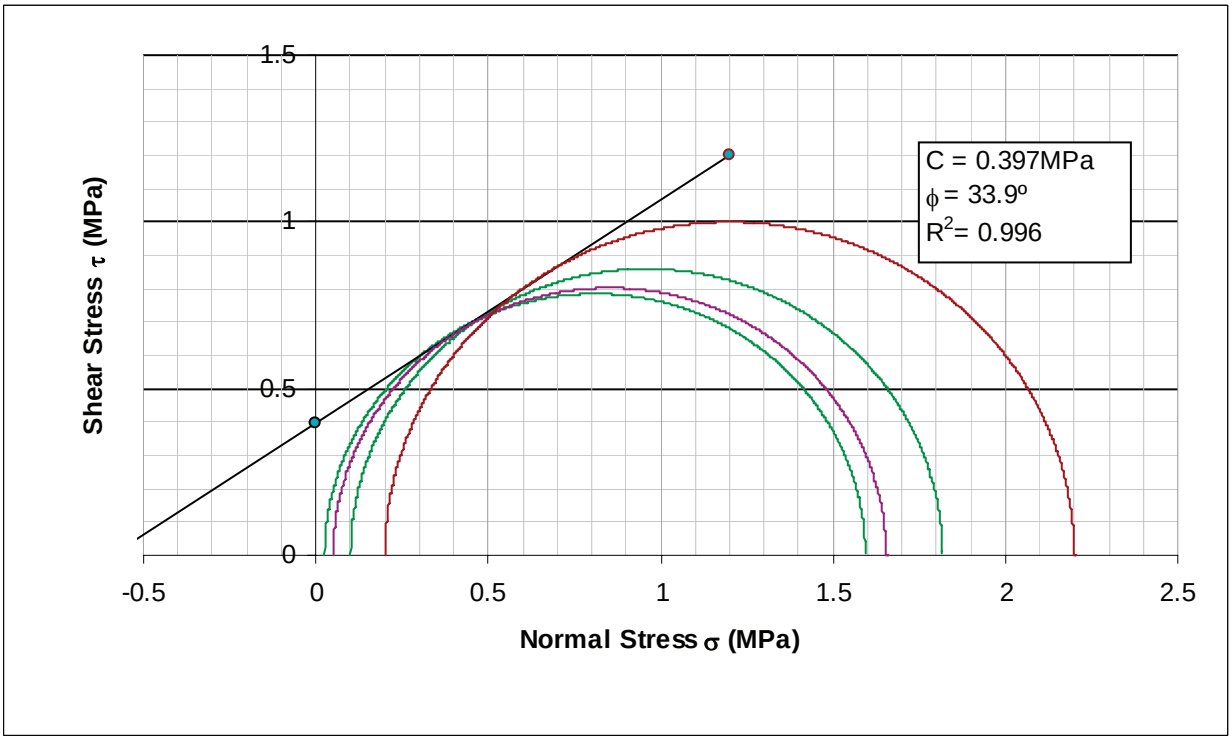
1.5
1
0.5
0
Shear Stress τ (MPa)
-0.5
0
0.5
1
1.5
2
2.5
Normal Stress σ (MPa)
C = 0.397MPa
ϕ = 33.9º
R2= 0.996

**Mix B-75M-0**

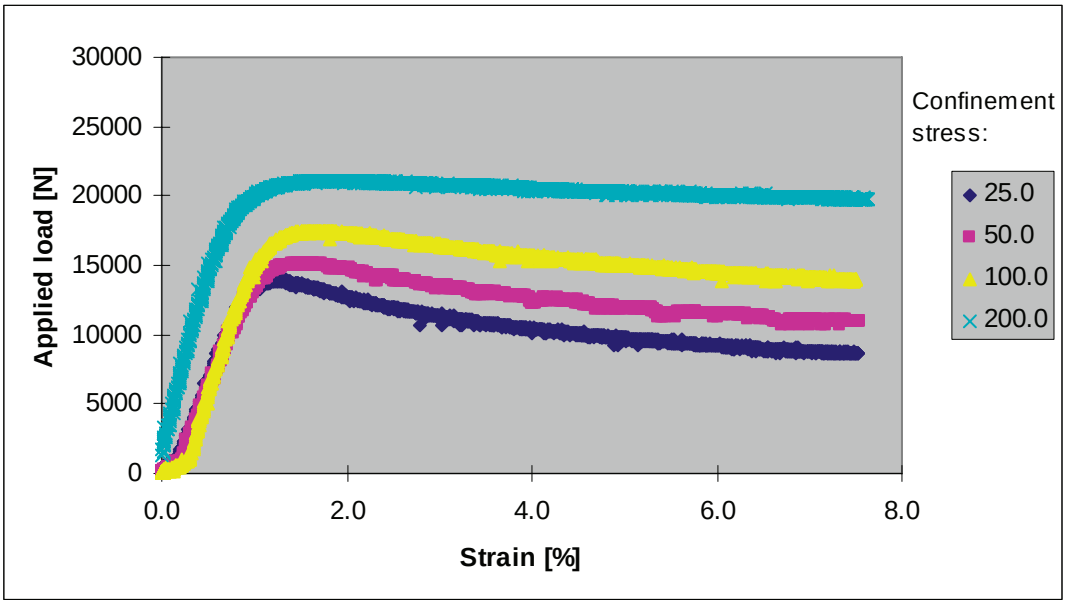
30000
25000
20000
15000
10000
5000
0
Applied load [N]
0.0
2.0
4.0
6.0
8.0
Strain [%]
Confinement stress:
25.0
50.0
100.0
200.0

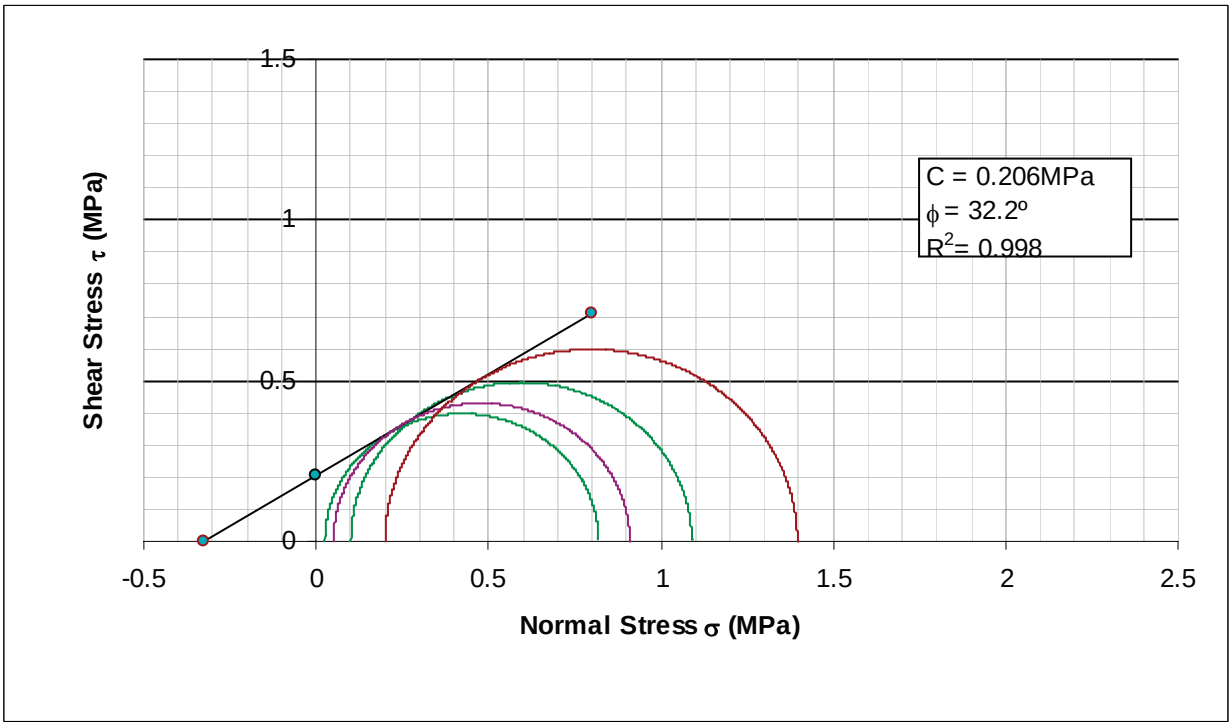
1.5
1
0.5
0
Shear Stress τ (MPa)
-0.5
0
0.5
1
1.5
2
2.5
Normal Stress σ (MPa)
C = 0.206MPa
ϕ = 32.2º
R2= 0.998

**Mix C-75C-0**

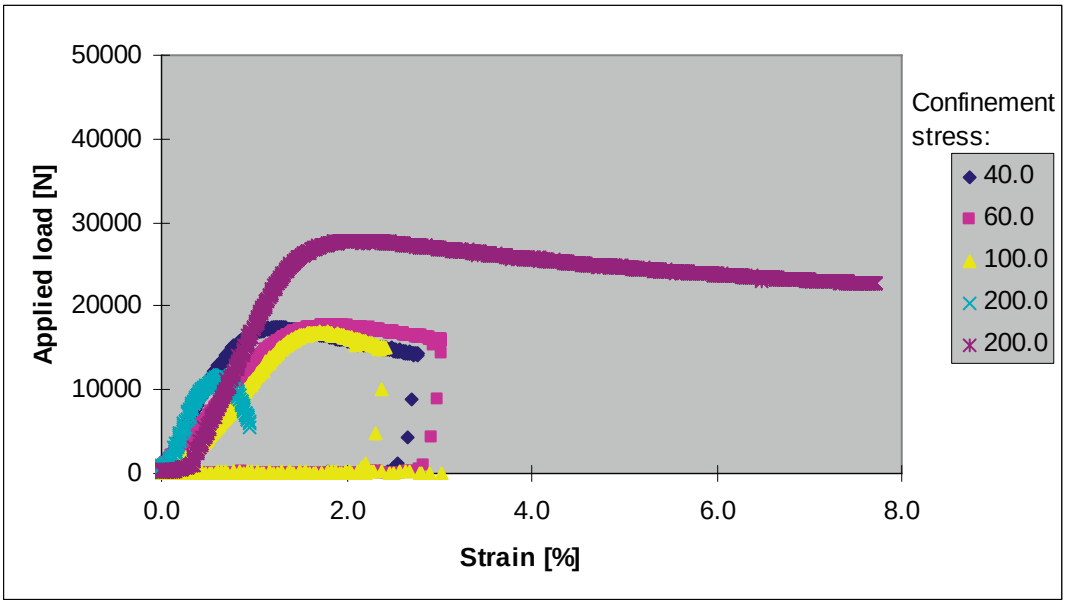


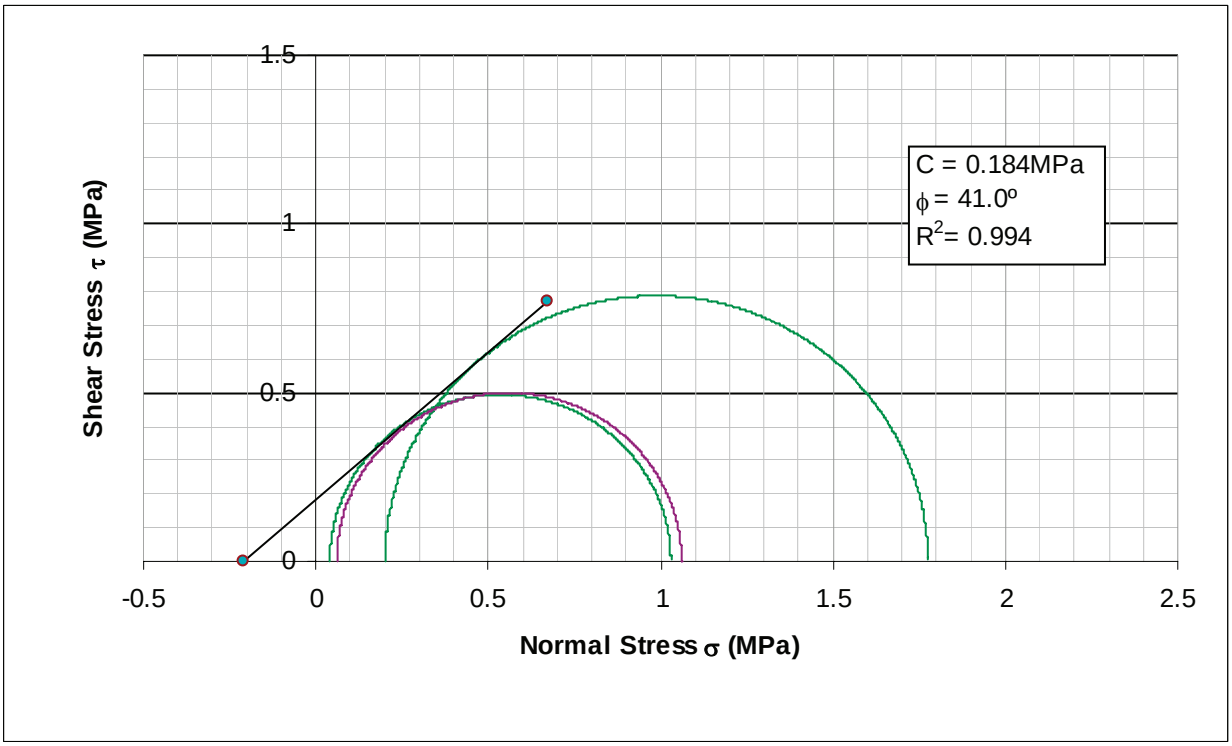


**Mohr-Coulomb diagram excluding circle for $\sigma_3$ = 100 kPa**

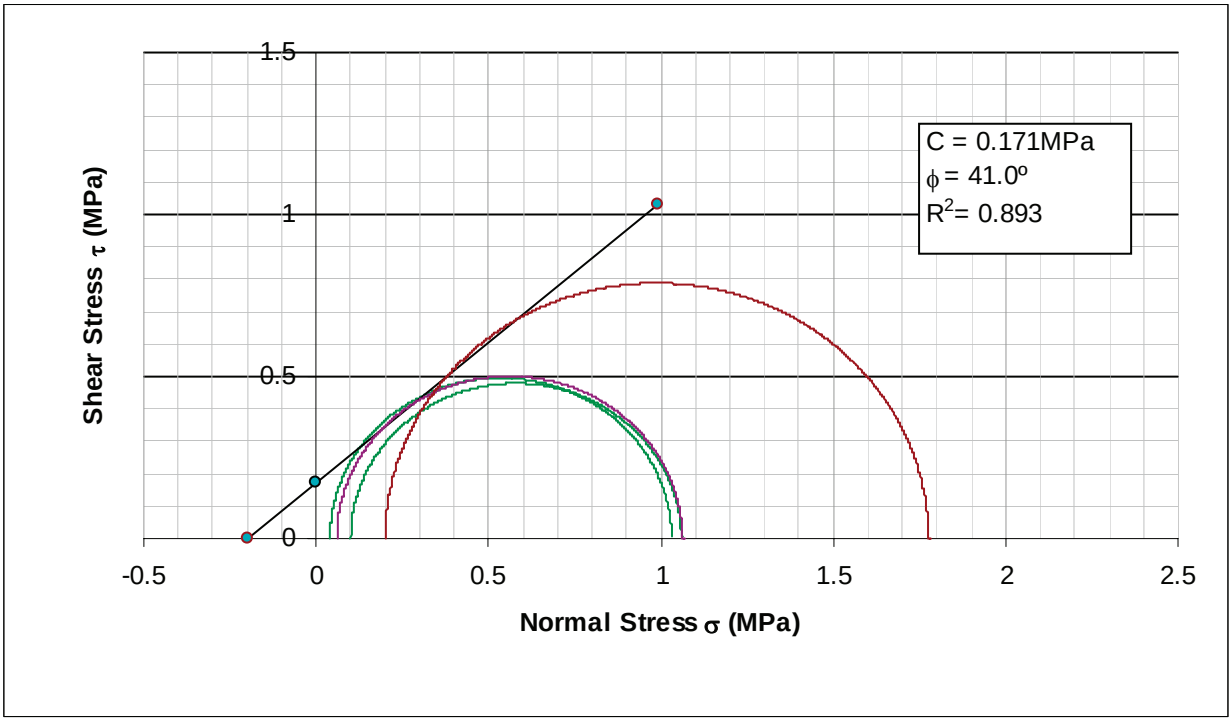


**Mohr-Coulomb diagram including circle for $\sigma_3$ = 100 kPa**

**Mix C-75C-1**

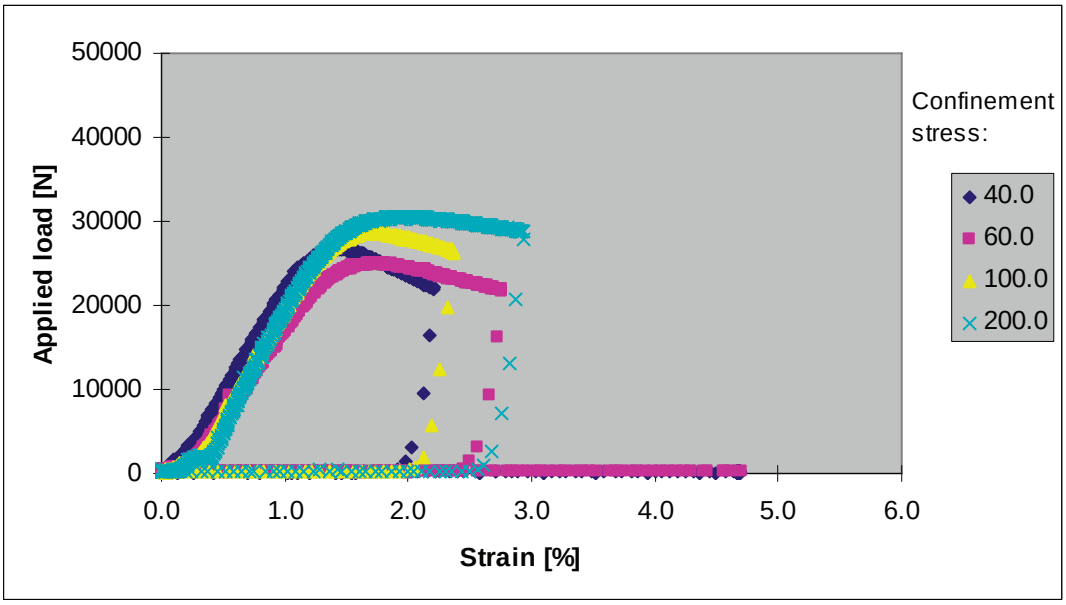


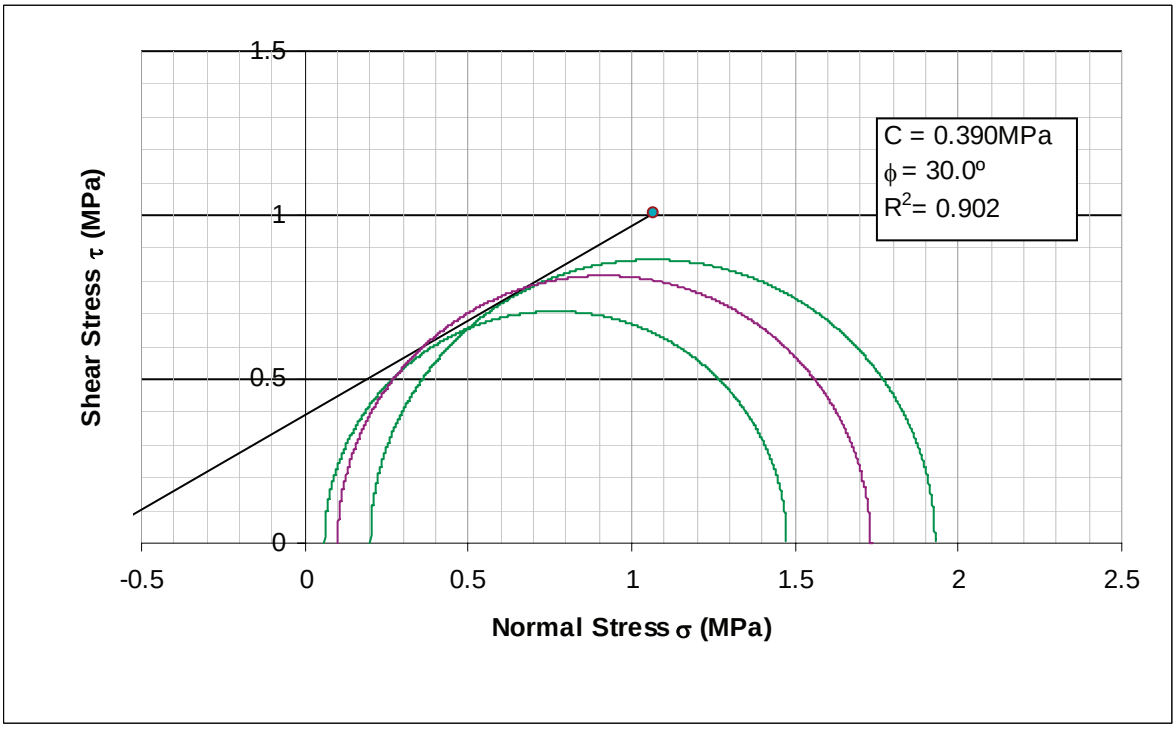


**Mohr-Coulomb diagram excluding circle for $\sigma_3$ = 40 kPa**

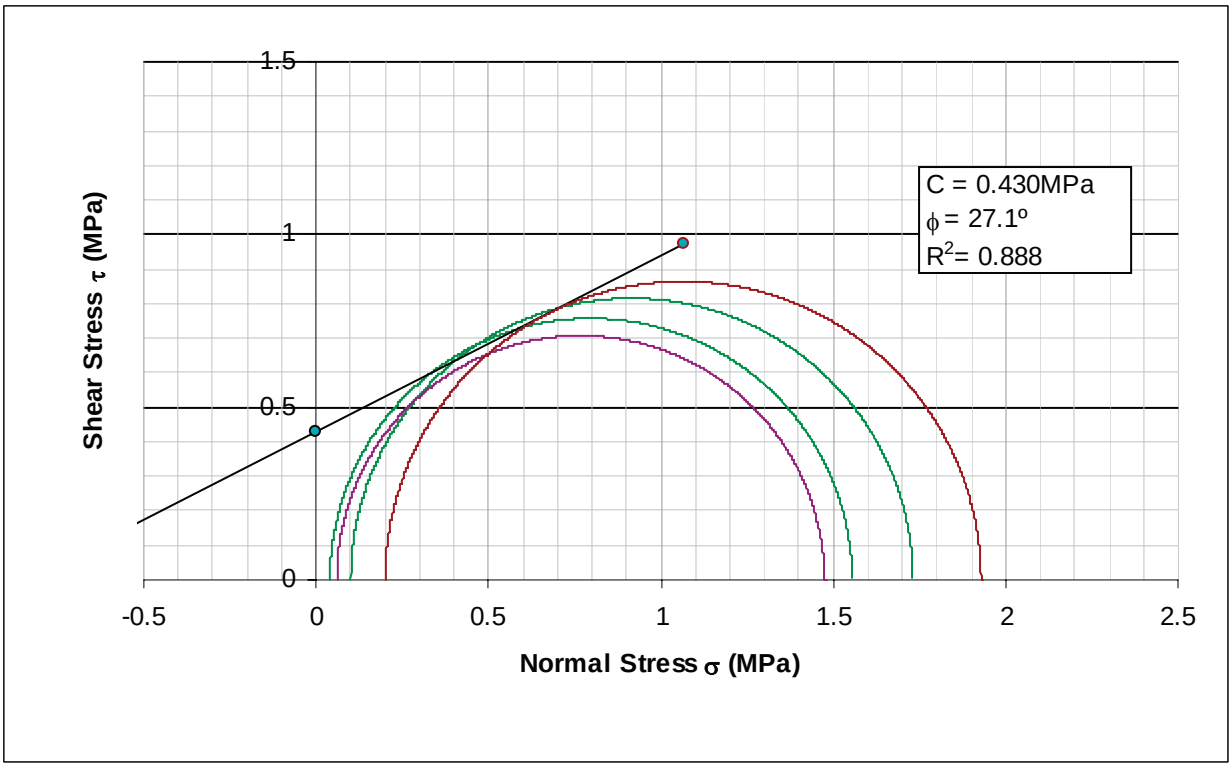


**Mohr-Coulomb diagram including circle for $\sigma_3$ = 40 kPa**

**Mix C-75M-0**

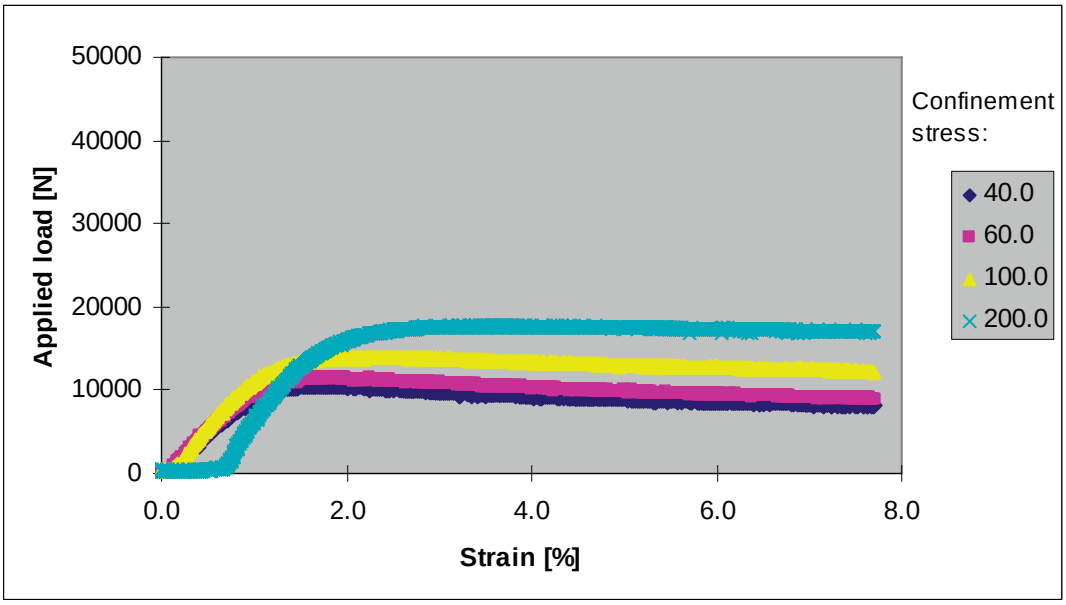
50000
40000
30000
20000
10000
0
Applied load [N]
0.0
2.0
4.0
6.0
8.0
Strain [%]
Confinement stress:
40.0
60.0
100.0
200.0

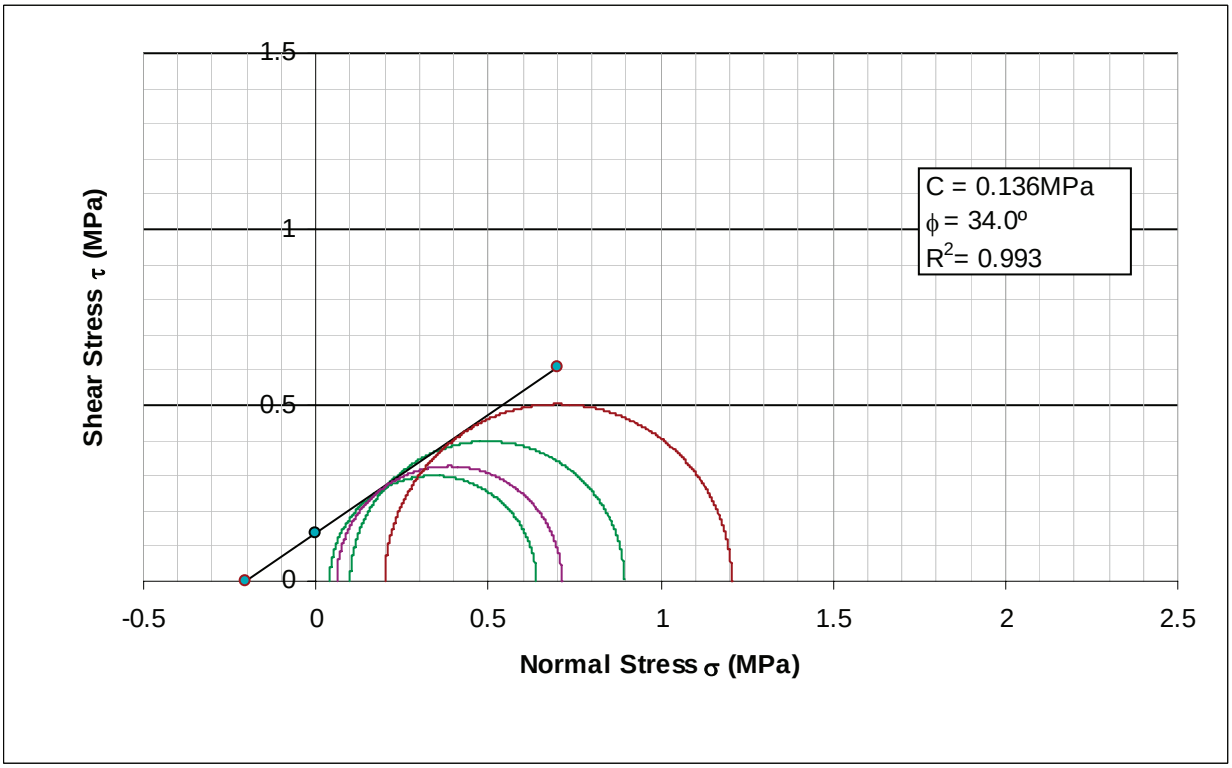
1.5
1
0.5
0
Shear Stress τ (MPa)
-0.5
0
0.5
1
1.5
2
2.5
Normal Stress σ (MPa)
C = 0.136MPa
ϕ = 34.0º
R2= 0.993

This page is left blank intentionally.

# APPENDIX F: RESILIENT MODULUS TESTING RESULTS

Table 1: Resilient modulus test results for the 75C-0 mixes (2 Hz and 25ºC)

| Confinement pressure $\sigma_3$ [kPa] | Target deviator stress ratio[1] $\sigma_d/\sigma_{d,f}$ [-] | Resilient modulus per binder type [MPa] | | | | | | |
|---|---|---|---|---|---|---|---|---|
| | | A | | B | | | C | |
| | | test a | test b | test a[2] | test b[3] | test c[4] | test a | test c[4] |
| 25 | 0.10 | 480 | 604 | 965 | 545 | 940 | 1127 | 594 |
| | 0.15 | 578 | 664 | 1027 | 528 | 954 | 866 | 782 |
| | 0.20 | 664 | 656 | 1107 | 594 | 1030 | 753 | 778 |
| | 0.25 | 675 | 707 | 1144 | 625 | 1027 | 808 | 850 |
| | 0.30 | 729 | 729 | 1145 | 639 | 1035 | 792 | 855 |
| 50 | 0.15 | 713 | 682 | | 590 | 1133 | 920 | 693 |
| | 0.20 | 723 | 716 | | 625 | 1142 | 822 | 721 |
| | 0.25 | 758 | 743 | 941 | 666 | 1093 | 876 | 801 |
| | 0.30 | 784 | 819 | 1145 | 687 | 1075 | 836 | 848 |
| | 0.35 | 703 | 833 | 841 | 693 | 1050 | 822 | 811 |
| 100 | 0.15 | 867 | 795 | 557 | 648 | 1345 | 865 | 669 |
| | 0.20 | 846 | 795 | 618 | 676 | 1334 | 887 | 786 |
| | 0.25 | 838 | 889 | 639 | 715 | 1305 | 837 | 814 |
| | 0.30 | 843 | 874 | 658 | 744 | 1377 | 874 | 837 |
| | 0.35 | 853 | 919 | 669 | 597 | 1369 | 884 | 880 |
| | 0.40 | - | - | - | - | - | 874 | - |
| 200 | 0.15 | 920 | 1007 | 710 | 749 | 1633 | 969 | |
| | 0.20 | 962 | 1044 | 720 | 708 | 1743 | 946 | |
| | 0.25 | 961 | 962 | 743 | - | 1776 | 903 | |
| | 0.30 | 969 | 1021 | 747 | - | 1734 | 953 | |
| | 0.40 | 994 | 1035 | 785 | - | 1885 | 915 | |
| | 0.50 | 1008 | 1036 | 820 | - | 1839 | 929 | |
| | 0.60 | - | 1090 | - | - | - | - | |

Note 1 : The difference between the target stress ratio and actually applied stress ratio did not exceed an absolute value of 0.02.

2 : Not all LVDT's recorded properly during this test. This resulted in incorrect average axial deformation and lower resilient moduli at 100 and 200 kPa confinement pressure.

3 : The specimen deformed to such an extent after the first two tests at the 200 kPa confinement pressure, that the LVDT's went out of range.

4 : Tests c are repeat tests carried out at the end of testing phase of this study. The specimen during test C-75C-0-b had failed during conditioning.

Table 2: Resilient modulus test results for the 75C-1 mixes (2 Hz and 25ºC)

| Confinement pressure $\sigma_3$ [kPa] | Target deviator stress ratio[1] $\sigma_d/\sigma_{d,f}$ [-] | Resilient modulus per binder type [MPa] | | | | | |
|---|---|---|---|---|---|---|---|
| | | A | | B | | C | |
| | | test a | test b | test a | test b | test a | test b |
| 25 | 0.10 | 826 | 935 | - | 1166 | 1495 | 1213 |
| | 0.15 | 720 | 1007 | 1222 | 1211 | 1304 | 1214 |
| | 0.20 | 844 | 1141 | 1321 | 1434 | 1447 | 1184 |
| | 0.25 | 1086 | 1218 | 1271 | 1363 | 1499 | 1352 |
| | 0.30 | 1116 | 1287 | 1394 | 1457 | 1460 | 1297 |
| 50 | 0.15 | 1036 | 1076 | 1202 | 1239 | 1532 | 1140 |
| | 0.20 | 1107 | 1182 | 1204 | 1512 | 1476 | 1256 |
| | 0.25 | 1172 | 1112 | 1337 | 1459 | 1450 | 1306 |
| | 0.30 | 1073 | 1328 | 1363 | 1507 | 1523 | 1382 |
| | 0.35 | 1244 | 1362 | 1362 | 1542 | 1501 | 1309 |
| 100 | 0.15 | 1091 | 1147 | 1253 | 1549 | 1554 | 1338 |
| | 0.20 | 1109 | 1319 | 1254 | 1505 | 1476 | 1309 |
| | 0.25 | 1274 | 1319 | 1293 | 1580 | 1581 | 1307 |
| | 0.30 | 1265 | 1382 | 1377 | 1617 | 1523 | 1379 |
| | 0.35 | 1142 | 1447 | 1368 | 1584 | 1501 | 1389 |
| | 0.40 | - | - | - | 1607 | - | - |
| 200 | 0.15 | 1317 | 1498 | 1269 | 1485 | 1797 | 1593 |
| | 0.20 | 1400 | 1465 | 1269 | 1702 | 1859 | 1614 |
| | 0.25 | 1397 | 1540 | 1264 | 1638 | 1733 | 1400 |
| | 0.30 | 1435 | 1538 | 1332 | 1597 | 1570 | 1372 |
| | 0.40 | 1441 | 1590 | 1275 | 1663 | 1551 | 1432 |
| | 0.50 | - | 1562 | 1334 | 1714 | 1491 | 1305 |
| | 0.60 | - | 1569 | - | - | 1481 | 1254 |

Note 1 : The difference between the target stress ratio and actually applied stress ratio did not exceed an absolute value of 0.02.

Table 3: Resilient modulus test results for the 75M-0 mixes (2 Hz and 25ºC)

| Confinement pressure $\sigma_3$ [kPa] | Target deviator stress ratio[1] $\sigma_d/\sigma_{d,f}$ [-] | Resilient modulus per binder type [MPa] | | | | | |
|---|---|---|---|---|---|---|---|
| | | A | | B | | C | |
| | | test a | test b | test a | test b | test a | test b |
| 25 | 0.10 | 982 | 1366 | 987 | 1201 | 641 | 647 |
| | 0.15 | 1344 | 1455 | 1069 | 1044 | 989 | 914 |
| | 0.20 | 1113 | 1530 | 1309 | 688 | 1004 | 867 |
| | 0.25 | 981 | 1338 | 1097 | 582 | 1117 | 872 |
| | 0.30 | 885 | 1168 | 1025 | 417 | 1074 | 884 |
| 50 | 0.15 | 1309 | 1607 | 1249 | 1239 | 1404 | 971 |
| | 0.20 | 1188 | 1577 | 1237 | 931 | 1167 | 1036 |
| | 0.25 | 1034 | 1271 | 1150 | 815 | 1136 | 924 |
| | 0.30 | 935 | 1181 | 1096 | 791 | 1006 | 972 |
| | 0.35 | 903 | 1107 | 1001 | 525 | 947 | 950 |
| 100 | 0.15 | 1297 | 1568 | 1338 | 1251 | 1108 | 1075 |
| | 0.20 | 1140 | 981 | 1308 | 1091 | 1090 | 1076 |
| | 0.25 | 1015 | 1022 | 1073 | 1074 | 1075 | 962 |
| | 0.30 | 947 | 1027 | 1094 | 1049 | 1027 | 885 |
| | 0.35 | 954 | 1049 | 1000 | 1017 | 962 | 911 |
| | 0.40 | - | - | 1020 | - | 973 | 921 |
| 200 | 0.15 | 1210 | 1385 | 1120 | 1466 | 1195 | 821 |
| | 0.20 | 1115 | 1378 | 1120 | 1410 | 1015 | 995 |
| | 0.25 | 1123 | 1263 | 1026 | 1257 | 1140 | 981 |
| | 0.30 | 1050 | 1231 | 1032 | 1264 | 961 | 974 |
| | 0.40 | 1033 | 1138 | 997 | 1171 | 976 | 930 |
| | 0.50 | 1020 | 1117 | 1027 | 1251 | 877 | 935 |
| | 0.60 | - | 1040 | 1039 | 1314 | - | - |

Note 1 : The difference between the target stress ratio and actually applied stress ratio did not exceed an absolute value of 0.02.

**Mix A-75C-0-a**

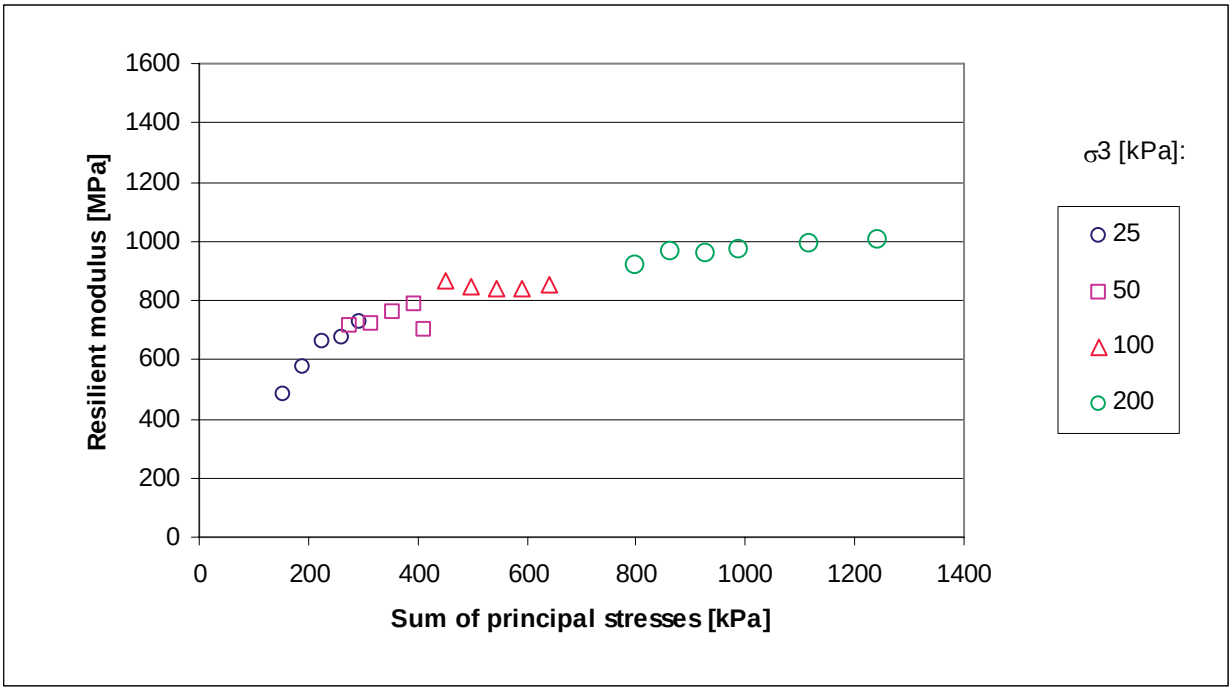
1600
1400
1200
1000
800
600
400
200
0
Resilient modulus [MPa]
0
200
400
600
800
1000
1200
1400
Sum of principal stresses [kPa]
σ3 [kPa]:
25
50
100
200

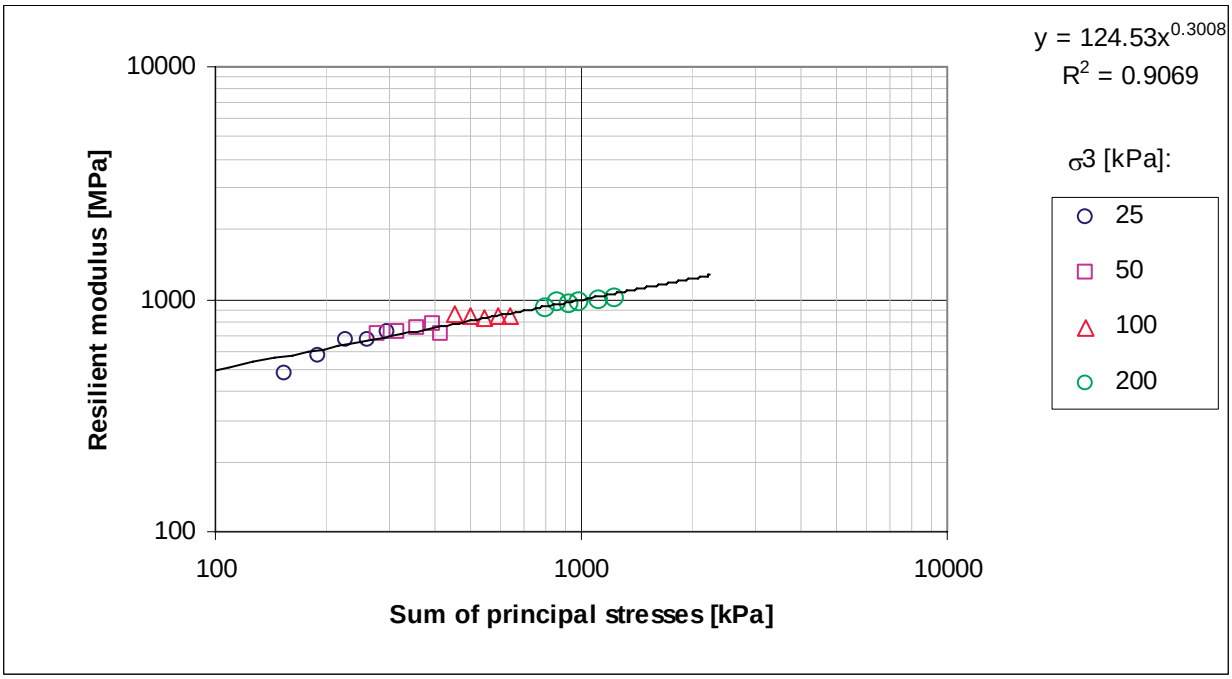
y = 124.53x^0.3008
R2 = 0.9069
10000
1000
100
Resilient modulus [MPa]
100
1000
10000
Sum of principal stresses [kPa]
σ3 [kPa]:
25
50
100
200

**Mix A-75C-0-b**

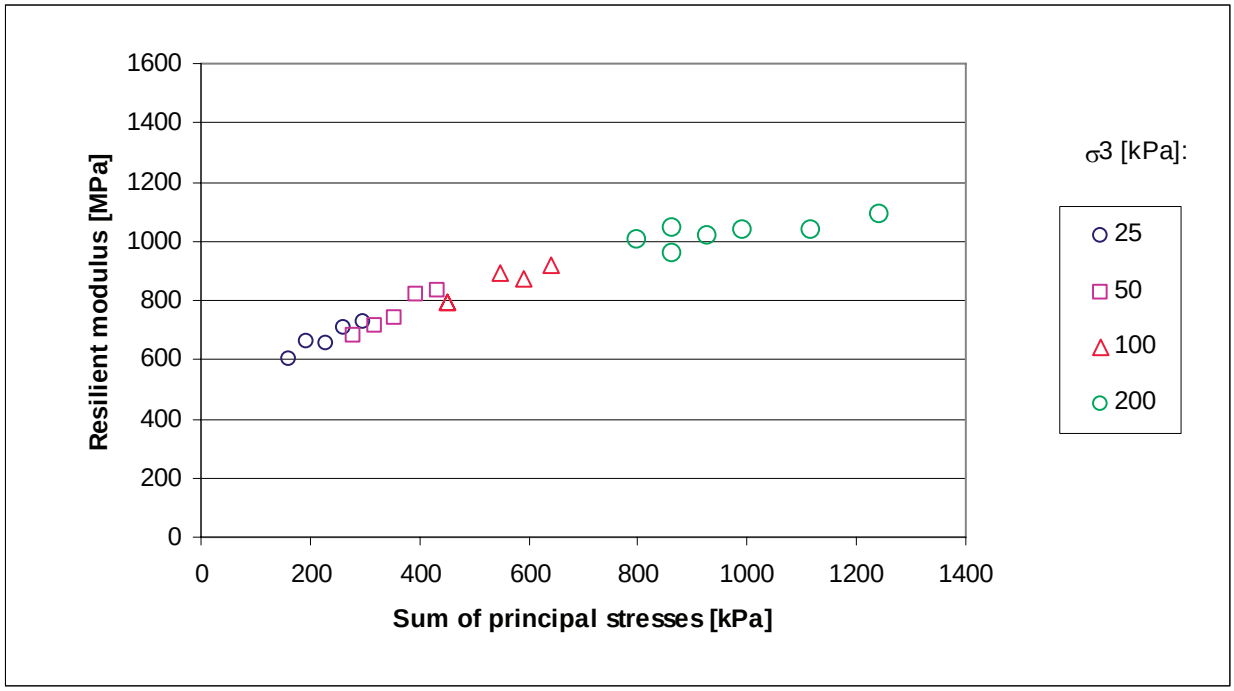
1600
1400
1200
1000
800
600
400
200
0
0
200
400
600
800
1000
1200
1400
Resilient modulus [MPa]
Sum of principal stresses [kPa]
σ3 [kPa]:
25
50
100
200

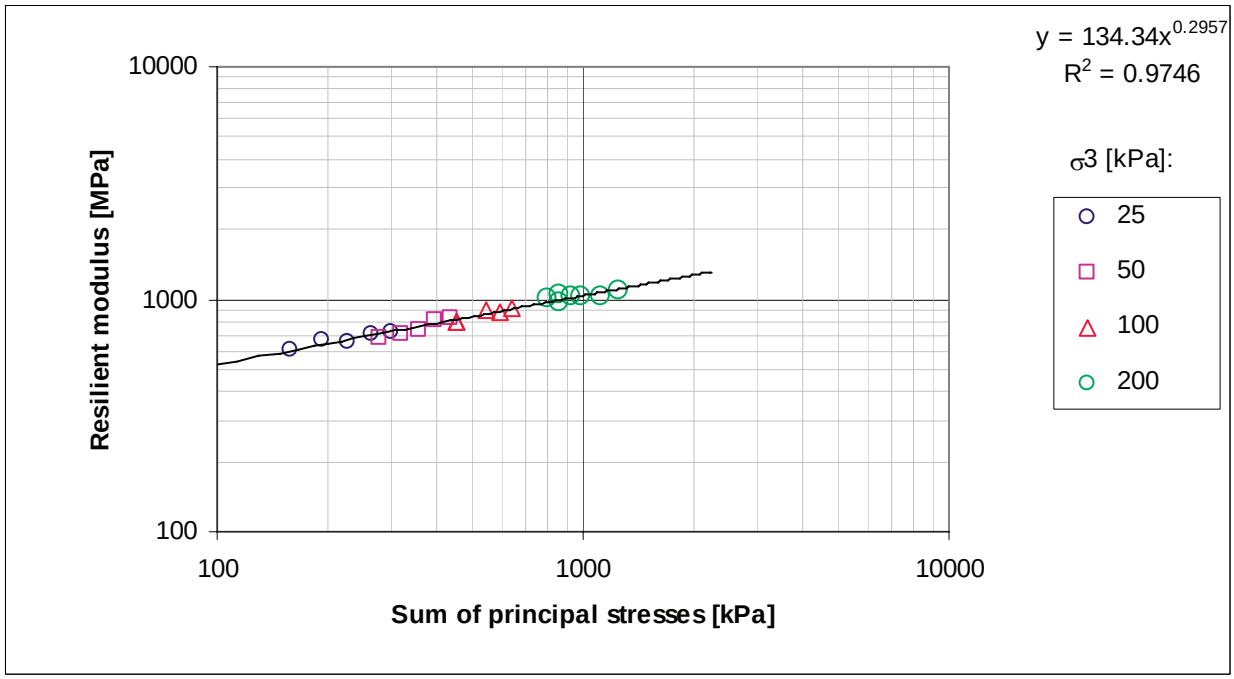
y = 134.34x^0.2957
R2 = 0.9746
10000
1000
100
100
1000
10000
Resilient modulus [MPa]
Sum of principal stresses [kPa]
σ3 [kPa]:
25
50
100
200

**Mix A-75C-1-a**

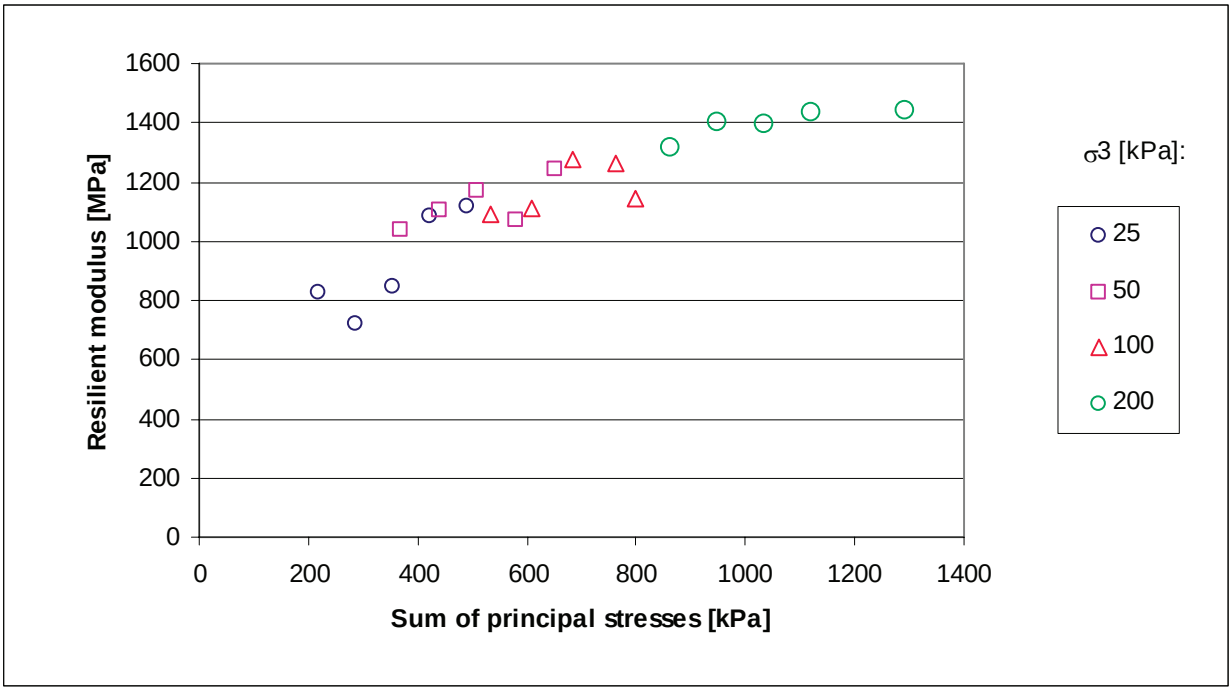
1600
1400
1200
1000
800
600
400
200
0
0
200
400
600
800
1000
1200
1400
Resilient modulus [MPa]
Sum of principal stresses [kPa]
σ3 [kPa]:
25
50
100
200

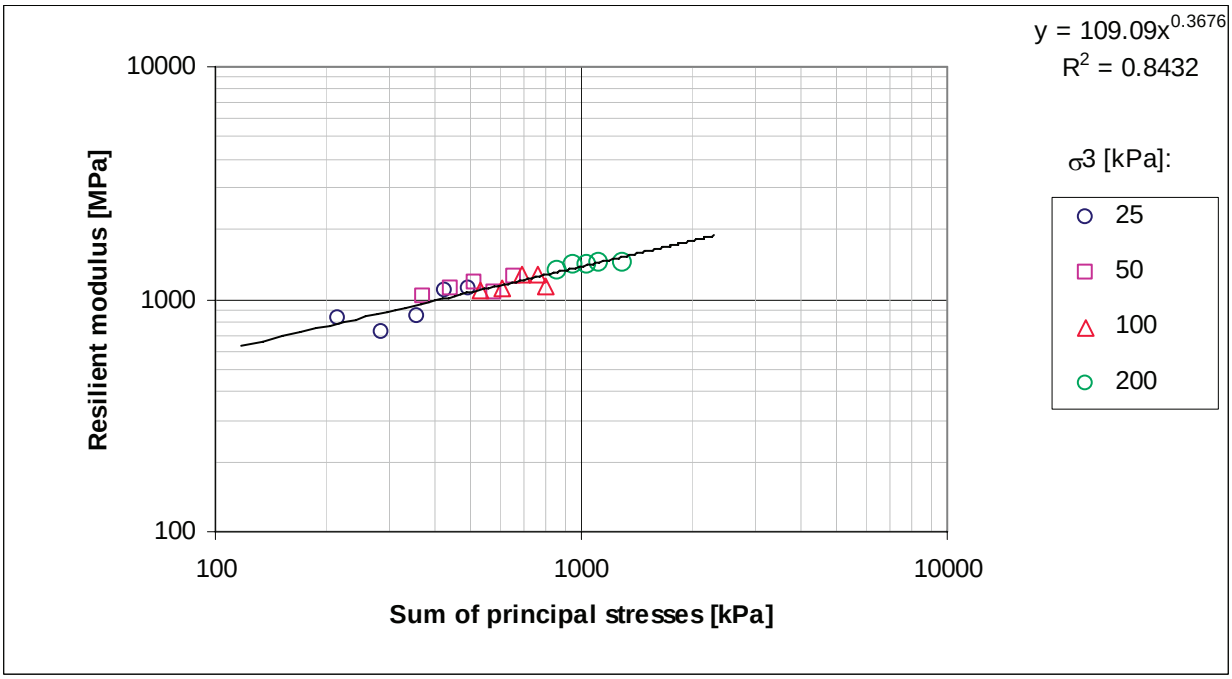
y = 109.09x^0.3676
R2 = 0.8432
10000
1000
100
100
1000
10000
Resilient modulus [MPa]
Sum of principal stresses [kPa]
σ3 [kPa]:
25
50
100
200

**Mix A-75C-1-b**

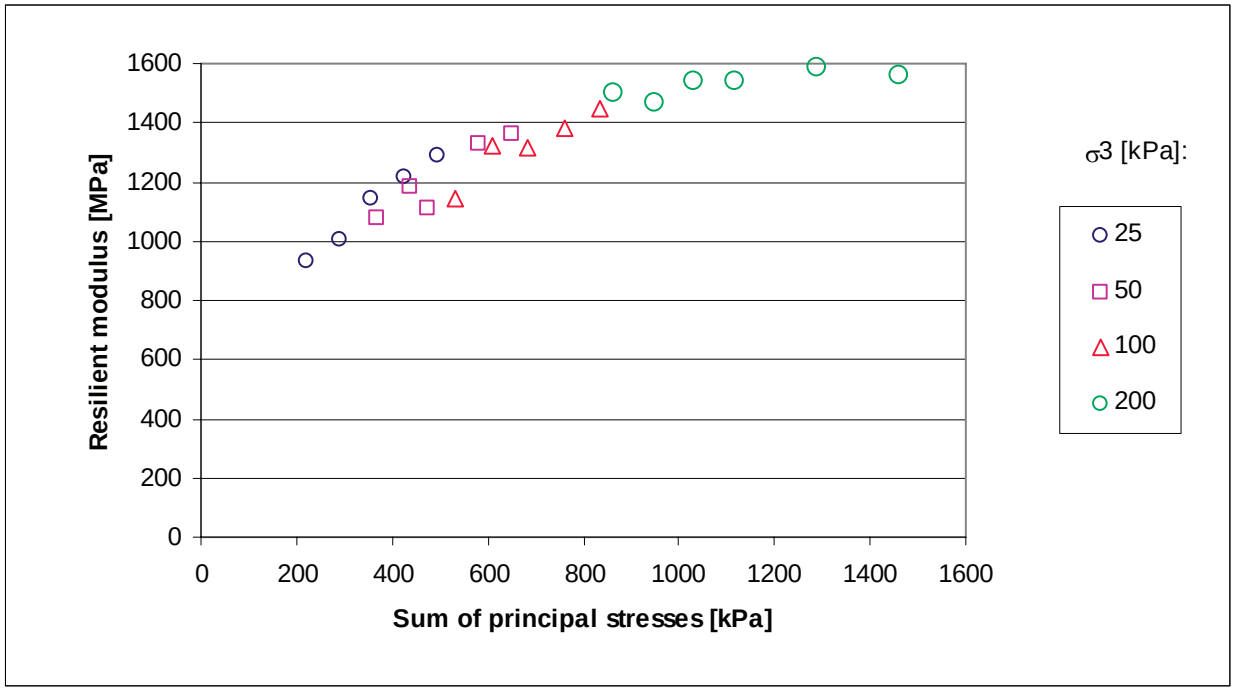
Resilient modulus [MPa]
1600
1400
1200
1000
800
600
400
200
0
0
200
400
600
800
1000
1200
1400
1600
Sum of principal stresses [kPa]
σ3 [kPa]:
25
50
100
200

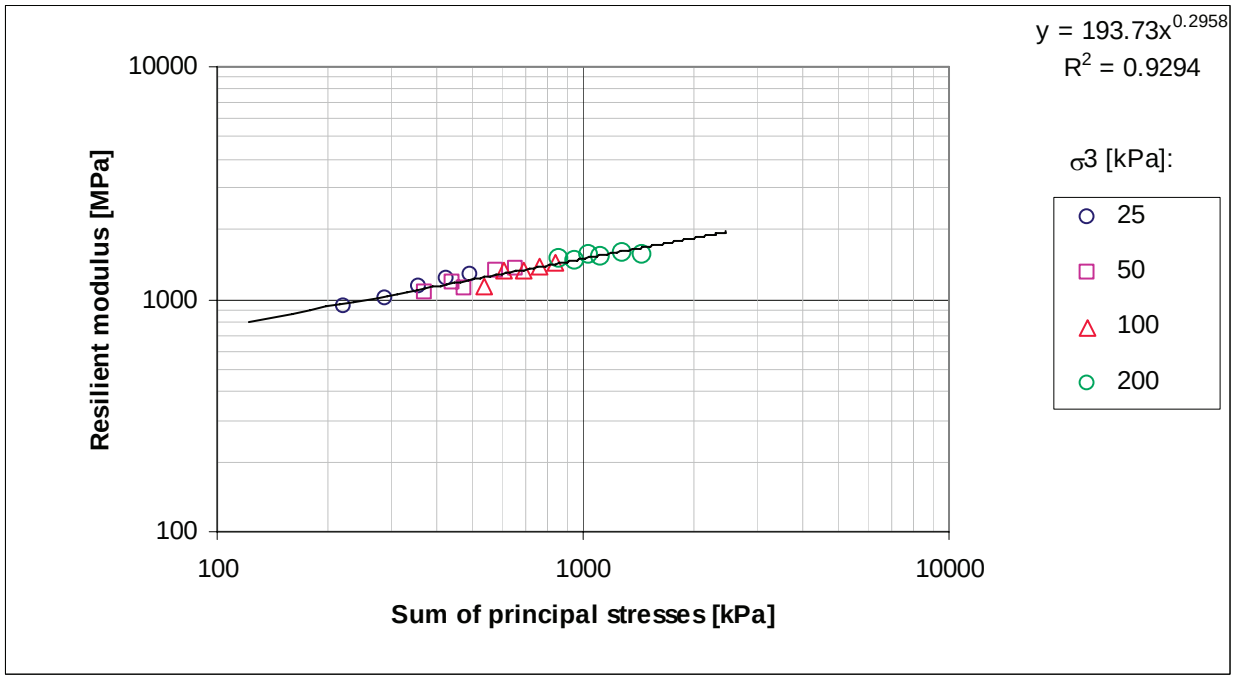
y = 193.73x^0.2958
R2 = 0.9294
Resilient modulus [MPa]
10000
1000
100
100
1000
10000
Sum of principal stresses [kPa]
σ3 [kPa]:
25
50
100
200

**Mix A-75M-0-a**

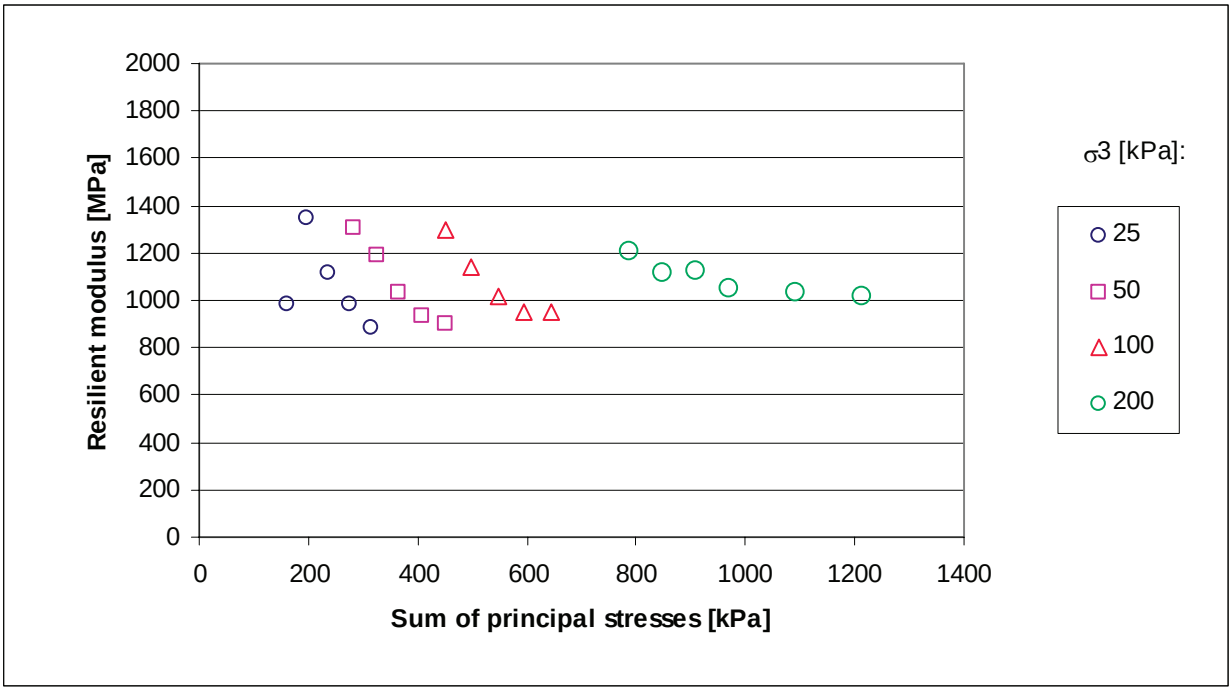
Resilient modulus [MPa]
2000
1800
1600
1400
1200
1000
800
600
400
200
0
0
200
400
600
800
1000
1200
1400
Sum of principal stresses [kPa]
σ3 [kPa]:
25
50
100
200

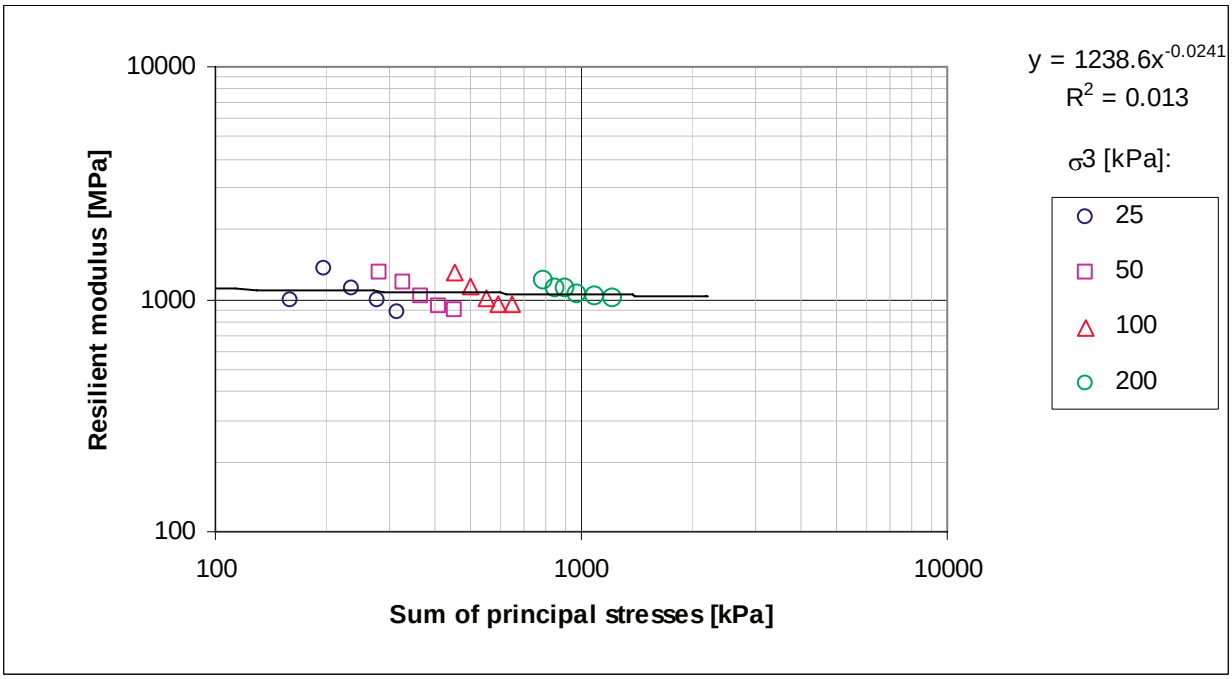
Resilient modulus [MPa]
10000
1000
100
100
1000
10000
Sum of principal stresses [kPa]
y = 1238.6x-0.0241
R2 = 0.013
σ3 [kPa]:
25
50
100
200

**Mix A-75M-0-b**

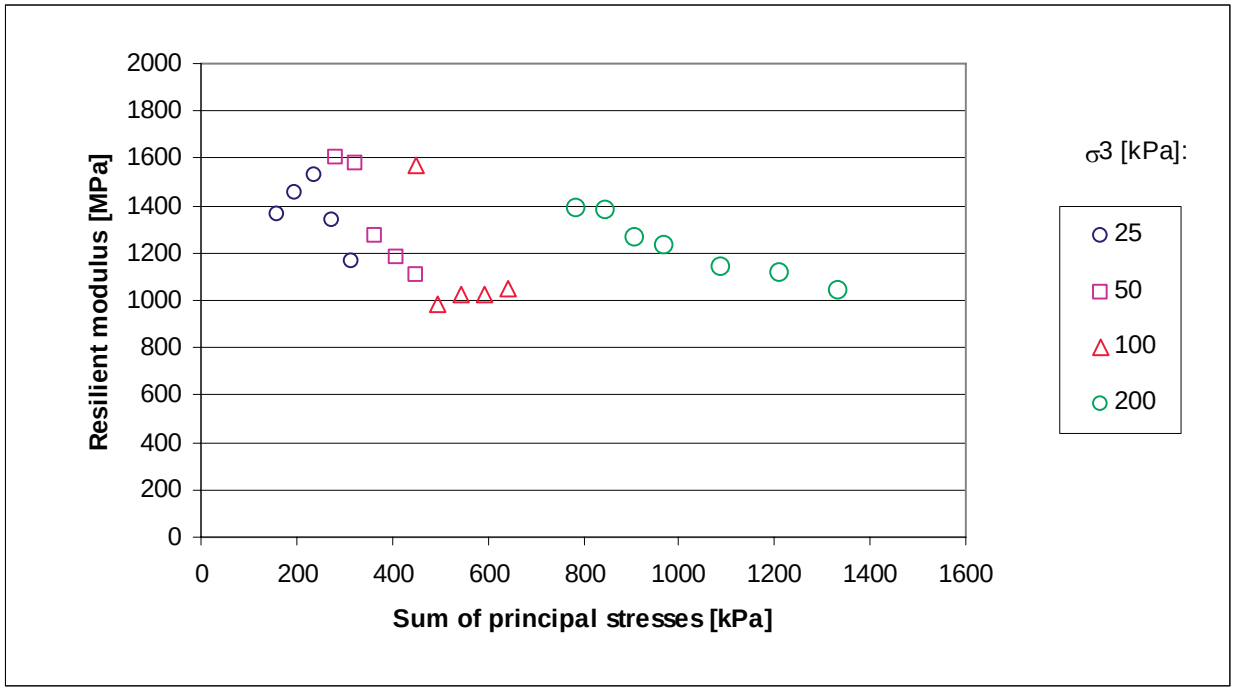
Resilient modulus [MPa]
2000
1800
1600
1400
1200
1000
800
600
400
200
0
0
200
400
600
800
1000
1200
1400
1600
Sum of principal stresses [kPa]
σ3 [kPa]:
25
50
100
200

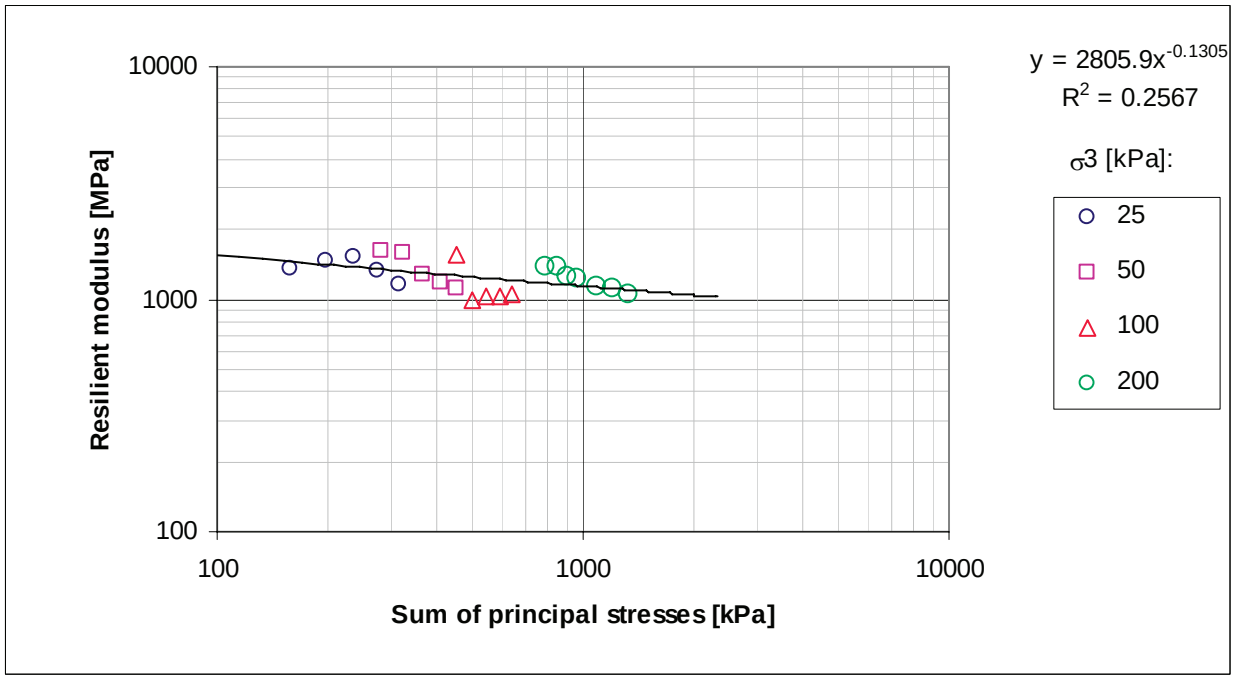
Resilient modulus [MPa]
10000
1000
100
100
1000
10000
Sum of principal stresses [kPa]
y = 2805.9x-0.1305
R2 = 0.2567
σ3 [kPa]:
25
50
100
200

**Mix B-75C-0-a**

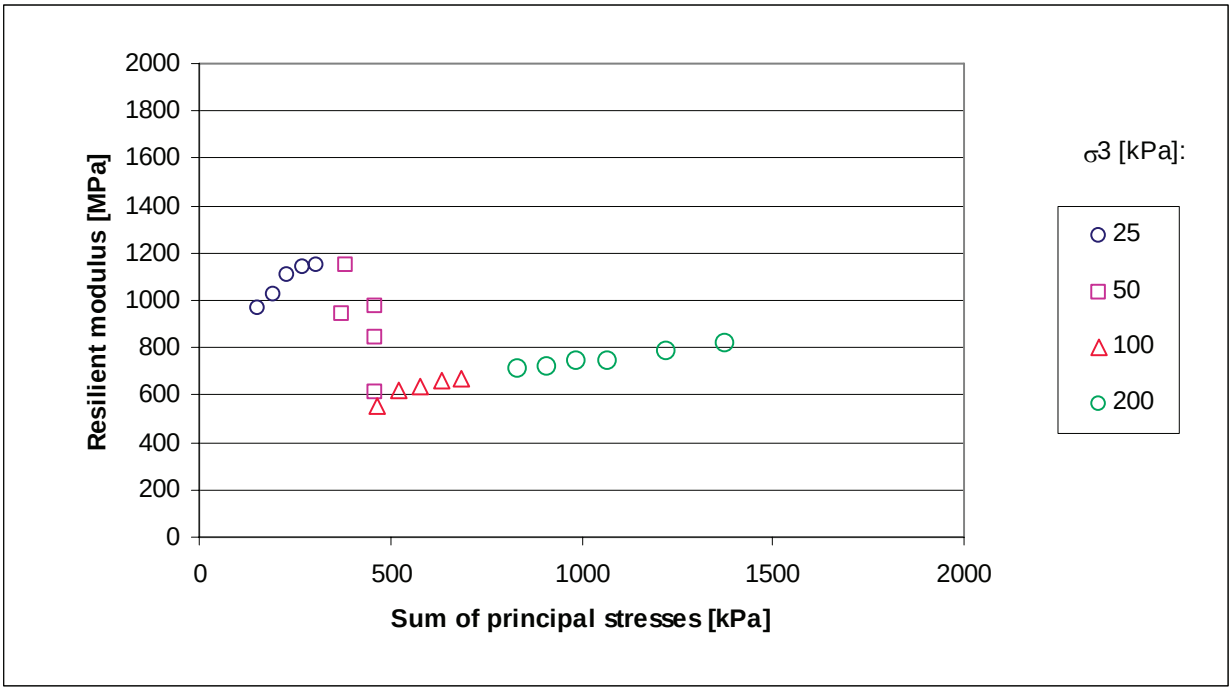
Resilient modulus [MPa]
2000
1800
1600
1400
1200
1000
800
600
400
200
0
0
500
1000
1500
2000
Sum of principal stresses [kPa]
σ3 [kPa]:
25
50
100
200

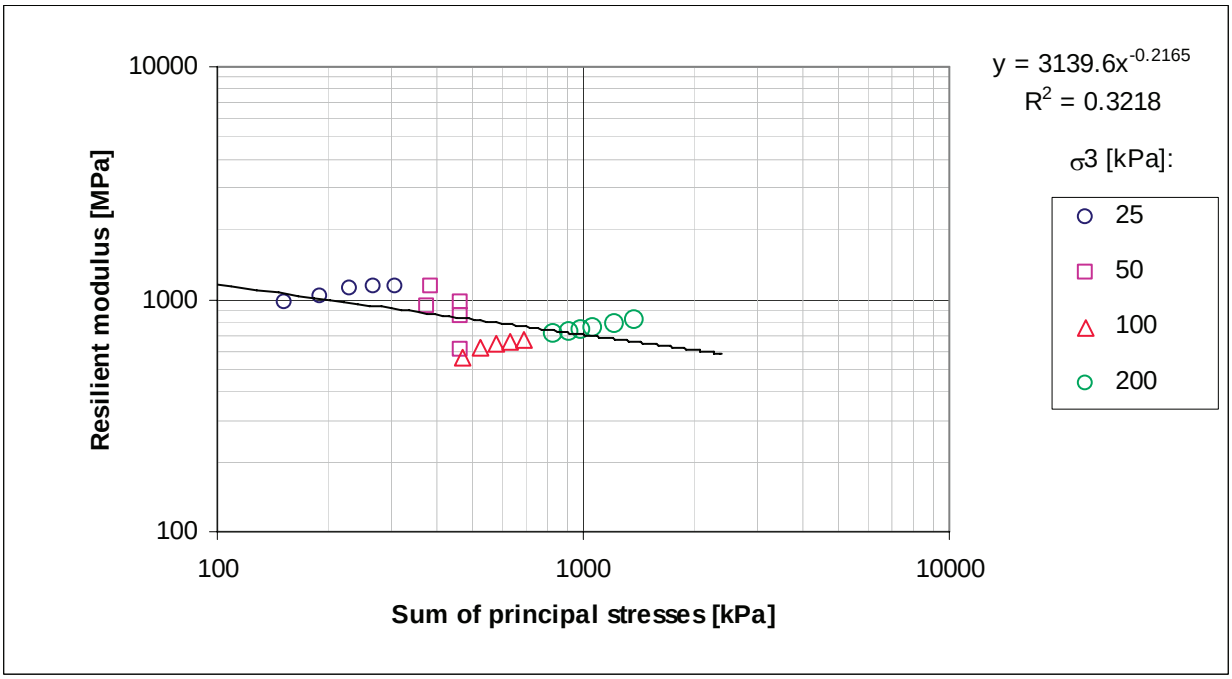
y = 3139.6x-0.2165
R2 = 0.3218
Resilient modulus [MPa]
10000
1000
100
100
1000
10000
Sum of principal stresses [kPa]
σ3 [kPa]:
25
50
100
200

**Mix B-75C-0-b**

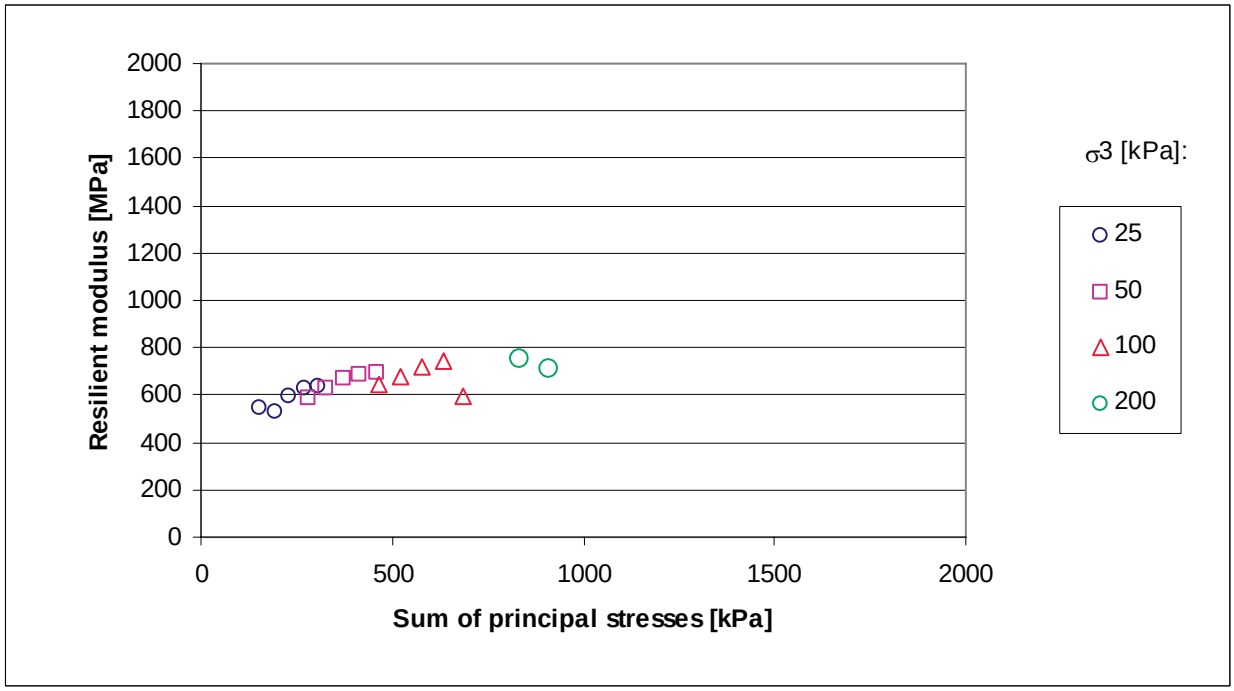
Resilient modulus [MPa]
2000
1800
1600
1400
1200
1000
800
600
400
200
0
0
500
1000
1500
2000
Sum of principal stresses [kPa]
σ3 [kPa]:
25
50
100
200

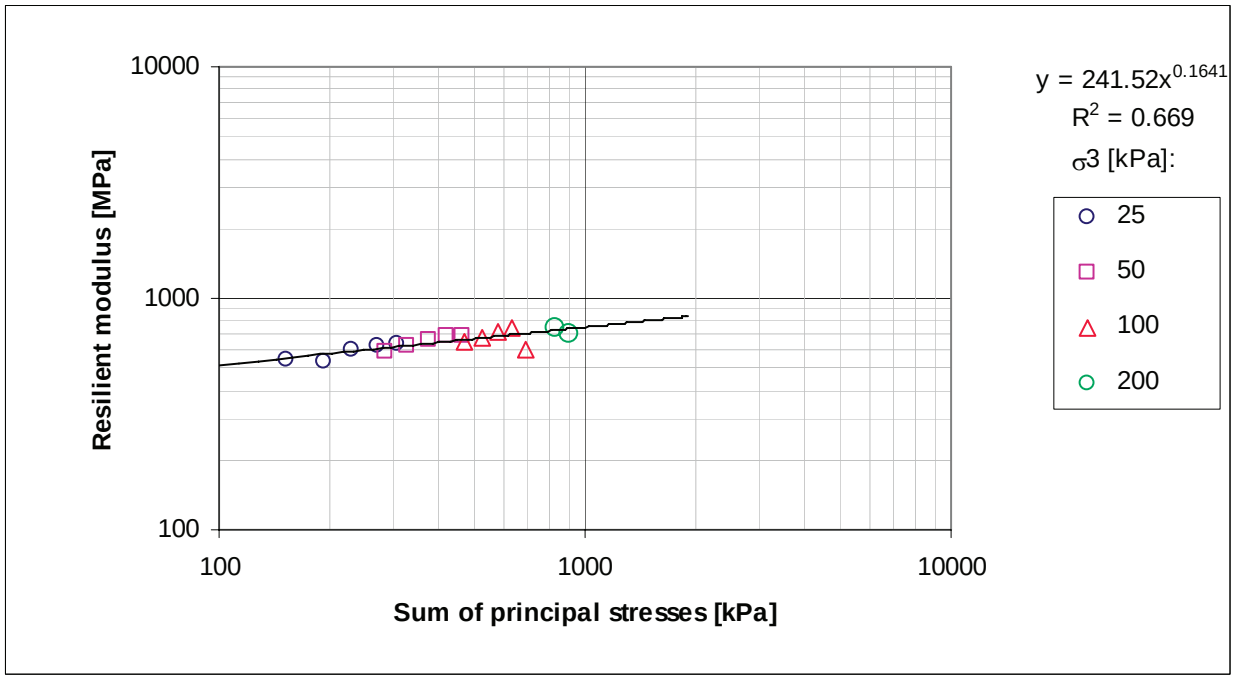
Resilient modulus [MPa]
10000
1000
100
100
1000
10000
Sum of principal stresses [kPa]
y = 241.52x^0.1641
R2 = 0.669
σ3 [kPa]:
25
50
100
200

**Mix B-75C-0-c**

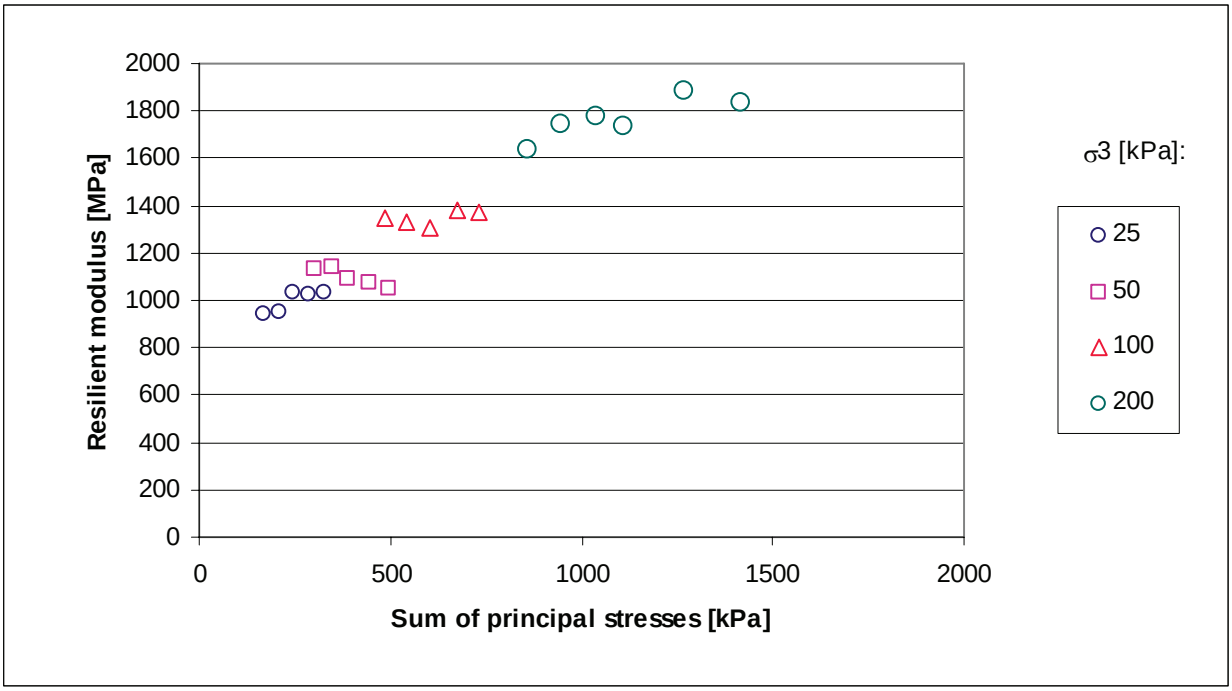
Resilient modulus [MPa]
2000
1800
1600
1400
1200
1000
800
600
400
200
0
0
500
1000
1500
2000
Sum of principal stresses [kPa]
σ3 [kPa]:
25
50
100
200

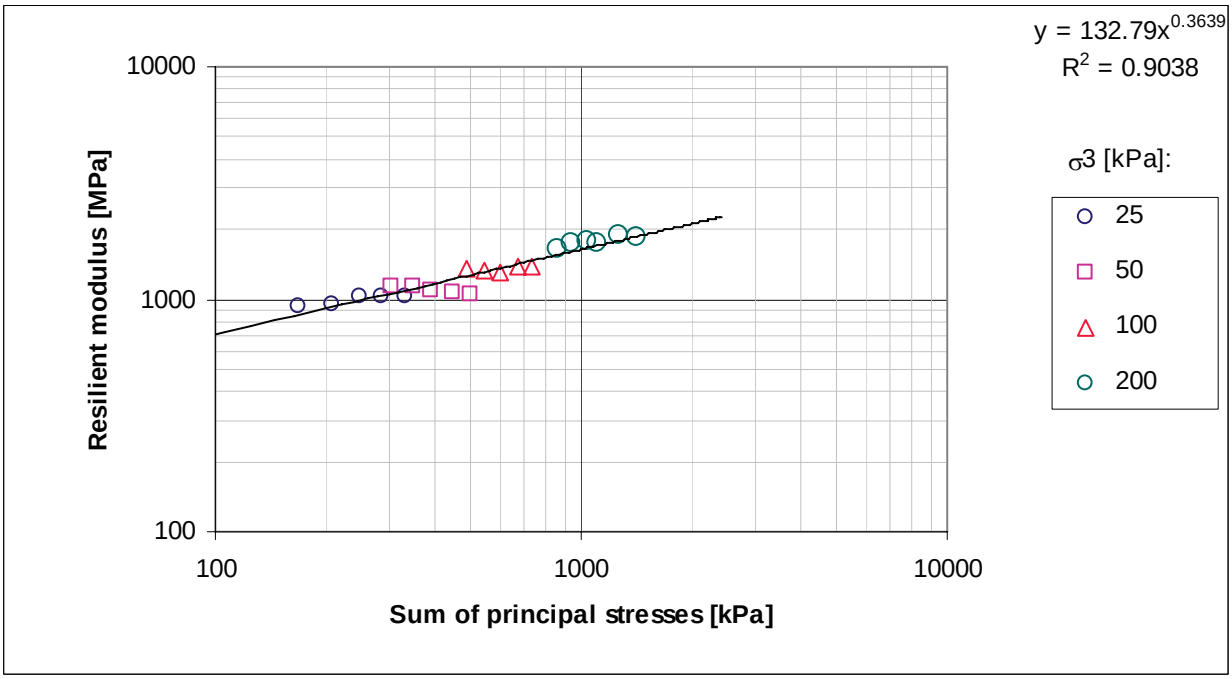
y = 132.79x^0.3639
R2 = 0.9038
Resilient modulus [MPa]
10000
1000
100
100
1000
10000
Sum of principal stresses [kPa]
σ3 [kPa]:
25
50
100
200

**Mix B-75C-1-a**

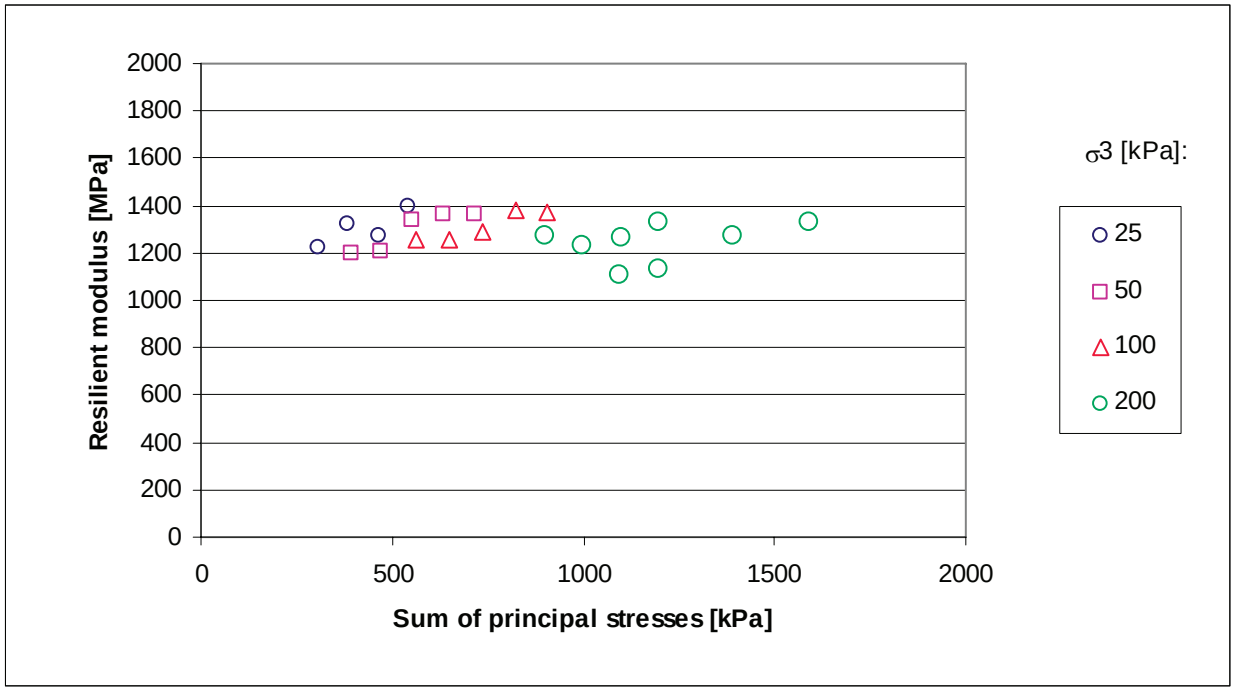
Resilient modulus [MPa]
2000
1800
1600
1400
1200
1000
800
600
400
200
0
0
500
1000
1500
2000
Sum of principal stresses [kPa]
σ3 [kPa]:
25
50
100
200

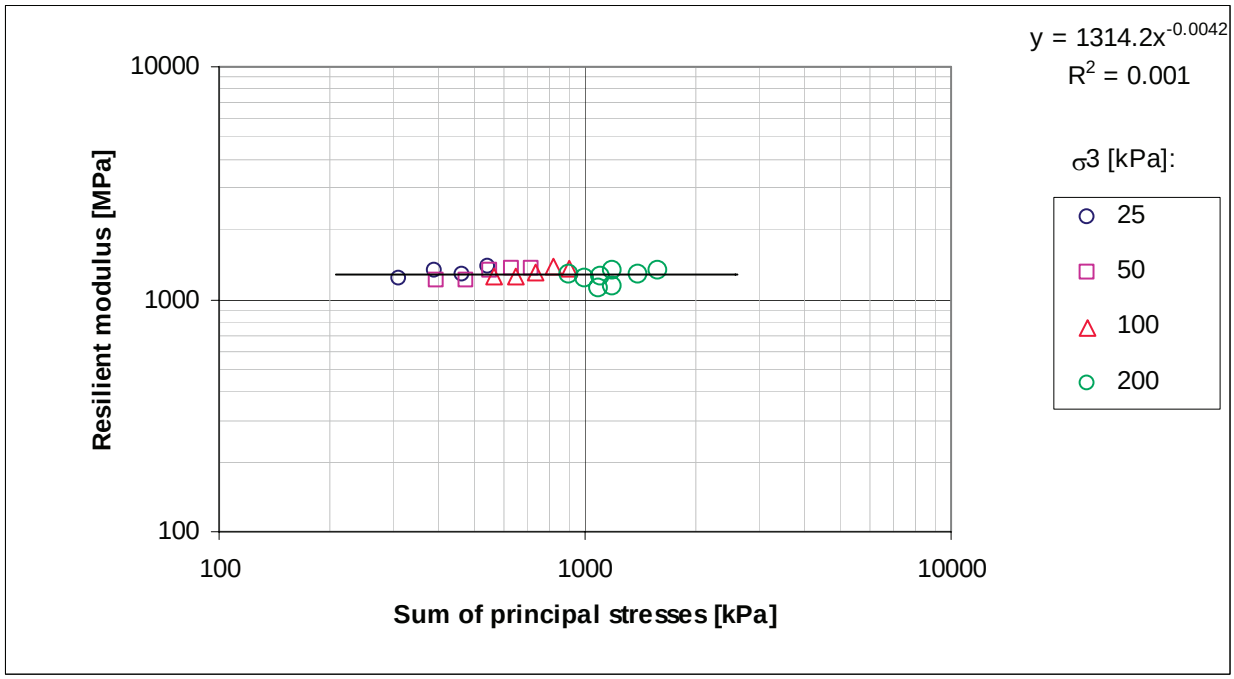
y = 1314.2x-0.0042
R2 = 0.001
Resilient modulus [MPa]
10000
1000
100
100
1000
10000
Sum of principal stresses [kPa]
σ3 [kPa]:
25
50
100
200

**Mix B-75C-1-b**

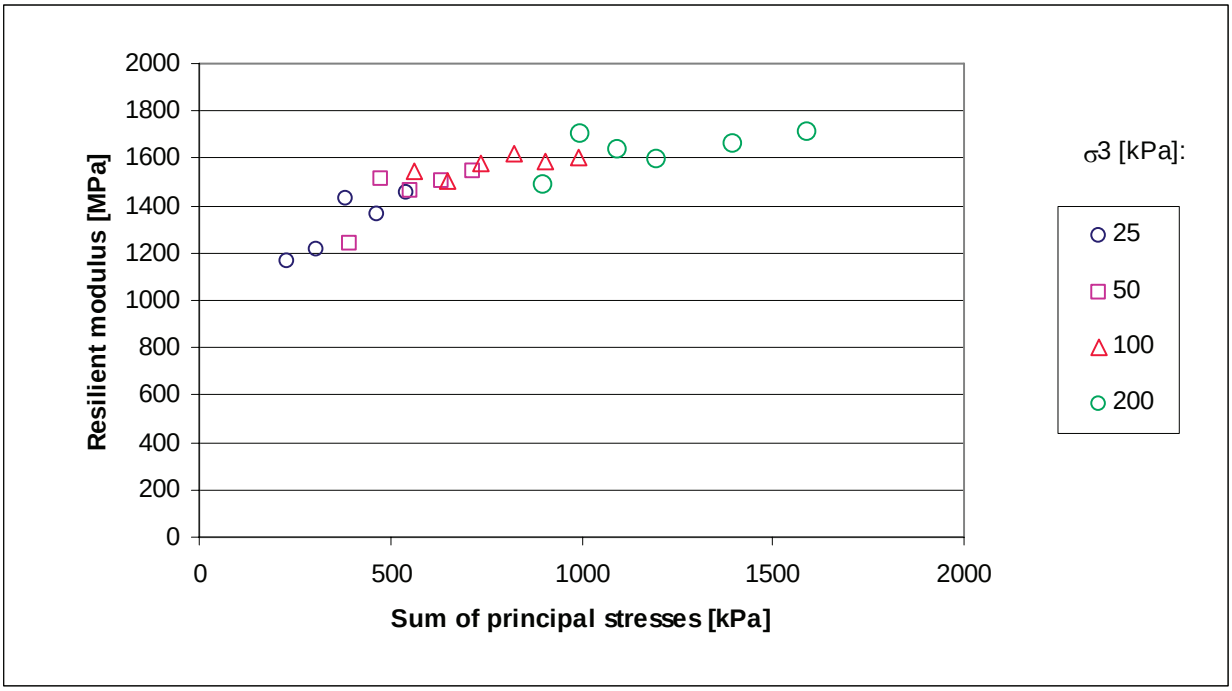
Resilient modulus [MPa]
2000
1800
1600
1400
1200
1000
800
600
400
200
0
0
500
1000
1500
2000
Sum of principal stresses [kPa]
σ3 [kPa]:
25
50
100
200

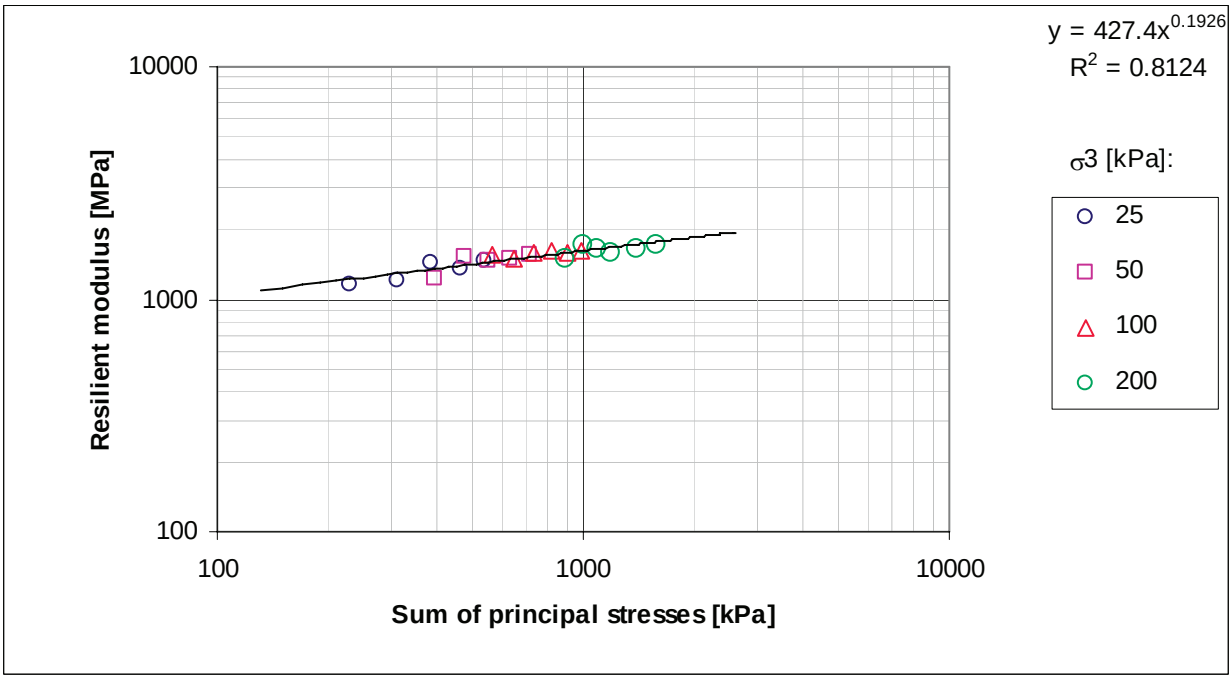
y = 427.4x^0.1926
R2 = 0.8124
Resilient modulus [MPa]
10000
1000
100
100
1000
10000
Sum of principal stresses [kPa]
σ3 [kPa]:
25
50
100
200

**Mix B-75M-0-a**

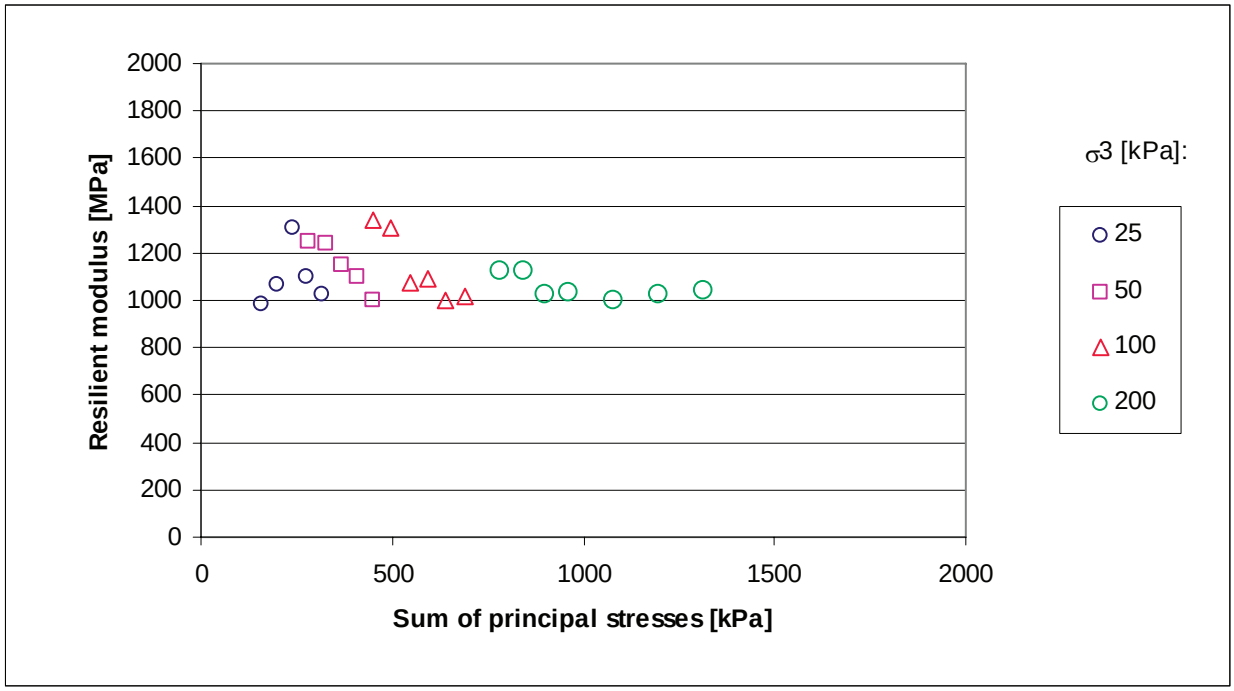
Resilient modulus [MPa]
2000
1800
1600
1400
1200
1000
800
600
400
200
0
0
500
1000
1500
2000
Sum of principal stresses [kPa]
σ3 [kPa]:
25
50
100
200

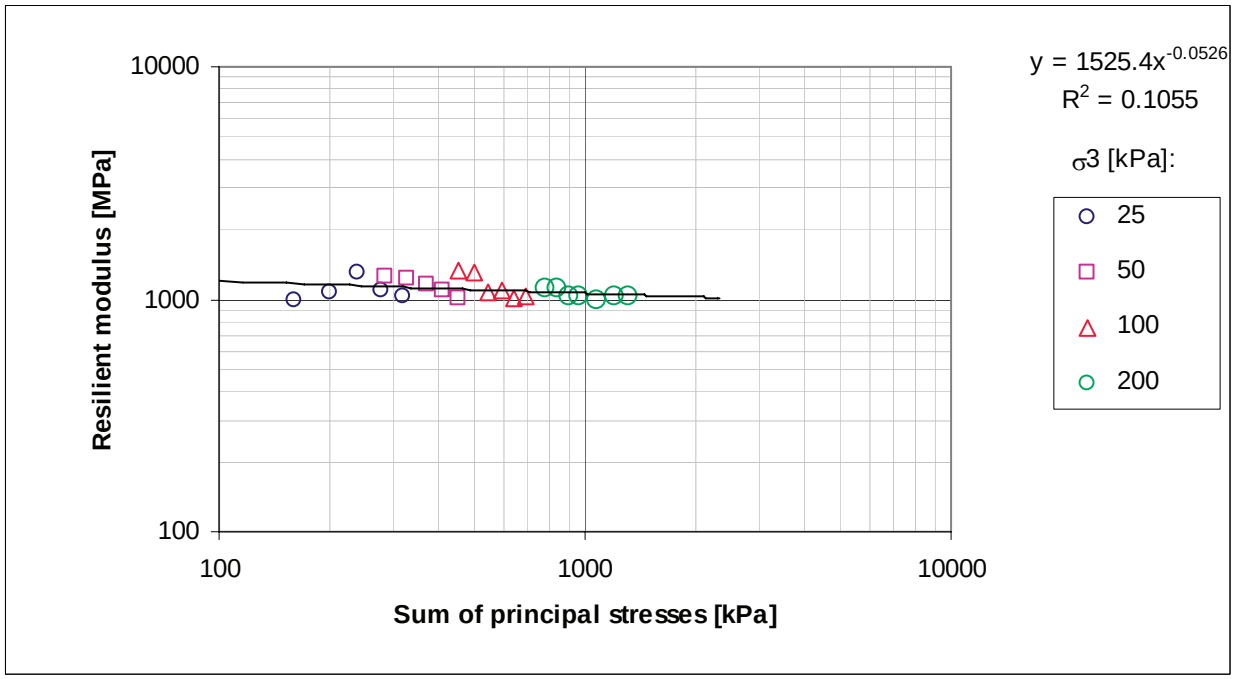
Resilient modulus [MPa]
10000
1000
100
100
1000
10000
Sum of principal stresses [kPa]
y = 1525.4x-0.0526
R2 = 0.1055
σ3 [kPa]:
25
50
100
200

**Mix B-75M-0-b**

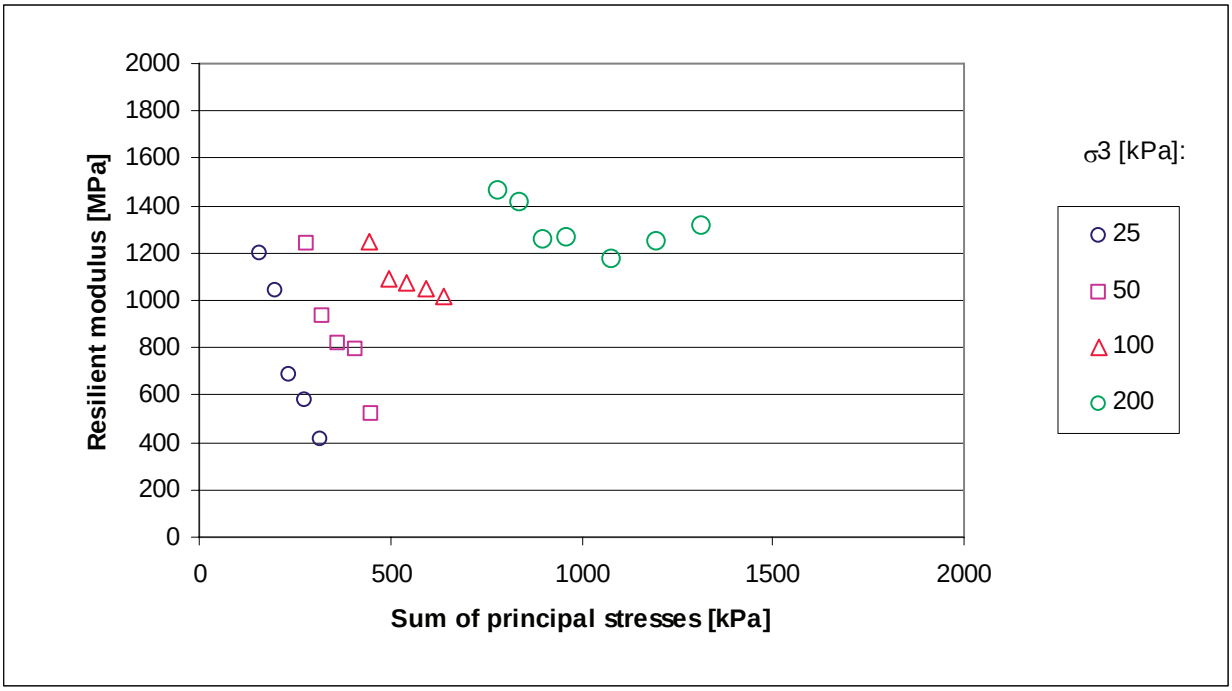
2000
1800
1600
1400
1200
1000
800
600
400
200
0
Resilient modulus [MPa]
0
500
1000
1500
2000
Sum of principal stresses [kPa]
σ3 [kPa]:
25
50
100
200

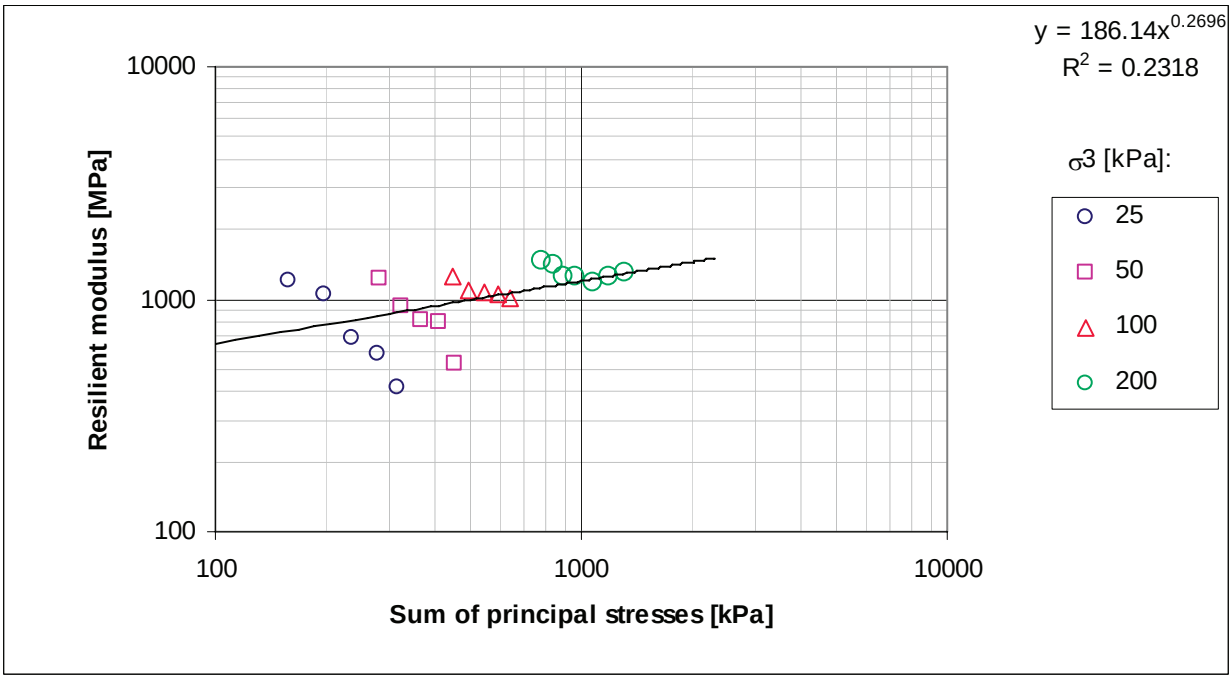
y = 186.14x^0.2696
R2 = 0.2318
10000
1000
100
Resilient modulus [MPa]
100
1000
10000
Sum of principal stresses [kPa]
σ3 [kPa]:
25
50
100
200

**Mix C-75C-0-a**

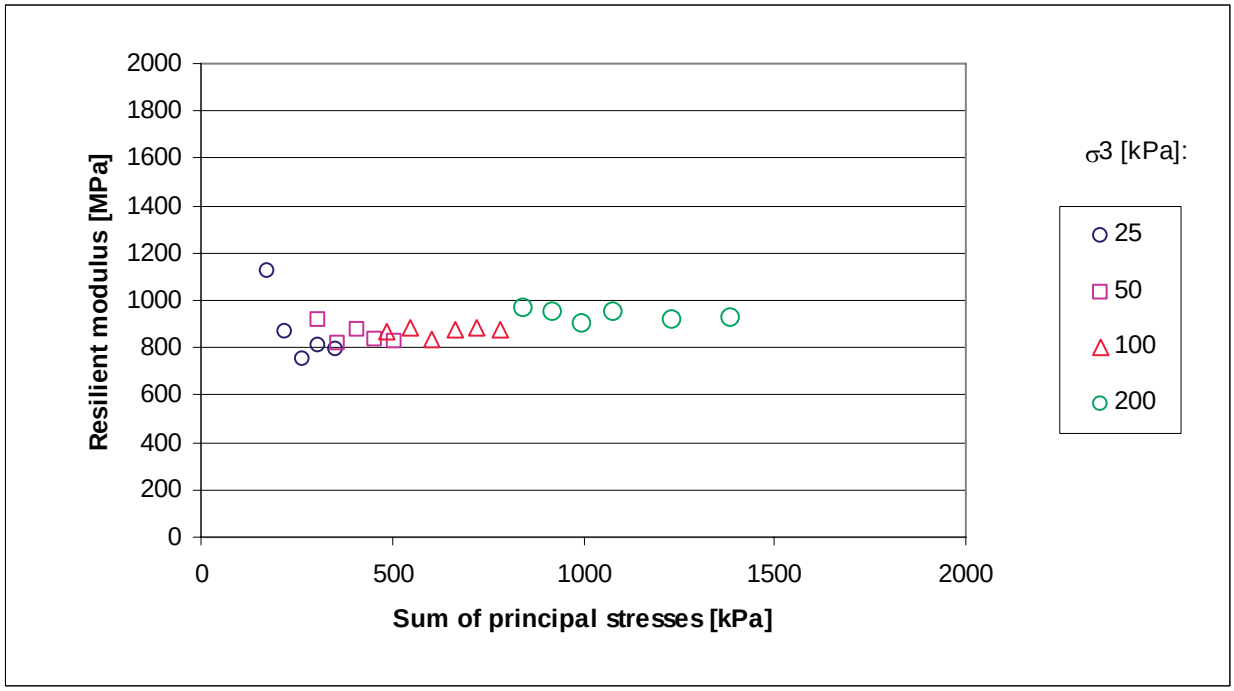


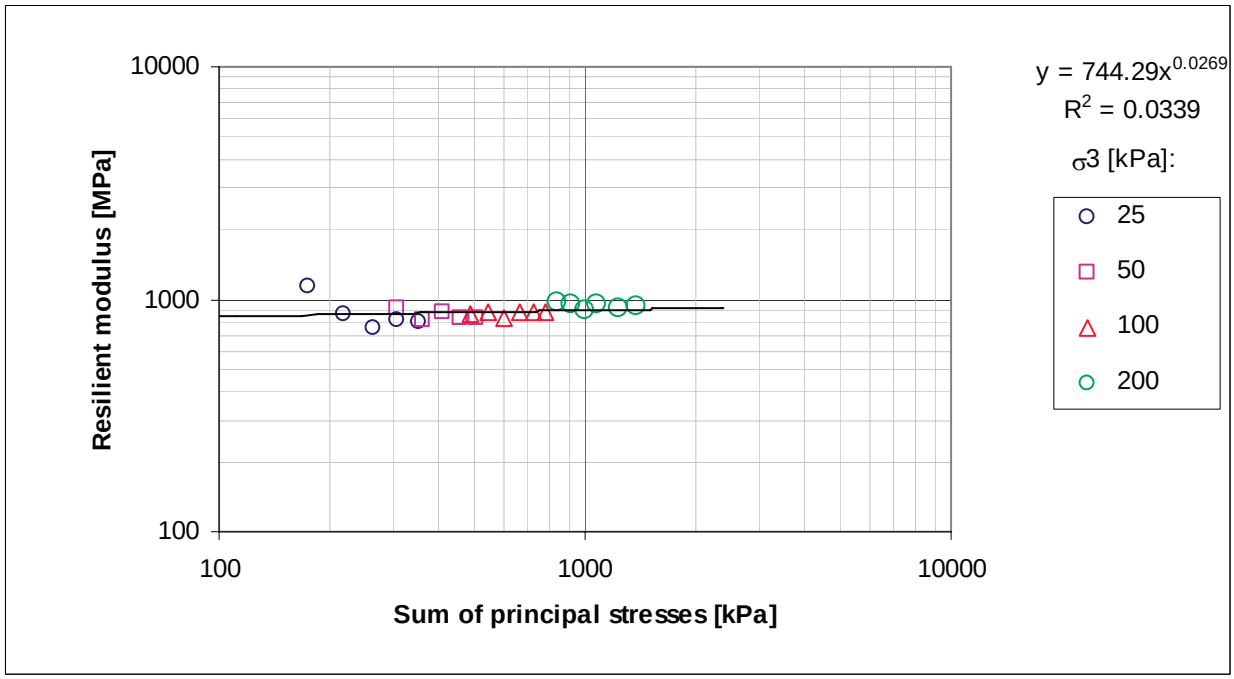


**Mix C-75C-0-b**

No data has been recorded for test b. The specimen had failed during conditioning

## Mix C-75C-0-c

Note: Data recorded at 200 kPa not useable

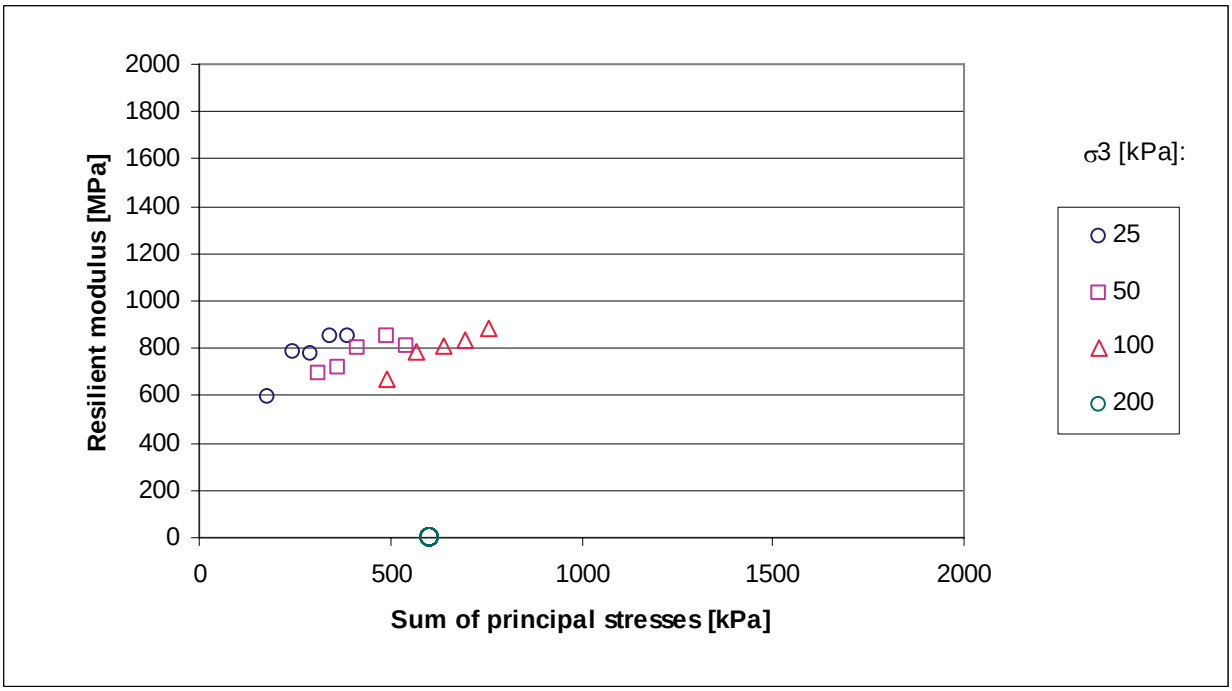


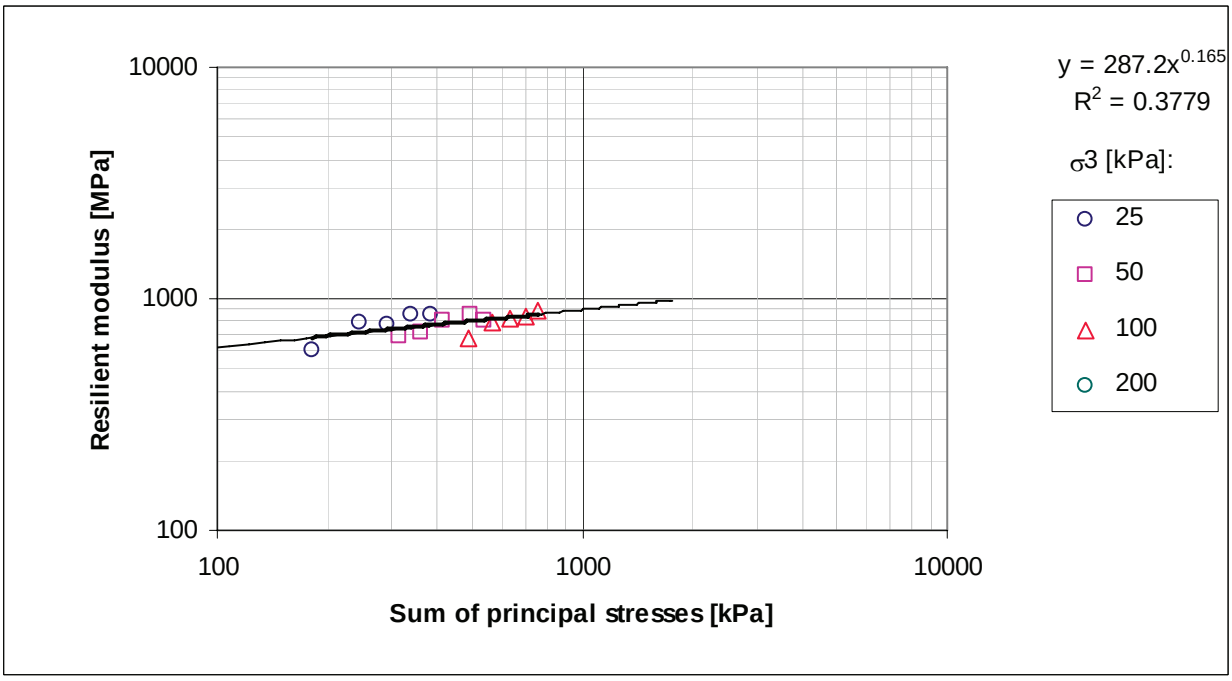

**Mix C-75C-1-a**

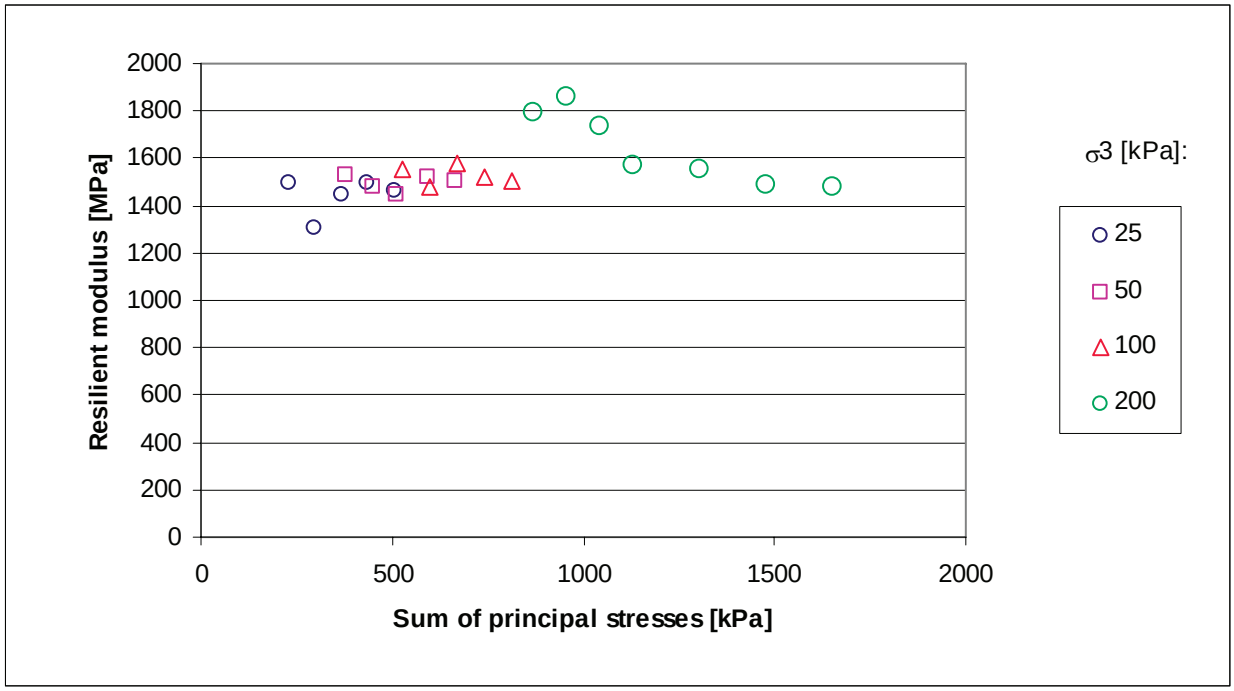
Resilient modulus [MPa]
2000
1800
1600
1400
1200
1000
800
600
400
200
0
0
500
1000
1500
2000
Sum of principal stresses [kPa]
σ3 [kPa]:
25
50
100
200

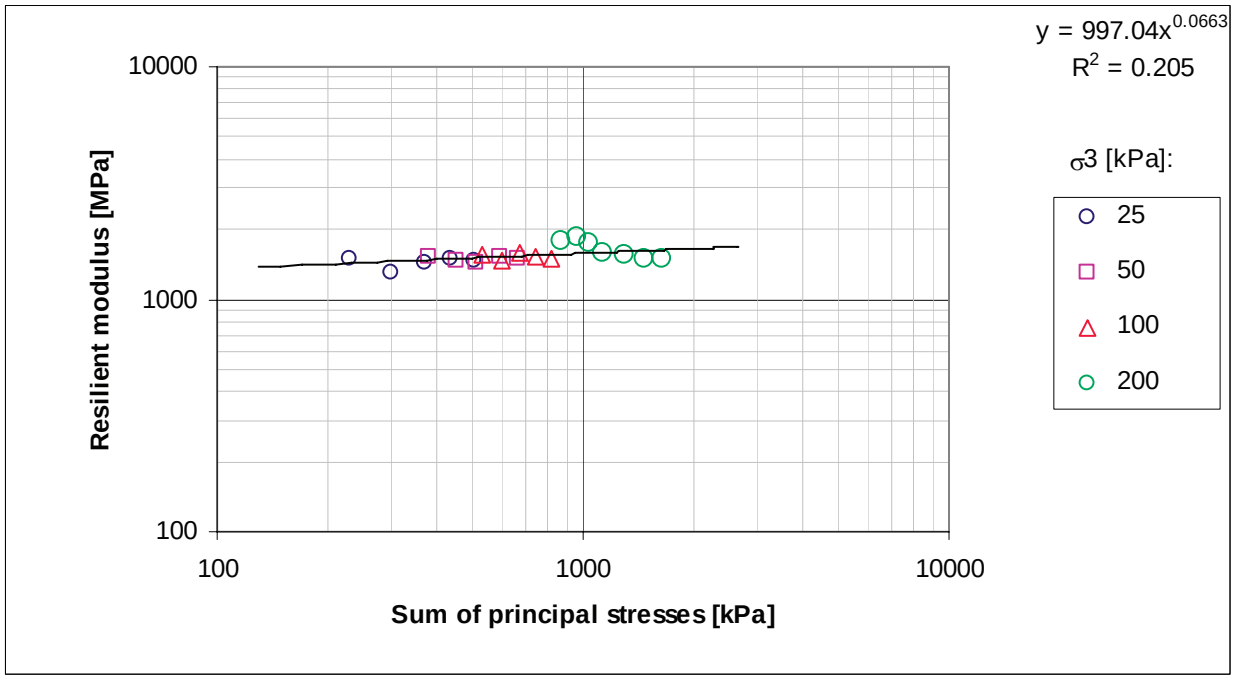
y = 997.04x^0.0663
R2 = 0.205
Resilient modulus [MPa]
10000
1000
100
100
1000
10000
Sum of principal stresses [kPa]
σ3 [kPa]:
25
50
100
200

**Mix C-75C1-b**

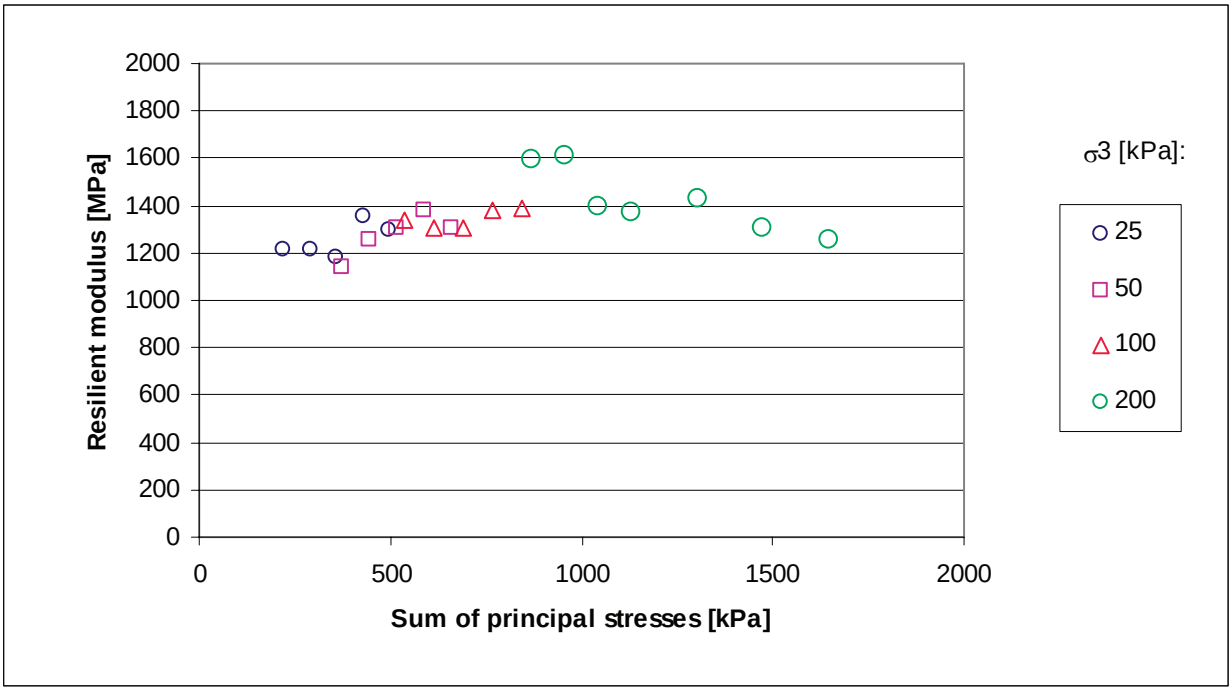
2000
1800
1600
1400
1200
1000
800
600
400
200
0
Resilient modulus [MPa]
0
500
1000
1500
2000
Sum of principal stresses [kPa]
σ3 [kPa]:
25
50
100
200

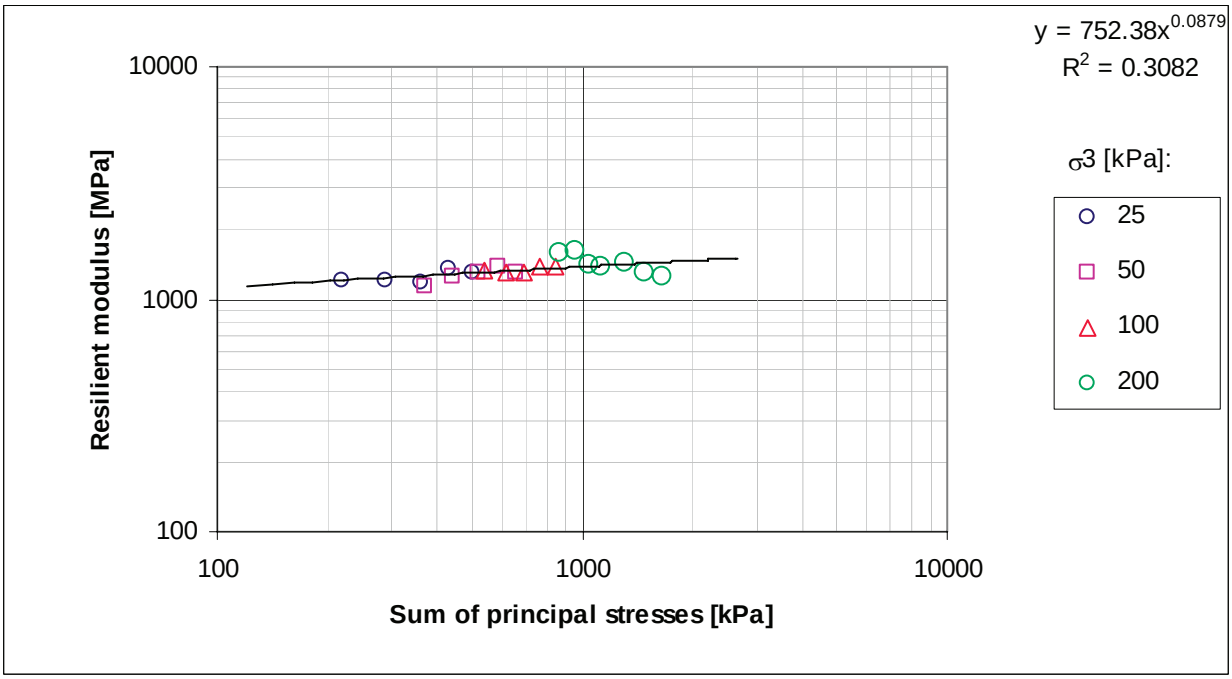
y = 752.38x^0.0879
R2 = 0.3082
10000
1000
100
Resilient modulus [MPa]
100
1000
10000
Sum of principal stresses [kPa]
σ3 [kPa]:
25
50
100
200

**Mix C-75M-0-a**

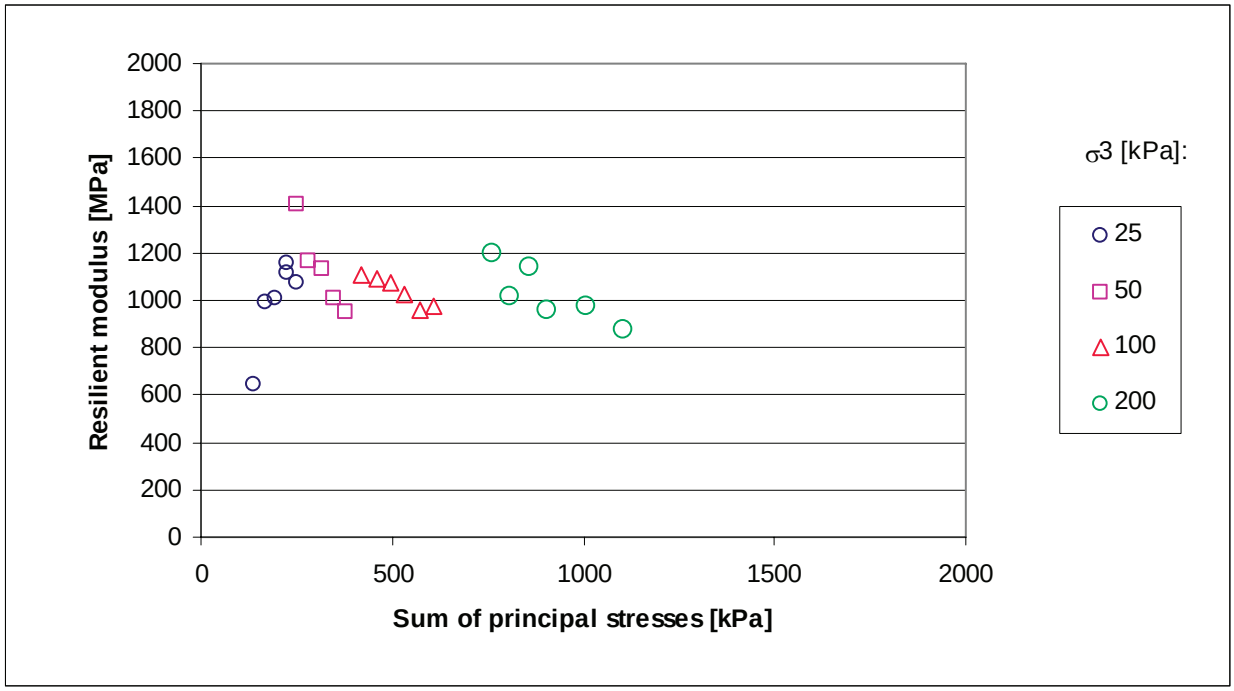
Resilient modulus [MPa]
2000
1800
1600
1400
1200
1000
800
600
400
200
0
0
500
1000
1500
2000
Sum of principal stresses [kPa]
σ3 [kPa]:
25
50
100
200

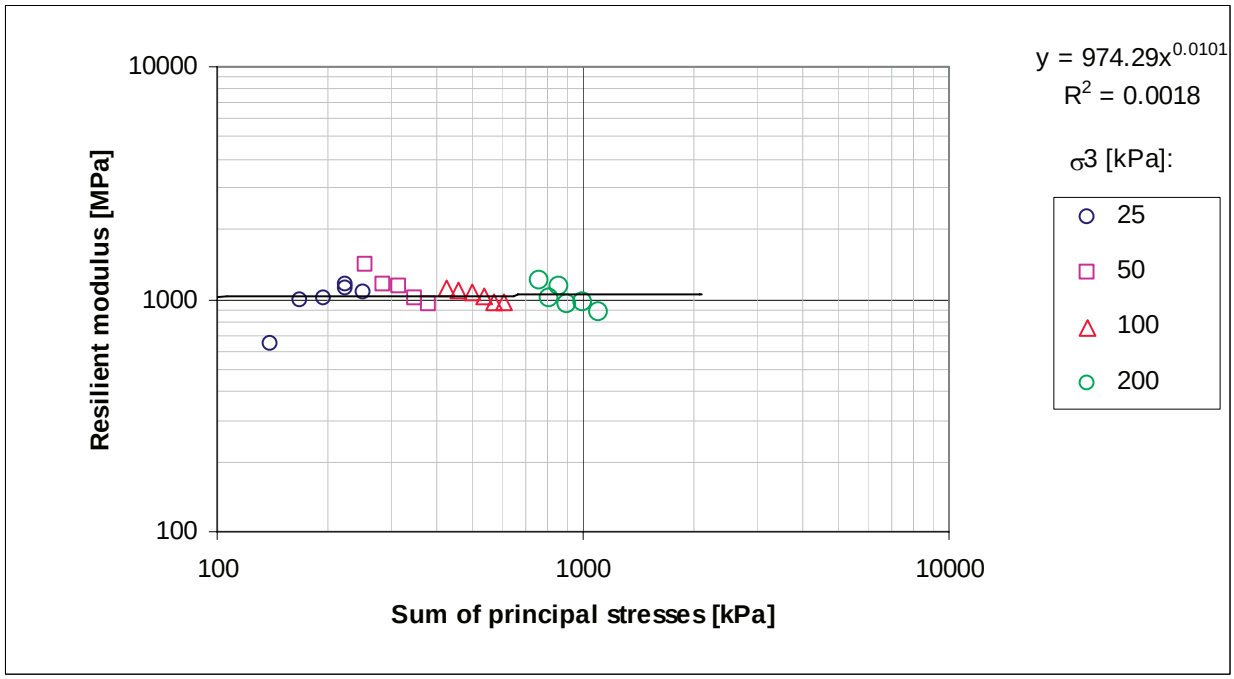
Resilient modulus [MPa]
10000
1000
100
100
1000
10000
Sum of principal stresses [kPa]
y = 974.29x^0.0101
R2 = 0.0018
σ3 [kPa]:
25
50
100
200

**Mix C-75M-0-b**

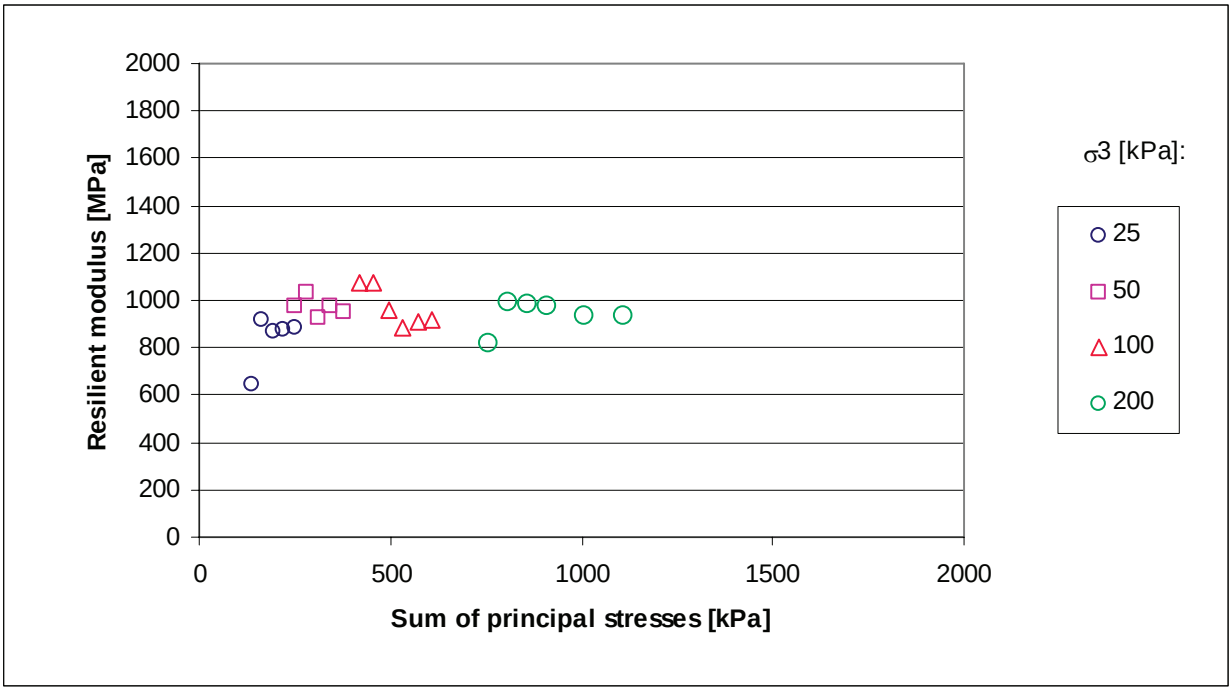
Resilient modulus [MPa]
2000
1800
1600
1400
1200
1000
800
600
400
200
0
0
500
1000
1500
2000
Sum of principal stresses [kPa]
σ3 [kPa]:
25
50
100
200

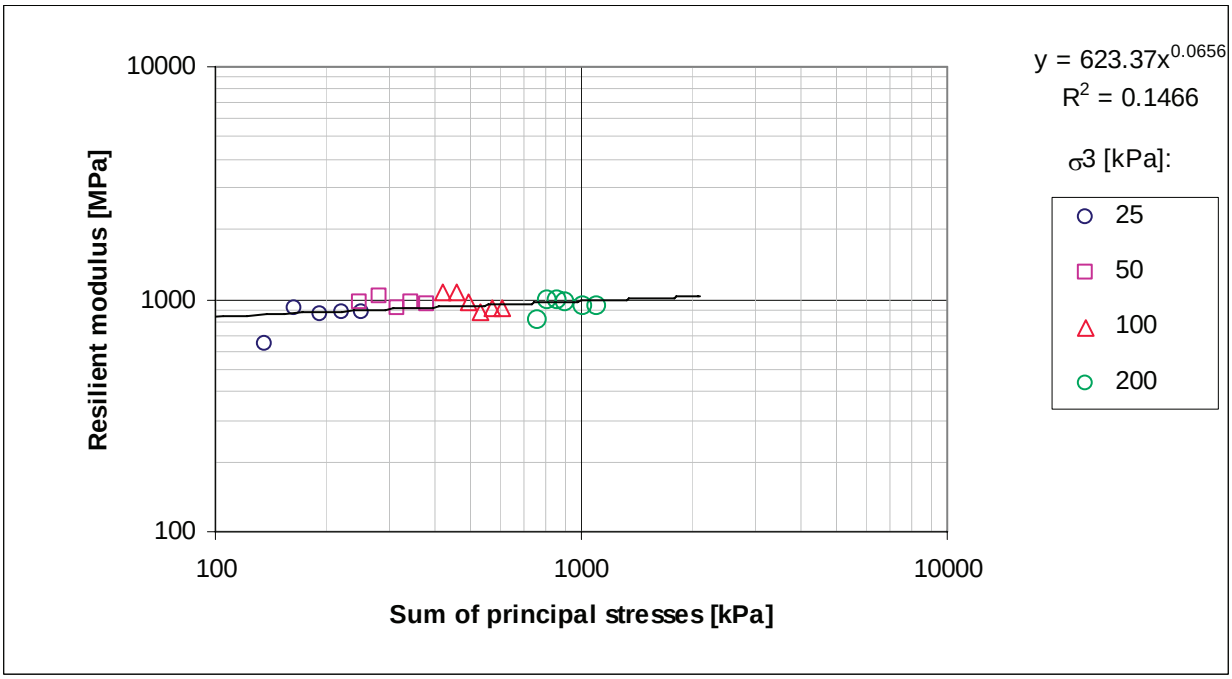
y = 623.37x^0.0656
R² = 0.1466
Resilient modulus [MPa]
10000
1000
100
100
1000
10000
Sum of principal stresses [kPa]
σ3 [kPa]:
25
50
100
200

## SUPERIMPOSED PLOTS REPEAT TESTS

### Mix A-75C-0

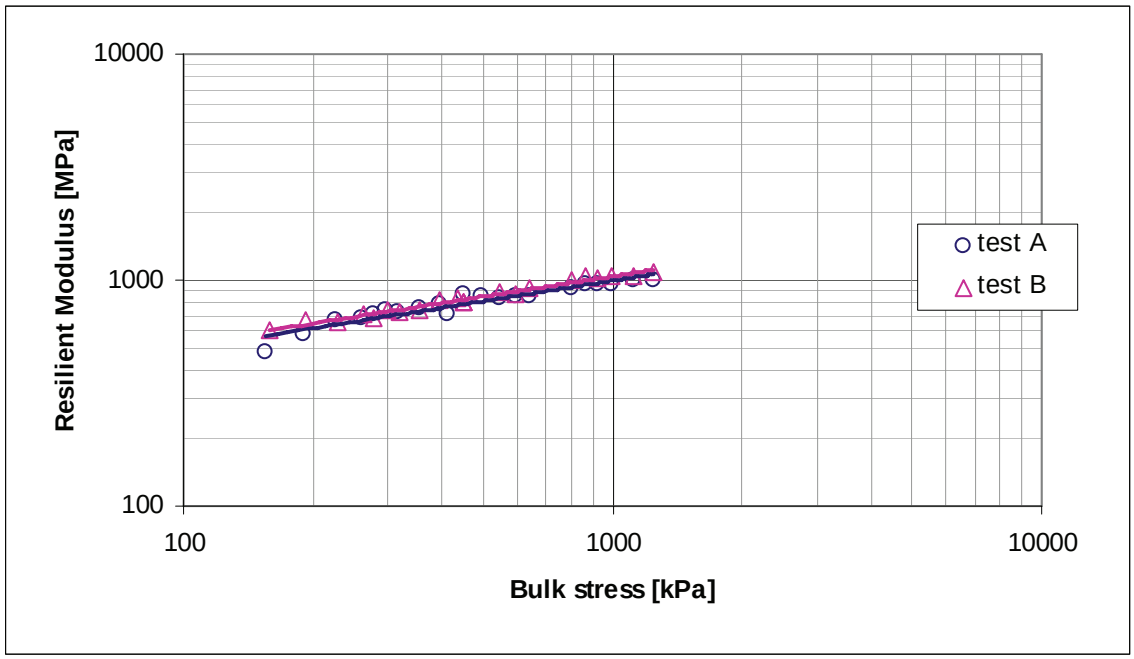


### Mix A-75C-1

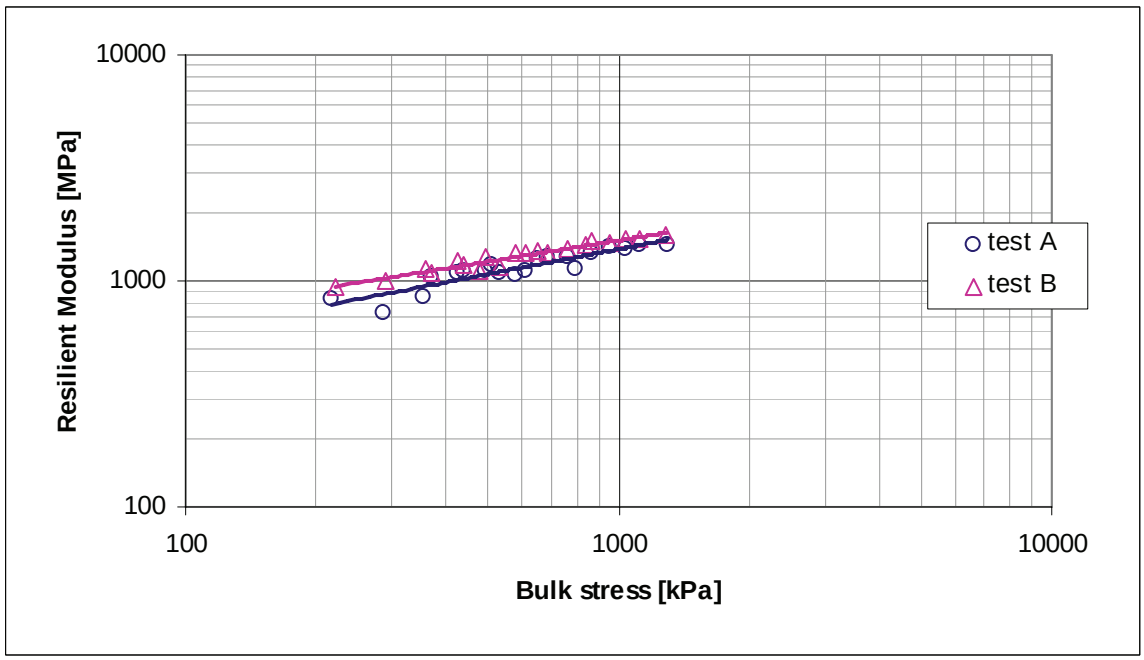

**Mix A-75M-0**

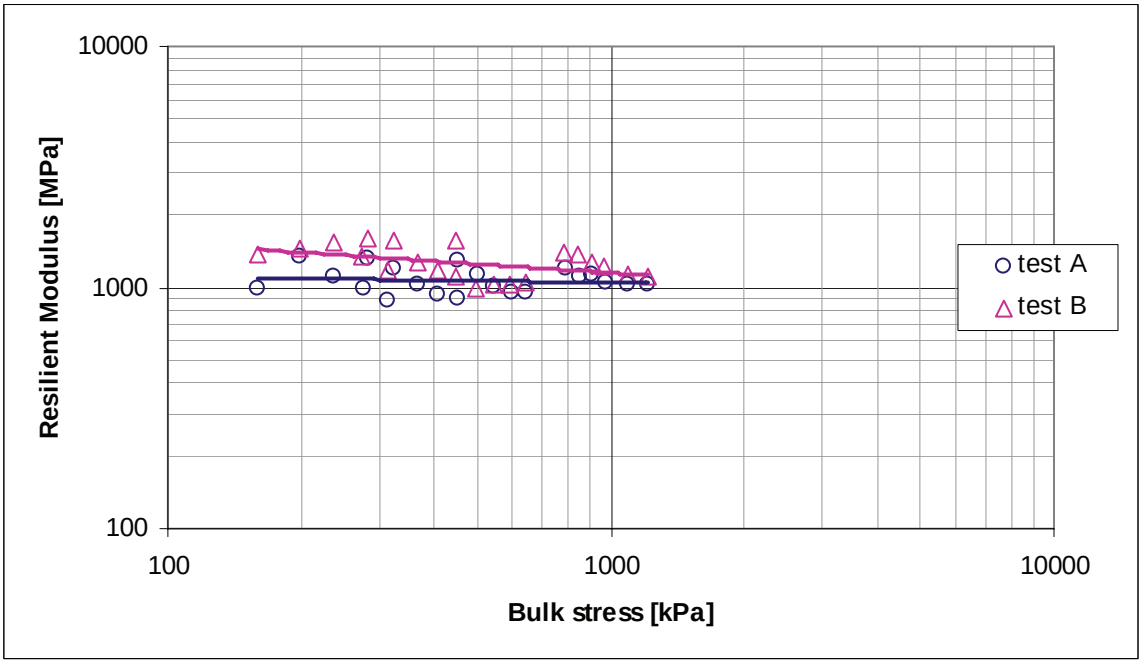


**Mix B-75C-0**

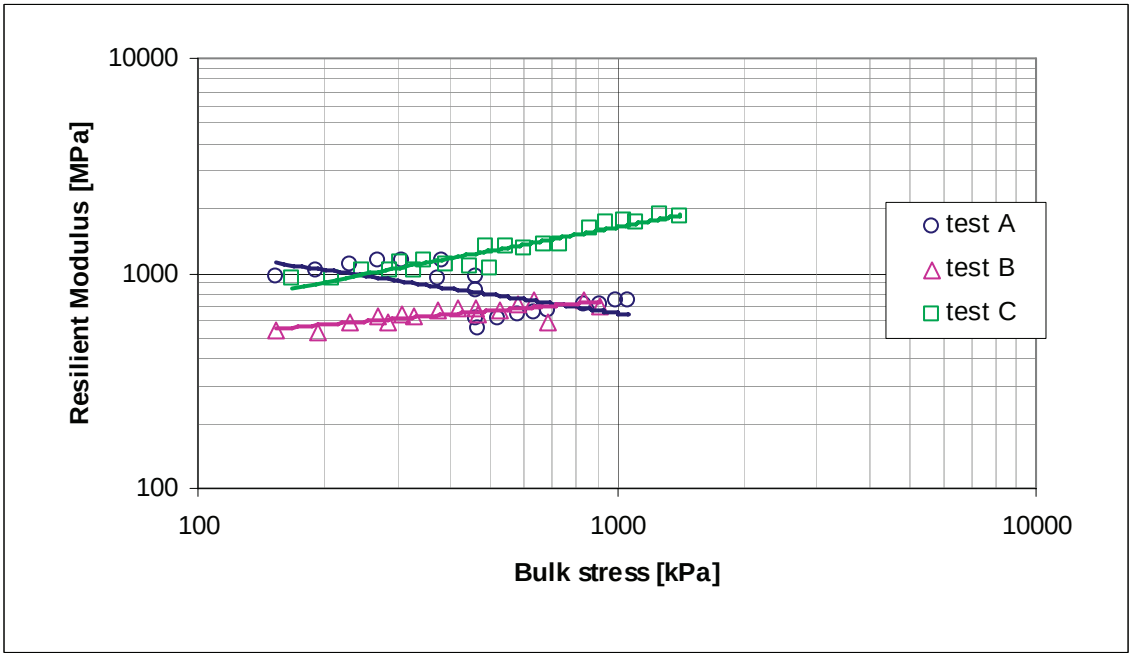

**Mix B-75C-1**

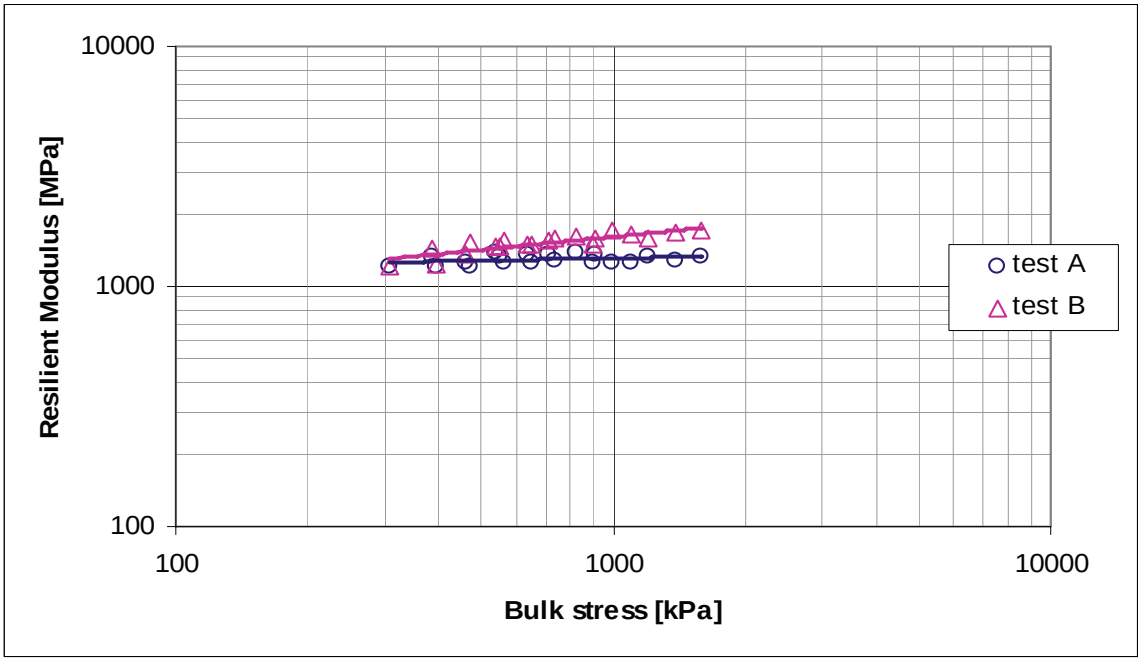


**Mix B-75M-0**

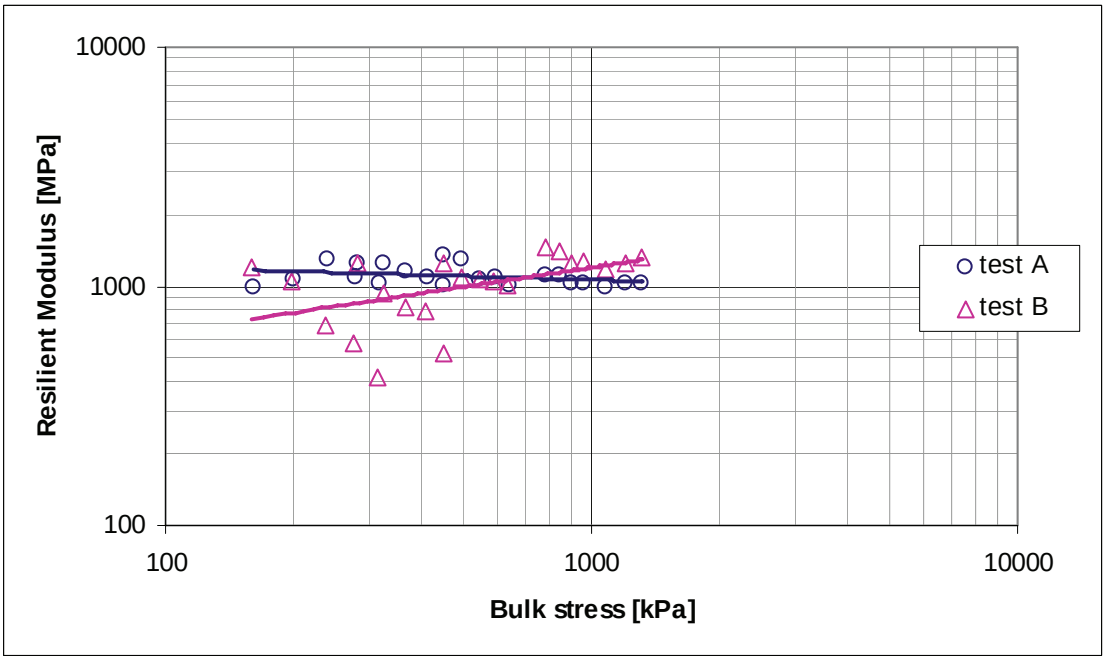

**Mix C-75C-0**

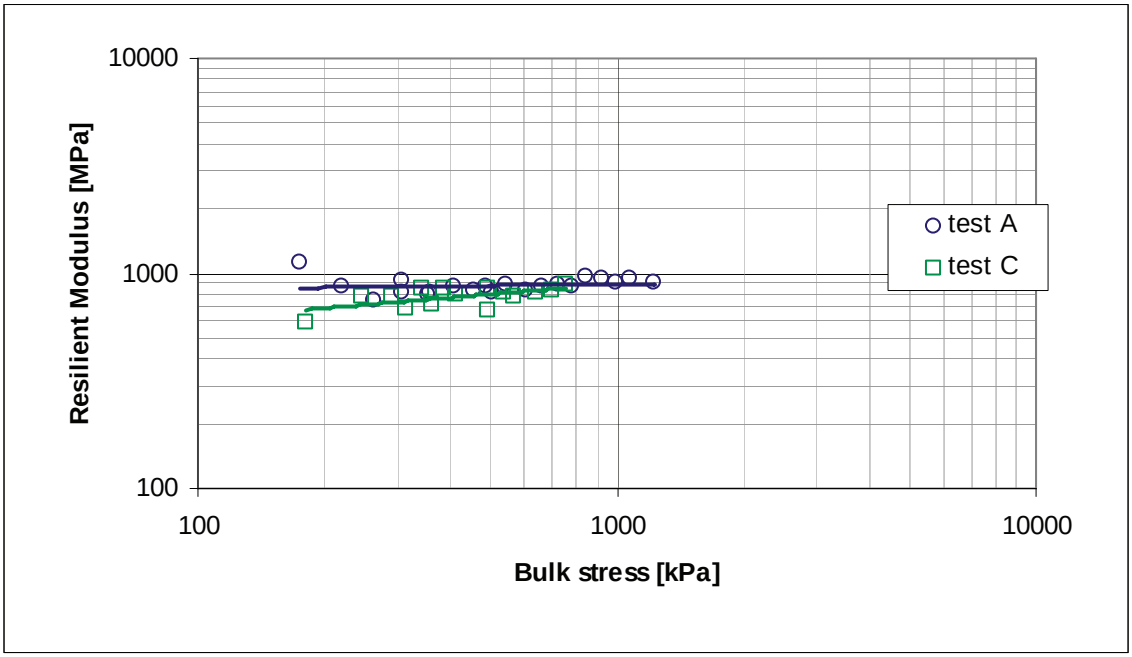


**Mix C-75C-1**

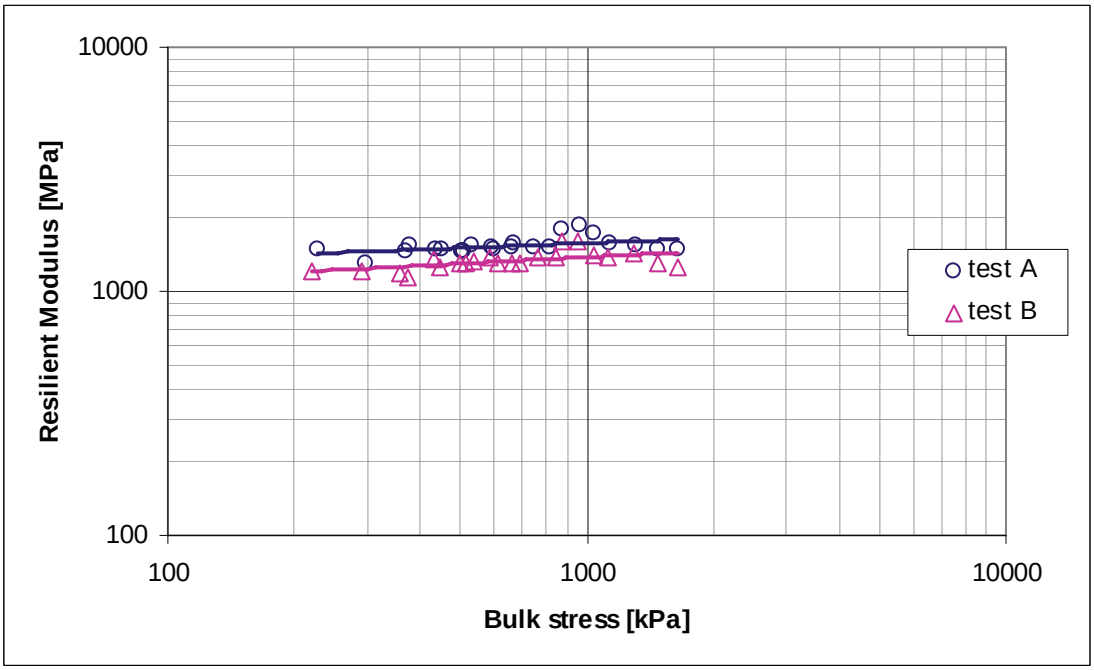

**Mix C-75M-0**

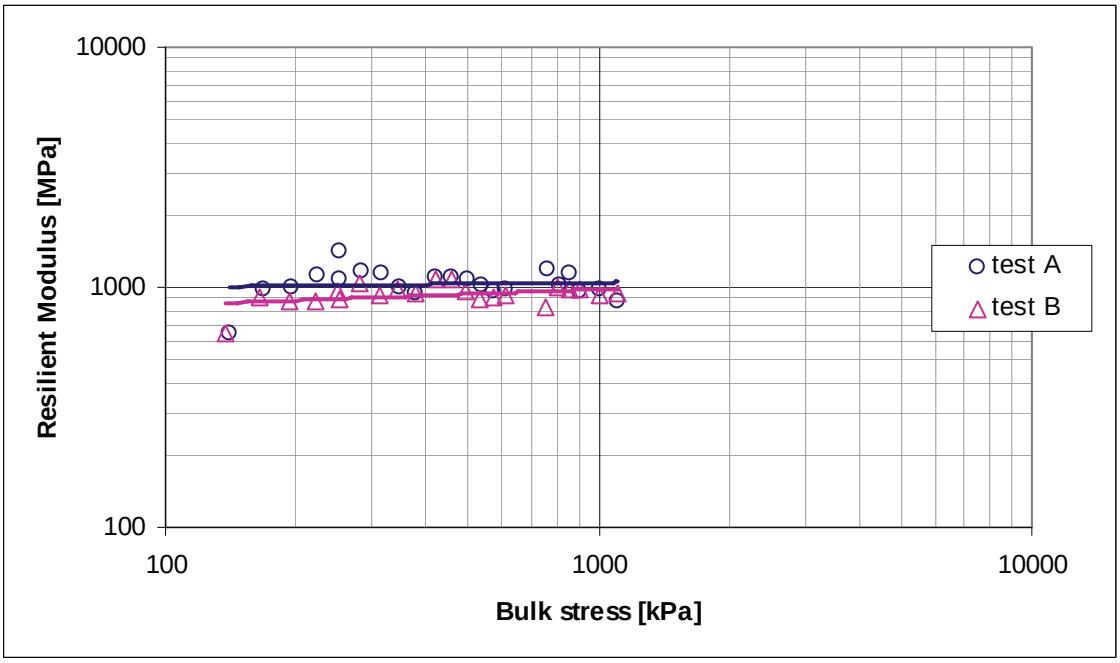
10000
1000
100
Resilient Modulus [MPa]
100
1000
10000
Bulk stress [kPa]
test A
test B

This page is left blank intentionally

# APPENDIX G: PERMANENT DEFORMATION TESTING RESULTS

**Mix A-75C-0**

Deviator stress ratio 0.25

| No. of load reps [-] | displacement recorded [mm] | relative displacement [mm] | relative strain [%] |
|---|---|---|---|
| 0 | 6.659 | | |
| 20 | 6.417 | 0.000 | 0.000 |
| 50 | 6.356 | 0.061 | 0.024 |
| 100 | 6.288 | 0.129 | 0.051 |
| 200 | 6.222 | 0.195 | 0.077 |
| 500 | 6.144 | 0.273 | 0.108 |
| 1001 | 6.095 | 0.322 | 0.128 |
| 2052 | 6.016 | 0.401 | 0.159 |
| 5001 | 5.953 | 0.464 | 0.184 |
| 10085 | 5.866 | 0.551 | 0.219 |
| 22320 | 5.782 | 0.635 | 0.252 |
| 49769 | 5.710 | 0.707 | 0.281 |
| 104216 | 5.647 | 0.770 | 0.306 |
| 137201 | 5.624 | 0.793 | 0.315 |
| 167821 | 5.608 | 0.809 | 0.321 |
| 202719 | 5.607 | 0.810 | 0.321 |
| 295865 | 5.601 | 0.816 | 0.324 |
| 402812 | 5.587 | 0.830 | 0.329 |
| 502703 | 5.568 | 0.849 | 0.337 |
| 586909 | 5.553 | 0.864 | 0.343 |
| 676411 | 5.549 | 0.868 | 0.344 |
| 726727 | 5.544 | 0.873 | 0.346 |
| 836161 | 5.542 | 0.875 | 0.347 |
| 901869 | 5.539 | 0.878 | 0.348 |
| 1000000 | 5.5370 | 0.880 | 0.349 |

Deviator stress ratio 0.35

| No. of load reps [-] | displacement recorded [mm] | relative displacement [mm] |
|---|---|---|
| 0 | 2.9740 | |
| 20 | 2.7450 | 0.000 |
| 50 | 2.6370 | 0.108 |
| 100 | 2.5580 | 0.187 |
| 200 | 2.5100 | 0.235 |
| 500 | 2.4240 | 0.321 |
| 1000 | 2.3650 | 0.380 |
| 2000 | 2.2780 | 0.467 |
| 5500 | 2.1990 | 0.546 |
| 20700 | 2.1100 | 0.635 |
| 53350 | 2.0100 | 0.735 |
| 113250 | 1.9600 | 0.785 |
| 154000 | 1.9220 | 0.823 |
| 183000 | 1.8540 | 0.891 |
| 201861 | 1.7870 | 0.958 |
| 230227 | 1.6630 | 1.082 |
| 313750 | 1.2340 | 1.511 |
| 348330 | 0.9550 | 1.790 |
| 400500 | 0.4020 | 2.343 |
| 491300 | -0.5880 | 3.333 |
| 562831 | -2.0370 | 4.782 |
| 659832 | -7.8780 | 10.623 |

Deviator stress ratio 0.40

| No. of load reps [-] | displacement recorded [mm] | relative displacement [mm] | relative strain [%] |
|---|---|---|---|
| 0 | 5.700 | | |
| 20 | 5.499 | 0.000 | 0.000 |
| 51 | 5.398 | 0.101 | 0.040 |
| 100 | 5.307 | 0.192 | 0.076 |
| 201 | 5.215 | 0.284 | 0.113 |
| 501 | 5.088 | 0.411 | 0.163 |
| 1000 | 4.984 | 0.515 | 0.204 |
| 1999 | 4.887 | 0.612 | 0.243 |
| 5209 | 4.733 | 0.766 | 0.304 |
| 10426 | 4.632 | 0.867 | 0.344 |
| 21535 | 4.506 | 0.993 | 0.394 |
| 48608 | 4.363 | 1.136 | 0.451 |
| 85030 | 4.279 | 1.220 | 0.484 |
| 94608 | 4.261 | 1.238 | 0.491 |
| 156172 | 4.130 | 1.369 | 0.543 |
| 190600 | 4.059 | 1.440 | 0.571 |
| 201005 | 4.047 | 1.452 | 0.576 |
| 259071 | 3.966 | 1.533 | 0.608 |
| 344370 | 3.855 | 1.644 | 0.652 |
| 426808 | 3.791 | 1.708 | 0.678 |
| 517981 | 3.702 | 1.797 | 0.713 |
| 592631 | 3.673 | 1.826 | 0.725 |
| 688327 | 3.635 | 1.864 | 0.740 |
| 768270 | 3.560 | 1.939 | 0.769 |
| 867750 | 3.4320 | 2.067 | 0.820 |
| 908566 | 3.3850 | 2.114 | 0.839 |
| 974347 | 3.2940 | 2.205 | 0.875 |
| 1051901 | 3.1960 | 2.303 | 0.914 |
| 1105919 | 3.1450 | 2.354 | 0.934 |

Deviator stress ratio 0.60

| No. of load reps [-] | displacement recorded [mm] | relative displacement [mm] | relative strain [%] |
|---|---|---|---|
| 0 | 5.3800 | | |
| 19 | 5.0510 | 0.000 | 0.000 |
| 50 | 4.8620 | 0.189 | 0.075 |
| 101 | 4.7020 | 0.349 | 0.138 |
| 200 | 4.5390 | 0.512 | 0.203 |
| 500 | 4.2610 | 0.790 | 0.313 |
| 1000 | 3.9920 | 1.059 | 0.420 |
| 2001 | 3.6580 | 1.393 | 0.553 |
| 5000 | 3.1240 | 1.927 | 0.765 |
| 10675 | 2.6020 | 2.449 | 0.972 |
| 21187 | 2.1890 | 2.862 | 1.136 |
| 31500 | 2.0220 | 3.029 | 1.202 |
| 43741 | 1.9000 | 3.151 | 1.250 |
| 80850 | 1.6270 | 3.424 | 1.359 |
| 132196 | 1.4950 | 3.556 | 1.411 |
| 160433 | 1.3890 | 3.662 | 1.453 |
| 200000 | 0.2830 | 4.768 | 1.892 |
| 215230 | -0.8190 | 5.870 | 2.329 |
| 243904 | -4.3870 | 9.438 | 3.745 |
| 257627 | -7.9240 | 12.975 | 5.149 |

## Mix A-75C-1

Deviator stress ratio 0.40

| No. of load reps [-] | displacement recorded [mm] | relative displacement [mm] | relative strain [%] |
|---|---|---|---|
| 0 | not recorded | | |
| 21 | 5.180 | 0.000 | |
| 52 | 5.031 | 0.149 | 0.059 |
| 101 | 4.928 | 0.252 | 0.100 |
| 201 | 4.815 | 0.365 | 0.145 |
| 501 | 4.651 | 0.529 | 0.211 |
| 1000 | 4.491 | 0.689 | 0.275 |
| 2001 | 4.289 | 0.891 | 0.355 |
| 5132 | 3.964 | 1.216 | 0.484 |
| 10124 | 3.690 | 1.490 | 0.594 |
| 22948 | 3.265 | 1.915 | 0.763 |
| 52360 | 2.899 | 2.281 | 0.909 |
| 132338 | 2.582 | 2.598 | 1.035 |
| 161366 | 2.556 | 2.624 | 1.045 |
| 193194 | 2.533 | 2.647 | 1.055 |
| 239643 | 2.503 | 2.677 | 1.067 |
| 331151 | 2.442 | 2.738 | 1.091 |
| 395142 | 2.388 | 2.792 | 1.112 |
| 483229 | -4.482 | 9.662 | 3.849 |
| 497370 | -7.862 | 13.042 | 5.196 |

Deviator stress ratio 0.40 repeat

| No. of load reps [-] | displacement recorded [mm] | relative displacement [mm] | relative strain [%] |
|---|---|---|---|
| 0 | 3.200 | | |
| 21 | 2.976 | 0.000 | |
| 50 | 2.858 | 0.118 | 0.047 |
| 100 | 2.745 | 0.231 | 0.092 |
| 201 | 2.634 | 0.342 | 0.136 |
| 501 | 2.480 | 0.496 | 0.198 |
| 1001 | 2.340 | 0.636 | 0.253 |
| 2001 | 2.207 | 0.769 | 0.306 |
| 6442 | 1.934 | 1.042 | 0.415 |
| 11292 | 1.780 | 1.196 | 0.476 |
| 21965 | 1.594 | 1.382 | 0.551 |
| 59650 | 1.276 | 1.700 | 0.677 |
| 131146 | 0.653 | 2.323 | 0.925 |
| 163439 | 0.159 | 2.817 | 1.122 |
| 178752 | -0.078 | 3.054 | 1.217 |
| 198992 | -5.423 | 8.399 | 3.346 |
| 200322 | -7.800 | 10.776 | 4.293 |

Deviator stress ratio 0.45

| No. of load reps [-] | displacement recorded [mm] | relative displacement [mm] | relative strain [%] |
|---|---|---|---|
| 0 | 3.490 | | |
| 23 | 3.132 | 0.000 | |
| 53 | 2.982 | 0.150 | 0.060 |
| 102 | 2.840 | 0.292 | 0.116 |
| 202 | 2.679 | 0.453 | 0.180 |
| 500 | 2.436 | 0.696 | 0.277 |
| 1001 | 2.218 | 0.914 | 0.364 |
| 2001 | 1.966 | 1.166 | 0.465 |
| 5001 | 1.564 | 1.568 | 0.625 |
| 10281 | 1.207 | 1.925 | 0.767 |
| 20322 | 0.745 | 2.387 | 0.951 |
| 32990 | 0.210 | 2.922 | 1.164 |
| 48978 | -0.337 | 3.469 | 1.382 |
| 88808 | -1.822 | 4.954 | 1.974 |
| 121150 | -3.933 | 7.065 | 2.815 |
| 150210 | -7.874 | 11.006 | 4.385 |

Deviator stress ratio 0.50

| No. of load reps [-] | displacement recorded [mm] | relative displacement [mm] | relative strain [%] |
|---|---|---|---|
| 0 | 3.450 | | |
| 20 | 3.114 | 0.000 | |
| 51 | 2.910 | 0.204 | 0.081 |
| 106 | 2.696 | 0.418 | 0.167 |
| 200 | 2.463 | 0.651 | 0.259 |
| 501 | 2.032 | 1.082 | 0.431 |
| 1000 | 1.263 | 1.851 | 0.737 |
| 2001 | 0.872 | 2.242 | 0.893 |
| 5039 | -0.731 | 3.845 | 1.532 |
| 7501 | -2.066 | 5.180 | 2.064 |
| 10066 | -3.827 | 6.941 | 2.765 |
| 13005 | -6.583 | 9.697 | 3.863 |
| 14103 | -7.955 | 11.069 | 4.410 |

Deviator stress ratio 0.60

| No. of load reps [-] | displacement recorded [mm] | relative displacement [mm] | relative strain [%] |
|---|---|---|---|
| 0 | 3.500 | | |
| 20 | 3.134 | 0.000 | |
| 51 | 2.917 | 0.217 | 0.086 |
| 100 | 2.705 | 0.429 | 0.171 |
| 200 | 2.431 | 0.703 | 0.280 |
| 501 | 1.912 | 1.222 | 0.487 |
| 1000 | 1.263 | 1.871 | 0.745 |
| 2038 | 0.097 | 3.037 | 1.210 |
| 3000 | -0.978 | 4.112 | 1.638 |
| 4500 | -2.902 | 6.036 | 2.405 |
| 6001 | -5.622 | 8.756 | 3.488 |
| 6850 | -7.803 | 10.937 | 4.357 |

## Mix A-75M-0

Deviator stress ratio 0.38

| | No. of load reps [-] | displacement recorded [mm] | relative displacement [mm] | relative strain [%] |
|---|---|---|---|---|
| | 0 | 4.900 | | |
| | 21 | 4.787 | 0.000 | |
| | 50 | 4.689 | 0.098 | 0.039 |
| | 100 | 4.595 | 0.192 | 0.076 |
| | 201 | 4.466 | 0.321 | 0.128 |
| | 500 | 4.280 | 0.507 | 0.202 |
| | 1001 | 4.090 | 0.697 | 0.278 |
| | 2045 | 3.855 | 0.932 | 0.371 |
| | 5200 | 3.441 | 1.346 | 0.536 |
| | 11500 | 2.982 | 1.805 | 0.719 |
| | 20500 | 2.537 | 2.250 | 0.896 |
| | 56501 | 1.601 | 3.186 | 1.269 |
| | 90100 | 1.068 | 3.719 | 1.482 |
| | 192700 | 0.046 | 4.741 | 1.889 |
| | 344600 | -0.503 | 5.290 | 2.108 |
| | 407074 | -0.678 | 5.465 | 2.177 |
| | 542692 | -1.012 | 5.799 | 2.310 |
| | 589959 | -1.127 | 5.914 | 2.356 |
| | 751172 | -1.467 | 6.254 | 2.492 |
| | 803752 | -1.562 | 6.349 | 2.529 |
| | 882484 | -1.696 | 6.483 | 2.583 |
| power cut | 935306 | -1.550 | 6.337 | 2.525 |
| | 935500 | -1.616 | 6.403 | 2.551 |
| | 936000 | -1.657 | 6.444 | 2.567 |
| | 939000 | -1.724 | 6.511 | 2.594 |
| | 1053756 | -2.025 | 6.812 | 2.714 |
| | 1056404 | -2.027 | 6.814 | 2.715 |

Deviator stress ratio 0.45

| No. of load reps [-] | displacement recorded [mm] | relative displacement [mm] | relative strain [%] |
|---|---|---|---|
| 0 | 4.360 | | |
| 20 | 4.145 | 0.000 | |
| 50 | 4.034 | 0.111 | 0.044 |
| 100 | 3.918 | 0.227 | 0.090 |
| 200 | 3.775 | 0.370 | 0.147 |
| 500 | 3.528 | 0.617 | 0.246 |
| 1001 | 3.275 | 0.870 | 0.347 |
| 2229 | 2.914 | 1.231 | 0.490 |
| 5000 | 2.405 | 1.740 | 0.693 |
| 7902 | 2.140 | 2.005 | 0.799 |
| 7999 | 2.086 | 2.059 | 0.820 |
| 8501 | 1.950 | 2.195 | 0.875 |
| 10100 | 1.736 | 2.409 | 0.960 |
| 20166 | 1.023 | 3.122 | 1.244 |
| 61400 | -0.294 | 4.439 | 1.769 |
| 138120 | -2.161 | 6.306 | 2.512 |
| 167263 | -2.683 | 6.828 | 2.720 |
| 191259 | -3.047 | 7.192 | 2.865 |
| 245337 | -3.760 | 7.905 | 3.149 |
| 317040 | -4.485 | 8.630 | 3.438 |
| 380000 | -4.961 | 9.106 | 3.628 |
| 505839 | -5.704 | 9.849 | 3.924 |

Deviator stress ratio 0.50

| No. of load reps [-] | displacement recorded [mm] | relative displacement [mm] | relative strain [%] |
|---|---|---|---|
| 0 | 2.290 | | |
| 21 | 2.110 | 0.000 | |
| 52 | 1.990 | 0.120 | 0.048 |
| 101 | 1.866 | 0.244 | 0.097 |
| 200 | 1.702 | 0.408 | 0.163 |
| 501 | 1.405 | 0.705 | 0.281 |
| 1000 | 1.110 | 1.000 | 0.398 |
| 2000 | 0.833 | 1.277 | 0.509 |
| 5000 | 0.367 | 1.743 | 0.694 |
| 10000 | -0.170 | 2.280 | 0.908 |
| 19501 | -1.022 | 3.132 | 1.248 |
| 31824 | -1.876 | 3.986 | 1.588 |
| 49003 | -2.480 | 4.590 | 1.829 |
| 69010 | -4.771 | 6.881 | 2.741 |
| 109373 | -7.874 | 9.984 | 3.978 |

Deviator stress ratio 0.55

| No. of load reps [-] | displacement recorded [mm] | relative displacement [mm] | relative strain [%] |
|---|---|---|---|
| 0 | 3.200 | | |
| 20 | 3.033 | 0.000 | |
| 51 | 2.885 | 0.148 | 0.059 |
| 100 | 2.714 | 0.319 | 0.127 |
| 200 | 2.475 | 0.558 | 0.222 |
| 500 | 1.972 | 1.061 | 0.423 |
| 1063 | 1.290 | 1.743 | 0.694 |
| 2102 | 0.305 | 2.728 | 1.087 |
| 5709 | -2.346 | 5.379 | 2.143 |
| 10000 | -4.954 | 7.987 | 3.182 |
| 15000 | -7.605 | 10.638 | 4.238 |

Deviator stress ratio 0.60

| No. of load reps [-] | displacement recorded [mm] | relative displacement [mm] | relative strain [%] |
|---|---|---|---|
| 0 | 1.330 | | |
| 20 | 1.060 | 0.000 | |
| 50 | 0.876 | 0.184 | 0.073 |
| 100 | 0.687 | 0.373 | 0.149 |
| 200 | 0.431 | 0.629 | 0.251 |
| 503 | 0.000 | 1.060 | 0.422 |
| 1060 | -0.540 | 1.600 | 0.637 |
| 2109 | -1.288 | 2.348 | 0.935 |
| 5001 | -2.830 | 3.890 | 1.550 |
| 8513 | -4.407 | 5.467 | 2.178 |
| 11000 | -5.459 | 6.519 | 2.597 |
| 14160 | -6.775 | 7.835 | 3.122 |
| 16000 | -7.555 | 8.615 | 3.432 |
| 16882 | -7.900 | 8.960 | 3.570 |

**Mix B-75C-0**

Deviator stress ratio 0.50

| No. of load reps [-] | displacement recorded [mm] | relative displacement [mm] | relative strain [%] |
|---|---|---|---|
| 0 | 4.980 | | |
| 20 | 4.774 | 0.000 | |
| 51 | 4.672 | 0.102 | 0.041 |
| 101 | 4.583 | 0.191 | 0.076 |
| 201 | 4.494 | 0.280 | 0.112 |
| 500 | 4.361 | 0.413 | 0.165 |
| 999 | 4.241 | 0.533 | 0.212 |
| 2000 | 4.114 | 0.660 | 0.263 |
| 5309 | 3.901 | 0.873 | 0.348 |
| 10804 | 3.745 | 1.029 | 0.410 |
| 15927 | 3.643 | 1.131 | 0.451 |
| 20720 | 3.574 | 1.200 | 0.478 |
| 52806 | 3.432 | 1.342 | 0.535 |
| 108823 | 3.379 | 1.395 | 0.556 |
| 162281 | 3.358 | 1.416 | 0.564 |
| 218089 | 3.340 | 1.434 | 0.571 |
| 312089 | 3.313 | 1.461 | 0.582 |
| 348743 | 3.304 | 1.470 | 0.586 |
| 388299 | 3.301 | 1.473 | 0.587 |
| 488556 | 3.267 | 1.507 | 0.600 |
| 515357 | 3.254 | 1.520 | 0.606 |
| 559879 | 3.237 | 1.537 | 0.612 |
| 663963 | 3.201 | 1.573 | 0.627 |
| 739550 | 3.160 | 1.614 | 0.643 |
| 861358 | 3.075 | 1.699 | 0.677 |

Deviator stress ratio 0.55

| No. of load reps [-] | displacement recorded [mm] | relative displacement [mm] | relative strain [%] |
|---|---|---|---|
| 0 | 5.700 | | |
| 20 | 5.455 | 0.000 | |
| 50 | 5.332 | 0.123 | 0.049 |
| 100 | 5.220 | 0.235 | 0.094 |
| 219 | 5.089 | 0.366 | 0.146 |
| 500 | 4.870 | 0.585 | 0.233 |
| 1010 | 4.702 | 0.753 | 0.300 |
| 2107 | 4.542 | 0.913 | 0.364 |
| 5230 | 4.342 | 1.113 | 0.443 |
| 10000 | 4.205 | 1.250 | 0.498 |
| 20900 | 4.064 | 1.391 | 0.554 |
| 60000 | 3.660 | 1.795 | 0.715 |
| 140222 | 2.400 | 3.055 | 1.217 |
| 192300 | -0.728 | 6.183 | 2.463 |
| 203600 | -4.284 | 9.739 | 3.880 |
| 207277 | -7.800 | 13.255 | 5.281 |

Deviator stress ratio 0.60

| No. of load reps [-] | displacement recorded [mm] | relative displacement [mm] | relative strain [%] |
|---|---|---|---|
| 0 | 4.700 | | |
| 21 | 4.414 | 0.000 | |
| 52 | 4.265 | 0.149 | 0.059 |
| 100 | 4.134 | 0.280 | 0.112 |
| 201 | 3.962 | 0.452 | 0.180 |
| 500 | 3.706 | 0.708 | 0.282 |
| 1000 | 3.442 | 0.972 | 0.387 |
| 2101 | 3.096 | 1.318 | 0.525 |
| 5200 | 2.479 | 1.935 | 0.771 |
| 10332 | 2.259 | 2.155 | 0.859 |
| 24701 | 2.077 | 2.337 | 0.931 |
| 69879 | 1.870 | 2.544 | 1.014 |
| 138908 | -0.334 | 4.748 | 1.892 |
| 156100 | -0.578 | 4.992 | 1.989 |
| 175416 | -0.798 | 5.212 | 2.076 |
| 200280 | -1.028 | 5.442 | 2.168 |
| 247593 | -1.379 | 5.793 | 2.308 |
| 312517 | -1.824 | 6.238 | 2.485 |
| 357517 | -2.292 | 6.706 | 2.672 |
| 382283 | -2.707 | 7.121 | 2.837 |
| 462425 | -7.892 | 12.306 | 4.903 |

Deviator stress ratio 0.70

| No. of load reps [-] | displacement recorded [mm] | relative displacement [mm] | relative strain [%] |
|---|---|---|---|
| 0 | 4.510 | | |
| 20 | 4.082 | 0.000 | |
| 50 | 3.835 | 0.247 | 0.098 |
| 101 | 3.598 | 0.484 | 0.193 |
| 200 | 3.312 | 0.770 | 0.307 |
| 501 | 2.729 | 1.353 | 0.539 |
| 1000 | 1.895 | 2.187 | 0.871 |
| 2046 | 0.026 | 4.056 | 1.616 |
| 5048 | -5.562 | 9.644 | 3.842 |
| 5773 | -7.677 | 11.759 | 4.685 |

**Mix B-75C-1**

Deviator stress ratio 0.38

| | No. of load reps [-] | displacement recorded [mm] | relative displacement [mm] | relative strain [%] |
|---|---|---|---|---|
| | 0 | 3.580 | | |
| | 21 | 3.400 | 0.000 | |
| | 51 | 3.303 | 0.097 | 0.039 |
| | 101 | 3.213 | 0.187 | 0.075 |
| | 201 | 3.116 | 0.284 | 0.113 |
| | 501 | 2.961 | 0.439 | 0.175 |
| | 1000 | 2.830 | 0.570 | 0.227 |
| | 2000 | 2.692 | 0.708 | 0.282 |
| | 5000 | 2.496 | 0.904 | 0.360 |
| | 10000 | 2.343 | 1.057 | 0.421 |
| | 20000 | 2.192 | 1.208 | 0.481 |
| | 57084 | 1.957 | 1.443 | 0.575 |
| | 73874 | 1.887 | 1.513 | 0.603 |
| | 137732 | 1.710 | 1.690 | 0.673 |
| | 173751 | 1.649 | 1.751 | 0.698 |
| | 198903 | 1.613 | 1.787 | 0.712 |
| | 238776 | 1.568 | 1.832 | 0.730 |
| | 315201 | 1.499 | 1.901 | 0.757 |
| | 377535 | 1.442 | 1.958 | 0.780 |
| HPS off interlock | 398000 | 1.505 | 1.895 | 0.755 |
| | 412730 | 1.311 | 2.089 | 0.832 |
| | 433135 | 1.192 | 2.208 | 0.880 |
| | 443261 | 1.141 | 2.259 | 0.900 |
| | 453522 | 1.089 | 2.311 | 0.921 |
| | 486728 | 0.950 | 2.450 | 0.976 |
| | 562097 | 0.738 | 2.662 | 1.061 |
| | 674623 | 0.476 | 2.924 | 1.165 |
| | 834402 | -0.134 | 3.534 | 1.408 |
| | 927466 | -0.945 | 4.345 | 1.731 |
| | 973500 | -1.808 | 5.208 | 2.075 |
| | 989104 | -2.268 | 5.668 | 2.258 |
| | 1028329 | -4.4500 | 7.850 | 3.127 |
| | 1046370 | -7.8740 | 11.274 | 4.492 |

Deviator stress ratio 0.45

| No. of load reps [-] | displacement recorded [mm] | relative displacement [mm] | relative strain [%] |
|---|---|---|---|
| 0 | 6.000 | | |
| 21 | 5.805 | 0.000 | |
| 52 | 5.655 | 0.150 | 0.060 |
| 122 | 5.481 | 0.324 | 0.129 |
| 201 | 5.370 | 0.435 | 0.173 |
| 500 | 5.143 | 0.662 | 0.264 |
| 1160 | 4.900 | 0.905 | 0.361 |
| 2001 | 4.724 | 1.081 | 0.431 |
| 5116 | 4.385 | 1.420 | 0.566 |
| 10224 | 4.115 | 1.690 | 0.673 |
| 18019 | 3.870 | 1.935 | 0.771 |
| 38900 | 3.438 | 2.367 | 0.943 |
| 51506 | 3.220 | 2.585 | 1.030 |
| 100469 | 2.307 | 3.498 | 1.394 |
| 169538 | 1.159 | 4.646 | 1.851 |
| 212825 | -0.861 | 6.666 | 2.656 |
| 229034 | -2.442 | 8.247 | 3.286 |
| 247342 | -7.874 | 13.679 | 5.450 |

Deviator stress ratio 0.50

| No. of load reps [-] | displacement recorded [mm] | relative displacement [mm] | relative strain [%] |
|---|---|---|---|
| 0 | 6.250 | | |
| 21 | 5.803 | 0.000 | |
| 52 | 5.562 | 0.241 | 0.096 |
| 100 | 5.366 | 0.437 | 0.174 |
| 201 | 5.137 | 0.666 | 0.265 |
| 500 | 4.782 | 1.021 | 0.407 |
| 1600 | 4.159 | 1.644 | 0.655 |
| 2501 | 3.847 | 1.956 | 0.779 |
| 5124 | 3.206 | 2.597 | 1.035 |
| 10001 | 2.325 | 3.478 | 1.386 |
| 20010 | 0.775 | 5.028 | 2.003 |
| 41132 | -5.534 | 11.337 | 4.517 |

Deviator stress ratio 0.60

| No. of load reps [-] | displacement recorded [mm] | relative displacement [mm] | relative strain [%] |
|---|---|---|---|
| 0 | 2.690 | | |
| 21 | 2.369 | 0.000 | |
| 51 | 2.180 | 0.189 | 0.075 |
| 101 | 1.984 | 0.385 | 0.153 |
| 201 | 1.746 | 0.623 | 0.248 |
| 500 | 1.295 | 1.074 | 0.428 |
| 1000 | 0.809 | 1.560 | 0.622 |
| 2000 | -0.023 | 2.392 | 0.953 |
| 4000 | -1.695 | 4.064 | 1.619 |
| 7905 | -5.505 | 7.874 | 3.137 |
| 9300 | -7.730 | 10.099 | 4.024 |

**Mix B-75M-0**

Deviator stress ratio 0.38

| No. of load reps [-] | displacement recorded [mm] | relative displacement [mm] | relative strain [%] |
|---|---|---|---|
| 0 | 5.900 | | |
| 21 | 5.635 | 0.000 | |
| 51 | 5.499 | 0.136 | 0.054 |
| 101 | 5.366 | 0.269 | 0.107 |
| 200 | 5.237 | 0.398 | 0.159 |
| 500 | 5.036 | 0.599 | 0.239 |
| 1000 | 4.852 | 0.783 | 0.312 |
| 2000 | 4.640 | 0.995 | 0.396 |
| 5201 | 4.279 | 1.356 | 0.540 |
| 10631 | 3.952 | 1.683 | 0.671 |
| 20500 | 3.612 | 2.023 | 0.806 |
| 53110 | 3.106 | 2.529 | 1.008 |
| 127000 | 2.600 | 3.035 | 1.209 |
| 185620 | 2.382 | 3.253 | 1.296 |
| 308150 | 2.124 | 3.511 | 1.399 |
| 377250 | 2.028 | 3.607 | 1.437 |
| 522560 | 1.882 | 3.753 | 1.495 |
| 700450 | 1.732 | 3.903 | 1.555 |
| 856500 | 1.577 | 4.058 | 1.617 |
| 923000 | 1.518 | 4.117 | 1.640 |
| 1031700 | 1.428 | 4.207 | 1.676 |

Deviator stress ratio 0.45

| No. of load reps [-] | displacement recorded [mm] | relative displacement [mm] | relative strain [%] |
|---|---|---|---|
| 0 | 5.500 | | |
| 26 | 5.280 | 0.000 | |
| 55 | 5.154 | 0.126 | 0.051 |
| 101 | 5.015 | 0.265 | 0.107 |
| 200 | 4.837 | 0.443 | 0.179 |
| 500 | 4.538 | 0.742 | 0.299 |
| 1000 | 4.242 | 1.038 | 0.419 |
| 2000 | 3.857 | 1.423 | 0.574 |
| 5001 | 3.155 | 2.125 | 0.857 |
| 10000 | 2.412 | 2.868 | 1.156 |
| 20650 | 1.391 | 3.889 | 1.568 |
| 51750 | -0.323 | 5.603 | 2.259 |
| 80602 | -1.255 | 6.535 | 2.635 |
| 161750 | -2.728 | 8.008 | 3.229 |
| 256300 | -3.553 | 8.833 | 3.562 |
| 334011 | -3.995 | 9.275 | 3.740 |
| 376176 | -4.214 | 9.494 | 3.828 |
| 398100 | -4.322 | 9.602 | 3.872 |
| 523621 | -4.931 | 10.211 | 4.117 |

Deviator stress ratio 0.60

| No. of load reps [-] | displacement recorded [mm] | relative displacement [mm] | relative strain [%] |
|---|---|---|---|
| 0 | 4.500 | | |
| 19 | 4.263 | 0.000 | |
| 50 | 4.092 | 0.171 | 0.068 |
| 100 | 3.927 | 0.336 | 0.134 |
| 200 | 3.726 | 0.537 | 0.214 |
| 501 | 3.371 | 0.892 | 0.355 |
| 1000 | 2.999 | 1.264 | 0.504 |
| 2000 | 2.509 | 1.754 | 0.699 |
| 5112 | 1.513 | 2.750 | 1.096 |
| 10001 | 0.350 | 3.913 | 1.559 |
| 15200 | -0.623 | 4.886 | 1.947 |
| 24524 | -2.080 | 6.343 | 2.527 |
| 36201 | -3.619 | 7.882 | 3.140 |
| 46900 | -4.711 | 8.974 | 3.575 |
| 79035 | -7.874 | 12.137 | 4.835 |

Deviator stress ratio 0.70

| No. of load reps [-] | displacement recorded [mm] | relative displacement [mm] | relative strain [%] |
|---|---|---|---|
| 0 | 4.800 | | |
| 21 | 4.513 | 0.000 | |
| 52 | 4.295 | 0.218 | 0.087 |
| 100 | 4.060 | 0.453 | 0.180 |
| 201 | 3.750 | 0.763 | 0.304 |
| 500 | 3.129 | 1.384 | 0.551 |
| 1000 | 2.383 | 2.130 | 0.849 |
| 2000 | 1.176 | 3.337 | 1.329 |
| 5001 | -1.846 | 6.359 | 2.533 |
| 8000 | -4.721 | 9.234 | 3.679 |
| 11151 | -7.859 | 12.372 | 4.929 |

## Mix C-75C-0

Deviator stress ratio 0.30

| No. of load reps [-] | displacement recorded [mm] | relative displacement [mm] | relative strain [%] |
|---|---|---|---|
| 0 | 7.000 | | |
| 20 | 6.755 | 0.000 | |
| 50 | 6.550 | 0.205 | 0.083 |
| 100 | 6.391 | 0.364 | 0.147 |
| 200 | 6.226 | 0.529 | 0.213 |
| 500 | 5.970 | 0.785 | 0.317 |
| 1000 | 5.734 | 1.021 | 0.412 |
| 2000 | 5.462 | 1.293 | 0.521 |
| 6701 | 5.055 | 1.700 | 0.685 |
| 12250 | 4.879 | 1.876 | 0.756 |
| 20751 | 4.765 | 1.990 | 0.802 |
| 52800 | 4.568 | 2.187 | 0.882 |
| 97778 | 4.457 | 2.298 | 0.927 |
| 170050 | 4.406 | 2.349 | 0.947 |
| 259505 | 4.370 | 2.385 | 0.962 |
| 353300 | 4.335 | 2.420 | 0.976 |
| 445711 | 4.327 | 2.428 | 0.979 |
| 554500 | 4.307 | 2.448 | 0.987 |
| 747200 | 4.270 | 2.485 | 1.002 |
| 912500 | 4.264 | 2.491 | 1.004 |
| 1088400 | 4.254 | 2.501 | 1.008 |

Deviator stress ratio 0.40

| No. of load reps [-] | displacement recorded [mm] | relative displacement [mm] | relative strain [%] |
|---|---|---|---|
| 0 | 6.000 | | |
| 20 | 5.595 | 0.000 | |
| 50 | 5.407 | 0.188 | 0.076 |
| 100 | 5.244 | 0.351 | 0.142 |
| 200 | 5.060 | 0.535 | 0.216 |
| 500 | 4.764 | 0.831 | 0.335 |
| 1000 | 4.456 | 1.139 | 0.459 |
| 2050 | 4.064 | 1.531 | 0.617 |
| 5555 | 3.336 | 2.259 | 0.911 |
| 11701 | 2.636 | 2.959 | 1.193 |
| 20700 | 2.054 | 3.541 | 1.428 |
| 40000 | 1.519 | 4.076 | 1.644 |
| 80880 | 0.985 | 4.610 | 1.859 |
| 159701 | 0.501 | 5.094 | 2.054 |
| 218000 | 0.405 | 5.190 | 2.093 |
| 345500 | 0.306 | 5.289 | 2.133 |

Deviator stress ratio 0.50

| No. of load reps [-] | displacement recorded [mm] | relative displacement [mm] | relative strain [%] |
|---|---|---|---|
| 0 | 6.000 | | |
| 20 | 5.240 | 0.000 | |
| 50 | 4.808 | 0.432 | 0.172 |
| 100 | 4.316 | 0.924 | 0.368 |
| 200 | 3.648 | 1.592 | 0.634 |
| 500 | 2.173 | 3.067 | 1.222 |
| 999 | -0.094 | 5.334 | 2.125 |
| 2000 | -5.535 | 10.775 | 4.293 |
| 2358 | -7.800 | 13.040 | 5.195 |

Deviator stress ratio 0.60

| No. of load reps [-] | displacement recorded [mm] | relative displacement [mm] | relative strain [%] |
|---|---|---|---|
| 0 | 5.900 | | |
| 20 | 5.227 | 0.000 | |
| 50 | 4.892 | 0.335 | 0.133 |
| 100 | 4.553 | 0.674 | 0.269 |
| 200 | 4.121 | 1.106 | 0.441 |
| 500 | 2.716 | 2.511 | 1.000 |
| 1056 | 0.173 | 5.054 | 2.014 |
| 2000 | -7.863 | 13.090 | 5.215 |

## Mix C-75C-1

Deviator stress ratio 0.40

| | No. of load reps [-] | displacement recorded [mm] | relative displacement [mm] | relative strain [%] |
|---|---|---|---|---|
| | 0 | 7.700 | | |
| | 20 | 7.413 | 0.000 | |
| | 50 | 7.281 | 0.132 | 0.053 |
| | 100 | 7.180 | 0.233 | 0.094 |
| | 200 | 7.064 | 0.349 | 0.141 |
| | 500 | 6.917 | 0.496 | 0.200 |
| | 1002 | 6.801 | 0.612 | 0.247 |
| | 2000 | 6.682 | 0.731 | 0.295 |
| | 5200 | 6.525 | 0.888 | 0.358 |
| | 10500 | 6.397 | 1.016 | 0.410 |
| | 22020 | 6.262 | 1.151 | 0.464 |
| | 75000 | 6.056 | 1.357 | 0.547 |
| | 155300 | 5.955 | 1.458 | 0.588 |
| | 214000 | 5.923 | 1.490 | 0.601 |
| temp low | 344300 | 5.850 | 1.563 | 0.630 |
| | 405650 | 5.853 | 1.560 | 0.629 |
| | 518500 | 5.800 | 1.613 | 0.650 |
| | 711811 | 5.743 | 1.670 | 0.673 |
| | 896250 | 5.718 | 1.695 | 0.683 |
| | 1072320 | 5.693 | 1.720 | 0.694 |

Deviator stress ratio 0.50

| No. of load reps [-] | displacement recorded [mm] | relative displacement [mm] | relative strain [%] |
|---|---|---|---|
| 0 | 7.000 | | |
| 20 | 6.730 | 0.000 | |
| 54 | 6.580 | 0.150 | 0.060 |
| 104 | 6.477 | 0.253 | 0.101 |
| 200 | 6.365 | 0.365 | 0.145 |
| 499 | 6.110 | 0.620 | 0.247 |
| 1000 | 5.994 | 0.736 | 0.293 |
| 2000 | 5.875 | 0.855 | 0.341 |
| 5000 | 5.706 | 1.024 | 0.408 |
| 10206 | 5.598 | 1.132 | 0.451 |
| 23499 | 5.484 | 1.246 | 0.496 |
| 69820 | 5.256 | 1.474 | 0.587 |
| 141351 | 4.964 | 1.766 | 0.704 |
| 210999 | 4.746 | 1.984 | 0.790 |
| 358012 | 4.616 | 2.114 | 0.842 |
| 541050 | 3.728 | 3.002 | 1.196 |
| 618500 | 2.066 | 4.664 | 1.858 |
| 658292 | -7.800 | 14.530 | 5.789 |

Deviator stress ratio 0.55

| No. of load reps [-] | displacement recorded [mm] | relative displacement [mm] | relative strain [%] |
|---|---|---|---|
| 0 | 7.200 | | |
| 22 | 6.817 | 0.000 | |
| 50 | 6.657 | 0.160 | 0.064 |
| 100 | 6.501 | 0.316 | 0.126 |
| 201 | 6.345 | 0.472 | 0.188 |
| 500 | 6.111 | 0.706 | 0.281 |
| 1000 | 5.909 | 0.908 | 0.362 |
| 2131 | 5.685 | 1.132 | 0.451 |
| 5000 | 5.349 | 1.468 | 0.585 |
| 10201 | 4.980 | 1.837 | 0.732 |
| 20500 | 4.415 | 2.402 | 0.957 |
| 47600 | 3.552 | 3.265 | 1.301 |
| 82541 | -7.800 | 14.617 | 5.824 |

Deviator stress ratio 0.60

| No. of load reps [-] | displacement recorded [mm] | relative displacement [mm] | relative strain [%] |
|---|---|---|---|
| 0 | 6.700 | | |
| 20 | 6.460 | 0.000 | |
| 50 | 6.335 | 0.125 | 0.050 |
| 100 | 6.231 | 0.229 | 0.091 |
| 200 | 6.109 | 0.351 | 0.140 |
| 500 | 5.926 | 0.534 | 0.213 |
| 1056 | 5.740 | 0.720 | 0.287 |
| 2000 | 5.547 | 0.913 | 0.364 |
| 6200 | 5.070 | 1.390 | 0.554 |
| 10606 | 4.764 | 1.696 | 0.676 |
| 22003 | 4.122 | 2.338 | 0.931 |
| 37400 | 2.724 | 3.736 | 1.488 |
| 51800 | -3.375 | 9.835 | 3.918 |
| 53066 | -7.800 | 14.260 | 5.681 |

Deviator stress ratio 0.70

| No. of load reps [-] | displacement recorded [mm] | relative displacement [mm] | relative strain [%] |
|---|---|---|---|
| 0 | 7.100 | | |
| 19 | 6.704 | 0.000 | |
| 50 | 6.510 | 0.194 | 0.077 |
| 100 | 6.330 | 0.374 | 0.149 |
| 200 | 6.109 | 0.595 | 0.237 |
| 501 | 5.715 | 0.989 | 0.394 |
| 1000 | 5.251 | 1.453 | 0.579 |
| 2000 | 4.407 | 2.297 | 0.915 |
| 3200 | 3.200 | 3.504 | 1.396 |
| 4000 | 1.899 | 4.805 | 1.914 |
| 5000 | -3.989 | 10.693 | 4.260 |
| 5098 | -7.800 | 14.504 | 5.778 |

**Mix C-75M-0**

Deviator stress ratio 0.45

| No. of load reps [-] | displacement recorded [mm] | relative displacement [mm] | relative strain [%] |
|---|---|---|---|
| 0 | 7.100 | | |
| 20 | 6.954 | 0.000 | |
| 50 | 6.856 | 0.098 | 0.039 |
| 100 | 6.785 | 0.169 | 0.067 |
| 201 | 6.707 | 0.247 | 0.098 |
| 500 | 6.577 | 0.377 | 0.150 |
| 1000 | 6.463 | 0.491 | 0.196 |
| 2000 | 6.331 | 0.623 | 0.248 |
| 5350 | 6.110 | 0.844 | 0.336 |
| 10151 | 5.939 | 1.015 | 0.404 |
| 20600 | 5.728 | 1.226 | 0.488 |
| 51750 | 5.404 | 1.550 | 0.618 |
| 96100 | 5.197 | 1.757 | 0.700 |
| 171261 | 5.007 | 1.947 | 0.776 |
| 277120 | 4.827 | 2.127 | 0.847 |
| 351601 | 4.725 | 2.229 | 0.888 |
| 407300 | 4.669 | 2.285 | 0.910 |
| 531200 | 4.555 | 2.399 | 0.956 |
| 589700 | 4.329 | 2.625 | 1.046 |
| 725100 | 3.727 | 3.227 | 1.286 |
| 812060 | 3.340 | 3.614 | 1.440 |
| 915800 | 3.248 | 3.706 | 1.476 |
| 1065600 | 3.139 | 3.815 | 1.520 |

Deviator stress ratio 0.60

| No. of load reps [-] | displacement recorded [mm] | relative displacement [mm] | relative strain [%] |
|---|---|---|---|
| 0 | 6.100 | | |
| 20 | 5.896 | 0.000 | |
| 50 | 5.785 | 0.111 | 0.044 |
| 100 | 5.685 | 0.211 | 0.084 |
| 200 | 5.568 | 0.328 | 0.131 |
| 500 | 5.391 | 0.505 | 0.201 |
| 1001 | 5.228 | 0.668 | 0.266 |
| 2001 | 5.043 | 0.853 | 0.340 |
| 5000 | 4.781 | 1.115 | 0.444 |
| 10121 | 4.521 | 1.375 | 0.548 |
| 23800 | 4.162 | 1.734 | 0.691 |
| 53151 | 3.724 | 2.172 | 0.865 |
| 90550 | 3.371 | 2.525 | 1.006 |
| 164101 | 2.786 | 3.110 | 1.239 |
| 222600 | 2.518 | 3.378 | 1.346 |
| 346220 | 1.963 | 3.933 | 1.567 |
| 405200 | 1.689 | 4.207 | 1.676 |
| 528120 | 0.960 | 4.936 | 1.967 |
| 583150 | 0.595 | 5.301 | 2.112 |
| 709609 | -0.368 | 6.264 | 2.496 |
| 816250 | -1.452 | 7.348 | 2.927 |
| 925501 | -2.934 | 8.830 | 3.518 |
| 988506 | -3.976 | 9.872 | 3.933 |
| 1084100 | -6.200 | 12.096 | 4.819 |
| 1104631 | -7.800 | 13.696 | 5.457 |

Deviator stress ratio 0.75

| No. of load reps [-] | displacement recorded [mm] | relative displacement [mm] | relative strain [%] |
|---|---|---|---|
| 0 | 5.000 | | |
| 20 | 4.742 | 0.000 | |
| 51 | 4.595 | 0.147 | 0.059 |
| 101 | 4.467 | 0.275 | 0.111 |
| 200 | 4.308 | 0.434 | 0.175 |
| 500 | 4.037 | 0.705 | 0.284 |
| 1000 | 3.776 | 0.966 | 0.390 |
| 2000 | 3.462 | 1.280 | 0.516 |
| 5000 | 2.943 | 1.799 | 0.725 |
| 10000 | 2.359 | 2.383 | 0.961 |
| 21200 | 1.415 | 3.327 | 1.342 |
| 41499 | -0.059 | 4.801 | 1.936 |
| 41601 | -0.085 | 4.827 | 1.946 |
| 51550 | -0.841 | 5.583 | 2.251 |
| 74150 | -2.607 | 7.349 | 2.963 |
| 134631 | -7.800 | 12.542 | 5.057 |

Deviator stress ratio 0.85

| No. of load reps [-] | displacement recorded [mm] | relative displacement [mm] | relative strain [%] |
|---|---|---|---|
| 0 | 5.400 | | |
| 20 | 5.114 | 0.000 | |
| 50 | 4.922 | 0.192 | 0.076 |
| 100 | 4.724 | 0.390 | 0.155 |
| 200 | 4.523 | 0.591 | 0.235 |
| 500 | 4.219 | 0.895 | 0.357 |
| 1000 | 3.911 | 1.203 | 0.479 |
| 2001 | 3.437 | 1.677 | 0.668 |
| valve confinement pressure closed due to bouncing 5500 | -0.639 | 5.753 | 2.292 |
| 6989 | -7.800 | 12.914 | 5.145 |

Deviator stress ratio 0.85 repeat

| No. of load reps | displacement recorded | relative displacement | relative strain |
|---|---|---|---|
| [-] | [mm] | [mm] | [%] |
| 0 | 5.500 | | |
| 20 | 5.232 | 0.000 | |
| 50 | 5.100 | 0.132 | 0.053 |
| 100 | 4.970 | 0.262 | 0.104 |
| 200 | 4.809 | 0.423 | 0.169 |
| 500 | 4.543 | 0.689 | 0.275 |
| 1000 | 4.282 | 0.950 | 0.378 |
| 2099 | 3.923 | 1.309 | 0.522 |
| 5000 | 3.326 | 1.906 | 0.759 |
| 11623 | 2.282 | 2.950 | 1.175 |
| 20200 | 0.932 | 4.300 | 1.713 |
| 52202 | -6.514 | 11.746 | 4.680 |
| 56586 | -7.800 | 13.032 | 5.192 |

## DEFORMATION PLOTS ON NORMAL SCALE (i.o. DOUBLE-LOG SCALE)

### Mix A-75C-0

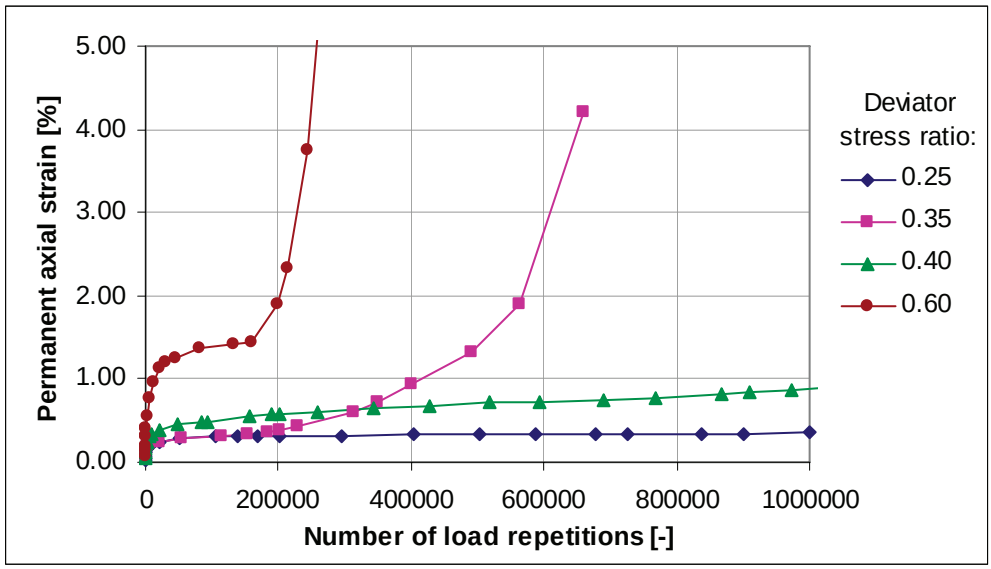


### Mix A-75C-1

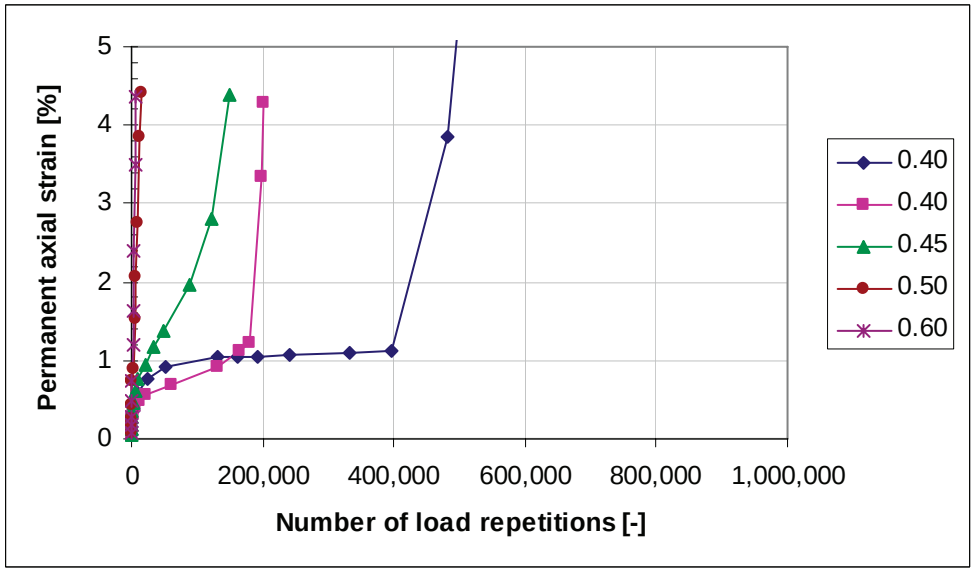

**Mix A-75M-0**

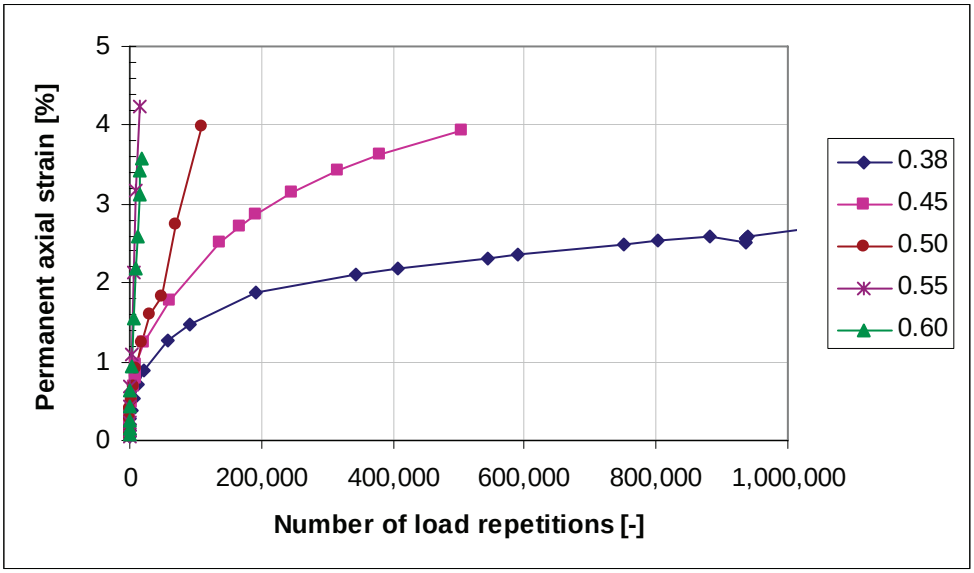


**Mix B-75C-0**

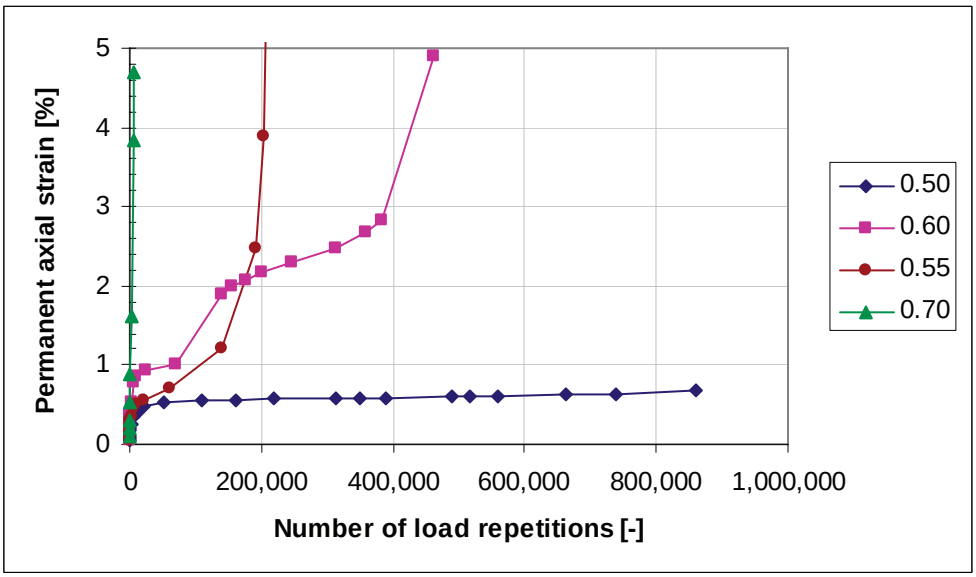

**Mix B-75C-1**

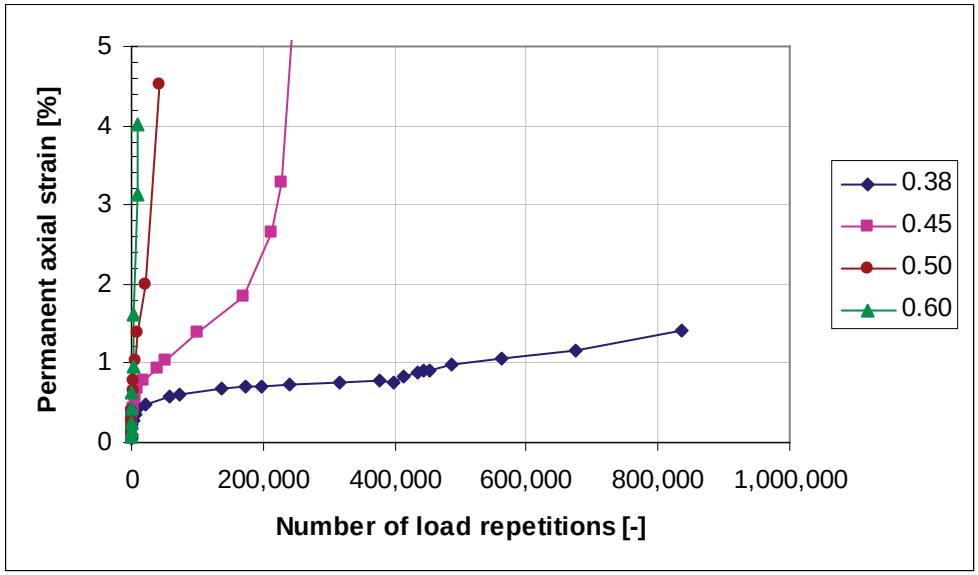


**Mix B-75M-0**

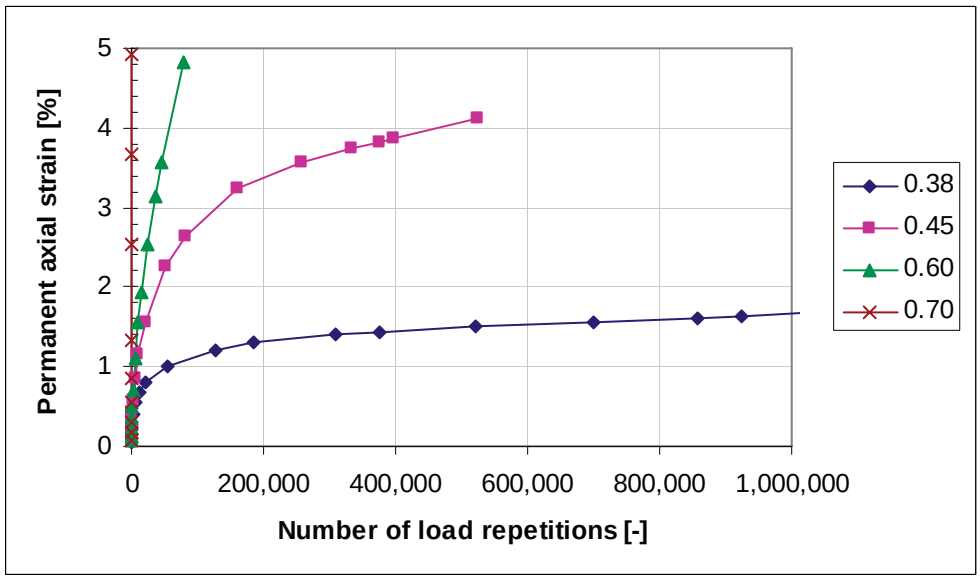

**Mix C-75C-0**

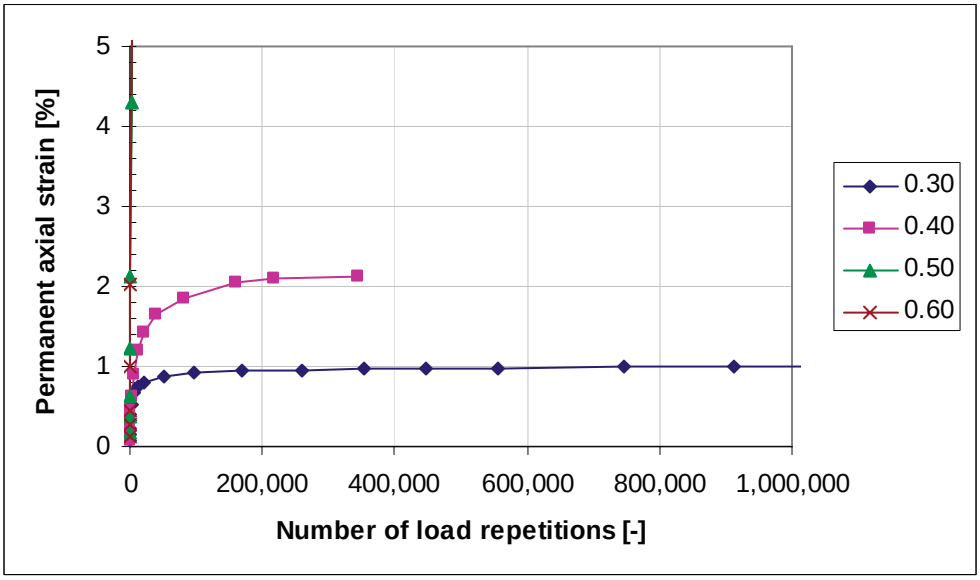


**Mix C-75C-1**

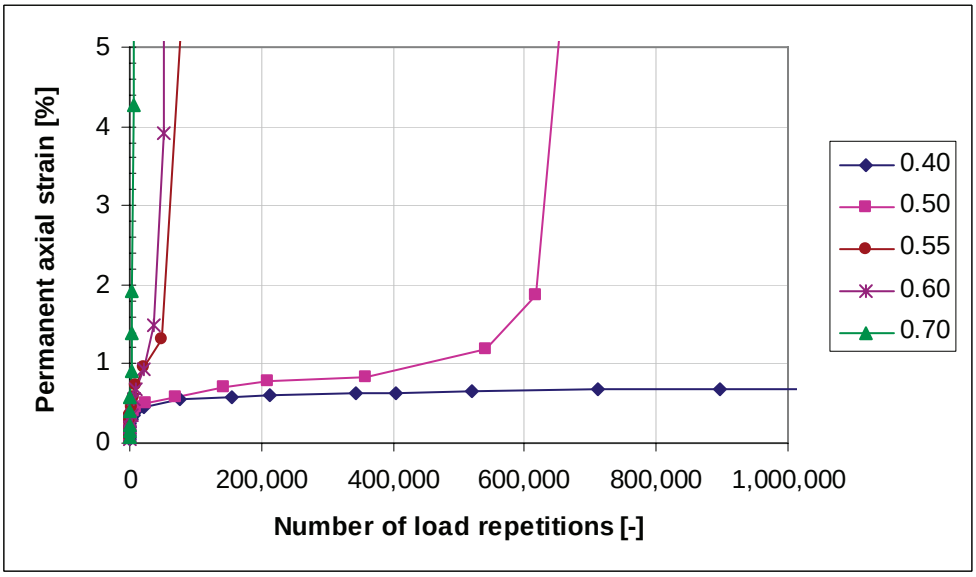

**Mix C-75M-0**

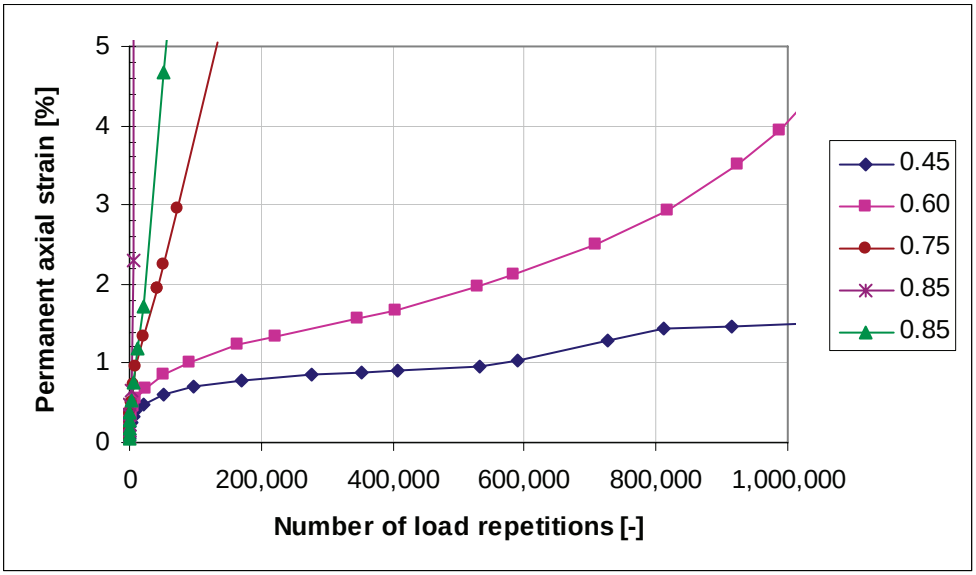
Permanent axial strain [%]
0
1
2
3
4
5
0
200,000
400,000
600,000
800,000
1,000,000
Number of load repetitions [-]
0.45
0.60
0.75
0.85
0.85

## General Permanent Deformation Law Model Fits

### A-75C-0

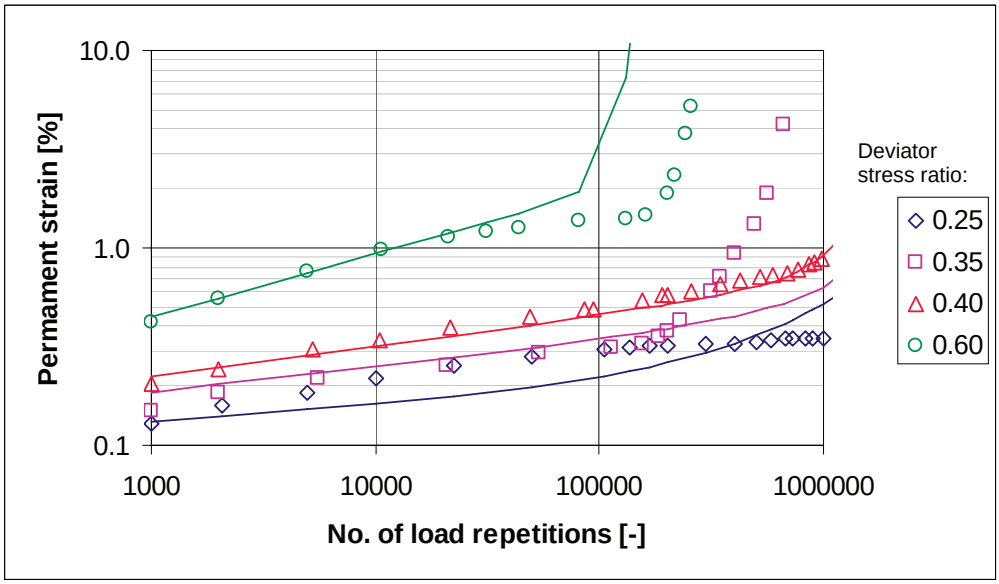


### A-75C-1

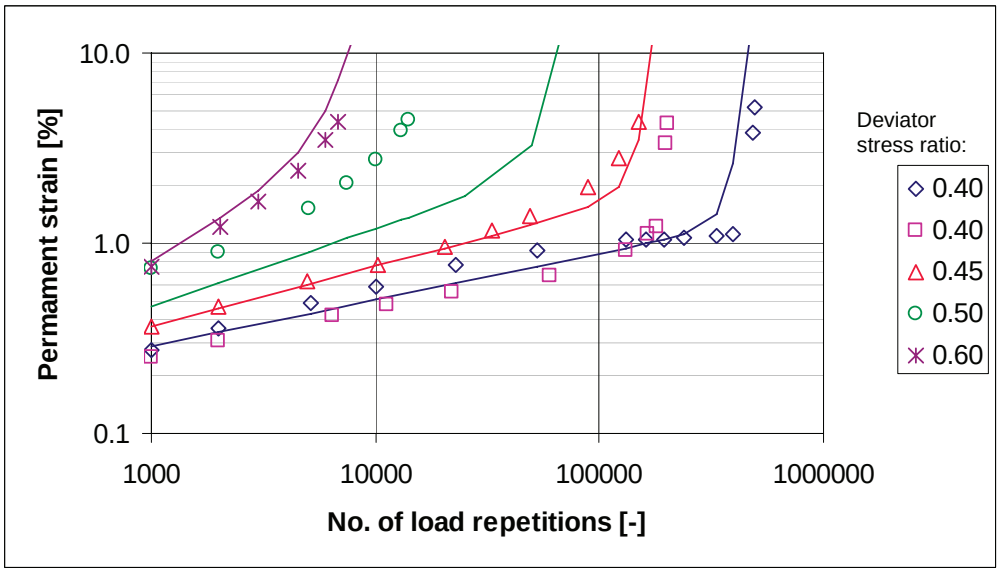

**A-75M-0**

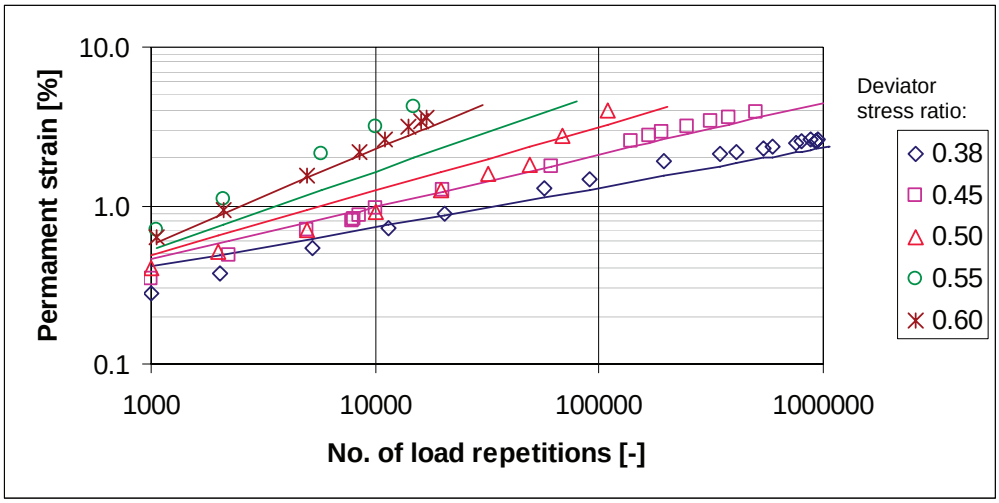
10.0
1.0
0.1
Permament strain [%]
1000
10000
100000
1000000
No. of load repetitions [-]
Deviator stress ratio:
0.38
0.45
0.50
0.55
0.60

**B-75C-0**

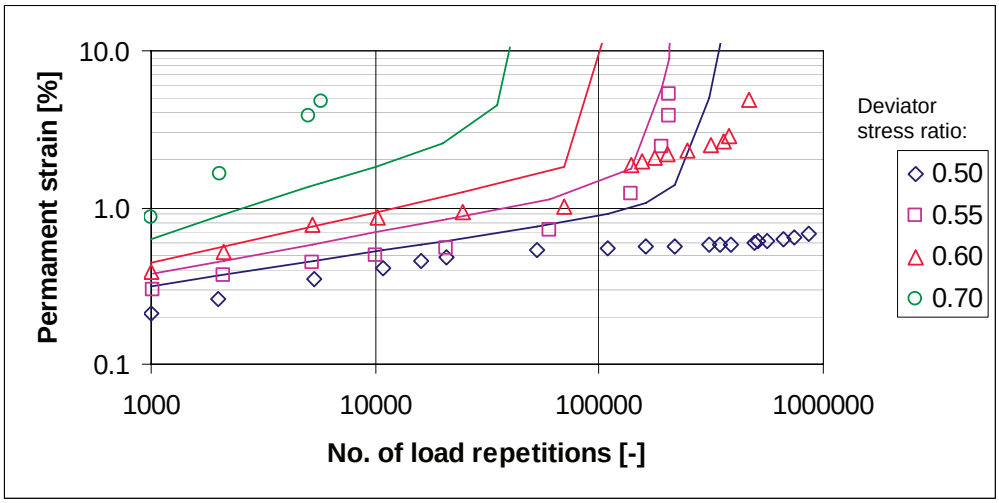
10.0
1.0
0.1
Permament strain [%]
1000
10000
100000
1000000
No. of load repetitions [-]
Deviator stress ratio:
0.50
0.55
0.60
0.70

**B-75C-1**

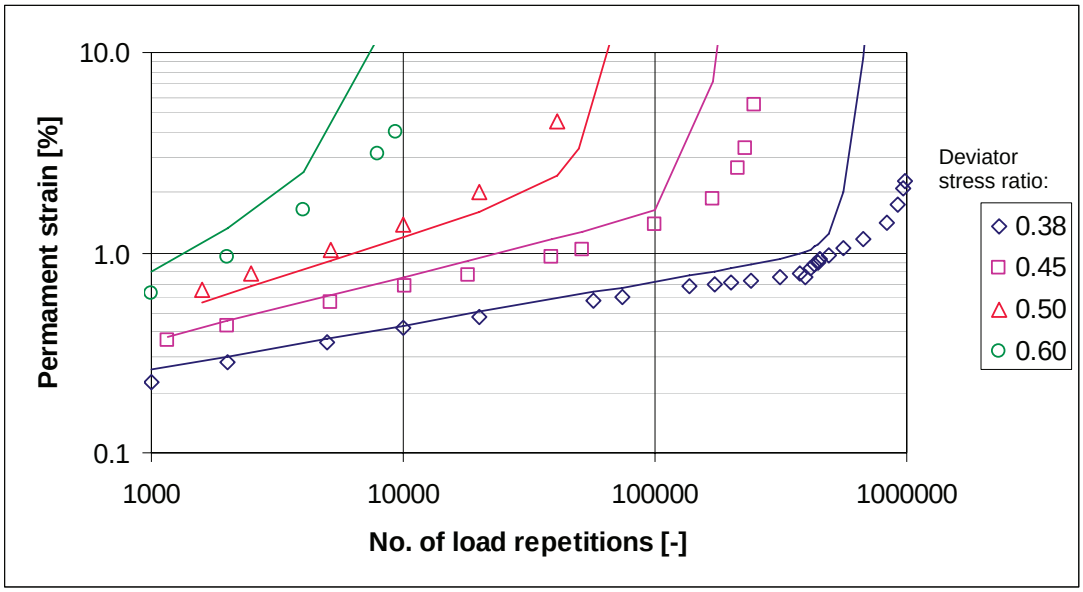
10.0
1.0
0.1
Permament strain [%]
1000
10000
100000
1000000
No. of load repetitions [-]
Deviator stress ratio:
0.38
0.45
0.50
0.60

**B-75M-0**

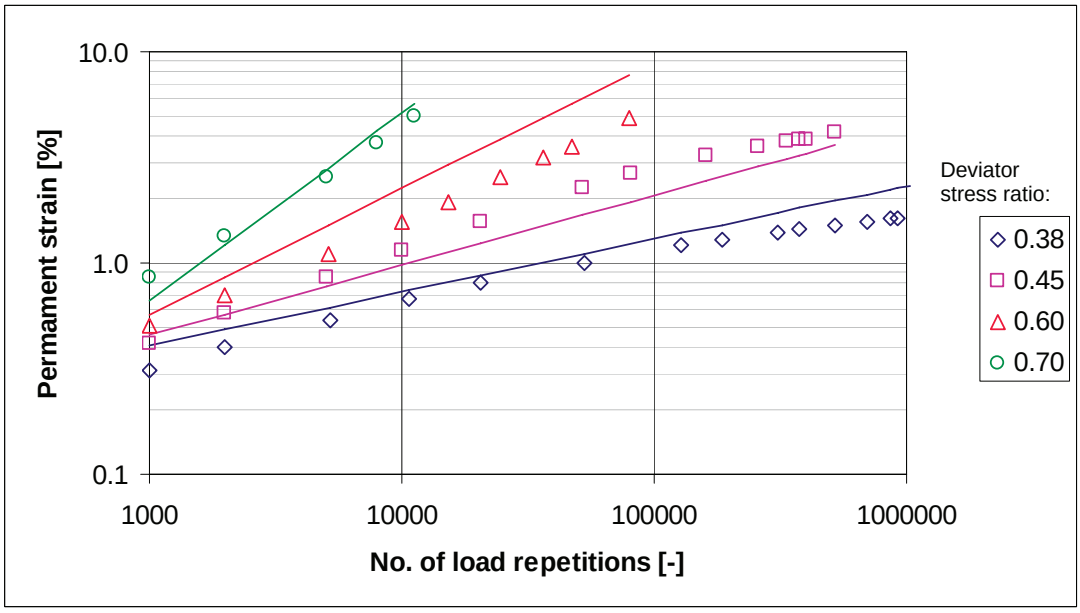
10.0
1.0
0.1
Permament strain [%]
1000
10000
100000
1000000
No. of load repetitions [-]
Deviator stress ratio:
0.38
0.45
0.60
0.70

**C-75C-0**

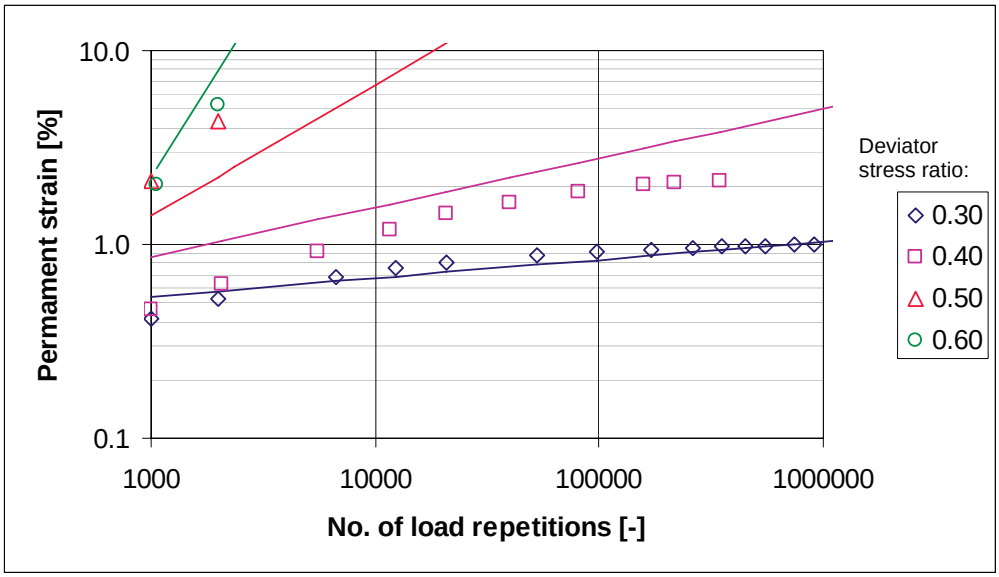
10.0
1.0
0.1
Permament strain [%]
1000
10000
100000
1000000
No. of load repetitions [-]
Deviator stress ratio:
0.30
0.40
0.50
0.60

**C-75C-1**

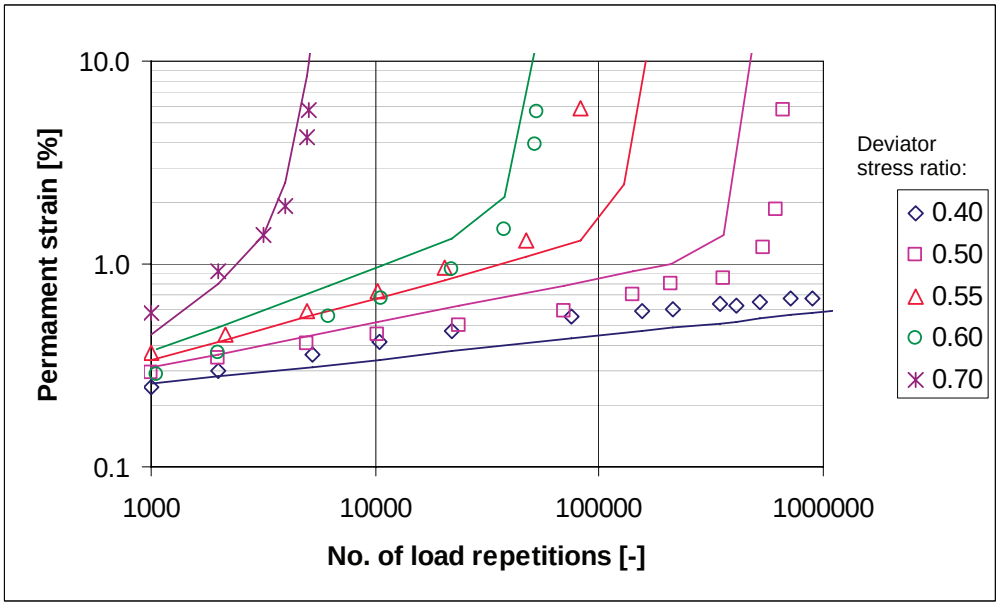
10.0
1.0
0.1
Permament strain [%]
1000
10000
100000
1000000
No. of load repetitions [-]
Deviator stress ratio:
0.40
0.50
0.55
0.60
0.70

**C-75M-0**

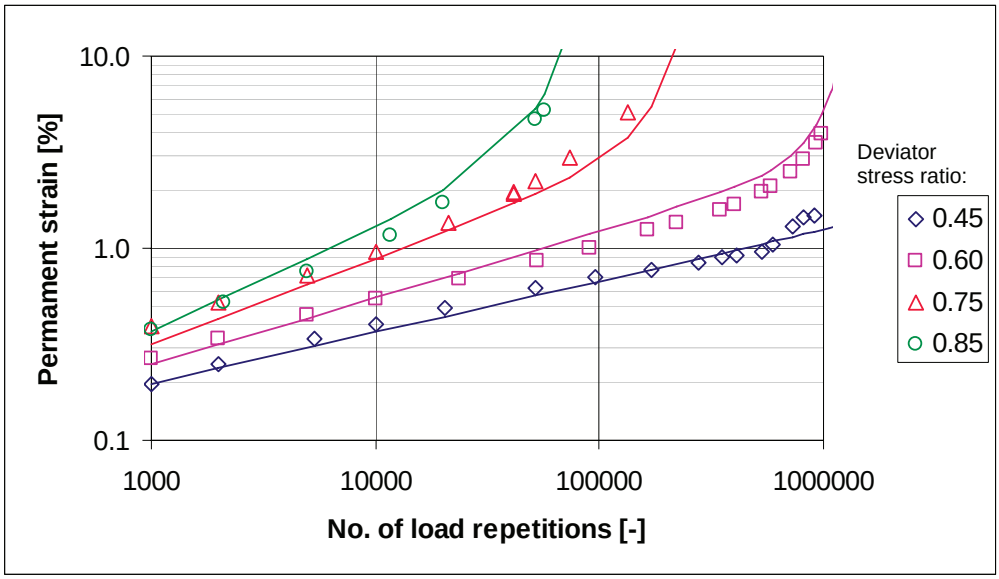
10.0
1.0
0.1
Permament strain [%]
1000
10000
100000
1000000
No. of load repetitions [-]
Deviator stress ratio:
0.45
0.60
0.75
0.85

# APPENDIX H : STRAIN-AT-BREAK TESTING RESULTS

**A-75C-0**

| Beam | Actuator displacement at peak load [mm] | Displacement converted to on-specimen LVDT [mm] | Peak load [kN] | height of beam [mm] | Strain-at-break [micron] |
|---|---|---|---|---|---|
| F1 | 3.5 | 1.018 | -0.053 | 52.28 | 1978 |
| F2 | 2.6 | 1.492 | -0.073 | 51.43 | 2850 |
| F3 | 3.2 | 1.754 | -0.082 | 51.28 | 3342 |

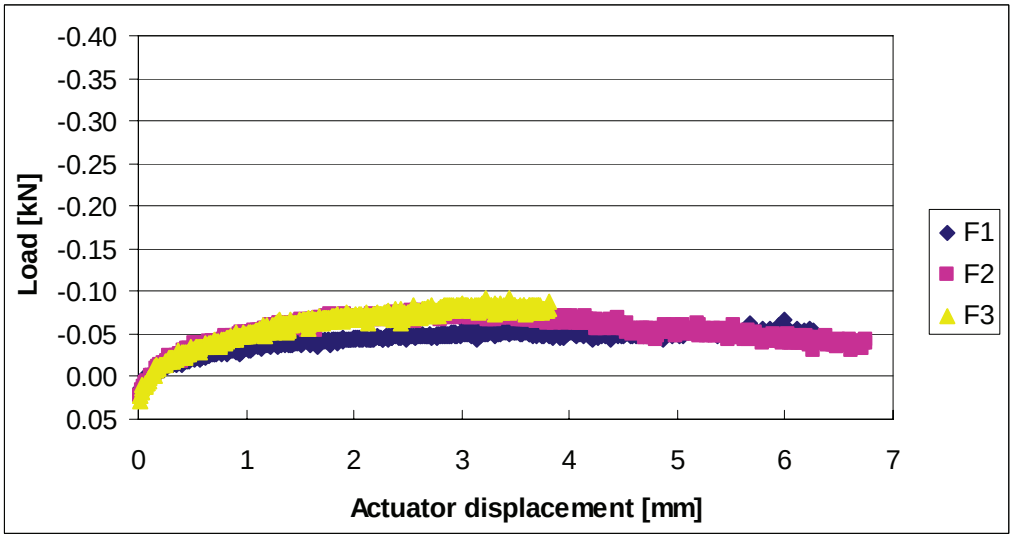

**A-75C-1**

| Beam | Actuator displacement at peak load [mm] | Displacement converted to on-specimen LVDT [mm] | Peak load [kN] | height of beam [mm] | Strain-at-break [micron] |
|---|---|---|---|---|---|
| D1 | 2.0 | 1.135 | -0.090 | 50.95 | 2149 |
| D2 | 5.9 | 2.059 | -0.037 | 51.12 | 3910 |
| D3 | 2.1 | 1.190 | -0.119 | 51.27 | 2268 |

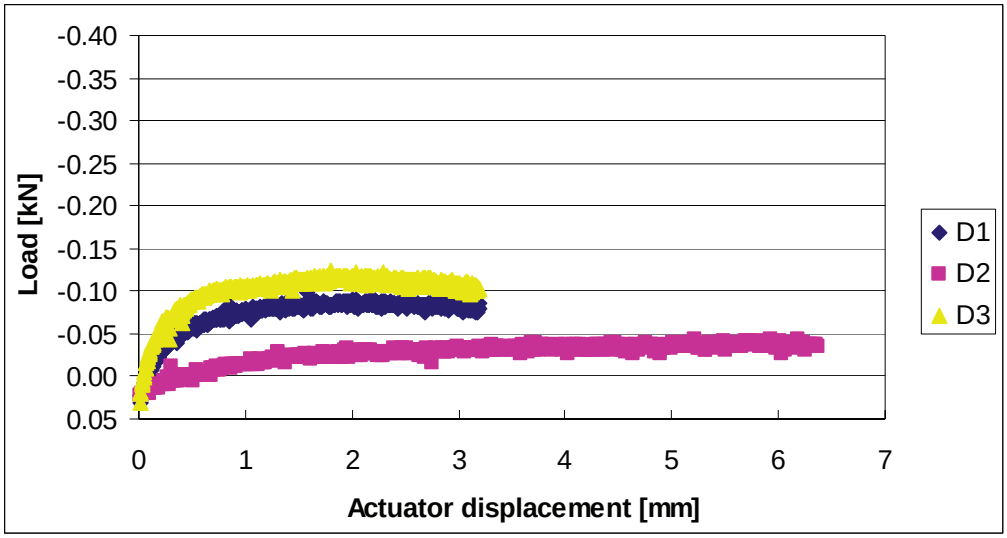

## A-75M-0

| Beam | Actuator displacement at peak load [mm] | Displacement converted to on-specimen LVDT [mm] | Peak load [kN] | height of beam [mm] | Strain-at-break [micron] |
|---|---|---|---|---|---|
| Y5 | 1.6 | 0.989 | -0.105 | 51.10 | 1878 |
| Z2 | 3.0 | 1.800 | -0.100 | 51.15 | 3421 |
| Z3 | 3.3 | 2.002 | -0.079 | 51.05 | 3798 |

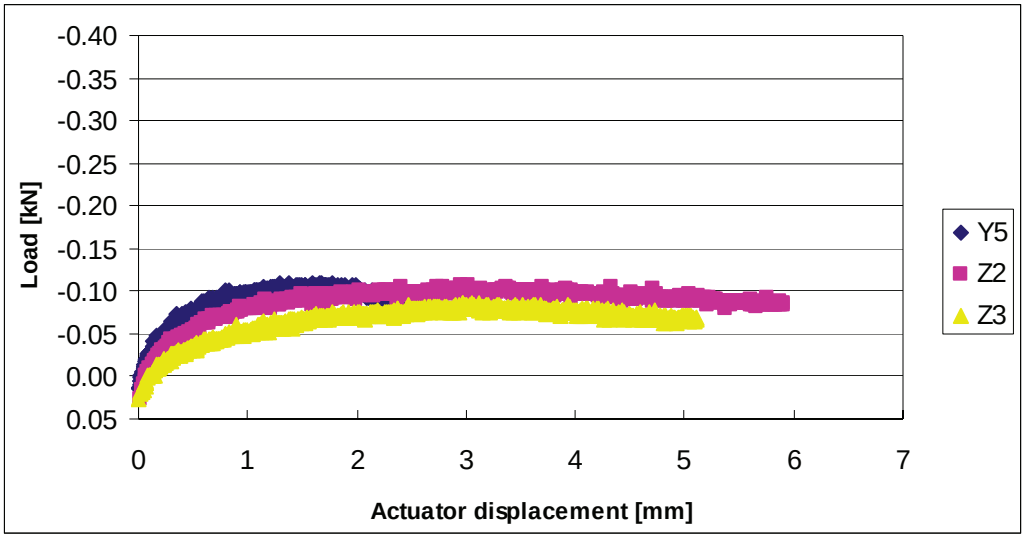

**B-75C-0**

| Beam | Actuator displacement at peak load [mm] | Displacement converted to on-specimen LVDT [mm] | Peak load [kN] | height of beam [mm] | Strain-at-break [micron] |
|---|---|---|---|---|---|
| C1 | 1.5 | 0.852 | -0.190 | 49.80 | 1577 |
| C5 | 2.0 | 1.177 | -0.123 | 50.65 | 2214 |
| C6 | 1.5 | 0.904 | -0.230 | 50.20 | 1686 |

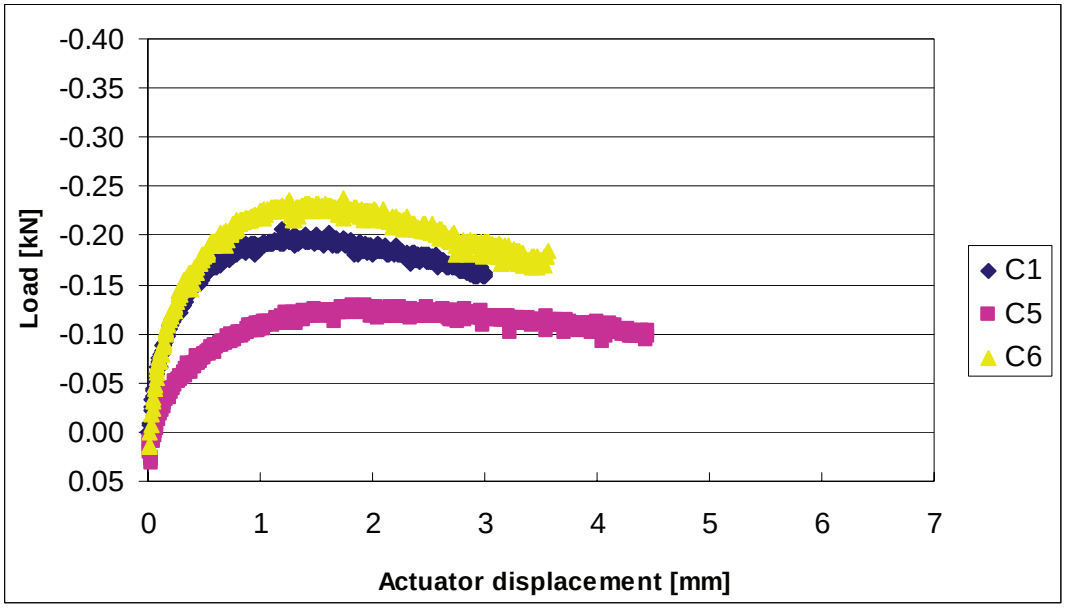

**B-75C-1**

| Beam | Actuator displacement at peak load [mm] | Displacement converted to on-specimen LVDT [mm] | Peak load [kN] | height of beam [mm] | Strain-at-break [micron] |
|---|---|---|---|---|---|
| D1 | 1.0 | 0.601 | -0.160 | 50.47 | 1127 |
| D3 | 0.6 | 0.409 | -0.115 | 50.80 | 771 |
| D4 | 1.1 | 0.633 | -0.160 | 50.40 | 1184 |

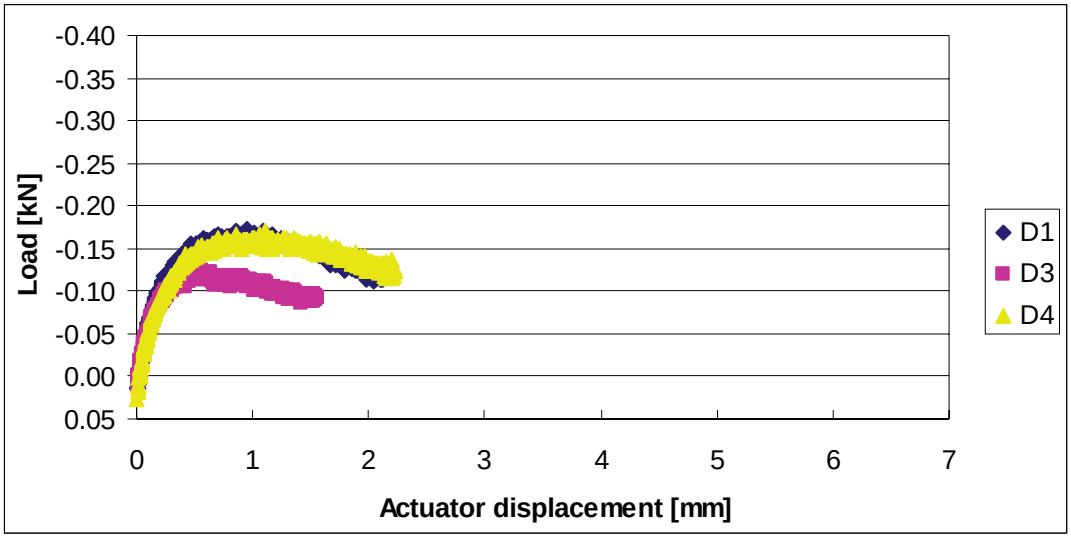

**B-75M-0**

| Beam | Actuator displacement at peak load [mm] | Displacement converted to on-specimen LVDT [mm] | Peak load [kN] | height of beam [mm] | Strain-at-break [micron] |
|---|---|---|---|---|---|
| C1 | 1.4 | 0.807 | -0.334 | 50.53 | 1516 |
| C2 | 0.8 | 0.478 | -0.165 | 49.80 | 885 |
| C5 | 0.65 | 0.434 | -0.177 | 50.47 | 814 |
| C6 | 0.9 | 0.557 | -0.198 | 50.33 | 1042 |

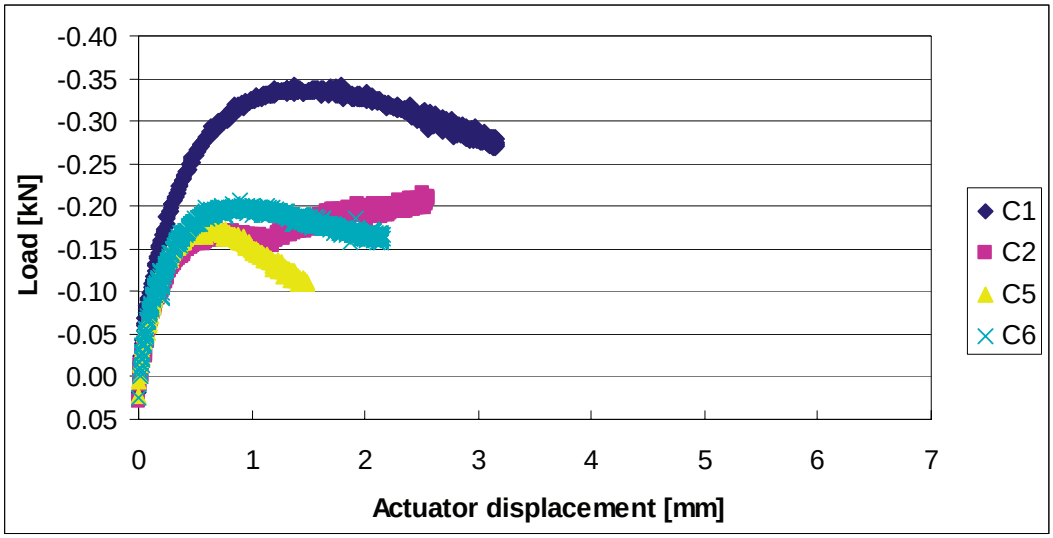

**C-75C-0**

| Beam | Actuator displacement at peak load [mm] | Displacement converted to on-specimen LVDT [mm] | Peak load [kN] | height of beam [mm] | Strain-at-break [micron] |
|---|---|---|---|---|---|
| C2 | 1.2 | 0.697 | -0.154 | 49.63 | 1285 |
| C5 | 1.5 | 0.887 | -0.190 | 50.20 | 1655 |
| C6 | 1.6 | 1.045 | -0.156 | 50.20 | 1950 |

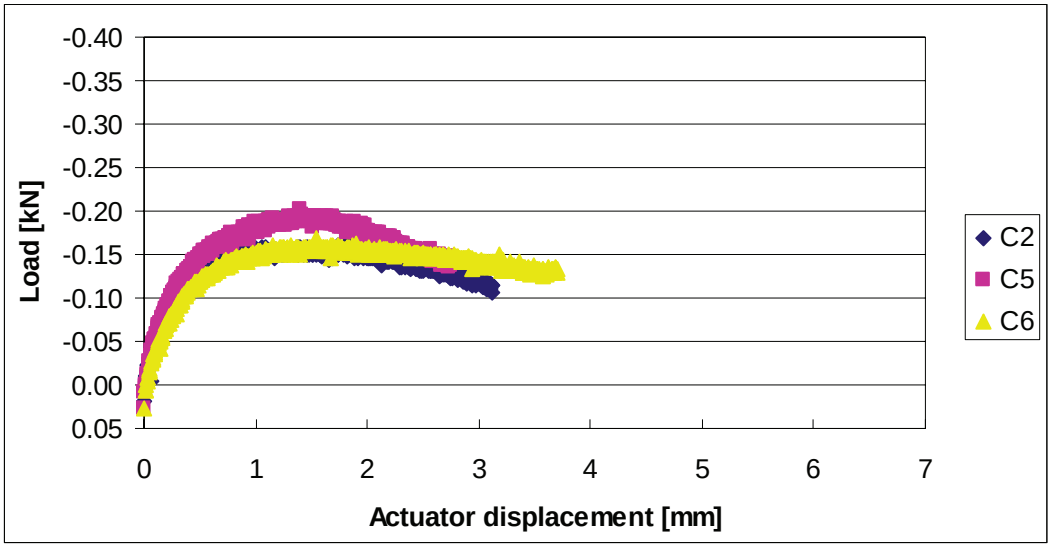

**C-75C-1**

| Beam | Actuator displacement at peak load [mm] | Displacement converted to on-specimen LVDT [mm] | Peak load [kN] | height of beam [mm] | Strain-at-break [micron] |
|---|---|---|---|---|---|
| C3 | 0.9 | 0.615 | -0.150 | 50.68 | 1158 |
| C5 | 2.4 | 1.289 | -0.158 | 49.48 | 2370 |
| C6 | 1.8 | 1.061 | -0.125 | 50.12 | 1976 |
| C1 | 2.8 | 1.533 | -0.248 | 50.30 | 2866 |

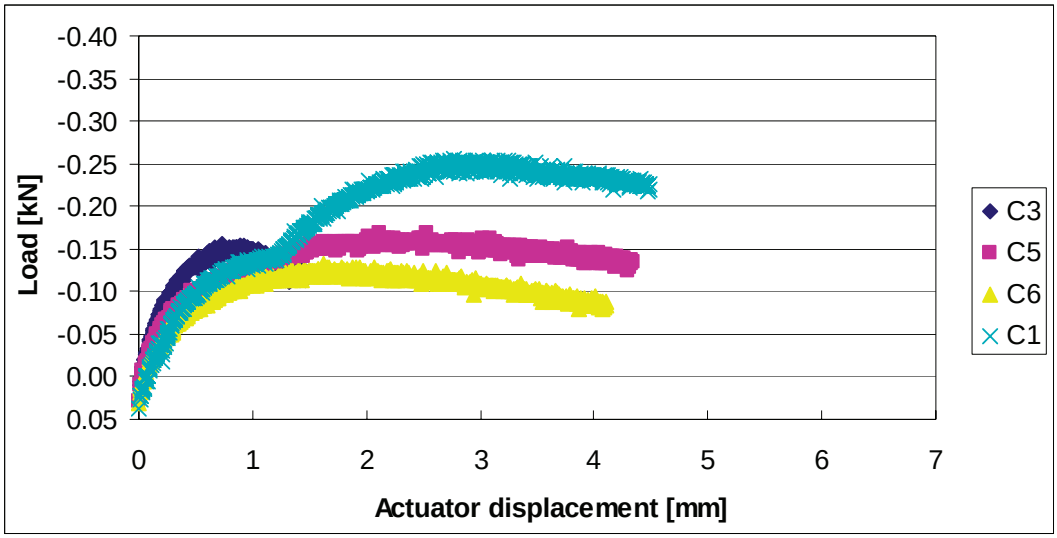

**C-75M-0**

| Beam | Actuator displacement at peak load [mm] | Displacement converted to on-specimen LVDT [mm] | Peak load [kN] | height of beam [mm] | Strain-at-break [micron] |
|---|---|---|---|---|---|
| B1 | 0.9 | 0.548 | -0.105 | 49.30 | 1004 |
| B2 | 1.1 | 0.651 | -0.138 | 50.70 | 1226 |
| B3 | 1.3 | 0.750 | -0.125 | 50.70 | 1412 |

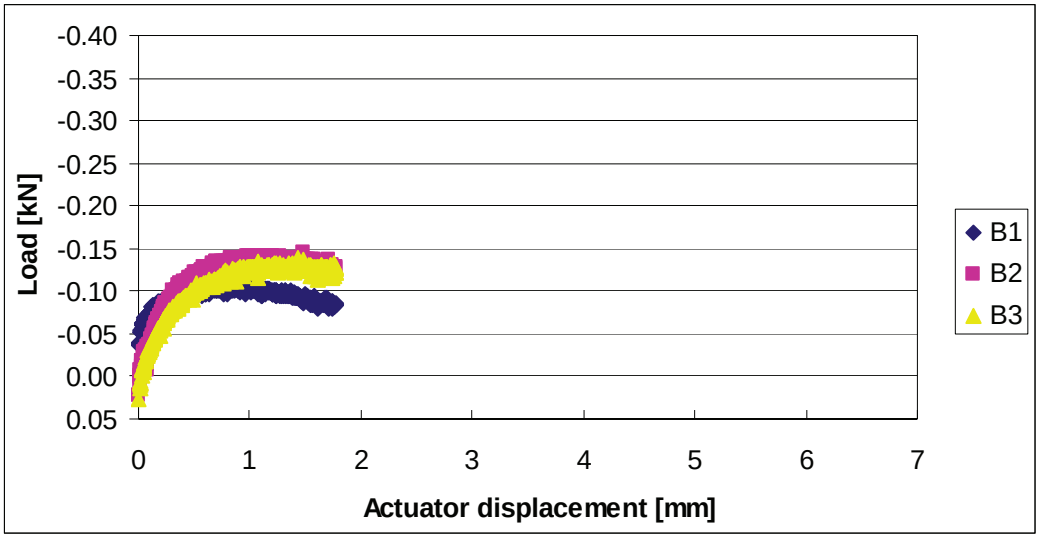

This page is left blank intentionally.

# APPENDIX I : FLEXURAL STIFFNESS TESTING RESULTS

Table 1: Flexural stiffness modulus for the 75C-0 mixes

| Test temperature [ºC] | Frequency [Hz] | Flexural stiffness modulus per binder type [MPa] | | | | | |
|---|---|---|---|---|---|---|---|
| | | A | | B | | C | |
| | | Beam E5 | Beam E6 | Beam D3 | Beam D4 | Beam C3 | Beam C4 |
| 5 | 0.5 | 2024 | 1841 | 2029 | 2010 | 1822 | 1788 |
| | 1 | 2317 | 1983 | 2329 | 2167 | 1937 | 1905 |
| | 2 | 2609 | 2018 | 2481 | 2310 | 2130 | 1970 |
| | 5 | 2976 | 2290 | 2950 | 2543 | 2333 | 2234 |
| | 10 | 3354 | 2565 | 3393 | 2828 | 2477 | 2430 |
| 10 | 0.5 | 1980 | 1808 | 1816 | 1610 | 1607 | 1682 |
| | 1 | 2218 | 1911 | 1997 | 1800 | 1741 | 1786 |
| | 2 | 2365 | 2011 | 2075 | 1950 | 1805 | 1895 |
| | 5 | 2664 | 2150 | 2451 | 2180 | 2000 | 2013 |
| | 10 | 2951 | 2370 | 2649 | 2355 | 2194 | 2249 |
| 15 | 0.5 | 1573 | 1499 | 1324 | 1290 | 1251 | 1392 |
| | 1 | 1710 | 1592 | 1475 | 1440 | 1381 | 1436 |
| | 2 | 1767 | 1695 | 1609 | 1520 | 1532 | 1536 |
| | 5 | 2102 | 1865 | 1775 | 1720 | 1650 | 1669 |
| | 10 | 2321 | 1933 | 1955 | 1850 | 1751 | 1901 |
| 20 | 0.5 | 1225 | 1147 | 1129 | 1044 | 1082 | 1174 |
| | 1 | 1305 | 1275 | 1224 | 1128 | 1181 | 1267 |
| | 2 | 1383 | 1348 | 1355 | 1303 | 1256 | 1358 |
| | 5 | 1658 | 1426 | 1467 | 1468 | 1345 | 1460 |
| | 10 | 1774 | 1550 | 1600 | 1625 | 1445 | 1555 |
| 25 | 0.5 | 1011 | 1018 | 1020 | 916 | 999 | 1053 |
| | 1 | 1038 | 1123 | 1029 | 1091 | 1039 | 1072 |
| | 2 | 1129 | 1073 | 1080 | 1087 | 1077 | 1136 |
| | 5 | 1172 | 1147 | 1180 | 1135 | 1198 | 1087 |
| | 10 | 1292 | 1218 | 1221 | 1266 | 1289 | 1151 |

Table 2: Flexural stiffness modulus for the 75C-1 mixes

| Test temperature [ºC] | Frequency [Hz] | Flexural stiffness modulus per binder type [MPa] | | | | | |
|---|---|---|---|---|---|---|---|
| | | A | | B | | C | |
| | | Beam C2 | Beam C3 | Beam D5 | Beam D6 | Beam C2 | Beam C4 |
| 5 | 0.5 | 2763 | 2957 | 2419 | 2460 | 1725 | 2017 |
| | 1 | 2984 | 3204 | 2561 | 2565 | 1750 | 2028 |
| | 2 | 3187 | 3490 | 2702 | 2813 | 1872 | 2079 |
| | 5 | 3388 | 3841 | 2910 | 3114 | 2029 | 2157 |
| | 10 | 3735 | 4228 | 3273 | 3354 | 2106 | 2291 |
| 10 | 0.5 | 2255 | 2639 | 1935 | 2046 | 1451 | 1692 |
| | 1 | 2460 | 2828 | 2000 | 2176 | 1533 | 1756 |
| | 2 | 2552 | 3104 | 2115 | 2335 | 1537 | 1811 |
| | 5 | 2749 | 3502 | 2396 | 2643 | 1573 | 1933 |
| | 10 | 2837 | 3768 | 2728 | 2853 | 1585 | 1973 |
| 15 | 0.5 | 2019 | 2194 | 1567 | 1690 | 1260 | 1373 |
| | 1 | 2087 | 2441 | 1731 | 1846 | 1335 | 1469 |
| | 2 | 2157 | 2593 | 1811 | 1947 | 1387 | 1501 |
| | 5 | 2284 | 2897 | 1942 | 2130 | 1421 | 1605 |
| | 10 | 2456 | 3043 | 2229 | 2315 | 1497 | 1662 |
| 20 | 0.5 | 1715 | 1904 | 1138 | 1303 | 1087 | 1220 |
| | 1 | 1868 | 2038 | 1423 | 1484 | 1183 | 1284 |
| | 2 | 1930 | 2166 | 1364 | 1540 | 1190 | 1343 |
| | 5 | 2054 | 2501 | 1542 | 1710 | 1238 | 1430 |
| | 10 | 2123 | 2642 | 1779 | 1852 | 1265 | 1479 |
| 25 | 0.5 | 1391 | 1528 | 1059 | 1108 | 957 | 1000 |
| | 1 | 1541 | 1653 | 1160 | 1175 | 1012 | 1089 |
| | 2 | 1592 | 1794 | 1178 | 1258 | 1054 | 1043 |
| | 5 | 1689 | 1971 | 1268 | 1406 | 1065 | 1062 |
| | 10 | 1765 | 1957 | 1383 | 1558 | 1128 | 1110 |

Table 3: Flexural stiffness modulus for the 75M-0 mixes

| Test temperature [ºC] | Frequency [Hz] | Flexural stiffness modulus per binder type [MPa] | | | | | |
|---|---|---|---|---|---|---|---|
| | | A | | B | | C | |
| | | Beam C5 | Beam C6 | Beam C3 | Beam C4 | Beam C3 | Beam C4 |
| 5 | 0.5 | 1730 | 1439 | 1863 | 2330 | 1423 | 1448 |
| | 1 | 1887 | 1513 | 1965 | 2336 | 1573 | 1493 |
| | 2 | 1965 | 1555 | 2090 | 2522 | 1601 | 1584 |
| | 5 | 2143 | 1701 | 2386 | 2854 | 1714 | 1672 |
| | 10 | 2433 | 1701 | 2667 | 3179 | 1758 | 1762 |
| 10 | 0.5 | 1582 | 1324 | 1646 | 1854 | 1210 | 1261 |
| | 1 | 1737 | 1425 | 1790 | 2018 | 1324 | 1348 |
| | 2 | 1842 | 1488 | 1932 | 2232 | 1374 | 1422 |
| | 5 | 1868 | 1653 | 2105 | 2528 | 1538 | 1510 |
| | 10 | 2078 | 1638 | 2335 | 2710 | 1570 | 1594 |
| 15 | 0.5 | 1333 | 1145 | 1449 | 1526 | 1069 | 1054 |
| | 1 | 1465 | 1246 | 1550 | 1575 | 1154 | 1100 |
| | 2 | 1547 | 1307 | 1664 | 1777 | 1180 | 1144 |
| | 5 | 1597 | 1362 | 1822 | 1968 | 1232 | 1314 |
| | 10 | 1672 | 1427 | 2030 | 2076 | 1300 | 1320 |
| 20 | 0.5 | 1076 | 976 | 1171 | 1217 | 984 | 977 |
| | 1 | 1140 | 1002 | 1286 | 1324 | 1041 | 957 |
| | 2 | 1184 | 1004 | 1397 | 1416 | 950 | 989 |
| | 5 | 1245 | 1116 | 1552 | 1603 | 1099 | 1053 |
| | 10 | 1314 | 1144 | 1686 | 1716 | 1156 | 1061 |
| 25 | 0.5 | 946 | 842 | 983 | 1028 | 919 | 781 |
| | 1 | 1038 | 898 | 1094 | 1095 | 937 | 859 |
| | 2 | 946 | 911 | 1193 | 1202 | 904 | 887 |
| | 5 | 964 | 887 | 1206 | 1286 | 888 | 871 |
| | 10 | 996 | 836 | 1333 | 1444 | 939 | 866 |

This page is left blank intentionally.

# APPENDIX J : FATIGUE TESTING RESULTS

It should be noted that, as explained in Section 4.6.3, the fatigue performance at the reported strain levels are unconservative and an over-estimation of the actual fatigue performance of the material. The fatigue lives as reported should be associated with strain levels that are anything between 0 % and 50 % lower than the reported strain levels, depending on the type of mix and specified strain levels.

Table 1: Number of load repetitions to failure of mixes with aggregate blend 75C-0 (at 10 Hz and 5ºC)

| Binder type | Beam specimen | Strain level [με] | Initial flexural stiffness [MPa] | Number of load repetitions to failure [-] |
|---|---|---|---|---|
| A | E1 | 370 | 2 239 | 7 010 |
| | D5 | 350 | 2 444 | 72 000 |
| | E2 | 270 | 2 614 | 204 900 |
| | F4 | 200 | 2 210 | 518 800 |
| B | A2 | 470 | 1 672 | 7 674 |
| | A5 | 450 | 1 572 | 7 059 |
| | A1 | 430 | 2 059 | 11 114 |
| | A3 | 400 | 1 521 | 9 323 |
| | A4 | 380 | 1 753 | 10 215 |
| | A6 | 350 | 2 349 | 15 050 |
| | B1 | 330 | 3 621 | 23 020 |
| | B6 | 300 | 3 563 | 95 250 |
| | B2 | 250 | 2 799 | 316 220 |
| | B3 | 230 | 2 626 | 132 350 |
| | B5 | 200 | 3 544 | 1 177 900 |
| | B4 | 180 | 3 177 | 416 860 |
| C | D5 | 470 | 2040 | 3 942 |
| | C1 | 450 | 1763 | 7 680 |
| | D3 | 430 | 1695 | 2 390 |
| | D4 | 400 | 2451 | 22 550 |
| | D6 | 380 | 2276 | 34 400 |
| | B4 | 350 | 614 | 42 000 |
| | D1 | 330 | 1836 | 66 000 |
| | B3 | 300 | 817 | 420 000 |
| | B5 | 250 | 725 | 3 420 000[1] |
| | D2 | 230 | 2858 | 732 820 |
| | A6 | 200 | 986 | 1 620 000[1] |
| | A5 | 180 | 1022 | 3 600 000[1] |

Table 2: Number of load repetitions to failure of mixes with aggregate blend 75C-1 (at 10 Hz and 5ºC)

| Binder type | Beam specimen | Strain level [με] | Initial flexural stiffness [MPa] | Number of load repetitions to failure [-] |
|---|---|---|---|---|
| A | C6 | 520 | 1 736 | 5 050 |
| | A2 | 450 | 2 813 | 4 630 |
| | B3 | 430 | 2 950 | 2 490 |
| | A3 | 400 | 2 544 | 46 650 |
| | B4 | 370 | 2 913 | 90 960 |
| | A1 | 350 | 2 499 | 56 810 |
| | C5 | 300 | 3 346 | 593 380 |
| | A6 | 270 | 2 020 | 177 640 |
| | C1 | 220 | 2 803 | 443 470 |
| | B2 | 200 | 3 840 | 984 820 |
| B | C4 | 450 | 1694 | 1 819 |
| | C1 | 420 | 1 270 | 5 713 |
| | C6 | 380 | 2 524 | 16 986 |
| | B1 | 350 | 1 674 | 23 612 |
| | B2 | 300 | 1 616 | 88 200[1] |
| | B3 | 280 | 2 101 | 21 300 |
| | B6 | 250 | 1 617 | 560 000[1] |
| | B5 | 200 | 1 832 | 172 000[1] |
| | D4 | 190 | 2 850 | 94 000 |
| | B4 | 180 | 2 370 | 800 000 |
| | C3 | 140 | 2 785 | 2 400 000[1] |
| | C5 | 120 | 3 093 | 1 700 000[1] |
| C | A4 | 470 | 1583 | 19 150 |
| | B5 | 450 | 1789 | 16 460 |
| | A2 | 400 | 1449 | 115 000 |
| | B3 | 380 | 1546 | 58 200 |
| | A3 | 350 | 1826 | 122 000 |
| | B2 | 330 | 1720 | 91 000 |
| | A1 | 300 | 1518 | 840 000 |
| | B4 | 280 | 1447 | 550 000 |
| | A5 | 250 | 1673 | 3 310 000 |
| | B1 | 230 | 1271 | 822 000[1] |
| | A6 | 200 | 1480 | 1 236 000 |
| | B6 | 180 | 1800 | 5 680 000[1] |

Note: 1) These results were obtained by extrapolation, see Chapter 6

Table 3: Number of load repetitions to failure of mixes with aggregate blend 75M-0 (at 10 Hz and 5ºC)

| Binder type | Beam specimen | Strain level [με] | Initial flexural stiffness [MPa] | Number of load repetitions to failure [-] |
|---|---|---|---|---|
| A | Z6 | 350 | 1 630 | 19 150 |
| | Y1 | 250 | 1 461 | 65 060 |
| | Z5 | 160 | 1 744 | 1 079 770 |
| B | B5 | 470 | 3658 | 1 748 |
| | A3 | 450 | 2 893 | 4 573 |
| | A4 | 400 | 3 346 | 7 706 |
| | B2 | 380 | 4173 | 8 000 |
| | B6 | 370 | 4 061 | 7 120 |
| | B4 | 350 | 3910 | 15 440 |
| | A1 | 300 | 4 035 | 27 130 |
| | A2 | 250 | 4 045 | 132 000 |
| | A6 | 230 | 3 850 | 168 520 |
| | B1 | 200 | 4 391 | 1 345 510 |
| | A5 | 180 | 3 593 | 1 260 000[1] |
| | B3 | 150 | 3750 | 2 630 000[1] |
| C | C5 | 470 | 1072 | 19 300 |
| | C4 | 450 | 789 | 14 790 |
| | B4 | 400 | 1410 | 26 000 |
| | A3 | 380 | 896 | 39 600 |
| | A1 | 350 | 842 | 205 000 |
| | C2 | 330 | 1052 | 310 762 |
| | A2 | 300 | 682 | 212 588 |
| | C1 | 280 | 634 | 194 177[1] |
| | A6 | 250 | 924 | 830 000 |
| | B5 | 230 | 1693 | 410 000 |
| | A5 | 200 | 1096 | 1 850 000[1] |
| | B6 | 180 | 1444 | 3 520 000[1] |

Note: 1) These results were obtained by extrapolation, see Chapter 6

This page is left blank intentionally.

# APPENDIX K: BURGERS MODEL PARAMETERS

Table 1: Burgers Model Parameters at 5ºC

| Parameter | A-75C-0 | A-75C-1 | A-75M-0 | B-75C-0 | C-75C-0 | C-75C-1 | C-75M-0 |
|---|---|---|---|---|---|---|---|
| $E_0$ [MPa] | 3644 | 3980 | 2796 | 3600 | 2906 | 2612 | 2231 |
| $E_1$ [MPa] | 5495 | 10869 | 5402 | 6720 | 5499 | 9577 | 4485 |
| $\lambda_1$ [MPa/s] | 1398 | 3126 | 1298 | 1659 | 1554 | 1236 | 1033 |
| $\lambda_0$ [MPa/s] | 317 | 559 | 263 | 341 | 318 | 204 | 206 |

Table 2: Burgers Model Parameters at 10ºC

| Parameter | A-75C-0 | A-75C-1 | A-75M-0 | B-75C-0 | C-75C-0 | C-75C-1 | C-75M-0 |
|---|---|---|---|---|---|---|---|
| $E_0$ [MPa] | 3553 | 3384 | 2414 | 3227 | 2632 | 2291 | 2045 |
| $E_1$ [MPa] | 5814 | 7619 | 5668 | 5015 | 4582 | 6765 | 3670 |
| $\lambda_1$ [MPa/s] | 1316 | 2098 | 1171 | 1212 | 1191 | 1633 | 734 |
| $\lambda_0$ [MPa/s] | 287 | 401 | 220 | 271 | 253 | 285 | 154 |

Table 3: Burgers Model Parameters at 15ºC

| Parameter | A-75C-0 | A-75C-1 | A-75M-0 | B-75C-0 | C-75C-0 | C-75C-1 | C-75M-0 |
|---|---|---|---|---|---|---|---|
| $E_0$ [MPa] | 2965 | 2794 | 2214 | 2590 | 2267 | 2016 | 1839 |
| $E_1$ [MPa] | 4042 | 7504 | 4171 | 3521 | 3094 | 4627 | 2873 |
| $\lambda_1$ [MPa/s] | 870 | 1744 | 781 | 731 | 680 | 1108 | 580 |
| $\lambda_0$ [MPa/s] | 208 | 314 | 160 | 175 | 162 | 210 | 129 |

Table 4: Burgers Model Parameters at 20ºC

| Parameter | A-75C-0 | A-75C-1 | A-75M-0 | B-75C-0 | C-75C-0 | C-75C-1 | C-75M-0 |
|---|---|---|---|---|---|---|---|
| $E_0$ [MPa] | 2342 | 2665 | 1809 | 2192 | 1981 | 1883 | 1320 |
| $E_1$ [MPa] | 2911 | 5324 | 2912 | 2806 | 2751 | 3953 | 3491 |
| $\lambda_1$ [MPa/s] | 161 | 258 | 123 | 141 | 143 | 173 | 114 |
| $\lambda_0$ [MPa/s] | 640 | 1291 | 562 | 572 | 604 | 888 | 629 |

Table 5: Burgers Model Parameters at 25ºC

| Parameter | A-75C-0 | A-75C-1 | A-75M-0 | B-75C-0 | C-75C-0 | C-75C-1 | C-75M-0 |
|---|---|---|---|---|---|---|---|
| $E_0$ [MPa] | 1802 | 2271 | 1074 | 1841 | 1842 | 1363 | 1049 |
| $E_1$ [MPa] | 2559 | 3971 | 4724 | 2405 | 2398 | 3783 | 4632 |
| $\lambda_1$ [MPa/s] | 475 | 980 | 699 | 474 | 505 | 674 | 687 |
| $\lambda_0$ [MPa/s] | 111 | 207 | 110 | 116 | 123 | 120 | 108 |

**A-75C-0**

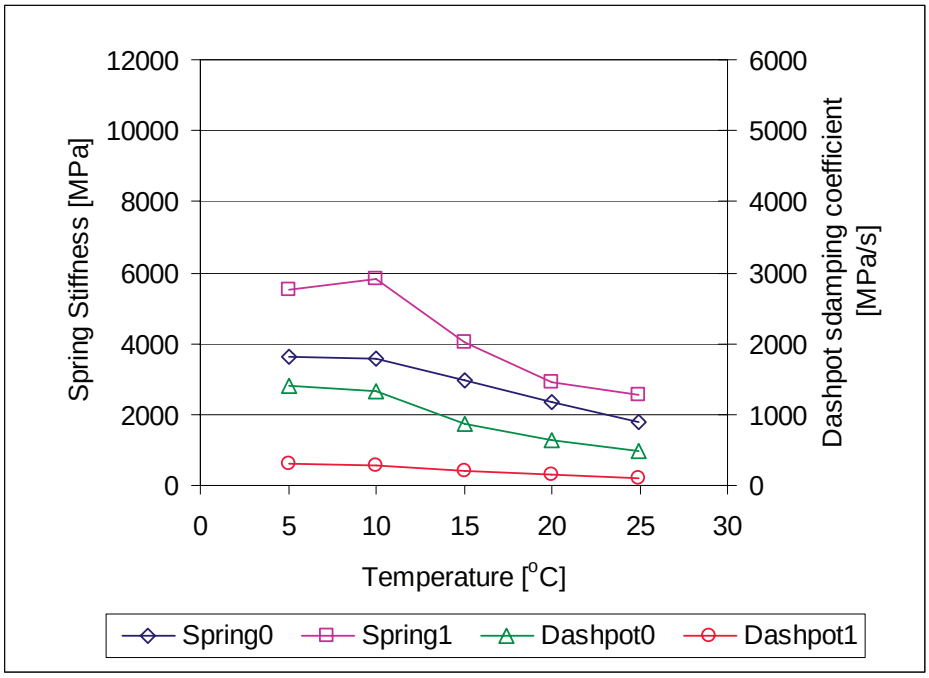
12000
10000
8000
6000
4000
2000
0
Spring Stiffness [MPa]
6000
5000
4000
3000
2000
1000
0
Dashpot sdamping coefficient [MPa/s]
0
5
10
15
20
25
30
Temperature [°C]
Spring0
Spring1
Dashpot0
Dashpot1

**A-75C-1**

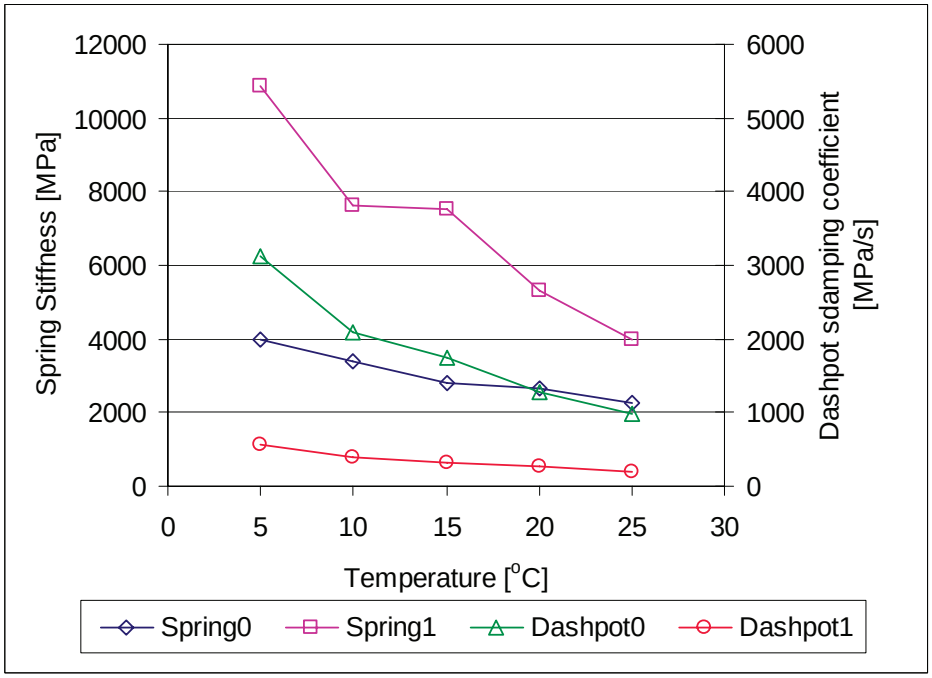
12000
10000
8000
6000
4000
2000
0
Spring Stiffness [MPa]
6000
5000
4000
3000
2000
1000
0
Dashpot sdamping coefficient [MPa/s]
0
5
10
15
20
25
30
Temperature [°C]
Spring0
Spring1
Dashpot0
Dashpot1

**A-75M-0**

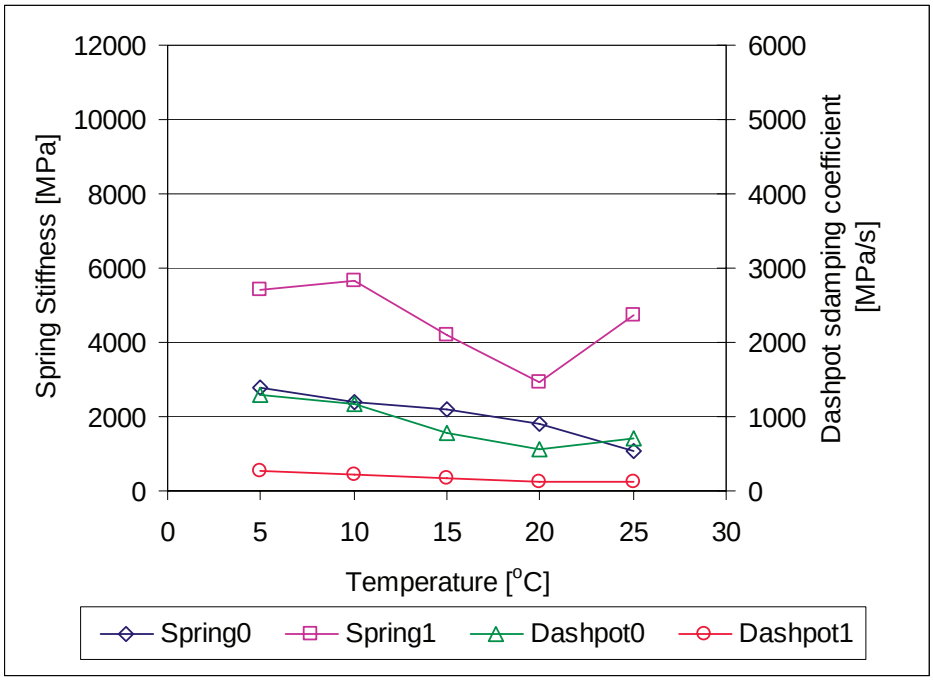
12000
10000
8000
6000
4000
2000
0
Spring Stiffness [MPa]
6000
5000
4000
3000
2000
1000
0
Dashpot sdamping coefficient [MPa/s]
0
5
10
15
20
25
30
Temperature [°C]
Spring0
Spring1
Dashpot0
Dashpot1

**B-75C-0**

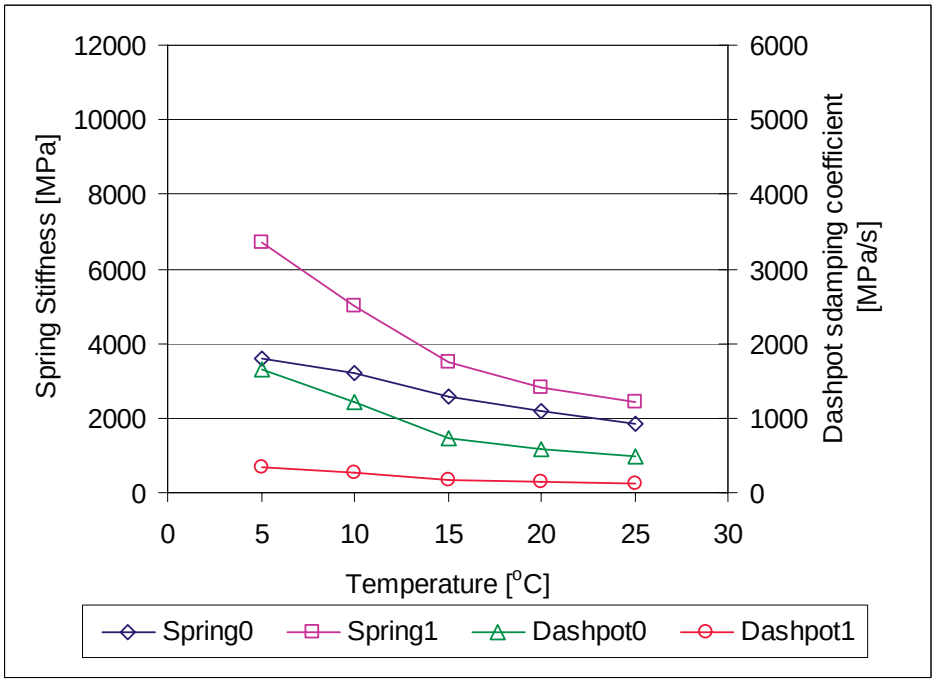
12000
10000
8000
6000
4000
2000
0
Spring Stiffness [MPa]
6000
5000
4000
3000
2000
1000
0
Dashpot sdamping coefficient [MPa/s]
0
5
10
15
20
25
30
Temperature [°C]
Spring0
Spring1
Dashpot0
Dashpot1

**B-75C-1**

Not determined.

**B-75M-0**

Not determined

**C-75C-0**

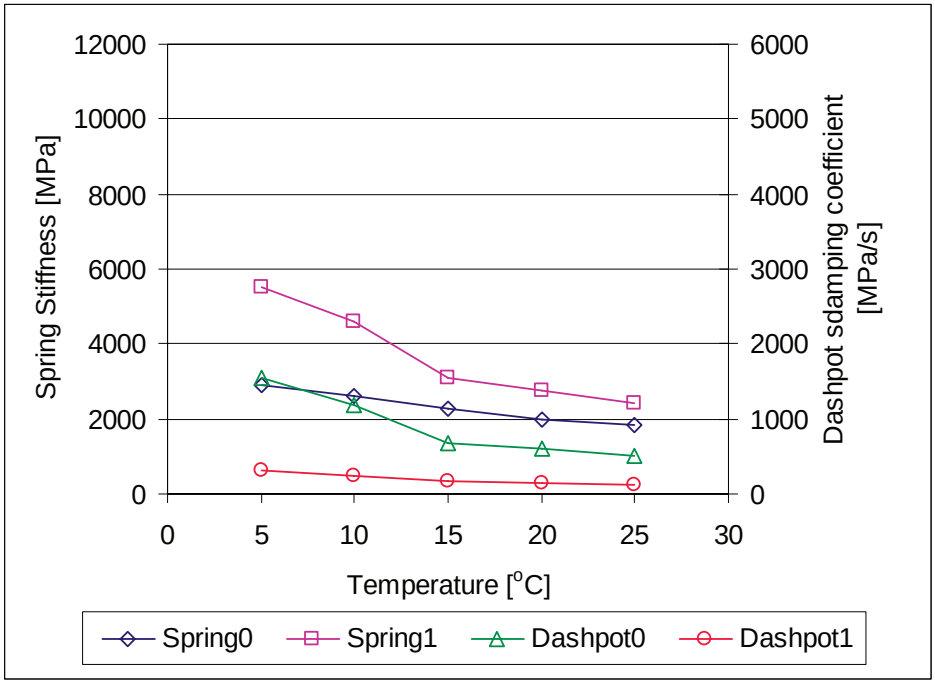

**C-75C-1**

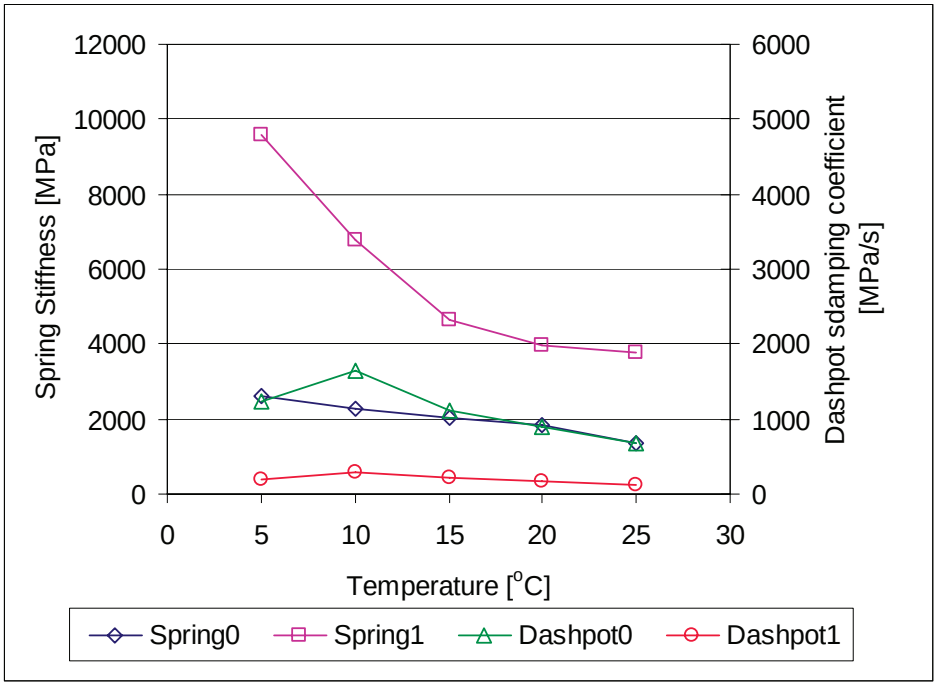
12000
10000
8000
6000
4000
2000
0
Spring Stiffness [MPa]
6000
5000
4000
3000
2000
1000
0
Dashpot sdamping coefficient [MPa/s]
0
5
10
15
20
25
30
Temperature [°C]
Spring0
Spring1
Dashpot0
Dashpot1

**C-75M-0**

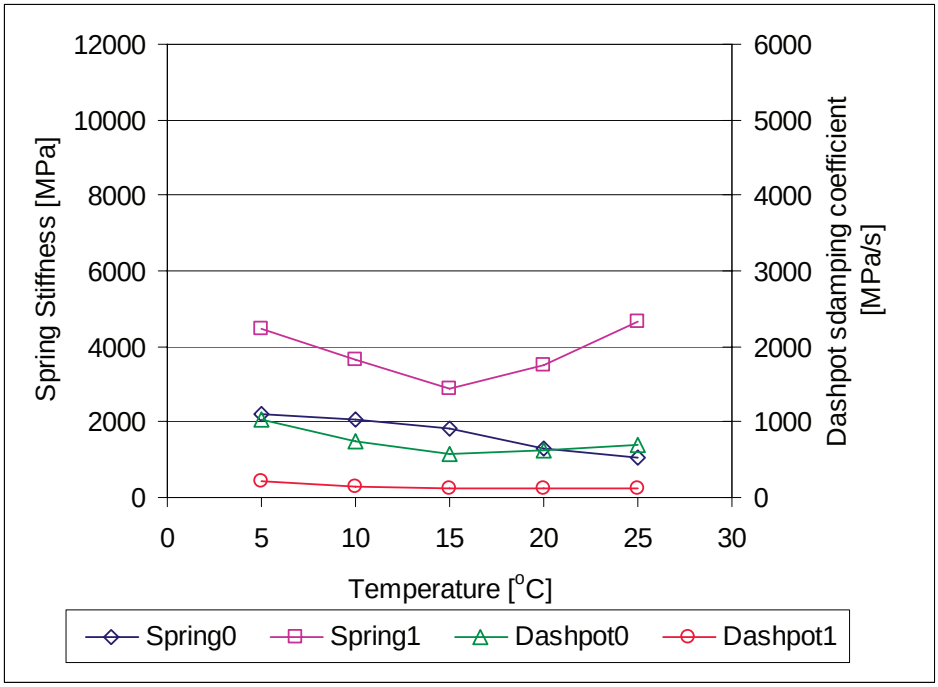
12000
10000
8000
6000
4000
2000
0
Spring Stiffness [MPa]
6000
5000
4000
3000
2000
1000
0
Dashpot sdamping coefficient [MPa/s]
0
5
10
15
20
25
30
Temperature [°C]
Spring0
Spring1
Dashpot0
Dashpot1

This page is left blank intentionally.